Impacts of fire, climate and land-use change on terrestrial ecosystems

Submitted by Chantelle Burton to the University of Exeter
as a thesis for the degree of
Doctor of Philosophy (PhD) in Geography
In December 2018

I certify that all material in this thesis which is not my own work has been identified and that no material has previously been submitted and approved for the award of a degree by this or any other University.

Signature: ……..

Abstract

Fire is an important component of the Earth system, affecting the land surface, releasing gases to the atmosphere, and altering the water cycle. Yet many Earth System Models lack full representation of this process, giving rise to uncertainty about its contribution to the development and stability of ecosystems now and in the future. In this PhD I investigate the impact of fire on the land surface today, and how this might change with drought events and with climate change in the future by developing the land surface model JULES to represent fire-vegetation interactions for the first time. I introduce a new fire disturbance term based on burnt area from the INFERNO fire model, and analyse the results of the coupling, together with changes in land-use, against observations of present day vegetation cover. I find that the simulation of vegetation cover is improved when disturbance is included, and that fire is important in the development of savanna regions. I apply the new modelling capability to assess the impact of the 2015/16 El Niño event on fire, where projections show that burned area and fire emissions were higher due to the El Niño. The largest impact was across South America, where carbon uptake was reduced due to increases in fire, inducing a shift from a net sink of carbon to a net source. Fire danger may be further exacerbated in years of higher temperatures and drought in the future as a result of climate change. I apply the capability to model different aspects of the fire regime with future scenarios of climate and land-use change across a range of emission scenarios. Using Representative Concentration Pathway scenarios, I show that burned area is projected to increase in the future, with hotter, drier conditions increasing with higher emission scenarios and greater changes in land-use, especially across South America but not homogeneously. Using a theoretical scenario of Solar Radiation Management to limit temperature rise to 1.5°C above pre-industrial, I show that meteorological fire danger is generally reduced compared to 2.0°C, although there are regional variations and some regions show an increase including USA and Asia. This work furthers our current modelling capability around fire vegetation interactions, and enhances our understanding of the response of ecosystems to changes in fire, climate and land-use.

Contents

List of figures

List of tables

Author's declaration

All of the work presented in this thesis is my own, except where referenced. Parts of the work presented here have been published as follows:

Burton, C., Betts, R.A., Jones, C.D., Williams, K. (2018): Will fire danger be reduced by using Solar Radiation Management to limit global warming to 1.5°C compared to 2.0°C? Geophysical Research Letters. Apr 28;45(8):3644-52.

Burton, C., Betts, R., Cardoso, M., Feldpausch, T. R., Harper, A., Jones, C. D., Kelley, D. I., Robertson, E., and Wiltshire, A. (2019): Representation of fire, land-use change and vegetation dynamics in the Joint UK Land Environment Simulator vn4.9 (JULES), Geosci. Model Dev., 12, 179-193, https://doi.org/10.5194/gmd-12-179-2019.

Acknowledgements

I would like to extend my sincerest thanks and gratitude to my supervisors Richard Betts, Chris Jones and Ted Feldpausch, who have guided and encouraged me over the last three years, have given up their time to supervise me, and who had enough faith to take me on as their student.

I would also like to thank my colleagues at the Met Office who have been so patient and willing to offer help and support, particularly Andy Wiltshire, Eddy Robertson and Karina Williams who I couldn't have done this without. Thanks also to my collaborators at CEH, Exeter University and INPE, including Doug Kelley, Manoel Cardoso and Anna Harper who have been fantastic to work with. I would like to give my deepest thanks to Stephen Belcher and Kirstine Dale for their encouragement and belief in me, and for making this opportunity possible.

Finally, this research would not have been possible without the generous support of my funders. This work was supported by the Newton Fund through the Met Office Climate Science for Service Partnership Brazil (CSSP Brazil), and the European Commission's 7th Framework Programme (EU/FP7) under Grant Agreement 603864 (HELIX, Chapter 6).

Abbreviations

AMO	Atlantic Multidecadel Oscillation
AOD	Aerosol Optical Depth
ATSR	Along-Track Scanning Radiometer
AVHRR	Advanced Very High Resolution Radiometer
BECCS	Bioenergy Carbon Capture and Storage
BL	Broadleaf vegetation
BS	Bare soil / ground
C3	C3 grass
C4	C4 grass
CCI	Climate Change Initiative
CDR	Carbon Dioxide Removal
CLM	Community Land Model
CO_2	Carbon dioxide
COP	Conference of Parties
CRU	Climate Research Unit
CSIRO	Commonwealth Scientific and Industrial Research Organisation (Australia)
CTEM-fire	Canadian Terrestrial Ecosystem Model (fire model)
DGVM	Dynamic Global Vegetation Model
DPM	Decomposable Plant Material
DVF	Disturbed Vegetation Fraction
Embrapa	Brazilian Agricultural Research Corporation
ENSO	El Niño Southern Oscillation
ERF	Effective Radiative Forcing
ESA	European Space Agency
ESM	Earth System Model
ET	Evapotranspiration
EVI	Enhanced Vegetation Index
FFDI	McArthur Forest Fire Danger Index
FireMIP	Fire Model Intercomparison Project
FMI	Sharples Fuel Moisture Index
FSS	Fire Season Severity
FSSI	Fire Season Severity Index

FWI	Forest Fire Weather Index
GBS	Global Burnt Surfaces project
GCM	Global Climate / Circulation Model
GCP	Global Carbon Project
GDP	Gross Domestic Product
GFDI	Grassland Fire Danger Index
GFED	Global Fire Emissions Database
GHG	Greenhouse gas
Glob-FIRM	GLOBal FIRe Model
GOES	Geostationary Operational Environmental Satellites
GPP	Gross Primary Productivity
GRACE	Gravity Recovery and Climate Experiment (satellite)
HadCM	Met Office Hadley Centre Climate Model
HadCM3LC	MOHC Climate model version 3, with low ocean resolution and carbon-cycle included
HadGEM2-ES	Met Office Hadley Centre Global Environmental Model version 2 Earth System configuration
HadOCC	Ocean-carbon cycle model
HDF	Hierarchical Data Format
HYDE	History Database of the Global Environment
IBAMA	Brazilian Institute of Environment and Renewable Natural Resources
IBIS-INLAND	Integrated Biosphere Simulator - Brazilian Integrated Model of Land Surface Process
INFERNO	INteactive Fire and Emission algoRithm for Natural envirOnments
INPE	Brazilian National Institute for Space Research
IPCC AR5	Intergovernmental Panel for Climate Change, 5th Assessment Report (AR4: 4th Assessment Report)
JSBACH	Land component of the Max Planck Institute Earth System Models MPI-ESM and ICON-ESM
JULES	Joint UK Land Environment Simulator
LAI	Leaf Area Index
LMfire	Lausanne-Mainz fire model
LPJ	Lund-Potsdam-Jena DGVM

LPJ-GUESS	Lund-Potsdam-Jena General Ecosystem Simulator
LPX	Land surface Process and eXchanges model
LSM	Land Surface Model
LUC	Land-use change
LULCC	Land-use and land cover change
MCFire	MAPPS-Century DGVM with fire
MOSES	Met Office Surface Exchange Scheme
MODIS	Moderate Resolution Imaging Spectroradiometer
MOHC	Met Office Hadley Centre
MMA	Brazilian Ministry of the Environment
NASA	National Aeronautics and Space Administration
NBP	Net Biome Production / Productivity
NCEP	National Centres for Environmental Prediction
NDVI	Normalized Difference Vegetation Index
NEP	Net Ecosystem Production
NFDRS	National Fire Danger Rating System
NL	Needleleaf vegetation
NOAA	National Oceanic and Atmospheric Administration
NPP	Net Primary Productivity
ONI	Ocean Nino Index
ORCHIDEE	Organizing Carbon and Hydrology In Dynamic Ecosystems
PI	Pre-Industrial
PFT	Plant Functional Type
PRODES	Program for the Estimation of Deforestation in the Brazilian Amazon
PVM	Potential Vegetation Model
RCP	Representative Concentration Pathways
Reg-FIRM	Regional Fire Model
RPM	Resistant Plant Material
SAGE	Centre for Sustainability and the Global Environment
SAMS	South American Monsoon System
SB	Shrub
SDGVM	Sheffield Dynamic Global Vegetation Model
SPITFIRE	Spread and InTensity of FIRE (fire model)
SRES	Special Report on Emissions Scenarios

SRM	Solar Radiation Management
SST	Sea surface temperature
TRENDY	Trends in net land carbon exchange project
TRIFFID	Top-down Representation of Interactive Foliage and Flora Including Dynamics
TRMM	Tropical Rainfall Measuring Mission
UNFCCC	United Nations Framework Convention on Climate Change
VIRS	Visible and Infrared Scanner

Chapter 1: Background & context

1.1 Introduction to thesis and aims

Fire is one of the most important disturbances in the Earth system (Bowman *et al*, 2009). It can impact vegetation dynamics through mortality and regrowth (Lasslop *et al*., 2016), atmospheric chemistry and the carbon cycle through the release of gases and particulate matter (Ward *et al*., 2012), and the hydrological cycle through reduction in evapotranspiration (Shakesby and Doerr, 2006), which is impacted by and feeds back onto anthropogenic impacts. It is therefore a crucial process to represent in both land surface models and Earth System Models (ESMs) (Hantson *et al*., 2016; Rabin *et al*., 2017). The representation of fire in models is still a relatively new process, especially in ESMs so there is still much uncertainty in the projection of burned area and its impacts (Ciais *et al*., 2013; Flato *et al*., 2013; Settele *et al*., 2014; Kloster and Lasslop *et al*., 2017). While many land surface models now include fire, the modelling capability and extent of interactions varies greatly across models (Rabin *et al*., 2017). It is therefore important for the community to continue to develop our current capability to improve our understanding of interactions in the terrestrial carbon cycle and ultimately within the Earth system. This thesis aims to further our understanding of the biogeophysical interactions surrounding fire and disturbance spatially and temporally, by improving our fire modelling capability within the UK land surface model JULES (Joint UK Land Environment Simulator) using a simple fire model INFERNO (INteactive Fire and Emission algoRithm for Natural envirOnments) and coupling it to dynamic vegetation.

Studies have shown both a potential increase in fire danger in some regions in the future, including increased risk of uncontrolled fire spread (Aragão *et al*., 2018) under extreme hot/dry conditions, and conversely a decreasing trend of fire occurrence over the last 20 years (Andela *et al*., 2017), leading to continuing uncertainty about the role that this important process will play in ecosystems over the coming decades. Fire occurrence is a function of local environmental and anthropogenic processes, and both its history and its future impacts will not be spatially homogeneous.

This thesis focuses on the impacts of fire, climate and land-use change globally but with a particular focus on South America and the ecosystems of Brazil. The Brazil region is one of the areas with the most uncertainty in future projections of fire (Kloster *et al*., 2012; Moritz *et al*., 2012; Betts *et al*., 2015). The Amazon rainforest itself (henceforth referred to as 'the Amazon') is scientifically important because of its capacity to store and release carbon, as a source of biodiversity, regulator of regional and global scale water and climate, and its historical socio-political focus as a site of extensive deforestation and degradation (Soares-Filho *et al*. 2006; Malhi *et al*., 2009; Brienen, 2015; Fauset *et al*., 2015). The Amazon is also a key region where there is still much uncertainty about how the links between climate, increased CO_2 and land-use will impact the occurrence of fire in the future (Good *et al*., 2014), and considering its importance in the Earth system, more work is needed to understand how fire danger may change here. However this needs to be placed in the context of other ecosystems across the country and continent according to the question being addressed. The regions of high fire for example effect the southern Amazon across the Cerrado of Brazil, pushing the frontiers of the Amazon further North, and to understand the drivers of these fire patterns it is useful to consider meteorological and climatological changes across the rest of the continent and globally. In the context of extreme events such as El Niño, it is useful to compare fire occurrence with other regions of high fire such as across Africa or Asia, to understand patterns and drivers across different ecosystems and put the results in a global context.

This PhD aims to further the knowledge in this area, by assessing the impact of fire on vegetation dynamics historically, for the present day, and in the future under different scenarios of climate and land-use change using improved fire modelling capability. The land surface model JULES will be used for this work, and the capability of the fire model INFERNO will be developed so that it interacts with the dynamic vegetation within JULES to produce an interactive response to fire. Scenarios will then be assessed for the historical period against observations, and the model tuned to give the best estimate of present day results. The model will be used to investigate the impact of the 2015/16 El Niño on fire, and driven with standard future scenarios of climate change to give a projected range of response to 2100 (high, medium and low emission scenarios).

Fire danger indices will also be used to give an indicative guide of the impact of alternative solutions, including mitigation efforts to limit temperature rise to 1.5ºC.

This research aims to further our understanding of the interaction of fire, climate and land-use change by developing current modelling capability, and using this to answer key questions about how ecosystems are affected by fire and disturbance today, and how and why this might change under different future scenarios.

The structure is as follows:

- Chapter 1: Background & context
  This chapter will give an overview of the current status of modelling fire and land-use, including use of observations, fire indices and fire models. This is placed in the context of existing literature, with a particular focus on a number of studies that have previously linked fire, land-use and climate change in Brazil. It highlights the gap in current research which this thesis will address.
    - Fire and land-use in context
    - Research gap and motivation for study
    - Overview of observations
    - Overview of fire indices
    - Current status of fire modelling
- Chapter 2: Introduction to land-use and land surface modelling
  This chapter will investigate the impact of land-use change globally and over Brazil, with a focus on the land carbon sink. A multi-model analysis shows large uncertainty in the land-use contribution of carbon allocation across models. I use four future RCP scenarios to analyse the implications for future land-use in Brazil.
    - Introduction to land-use change
    - Representation of land-use across models
    - Contribution of land-use to carbon allocation
    - Future RCP scenarios of land-use
- Chapter 3: Interactive INFERNO: fire-vegetation interactions in JULES
  This chapter will outline the work that has been done to develop the fire modelling capability in INFERNO, to couple fire to dynamic vegetation and

the results of the coupling. These will be compared against observations, and the model tuned to produce a standard set up with interactive fire. Results will be analysed for Brazil.

  - Developing fire modelling capability in JULES
  - Impact of disturbance on vegetation cover
  - Impact of fire on development of savannas in Brazil

- Chapter 4: Impacts of the 2015-2016 El Niño

  A range of variables will be assessed with JULES-INFERNO to understand what impacts the 2015-2016 El Niño had on fire and the terrestrial ecosystem.

  - What was the impact of the 2015/16 El Niño on fire? Did this vary globally, and why?
  - What impact did the El Niño have on the carbon sink globally and regionally when fire is taken into account?
  - How did the impacts of the 2015/16 El Niño vary spatially and in time across South America?

- Chapter 5: Future projections of fire, climate and land-use change

  JULES-INFERNO is used to assess the standard RCP scenarios of future emission pathways, with a focus on vegetation dynamics in the region of Brazil.

  - How is burnt area projected to change with climate change in the future and, together with changes in land-use, what impact does this have on vegetation coverage?
  - What is the impact of different warming levels, and does the pathway to reach them alter the impacts on the land surface?
  - Could fire lead to a change in state from tropical forest to savanna by 2100?

- Chapter 6: New horizons: limiting temperature rise to 1.5°C with SRM

  Fire danger indices are used to understand potential impacts of limiting temperature rise to 1.5ºC based on new policy developments under the ‘Paris Agreement’.

  - Impacts of limiting temperature rise to 1.5°C on fire danger
  - Drivers of regional differences in fire

- Chapter 7: Synthesis and conclusions

  The final chapter will summarise the results found over the course of this PhD, draw conclusions about the implications and recommend steps for further research.

  - Summary of key findings
  - Future work
  - Wider implications of this work

The high-level findings can be summarised as follows:

- Disturbance is important for accurate simulation of vegetation cover within JULES
- Fire is important for the representation of the Cerrado in Brazil in JULES, and improves the simulation of land-use emissions from this region
- El Niño events can increase fire danger in some areas, as was the case with the 2015-16 El Niño in South America due to hotter and (in some areas) drier conditions.
- The Amazon biome has the potential to change from a sink to a source of carbon in hot, dry years
- Fire danger is projected to increase in the future due to hotter and drier conditions, but not homogeneously
- The pathway taken to specific levels of warming has different regional impacts, with hotter temperatures and higher burnt area projected in NE Brazil in scenario RCP8.5 at global mean temperatures of 2.0˚C compared to other RCP scenarios, leading to reduced evapotranspiration and higher albedo
- Fires may reduce dry season resilience of tropical ecosystems and bring them closer to a tipping point in the future
- Fire danger is reduced at lower temperatures, but not homogeneously due to changing patterns of temperature and moisture availability

The ultimate goal of this PhD will be to represent interactive fire disturbance processes in JULES with dynamic vegetation in the present day, and understand the implications of this for the Amazon historically and in the future. This is the first step towards including interactive fire from INFERNO within an Earth System Model, which will ultimately contribute to the wider field of climate science by

improving our ability to properly simulate the complete Earth system. This will enable us to create more realistic projections of the future, and thus aid policy by providing a better understanding of the implications of climate change and how to best mitigate and or adapt to these coming changes.

1.2 Fire, climate and land-use in context

1.2.1 Introduction to fire modelling

Fire events exist in the confluence of temporal and spatial scales. Fires are experienced as a local phenomenon, yet are recognised as a global scale environmental process with importance and impacts at the Earth system level (Rabin *et al*, 2017). In terms of hazard management and action planning, we consider individual fires that occur over days to weeks, but fire danger and change in regimes are studied on a seasonal basis, with implications for the atmosphere and biosphere on timescales of hundreds to millions of years (Pechony and Shindell, 2010; Koele *et al*., 2017; Goulart *et al*., 2017).

Fundamentally, the occurrence of fire depends on the availability of fuel, oxygen and ignition, but the nature of the fire regime including frequency, seasonality, size, intensity, and ecosystem effects, depends on a number of processes. These include fuel connectivity, fuel type, resistance of fuel to fire, density and dryness, conditions such as topography, temperature, moisture, wind, anthropogenic factors of ignition, management and suppression, and natural factors such as lightning ignition (see Figure 1.1).

Fire can have a significant impact both on a global and a local scale. Fire affects global vegetation composition and dynamics through mortality, regrowth and species diversity (Barlow and Peres, 2008), atmospheric chemistry through emissions of gases including carbon dioxide, carbon monoxide, methane, sulphur dioxide, and nitrous oxides, the carbon cycle through the release of carbon from vegetation, the hydrological cycle through reduction of evapotranspiration and release of particulate matter, as well as altering the surface albedo from burnt area, black carbon, and changing vegetation cover (Hantson *et al*, 2016). It has been claimed that fire is the single most important disturbance of vegetation

globally (Hantson *et al*, 2016). Worldwide, annual burned area reaches approximately 350 million hectares or 3.4 Mkm^2 per year, and resultant CO_2 emissions in the past have been as much as 50% of fossil fuel emissions (Jolly *et al*., 2015; Bowman *et al*., 2009). For example, in 1997 carbon emissions from Indonesian fires alone was between 0.81 and 3 GtC (Page *et al*., 2002; van der Werf *et al*., 2004; GFED data), compared to 6.55 GtC of total global fossil fuel emissions that year (Le Quèrè *et al*., 2017). Today total fossil fuel emissions have risen to ~10.0 GtC yr^{-1} (Global Carbon Project, emissions for 2016[1]), and fire emissions are slightly lower (1.869 GtC in 2016, and estimated 1.822 GtC in 2017, GFED[2]), amounting to around 20% of global emissions.

Fires also have social and economic dimensions, making it challenging to represent fire events holistically in models. For example the 2017 Californian fires are estimated to have impacted over 10,878,000 people (US CENSUS BUREAU[3]), killed 43 people (Cal Fire) and estimates of economic cost for this fire event alone are up to $180 billion (Accuweather[4]). One study estimated that wildfires are responsible for 339,000 deaths worldwide every year[5], and the annual economic burden has been estimated to be between $71.1 billion and $347.8 billion ($2016 US) (Thomas *et al*, 2017). They can impact air quality, and can destroy lives and infrastructure, and yet can also be a vital process for successful ecosystem functioning (e.g. maintaining savanna ecosystems; Andela *et al*. 2017), vegetation succession (e.g. seed release and resprouting in *lodgepole pine*, *Eucalyptus*, *Banksia*; post-fire flowering in Australian grass tree and Cyrtanthus[6]) and small-scale farming (waste disposal, land clearance, disease and pest control (Brandt, 1966)), increasing soil fertility (Santin *et al*, 2016), soil carbon (Koele *et al*., 2017) and encouraging new growth for grazing animals[7].

[1] Global Carbon Project 'global budget' http://www.globalcarbonproject.org/carbonbudget/17/data.htm
[2] GFED emissions https://www.geo.vu.nl/~gwerf/GFED/GFED4/tables/GFED4.1s_C.txt
[3] US Census: https://www.census.gov/topics/preparedness/events/wildfires/2017-ca-wildfires.html
[4] ACCUWEATHER: https://www.accuweather.com/en/weather-news/accuweather-predicts-2017-california-wildfire-season-cost-to-rise-to-180-billion/70003495
[5] Wildfire deaths: http://newsinfo.inquirer.net/148611/wildfires-kill-339000-people-per-year-study
[6] Fire vegetation adaptation: https://www.britannica.com/list/5-amazing-adaptations-of-pyrophytic-plants
[7] Swaling: http://www.exmoor-nationalpark.gov.uk/living-and-working/info-for-farmers-and-land-managers/swaling

1.2.2 Global impacts of land-use change

Humans have been changing the land surface since prehistoric times, converting natural vegetation to crops, pastures and savanna through the use of fires and deforestation, using wood harvesting for fuel and construction which has only increased as population levels have continued to grow (Williams, 2006 in Wilkenskjeld, 2014). Over 50% of the land surface has been affected by land-use activities over the last 300 years; 25% of global forest area has been lost, and agriculture now accounts for around 30% of the land surface (Turner *et al*, 1990), which continues to grow at a rate of 13 million hectares per year (Zhang and Wiltshire, 2014). These land-use transitions not only create important primary changes to ecosystems (e.g. through cutting of forests and planting of crops etc.), but also leave behind secondary land in various stages of regrowth (Hurtt *et al*, 2011). Vegetation influences the surface fluxes of radiation, heat and moisture, where conversion to crops or pastureland can reduce the aerodynamic roughness and alter evaporation patterns, soil moisture and latent heat (Betts, 2005).

Land-use and land-cover change (LULCC) is both a cause and a consequence of climate change (Settele *et al*, 2014). As well as directly affecting the land surface, land-use changes also impact the regional and global climate by altering greenhouse gas (GHG) concentrations in the atmosphere, the surface-energy budget, surface and cloud albedo, wind profiles and changing the natural carbon cycle through removal of carbon from natural vegetation and increasing carbon emissions (Pielke *et al*, 2002), or visa versa through reforestation. Changes in land-use have altered other basic cycles as well, including the nitrogen and water cycle. These are all critically important factors in the climate system, and can act to enhance or dampen the global thermodynamics of climate change.

The largest impact on global mean temperatures comes from emissions of GHGs and aerosols, and as a result land-use change has previously been overlooked in many ESMs. However, cumulatively land-use emissions of carbon are not insignificant; changes in land-use have contributed almost 30% to the total anthropogenic CO_2 emissions since 1750 (180±80 PgC out of 555 PgC) with a major contribution from deforestation in tropical South America (Ciais *et al*, 2013). LUC is the second largest source of total GHG emissions globally (Don *et al*,

2011). Using HadGEM2-ES simulations to assess the impacts of climate change and land-use change over the four future Representative Concentration Pathway (RCP) scenarios, Betts *et al*. (2015) show that land-use has a greater effect on projected changes in global terrestrial ecosystems than climate change on a regional scale. Without adding in carbon loss from land-use change, we also risk overestimating carbon budgets. Strong evidence suggests that LUC can be as important as these larger forcings on a regional scale (Christidis, 2013). Change in biomass in the Amazon ecosystem has been found to be larger as a result of LUC than other drivers including climate change, fire and CO_2 fertilisation (Zhang *et al*., 2015). Recent analysis has shown the importance of land-use change in Effective Radiative Forcing (ERF) over the 20th century in HadGEM2-ES. While the magnitude of land-use change forcing is comparatively small on a global scale (albedo forcing alone =-0.15+/-0.1Wm^{-2}, total land-use ERF in HadGEM2-ES ~=-0.4Wm^{-2}, Andrews *et al*, 2017), it can have a large impact on regional climate and extremes. It is therefore a fundamentally important process that needs to be included in model simulations in order to get an accurate picture of how the climate is changing, and how it is likely to change in the future.

A major innovation in the terrestrial carbon component of ESMs since AR4 is the inclusion of the effects of land-use change associated with the spread of agriculture, urbanisation and deforestation. However, this increasing complexity introduces greater spread in climate model projections (Flato *et al*, 2013).

1.2.3 Interaction of climate, fire, and land-use

LUC can be a cause of both fire initiation and suppression. Globally biomass burning increased from around the year 1750 as a result of land-conversion and population growth together with increasing temperatures. After 1870 there was a sharp decline in biomass burning despite increasing population and agriculture, indicating a shift in the way fire is used in agriculture from land-clearance to suppression (Marlon *et al*, 2008). Many studies have demonstrated the close link between land-use and fire trends (e.g. Aragao *et al*, 2008, Cardoso *et al*, 2003), mostly demonstrating increases in fire with human activity in the tropics, although on a global scale expansion of agriculture has generally led to fire suppression (Bistinas *et al*., 2014). Andela *et al*. (2017) have shown that global burned area has declined in the last 20 years, with the largest decline in savannas due to

increasing use of agriculture. This trend is not reproduced in most fire models as the interaction of fire and LUC is not yet properly represented. However this global average may mask regional variation in fire trends that are a function of the environment and changing anthropogenic land-use trends. It is also a function of human fire suppression, which can conceal changes in fire trends due to a changing climate.

Underlying changes in ignition and fuel availability, is a background of meteorologically-driven changes in fire. A number of studies have suggested that there have been increases in fire occurrence in some areas that reflect recent changes in the climate. Westerling *et al*. (2006) showed that fire activity in the western United States has increased the area of forest burned by six times compared to 1970-1986 as a result of warmer temperatures and longer dry summers. Increases in wildfires in Canada from 1992-1999 have been directly attributed to human-induced warming (Gillett *et al*., 2004), extreme fire risk in Western Canada linked to human emissions (Kirchmeier-Young *et al*., 2017), and an increase in fire risk in California has been attributed to human-induced climate change (Yoon *et al*., 2014). There is still much uncertainty around future changes in fire associated with climate change (Mortiz *et al*., 2012), but the potential consequences of the social and economic impacts, impacts on human heath, changes in ecosystem functioning and services, and feedbacks on climate make this area of research particularly important and pertinent (Rabin *et al*., 2017).

The interaction of LUC, climate change and fire is complex (Coe *et al*., 2013) and in order to understand the multiple positive feedbacks comprehensively, it is necessary to consider all of these elements together (Aragão *et al*., 2008). Figures 1.1 and 1.2 below illustrate the complexity of the problem and how many feedback loops can exist between these three processes.

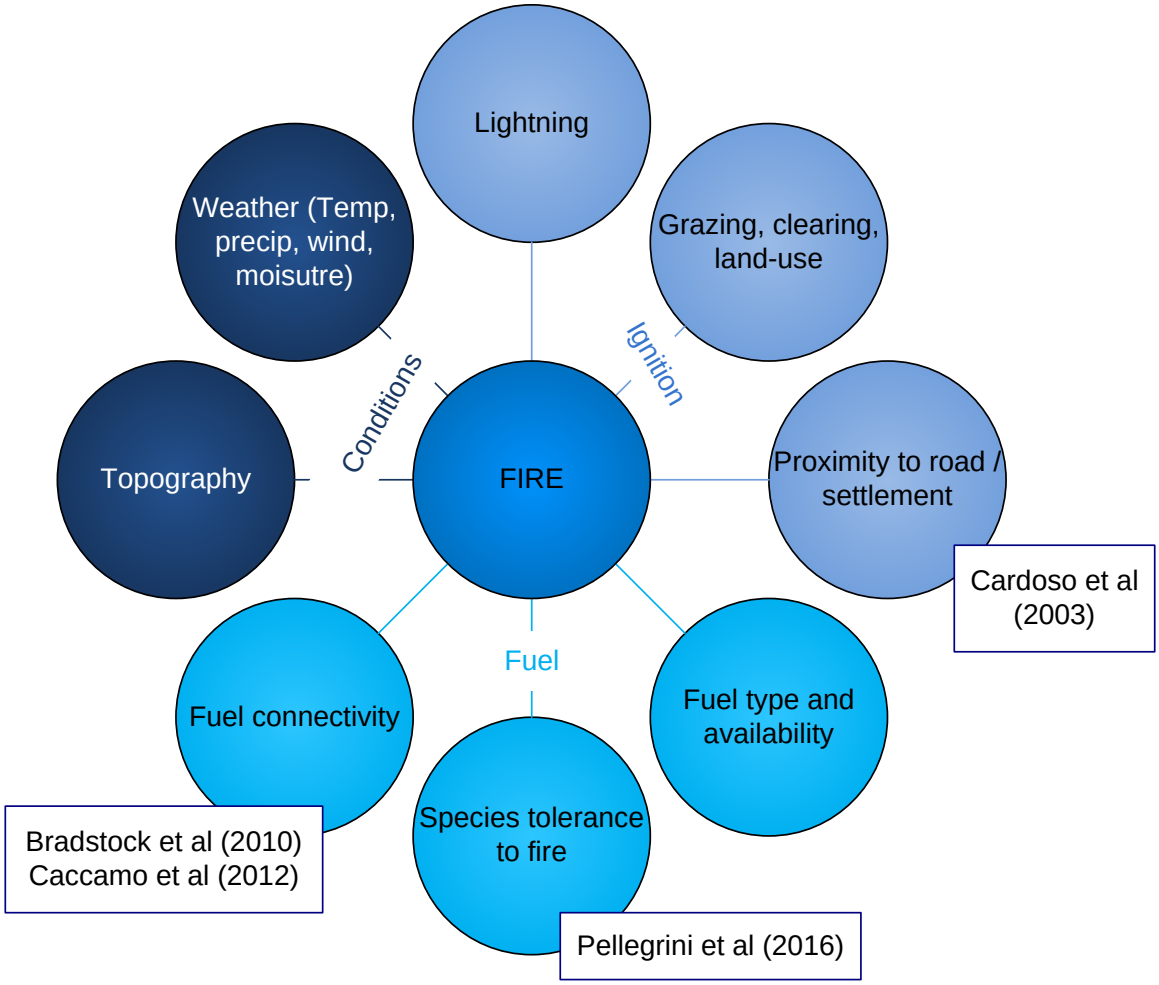

Figure 1.1 Factors influencing fire
Simple diagram showing the main factors influencing forest fires, and references to key literature

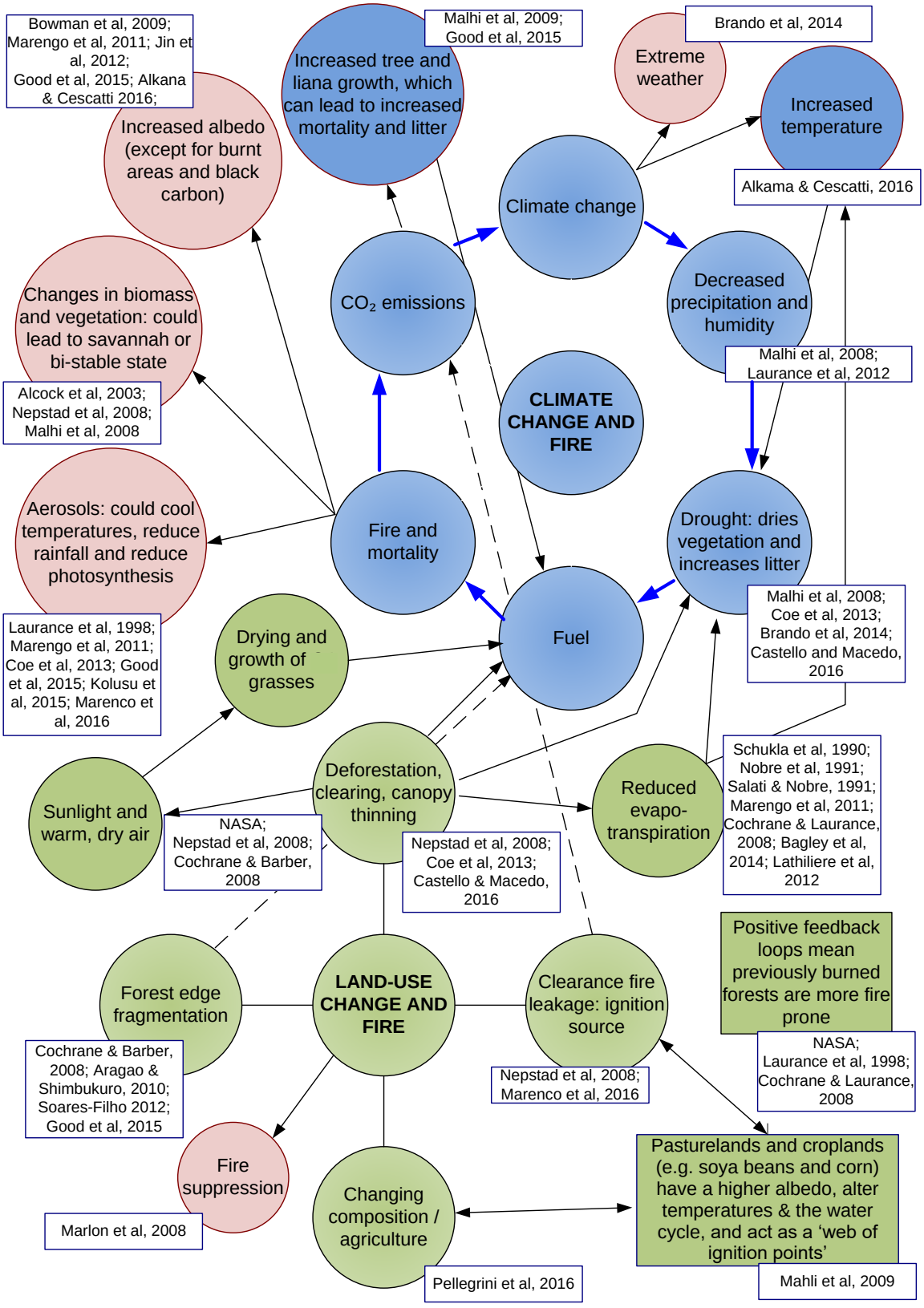

Figure 1.2: Feedbacks between fire, climate change and land-use change.
Multiple factors and feedback loops exist between fire, climate change and land-use change. Blue colours represent the positive feedbacks between fire and climate change, green represents the positive feedbacks between fire and land-use change, and pink represents uncertain or mixed positive and negative feedbacks (original figure, with references to key literature associated with certain interactions included)

The representation of fires is beginning to become a focus for model development, with the recognition of the important contribution that they make within the Earth system. The development of Dynamic Global Vegetation Models (DGVMs) and ESMs with fires is continually progressing, albeit with large variation in complexity across models (Rabin *et al*., 2017).

1.2.4 Introduction to the region of study: the Amazon

The Amazon forest biome is one of the largest and most important carbon sinks in the world (Brienen *et al*., 2015), as well as being one of the richest sources of biodiversity, and a major component of the global hydrological cycle (Moran, 1993) and the Earth system itself (Malhi *et al*., 2008). Covering 5.3 million km², the Amazon forest contains 90–140 billion tons of carbon (Soares-Filho *et al*. 2006), accounting for 17% of the global total terrestrial vegetation carbon (Fauset *et al*., 2015). Amazonia contains around a quarter of the world's total biodiversity (Malhi *et al*., 2009) ~16,000 tree species (ter Steege *et al*., 2013), and the Amazon river has the largest average discharge in the world, releasing over 200,000 m³/second of freshwater into the oceans (~20% of global total river discharge, Gupta 2007), with approximately eight trillion tons of water evaporating from Amazon forests every year (Nepstad, 2008).

These colossal figures alone would make the Amazon an interesting focus of study, and combined with significant pressure on land-use, historical deforestation on an unprecedented scale (Laurence, 1998), and potentially devastating projected changes in climate (e.g. Cox *et al*., 2000) and fire danger (Golding and Betts, 2008) as discussed further below, this region has become one of the most important areas of research today. Changes in this finely balanced ecosystem will have a direct impact on the global carbon cycle, nitrogen cycle, and water cycle, as well as regional and even global climate (Good *et al*., 2011). Global Climate Models (GCMs) and ESMs can give useful indications of how the system may change over the coming decades as a result of changes to the climate, but in order for these to be as realistic as possible it is important that the complexity of the system is properly represented. We need to fully understand the multifaceted interactions that will affect fire in this region, and its resilience over the coming century, which will have important implications for policy decisions.

The main vegetation type in the Amazon is evergreen tropical broadleaf rainforest (Figure 1.3), which is not well adapted to fire. The Amazon region has high levels of precipitation year-round (Figure 1.4), which historically has led to low occurrence of fire. Maximum burned area in Brazil occurs primarily in the Cerrado region, which comprises savannah vegetation made up of shrubs and grasses, and a hot dry climate. Here vegetation is much more adapted to frequent fire occurrence. In the East, an area of hot dry scrub vegetation makes up the semi-arid Caatinga, which is fuel limited in supporting fire. Further south the tropical semi-deciduous Atlantic forest has a cooler climate. The fire regime across Brazil is therefore a function of climate and fuel, as well as human land management and ignition.

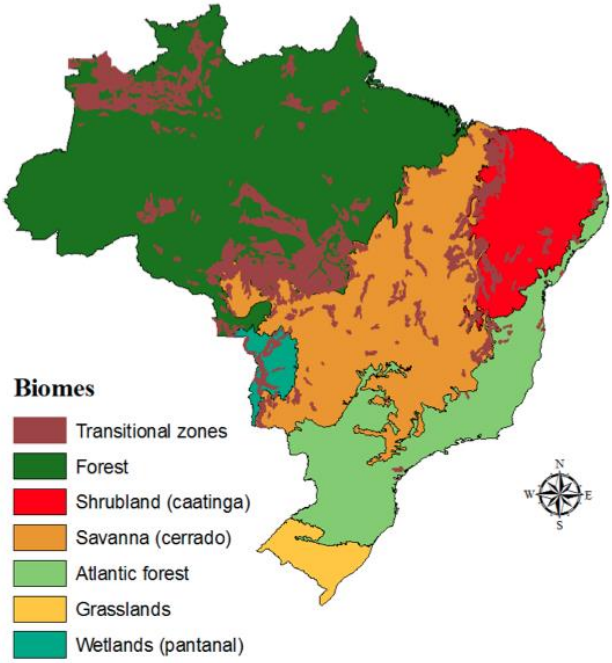

Figure 1.3: Distribution of biomes and transition zones of Brazil
Source: Brazilian Institute of Geography and Statistics (IBGE)

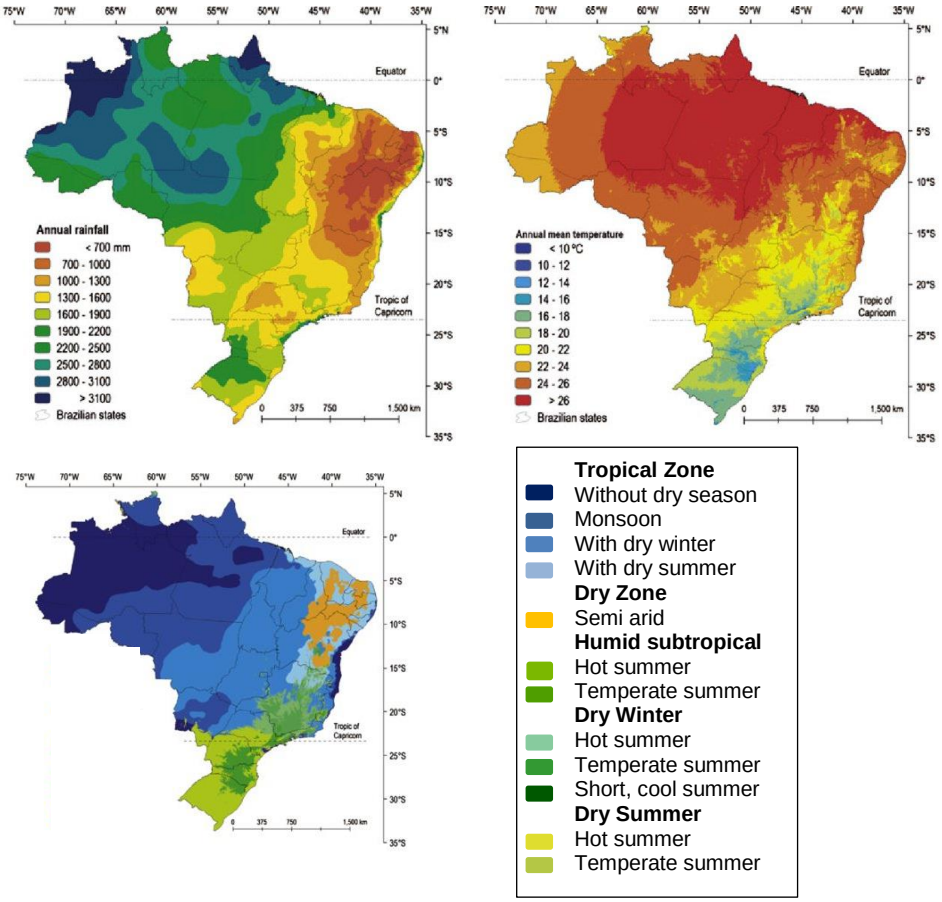

Figure 1.4: Climatic zones of Brazil
Top left: Annual rainfall (mm). Top right: Annual mean temperature (°C). Bottom left: Climatic zones, with legend to right. Source: Alvares *et al.* (2014)

1.2.5 History of projections for the Amazon

In 1999, White *et al*. published an important study on the impacts of climate change on ecosystems and the terrestrial carbon sink, using output from two Met Office Hadley Centre climate models, HadCM2 and HadCM3. As a result of a strong warming (7°C increase) and drying (decreased rainfall of up to 500 mm/y^{-1}) signal over South America, HadCM3 in particular predicted large areas of Amazon dieback and conversion of tropical evergreen forests to savanna, grassland and desert by 2080s. Also based on output from HadCM3LC, Cox *et al*. (2000) showed that the inclusion of an interactive carbon cycle makes a significant contribution to future warming projections, with carbon emissions around 280ppmv higher by 2100 compared to simulations that exclude this feedback, leading to significant Amazon dieback as a result of climate change. Using HadCM3 coupled to the ocean-carbon cycle model "HadOCC" and the

DGVM “TRIFFID” (Top-down Representation of Interactive Foliage and Flora Including Dynamics), Cox *et al*. (2004) showed that the increased temperatures and decreased rainfall from HadCM3LC projections, with potential implications for drought and fire danger, give rise to a reduction in vegetation carbon of around 73GtC over 1860-2100 in South America.

A number of subsequent studies using DGVMs based on HadCM3 supported this large-scale forest loss in future scenarios; Scholze *et al*. (2006) showed high risk of climate-induced forest loss from drought and wildfire, and Sitch *et al*. (2008) showed projections of year-round temperature increases and decrease in rainfall rates across Amazonia, and a resultant increase in wildfire frequency. All models used in the Sitch *et al*. (2008) study simulate a decrease in vegetation carbon over the Amazon, with TRIFFID simulating the strongest dieback scenarios where forest is replaced by grasses. Jones *et al*. (2009) proved that a lag in the terrestrial ecosystem means that full vegetation response to climate change may take decades to be fully realised, long after stabilization of radiative forcing, significantly increasing the risk of a loss in Amazonian forest cover with rising temperatures.

All of these studies showing significant Amazonian dieback are based on the Hadley Centre model HadCM3. As Cochrane and Barber (2009) suggest, “such apocalyptic scenarios of environmental devastation make it necessary to critically examine the climate model simulation driving speculation about a massive dieback of the Amazon”. Huntingford *et al*. (2004) compared simulations of HadCM3 precipitation with observations over the Amazon, and showed that the model was on average predicting precipitation that was 25% too low. Betts *et al*. (2004) reviewed the forcings and feedbacks within HadCM3LC, and concluded that a range of biogeophysical and biogeochemical feedbacks (such as stomatal closure) that are not included in other GCMs could cause a higher drying signal over the Amazon, which leads to the projected dieback scenarios. This has important implications for the reliability of the HadCM3 projections (Cochrane and Barber, 2009), and successive Hadley Centre climate models have not shown such a dramatic drying in this region.

Many of the other GCMs used in the AR4 report underestimate current rainfall (Yin *et al*., 2013), making a shift to seasonal forest potentially a more likely

outcome than transition to savanna (Malhi *et al*., 2009). In 2014 the Intergovernmental Panel on Climate Change (IPCC) Fifth Assessment Report (AR5) concluded that large-scale dieback due to climate change alone is unlikely by the end of this century (medium confidence). However, new observations have provided evidence of critical ecological thresholds and positive feedbacks whereby drought, land-use change (LUC) and fire could interact and catalyse a self-reinforcing transition to low-biomass fire-adapted vegetation (Settele *et al*., 2014).

So whilst dieback from climate change alone is no longer seen as a likely scenario over the course of this century, when combined with changes in land-use and fire, this worst-case scenario cannot be completely ruled out (Barlow *et al*., 2003; Nepstad *et al*., 2008; Malhi *et al*., 2009; Settele *et al*., 2014; Nobre *et al* 2016; Aragão *et al*., 2018; Lovejoy and Nobre, 2018). Research has shown that despite a recent decrease in LUC in the Amazon, fire incidence has not decreased (Cano-Crespo *et al*., 2015), and conversely drought-related fires, including escaped management fires, increased by 36% as a result of the recent El Niño in 2015 (Aragão *et al*., 2018). These changing trends suggest a decoupling of fire and LUC, and a transition to a more climate-driven fire regime which could increase as the climate warms.

The AMAZALERT[8] research project (2011-2014) focused on the impacts of climate change and LUC in Amazonia. The current generation of CMIP5 models simulates strong warming of up to 5.6°C over Amazonia, but observations made throughout the AMAZALERT project suggest that forests could be more resilient to temperature increase than previously thought. The results of the project confirmed that most of the Amazon is unlikely to degrade severely as a result of climate change this century, but the south-east Amazon forest is more vulnerable, and there are still high uncertainties around the sensitivity of the forest to climate and LUC, including response to fire dynamics, incidence of drought, CO_2 fertilisation and socio-economic developments (AMAZALERT-D6.7). It was also concluded that if climate-induced degradation does occur, it is likely to happen quickly and without warning and will therefore be difficult to mitigate. Signals of change may only come after a biophysical threshold has been passed and when

[8] AMAZALERT: http://www.eu-amazalert.org/publications/deliveryreports

decline is already irreversible, and may be brought on by extreme weather events.

1.2.6 Risk of abrupt change

In 2008, Lenton *et al*. coined the term 'tipping element' to refer to a large-scale (subcontinental or larger) component of the Earth system that may induce a mass tipping point or abrupt change. This refers to a critical threshold whereby a small perturbation can rapidly and qualitatively alter the state and dynamics of the system, producing large-scale and long-term consequences on human and ecological systems which persist even if the drivers of the change are abated (Settele *et al*., 2014).

The dieback of the Amazon rainforest is included as one of these tipping elements, which has been predicted to occur under 3-4°C of warming (Lenton *et al*., 2008; Kriegler *et al*., 2009), and/or drought (Reyer *et al*., 2015). Here LUC is acknowledged as a potentially critical factor, which alone could bring forest cover to a critical threshold, especially through the interaction with fire (Lenton *et al*., 2008). Good *et al*. (2011) show that in terms of dry season resilience, the Amazon is the most vulnerable and closer to a threshold than other tropical forests. For example the dry season in Amazonia is cloudless which can lead to higher water stress than in the West African tropics where the dry season is characterised by overcast conditions (Charles-Dominique *et al*., 1998). Each tipping element could also interact with other elements in the system, for example Cai *et al*. (2016) shows that a tipping of the El Niño Southern Oscillation (ENSO) into a more persistent regime could increase drying of the Amazon, increasing the likelihood of the Amazon tipping.

According to AR5, there is a high risk (but low confidence) that high rates of climate change will result in abrupt and irreversible change in Amazonia this century as a result of combined effects of fire, LUC and drought (Settele *et al*., 2014). The outcome of passing this critical threshold is uncertain, but it has been suggested that even with a change towards a warmer, drier climate, there is some resilience in the forest ecosystems that means that a seasonal forest may persist in Amazonia (Malhi *et al*., 2009). For example, the existence of a dual bi-stable state of forest and savanna has been postulated under drought conditions (Oyama and Nobre 2003; Staver *et al*. 2011). However, this semi-stable state

would collapse if fire occurrence were to increase, and a transition to low-biomass savanna could occur (Hoffmann and Jackson, 2000) known as ‘savannization’ (Silverio *et al*., 2013). Fire can be a key determinant in self-reinforcing scenarios of vegetation. It can promote savanna vegetation where open, dry grasses create flammable conditions, but when tree cover becomes dense, grass growth is inhibited and conditions become too moist to support fires, leading to a self-propagating shift to closed forest (Hirota *et al*., 2011).

1.2.7 Projections of future climate

Models generally show a signal of warming over the Amazon Basin throughout this century (Cochrane and Laurence, 2008; Zhang *et al*., 2015). Projections of rainfall over the Amazon region are mixed; Mortiz *et al*. (2012) show general agreement in 16 GCMs for increased precipitation over the tropics based on CMIP3, whereas other models including the CMIP5 mean model projections forecast drying (Stocker *et al*., 2013) and a lengthening and intensification of dry seasons, especially in the south-east (Malhi *et al*. 2008; 2009), along with increased warming. Indeed recent work by Jolly *et al*. (2015) has shown that the fire weather season in South America has already increased by an average of 33 days over the last 35 years as a result of climate change, and the dry season length in Amazonia has increased by 6.5 (±2.5 days) per decade since 1979, resulting in a longer fire season (Fu *et al*., 2013). Deforestation may also increase dry season length (Costa and Pires, 2010), and there is high confidence that moist-tropical forests have many tree species that are vulnerable to drought and fire during extreme dry periods (Settele *et al*., 2014). This is based on numerous observational studies of increased tree mortality during previous severe droughts, e.g. 2005 (Philips *et al*., 2009), and 2010 (Gatti *et al*., 2014; Feldpausch *et al*., 2016). Episodes of even modest warming in the past have demonstrated increased fire occurrences in drier parts of the Amazon (Settele *et al*., 2014), and in such times the net Amazon carbon sink can change to a source of carbon (Anderson *et al*., 2015).

An increase in atmospheric CO_2 could partially offset this risk and vulnerability to drought, through increased photosynthesis and carbon uptake, as well as greater water use efficiency which would result in higher growth rates (Ciais *et al*., 2013). However there is still much uncertainty around this hypothesis due to lack of

observations. For example the effect may be limited by nutrient and water availability, and some studies suggest that increased CO_2 will reduce transpiration and result in further localised drying and warming (Myhre *et al*., 2013). It has been proposed that CO_2 is one of the main drivers of rainfall change in tropical regions, due to the biogeophysical effects on plant stomata and transpiration rates (Chadwick *et al*., 2016). Corresponding increases in growth of parasitic vines like lianas could also increase tree mortality and undermine the effects of the CO_2 fertilisation (Good *et al*., 2014).

1.2.8 Land-use change in the Amazon

LUC has affected 1.4 million km², around 20% of the Amazon basin so far (Castello and Macedo, 2016). The peak of deforestation in the Amazon was 27,772 km²/yr^{-1} in 2004, (AMAZALERT-D4.2) which was primarily the result of cattle ranching (Moran, 1993; Nepstad, 2006), but soybean production has also been expanding (Settele *et al*., 2014). Palm oil is one of the main biofuel crops, and while its current use is still relatively small, Brazil has the largest potential for expansion in South America as around half of the Amazon is suitable for its cultivation (Butler and Laurance, 2009). Fire is often used as a quick and cost-effective way of clearing the land for alternative use, which together with higher temperatures and drier conditions, can lead to increased fire danger.

Post 2004, official estimates show that the rate of deforestation has reduced considerably to ~6,000 km²/yr^{-1} (Aguiar *et al*., 2016) although illegal deforestation is still rife (AMAZALERT-D4.2). Gross emissions from tropical deforestation and degradation were 3.0±0.5 PgC/yr^{-1} for the 1990s and 2.8±0.5 PgC/yr^{-1} for the 2000s (Ciais *et al*., 2013). However, even with technological changes that could result in agricultural intensification, LUC and expansion of pasture and crop lands may continue from an increasing global demand for food and biofules (see Chapter 2).

The south-east (SE) region of the Amazon has been identified as the most vulnerable region to small climatic changes, because of the combination of severe historical deforestation, as well as spanning the geographic transition zone between rainforest and savanna. The region has become known as the ‘arc of deforestation’ due to the intensity with which it has been depleted (Malhi *et al*., 2008). Coe *et al*. (2013) identified South-SE Amazonia as a region that has

already experienced decreased evapotranspiration as a result of deforestation, as well as more frequent and intense fires and droughts, which are likely to increase with continued changes to climate and land-use.

1.2.9 Land-use change and fire danger in the Amazon

LUC is known to be one of the most important influencing factors in scenarios of Amazon decline in a number of ways: directly through deforestation and canopy thinning (cutting as well as use of fire for clearance), and through fire-leakage which can extend deforestation into much larger areas than planned. Forest fragmentation is also an important contributing factor, where lengthened forest edge increases the spread of fire into the forest (Soares-Filho *et al*., 2012; Coe *et al*., 2013; Good *et al*., 2014). This can be the result of land clearance for agriculture, and for urban expansion. For example there is a clear correlation between distance to roads and increased fire danger (Cardoso *et al*., 2003). The impact of this edge effect can vary from region to region though, with some research showing a more limited effect in the southwest Amazon region, likely counteracted by nutrient-rich soils and faster forest recovery (Numata *et al*., 2017).

LUC can have important impacts on regional climate, and has been shown to reduce evapotranspiration (Cochrane and Laurance, 2008), and decrease precipitation and induce drought over the Amazon (Bagley *et al*., 2014), which can in turn initiate abrupt increases in fire-induced tree mortality (Brando *et al*., 2014; Castello and Macedo, 2016). Even when deforestation itself declines, fire incidence can still remain high due to increased agricultural frontiers where accidental fires burn out of control (Aragão and Shimabukuro, 2010). Nelson and Chomitz (2011) found that protected areas (especially multi-use protected areas) reduce the incidence of fire substantially; however, Carmenta *et al*. (2016) recently published a study investigating the incidence of fire in reserves, and found that fires are only less prevalent in reserves where the population is lower, and that reserve creation itself has no discernible impact on fire density.

Due to their humid climate and high precipitation, tropical forests have not in recent history been at high risk of wildfire, although there is paleo evidence that suggests that the climate was dry enough ~10,000 years ago to sustain natural fires in these areas (Charles-Dominique *et al*., 1998). Today, fires are almost all

anthropogenically initiated in tropical regions (Aldersley *et al*., 2011; Cochrane and Barber, 2009). Traditional agriculture in Amazonia has used the 'slash-and-burn' method of using fire to clear land at the end of the dry season. This depends on the fuel being dry enough to maintain a fire, otherwise the land must be left fallow. However, in very dry years (i.e. with El Niño) there is risk of these small-scale fires escaping and burning large areas of forest, as was the case in 1988 where over 80,000km² of rainforest in southern Brazil was damaged by fire (Charles-Dominique *et al*., 1998). This risk may be increasing with hotter, drier conditions and more points of ignition through forest fragmentation and agriculture. This historically low fire incidence rate also means that the tropical vegetation is not adapted to cope with frequent fire in the same way that vegetation in the Cerrado is, for example, where wildfire occurs often (Malhi *et al*., 2008). The fires in the Amazon may be low intensity and slow-moving, burning for long periods of time over vast areas, powered by dead leaf litter on the forest floor (NASA[9]; Morton *et al*., 2013). These fires often kill trees, especially the small thin-barked trees (Pellegrini *et al*., 2017), but do not fully consume them; more fuel is created from the dead tree and the gap in the canopy lets air circulate and more sunlight in which dries out the forest floor and leaves it at higher risk of burning again (Laurance, 1998; Cochrane and Barber, 2009).

In addition to having important implications for ecosystems and vegetation, fires can also cause social and economic disruption (Lohberger *et al*., 2018); for example, smoke from fires in 1997 forced the temporary closure of airports at Manaus and Boa Vista, and an increase in respiratory-related hospital admissions of 40-100% (Laurance, 1998). Tropical forests are increasingly being affected by fire, which drives degradation, biodiversity loss, disruption to ecosystem functioning and services, and reduction of carbon stocks (Oliveras *et al*., 2018). Globally, biomass burning is the second largest source of anthropogenic aerosols and South America is one of the major source regions (Marenco *et al*., 2016). In addition, fire-derived aerosol particles can decrease incoming solar radiation and photosynthesis, contributing further to forest degradation (Coe *et al*., 2013).

[9] NASA Amazon fires: https://earthobservatory.nasa.gov/Features/AmazonFire/amazon_fire2.php

Future fire activity will depend on a combination of both anthropogenic and climatic factors. Forest susceptibility to fire is projected to change little for low emissions scenarios, but substantially for high emissions scenarios (Settele *et al*., 2014). Because the frequency of fires increases with temperature, the incidence of fires is expected to rise over the 21st Century (Flato *et al*., 2013). For the Amazon it is estimated that currently 58% of the area is too humid to support fires, but climate change might reduce this area to 37% by 2050 (Ciais *et al*., 2013) or even lower (Le Page *et al*., 2010). Golding and Betts (2008) used the McArthur Forest Fire Danger Index (FFDI) to calculate the change in fire danger in the Amazon with the simulated changes in climate, and found that high fire danger for over 50% of the forest is simulated by 2080, and these areas correlate with those projected to be most impacted by deforestation. They estimate that future vulnerability to fire may depend nonlinearly on both climate change and deforestation. According to IPCC AR5 (Settele *et al*., 2014), there is low agreement in the models on whether climate change will cause fires to become more or less frequent on a regional scale due to the complexity of interactions and feedbacks and lack of proper representation in models..

There is also mounting evidence that extreme weather events can interact with LUC to change fire danger. A number of studies have looked at the incidence of drought and fire related to ENSO (e.g. Latif and Keenlysie, 2008). El Niño years are associated with the largest fire events in the Amazon, due to the hotter, drier conditions experienced over the South American continent (Cochrane and Barber, 2009), and some projections suggest that El Niño droughts may increase in severity or frequency under a warmer climate (Laurance, 1998). Gatti *et al*. (2014) showed that the Amazon switched to become a source of carbon rather than a sink during the 2010 drought, which is a cause for concern if this trend of extremes continue given the large potential source of carbon in the Amazon. AR5 (Settele *et al*., 2014) concluded that there is high confidence that forest fire frequency and severity is increasing through the interaction of severe droughts and land-use. Work by Saatchi *et al*. (2013) also showed the slow recovery rate of the canopy in the Amazon following a major drought, such that if droughts were to occur more frequently there may be permanent changes in the canopy. However, Feldpausch *et al*. (2016) found that closely occurring droughts-such as the 2005 and 2010 droughts in Amazonia did not compound carbon loss. Data

from Brienen *et al*. (2015) suggests that there is a decreasing trend of carbon accumulation in the Amazon, as a result of levelling growth rates but increasing biomass mortality that is contrary to model projections. There is clearly still much uncertainty around the potential response of the forest to future changes in the climate.

1.2.10 Work to date on fire danger

The first study to assess changing fire danger over the Amazon in detail was Golding and Betts (2008). They used the McArthur FFDI to calculate the change in fire danger in the Amazon with simulated changes in climate, and found a significant increase in central and eastern Amazonia by 2020, and high fire danger for over 50% of the forest by 2080. However, this study was also based on HadCM3, which was subsequently shown to have a dry-bias in this region.

In 2015, Betts *et al*. repeated the study using HadGEM2-ES at N96 atmospheric resolution with 38 levels and 1 degree ocean resolution with 40 levels, together with 4 RCP scenarios. Land surface processes were included through MOSES II (Met Office Surface Exchange Scheme) with vegetation dynamics simulated by TRIFFID, and LUC was also included in the RCP scenarios based on the Hurtt *et al*. (2011) data sets. However disturbance was prescribed as a uniform rate in the model that remains constant over time, with no representation of the effects of climate on disturbances such as fire. They showed that there was little difference as a result of climate-related changes between scenarios, and the dominant driver for large-scale ecosystem change is from LUC. In terms of fire danger, the FFDI was shown to perform well over the tropics when compared with observed burnt area. Future projections show a general increase in FFDI for all RCPs by the end of the century, with greater increases at higher levels of warming. Areas of particularly large increase in FFDI under RCP 8.5 included eastern Amazonia. There is a lack of consensus across models on the projected change in fire danger across the tropics (Kloster *et al*., 2012; Moritz *et al*., 2012), and the aim of this work will be to further the capability of how fire is represented in models and investigate the implications for future fire danger.

In 2014 AMAZALERT published a report (AMAZALERT-D3.3) on ‘Quantifying impacts of fire on climate’. The report recognised the need for incorporating fire into coupled models that will allow climate change, fire and LUC to interact and

give an indication of potential feedbacks within the Earth system. In this study, a fire module was implemented in HadGEM2-ES and the Brazilian land surface model IBIS-INLAND (Integrated Biosphere Simulator- IBIS, Brazilian Integrated Model of Land Surface Process- INLAND). In HadGEM2-ES, burnt area was estimated from soil and atmospheric moisture, assuming constant rates of ignition, based on the work of Kasikowski *et al*. (unpublished, see Bibliography) designed for HadCM3. This was an offline estimation of burning extent, and plant mortality was not included. Within IBIS-INLAND, an estimation of fire potential from biomass and flammability was used to calculate vegetation dynamics, biomass, leaf area index and net primary productivity, using two RCP scenarios out to 2100 and AMAZALERT LUC scenarios. Under the climate change-only runs, an increase in biomass was observed, likely as a result of the CO_2 fertilisation effect, whereas when fire was included there was a shift in vegetation from forest to grass. In both scenarios a drying and lengthening of the dry season was predicted, especially in the south and east of the Amazon Basin, which was increased by deforestation. One surprising result was the relatively small impact of LUC, and the report concluded that this requires further investigation.

1.2.11 Missing processes

This review has aimed to show the importance of considering the interactions of fire, climate change and LUC in the critical ecosystem of the Amazon. With mounting pressure from LUC and climate change, it is likely that fire danger is going to become an increasing concern over this century in some areas. Yet this is one critical area that has been missing in climate modelling processes.

It has been well-documented that models are still at their early stages in dealing with land-use, LUC and forestry, and in particular, disturbances from fire, drought, and tree mortality are either poorly characterised and treated crudely as uniform disturbances without any representation of the underlying physical processes (Nepstad 2008; Costa *et al*., 2010; Pan 2011; Hirota 2011; Coe *et al*., 2013; Brando *et al*., 2014; Ciais *et al*., 2013; Betts *et al*., 2015; Malhi *et al*., 2018), or are missing completely (Ciais *et al*., 2013; Flato *et al*., 2013; Collins *et al*., 2013).

The mechanisms and links between fire, drought and LUC are still poorly understood (De Faria *et al*., 2017). Our understanding is currently limited to a small number of studies in dry temperate or boreal forests, and likely response in

the Amazon is still unclear (Coe *et al*., 2013). ESMs also are not always able to account for alternative stable states such as tropical forest or savanna (Ciais *et al*., 2013), which is a possible outcome of change in the Amazon (see Chapter 5). This means there is low confidence in many of the future projections of terrestrial carbon storage. Although more recent studies have found that climate-driven Amazon dieback such as that described by Cox *et al*. (2000) is unlikely (Settele *et al*., 2014), the missing process of fire and associated feedbacks mean that we cannot rule this possibility out.

> 'At present, the tropical forest biome constitutes the largest terrestrial carbon sink, but it is also associated with the largest uncertainties.'
> (Good *et al*., 2014)

According to Cavaleri *et al*. (2015), over the next 20 years it is likely that the tropics in particular will experience unprecedented warming, yet model variation in this region is vast and there is still 'exceedingly high uncertainty' about future changes in precipitation, and vegetation responses to climate change, including changes in temperature and levels of CO_2 due to their inherent complexity, wide range of possible feedbacks and nonlinearities, and interplay between climate and LUC. An important part of this response is how fire danger will change, and the resilience of the forests to this risk. Zhang *et al*. (2015) identifies an 'important need' to evaluate model predictions of fire dynamics for the Amazon. The early detection and prediction of changing fire danger is therefore still an area of active research (Settele *et al*., 2014; Reyer *et al*., 2015).

The AMAZALERT project showed that fire incidence rises substantially in the presence of drought and land-use, and recommended that future research focus on the balance of CO_2 fertilisation, temperature increase, drought, LUC and fire dynamics.

1.3 Observations

There are a large range of observational products available for data of burned area, vegetation cover and land-use which are useful to this study. Here I outline a selection of well-known and relevant products, giving an overview of their scope, how they were created / collected, and some of the uncertainties that are associated with their use.

1.3.1 Burned Area

As interest in fire as part of Earth system modelling grows, a number of observational datasets are now available that give information on burned area. On a global scale, the best source of observational data is via satellite imagery. These include for example: L3JRC (1km resolution, 2000-2007, produced from SPOT VEGETATION imagery and Global Burnt Area algorithm) (Tansey *et al*., 2004); GLOBCARBON (1km resolution, 1998-2007 also based on SPOT VEGETATION plus ATSR-2 and AATSR) (Giglio *et al*., 2010); and NOAA products AVHRR and GOES-8 (Cardoso *et al*., 2003). Observations are essential in comparing against historical projections of burned area or fire danger to get an indication of how accurate a model or fire index is. If patterns of burned area are accurately represented in historical simulations, we can have more confidence in future projections. Two of the most popular observational products are MODIS and GFED, outlined below.

- **Moderate Resolution Imaging Spectroradiometer (MODIS)**

NASA provides MODIS data from polar-orbiting Terra and Aqua satellites, as well as high-resolution Landsat data. Satellites are effective at covering large regions in short time periods, and are able to map temperature changes so can be useful in helping to estimate fire occurrence, intensity and extent. However, there are multiple sources of uncertainty in the data, for example clouds can hide fires, very reflective surfaces may be confused with burned area, and omission errors may occur when satellites are not passing over (AMAZALERT-D3.3). Small understory fires are also undetectable in many cases, hidden from satellites by tree canopies (Morton *et al*., 2013).

MODIS also provide active fire and burned area. The active fire products detect fires over 1km resolution. Burned areas are made up of deposits of charcoal and ash and alteration/removal of vegetation. Using changes in daily surface reflectance, an algorithm is used to calculate approximate date of burning, given at 500m for recent fires[10].

[10] MODIS: http://modis-fire.umd.edu/index.php

The National Institute of Space Research (INPE) also make use of geostationary (GOES, MSG) satellites for regional-scale burned area information over the Amazon as part of their fire monitoring programme[11]. In addition INPE use AVHRR/3, NOAA-15, NOAA-18, NOAA-19 and METOP-B polar satellites which have optical sensors in a 4m thermal range, all for fire detection purposes. Each polar orbiting satellite produces at least two images a day, while geostatic satellites generate several images an hour. Current data for fire danger and occurrence are made available on their website, along with statistics around historical fire counts (see Appendix 4).

- **Burned area from Global Fire Emissions Database (GFED)**

GFED provides gridded data on burned area and fire emissions based on observations from MODIS, ATSR, TRMM, and VIRS (Giglio *et al*., 2010). The latest data are available at 0.25° resolution from 1997-present, including gridded burned area, 3-hourly and daily emissions, monthly emissions, and global emission totals. Annual emissions are available but contain large uncertainties and missing data. Burned area estimates are derived from active fires detected by 500m MODIS after 2001; prior to 2001 fire observations are derived from the Tropical Rainfall Measuring Mission (TRMM), visible and Infrared Scanner (VIRS), and the Along-Track Scanning Radiometer (ATSR)[12]. The original GFED4 data are in HDF format, and do not include small fires (Giglio *et al*., 2013).

However it is recognised that the small understory fires which are difficult to detect via satellites are important to total emissions and burned area, adding up to as much as 35% to the global total burned area (Randerson *et al*., 2012). These fires are currently below the detection capability of satellite products using reflectance imagery, and whilst they can be detected by thermal anomalies they have not historically been quantified for inclusion in global fire products. Recently work has been done to include the representation of an 'experimental' small fire estimate in the updated HDF5 burned area dataset, GFED4.1s (van der Werf *et al*., 2017), based on 1km thermal anomaly and 500m burned area data products. The number of active small fires outside of the existing 500m burned area were estimated by using the normalised burn ratio for each product individually and

[11] INPE fire data: http://www.inpe.br/queimadas/portal
[12] GFED data: https://daac.ornl.gov/VEGETATION/guides/fire_emissions_v4.html

then combining the information from both products along with ground based information[12]. The GFED3 biogeochemical model was then used to estimate resultant emissions, which were added to the GFED4 emissions data as a 'boost' to create the new GFED4.1s product including small fires.

There are also a number of older products from historical projects that have looked at burnt area datasets, including the Global Burnt Areas 2000-2007 (L3JRC project), Global Burnt Area Project 2000, Global Burnt Surfaces (GBS) 1982-1999, and GLOBSCAR 2000[13].

Satellite data can provide a good indication of burned area; however, they cannot give information on tree mortality rate. For this more local fieldwork is required. Furthermore, not all fires are the same; wildfire in dense vegetation or for deforestation will produce more CO_2 than from fires used to manage pasture and grassland. Anderson *et al*. (2015) show that there is a highly anti-correlated relationship between biomass and fire rate where, as biomass increases, the forest climate becomes wetter and cooler which reduces fire intensity. There may also be a lag in the mortality rate, where some trees may take months or years to die as a result of a fire event (Barlow *et al*., 2003). This information needs to be taken into account when modelling dynamic vegetation.

Many satellites of coarse resolution also have difficulty capturing smaller, understory fires, which has partly been addressed now with the introduction of new datasets such as GFED4.1s. Use of landsat data, if available, may be another solution to this, or using a Burn Damage Recovery algorithm as presented in Morton *et al*. (2013).

[13] GLOBSCAR: http://due.esrin.esa.int/page_project24.php

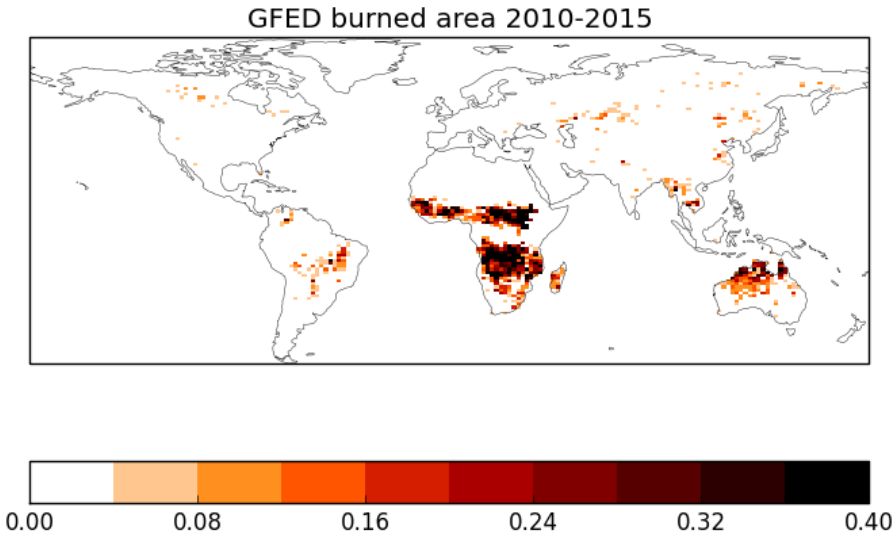

Figure 1.5: GFED4.1s mean burned area fraction 2010-2015

1.3.2 Vegetation and land-use change

There are a number of data products available today which represent various aspects of LULCC. Ultimately many of these could be used together to produce a blended product that would be useful for an improved observational product that could be used with models, driving improvements in land-use changes. An overview of available products is provided here, starting with global datasets and then focusing on those available over the Amazon region.

- **HYDE**

The global HYDE (History Database of the Global Environment) dataset is developed by the Netherlands Environmental Assessment Agency, based on UN Food and Agriculture Organisation (FAO, 2015) data. It comprises a gridded time series of land-use data and population covering the last 12,000 years, as well as Gross Domestic Product (GDP), agriculture, greenhouse gas emissions and industrial production data for the last century[14] (Klein Goldewijk *et al*., 2011). There are few global-scale products of historical land-use data that cover the pre-observational period, and a variety of methods exist for reconstructing land-use patterns. Some products use hindcast modelling to extrapolate historical cropland data, while other products use a book-keeping method to estimate carbon fluxes.

[14] HYDE: http://themasites.pbl.nl/tridion/en/themasites/hyde/introduction/index-2.html

The HYDE product uses a land-use per capita calculation based on historical statistics and computation for the entire Holocene period (10,000 BC to 2000 AD) at a temporal resolution of 1000 years for the BC period, 100 years for pre-1700, and 10 years for 1700-2000 (Klein Goldewijk and Verburg, 2013).

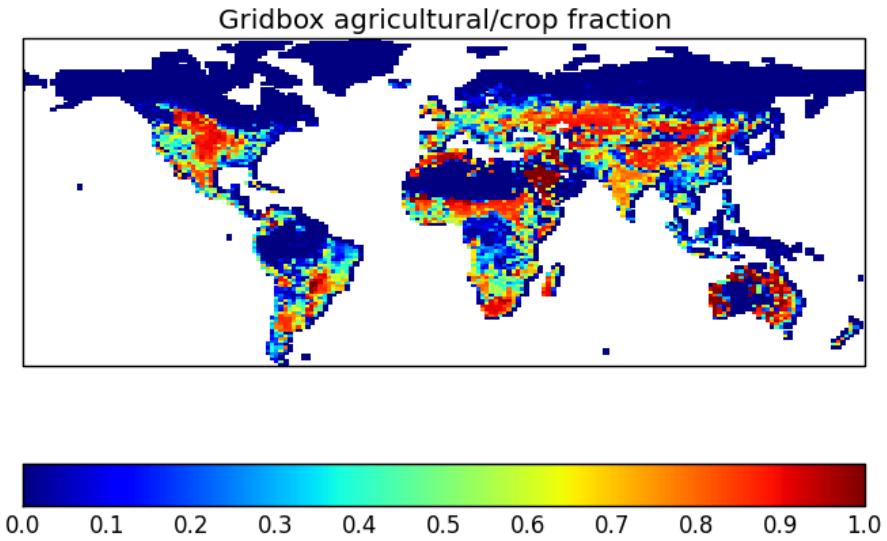

Figure 1.6: HYDE present day agricultural fraction

- **Hurtt / LUH2**

LUH2 is a harmonised land-use change dataset (Hurtt *et al*., 2011) based on HYDE, available for the period 1500-2100 at half a degree spatial resolution (Le Quere *et al*., 2018). The harmonisation applied by the Global Land-Use Model to create the dataset attempts to preserve regional crop and pasture changes, grid data where required, and to smooth the transition across time periods from past to future (Jones *et al*., 2011). This results in final land use states being presented, as well as transitions between all land cover states of forests and agricultural land, and distinguishes between rangeland and pastureland.

- **Pongratz (800-1992)**

The Pongratz dataset contains reconstructions of global land-use and land cover from AD800 to 1992. Before 1700, the land-use is estimated using population data (McEvedy and Jones 1978) using the maximum range, and post-1700 the data is based on HYDE and SAGE (Centre for Sustainability and the Global Environment) products from Ramankutty and Foley (1999), Foley *et al*. (2003) and Klein Goldewijk (2001). The vegetation includes three agricultural land-use

types (crops, C3 pasture, C4 pasture) and 11 natural vegetation types[15] (Pongratz *et al*., 2008).

- **MODIS**

Both burned area and vegetation maps are provided on a global scale through MODIS. The MODIS Vegetation Indices (VI) are produced at multiple spatial resolutions, retrieved from surface reflectance from Terra and Aqua satellites and show empirical measures of vegetation activity on the land surface. There are two products available globally for land regions. The first is the standard Normalized Difference Vegetation Index (NDVI) which runs from 1981-2015 from NOAA-AVHRR. The second is the Enhanced Vegetation Index (EVI), which has improved vegetation monitoring and sensitivity capability[10] (Justice *et al*., 2002).

- **ESA CCI land cover data**

The European Space Agency (ESA) Climate Change Initiative (CCI) programme provides an annual global land cover time series from 1992 – present day, made up of daily observational data from 5 different satellites (NOAA-AVHRR HRPT, SPOT-Vegetation, ENVISAT-MERIS FR and RR, ENVISAT-ASAR, and PROBA-V). It includes 22 different land cover classes, defined by the UN Land Cover Classification System to support the conversion to Plant Functional Types (PFTs) used in climate and land surface models (ESA, 2010[16]). Work has been done to translate these data into the PFTs that are used within JULES to enable comparison of model output with observations (Hartley *et al*., 2017). The plots below show the output of these observational products for the standard 5 PFTs used in JULES (Broadleaf trees, Needleleaf trees, C3 grass, C4 grass and Shrubs). Here the reference values are used, but it should also be considered that there is a range of uncertainty with any observational dataset, as explained in section 1.3.3. The latest dataset available including this translation is 2010.

[15] RECON: http://cera-www.dkrz.de/WDCC/ui/Entry.jsp?acronym=RECON_LAND_COVER_800-1992
[16] ESA CCI https://www.esa-landcover-cci.org/?q=node/175

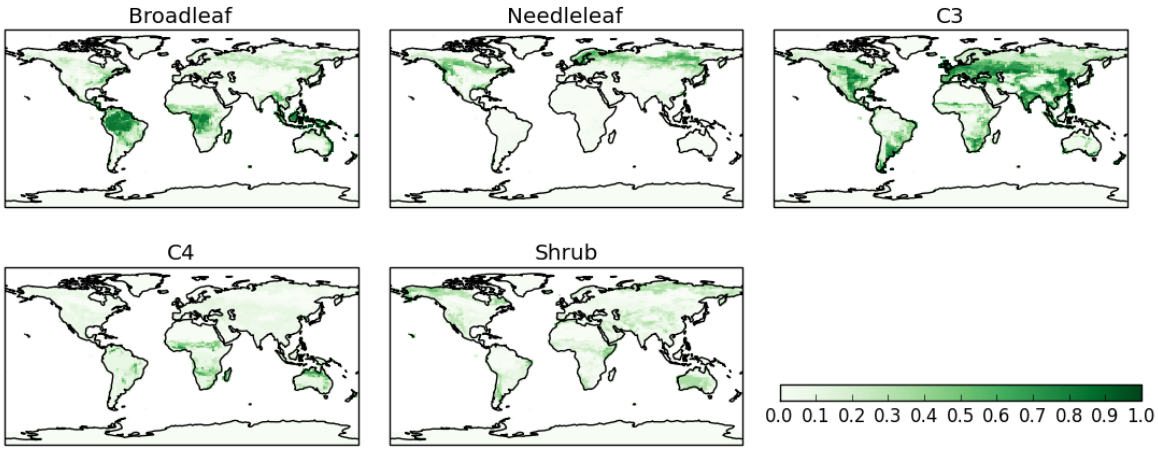

Figure 1.7: N96 resolution ESA land cover map, 5 PFTs (2010) by fraction of gridbox

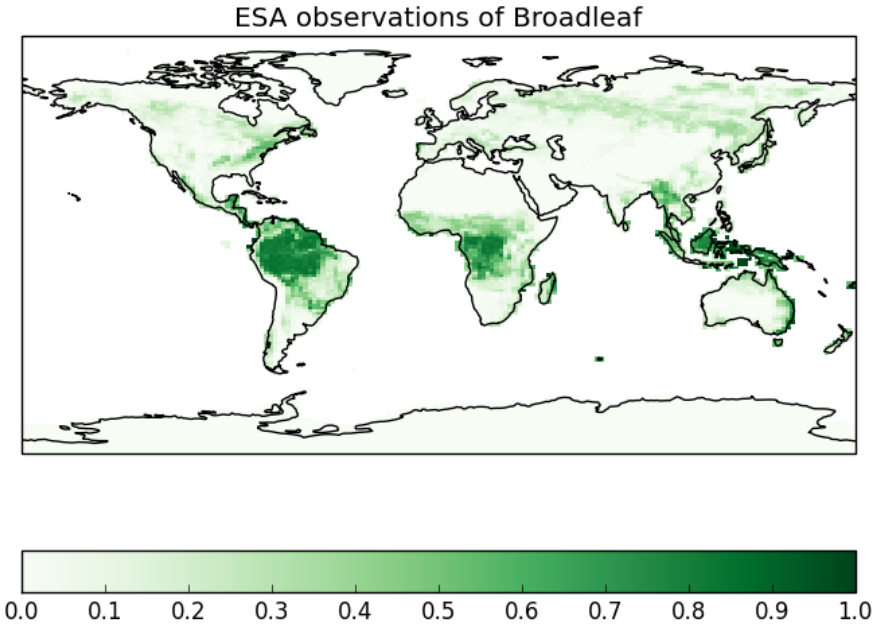

Figure 1.8: N96 resolution ESA land cover map of Broadleaf fraction (2010)

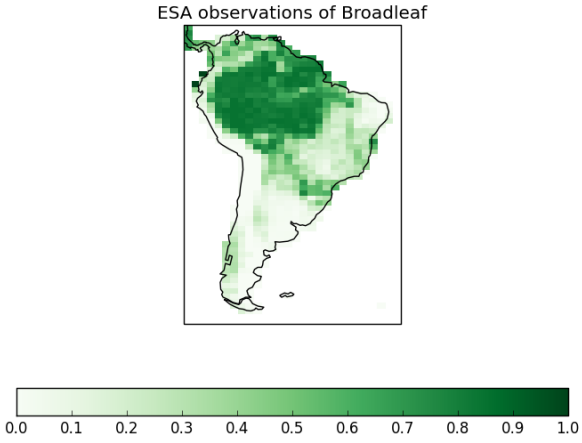

Figure 1.9: N96 resolution ESA land cover map of Broadleaf fraction over South America (2010)

- **Terraclass**

The Terraclass dataset is available from INPE, and gives information on land cover for the Amazon region in Brazil (Almeida *et al*., 2016). Currently only available for Brazilian Amazonia, there are ambitions to extend the data further into Brazil. The product uses a number of land-use classifications, which determine forest from agricultural regions, four different types of pasture land, farming, urban, mining, secondary vegetation and deforested areas. The data is obtained from satellite information, from Embrapa (the Brazilian Agricultural Research Corporation), and is available from 2008 (Figure 1.10).

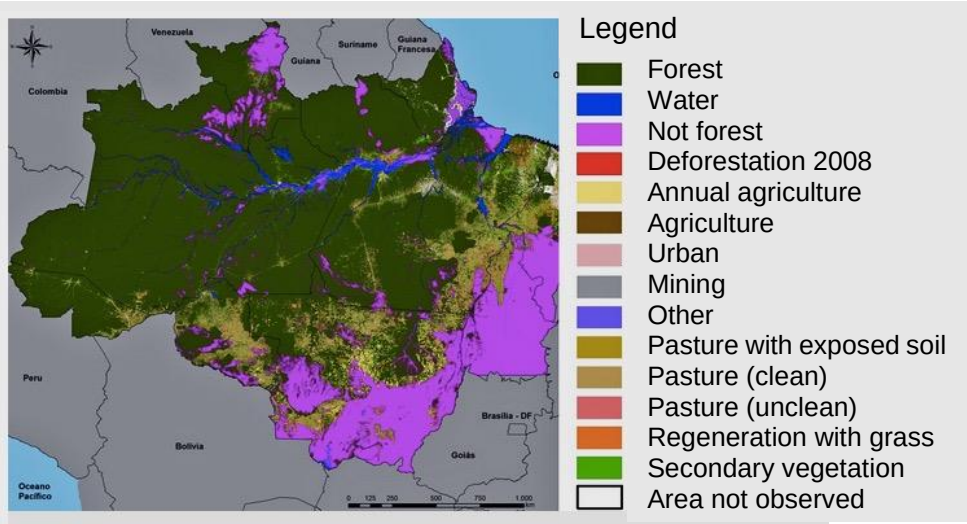

Figure 1.10: TerraClass land cover map for 2008.
Data from INPE and Embrapa

- **PRODES**

The PRODES (Program for the Estimation of Deforestation in the Brazilian Amazon) dataset is also made available by INPE, in collaboration with the Ministry of the Environment (MMA) and the Brazilian Institute of Environment and Renewable Natural Resources (IBAMA), and gives information on annual deforestation rates in the Brazilian Legal Amazon. The dataset runs from 1988, using Landsat images as well as imagery from CBERS, Resourcesat and UK2-DMC. This information is available online, with data from 1997-2000, and annual deforestation data from 2000 to present day17 (INPE, “PRODES” 2014).

[17] PRODES, funded by the Brazilian Ministry of Science, Technology and Communications (MCTIC) through the "Monitoramento Ambiental da Amazônia" (Environmental Monitoring of

- **Avitabile**

Avitabile *et al*. (2016) have created a pan-tropical above ground biomass dataset at 1km resolution by combining two existing datasets of observations and high-resolution maps. The data integration technique uses bias correction and weighted linear averaging resulting in very low bias estimates. The AGB stock for the tropics is 9-18% lower than previous estimates using this technique (Avitabile *et al*., 2016).

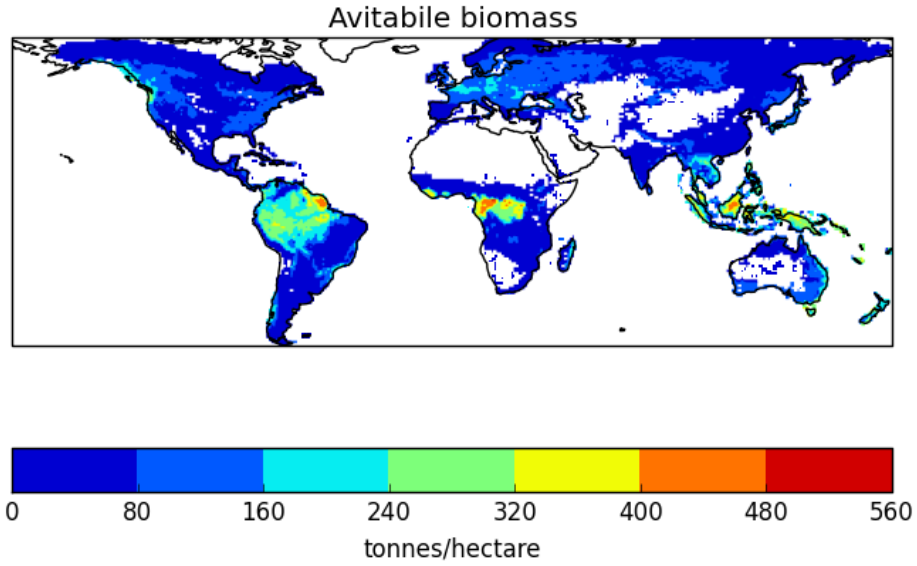

Figure 1.11: Avitabile aboveground biomass

- **WWF Biomes**

The World Wildlife Fund has created a 'Terrestrial Ecoregions of the World' product which divides the Earth's terrestrial biodiverse ecoregions into 14 biomes, defined as 'relatively large units of land or water containing a distinct assemblage of natural communities sharing a large majority of species, dynamics and environmental conditions'[18]. The product is intended for use in conservation strategies and planning (Olson *et al*., 2001).

Amazônia) program at INPE:
http://www.obt.inpe.br/OBT/assuntos/programas/amazonia/prodes
https://www.arcgis.com/home/item.html?id=4160f715e12d46a98c989bdbe7e5f4d6

[18] WWF ecoregions: https://www.worldwildlife.org/publications/terrestrial-ecoregions-of-the-world

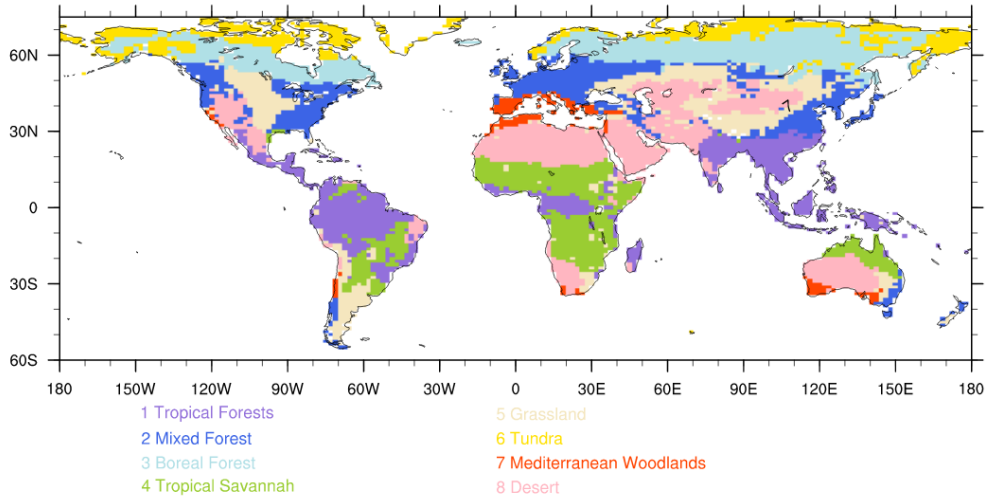

Figure 1.12: WWF biomes and ecoregions
Major global biomes based on 14 World Wildlife Fund's ecoregions. Some ecoregions have been combined to reduce the total number to 8: Tropical forests = all tropical and subtropical forests plus mangroves; Mixed forest = temperate broadleaf and mixed forests plus temperate conifer forests; tropical savannas = tropical/sub-tropical grasslands, savanna, and shrubland; Grassland = temperate grasslands, savannas, shrublands, flooded grasses, montane grasses. Reproduced from Harper *et al*. (2016), Figure 3b.

1.3.3 Observational uncertainty

Across all observational products there is a degree of uncertainty associated with the data. These can stem from flaws in data collection. For example in satellite data, overpass time, clouds and spatial resolution hinder output, which affect most burned area products in use today. As outlined in Hantson *et al*. (2016), there are multiple burned area products such as g. GFED4, L3JRC, MCD45, MODIS and Fire_cci, some of which have been mentioned here, all giving different results and with different ranges of uncertainty. Similarly with land-use data, the HYDE LULCC dataset for example has been developed from a combination of model, satellite and historical reconstructions of agricultural and population data to cover the entire period 10,000 AD to present day, long before observational records began, and the biomass quantities are noted to contain uncertainties due to lack of direct observations from the historical period (Klein Goldewijk and Verburg, 2013; Hurtt *et al*., 2011). Uncertainties can also stem from data interpretation. The ESA CCI land cover data is the product most commonly used as observations for use with JULES, mostly due to the work invested in classifying the data into the JULES PFTs for improved comparison. I therefore focus on this product for comparison with my results. However, the process of translating global vegetation cover into the 5 PFTs that are used in

JULES (Poulter *et al*., 2015), and through the process of data collection and classification, a number of uncertainties are introduced which result in a range of possible outcomes for land cover distribution (see Hartley *et al*., 2017). These uncertainties can include for example variation in classifying the surface reflectance products into the 22 land cover classes, and aggregating these by dominant vegetation type into just 5 PFTs for JULES by a consultative cross-walking technique. This classification also needs to take into account seasonal variation in NDVI (greenness), burned area, cloud cover and snow occurrence that can all vary throughout the year, giving a large range between the minimum and maximum possible vegetation cover for any one PFT, as shown below. A classification algorithm is used to determine vegetation type using satellite-derived radiance and ground-based observations, and the most likely class is then chosen. This is referenced with a cross-walking technique, aggregation, and post-processing, to result in a 'most likely' case for vegetation cover referred to as the 'reference' case (Hartley *et al*., 2017). The 'reference' dataset is the one commonly used in analysis.

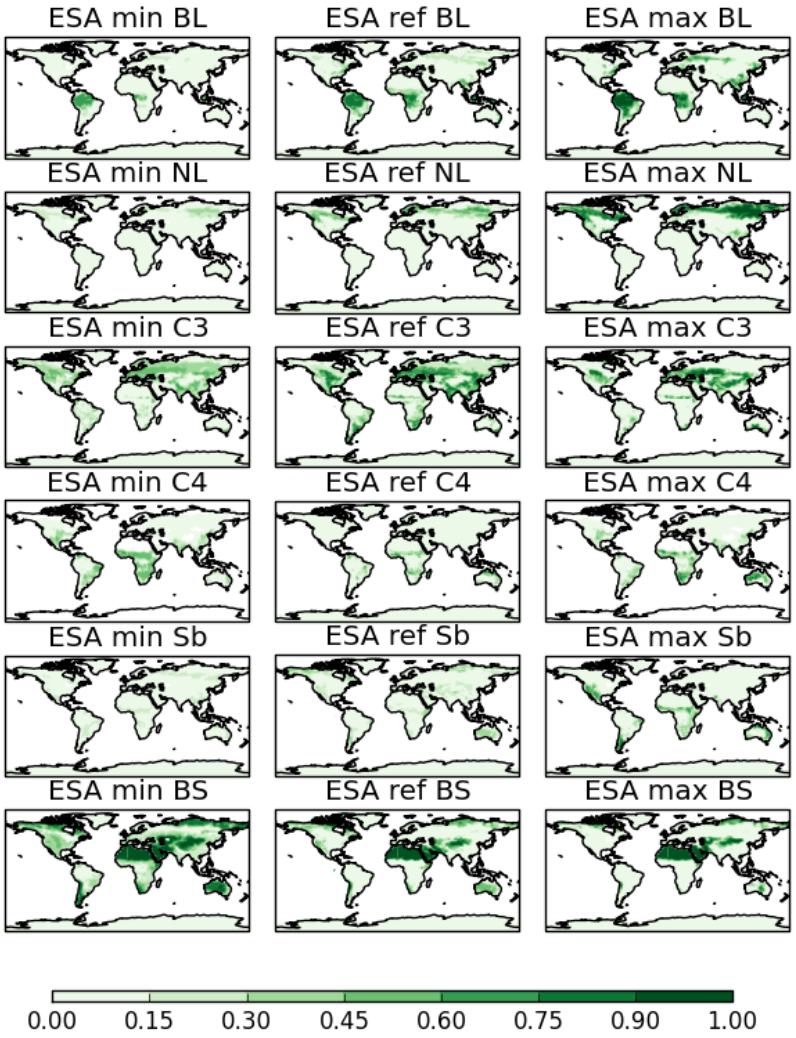

Figure 1.13: ESA CCI land cover uncertainty
ESA CCI fraction of vegetation cover. Minimum cover shown in left column, reference data in centre column, and maximum cover in right column. BL = broadleaf, NL = needleleaf, C3 = C3 grass, C4 = C4 grass, Sb = Shrub, BS = bare soil.

It is not within the scope of this PhD to attempt to reduce observational uncertainty within the datasets used. However it must be borne in mind when comparing the model results with the observations that there are uncertainties associated with the products, and they should not be taken as perfect representations of the real world.

1.4 Fire indices

Forest fires are greatly affected by meteorological conditions, where fire occurrence is highest during dry summer periods when temperatures are high, humidity is low and fuel moisture is reduced (Pinol *et al*. 1998). Based on this, a number of fire indices have been developed that can give information on the

potential behaviour of fires as a result of varying conditions. An overview of the more common fire indices is give here.

1.4.1 McArthur Mark 5 Forest Fire Danger Index (FFDI)

(Noble *et al*. 1980)

The McArthur FFDI was developed in 1960 by the CSIRO scientist A.G. McArthur, based on the degree of fire danger in Australia. It uses meteorological data to calculate the change of a fire igniting, its rate of spread, and the difficulty of suppression, using the following equation:

$$\boldsymbol{FFDI = 2.0 * exp(-0.450 + 0.987 * ln(D) - 0.0345 * H + 0.338 * T + 0.234 * V)}$$

Or simplified:

$$\boldsymbol{FFDI = 1.25 * D * exp\left[\frac{T - H}{30.0} + 0.0234 * V\right]}$$

Where:

D = drought factor, calculated as follows:

$$\boldsymbol{D = \frac{0.191 * (I + 104) * (N + 1)^{1.5}}{3.52 * (N + 1)^{1.5} + P - 1}}$$

Table 1.1: Input to McArthur FFDI

Symbol	Meaning	Units
I	Based on Keetch-Byram drought index	mm equivalent
H	Relative humidity	%
T	Air temperature	˚C
V	Average wind velocity in the open at a height of 10m	km hr^{-1}
N	Number of days since last rain	days
P	Amount of precipitation	mm equivalent

The McArthur FFDI is measured on a scale of 1-100, as shown in Table 1.2.

Table 1.2: McArthur FFDI scale of fire danger.

Category	Forest Fire Danger Index
Catastrophic* (code red)	100+
Extreme	75 - 99
Severe	50 – 74
Very high	25 – 49
High	12 - 24
Low - Moderate	0 - 11

***Catastrophic refers to fires that spread so quickly that they present a threat to life and safety**

This index is widely used, and has been applied by Golding and Betts (2008), Betts *et al*. (2015) and was cited in IPCC AR5 to assess fire danger globally and in the Amazon. It is useful in providing an indication of fire danger, and includes a number of meteorological variables as well as a drought index which enhance its accuracy. It does however still have notable limitations, in that it was designed for Australian vegetation, and therefore its applicability outside of this region is less certain. The power function and inability to measure inputs precisely also means there is a large uncertainty range. (Note there is also a McArthur Mark 4 Grassland Fire Danger Index (GFDI), but this is outside the scope of this work so is not considered here.)

1.4.2 Canadian Forest Fire Weather Index (FWI)

(de Groot, 1987)

The FWI was developed in 1970, based on the effects of weather parameters on forest floor fuel moisture conditions. This index assesses the fixed and variable factors of the fire environment, which determine the ease of ignition, rate of spread, difficulty of control and potential fire impact. Its purpose is to account for the effects of weather on forest fuels and forest fires, and is based on a number of inputs, as shown in Figure 1.14:

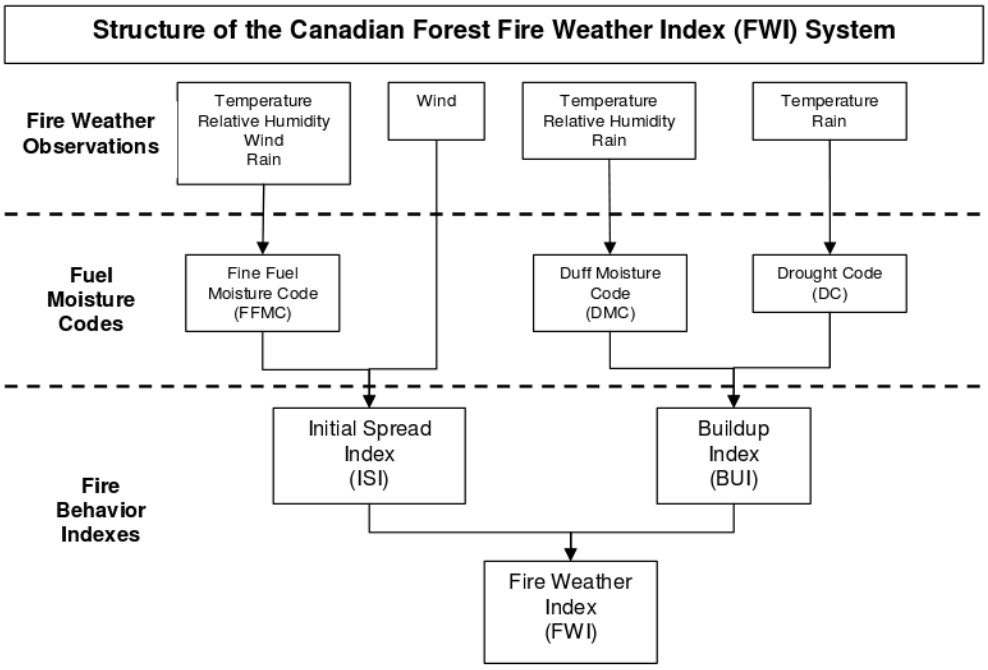

Figure 1.14: Structure of the Canadian FWI.
Reproduced from de Groot, 1987. Input variables include temperature, relative humidity, wind speed, and rainfall in previous 24 hours

This is a complex index with many input variables (Appendix 1). It was developed to forecast fire danger in Canadian pine forests so, similar to the FFDI, can give an indication of fire danger in other regions such as the Amazon, but its applicability can only extended so far and does not account for the difference in flammability of different vegetation types.

Bedia *et al*. (2015) investigate the sensitivity globally to fire-weather using the FWI, and find that the Amazon is one of the most susceptible regions to fire-weather fluctuations, which may result in severe impacts on future fire regimes with climate change.

These complex fire rating systems integrate sub-models and drought indices within the calculation. A drought index quantifies fuel flammability by representing the cumulative moisture deficiency as a net effect of evapotranspiration and precipitation (Mantzavelas *et al*., 2006). However, because of the complexity of drought there are many indices and no single index has been able to adequately represent the severity, intensity and potential impacts for so many different users. Some drought indices are used on their own to indicate fire danger, such as the Angström and Nesterov indices, as described below.

1.4.3 Angström Index

One of the simplest drought indices, the Angström Index was devised in Sweden and has been used all over Scandinavia. It was designed to be computed mentally.

The index, I, is given by:

$$I = \left(\frac{R}{20}\right) + \left(\frac{27 - T}{10}\right)$$

Where:

R = Relative humidity (%)

T = Air temperature (°C)

This is measured on a reverse scale where a low index pertains to a high fire likelihood, as shown in Table 1.3.

Table 1.3: Angström Index scale of fire danger

Index Value	Meaning
I > 4.0	Fire occurrence unlikely
4.0 > I > 2.5	Fire conditions unfavourable
2.5 > I > 2.0	Fire conditions favourable
I < 2.0	Fire occurrence very likely

1.4.4 Nesterov Index

(Mantzavelas *et al*., 2006)

This drought index was developed by Professor V.G. Nesterov in 1967 for use in Russia for fire danger rating, and uses synoptic daytime data of temperature, humidity and precipitation:

$$NI = \sum_{i=1}^{W} (t_i - D_i) * t_i$$

Where:

NI = Nesterov Index, W = number of days since last rainfall > 3 mm,
T = mid-day temperature (°C), and D = dew point temperature (°C).

Table 1.4: Nesterov scale of fire danger

Index Value	Meaning
N < 300	No fire danger
301 < N < 1000	Low fire danger
1001 < N < 4000	Medium fire danger
4001 < N < 10,000	High fire danger
N > 10,001	Extremely high fire danger

This is a simple equation which doesn't require wind speed or daily humidity, for which accurate data are difficult to obtain. However it does require sub-daily meteorological information which may not be easily available. This is available as a stand-alone fire-danger index in JULES.

None of these indices were designed for use in tropical humid ecosystems, probably because historically there have been few fires in these regions due to the high moisture levels. Some of these indices have been shown to do a reasonable job of predicting fire danger over the Amazon (e.g. the FFDI is assessed in Betts *et al*. (2015) against observed burned area), but there is a question over whether this could be improved with an index based specifically on tropical vegetation.

Currently in JULES the FFDI, FWI and the Nesterov fire indices are available. Fire indices can give a good indication of changes in fire danger to give information on the probability of fire occurring in a particular location based on only meteorological and climatological conditions. This is different to burned area, which is where fires occur given meteorological conditions, available fuel and ignitions. Global observed burned area for example inherently includes human land management which can increase and supress ignitions according to policies and cultural practices, and may not reveal changes in the susceptibility of ecosystems to fire as a result of changes in the climate. However with fire indices, the risk of fire is not quantitatively related to burned area, emissions or fuel consumption (Hantson *et al*., 2016), and does not include ignition. These factors can be crucial in determining where fires occur; without natural or anthropogenic ignition, an area can have high fire danger but will never burn. Similarly there is

high fire danger over desert areas, but with limited fuel fire is not a hazard. The complete assessment of burnt area and interaction with climate and vegetation therefore needs to be addressed by more sophisticated land surface and Earth system models.

1.5 Fire models

1.5.1 Overview of fire models

Despite the relative lack of progress so far in implementing fire as a standard process across ESMs (Ciais *et al*., 2013) a large number of fire models exist today, varying greatly in complexity. Although many different streams of work in fire modelling have been started, there has been little evaluation across these different models until now, and there is therefore a lack of consensus on how well the individual models perform, and over the degree of complexity that is required to model fire accurately (Hantson *et al*. 2016). The current FireMIP (Model Intercomparison Project) activity aims to provide this independent evaluation across models, and therefore provide an authoritative voice on fire modelling.

One of the main points on which models vary is around ignition, and there are differing perspectives on the best way to model human-induced fire starts. For example some empirical models use a constant estimated rate of ignition, whereas some include algorithms that estimate lightning frequency and population density, and others give the option of reading in observed data. Pechony and Shindell (2009) proposed that fires increase with population due to higher ignition potential, until an optimum maximum point, beyond which fire occurrence decreases with increased population due to anthropogenic intervention and management (fire suppression). The simulated number of fires then translates into burned area. Other schemes simulate human ignition as a result of land-use change (LUC), e.g. Kloster *et al*. (2010) includes burned area as an assumed fraction of cleared biomass. Li, Levis and Ward (2013) propose fire-rates based on deforestation and weather in closed tropical forests, plus cropland management. Other DGVMs, such as Sheffield (SDGVM), include fire modules, but assume ignition is not limited (Bond, Woodward and Midgley 2005) (see section 1.5.2). This section provides an overview of the development of a selection of fire models.

- **MAPSS-CENTURY Fire (MC-FIRE)** (Lenihan *et al*., 1998)
    - Uses a rate of spread model (based on Rothermel equations (1972)
    - Simulates large, intense fires where all of the grid cell is assumed to burn (later version includes low-intensity fires)
    - Includes meteorological input (moisture availability)
    - Allows only one ignition per grid cell per year
    - Embedded in MC1 DGVM
- **GLOBal FIRe Model (Glob-FIRM)** (Thonicke *et al*. 2001)
    - First global fire model
    - Assumes vegetation burns at a constant rate for each PFT
    - If fuel is sufficient, burned area depends on length of fire season (function of soil moisture)
    - Calibrated using site-based observations
    - Threshold value of 200 gC/m² (point at which fuel becomes discontinuous and fire occurrence = 0)
    - Coupled in LPJ, CLM, ORCHIDEE, LPJ-GUESS, BETHY
    - Does not specify ignition sources
- **Regional Fire Model (Reg-FIRM)** (Venevsky *et al*. 2002)
    - Based on Glob-FIRM
    - Simulates burnt area as a product of number of fires and average fire size
    - Assumes constant lightning ignition rate, and human ignitions dependent on population density
    - Includes Nesterov Index
    - Uses simplified Rothermel equations to simulate rate of spread
    - Vegetation mortality is a prescribed parameter
    - Used in LPJ
- **Canadian Terrestrial Ecosystem Model (CTEM-fire)** (Arora and Boer 2005)
    - Based on Reg-FIRM
    - Simulates the feedback between vegetation and fires using a simplified parameterised approach
    - Models rate of spread
    - Completeness of combustion depends on PFT, but does not vary with fire intensity
- **HADLEY-FIRE** (Venevsky *et al*., 2007)
    - Based on Reg-FIRM
    - Prototype fire model in HadCM3LC, and off-line version in JULES using IMOGEN/climate emulator for fine tuning
    - Number of ignitions is constant
    - No interaction with vegetation
    - No fire suppression
    - Fuel threshold determined by total fraction of vegetation in grid cell
    - 2.5° x 3.75° resolution, 30 min timesteps
    - Validation against MODIS
    - Output: fire weather risk (0,1) and burnt area (m²)
- **Spread and InTensity of FIRE (SPITFIRE)** (Thonicke *et al*. 2010)
    - Based on Reg-FIRM and rate of spread, but maximum fire duration limited to 4 hours, and population density is regionally tuned

    - Builds on Nesterov Index
    - Explicit representation of ignitions, spread and intensity
    - Coupled with ecosystem dynamics, included in LPJ, and in ORCHIDEE, JSBACH, LPJ-GUESS and CLM-ED with modifications
    - Completeness of combustion depends dynamically on moisture, fire intensity, and PFT
    - Mortality varies with bark-thickness which scales with tree size
    - Used to explore the impact of fire on the terrestrial carbon cycle
    - Estimates an average release of 2.24 $PgCyr^{-1}$ as CO_2 from biomass burning over 1980s-1990s
    - Reproduces broadly accurate geographic patterns for peak fire seasons, although this can be late and too long in some areas, as validated by MODIS and GBS
    - Implemented in historic versions of JULES but no longer available
- **Land surface Process and eXchanges model (LPX)** (Prentice, Harrison and Bartlein 2011)
    - Based on SPITFIRE
    - Realistic representation of lightning by including precipitation data
    - Does not include human ignition
    - Only model to date that includes fire-triggered regeneration (resprouting)
- **Lausanne-Mainz fire model (LMfire)** (Pfeiffer, Spessa and Kaplan 2013)
    - Based on SPITFIRE
    - Limits lightning ignition to rain-days, by interannual variability, and by fraction of land already burned
    - Separates population into three categories: hunter-gatherer, pastoralist, farmers
- **INteactive Fire and Emission algoRithm for Natural envirOnments (INFERNO)** (Mangeon *et al*. 2016)
    - Fuel flammability is simulated using temperature, relative humidity, fuel density, precipitation and soil moisture
    - Flammability, fuel and ignition gives diagnostic burned area and emissions
    - Implemented as diagnostic fire model in JULES version 4.5
    - Does not include fire spread, or interactive vegetation
- **IBIS-INLAND** (AMAZALERT D3.3)
    - Based on CTEM
    - Represents major features of fire occurrence
    - Emphasis on ecosystems in Brazil
    - Focus on simulation of fire probability (based on fuel, flammability and source of ignition) and effects on vegetation dynamics only
    - Ignition is taken into account, but it is currently considered random
    - IBIS-INLAND fire model is not properly calibrated yet

The representation of fire in models can be organised according to different aspects of the fire regime, as summarised in Table 1.5.

Table 1.5: Aspects of the fire regime

Model	Burnt Area	Fire danger / probability	Rate of Spread (ROS)	No. of fires	Fire Intensity	Fire duration	Fire Weather (e.g FDIs)	Vegetation mortality	Carbon Emissions	Ignition	Suppression
Vegetation-Fire models											
MC-FIRE											
GlobFIRM											
RegFIRM											
CTEM											
HADLEY-FIRE											
SPITFIRE											
LPX											
LMfire											
INFERNO								This PhD			
IBIS-INLAND											
Fire Danger Indices											
McArthur FFDI											
Canadian FWI											
Angström											
Nesterov											

The characteristics of fire can be numerous and varying. There is no agreed consensus on what aspects should be included in the definition of a 'fire regime', and in some respects this depends on the temporal and spatial scales being studied. However, we can broadly categorise the main aspects of fire into groups such as size, pattern, frequency, seasonality, intensity and severity, which make up the 'fire regime'. For example, the nature of a fire depends on vegetation composition, type, and structure, previous fires, ignition, management, climate and weather, terrain (slope and exposure), and landscape patterns, which can effect the frequency, return interval, size, severity, seasonality, and extent of a fire, as well as the type of fire including surface, crown, understory / sub-canopy, ground, stand replacement, or mixed-severity fire[19]. It is very difficult to attempt to model all aspects of the fire regime at once, largely due to the inclusion of unconstrained model parameters and inputs from the base vegetation model, and models that include more inputs are generally more complex and harder to maintain within a constantly-developing modelling environment. In addition, the importance of each aspect depends on the research question being asked; for some research questions a simple fire index will be enough to give an indication of changing fire danger across an area, whereas for other questions a fully-coupled interactive fire model will be required. This provides some reasoning for why there are many different fire models that exist today, and why there is a large spread in results and uncertainty across the models.

1.5.2 Uncertainty in fire modelling

In addition to modelling different aspects of the fire regime, part of the reason why there is such variety across fire models is because there are still many areas of uncertainty in correctly simulating fire count and burned area. Firstly, as outlined in section 1.3, there are uncertainties in the observation datasets of burned area and vegetation resulting from methods of collection, which makes calibration of models difficult. Bachmann and Allgöwer (2002) identify fire spread through wind speed and direction to be a large source of uncertainty, together with fuel type, which impacts models such as SPITFIRE which aim to model fire spread. In terms of fuel, LSMs are necessarily a simplification of real world variation in vegetation type, which introduces a source of uncertainty in representing how fire and

[19] Fire Science Project, 'Fire History and Climate Change', Chapter 3: https://www.firescience.gov/JFSP_fire_history.cfm

vegetation interacts. In JULES for example there are just 5 PFTs as standard, or 9 PFTS if extended (Harper *et al*., 2016; Harper *et al*., 2018). In reality, some vegetation species will be more fire resilient than other species within each PFT class. For example, vegetation in high fire-risk areas often develops thicker bark for protection from fire, whereas other species may adapt to the fire and use it as a method of reproduction (Pellegrini *et al*., 2017). There is no consensus on the best way to model human ignition, with some models using population either as a unimodal relationship (e.g. Pechony and Shindell, 2009; Mangeon *et al*., 2016) or negative monotonic relationship (e.g. Bistinas *et al*., 2014), or some using distance to construction / roads (i.e. Cardoso *et al*., 2003; Song *et al*., 2017). Li *et al*. (2012) advocate the use of a combination of ignition sources: population and GDP (both negatively correlated with fire, reflecting that less populated and less developed regions are more likely to use fires in agricultural management, and more developed regions may have more resources for fire management and suppression) and socioeconomic factors (i.e. harvesting patterns) are taken into account for agricultural fires; positive correlation with deforestation rates are used for tropical forests such as the Amazon; climatic factors are used in simulating peat fires; and population and GDP by PFT is used for all other fire types. These differences result in a model spread of simulated burned area (Figure 1.15). However, due to equifinality of models (Beven, 2006), there are many different approaches and model assumptions used across fire models that can lead to similar patterns of burned area.

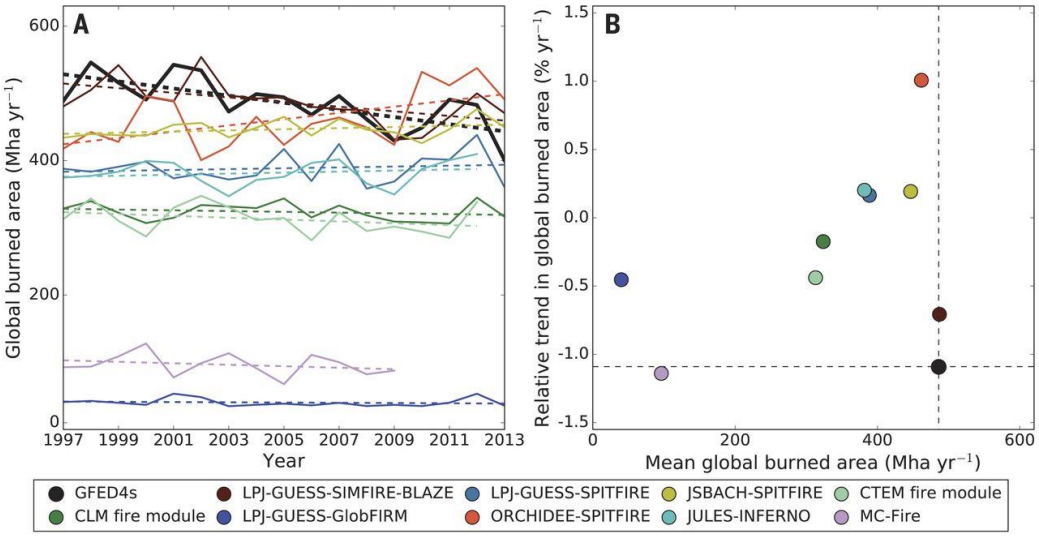

Figure 1.15: Uncertainty across fire models.
Global burned area time series (A) and annual mean (B) from observations and models in FireMIP. Reproduced from Andela *et al*. (2017), as their figure 3

1.5.3 Fire modelling in Brazil

Considering the whole country, one of the most important fire modelling applications in Brazil is the warning system for the fire monitoring program at the Brazilian Centre for Weather Forecasts and Climate Studies[11]. The system provides daily information on fire occurrence and risk for the whole of Brazil and some neighbouring countries, based on land-cover and meteorological information and fire detection from several satellite products. The information supports the operation of national parks and environmental protection institutions such as the Brazilian Institute of the Environment and Renewable Natural Resources (IBAMA) and Brazilian Ministry of the Environment (MMA) to avoid and control catastrophic fires. Preparedness and allocation of resources are concentrated in regions with indication of higher occurrence or risk of fires.

The model, based on several years of empirical observations of fires in Brazil (Setzer and Sismanoglu 2012), assumes that fire susceptibility is mainly driven by a lack of precipitation, where fire danger increases for longer dry periods and decreases for recent high precipitation. Vegetation is grouped into broad categories from grasslands to evergreen forests with progressively higher capacity to resist dry periods before becoming flammable. In addition to precipitation, the model considers recent data on minimum relative humidity, maximum temperature, and detection of active fires. Fire danger increases if the relative humidity is lower than 40%, and maximum temperature is above 30 °C. Places presenting low risk but detection of fires are reclassified to high susceptibility. The model then classifies the study regions into five main categories of minimum, low, medium, high and critical fire susceptibility.

The fire season severity (FSS) forecast lead by the University of California in cooperation with NASA Goddard Space Flight Center, Columbia University, University of Maryland and Duke University, based on Chen *et al*. (2011), was a service available from 2012-2016. It presented a range of information about the fire danger for the forthcoming dry season for 6 high-biomass burning sub-regions; Acre, Amazonas, Maranhão, Mato Grosso, Pará, and Rondônia[20]. A fire season severity index (FSSI) is given, based on active fire counts and two ocean climate indices, the ONI (Ocean Nino Index) and AMO (Atlantic Multidecadel

[20] FSSI: http://www.ess.uci.edu/~amazonfirerisk/ForecastWeb/SAMFSS2016.html

Oscillation index). The sea surface temperature (SST) anomalies are captured by the ONI 3-month mean SST anomaly from the NOAA National Weather Service Climate Prediction Centre, and the AMO 3-month mean from the NOAA Earth System Research Laboratory. Observations of fire counts are detected from thermal radiation anomalies via Moderate Resolution Imaging Spectroradiometer (MODIS) on board the NASA Terra satellite, and are ongoing throughout the season. The SSTs have a strong relationship with fire activity, and the empirical predictive model is based on a linear combination of the two ocean climate indices, and verified against observations. Although as the deviser of the method notes, actual fire severity depends on a complex interaction between multiple parameters including fuel moisture levels, precipitation, wind speeds, ignition sources and land-use decisions (Chen *et al*. 2011). A time series of fire counts 2001-2016 is also available. Terrestrial water storage is monitored by NASA's Gravity Recovery and Climate Experiment (GRACE) satellite to give further support to the FSSI, although is not directly used by it.

Other fire models are more complex and have been coupled to ecosystem models, such as the fire-susceptibility system *RisQue98* that was developed during the dry season of 1998 to map the vulnerability across the Amazon to fire, using historical observations also from the AVHRR satellite together with information on climate, soil properties, land-use. There are also the MAPSS-CENTURY Dynamic Vegetation Model and the Ecosystem Demography models. These model natural fire occurrence as a result of fuel availability and meteorological conditions, but do not include human ignitions, which are the cause of a large proportion of fires in this region.

Cardoso *et al*. (2003) presented a new fire model based on GOES-8 satellite data, which incorporates factors linked to land cover (forest cover), land-use (distance to road, presence of deforestation), and climate to give a yearly indication of large-scale fire patterns in Amazonia. When tested against observations it performed well in reproducing the spatial pattern of fire at large scales. This was more advanced than the previous fire danger models, as the input factors were spatially and temporally variable, however this model didn't interact with the climate or Earth system and so important dynamical feedbacks were absent. Fire pixels were the main focus of the study, and information on emitted carbon and impacts on vegetation was not included. Analysis of remote

sensing data has also been used as a way of determining the relationship between fire and land-use (Cardoso *et al*. 2005), but the extent of the burnt area and fraction of biomass is not easy to establish from this method alone. The CPTEC Potential Vegetation Model (PVM) has also been improved in recent years to include a new parameterization for long-term fire occurrence (Cardoso *et al*. 2008). This was based on a simple-empirical relationship of lighting occurrence combined with fuel availability using large-scale topography and climatological data, but did not account for human ignition.

As part of research on surface-atmosphere interactions at CCST/INPE[21], the Brazilian Integrated Model of Land Surface Process (INLAND) has been improved to incorporate fire processes as part of the AMAZALERT project 2011-2014 (see AMAZALERT Deliverable D3.3 'Impacts of fire on climate'). Based on work by Arora and Boer (2005), the model calculates fire potential using fuel, flammability and sources of ignition. The model uses the output of fire estimates to calculate vegetation dynamics, biomass, leaf area index, and net primary productivity (NPP), and fractional cover of forest and herbaceous canopies are modified as a result.

In this model, the minimum requirement for fuel in order to sustain a fire is 200gC/m², which is made up of stem and leaf biomass. Flammability is based on soil moisture in the top soil layer, and ignition is random:

Fire occurrence probability = Fuel x Flammability x Ignition

Vegetation disturbance from fire is assumed to be proportional to fire probability. Deforestation was not included as a direct relationship with fire, but was accounted for as an additional disturbance, affecting plant biomass, leaf area index and NPP. However the current version of the INLAND fire model still lacks proper calibration.

1.5.4 Fire modelling in Europe

From the above list of fire models used in Europe in 1.5.1, it is proposed that there are two contrasting approaches used in fire modelling; a process-based approach to model individual fires that is extrapolated up to the large scale, and

[21] CCST: http://www.ccst.inpe.br/projetos/inland/

an empirical approach using statistical relationships between fires and observations. Here SPITFIRE and INFERNO are used as examples of each approach respectively.

SPITFIRE is a relatively complex model with multiple inputs (Figure 1.16).

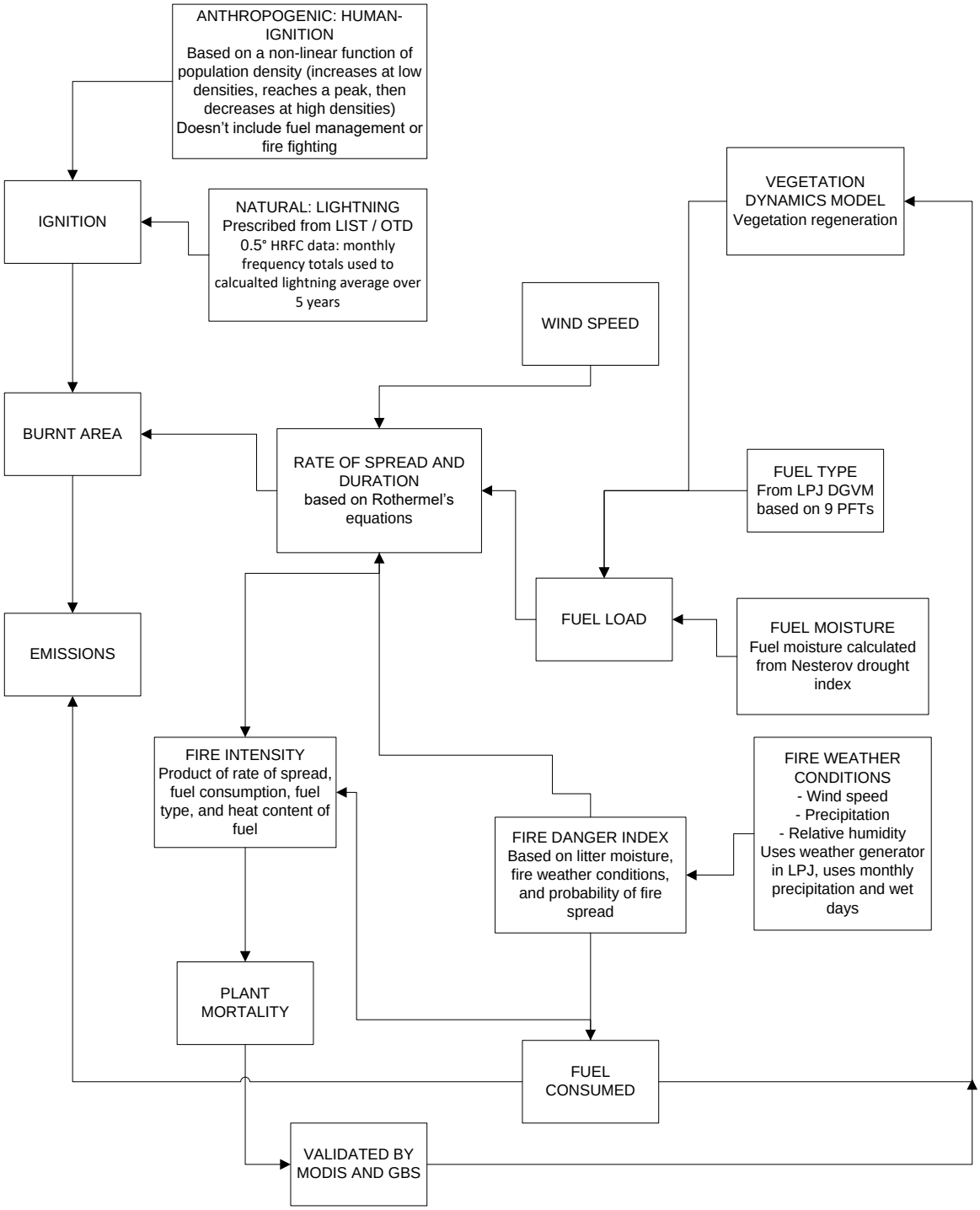

Figure 1.16: Overview of SPITFIRE.
Figure by C.Burton, based on information from Thonicke *et al*. (2010) and Spessa (2009)

SPITFIRE uses both anthropogenic and natural ignitions. The anthropogenic ignitions are again based on the unimodal relationship of population density with ignitions proposed by Pechony and Shindell (2009), with low ignitions at low population densities, rising with population to a peak, then decreasing at high population density. The lightning ignitions are prescribed from LIS lightning data.

In terms of geographic distribution and general timing of fires compared to data from MODIS, SPITFIRE has been shown to do well (Thonicke *et al*. 2001, Thonicke *et al*. 2010). However, the model does not allow for long-lasting fires, landscape heterogeneity, or fire suppression. There are also a couple of key regions over which the model performs poorly as outlined in Fletcher *et al*. (2014); for the interior of Australia which is a high fire-prone region, the model simulates very low vegetation due to low rainfall, and thus zero fire. The extent of low fire occurrence in northern latitudes also extends too far south in the model. This could be due to the use of monthly climate data, which are interpolated to quasi-daily values. There is little fire activity simulated over the Amazon due to the humid conditions, which fails to capture the high rate of human-induced fire which can be seen in the MODIS data, although later studies show the statistical representation of burned areas of the Amazon performs well at coarse resolution. SPITFIRE is also one of the more complex fire models, making it difficult to develop and maintain, and the underlying calculations are based on a number of weakly constrained input variables and datasets (Fletcher *et al*. 2014).

Despite their global importance, fires are a local phenomenon and are difficult to model at large scales. INFERNO was therefore developed on the premise of a reduced complexity approach and intended for decadal to centennial scale climate simulations on continental to global scales (Mangeon *et al*. 2016). See Figure 1.17 below.

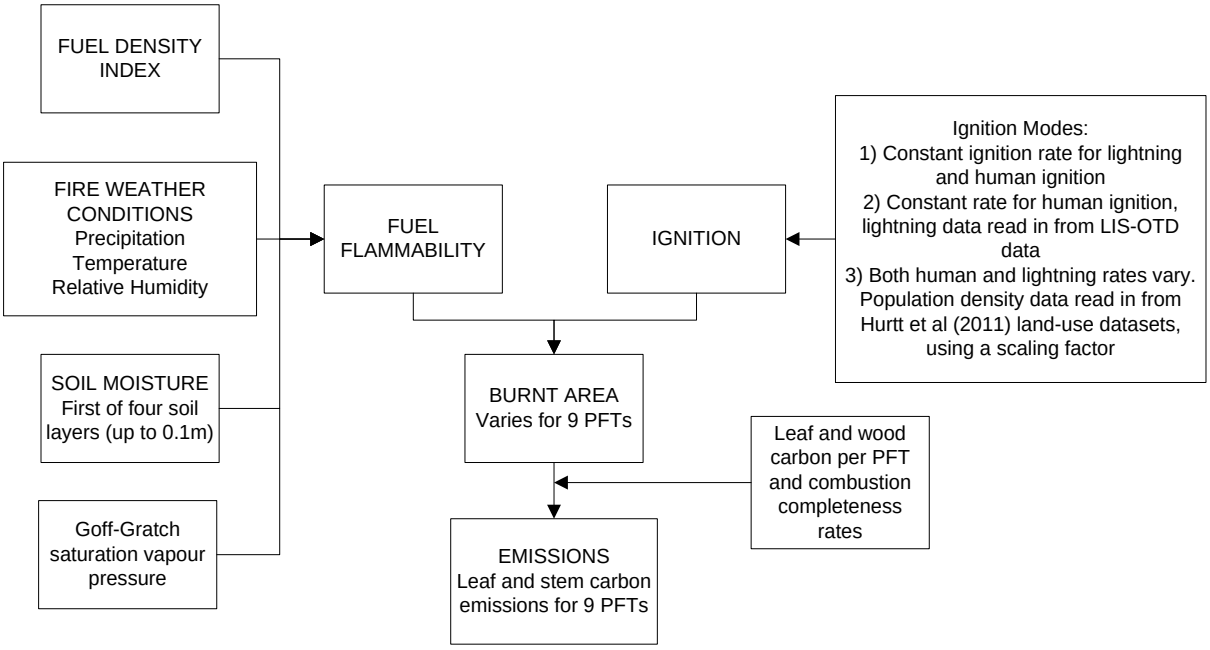

Figure 1.17: Overview of INFERNO.
Figure by C.Burton based on information from Mangeon *et al*. (2016)

Even though much reduced in complexity in comparison to SPITFIRE as highlighted by the figures above, INFERNO generally performs well for global fire occurrence and emissions, as detailed in Mangeon *et al*. (2016). INFERNO is also compared against the fire indices available in JULES in the same study, and on a global scale performs better compared to GFED observations of burnt area, and performs particularly well for low latitudes and equatorial regions. Current limiting factors in INFERNO are the lack of representation of peat, no estimation for rate of fire spread, and inability to interact dynamically with vegetation, so that it only acts a diagnostic to predict burnt area.

INFERNO uses inputs of surface air temperature, relative humidity, precipitation, soil moisture, fuel density and saturation vapour pressure (via the Goff-Gratch equation) to calculate flammability. It uses three interactive modes of ignition (see Figure 1.17), combined with flammability and an estimation of average burnt area by PFT to calculate burnt area. It then uses burnt area and flammability together with leaf and wood carbon per PFT and combustion completeness rates to calculate emissions of Carbon Monoxide, Carbon Dioxide, Methane, Nitrogen Oxides, Sulphur Dioxide, Organic Carbon and Black Carbon.

INFERNO has recently been implemented in JULES, and was purposefully designed as a reduced complexity model in order to be easier to maintain and develop. It has been shown to give good results compared to observations, and

is comparable to other fire models. However, as INFERNO is not yet developed to interact dynamically with the vegetation in JULES, this aspect will need to be implemented in order to obtain a realistic projection of future vegetation mortality. This was noted in Thonicke *et al*. (2010) as an important feature of a good fire model. For the purposes of this research, INFERNO will be used within the land surface model JULES.

Chapter 2: Introduction to land-use and land surface modelling

2.1 Abstract

The terrestrial biosphere is an important sink and potential source of carbon. Land-use and land cover change have significant implications for changes to this sink, releasing carbon through deforestation, and changing the biophysical properties of the landscape through agriculture, crop and biofuel production. There are still large uncertainties in how and where all of the emitted carbon is taken up within the Earth system, leading to what is known as the budget imbalance, or "missing sink". Working to reduce the uncertainties around land-use change should be a starting point to account for this missing sink. In this study I assess the impacts of land-use change (LUC) globally and over Brazil though a number of variables, and find that the land carbon sink is substantially impacted by LUC in this region, leading to a high vulnerability to climate variability and change in the future. I conduct a multi-model analysis for the region using TRENDY (Trends in net land carbon exchange project) model simulations, which show a high degree of uncertainty in the land-use contribution of carbon allocation, especially in the Cerrado region. I also review four future RCP scenarios and analyse the implications for future land-use in Brazil, finding that the highest emissions scenario (RCP8.5) and the highest mitigation scenario (RCP2.6) are projected to have the largest impact on LUC in the future.

2.2 Introduction

LUC (land-use change) is both driven by, and results in, changes in the climate system (Settele *et al.*, 2014). Deforestation and agriculture can be important sources of carbon emissions driving climate change, and at the same time changes in the climate are leading to changing patterns of land-use, both directly human-driven e.g. for biofuels, crop production, or land abandonment, and unintentional e.g. climatic forest expansion (Chapin *et al*., 2005) and savannization (Silverio *et al*., 2013).

The land surface has undergone countless changes since prehistoric times, many of which have resulted from natural processes, but since the Neolithic era

people have also been converting natural vegetation to agriculture to grow crops, and using wood for fuel and construction (Williams, 2006). This process has increased with population and food demand, and today over 50% of the ice-free land surface has been affected by land-use activities, with agriculture expanding from an estimated 300-400 million hectares in 1700 to 1500-1800 million hectares in 1990 (Lambin, Geist and Lepers 2003), which continues to grow at a rate of 13 million hectares per year (Zhang and Wiltshire, 2014). The main drivers of LUC are conversion of forested land to agricultural land including crop and pasture, as well as conversion to biofuels, and urban expansion, all of which are facing increasing pressure globally as the demand for food, energy and minerals increases (Flato *et al.,* 2013).

Despite LUC representing one of the most important drivers of change within Earth systems, the processes are still under-represented and over-simplified in many ESMs and Land Surface Models (LSMs), for a variety of reasons. These include, for example, difficulties in obtaining comprehensive ground-based datasets on how the land cover changes, and the building of model equations that reflect the information in these datasets and the actual processes occurring on the ground. This leads to large uncertainties in the estimates of emissions from LUC (Le Quéré *et al.*, 2016).

There has been some progress in implementing the effects of LUC since the IPCC AR4 report, where many of the CMIP3 (Climate Model Inter-comparison Project 3) models omitted these processes. The latest models used in CMIP5 now include carbon dioxide (CO_2) emissions from LUC and many simulate some of the biophysical effects as well (Flato *et al.,* 2013). However this increased complexity has also led to an increased spread in model projections, and there is an ongoing need for better representation of LUC and its associated impacts in models. These improvements will lead to better representation of vegetation and biomass structure and characteristics, which in turn leads to improved representation of vegetation dynamics, estimates of carbon fluxes, and understanding of biophysical feedbacks.

Disturbance as a result of LUC has manifold implications for biogeochemical and biophysical Earth system processes. Firstly it can be a primary cause of soil erosion and degradation. There are also impacts on local and global climate, causing changes in temperature, precipitation, evapotranspiration and runoff

which are regionally dependent (Settele *et al.*, 2014). Simulations of Amazon deforestation typically generate reductions in precipitation, lengthening of dry season, and increases in temperature as a result of reduced evapotranspiration, (although with some variation, see Marengo *et al*. 2006) which means changes in land-use could cause the forest to reach a critical threshold, leading either to dieback or a bi-stable forest/savanna state (Zemp *et al*., 2017). Christidis *et al*. (2013) show that a loss of trees and increase of grassland since preindustrial times has caused an overall cooling trend in both mean and extreme temperatures on a global scale due to increases in albedo, but note that physiological changes from land-use on regional scales may dominate in areas like the tropics. Agricultural expansion in the tropics for example has been associated with an increase in temperature of 0.23°C from 2000-2015, due to reduced evapotranspiration (Duveiller *et al*., 2018; Skinner *et al*., 2018). Vegetation changes influence the surface fluxes of radiation, heat and moisture, where conversion to crops or pastureland can reduce the aerodynamic roughness and alter wind profiles, soil moisture and latent heat (Betts 2005). The loss of forest cover also has a particularly large impact on runoff, as shown by Wei *et al*. (2018).

Another important impact of LUC is increased emissions and release of aerosols. Fire can be used as a quick method of land-clearance, leading to increased air pollution, greenhouse gas emissions, and release of particulate matter into the atmosphere either directly, or indirectly from escaped fire. For example Cano-Crespo *et al*. (2015) showed that up to 52% of burnt forest area in the vicinity of pasture lands in Amazonia is a result of escaped management fire. Globally, carbon emissions from fire amounts to approximately 2.8 ± 0.4 PgC yr^{-1}, largely from the tropics, which offsets the global terrestrial carbon sink resulting in a net carbon balance for global forests of 1.1 ± 0.8 Petagrams of Carbon per year (PgC yr^{-1}) (Ciais *et al.*, 2013). This could also lead to a positive feedback cycle, where hotter, drier conditions increase the risk of fire spread. For Amazonia for example, (Zhang *et al*. 2009) suggest that biomass-burning aerosols negatively impact the seasonal monsoon circulation transition leading to a reduction in dry season rainfall for southern Amazonia.

The change in land surface properties leads to alteration of the surface albedo, and the release of aerosols can lead to changes in cloud albedo, which results in

changes in the radiative energy balance. These impacts can oppose other biogeochemical effects, introducing further complexity. For example the release of greenhouse gases and decreases in evapotranspiration both create a warming effect and hence act as positive feedbacks, but increased albedo from aerosols and reduction in forest cover on average induces a cooling trend. However this can be regionally dependent, where some satellite observations suggest that the effect of conversion of the Brazilian savannas (cerrado) to pasture was to induce a local warming (Settele *et al*., 2014).

Accurately representing disturbance also requires adequate representation of the vegetation recovery time. Both of these processes are important for producing accurate simulations of present day vegetation, which can then be used for better predictions of changes in future vegetation cover.

There are a number of data products available today which represent various aspects of LUC. Ultimately many of these could be used together to produce a blended product that would be useful for an improved observational product that could be used with models, driving improvements in land-use changes. An overview of available products is provided in section 1.3.2.

In this study I aim to evaluate the impacts of land-use change globally and over Brazil, to understand the impact on the terrestrial carbon sink across a range of models. I review four future RCP scenarios and analyse the implications for future land-use in Brazil. This will underpin further research later in the thesis where the impacts of future fire and land-use change are assessed, as presented in Chapter 5.

2.3 Representation of land-use in models

Land-use in JULES

JULES (the Joint UK Land Environment Simulator) is a DGVM which represents the land component of the UK Hadley Centre family of models and is used to predict the response of vegetation to climate change. It was developed from the Met Office Surface Exchange Scheme (MOSES), and is based on a modular structure which gives various science options when running (Best *et al*., 2011). It uses 5 PFTs as standard, but extra PFTs up to 9 (with more in development) are available if required (Harper *et al*., 2016). The 5 PFT set up uses broadleaf trees,

needleleaf trees, C3 grass, C4 grass and shrub. Additional PFTs comprise tropical and temperate broadleaf evergreen trees, broadleaf deciduous trees, needleleaf evergreen and deciduous trees, C3 and C4 grasses, and evergreen and deciduous shrubs. JULES represents the land surface component within the new state of the art Earth System Model UKESM1 (Kuhlbrodt *et al*., 2018; see also ukesm.ac.uk[22]), developed jointly at the Met Office with Leeds University.

The land surface model JULES can represent changes in vegetation cover arising from both natural responses to changing climatic conditions and from direct human impact via land-use. In the current version of the model, there are two options for this. Firstly, land cover can be prescribed through an input data file, where all PFTs are prescribed either as static, or time varying for the length of the run. Alternatively, natural vegetation can be simulated via the dynamic vegetation scheme TRIFFID (Cox, 2001), and human land-use imposed on this by being prescribed through a data file as 'Disturbed Vegetation Fraction', representing both crop and pasture land as agriculture. This gives TRIFFID the boundary conditions of land-use from which woody PFTs are excluded, allowing just C3 and C4 grasses to grow in these agricultural areas, according to the climatic conditions. This Disturbed Vegetation Fraction input file can again either be static or time-varying. These data files for land cover / land-use can be created from a number of sources, for example from the HYDE dataset.

The total carbon flux for each grid box is made up of local litterfall, large-scale disturbance, and land-use, as represented by the following equation:

$$\Lambda_c = \sum_i V_i = \left(\Lambda_{li} + \gamma_{vi} C_{vi} + \Pi_i \sum_j C_{ij} V_j \right)$$

Where Λ is the total carbon lost from vegetation, $C_{ij}$are the competition coefficients, $\gamma_{vi}$is a large scale disturbance, Π is the NPP per unit of vegetation area, and V is the fractional coverage of PFT i after competition (Clark *et al*., 2011).

Carbon is lost from the vegetation carbon pools through the process of land-use change, with the amount determined by the prescribed land-use change data,

[22] UKESM: https://ukesm.ac.uk/

and transferred into product pools to represent the capture of carbon in wood products. There are three product pools that act on different timescales: a fast product pool for products that may be broken down quickly such as paper, with a turnover rate of 1 year; a medium pool that releases carbon more slowly over 10 years; and a slow product pool for products such as furniture where carbon may be locked away for many years, with a turnover rate of 100 years. Eventually these pools are broken down and release carbon back to the atmosphere.

In this version of JULES, fire is not represented as a separate process of disturbance, and its impact on the carbon cycle is subsumed within a large scale disturbance term.

TRENDY project

The Global Carbon Project (GCP) (Le Quéré, 2016) is a global, cross-organisational partnership that aims to establish a robust knowledge base about how the carbon cycle may be responding to climate change. The project focuses on both biophysical and human dimensions, carbon management and policy, variability in the carbon sink, and interactions and feedbacks in the Earth system. One of the most important aspects of this project is to establish an annual global carbon budget. One consortium sponsored by the GCP is TRENDY, which is a terrestrial carbon cycle model intercomparison project aiming to quantify the response of ecosystems to increasing atmospheric concentration of carbon dioxide, changes to the climate, and anthropogenic changes to the land surface (Sitch *et al.*, 2015). Many terrestrial carbon cycle groups contribute to this effort, submitting modelled simulations of the carbon balance of the terrestrial biosphere from pre-industrial to present day in order to compare land surface model results.

TRENDY is typically run annually with a set of 9-14 DGVMs in order to investigate trends in land-atmosphere model simulations. Climate forcing is based on the Climate Research Unit (CRU) observed monthly 0.5 degree climatology and the National Centre for Environmental Prediction (NCEP) reanalysis. Global atmospheric CO_2 is from ice core records. Land-use change is achieved through the implementation of the Hurtt LUC dataset for observed evolving cropland and grazing (crop + pasture) from HYDE.

Table 2.1 below gives a summary of a selection of these models (Ahlström *et al*., 2015; Le Quéré *et al*., 2018).

Table 2.1: Summary of TRENDY models

DGVM	Disturbance types
CABLE	Wood harvest, shifting cultivation
CLASS-CTEM	Tillage, fire
DLEM	Wood harvest, crop harvest, fire
ISAM	Wood harvest, crop harvest, grazing/mowing
JULES	-
LPJ	Crop harvest, grazing/mowing, fire
LPX-Bern	Crop harvest, fire
O-CN	Wood harvest, crop harvest
ORCHIDEE	Wood harvest, crop harvest, tillage
VEGAS	Fire
VISIT	Fire

However while some of these models simulate fire, none represent fire as a management tool.

TRENDY uses three scenarios: S0 = no forcing, S1 = CO_2 only, S2 = CO_2 plus climate (static land-use at 1860), S3 = CO_2, climate and land-use change. Here I focus on two simulations, S2 and S3 to show the impact of land-use change in the models. The results are presented as global means, and for the region of Brazil, for the period 1860-2015. First I focus on output from the JULES model. JULES is run here with TRIFFID dynamic vegetation.

2.4 Analysis and results

TRENDY: JULES results

Figure 2.1 below shows the disturbance as a result of land-use change over time, globally and over Brazil. In the global run, we can see there is a rapid increase in agricultural area from 1866-1966, after which the rate of change slows. Comparatively we can see that the land-use change continues to increase throughout the entire timeseries for Brazil. We can see the impact of this as we look at other variables in the model.

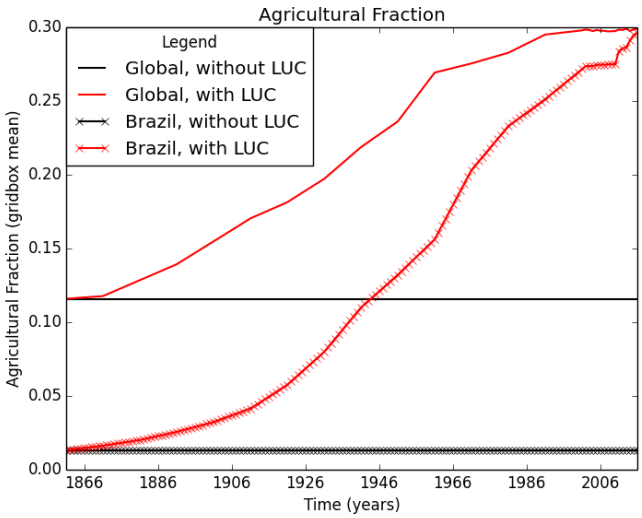

Figure 2.1: Agricultural / crop fraction change over time
Gridbox mean agricultural fraction time series 1860-2015 from JULES, with (red) and without (black) land-use change globally (solid line) and over Brazil (crosses)

From the model simulations, I assess how carbon distribution changes between the product pools over time (Figure 2.2). Here we can see that the fast product pool remains relatively stable over time in both the global and regional runs, whereas the medium product pool increases rapidly from 1866 to a peak around 1966, then declines as the slow product pool starts to increase gradually. Here the overall regional trend is not dissimilar to the global trend, except at the start of the run where the medium pool takes up carbon much faster in the global run than the regional run, reaching a first peak around 1900 whereas this comes much later in 1930 over Brazil. Note also the different scales, with Brazil an order of magnitude higher than the global mean (per square meter). These results suggest that most of the carbon from land-use change (Figure 2.1) ends up in the medium product pools, and more recently in the slow product pools.

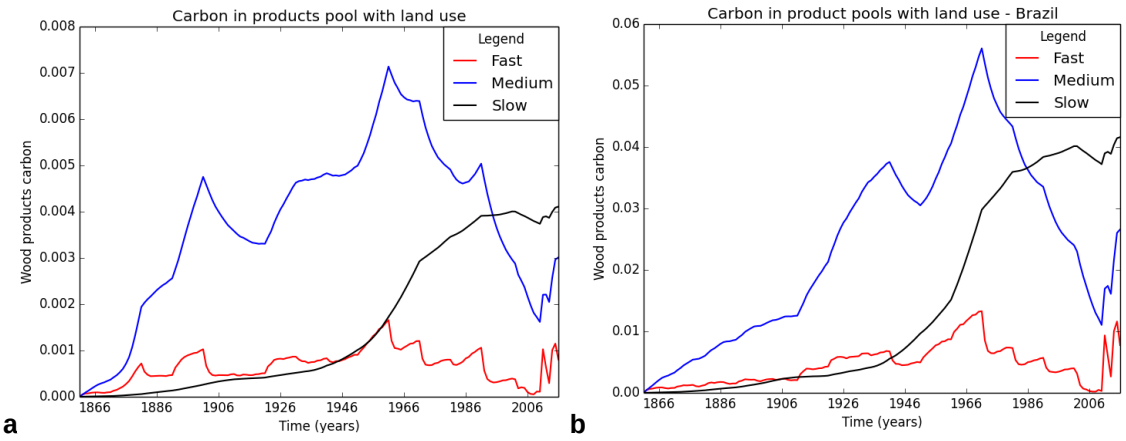

Figure 2.2: Carbon changes in the three product pools over time
Time series of carbon from wood product pools (kgC/m^2) 1860-2015 from JULES as a product of changes in land-use (S3). Panel (a) shows global mean, panel (b) shows mean over Brazil

Figure 2.3 shows how total vegetation carbon changes with and without land-use change. Here we can see that globally with LUC, vegetation carbon decreases to a minimum around 1966, and then starts to recover. Without LUC, vegetation carbon increases throughout the run. Over Brazil however, there is a continual decrease in vegetation carbon, reflecting the continuous trend of LUC shown in Figure 2.1. in terms of mean carbon per square meter, this has a more significant impact on vegetation carbon in Brazil compared to the global trend.

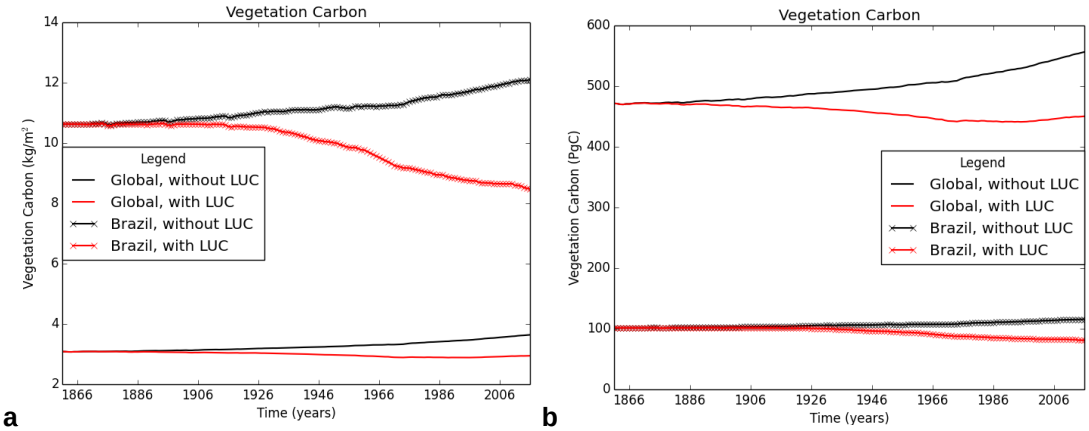

Figure 2.3: Time series of vegetation carbon
Time series of vegetation carbon 1860-2015 from JULES, with (red) and without (black) land-use change, globally (solid lines) and over Brazil (crosses). Panel (a) shows mean change (kgC/m^2), panel (b) shows total carbon (PgC).

Figure 2.4 shows the mean change in soil carbon over time. Here we can see that proportionally the global change with land-use is not large compared to no

land-use, however there is a substantial increase in soil carbon over Brazil with land-use (top panel). The difference in total carbon at present day is approximately 12PgC over Brazil and approximately 20PgC globally.

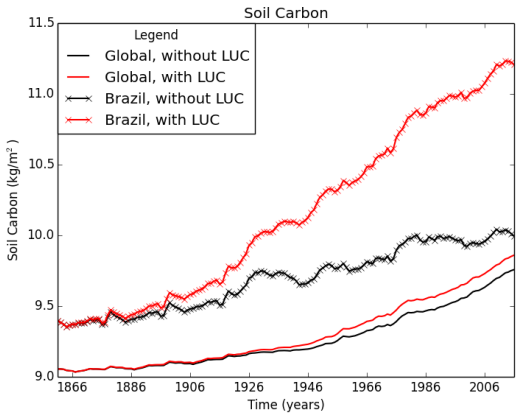

a

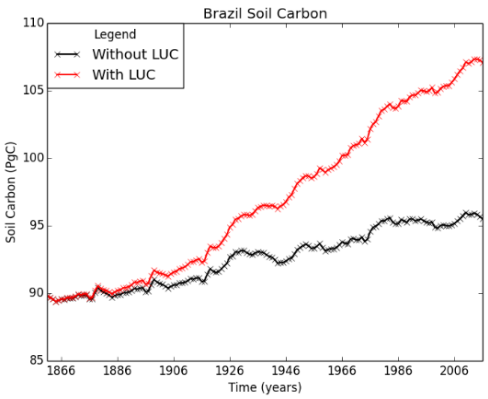

b

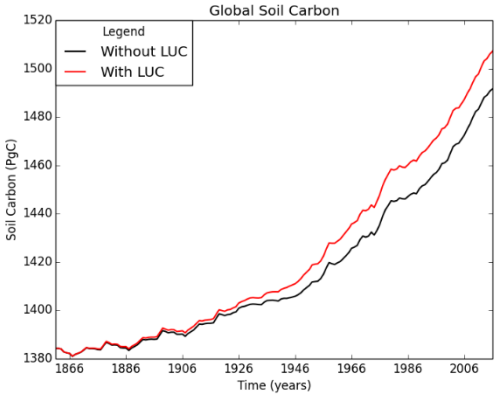

c

Figure 2.4: Time series of soil carbon
Time series of soil carbon 1860-2015 from JULES, with (red) and without (black) land-use change, globally (solid lines) and over Brazil (crosses). Panel a shows mean change (kgC/m^2), bottom panels show total carbon (PgC) for Brazil (b) and globally (c)

Figure 2.5 and Figure 2.6 show similar trends of productivity. Both GPP and NPP are proportionally much higher in Brazil than the global mean, and again LUC has more of an impact on the mean (totals also shown for context).

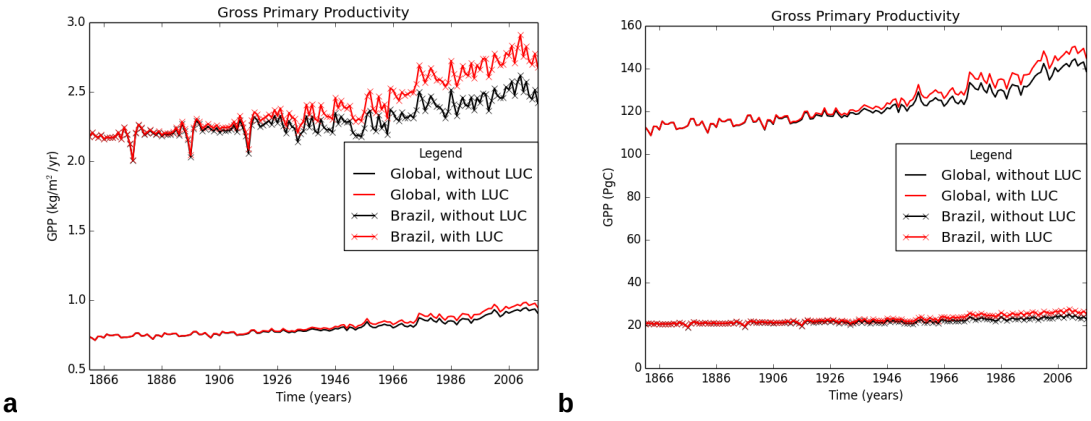

Figure 2.5: Time series of Gross Primary Productivity (GPP)
Time series of GPP 1860-2015 from JULES, with (red) and without (black) land-use change, globally (solid lines) and over Brazil (crosses). Panel (a) shows mean change (kg/m^2/yr), panel (b) shows total carbon (PgC)

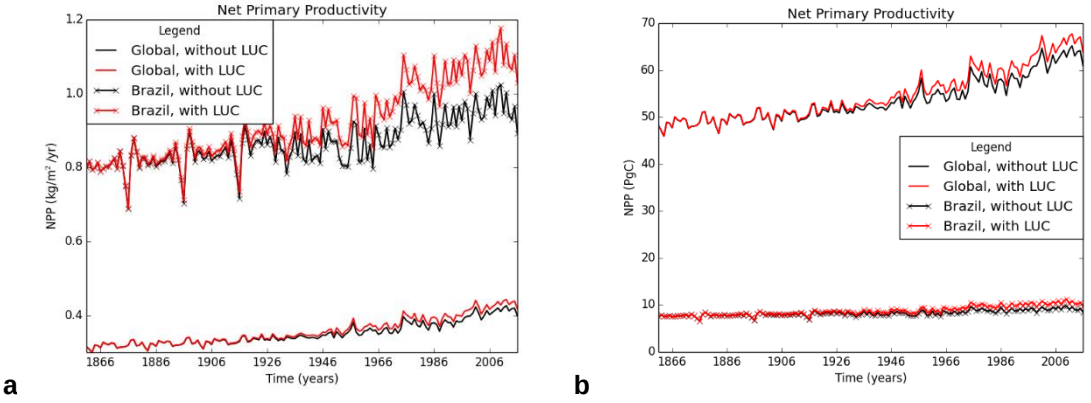

Figure 2.6: Time series of Net Primary Productivity (NPP)
Time series of NPP 1860-2015 from JULES, with (red) and without (black) land-use change, globally (solid lines) and over Brazil (crosses). Panel (a) shows mean change (kg/m^2/yr), panel (b) shows total carbon (PgC)

According to IPCC definitions[23], the Gross Primary Productivity (GPP) refers to the total amount of carbon fixed in the process of photosynthesis by plants. The NPP refers to the net production of organic matter which is equal to GPP minus autotrophic (plant) respiration. Net Ecosystem Production (NEP) is the net accumulation of carbon by an ecosystem, which is equal to NPP minus heterotrophic (soil) respiration. The Net Biome Production (NBP) is the net production of organic matter per biome, which is calculated as NEP minus carbon loss (NPP minus soil respiration and the total of the loss of carbon from the wood product pools).

[23] IPCC LUC: http://www.ipcc.ch/ipccreports/sres/land_use/index.php?idp=24

We can assess the NBP (Figure 2.7 and Table 2.2) to show how much carbon is accumulated in a system, after accounting for loss from harvesting and respiration. We can see that there is an overall increase in NBP globally and that this is larger without land-use change, whereas there is a net decrease in NBP over Brazil and this is larger with land-use change.

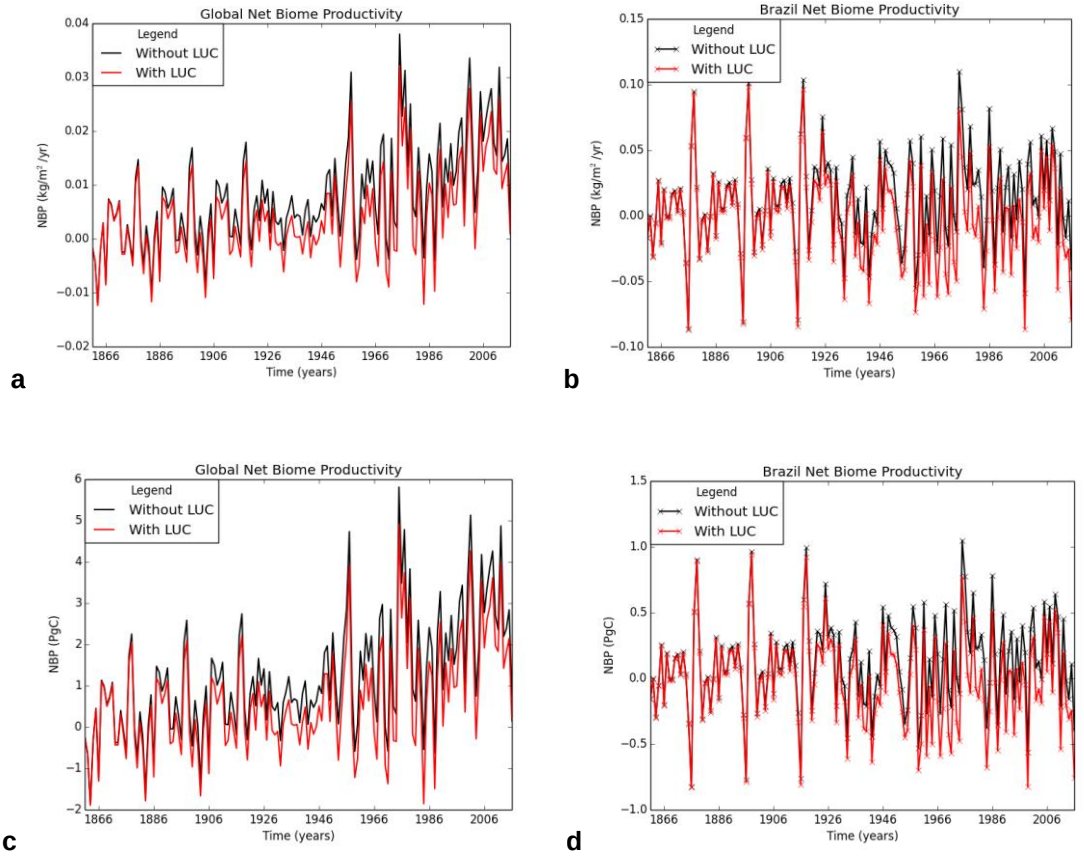

Figure 2.7: Time series of Net Biome Production (NBP)
Time series of NBP 1860-2015 from JULES, with (red) and without (black) land-use change, globally (left column) and over Brazil (right column). Top row shows mean NBP (kgC/m^2), bottom row shows total NBP (PgC).

Table 2.2: Summary of results for NBP, with and without land-use change from JULES

PgC	**Without land-use change**		**With land-use change**	
	Global	**Brazil**	**Global**	**Brazil**
Total 2016	0.76	-0.39	0.14	-0.76
Change 1861 to 2016	0.92	-0.23	0.30	-0.60

From Figure 2.8 below we can see more detail of how LUC affects different vegetation types over time. For broadleaf and needleleaf trees, with land-use changes over time we see a gradual decline in tree cover fraction. As this occurs,

we see a corresponding increase in C4 grasses. We also see a more substantial decrease in shrub cover with LUC, and a large increase in C3 grasses. We know that the growth of C3 and C4 grasses represents the increase in crops and pasture lands, and this analysis now gives more insight into the distribution across the different PFTs with the addition of land-use.

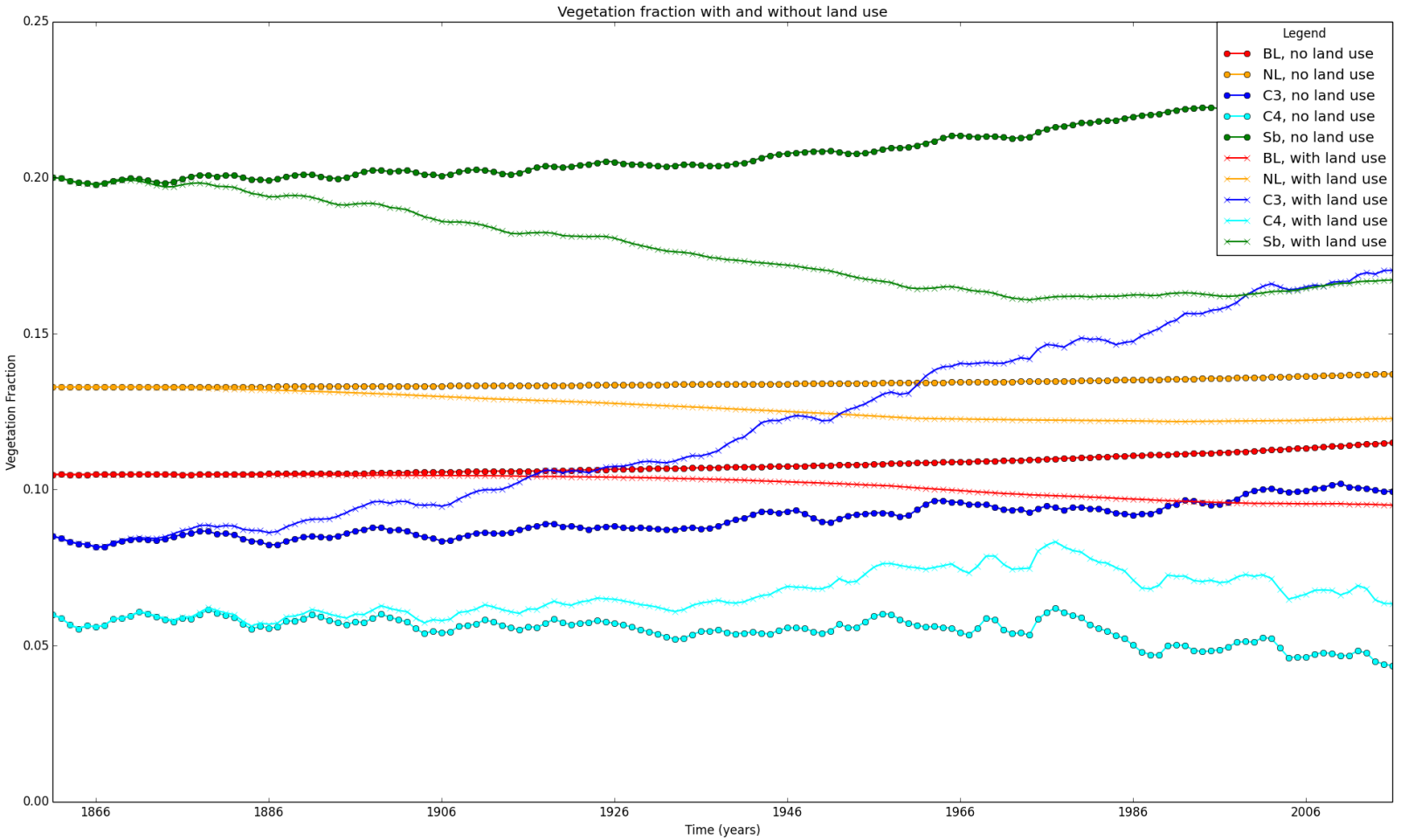

Figure 2.8: Global mean change in fraction of Plant Functional Type (PFT) over time.
BL = broadleaf (red), NL = needleleaf (yellow), C3 = C3 grasses (dark blue), C4 = C4 grasses (light blue), Sb = shrubs (green). Dotted lines represent vegetation fraction without land-use change from JULES

TRENDY: Multi-model analysis

I perform a multi-model review of the carbon contribution from land-use across the TRENDY models, as context for the JULES output. Here I use Brazil as a case study, using five ecosystem regions: Atlantic Forest, Amazon forest, Pantanal wetland, Cerrado and Caatinga.

Not all of the models in TRENDY have available land-use data, so here I use results from 6 models: CABLE, DLEM, ISAM, LPJ-GUESS, VEGAS, and JULES. Table 2.3 below shows the impact of LUC on the carbon balance of each ecosystem over the historical period (1860-2015), calculated as S3 - S2, where negative results show land-use emission (mean rate of carbon loss due to LUC, in PgC/yr).

Table 2.3: Carbon flux for each TRENDY model from LUC (PgC/yr), 1860-2015

	Atlantic Forest	Amazon	Pantanal	Caatinga	Cerrado
CABLE	-2.44168	-3.6511	-0.40663	-0.32488	-9.27507
DLEM	-5.29373	-2.02379	-0.12549	-0.18984	-4.26964
ISAM	-6.21358	-8.1601	-0.1018	-0.31383	-3.58486
LPJ_GUESS	-7.67722	-4.1563	-0.84143	-0.11815	-14.3983
VEGAS	-3.19863	1.75657	0.04636	-0.08492	-1.70009
JULES	-4.91821	-3.21025	-0.9709	-0.04072	-11.6607

Figure 2.9 below shows the uncertainty range across the models. The largest potential source of emissions as a result of LUC is in the Cerrado region, which also shows the largest uncertainty range across the models. The large uncertainty in carbon-climate feedbacks across the models is likely to be associated with the different sensitivities of simulated terrestrial carbon cycle

processes to changes in the climate and CO_2, as well as different approaches to simulating processes such as nutrient limitation, land-use and recovery. A potential factor here could also be the inclusion of fire in the models. Fire is not accounted for as a separate process in JULES for example, which has one of the highest rates of emissions from land-use change. Fire is included in the VEGAS model (Table 2.1), which has the lowest rate of land-use emissions from this area (Table 2.3). The Cerrado is a high fire danger region due to the hot, dry climatic conditions, so we could expect to see a contribution to emissions from fire rather than land-use in those models that include this as a separate process.

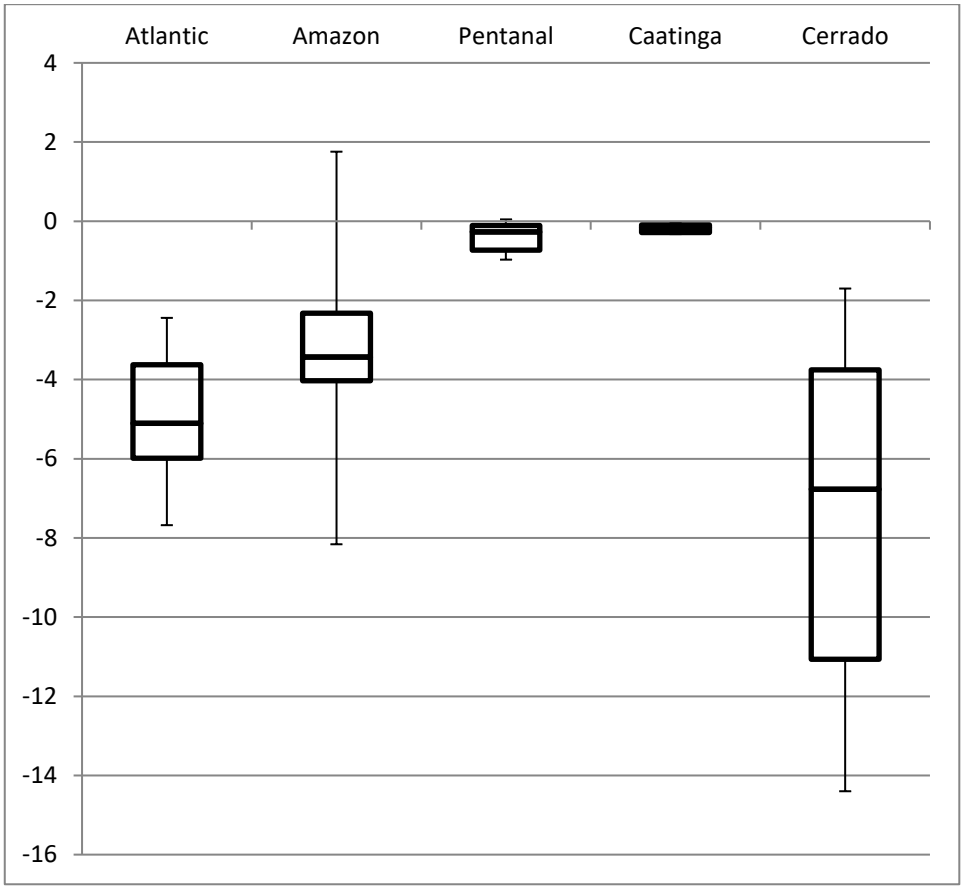

Figure 2.9: Uncertainty range of carbon loss due to land-use change in TRENDY models Carbon loss (PgC/yr),1860-2015

Considering JULES as an example of a model showing high emissions from the Cerrado, we can see that this region had high pre-industrial vegetation carbon and together with large changes in land use (Table 2.4), this results in high carbon flux values attributed to land-use change (Table 2.3).

Table 2.4: Change in agricultural fraction and vegetation carbon for JULES

Agricultural fraction (gridbox fraction)					
	Atlantic Forest	**Amazon**	**Pantanal**	**Caatinga**	**Cerrado**
1860	0.031613	0.000679	0.020501	0.02305	0.026535
2015	0.548756	0.089445	0.711089	0.548756	0.543046
Change	0.517143	0.088766	0.690588	0.525705	0.516511
Mean vegetation carbon, S3 (kg/m2)					
	Atlantic Forest	**Amazon**	**Pantanal**	**Caatinga**	**Cerrado**
1860	12.40017	12.77756	10.20659	0.580391	11.67313
2015	5.465484	13.45711	0.580391	0.612066	5.857612
Change	-6.93469	0.679555	-9.6262	0.031675	-5.81552
Total vegetation carbon, S3 (PgC)					
	Atlantic Forest	**Amazon**	**Pantanal**	**Caatinga**	**Cerrado**
1860	17.00827	59.97019	2.227475	0.498201	29.70806
2015	7.496542	63.15961	0.984663	0.525391	14.9076
Change	-9.51173	3.189424	-1.24281	0.027189	-14.8005

2.5 Future projections of land-use change in Brazil

When modelling future climate, an essential factor to evaluate is the level of GHGs we are likely to see in the future, in order to understand how the climate may change and what impact this will have on temperature and other factors. The levels of future emissions are highly uncertain, with many different variables that could change and interact in numerous complex ways, including policy options, technology, population levels, and land-use changes. The IPCC therefore introduced a number of emission scenarios that represent plausible pathways of how GHG concentrations may change over time (see Appendix 2).

RCP scenarios describe future releases of GHGs, aerosols, and other pollutants into the atmosphere and, along with information on LUC, provide inputs to climate models. They are based on assumptions about driving forces such as patterns of economic and population growth and technology development. They assist in climate change analysis, including climate modelling and the assessment of impacts, adaptation, and mitigation. There are large uncertainties around the future scenarios of LUC in the Amazon however (Aguiar *et al*., 2016), and multiple different estimates exist.

For IPCC AR5, four main future RCP scenarios were used from high mitigation (RCP 2.6), to business-as-usual with high emissions and no mitigation (RCP 8.5). These were based on previous IPCC SRES scenarios, but included the possibility of mitigation. Broad global assumptions around LUC are made within the scenarios, as outlined in detail in Appendix 2. Here I present a review of LUC over Brazil using these RCPs.

As outlined in Chapter 1, LUC has affected 1.4 million km², around 20% of the Amazon basin (Castello and Macedo, 2016). The peak of deforestation in 2004 was approximately 28,000 km²/yr (AMAZALERT-D4.2) resulting from cattle ranching (Nepstad, 2006) and soybean production (Settele *et al*., 2014). Palm oil is one of the main biofuel crops, and while its current use is still relatively small, Brazil has the largest potential for expansion in South America as around half of the Amazon is suitable for its cultivation (Butler and Laurance, 2009).

Using the RCP scenarios as an example of potential future pathways of land-use, LUC is not projected to increase directly in line with emissions in the future but reflects more complex assumptions (see Appendix 2). In RCP 2.6 and 8.5 LUC continues to increase to 2100 resulting from increasing use of croplands to feed a rapidly expanding population in RCP 8.5, and an increase in the use of biofuels in the high-mitigation scenario, RCP 2.6. Conversely, LUC is projected to decline in RCP 6.0 and 4.5, based on the assumption that there will be a decreasing use of grasslands (and croplands in RCP 4.5) due to dietary changes, and reforestation resulting from climate mitigation policies (Settele et al., 2014; see Appendix 2).

Here I use the output from Met Office Earth System Model HadGEM2-ES to understand how land-use has changed up to present day, and to see how assumptions made in RCP scenarios affect projections of LUC into the future. This will provide a basis for comparison with LUC scenarios when implemented in JULES.

The datasets are based on the Hurtt *et al*. (2011) harmonized datasets that were used in CMIP5 and IPCC AR5, which capture land-use transitions between cropland, pasture, primary land and secondary (recovering) land, including the effects of wood harvest and shifting cultivation, as well as transitions from/to

urban land. The dataset estimates fractional land-use patterns annually for 1500-2100, spatially gridded at 0.5° x 0.5° resolution. It should be noted that in the original Hurtt dataset, and most other CMIP5 models, the areas of crop and pasture land are treated separately and vary over time. However, in HadGEM2-ES they are added together and referred to as the 'Disturbed Fraction of Vegetation' (DFV). In other words, HadGEM2-ES assumes that any loss in trees or shrub equates to crop and pasture growth, and treats them together as 'grasses'. This may potentially mask important variation, as not all pasture is necessarily grass and may still include trees or shrubs, which could over-emphasize deforestation (Andrews *et al*., 2017).

In order to examine how LUC in Brazil varies over time based on RCPs, I analyse the DVF from HadGEM2-ES data. The graphs in Figure 2.10 show the historical trend of land-use globally and over Brazil, and I use the four RCPs to project how this may change over the rest of this century to 2100.

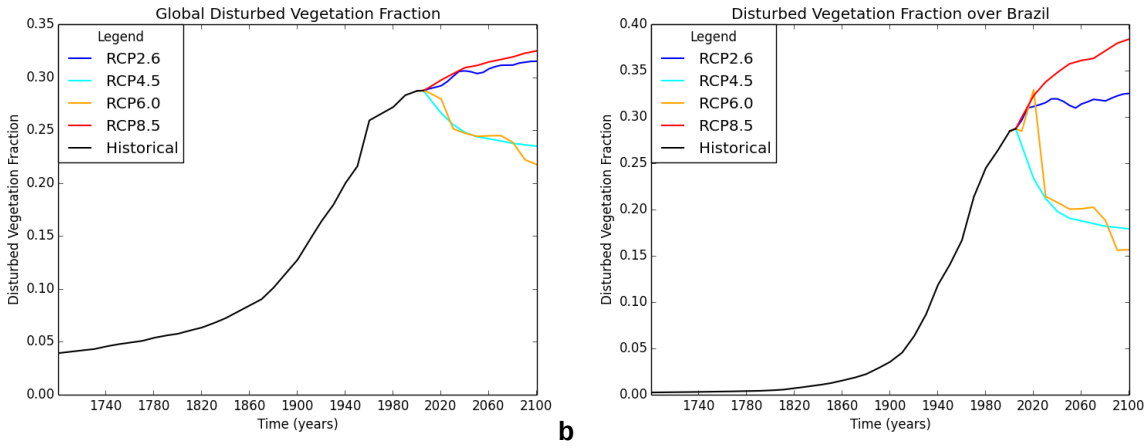

Figure 2.10: Disturbed vegetation fraction by RCP scenarios
Globally (a) and for Brazil (b), from HadGEM2-ES. Note different scales on Y axis.

The historical simulations show a trend of increasing disturbance, in line with a move from primary forest land to agriculture both globally and in Brazil. In Brazil there is little disturbance up until 1920, where there is a sharp increase in deforestation. For the future projections, we can see a marked divide between RCP scenarios, where in RCP 2.6 and 8.5 LUC increases to 2100, but declines in RCP 6.0 and 4.5. This reflects the assumptions made in the RCP scenarios (see Appendix 2), of increasing use of croplands for agriculture to feed a rapidly expanding population in RCP 8.5, and an increasing conversion to crops for the

use of biofuels in the high-mitigation scenario, RCP 2.6. In the two intermediate emission scenarios we see decreasing use of grasslands (and croplands in RCP 4.5) due to dietary changes and reforestation.

To see how this change in DVF varies geographically, Figure 2.11 shows the global DVF at 1860, 2005 and 2100 for the four RCP scenarios, and Figure 2.12 centres on Brazil to show this in more detail.

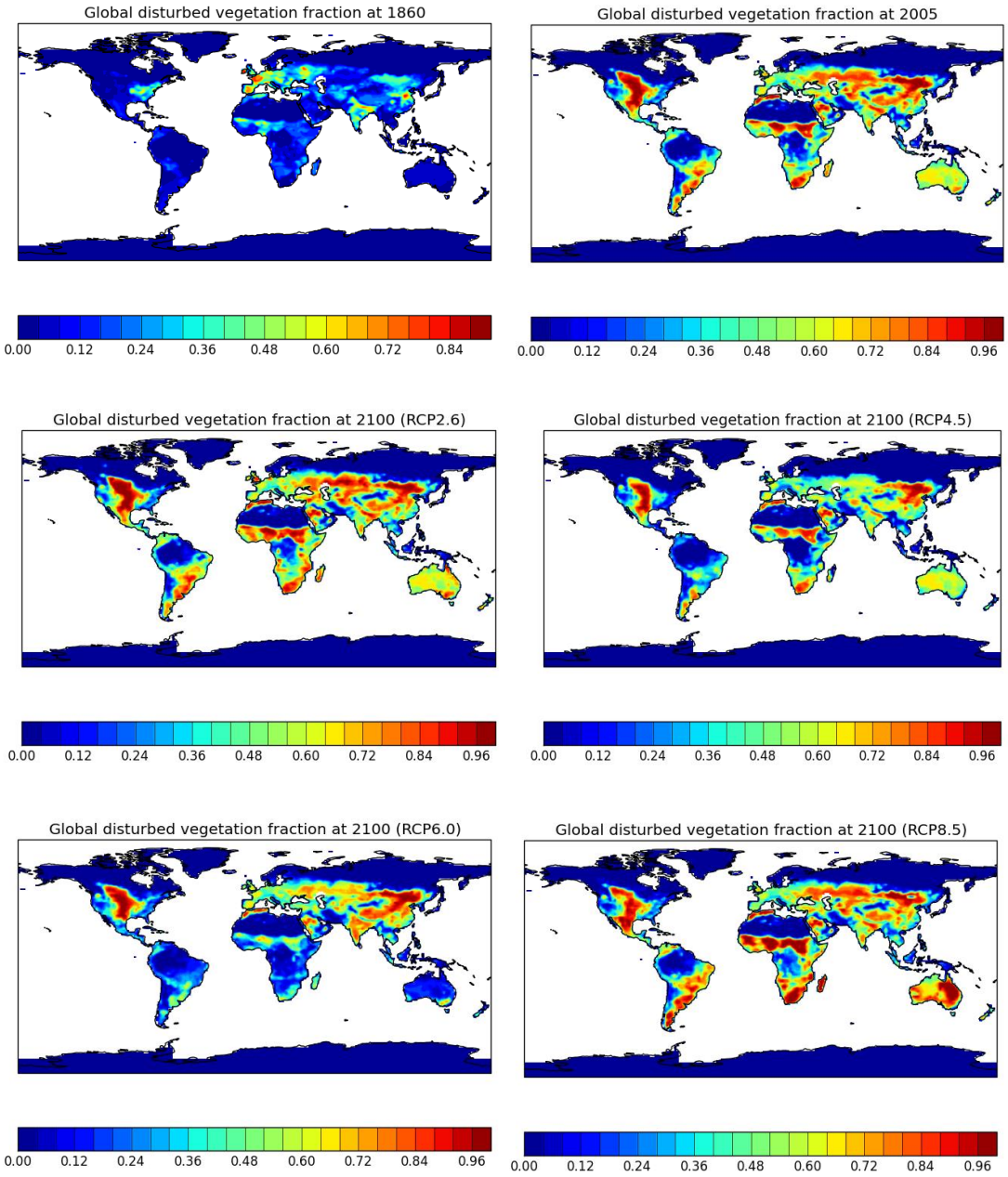

Figure 2.11: Global disturbed vegetation fraction
From HadGEM2-ES for 1860, 2005, 2100 and four RCP scenarios

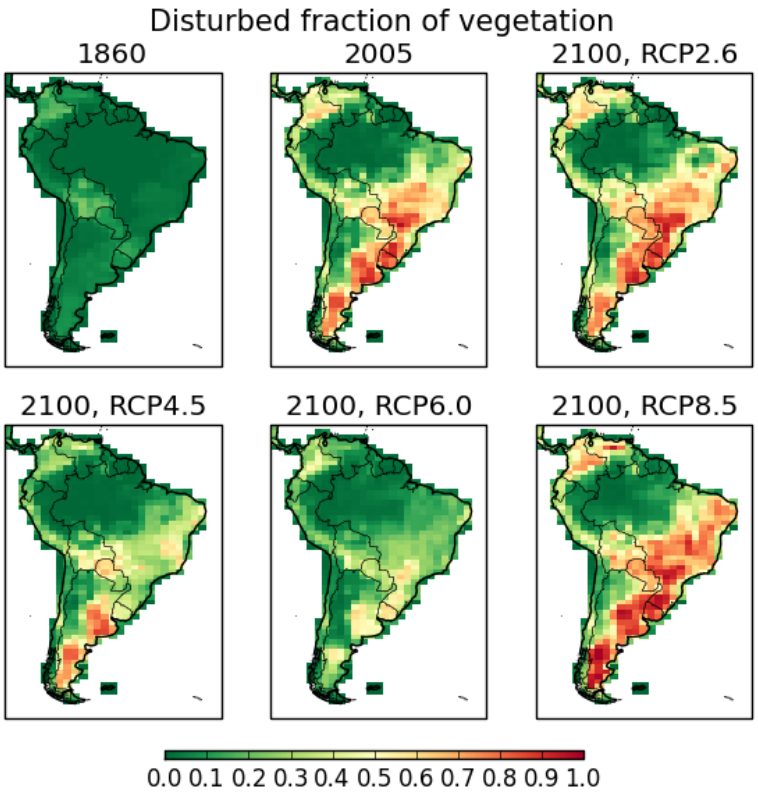

Figure 2.12: Disturbed vegetation fraction for Brazil
From HadGEM2-ES for 1860, 2005 and 2100 for four RCP scenarios

It is interesting to note that the Amazon forest remains mostly in tact in the future projections, with most of the DVF located in the South of Brazil in the Cerrado region, Atlantic forest, and into Paraguay, Uruguay and Argentina. However there is some degradation evident in the Eastern Amazon in scenarios RCP2.6 and RCP8.5 (Marengo *et al*., 2018). In these scenarios therefore LUC doesn't appear to be a major driver of forest loss in the future, however fire is not included in this and may be an important factor in determining future vegetation patterns.

2.6 Conclusion

The land and ocean absorb around half of the anthropogenic emissions of CO_2 every year, creating long term carbon sinks which are regulated through climate change and variability. We know that climate change is driven by anthropogenic activity, both directly through emissions but also through additional feedback on these carbon sources and sinks (Piao *et al*., 2013). Land-use change is an important element in this. Sitch *et al*. (2015) for example used a number of the TRENDY models to review the trends in regional sources and sinks, and concluded that the trend of increasing carbon uptake is driven by increasing NPP

primarily in the tropics. However that study did not include LUC, and recommended that further work should be undertaken to understand what impact LUC has on the carbon fluxes globally and regionally through time, as this is likely to have a significant impact on the results.

Here I have focused on metrics of terrestrial carbon fluxes over the Brazil region compared to global means in order to understand how this large store of carbon has changed over the historical period with land-use change. The results have shown that the land is increasingly being converted from forest to agricultural land, at a faster rate than the global average. This has led to a substantial decrease in vegetation carbon (Figure 2.3). It is here that we see the importance of land-use change in model simulations leading to a change in the sign of carbon uptake, where vegetation carbon is simulated to increase over the historical period without land-use change, but when LUC is added in vegetation carbon decreases. This also leads to increased soil carbon. GPP and NPP also increase with land-use change, but when we analyse the overall carbon uptake including carbon losses through respiration and disturbance (NBP), we see that the overall trend for Brazil is a slight decrease, which is larger with LUC. This seems to support the conclusion of (Cox *et al*., 2000) that the disturbances in this region are offsetting the positive effects of CO_2 fertilisation.

I have also shown the contributions to the carbon sink from different eco-regions in Brazil across the TRENDY models. This has offered an insight into the large uncertainties that still exist in the terrestrial biosphere across models, and has highlighted the Cerrado as a potentially important source of carbon. The Amazon biome still offers a potentially large carbon sink, but this also has the potential to become a source in adverse conditions such as during El Niño years (Cox *et al*., 2000).

The analysis of future land-use scenarios over Brazil show that there may be continued decreases in the carbon sink in this region as a result of climate and land-use change, especially in the high emission and high mitigation scenarios. This will underpin further work later in this thesis assessing the impact of future land-use and fire on the land surface in Chapter 5.

Chapter 3: Interactive INFERNO: fire-vegetation interactions in JULES

3.1 Background, motivation and initial testing

As presented in Chapter 1, it has been well-documented that many models are still in the relatively early stages in dealing with land-use, LUC and forestry, and in particular, disturbances from fire, drought, and tree mortality are often not well characterised and treated crudely as constant disturbances (Nepstad *et al*. 2008; Costa and Pires 2010; Pan *et al*. 2011; Hirota *et al*. 2011; Coe *et al*. 2013; Brando *et al*. 2014; Ciais *et al*., 2013; Betts *et al*. 2015), or are not represented at all (Ciais *et al*., 2013; Flato *et al*., 2013; Collins *et al*., 2013). ESMs also do not account for alternative stable states such as tropical forest or savanna yet (Ciais *et al*., 2013), which is a possible outcome of change in the Amazon. This means there is low confidence in many of the future projections of land carbon storage.

The aim of this research is therefore to develop the current status of fire modelling in order to improve the representation of vegetation and its disturbance, and create more robust projections of future changes.

Here I advance the current fire modelling capability in JULES, by developing the diagnostic fire parameterisation model INFERNO as presented in Mangeon *et al*. (2016) into a coupled fire-vegetation model. This has been achieved by introducing a new disturbance term within JULES for mortality due solely to fire, resulting in vegetation mortality and incorporating the resultant release of carbon into the atmosphere and soil.

The processes I have focused on developing here are the biogeophysical processes of vegetation cover, mortality and burnt area. I have therefore chosen to complete initial model development work in the JULES land surface model to test the interactions of fire and vegetation in a terrestrial capacity. This is the first necessary step before developing these processes into a fully coupled climate and Earth system model. I first undertake initial testing of the capability for coupling by simulating burnt area in a diagnostic form and comparing to present day vegetation cover. I then develop a basic coupling method by prescribing burnt area and assessing the impact on vegetation, before undertaking full modification

of the JULES model to include fire disturbance. I describe the coupling methods and represent this in the form of new equations for the JULES vegetation dynamics, and describe the tuning process undertaken as part of the coupling including tuning disturbance, burnt area by vegetation type, and dynamics relating to vegetation spreading. I then evaluate the simulation of present day vegetation with fire and land-use disturbance. I finish by exploring the implications of the new modelling capability for the focus region of Brazil.

3.1.1 Initial simulations using INFERNO

In its current form, INFERNO is a diagnostic fire model available in an offline land surface model. This means that the burnt area is calculated based on which areas of the land surface would burn given certain meteorological conditions, and given enough fuel and ignitions, but that the resultant area of fire occurrence does not affect the vegetation, atmosphere, climate or any other aspects of the Earth system. A diagnostic output of burnt area and emissions are provided by INFERNO, but this does not currently alter the vegetation cover. This is a necessary and important process to be able to represent in a land surface model for a number of reasons. One of the most important aspects of the land surface is the vegetation and soil cover, which affects the albedo, evapotranspiration, carbon stores, and circularly also affects subsequent fires through available fuel. In a fully interactive model these processes, together with fire emissions, would also affect the temperature, humidity, aerosols and organic matter, and radiative forcing. Furthermore, without a loss of fuel through fire occurrence, change in burnt area over time cannot be accurately represented. This makes the development of fire-vegetation coupling a top priority for JULES.

Before undertaking model development within JULES, it is important to first assess the potential impact of coupling fire to vegetation, by reviewing the current simulation of vegetation and diagnostic of burnt area from INFERNO. Here I use the TRENDY (Sitch *et al*. 2015) project scenarios to review the present day vegetation fractions simulated by JULES (Table 3.1), focusing on the S2 (no land-use change) scenario (Figure 3.1) and S3 (with land-use change) scenario (Figure 3.2). The primary changes to vegetation as a result of land-use change are a decrease of broadleaf vegetation in South America (Figure 3.3), a reduction

in shrub cover (except in the boreal region), and an increase in C3 - and to a lesser extent C4 -grasses.

Table 3.1: TRENDY experiments

TRENDY experiment	Forcings
S0	Constant pre-industrial (1860)
S1	CO_2
S2	CO_2, Climate
S3	CO_2, Climate, land-use change

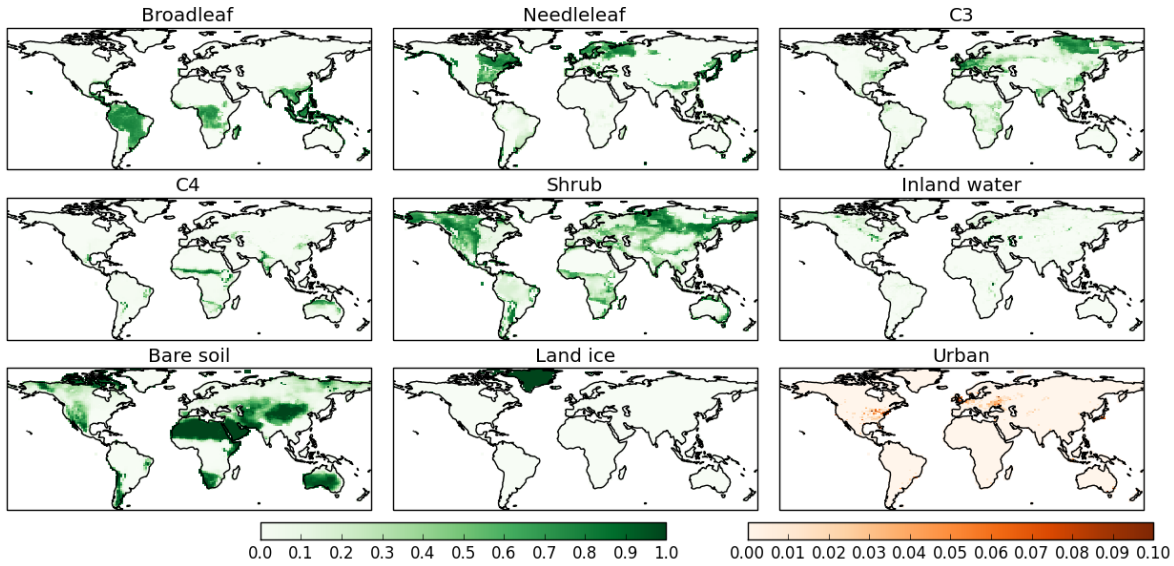

Figure 3.1: S2 land cover from JULES
2016 Fraction of land cover for 10 land cover types, S2 without land-use change, as modelled by JULES for the TRENDY 2017 project

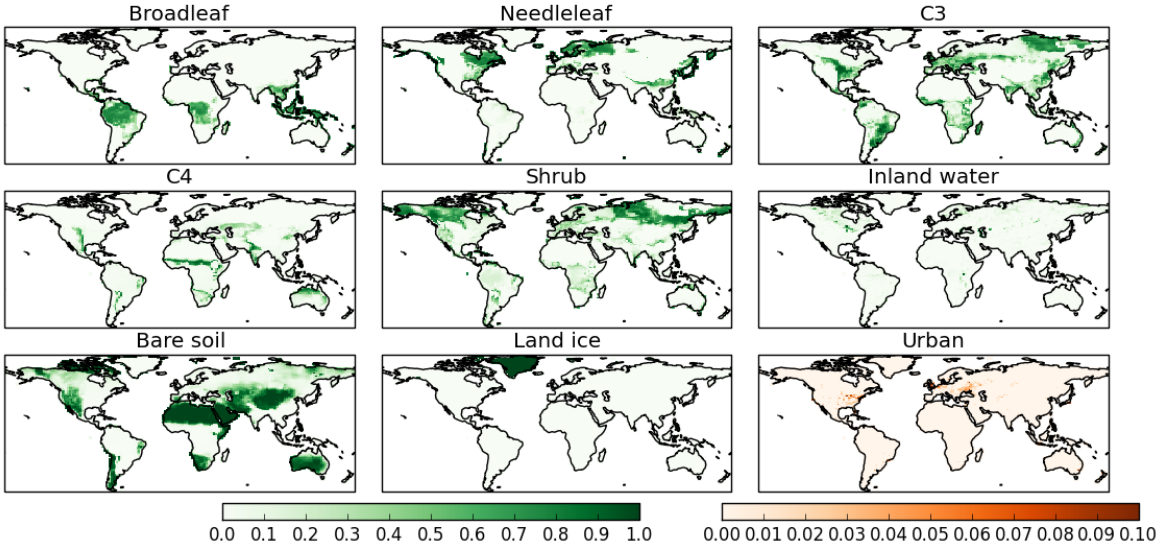

Figure 3.2: S3 land cover from JULES
2016 Fraction of land cover for 10 land cover types, S3 with land-use change, as modelled by JULES for the TRENDY 2017 project

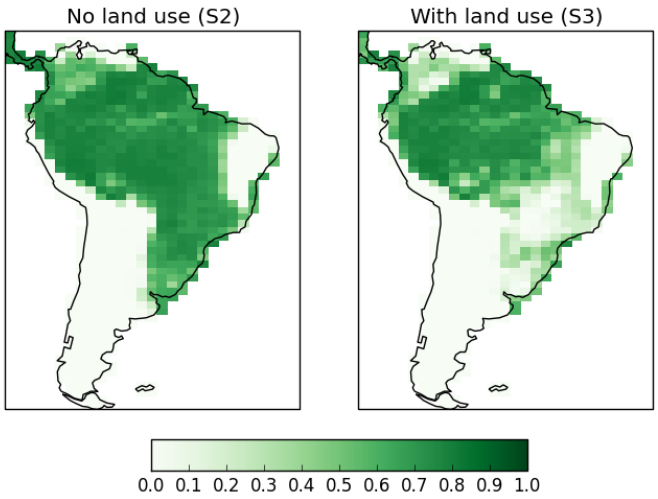

Figure 3.3 JULES simulations of broadleaf, South America
2016 Fraction of broadleaf cover with no land-use change (left) and with land-use change (right) as modelled by JULES for the TRENDY 2017 project

Compared to ESA observations (Figure 3.4) of land cover, the model has too much shrub, especially in the high latitudes, and C4 grass fraction is higher than observed, whereas the other PFTs are mostly too low in fraction and coverage. In particular needleleaf is lacking across the central Canada region in the model compared to observations. Broadleaf over South America is well modelled compared to this version of ESA observations when land-use is included (S3), but is too high without land-use (S2) (see also Figure 3.3).

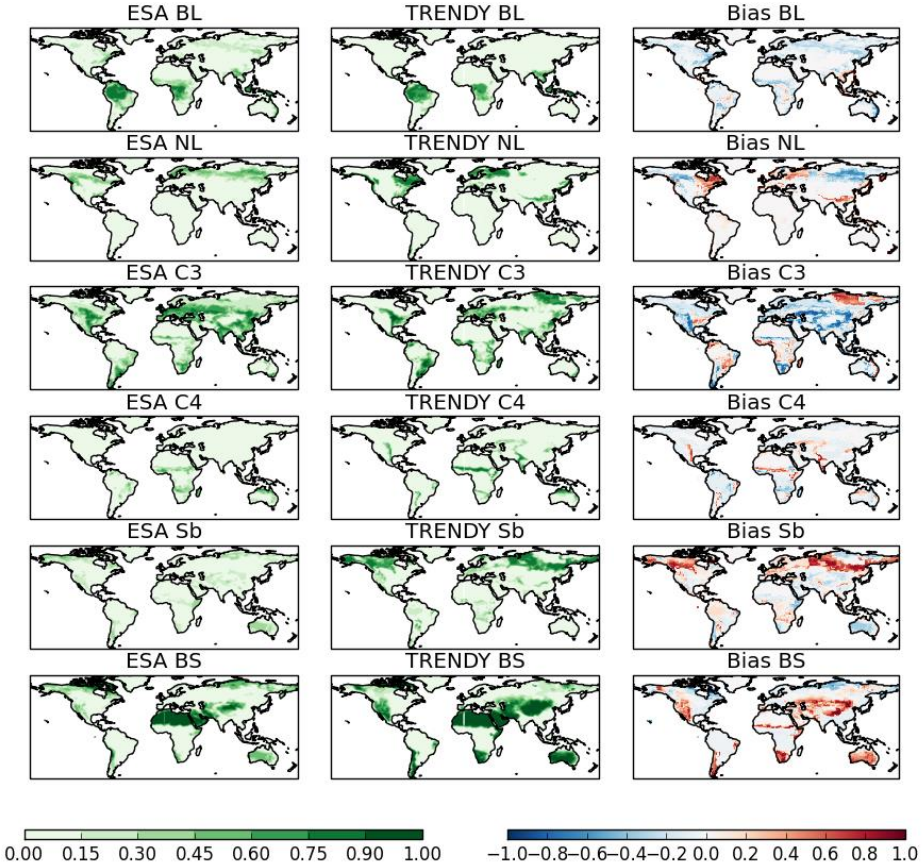

Figure 3.4: Modelled and observed vegetation cover
ESA CCI observations (left column), JULES 2016 modelled vegetation with land-use change (centre column), and difference (right column) for fraction of Broadleaf (BL), Needleleaf (NL), C3 grasses (C3), C4 grasses (C4), Shrub (Sb) and Bare Soil (BS)

Below I review the output of the diagnostic burnt area using all three ignition modes for comparison, without LUC. Mode 1 refers to constant ignitions, mode 2 refers to varying lightning ignitions, and mode 3 refers to varying population and lightning ignitions (as described in Mangeon *et al*., 2016). Constant ignitions are set to a global average of 1.67 ignitions km^{-2} $month^{-1}$; 1.5 ignitions km^{-2} $month^{-1}$ are attributed to humans, and 0.17 ignitions km^{-2} $month^{-1}$ are attributed lightning ignitions derived from a multi-year annual mean of 2.7 strikes km^{-2} $year^{-1}$ (Huntrieser *et al*., 2007) and assuming 75% of the strikes are cloud-to-ground (Prentice and Mackerras, 1977). For mode 2, human ignitions remain at 1.5 ignitions km^{-2} $month^{-1}$ but lightning ignitions are prescribed from an ancillary file and vary spatially and temporally, with all strikes assumed to ignite a fire. For mode 3, ignitions depend on spatially and temporally varying lightning and population data through a function which represents both ignition and

suppression based on population density (Venevsky *et al*., 2002; Pechony and Shindell, 2009), as follows.

$$I_T = (I_N + I_A)* f_{NS} \quad (1)$$

$$I_A = k(PD)\ PD\ \alpha \quad (2)$$

Where $k(PD) = 6.8*PD^{-0.6}$, and $\alpha = 0.03$ (representing number of potential ignitions per person per month per km^2). Both natural and anthropogenic ignitions can be suppressed, and the non-suppressed fraction (f_{NS}) is described as:

$$f_{NS} = 7.7\ (0.05 + 0.9 \times e^{-0.05\ PD}) \quad (3)$$

where 7.7 is used as a scaling factor for calibration to MODIS data (Pechony and Shindell, 2009; Mangeon *et al*., 2016), and where:

I_T : Total ignitions (Ignitions km^{-2} $month^{-1}$)

I_N : Natural ignitions (Ignitions km^{-2} $month^{-1}$)

I_A : Anthropogenic ignitions (Ignitions km^{-2} $month^{-1}$)

PD : Population density (People km^{-2})

Varying ignitions therefore refers to spatially and temporally varying ignitions based on lightning and population density; the function as shown in Figure 3.5 is based on the assumption that at very low levels of population there will be no anthropogenic ignition, which increases as population increases to a maximum point whereby the suppression curve reflecting active fire management, suppression and urbanisation reduces ignitions.

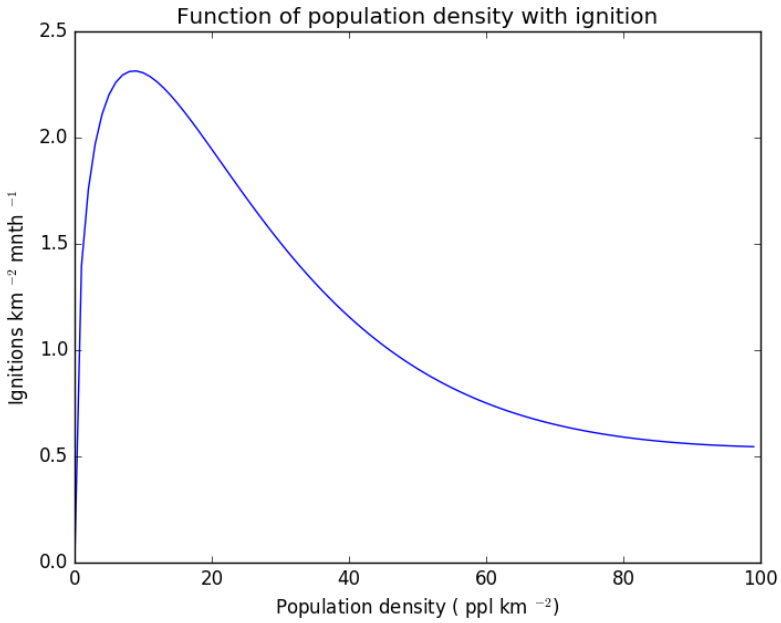

Figure 3.5: Function of ignitions relating to population density in INFERNO

Here I use one PFT, broadleaf vegetation, for comparison. Figure 3.6 shows plots of burnt area from JULES-INFERNO mode 1 (constant ignitions). The top row of plots show the burnt area as a fraction of gridbox. The middle row of plots show burnt area by PFT for broadleaf. If vegetation were allowed to grow in these regions, climatologically the areas marked in red are where high fire incidence rates would occur. However after natural competition and land-use, there is less vegetation in these areas and the bottom row of plots take account of available fuel (burnt area by PFT multiplied by broadleaf fraction), showing decreased burnt area. The desert regions of the Sahara and Kalahari in Africa are a good example of this; these are areas that provide favourable fire conditions, with hot, dry weather. If there were vegetation and ignition in these areas, fuel would burn readily. However there is little available fuel which is why we see little burnt fraction of vegetation in the bottom row of plots.

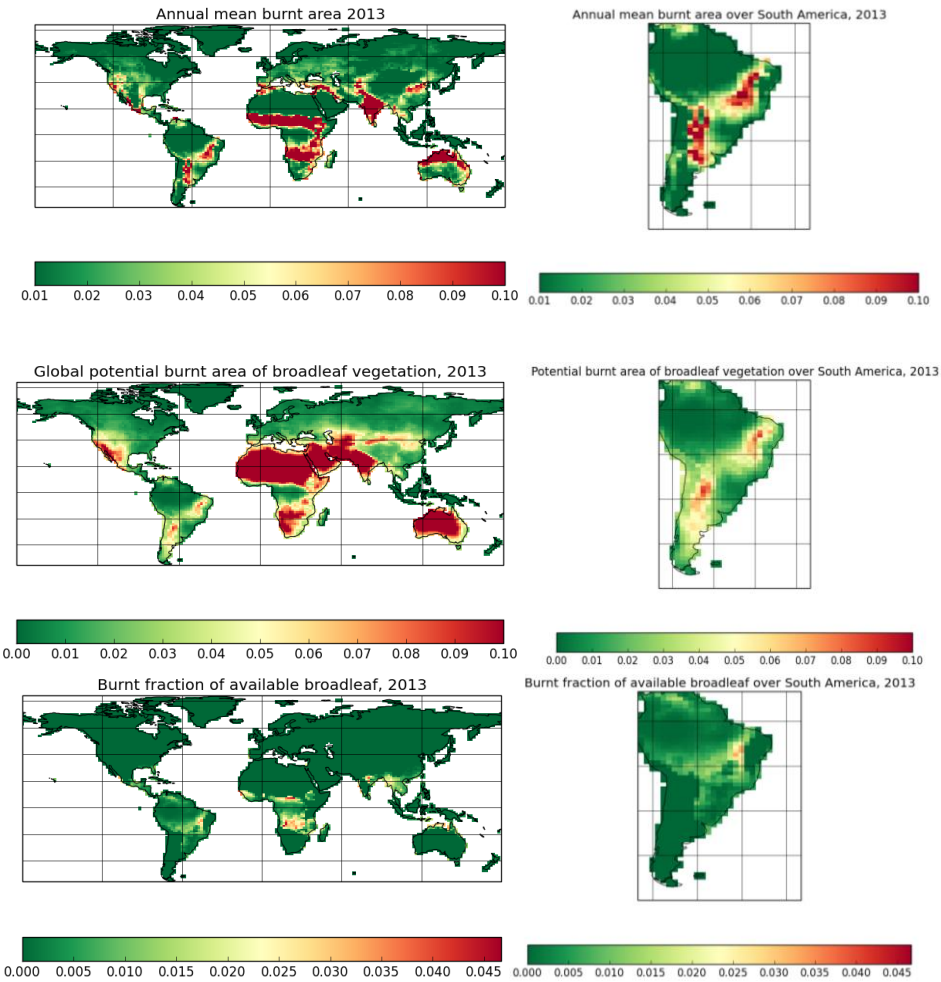

Figure 3.6: Output from INFERNO (mode 1)
From top to bottom: Annual mean burnt area fraction; potential area of broadleaf that would burn if there were sufficient fuel available; burnt fraction of available broadleaf vegetation. All means shown globally (left panels) and over South America (right panels) for one year (2013)

Figure 3.7 shows plots of burnt area from JULES-INFERNO mode 2 (constant human ignitions, varying natural ignitions). There are no obvious differences between mode 1 and mode 2 in terms of simulated burnt area.

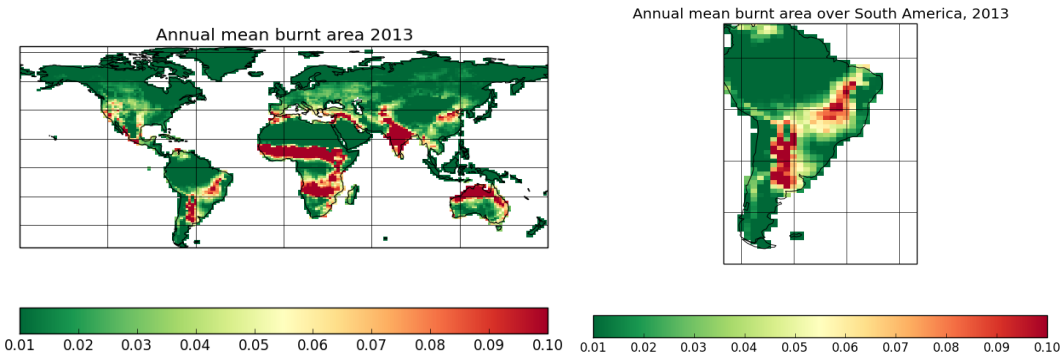

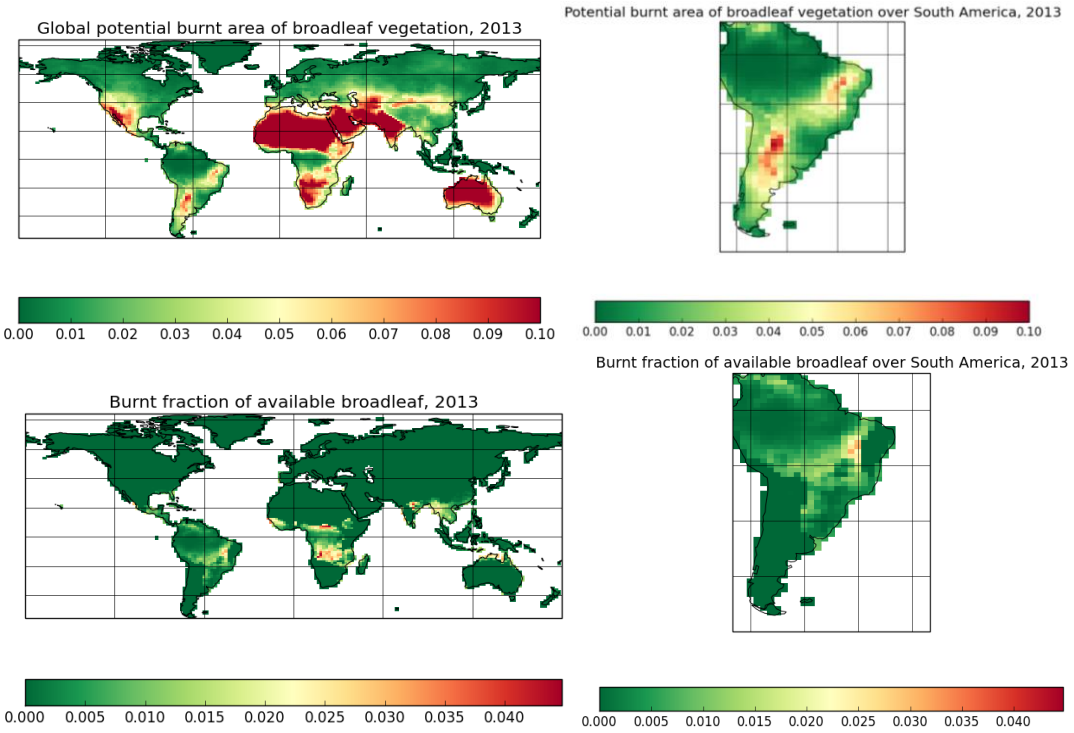

Figure 3.7: Output from INFERNO (mode 2)
From top to bottom: Annual mean burnt area fraction; potential area of broadleaf that would burn if there were sufficient fuel available; burnt fraction of available broadleaf vegetation. All means shown globally (left panels) and over South America (right panels) for one year (2013)

Compared to modes 1 and 2, mode 3 (Figure 3.8) simulates more potential burnt area of broadleaf vegetation, as well as mean burnt area. This implies that human ignitions make an important contribution to projected burnt area in the model. After taking account of vegetation however, the simulated burnt area is the same as in modes 1 and 2.

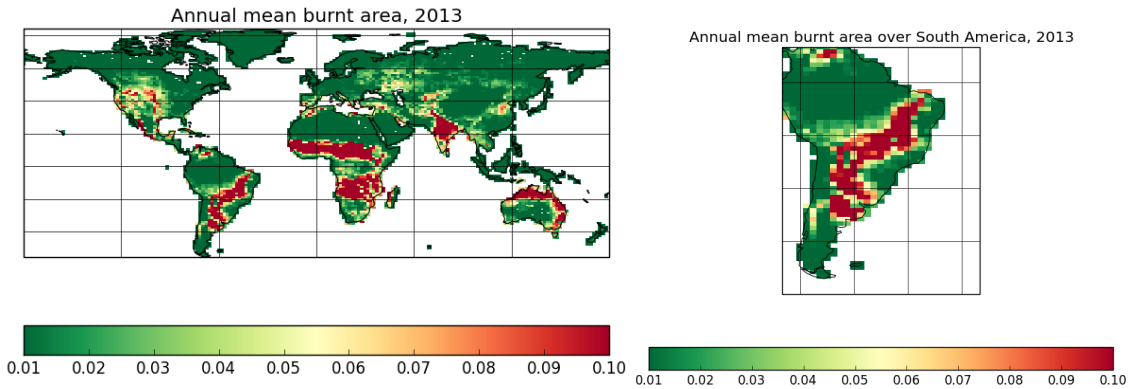

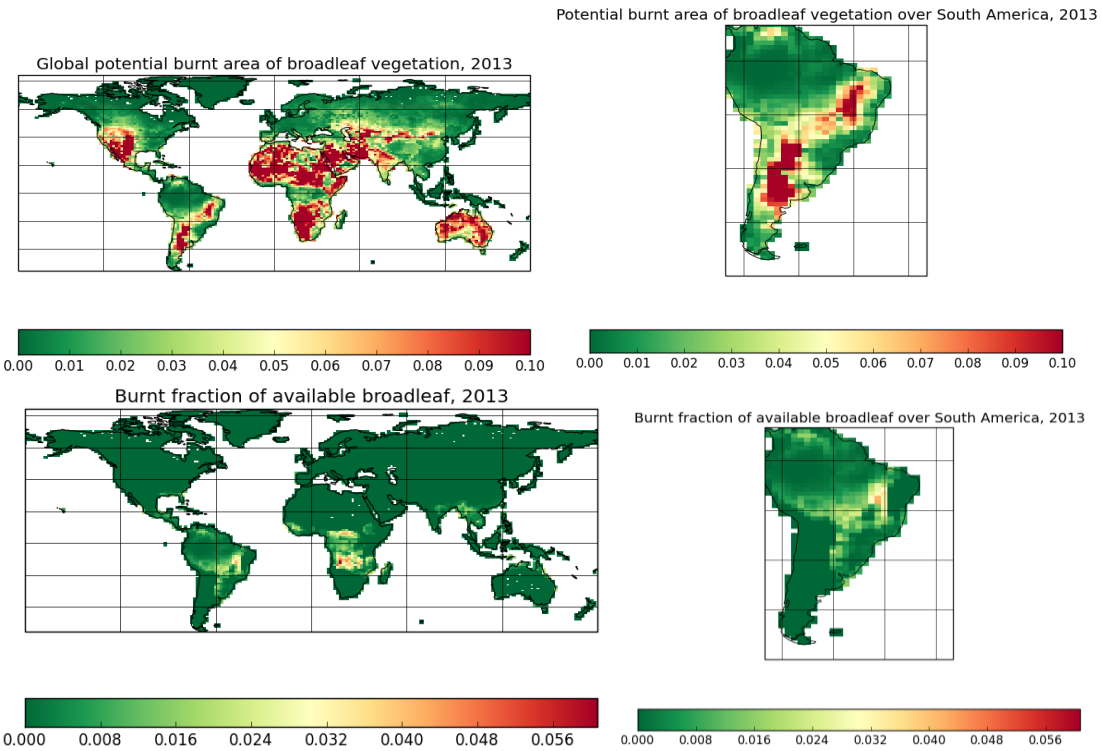

Figure 3.8: Output from INFERNO (mode 3) from top to bottom
Annual mean burnt area fraction; potential area of broadleaf that would burn if there were sufficient fuel available; burnt fraction of available broadleaf vegetation. All means shown globally (left panels) and over South America (right panels) for one year (2013)

Comparing annual mean burnt area as modelled by diagnostic INFERNO to GFED observations (Figure 3.9), it is apparent that although the general spatial pattern of burnt area is captured by the model, there is a larger area burnt in the model projections than in the observations. Certain areas show particularly high burnt area compared to observations, including India, the east coast of Australia, Central/Western USA and South America. This is something to consider when coupling the model with vegetation, as this may have a negative impact on the vegetation cover in these areas.

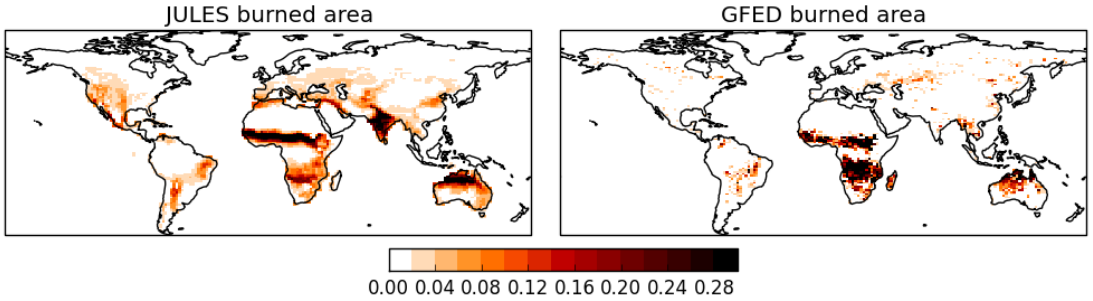

Figure 3.9: Modelled and observed burnt area fraction
As modelled by diagnostic INFERNO with constant ignitions (left) and observations from GFED4.1s (right), annual mean 2009-2014

3.1.2 Using prescribed burnt area

The first stage of the fire-vegetation coupling has been to update the disturbance term in JULES. Previously all vegetation disturbance was combined into one term. This included death due to natural mortality of vegetation, insects and diseases, windfall, and fire, among other causes. In order to separate out fire as a separate disturbance, I have now separated this into 'disturbance from fire', and 'all other disturbance'. I have added a switch so that fire can either be prescribed via an ancillary file (e.g. output from a run with INFERNO, or using burnt area data from MODIS or GFED), or if there is no ancillary file available in the run then the burnt area will be taken straight from the INFERNO module as the model runs.

Figure 3.10 shows initial results of disturbing the vegetation using prescribed burnt area from an ancillary file simulated by INFERNO. This removes broadleaf vegetation around the South of the Amazon, and C3 grass and shrubs increase around the same area. This is as expected, considering the burnt area in INFERNO is high in this region. Some needleleaf is also reduced in the boreal regions, and again shrub increases here also. Compared to observations, this means that vegetation is lower for trees, but grasses and shrubs are higher. This is likely to be a result of the quicker regrowth time of these PFTs in the model after disturbance.

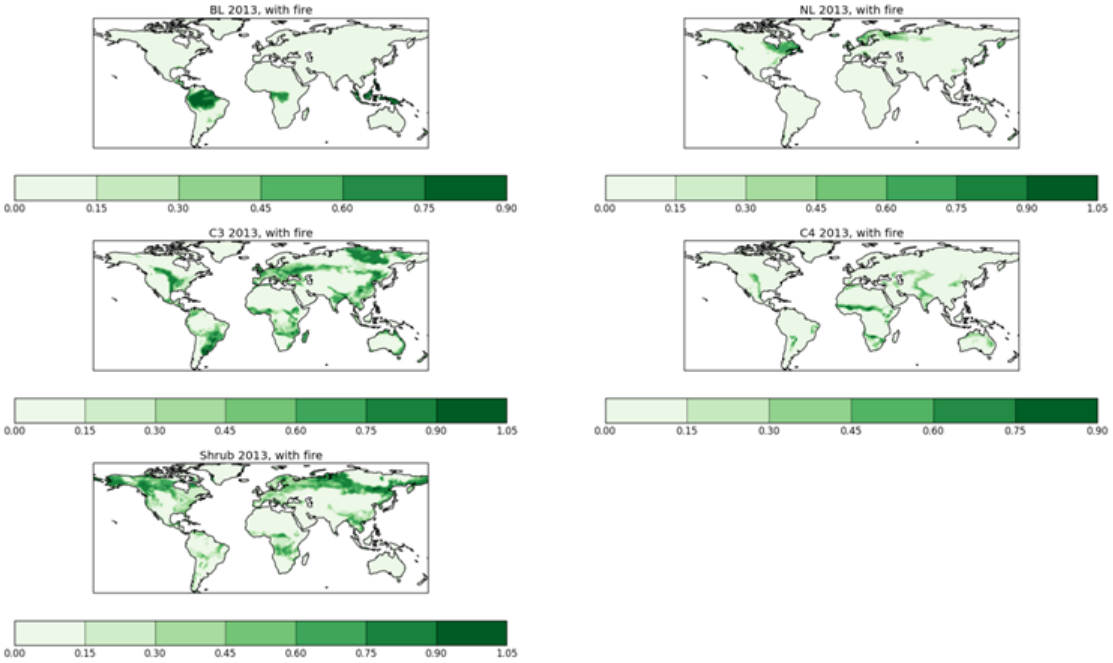

Figure 3.10: JULES Initial simulations with prescribed burnt area
Fraction of vegetation for each PFT (left to right, top to bottom: broadleaf, needleleaf, C3 grass, C4 grass and shrub)

Overall the results from the initial coupling are successful, which suggests that full coupling will also be successful. The original disturbance term will now need to be reduced to account for the new fire disturbance which has been introduced as a separate term.

3.1.3 Coupling fire and vegetation

The second stage of the coupling has been to introduce a new disturbance term in the dynamic vegetation scheme TRIFFID, to reduce the vegetation carbon as a result of fire disturbance, and further reduction of carbon in the soil carbon layers to represent burning litter. These modifications have now been accepted into the JULES trunk at version 4.8, as described in the next section.

3.2 Representing disturbance in JULES

The following is based on a manuscript accepted for publication in GMD (Burton *et al*., 2019), with additional information on the tuning work undertaken in developing the interactive fire model.

3.2.1 Abstract

Disturbance of vegetation is a critical component of land-cover, but is generally poorly constrained in land surface and carbon cycle models. In particular, land-use change and fire can be treated as large-scale disturbances without full representation of their underlying complexities and interactions. Here we describe developments to the land surface model JULES (Joint UK Land Environment Simulator) to represent land-use change and fire as distinct processes wich interact with simulated vegetation dynamics. We couple the fire model INFERNO (INteractive Fire and Emission algoRithm for Natural envirOnments) to dynamic vegetation within JULES and use the HYDE (History Database of the Global Environment) land cover dataset to analyse the impact of land-use change on simulation of present day vegetation. The explicit disturbances provide important contributions to the realistic modelling of vegetation on a global scale, although in some areas fire and land-use together result in over-disturbance. Overall, disturbance generally improves the simulation of vegetation compared to observations, with grasses showing a particularly large improvement (biases reduced from -66% to 13% respectively), but trees are often

represented as too sparse. This work provides a substantial contribution towards representing the full complexity and interactions between land-use change and fire that could be used in Earth System Models.

3.2.2 Introduction

JULES (Joint UK Land Environment Simulator) is a land surface model (LSM) which simulates surface fluxes of water, energy and carbon, along with the state of terrestrial hydrology, vegetation and carbon stores (Clark *et al*., 2011; Best *et al*., 2011). It forms the land-surface component in the Met Office Unified Model for Numerical Weather Prediction, as well as in the latest Climate and Earth System Models of the Hadley Centre family including HadGEM3 (Senior *et al*., 2016) and UKESM1, and can also be used as a stand-alone LSM, used to contribute to international scientific studies such as the Global Carbon Project and TRENDY (Trends in net land atmosphere carbon exchange model intercomparison project). As documented in Cox (2001) and Clark *et al*. (2011), vegetation cover was previously simulated as a function only of competition between plant species, and a large-scale, spatially-constant disturbance term. Here we document updates to the calculation of vegetation cover, including spatially and temporally varying changes in land-use, and introduce a new disturbance term from fire based on the fire model INFERNO (Mangeon *et al*., 2016) as separate from the large-scale disturbance factor for the first time in JULES. We use these processes together with dynamic vegetation to address the impact on global vegetation cover.

JULES can be used in a number of different configurations depending on the focus of research, and parameters can be switched on or off by the user accordingly. For example JULES can be used for studying river routing and runoff, snow cover and permafrost, or crop modelling *inter alia*. In this context, it is useful for the community to develop standard configurations that can be used widely, and are thus easily comparable. In this study we use a standard JULES configuration with dynamic vegetation, and focus on the impact of disturbance from fire and land-use on the simulation of vegetation cover.

Land-use change and fire are two of the most important processes which affect vegetation cover. These disturbances affect vegetation dynamics (e.g. Lasslop *et al*., 2016), atmospheric chemistry (Crutzen *et al*., 1979), the hydrological cycle

(Shakesby and Doerr, 2006) and the carbon cycle (Prentice *et al*., 2011), as well as surface albedo (López-Saldaña *et al*., 2015) and feedbacks on radiative forcing. Each year around 4% of vegetation is burnt (Giglio *et al*., 2013), releasing approximately 2 PgC which equates to around a quarter of emissions from fossil fuel combustion (Hantson *et al*., 2016; van der Werf *et al*., 2017). Land-use and land-cover change (LULCC) can include clearance through fire, as well as other forms of deforestation, conversion of natural vegetation to agricultural land, and abandonment of agricultural land with subsequent forest regrowth. At least 50% of the ice-free land surface has been affected by land-use activities over the last 300 years; 25% of global forest area has been lost, and agriculture now accounts for around 30% of the land surface (Hurtt *et al*., 2011). LULCC can result in changes to biogeochemical and biophysical properties of the Earth system, including changes to surface fluxes of radiation, aerodynamic roughness, heat and moisture, evaporation patterns, soil moisture and latent heat (Betts 2005). LULCC often represents deliberate conversion from one land cover type to another, such as forests to cropland, and this can be long-lasting until the area is subsequently abandoned based on various socio-economic conditions and decision making processes (Turner *et al*., 1995). Fires may be used in a similar way for land conversion, or otherwise may be unintentional (natural or escaped fire), and thus recovery may be more temporally variable than with LULCC.

LULCC is known to be one of the most important influencing factors in the decline of forests in several ways: directly through deforestation and canopy thinning (cutting as well as use of fire for clearance), and indirectly through fire-leakage which can extend forest losses into much larger areas than planned. Fragmentation is also an important contributing factor, causing increased tree mortality and carbon losses near the forest edges (Laurance *et al*., 2000), and increased risk of fire spread into the forest (Soares-Filho *et al*., 2006; Coe *et al*., 2013; Good *et al*., 2014). This can be the result of land clearance for agriculture, and for urban expansion. For example there is a clear correlation between distance to roads and increased fire danger in Amazonia (Cardoso *et al*., 2003). Even when deforestation itself declines, fire incidence can remain high due to increased agricultural frontiers where accidental fires burn out of control (Aragão and Shimabukuro 2010; Cano-Crespo *et al*., 2015) exacerbated by drought conditions (Aragão *et al*., 2018). Small-scale forest degradation is sometimes

included in the definition of LULCC and can be an important contributor to carbon and biomass loss, however more frequently these contributions are below the level of detection and are often not accounted for in estimates of LULCC (Watson *et al*., 2000; Arneth *et al*., 2017). Similarly small fires are difficult to detect by conventional satellite methods (Randerson *et al*., 2012), leading to potential underestimations in LULCC and emission reporting.

The interaction between fire and managed agricultural land is complex. Small scale croplands are often burnt to clear land before planting or harvesting, and can also be burnt after harvest to dispose of waste, where pasture lands may be burnt to fertilise the soils between crops (Rabin *et al*., 2017a). Agricultural land may therefore be an important contributing factor in fire emissions, and fire ignition. Conversely, larger agricultural lands may provide a fire break, where more active fire management takes place to prevent fires from spreading into crop areas unintentionally, and it has been shown that burnt area reduces as cropland area increases (Bistinas *et al*., 2014). Andela *et al*. (2017) has shown that fire occurrence has been reducing in many regions because of agricultural expansion and intensification, making fuel less readily available and decreasing ignitions.

While human ignitions are the main causes of fires in tropical (Cochrane, 2003) and Mediterranean (Mooney *et al*., 1977) regions, natural fires from lightning and volcanic activity are also important for shaping vegetation cover in temperate (Ogden *et al*., 1998) and boreal regions (Johnson, 1992; Veraverbeke *et al*., 2017). In addition, climate-induced land cover change has been shown to be as important in the long-term as anthropogenic LULCC (Davies-Barnard *et al*., 2015), and can continue to fluctuate for decades before a committed state is realised (Pugh *et al*., 2018), making it particularly important to incorporate dynamic vegetation processes in modelling (Seo and Kim., 2019). While previous modelling studies have considered the impact of each of these processes (e.g. Sitch *et al*., 2015; Betts *et al*., 2015; Seo and Kim, 2019), considering fire, LULCC and dynamic vegetation together is still a relatively recent development.

Future fire activity will depend on a combination of both anthropogenic and climatic factors. Forest susceptibility to fire is projected to change little for low emissions scenarios, but substantially for high emissions scenarios (Settele *et*

al., 2014; Burton *et al*., 2018). Because the frequency of fires increases with temperature, the IPCC AR5 report concluded that the incidence of fires is expected to rise over the 21st Century (Flato *et al*., 2013) although there is low agreement in the models on a regional scale due to the complexity of interactions and feedbacks and lack of proper representation in models (Settele *et al*., 2014). However while the meteorological conditions may become more conducive to fire danger in the future, the effects of future LULCC will also have a direct impact on how fire danger will change. LULCC can have important impacts on regional climate, and has been shown to reduce evapotranspiration (Cochrane and Laurance 2008), decrease precipitation and induce drought (Bagley *et al*., 2014), which can in turn initiate abrupt increases in fire-induced tree mortality (Brando *et al*., 2014; Castello and Macedo 2016). The interaction of LULCC, climate change and fire is complex (Coe *et al*., 2013) and in order to understand the multiple feedbacks comprehensively, it is necessary to consider all of these elements together (Aragão *et al*., 2008). To do this we need to be able to represent these processes explicitly within our models.

Currently the representation of disturbance, in particular fire, drought and tree mortality in models is poorly constrained, as identified in the most recent IPCC report (Ciais *et al*., 2013; Flato *et al*., 2013). The purpose of this paper is to document the developments to JULES to include the explicit representation of fire and LULCC and their coupling to vegetation dynamics, and to evaluate the impact of these developments on the simulation of vegetation within the model, with the aim of ultimately being able to represent these processes within a fully coupled Earth System Model. We begin by describing how dynamic vegetation is already simulated in JULES as documented in Cox (2001) and Clark *et al*. (2011), before describing the new processes of fire and land-use. We then outline the methods used in this study for simulating vegetation cover in a number of experiments, and describe the benchmarking approach used to quantify the change. We present results showing the impact of fire and LULCC on vegetation cover, which generally decreases woody vegetation cover and increase grass cover, contributing to an improved simulation of vegetation compared to observations.

3.2.3 Model description and developments

3.2.3.1 Model description

This section describes the representation of disturbance in the land surface model JULES, described in Clark *et al*. (2011) and Best *et al*. (2011). This is a community model, developed from the Met Office Surface Exchange Scheme (MOSES), and will act as the land surface component of the new Earth System Model UKESM. The model can be used offline, forced by observational data. The configuration considered here is the Carbon Cycle configuration of JULES, with dynamic vegetation.

JULES uses TRIFFID (top-down representation of interactive foliage and flora including dynamics) for modelling dynamic vegetation. TRIFFID models vegetation dynamics including the soil carbon, and the structure and coverage of five plant functional types (PFTs) within each gridbox, broadleaf tree, needleleaf tree, C3 grass, C4 grass, and shrub (Cox *et al*. 2000). More recent developments to JULES have included the option of modelling an extra 4 PFTs (Harper *et al*. 2016; Harper *et al*., 2018). TRIFFID models carbon fluxes for each vegetation type using climate and atmospheric CO_2 concentration provided by ancillaries, and this accumulates to update vegetation and soil carbon on a 10 day timestep.

The vegetation carbon density is related allometrically to changes in the balanced leaf area index (LAI) which in turn is separated into leaf (L_c), root (R_c) and stem (W_c) pools:

$$C_v = L_c + R_c + W_c \quad (1)$$

The change in vegetation carbon is based on Net Primary Productivity (NPP) minus litterfall:

$$\frac{dC_{vi}}{dt} = (1 - \lambda_i)\Pi_i - \Lambda_{li} \quad (2)$$

Where λ represents the fraction of NPP allocated to PFT area expansion, Π represents NPP per unit of vegetated area of PFT *i,* and Λ represents litter (Clark *et al*. 2011).

The model uses species competition based on the Lotka-Volterra approach, populating the available land surface with expansion by a dominance hierarchy of trees, shrubs then grasses (Cox *et al*. 2000). Therefore the vegetation competition is represented by the change in fractional coverage of PFT *i* (v_i) in a gridcell is:

$$C_v \frac{dv}{dt} = \lambda \Pi v_* \left\{ 1 - \sum_j c_{ij} v_j \right\} - \gamma_v v_* C_v \quad (3)$$

Where v_* = MAX {v,0.01}. c_{ij} is the competition coefficient describing the effect of PFT *i* on *j*, and γ_v is a large scale disturbance term. A proportion of this NPP (λ) is used to increase the fractional coverage of a PFT and the remainder (1- λ) increases the carbon content of the existing vegetated area (equation 2) (Cox *et al*., 2001).

Carbon and Nitrogen allocated to spreading allow the vegetation to expand onto bare ground. Where available area is limiting, the vegetation competes for space with some carbon being turned over as litter, and the competition code updates the vegetation fractions (v_i) accordingly.

Carbon is lost from the vegetation via a local scale litter term, as defined by:

$$\Lambda_{\mathrm{li}} = \gamma_{\mathrm{l}} \mathrm{L_c} + \gamma_{\mathrm{r}} \mathrm{R_c} + \gamma_{\mathrm{w}} \mathrm{W_c} \quad (4)$$

Where γ_{r} and γ_{w} are constant turnover rates for root and stem carbon, and γ_{l} is a temperature dependent turnover rate of leaf carbon defined to be consistent with the phenological state.

JULES was developed with one generic disturbance term to cover mortality from age, pests, disease, storms, and fire (γ_{v}), referred to as ‘g_area’. This included implicit fire disturbance, in a spatially constant turnover rate.

In the original formulation all vegetation carbon turnover was considered litterfall. Total litterfall for each grid box is made-up of the area-weighted sum of the local litterfall from each PFT, along with the previously described large-scale

disturbance rate (γ_v), and a density dependent component from PFT competition for space (Clark *et al*., 2011):

$$\Lambda_c = \sum_i v_j \left(\Lambda_{li} + \gamma_{vi} C_{vi} + \Pi_i \sum_j c_{ij} v_j \right)$$

(5)

The carbon lost from the total litterfall Λ_c is transferred to the soil carbon pool C_s. Some of this is broken down by microbial respiration and returned to the atmosphere as CO_2 (Clark *et al*., 2011):

$$\frac{dC_s}{dt} = (\Lambda_c) - R_s$$

(6)

The effect of land-use on vegetation distribution is included by modifying the competition term of equation 3 (Burton *et al*., 2019). In the competition term, c_{ij} is zero for dominant PFTs, meaning the whole gridbox is available for PFT i to expand into. For non-dominant PFTs, c_{ij} is 1 and expansion is scaled by the fraction of the gridbox where PFT i is dominant. Land-use is also represented by a limitation to the space available for a PFT to expand into. A fraction of each gridbox is prescribed as the "disturbed fraction", which represents the area covered by agriculture, with no distinction between cropland and pasture being made. When land-use is added, we have:

$$\frac{dv_i}{dt} = \frac{\lambda \Pi v_*}{C_{vi}} \left\{ 1 - \alpha a_i - \sum_j c_{ij} v_j \right\} - \gamma_v v_*$$

(7)

Where α is the disturbed fraction and a_i is 1 for non-woody PFTs and 0 for woody PFTs. The three woody PFTs (broadleaf trees, needle-leaf trees and shrubs) are prevented from growing in the disturbed fraction, while the two grass PFTs (C3 grass and C4 grass) can grow anywhere in the gridbox. Grass PFTs growing in the disturbed fraction are interpreted as agricultural grasses, although they are physiologically identical to "natural" grasses. α can increase or decrease over

time. As α increases, first “natural” grasses are relabelled as “agricultural” grasses, then an area of woody PFTs is replaced by bare soil, which can be replaced by the non-woody PFTs over time if they are viable. As α decreases, an area of “agricultural” grasses is relabelled as “natural” and becomes available for woody PFTs to expand into.

3.2.3.2 Model developments

Until now, JULES has not included fire as a separate disturbance. Here I have developed the model so that fire is separated into an independent disturbance which reduces the vegetation carbon pool accordingly. The carbon flux as a result of fire is calculated in a similar way as LULCC, although fire differs in the respect that it is an instantaneous occurrence based on fire danger conditions and ignition, whereas LULCC is maintained as agricultural fraction of land over time.

The disturbance from fire is calculated via the diagnostic fire model INFERNO which was recently implemented in JULES (Mangeon *et al*. 2016). This is a reduced-complexity global fire model, designed to represent fire variability at large scales. The model uses flammability, ignition and fuel to diagnose burnt area. Burnt area is accumulated to the TRIFFID timestep and used to calculate the fire disturbance term.

The effect of fire on vegetation distribution is included by modifying the disturbance rate, γ_v. Previously disturbance due to fire was implicitly included in γ_v, along with mortality due to pests, windfall and many other processes. Fire disturbance, β_i, is included as a PFT-dependent burnt area which can vary in space and time. β_i is calculated within JULES by the INFERNO fire model. Now that fire is explicitly represented, γ_v must be reduced accordingly, hence the representation of fire does not necessarily increase mortality, but makes it spatially and temporally variable. Table 3.2 shows the standard values of γ_v implicitly including fire disturbance. The developments to γ_v to account for fire disturbance will be described in section 3.2.4.

Table 3.2: The original disturbance rate, γ_v, implicitly including fire disturbance

PFT	Broadleaf Tree	Needle-leaf Tree	C3 Grass	C4 Grass	Shrub
Standard γ_v including implicit fire $(360\ days)^{-1}$	0.009	0.0036	0.10	0.10	0.05

The vegetation competition equation can now be updated with fire and land-use disturbance:

$$\frac{dv_i}{dt} = \frac{\lambda \Pi v_*}{C_{vi}} \left\{ 1 - \alpha a_i - \sum_j c_{ij}\, v_j \right\} - (\gamma_v + \beta_i)\, v_* \qquad (8)$$

The calculation of burnt area depends on soil carbon density, C_s, providing additional mechanisms by which fire and land-use can feedback onto vegetation distribution. The coupling of fire and the carbon cycle includes a direct impact of fire on C_s; some soil carbon is burnt, resulting in a flux of carbon from the soil to the atmosphere. The burnt soil carbon flux is diagnosed in INFERNO and we now allow the flux to effect the evolution of C_s. The carbon cycle in JULES does not explicitly represent a litter carbon store, however the model includes four soil carbon pools and two of these pools are used here as proxies for flammable litter. The decomposable plant material soil carbon pool, C_{dpm}, and the resistant plant material soil carbon pool, C_{rpm}, both receive the litter carbon flux from vegetation and have a relatively rapid turnover rates, making them reasonable proxies for the litter carbon store. The calculation of the burnt soil flux is based on the INFERNO diagnosis of burnt vegetation flux (equation 8 of Mangeon *et al*., 2016).

$$f_s = \left(\mu_{min,k} + \left(\mu_{max,k} - \mu_{min,k} \right)(1 - \theta) \right) C_k \sum_i \beta_i v_i \qquad (9)$$

The efficiency of soil burning is inversely proportional to the surface soil moisture, θ, with the values of the completeness of combustion parameters, μ, for each soil pool, k, being listed in Table 3.3. The burnt soil flux is proportional to the total available fuel, C_k, and the total burnt area, summed over all PFTs.

Table 3.3: Completeness of combustion parameters

Soil Carbon Pool	Decomposable plant material, C_{dpm}	Resistant plant material, C_{rpm}
μ_{min}	0.8	0.0
μ_{max}	1.0	0.2

Fire and land-use both affect the soil carbon store by altering the vegetation-to-soil litter flux. Without fire or land-use, the litter flux comprises a local litter fall rate, Λl, representing the turnover of leaves, roots and stems, litter due to disturbances and litter due to competition. The total litter fall is defined by Clark *et al*. (2011) as (their equation 63):

$$\Lambda_c = \sum_i v_i \left(\Lambda_{li} + \gamma_{vi} C_{vi} + \Pi_i \sum_j c_{ij} v_j \right) \quad (10)$$

Including both fire and land-use disturbance terms produces:

$$\Lambda_{CvLoss} = \sum_i v_i \left(\Lambda_{li} + (\gamma_{vi} + \beta_i) C_{vi} + \Pi_i \sum_j (\alpha a_i + c_{ij} v_j) \right) \quad (11)$$

Λ_{CvLoss} represents the loss of vegetation carbon. The carbon that is not combusted following a fire enters the soil carbon pools and is split between C_{dpm} and C_{rpm} according to PFT-specific parameters as described by Clark *et al*. (2011). To calculate the losses due to fire, the vegetation distribution (equation 8) and vegetation loss (equation 11) are calculated with and without fire, and the difference between the two values of Λ_{CvLoss} is attributed to the fire, following the same method as used for land-use change.

Carbon loss due to fire, Λ_{Fire}, is calculated by repeating equations 8 and 11 with no burnt area (β=0):

$$\Lambda_{Fire} = \Lambda_{CvLoss} - \sum_i v_{NoFire,i} \left(\Lambda_{li} + \gamma_{vi} C_{vi} + \Pi_i \sum_j (\alpha a_i + c_{ij} v_{NoFire,j}) \right) \quad (12)$$

Where v_{NoFire} is the PFT area calculated using equation 8 with β=0. 13% of the vegetation killed by fire emitted as CO_2 and the remainder enters the soil carbon pools (Li, Zeng and Levis 2012). All terms expressed in the above equations are summarised in Appendix 3.

The figures below show some initial results for 5 plant functional types following this update.

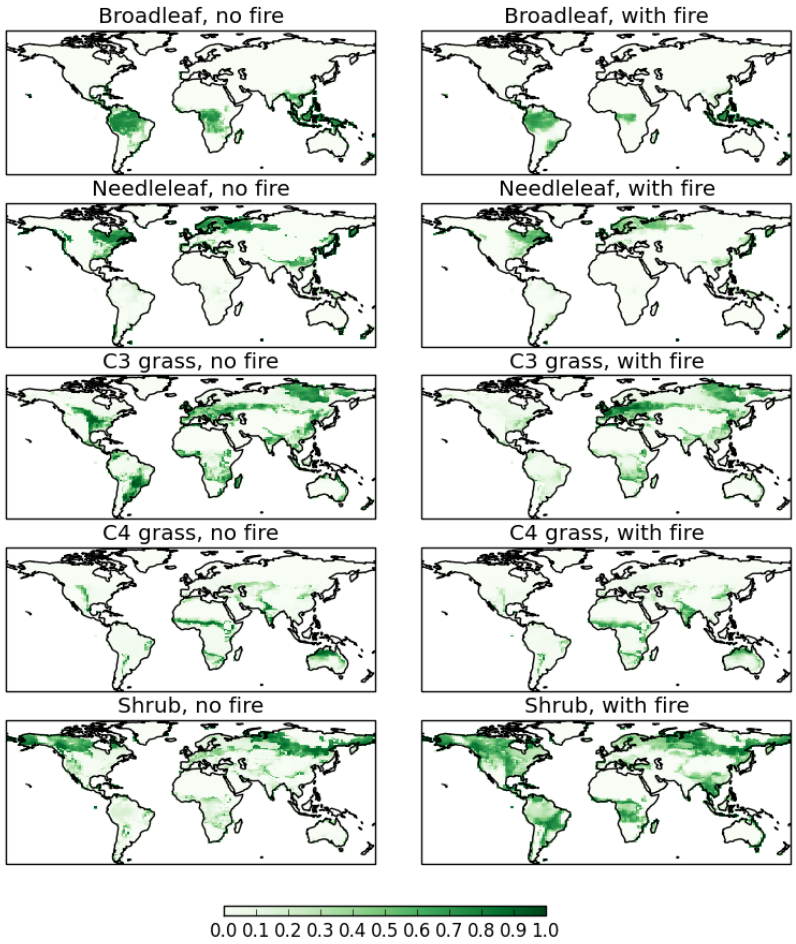

Figure 3.11: JULES vegetation fractions without (left) and with (right) fire. From top to bottom, PFTs are: broadleaf, needleleaf, C3 grass, C4 grass and shrub

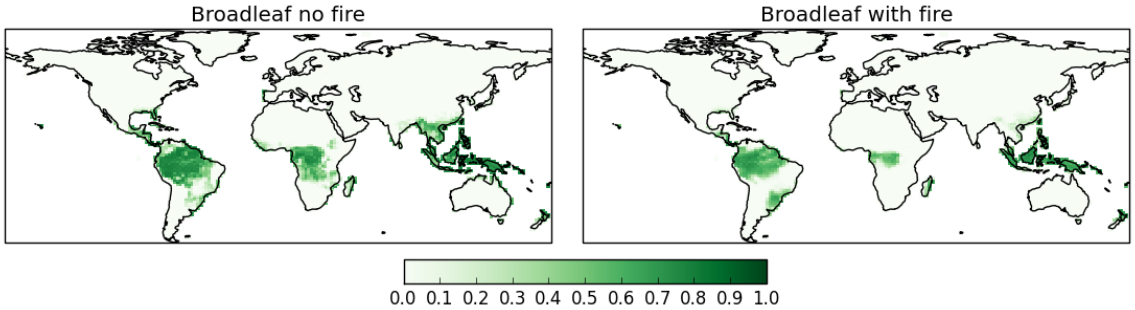

Figure 3.12: JULES broadleaf fractions, with and without fire

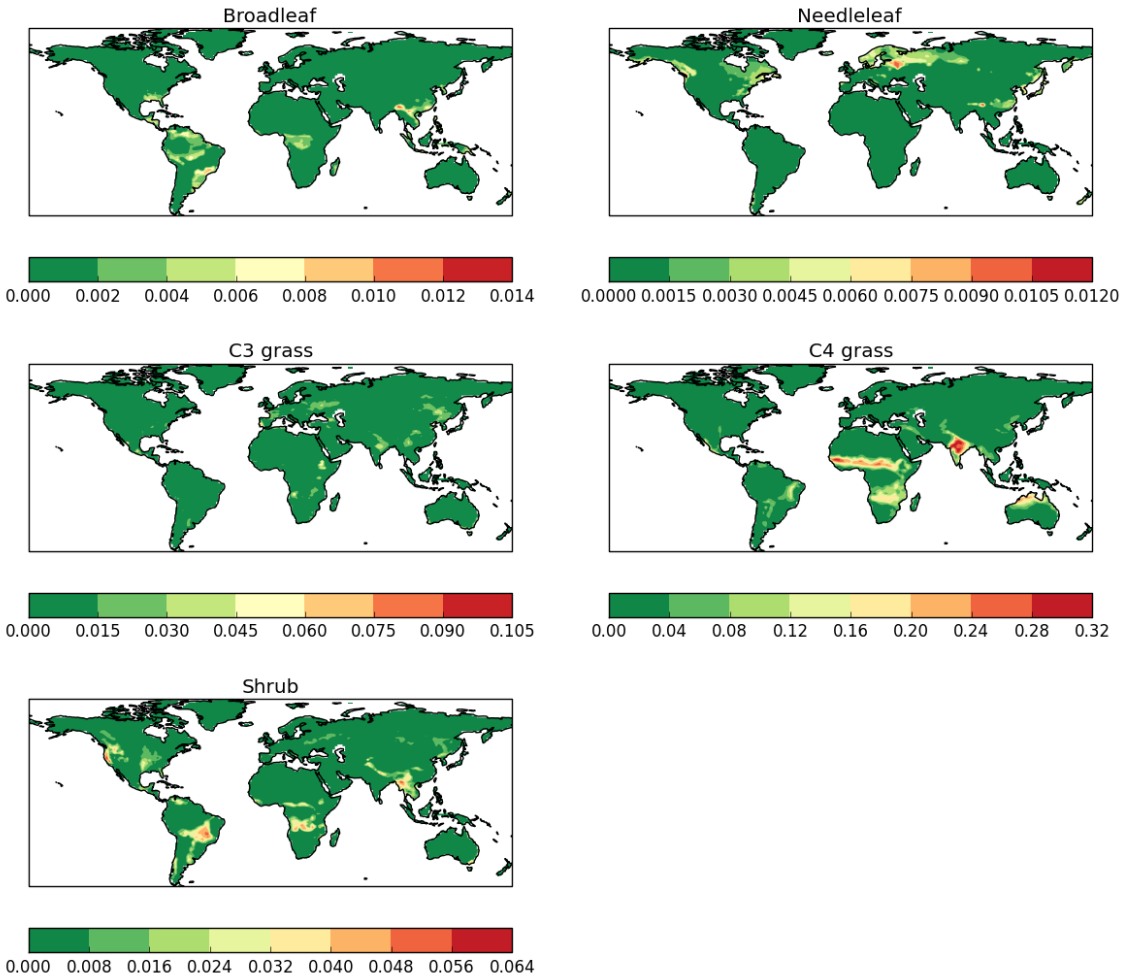

Figure 3.13: Plotted output of fire disturbance for each PFT
JULES fire disturbance (g_burn) fraction by PFT. Left to right, top to bottom: broadleaf, needleleaf, C3 grass, C4 grass, and shrub

Here interactive fire is working well, and following the pattern of burnt area that would be expected from INFERNO. The plots comparing fire to no fire (Figure 3.11 and Figure 3.12) show that fire is primarily decreasing broadleaf and needleleaf vegetation, with some reduction in C4 grasses, and increasing shrub and C3 vegetation. The amount of disturbance is currently relatively high, so

further work is now required to tune this to observations. Some of this is likely to be due to double-counting of fire, within the existing 'all disturbance' term (γ_v) which should be reduced now fire is separated out.

It should be noted that here burnt area is directly converted into vegetation mortality, as implemented in other simple schemes such as JSBACH (Lasslop *et al*., 2018), given that INFERNO calculates flammability based only on leaf carbon and DPM (Mangeon *et al*., 2016). There are no observational data available on scales relevant to global models that give information on the impact of fire on vegetation (Rabin *et al*., 2017) , which limits the ability to constrain this processes within models (Lasslop *et al*., 2018). However mortality is in fact likely to be highly variable depending on the duration, severity and intensity of the fire, the type of biomass burned and its resistance to fire, and the condition of the fuel (moisture level) *inter alia*.

3.2.4 Tuning the fire model

The uncertainties associated with fire modelling (see section 1.5.2) result in a range of potential values of projected burnt area. This range can be constrained to a certain extent by observations of burnt area, but there are also uncertainties associated with observations which should be taken into account (see section 1.3.3). Adding fire as a new disturbance term into the model now results in changes to the vegetation distribution and vegetation fractions, which can also be tuned to observations.

However, it should be noted that tuning the vegetation response is just one method of tuning the model with fire. Other methods could include tuning the emissions, burnt area, and ignitions. Here I focus on tuning the vegetation with the fire model for a number of reasons. Firstly the aim of this PhD is to understand the impact of fire on vegetation in JULES, and so modelling the vegetation fractions with accuracy for the historical period and present day narrows the range of uncertainty associated with future projections. Secondly, burnt area and emissions have already been tuned to some extent within the work of Mangeon *et al*. (2016) using GFED burnt area, and was shown to perform well against other fire models. Finally, there is still much uncertainty around the modelling of ignitions across the fire modelling community (see section 1.5.2) which is a

separate topic for research, so for now the best estimate for the calculation of ignitions based on the work of Pechony and Shindell (2010) is used here.

There are a number of ways of tuning the model so that the results reflect observations of vegetation, to stay within a range of uncertainty:

- Tuning disturbance
  Previously in JULES there was only one disturbance term 'g_area' (γ) which represented all disturbance to vegetation, including pests, disease, windthrow and also fire. Now there is a separate disturbance term for fire, the value of g_area needs to be reduced accordingly.
- Tuning with average burnt area
  The average burnt area per PFT was heuristically defined in Mangeon *et al*. (2016), and therefore is associated with inherent uncertainty. This can be reduced or increased within JULES
- Tuning Leaf Area Index
  'LAI_min' refers to a fraction (λ) of NPP that is used to increase the fractional coverage of vegetation.

I consider the impact of each of these methods in turn.

3.2.4.1 Tuning disturbance

Previously all vegetation disturbance in JULES was captured in the term (γ_{vi}), or 'g_area' (Jones *et al*., 2011). Now fire is represented as a separate disturbance, termed 'g_burn':

g_dist = g_area + g_burn

where 'g_dist' refers to overall disturbance. Thus g_area should be reduced. G_area (g_area_io) is a parameter value available in the JULES namelist files under the 'TRIFFID PFT parameters' which can be tuned according to a particular set up. The standard set up of JULES as used for the TRENDY experiments uses g_area values as outlined in Table 3.2.

Using the standard set up of JULES and the new interactive fire option, the vegetation fractions change significantly compared to results without fire, and depart further from observations (Figure 3.14). Particularly noticeable is the loss of broadleaf and needleleaf trees, and the increase in shrub fraction.

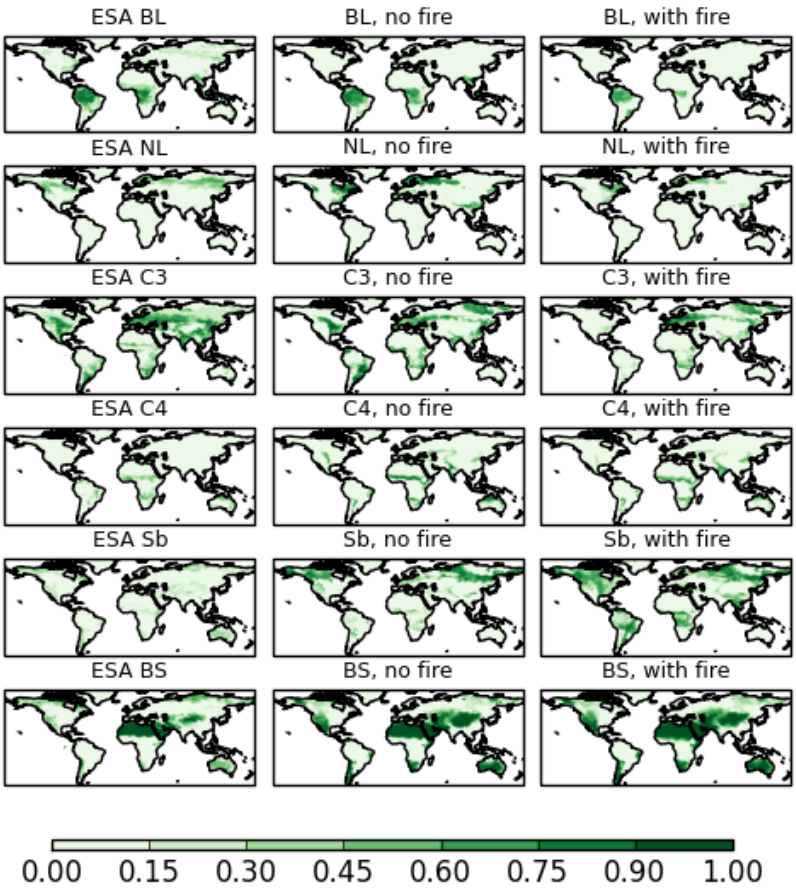

Figure 3.14: Results of initial coupling in JULES

Tuning with competition equation

One method of estimating disturbance is outlined in Harper *et al*. (2018a), using the competition equation within TRIFFID to calculate the level of disturbance required to achieve certain vegetation distributions per PFT. The method is based on a formula that calculates the equilibrium distribution of PFTs using the following equation (from Harper *et al*., 2018a, their equation 17):

$$\gamma_{vi} = \lambda_i \Pi_i \left[1 - \sum_{j=1}^{n_{pft}} c_{ij} v_j \right] \times \frac{1}{C_{V_I}} \quad (13)$$

Using this method with the initial simulations of interactive fire, new values for g_area were calculated, as outlined in Table 3.4.

Table 3.4: Values of g_area using competition

Broadleaf Tree	Needle-leaf Tree	C3 grass	C4 Grass	Shrub
0.005493	0.004704	0.08124	0.07023	0.04257

Running the model again with the new values of g_area shows improved results, but there is still a high loss of woody PFTs and too much shrub and grasses compared to observations (Figure 3.14).

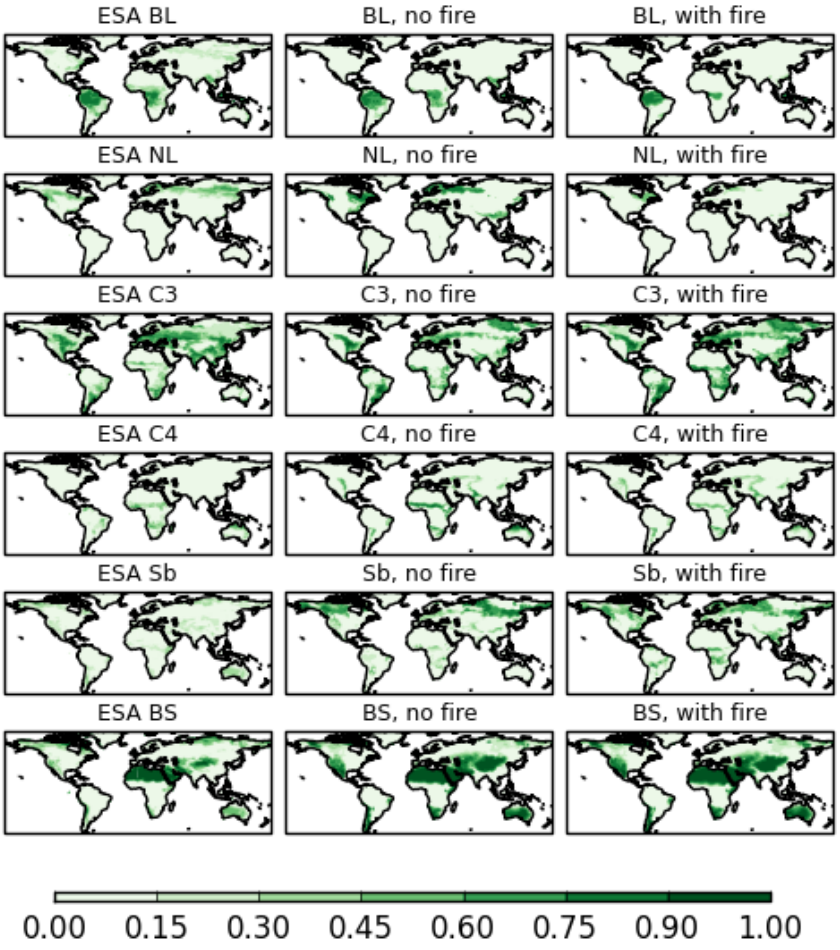

Figure 3.15: Results with tuned values for g_area in JULES

Tuning with observations

The results of the first tuning experiments show that there is still some discrepancy between the model output and the observations. The next step is

therefore to continue tuning g_area and other factors of fire disturbance as outlined above to try to improve the results.

To maximise growth of the larger woody PFTs and attempt to find the right level of grasses and shrubs, I reduce g_area in a number of test simulations, and based on the result continue to adjust the disturbance across the PFTs, as shown in Table 3.5.

Table 3.5: Tests for g_area values

G_area (360 days)$^{-1}$	**Broadleaf Tree**	**Needle-leaf Tree**	**C3 Grass**	**C4 Grass**	**Shrub**
Standard set up	0.009	0.0036	0.10	0.10	0.05
Test 1	0.0001	0.0001	0.33	0.8	0.45
Test 2	0.0001	0.0001	0.01	0.3	0.3
Test 3	0.0001	0.0001	0.03	0.4	0.2
Test 4	0.0001	0.0001	0.12	0.42	0.18
Test 5	0.0001	0.0001	0.15	0.43	0.19

Figure 3.16 below shows the results of test 5. Even by reducing the disturbance term to as little as 0.0001, the broadleaf and needleleaf trees still do not survive with interactive fire included. There could be a number of reasons for this. The regrowth timescale of trees in TRIFFID could be too slow which is a known issue in JULES, so that with frequent disturbance from fire the trees are unable to recover fast enough to sustain vegetation in areas of high fire occurrence. Research studies have shown that it takes around 30-50 years for a forest to recover following a fire (Oliveras *et al*., 2018; Houghton, 1999), whereas to grow a forest to full size in TRIFFID takes in excess of 800 years, with tropical forests taking over 950 years to recover (Oliver and Jones, unpublished data – see Appendix 3).

Another reason could be that the fire disturbance level as calculated by INFERNO is too high. Therefore the next step of tuning should be to assess the burnt area given by INFERNO against observations.

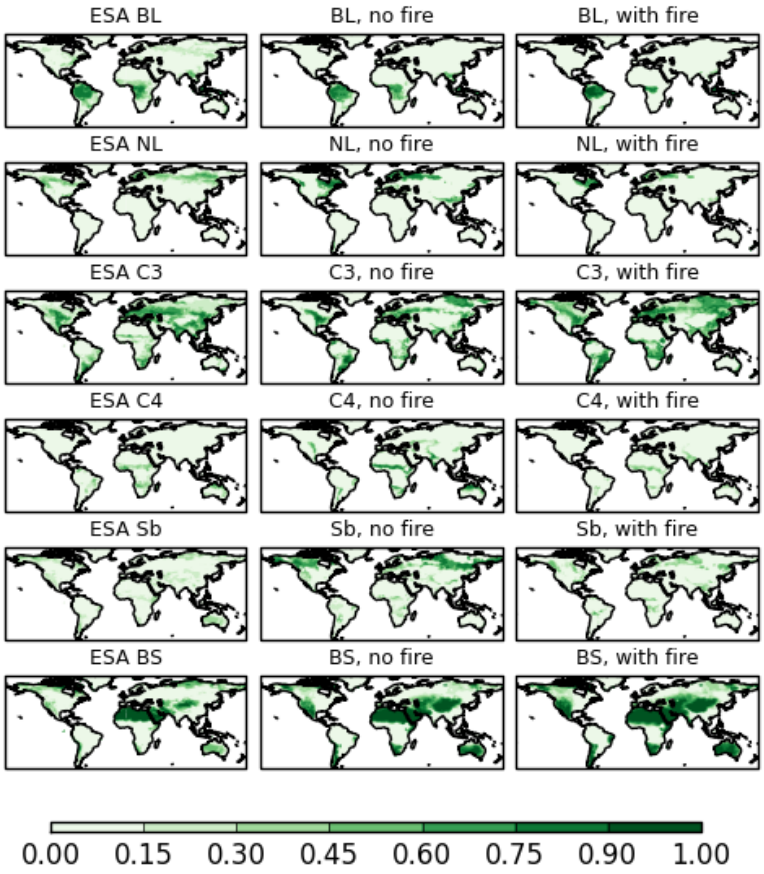

Figure 3.16: Results with further tuning of g_area in JULES

3.2.4.2 Tuning average burnt area

Different vegetation types have different propensities to burning (Pellegrini *et al*., 2017). Burnt area therefore depends to some extent on the vegetation type that is available at the site of a fire. Some studies have assessed this, however this has not been categorised by the 5 PFTs available within JULES and we cannot therefore draw strong conclusions about how these numbers should be represented in JULES. In the original set up of INFERNO, the average burnt area for each PFT is "heuristically" determined (Mangeon *et al*., 2016). There could therefore be some scope for further tuning this with vegetation. The parameters for the average burnt area by PFT are available in the namelist files in JULES (avg_ba_io within PFT parameters) and can be tuned within a suite. Burnt area is therefore a function of flammability, ignition, and the average burnt area by PFT, which then is translated into the new disturbance term g_burn. Within this calculated burnt area, 100% of the vegetation is then assumed to die and is converted either to emitted carbon or to soil carbon. The avg_ba parameter thus impacts the total burnt area for each PFT, influencing the mortality rate indirectly.

The original values of average burnt area are shown in Table 3.6.

Table 3.6: Standard values for burnt area by PFT

Broadleaf Tree	**Needle-leaf Tree**	**C3 Grass**	**C4 Grass**	**Shrub**
0.6km^2	0.6km^2	1.4km^2	1.4km^2	1.2km^2

To understand how much of an impact this parameter values makes on the results of vegetation distribution, I try a number of experiments focusing on the simulation of broadleaf fractions, as outlined in Table 3.7.

Table 3.7: Tests for burnt area by PFT values

avg_ba (km^2)	**Broadleaf Tree (BL)**	**Needle-leaf Tree (NL)**	**C3 Grass**	**C4 Grass**	**Shrub**	**Result (compared to obs)**
Standard set up	0.6	0.6	1.4	1.4	1.2	BL too low
Test 1	0.06	0.06	0.14	0.14	0.12	Burnt area too low
Test 2	0.3	0.3	0.7	0.7	0.7	BL too low
Test 3	0.1	0.3	0.7	0.7	0.7	Good (no loss of BL)
Test 4	0.2	0.4	0.8	0.7	0.8	BL too low
Test 5	0.15	0.4	0.7	0.8	0.7	Good (some loss of BL

As the burnt area is now being reduced, it is appropriate to increase the level of general disturbance again. In these tests I use the following values for g_area:

Table 3.8: Values for g_area (yr^{-1}) with modified burnt area

Broadleaf Tree	**Needle-leaf Tree**	**C3 Grass**	**C4 Grass**	**Shrub**
0.0045	0.0018	0.15	0.43	0.19

One of the largest differences in the simulation of vegetation when fire is added can be seen across the tropical regions of Brazil and the Congo. Therefore this is one of the regions I will focus on in the tests to look for improvement.

Without land-use change included (S2), the area of broadleaf vegetation was too high across South America in Test 1. Burnt area was also too low compared to observations. When fire is added with too low a burnt area, there is no visible impact on vegetation. Test 2 showed a reduction in the loss of broadleaf forest across South America, but still a high loss of the broadleaf forest around the Congo region. The burnt area is improved in test 3 although still lower than observations, but there was little impact on the vegetation of adding fire. Test 5 showed reduced loss of broadleaf in South America than in other tests, but broadleaf across the Congo was still lower than ESA CCI (Figure 3.17). In addition there was little impact on vegetation across South America without prescribing land-use, and burnt area was too low (right panel).

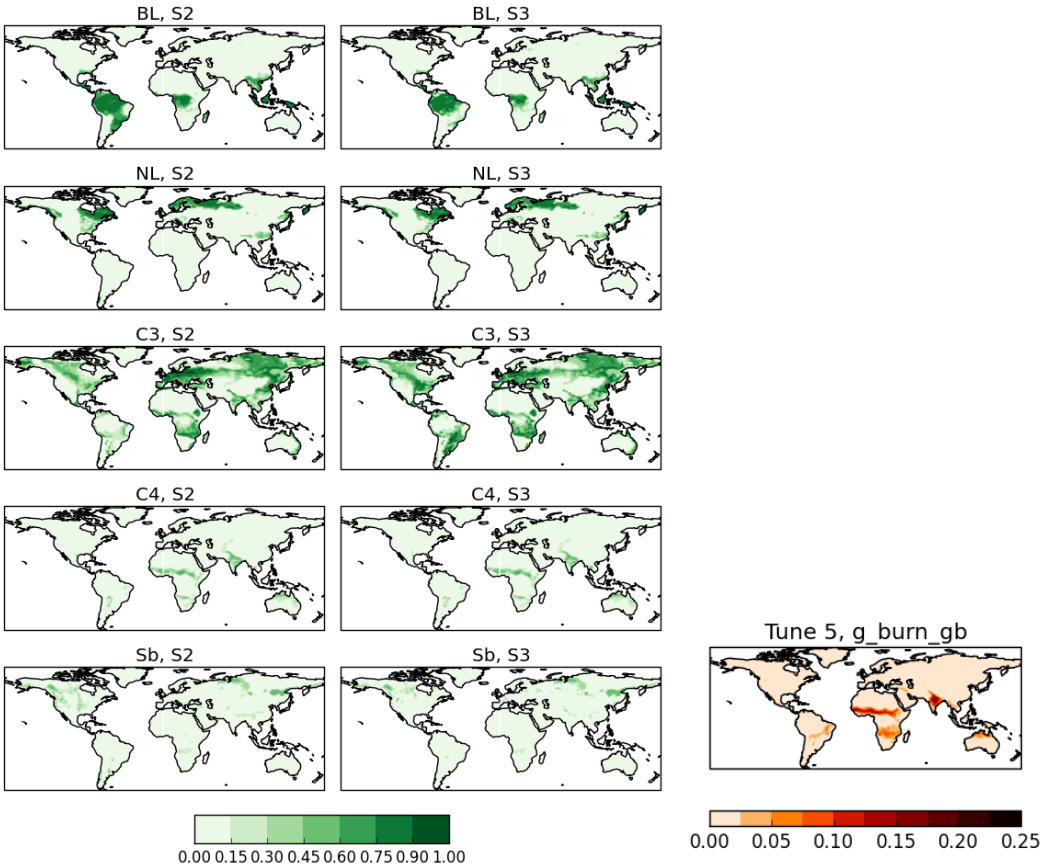

Figure 3.17: Tuning test 5 with burnt area by PFT
Fraction of vegetation by PFT for S2 without land-use (left column), S3 with land-use (right column) and gridbox total burnt area (right) in JULES

From Figure 3.18 it is apparent that although the results of reducing the burnt area may result in less vegetation disturbance across all PFTs, the total burnt area is much lower than observations.

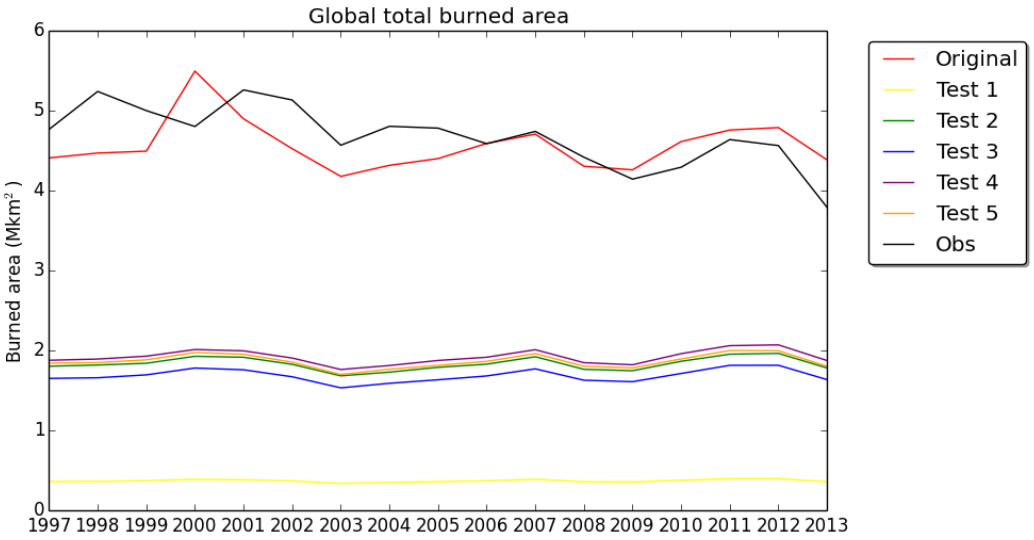

Figure 3.18: Total global burnt area
Total global burned area (Mkm^2) for GFED4.1s observation data and a selection of tuning tests in JULES as described above

The tests have shown that reducing the amount of area burnt per PFT has clear impacts on the resultant vegetation growth. By reducing the burnt area by an order of magnitude, there is virtually no impact of adding fire to the model: the broadleaf fraction is too high across South America as before, and there is little shrub coverage. By gradually reducing the burnt area for trees, it is possible to reduce the amount of disturbance around the Congo region and the shrubs remain low, giving good results compared to mean observations from ESA. However, when the burnt area for this set-up is compared to observations of burnt area (Figure 3.18) it is clear that overall levels of fire are too low.

Finally, I try a number of tests reducing the average burnt area for trees while increasing burnt area for grasses and shrubs to try to encourage tree growth while keeping grasses and shrubs lower (Table 3.9).

Table 3.9: Tests for reduced tree burnt area

	Broadleaf Tree (BL)	Needle-leaf Tree (NL)	C3 Grass	C4 Grass	Shrub
Standard set up					
G_area (yr^{-1})	0.009	0.0036	0.10	0.10	0.05
Avg_ba (km^2)	0.6	0.6	1.4	1.4	1.2
Test 6	0.0045	0.0018	0.05	0.1	0.1
	0.1	0.3	1.7	1.6	1.5
Test 7	0.0045	0.0018	0.05	0.1	0.1
	0.1	0.3	1.9	1.5	1.4
Test 8	0.0045	0.0018	0.4	0.08	0.1
	0.1	0.3	1.9	1.5	1.4
Test 9	0.0045	0.0018	0.2	0.12	0.12
	0.1	0.3	1.9	1.5	1.4

The final tests gives a higher burnt area compared to observations at present day, and no improvement in spatial tree cover globally (although total vegetation carbon is higher owing to higher density tree fraction).

In conclusion, by testing a range of values for burnt area by PFT I have shown that reducing the burnt area results in values of global burnt area that are too low compared to observations, and reducing the average burnt area for trees does not improve the tree cover. This again points to a need for increased recovery times for trees in TRIFFID to improve the results. I therefore progress with the original values of burnt are by PFT as published in Mangeon *et al*. (2016).

3.2.4.3 Tuning Leaf Area Index

The results of the initial tuning suggest a tendency of the model to reproduce fast-growing vegetation quickly, while the larger woody vegetation lags behind. One way to encourage new vegetation growth is to alter the value of LAI_min.

In JULES, TRIFFID assigns a fraction (λ) of NPP to use in increasing the carbon content of the existing vegetation, while the remainder increases fractional coverage of each PFT, with this boundary being determined by the value of

LAI_min. Thus, when LAI values are small, all of the NPP is used for growth, and when they are large all the NPP is used for spreading (Clark *et al*., 2011).

By reducing the LAI_min boundary term for broadleaf and needleleaf trees, the LAI values become larger and maximum spreading of these vegetation types is promoted. I will test what impact this has on the simulation of vegetation in JULES by altering the values as shown in Table 3.10.

Table 3.10: Altered values for LAI-min

PFT	Broadleaf Tree	Needle-leaf Tree	Shrub	C3 Grass	C4 Grass
LAI_min standard	3.0	3.0	1.0	1.0	1.0
LAI_min with fire	1.0	1.0	1.0	1.0	1.0

The results of the tests are shown through plots of global vegetation distribution at present day (Figure 3.19). Using this method of analysis there is little perceptible difference in vegetation distribution when LAI is modified. I then assess the changes in global mean vegetation fractions (Figure 3.20).

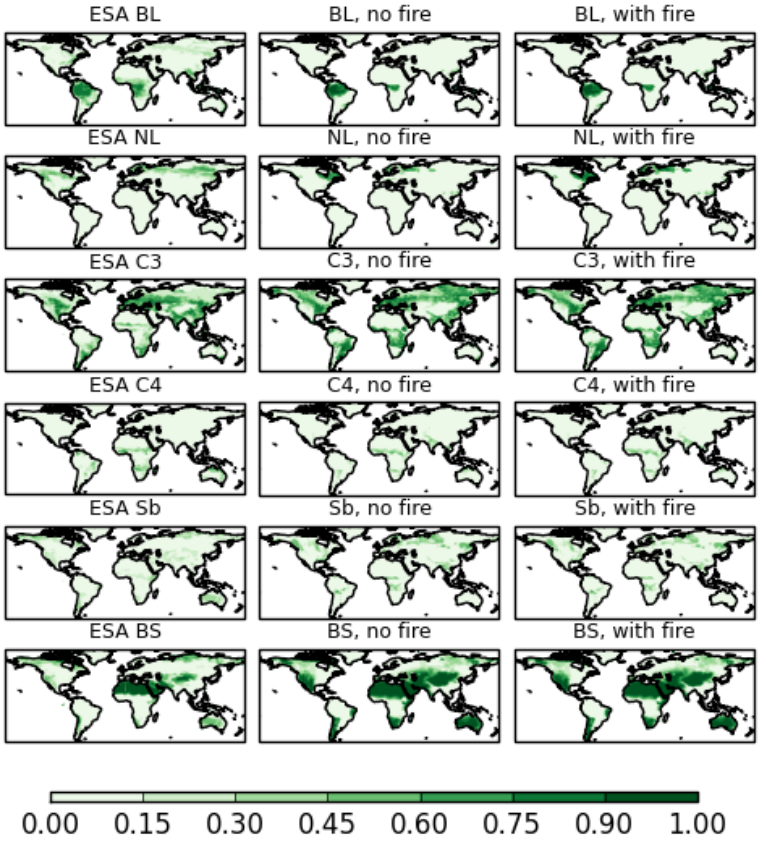

Figure 3.19: Vegetation fraction by PFT
ESA observations (left column), JULES using standard LAI (centre column) and JULES using modified LAI values (right column). From top to bottom BL= broadleaf, NL = needleleaf, C3 = C3 grass, C4 = C4 grass, Sb = shrub, BS = bare soil.

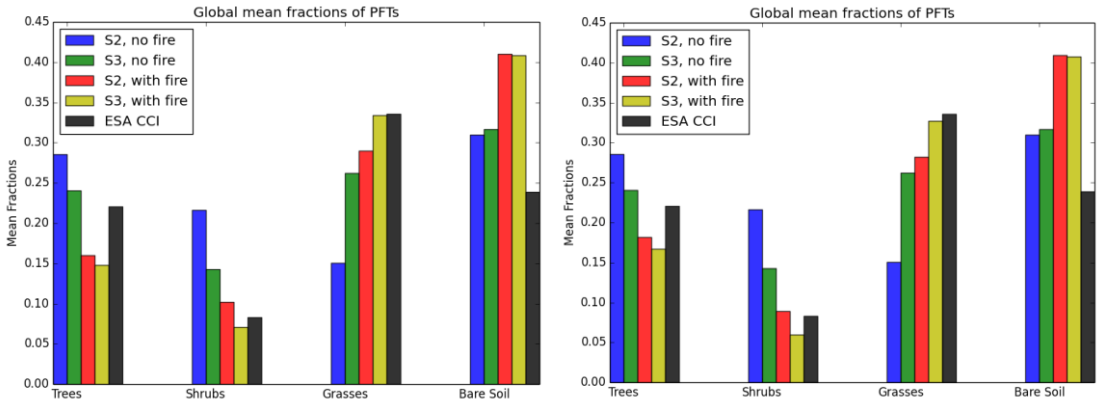

Figure 3.20: Global mean fractions of PFTs
JULES using standard LAI (left) and modified LAI (right). Trees = broadleaf and needleleaf, grasses = C3 and C4 grasses. S2 = no land-use. S3 = with land-use.

Decreasing the values of LAI_min for trees results in a slight increase in the global means. This appears to make a slight improvement to the results, so I will therefore continue to use this set-up in further tests.

3.2.4.4 Tuning within a range of observations

Having reviewed the g_area, burnt area and LAI for methods of tuning, I will now focus on assessing these results against a range of observations. As shown in section 1.3.2, ESA land cover CCI observations are often used for tuning models, and work has been done to categorise the land cover classes into the 5 JULES PFTs to make comparison between the model output and observations easier. Both in collecting the initial data and through this process of categorisation, uncertainty is introduced. To understand how this uncertainty impacts my results, I use the minimum and maximum values for the observations here, and tune the model further to ensure the total vegetation cover is within this uncertainty range. In these tests I try a new set of tuning tests with g_area, keeping the same values of burnt area per PFT and using the new values for LAI_min (Table 3.11).

Table 3.11: Tests for g_area with modified LAI_min

	Broadleaf Tree	Needle-leaf Tree	C3 Grass	C4 Grass	Shrub
Standard set up	0.009	0.0036	0.10	0.10	0.05
Test 6	0.0045	0.0018	0.30	0.30	0.19
Test 7	0.0045	0.0018	0.32	0.29	0.10
Test 8	0.0045	0.0018	0.36	0.28	0.17

The results of the additional tests show that with some small modifications to the g_area values for grasses and shrubs, it is possible to fit the results of the total modelled vegetation to be within the range of uncertainty values, although bare soil is too high (Figure 3.21). This does not solve the differences between the modelled distribution of vegetation and the mean observations, but it is another way of ensuring the results are reliable within certain bounds.

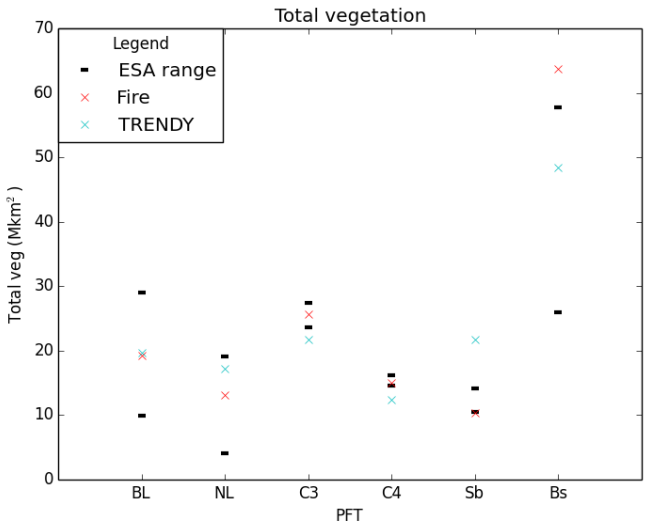

Figure 3.21: Tuning test 8 by PFT
Total vegetation cover (Mkm^2). BL = Broadleaf tree, NL = Needleleaf tree, C3 = C3 grass, C4 = C4 grass, SB = Shrub, Bs = Bare soil. Results of JULES test with fire shown in red crosses, compared to control run (JULES TRENDY S3 with land-use no fire). ESA uncertainty bars shown in black.

To check the burnt area still fits with observations, modelled burnt area is plotted here against GFED observations of total annual burnt area. The model does not capture the long term decline in burnt area that has been observed (Andela *et al*. 2017), but it is within the right order of magnitude.

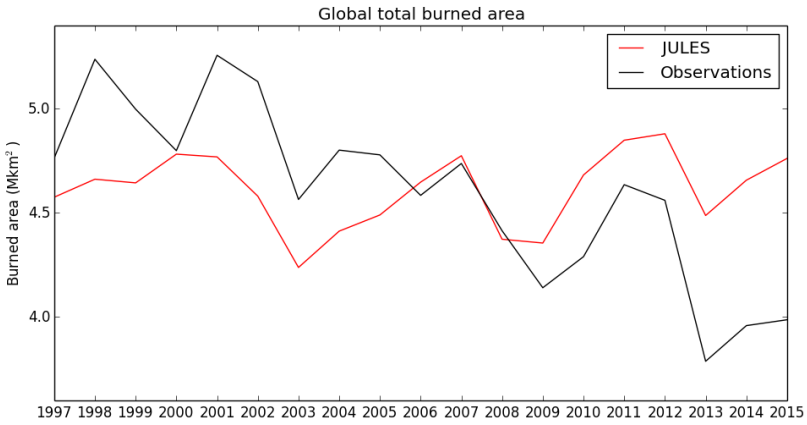

Figure 3.22: Global total burnt area
Global total burnt area (Mkm^2) using JULES (red) and GFED 4.1s (black).

Another way of achieving this may be to reduce fire disturbance for larger PFTs and increase fire disturbance for shrubs and grasses to achieve correct mean burnt area across all PFTs and improve the simulation of vegetation. This is reviewed in the following experiments (Table 3.12).

Table 3.12: Tests to reduce burnt area for trees

	Broadleaf tree	Needleleaf tree	C3 grasses	C4 grasses	Shrub	Notes
Test 10 g_area: avg_ba:	 0.0045 0.1	 0.0018 0.3	 0.05 1.9	 0.1 1.5	 0.1 1.4	Bare soil good, C3 too high, C4 slightly low
Test 11 g_area: avg_ba:	 0.0045 0.1	 0.0018 0.3	 0.4 1.9	 0.08 1.5	 0.1 1.4	C3 too low, C4 too high, shrub too high, bare soil slightly high
Test 12 g_area: avg_ba:	 0.0045 0.1	 0.0018 0.3	 0.2 1.9	 0.12 1.5	 0.12 1.4	All veg OK, bare soil still too high

The first tests showed an improvement in the simulation of bare soil, but some PFTs were too high. I reduced this by increasing g_area. The end result still shows bare soil as too high compared to observations, and the distribution of PFTs still shows large disturbance across the Congo and Cerrado regions similar to previous experiments. The burnt area is well simulated for the historical period, but the present day burnt area is too high.

In summary, the series of tuning experiments performed here have shown that when fire is included in the model, it is not possible to grow broadleaf vegetation in certain regions such as the Congo and Cerrado unless burnt area is reduced to very low levels that are much lower than observed. Competition in the model means that when trees cannot grow the carbon is allocated instead to grasses, resulting in high levels of grasses and shrubs with fire disturbance. When grasses are kept artificially low by increasing g_area in order to keep within an observed range, vegetation cannot be maintained and the bare soil fraction increases.

3.2.4.5 Diagnostic fuel consumption

As part of the fire model intercomparison project (FireMIP), factors of fuel consumption have been assessed across a number of fire models, where I have contributed JULES results (Mangeon *et al*., in prep). Within INFERNO, the combustion completeness can be set as a minimum and maximum value for leaves and wood for each PFT, which currently impacts the carbon that is emitted within the diagnostic framework for the calculation of diagnostic emissions. If this testing is successful, this could be another factor to include within the coupled model to improve results in future developments.

I started by decreasing values of combustion completeness within INFERNO for broadleaf, needleleaf and shrub vegetation. In theory, this should lead to less vegetation being converted into emitted carbon, and more remaining in the vegetation. The original and modified values are presented in Table 3.13.

Table 3.13: Tests for altering fuel consumption

Standard Values	**BL**	**NL**	**C3**	**C4**	**Sb**
ccleaf_max_io	1.0	1.0	1.0	1.0	1.0
ccleaf_min_io	0.8	0.8	0.8	0.8	0.8
ccwood_max_io	0.4	0.4	0.4	0.4	0.4
ccwood_min_io	0.0	0.0	0.0	0.0	0.0
Modified Values	**BL**	**NL**	**C3**	**C4**	**Sb**
ccleaf_max_io	0.5	0.5	1.0	1.0	0.9
ccleaf_min_io	0.4	0.4	0.8	0.8	0.8
ccwood_max_io	0.2	0.2	0.4	0.4	0.5
ccwood_min_io	0.0	0.0	0.0	0.0	0.0

The results of the model comparison are shown in Figure 3.23 (Mangeon *et al*., in prep). The first thing to note is that for tropical forests in particular there is a large range of uncertainty within the observations for fuel consumption, and a

large difference between field observations and GFED4s observation data. With the modified values, the results for INFERNO (JULES-INFERNO mod) are improved for grasses and boreal forests, but results for temperature forests are poorer. For tropical forests and croplands, the results are improved compared to field observations, and noticeably the range increases for tropical, boreal and croplands.

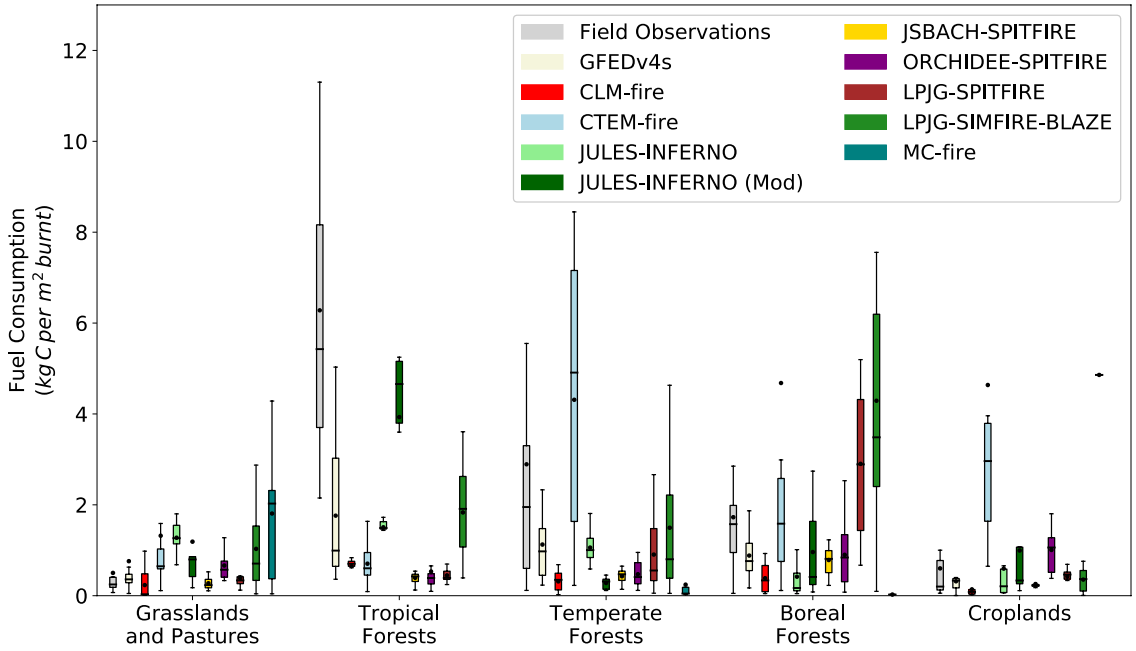

Figure 3.23: Fuel consumption across FireMIP models
By ecoregion (kgC/m^2 burnt). Figure reproduced from Mangeon *et al*. (2017), and updated for ongoing analysis to be included in Mangeon *et al*. (in prep)

The results indicate some improvement in altering values of combustion completeness for leaves and wood in certain biomes, but more work is needed to tune the values to each PFT within JULES, and by biome. In future developments of the model and when coupled to an atmospheric model or fully interactive ESM, this may be a useful area for further research.

3.2.4.6 Final set up

It is likely that a combination of all of the above factors will create the best results for modelling vegetation distribution. And again it should be reiterated that this is one method of tuning to observations, and does not take into account carbon stocks and emissions, productivity, or changes in the hydrological cycle. Furthermore, there are limitations on how much can be achieved by tuning the model to observations through modifying different parameters. To achieve a

fundamentally improved simulation of vegetation including fire disturbance, it is likely that a new vegetation dynamics scheme will be required that can represent age-class scaling so that the slow regrowth issue identified by Oliver and Jones (Appendix 3) can be addressed. This is a priority for the JULES community, and is starting to be addressed through the RED (Robust Ecosystem Demography) project, aimed at developing a new vegetation dynamics scheme which will enable smaller trees to be sustained without having to accumulate enough carbon for a full-height tree to be established (Moore *et al*., 2018).

This section has shown that there are a number of ways of tuning the model, and a number of potential outcomes compared to differing observational datasets. The mean ESA CCI land cover dataset (2010) is commonly used by the JULES community for evaluating the global vegetation cover as simulated in the model. I therefore use a compromise of the most appropriate parameters for the fire and LULCC configuration to achieve results comparable to this dataset, by halving general disturbance for trees and increasing shrub disturbance by a factor of three as shown below (Table 3.14).

The final set up of JULES with interactive fire is therefore as shown in Table 3.14.

Table 3.14: Final set up of JULES with interactive fire

PFT	Broadleaf Tree	Needle-leaf Tree	C3 grass	C4 grass	Shrub
g_area (γ) (360 days)$^{-1}$	0.0045	0.0018	0.10	0.10	0.15
LAI_min (λ) with fire	1.0	1.0	1.0	1.0	1.0
Average burnt area (km^2)	0.6	0.6	1.4	1.4	1.2

3.2.5 Trend analysis

As mentioned in the previous section 3.2.4 ‘Tuning the fire model’, JULES-INFERNO does not capture the decline in burned area that Andela *et al*. (2017)

show from the observed global burned area. Observed decreases in burned area mainly occurred in areas of low and intermediate tree cover such as savanna areas, driven primarily by agricultural expansion and intensification, whereas closed-canopy forests showed an increase (Andela *et al*., 2017). To explore this in more detail, I evaluate the burned area trend in each region individually in the model and using GFED4.1s observations.

Globally, there is a significant negative trend in burned area over the satellite period (1997-2016), whereas JULES-INFERNO projects a slight increase over the same period (Figure 3.24).

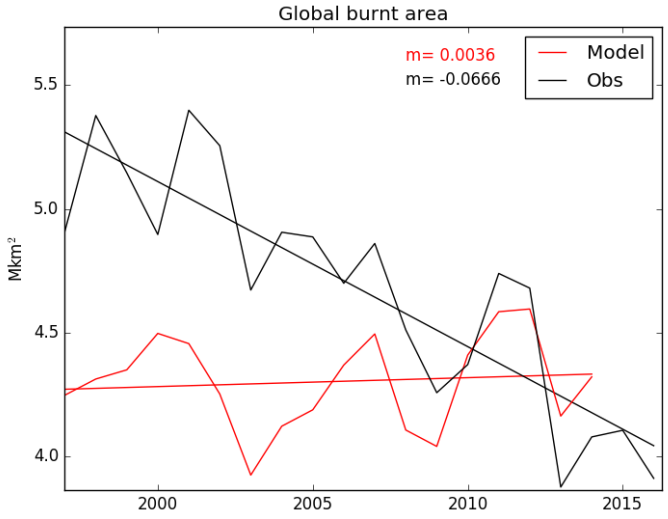

Figure 3.24: Global burned area trend
JULES-INFERNO modelled burned area (Mkm^2) shown in red, with GFED4.1s observations in black. Regression line included for each dataset, with gradient of regression line (m) shown next to legend

Looking in more detail at four key fire-prone regions, we can see that Africa shows the largest decline in the observations (gradient = -0.04), whereas SE Asia shows the smallest decline (gradient = -0.001). JULES-INFERNO projects an increase in burned area in Africa and SE Asia, but correctly captures a decrease in Australia and South America, with the trend in South America modelled reasonably well.

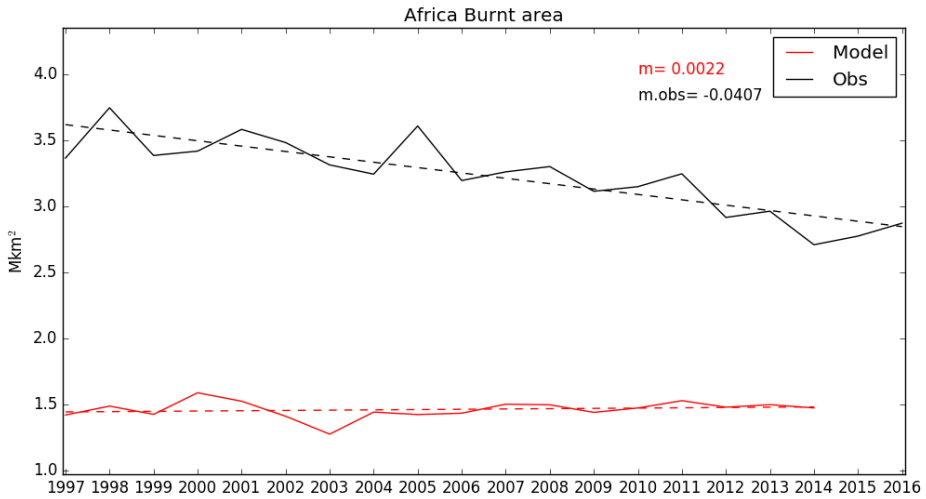
Africa Burnt area
Model
Obs
m= 0.0022
m.obs= -0.0407
Mkm²
4.0
3.5
3.0
2.5
2.0
1.5
1.0
1997 1998 1999 2000 2001 2002 2003 2004 2005 2006 2007 2008 2009 2010 2011 2012 2013 2014 2015 2016

a

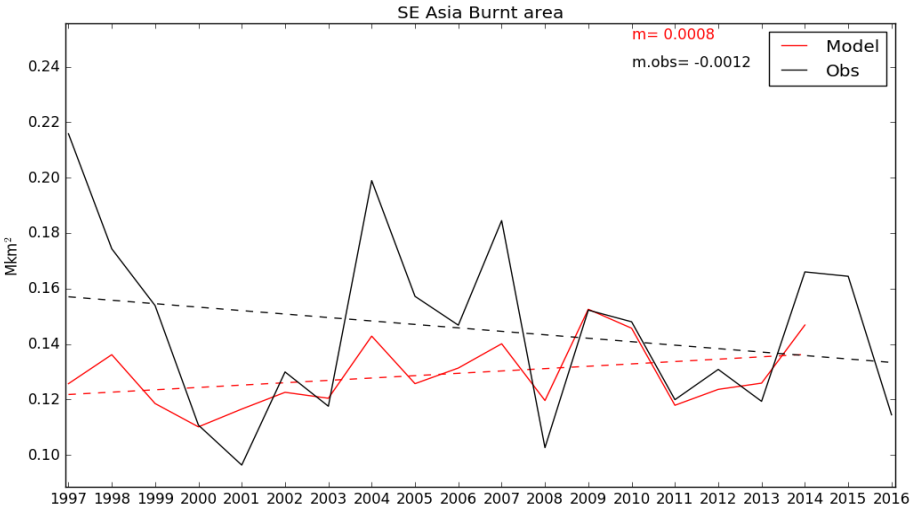
SE Asia Burnt area
Model
Obs
m= 0.0008
m.obs= -0.0012
Mkm²
0.24
0.22
0.20
0.18
0.16
0.14
0.12
0.10
1997 1998 1999 2000 2001 2002 2003 2004 2005 2006 2007 2008 2009 2010 2011 2012 2013 2014 2015 2016

b

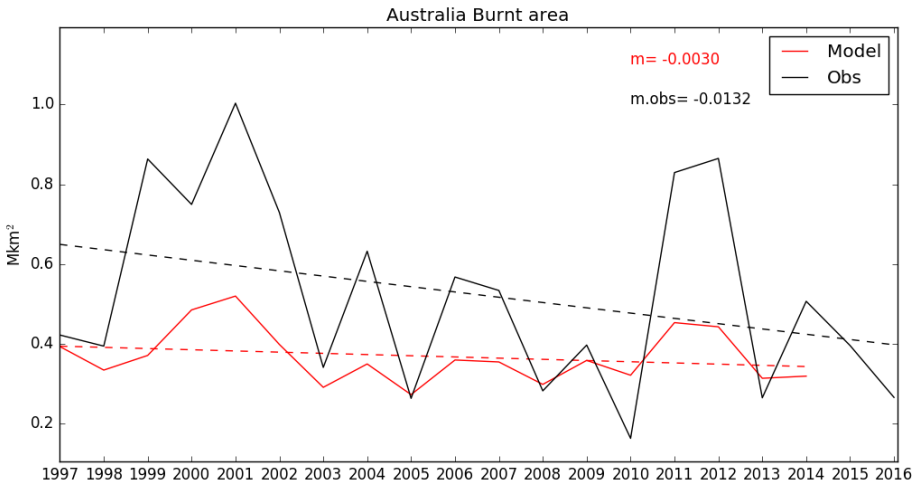
Australia Burnt area
Model
Obs
m= -0.0030
m.obs= -0.0132
Mkm²
1.0
0.8
0.6
0.4
0.2
1997 1998 1999 2000 2001 2002 2003 2004 2005 2006 2007 2008 2009 2010 2011 2012 2013 2014 2015 2016

c

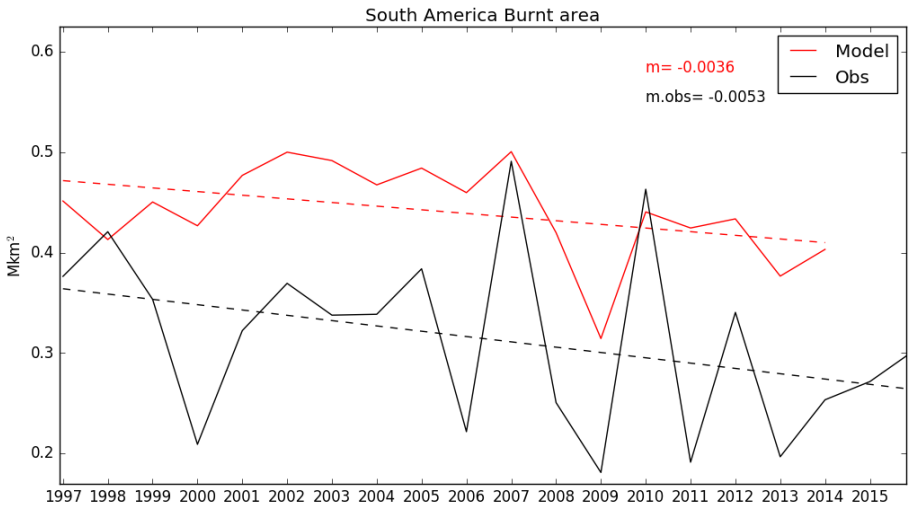

d

Figure 3.25: Burned area regional trends
Burned area trend by region. JULES-INFERNO modelled burned area (Mkm^2) shown in red, with GFED4.1s observations in black. Regression line included for each dataset, with gradient of regression line (m) shown next to legend. Regions as follows: Africa (a); SE Asia (b); Australia (c); South America (d)

The spatial trends are also plotted below, showing the gradient of each regression by gridpoint (Figure 3.26). It is apparent from the observations that there is a strong decline in northern hemisphere (NH) Africa which dominates; there are also declines across the Cerrado region of Brazil, Australia, and northern Asia. Conversely an increase is seen in east Brazil, southern hemisphere (SH) Africa, and the northern high latitude boreal regions. Much of this trend is actually captured well by JULES-INFERNO, including the boreal, Australia, South America and SH Africa. However the increase in east Brazil is not simulated by the model, and although a decrease is simulated in NH Africa, this is outweighed by a simulated increase further north which is not seen in the observations.

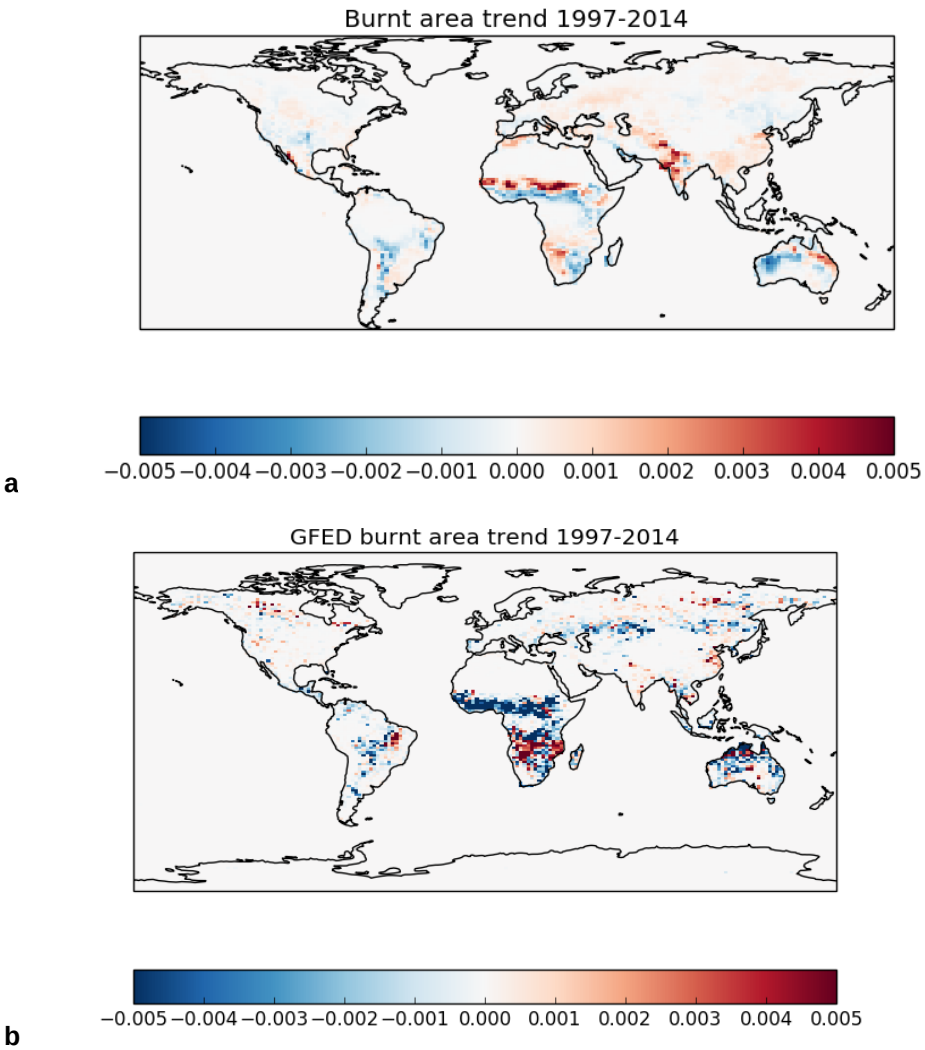

Figure 3.26: Map of trend in burned area
The gradient of the regression over 1997-2014 is plotted for each gridpoint as simulated by JULES-INFERNO (a) and as observed by GFED4.1s (b)

The decrease in burned area has been linked to change in land management practises and human suppression (Andela *et al*., 2017). These factors are not included in the model, and therefore it cannot be expected that these trends would be captured in the current configuration. An important next step to develop the model would therefore be to simulate fire suppression in cropland areas, which would diminish the large signals of increase seen in NH Africa and over India and would likely lead to the correct simulation of an overall decrease in global burned area over last 20 years.

3.2.6 Experimental configuration

JULES Vn4.9 was run here with CRU-NCEP7 forcing data, for climate and CO_2, and land-use ancillaries from HYDE (Hurtt *et al*., 2011; Le Quéré *et al*., 2016)

from 1860 to present day. The harmonised HYDE dataset estimates fractional land-use patterns and underlying transitions in land-use annually for 1500-2100, and is spatially gridded at 0.5° x 0.5° resolution. It does not include impacts of degradation, climate variability, forest management, fire management or pollution on land cover (Hurtt *et al*., 2006). This is then re-gridded for use in JULES at N96 resolution (1.25° latitude x 1.875° longitude).

For the fire experiments, the model was spun-up for 1000 years with fire on using pre-industrial land-use and CO_2 at 1860 prescribed as a climatology. INFERNO was run here with constant natural and anthropogenic ignitions, and interactive fire-vegetation on.

The model was tuned with fire towards a PFT distribution from the European Space Agency Climate Change Initiative (ESA CCI, 2010) observations, using maximum spreading (λ) as LAI_min= 1.0, and the large-scale disturbance term (γ_v) modified as per Table 3.14. Altering LAI_min is a way of increasing the rate of spread of vegetation to account for a known deficiency in the model associated with slow regrowth. The large-scale disturbance of trees has been halved and disturbance of shrub increased by a factor of three to be within the error bars of ESA observations as far as possible.

JULES was configured to the TRENDY set up (Sitch *et al*., 2015) using two experiments: S2 = CO_2 and climate forcing (with land-use constant at 1860, referred to as 'No LULCC'); and S3 = CO_2, climate and land-use forcing, initially not including explicit fire for the purposes of comparison. These two experimental configurations were repeated including the new separate fire term (SF2 and SF3).

3.2.7 Results

Here I present results showing the effect of LULCC and fire on the vegetation in JULES. First, I present global vegetation by PFT to assess the present day spatial distribution of vegetation as a result of LULCC disturbance compared to observations. I then move on to fire disturbance, first reviewing how the new fire disturbance term modelled by the coupled INFERNO model compares to GFED observations of burnt area as validation for the fire model. I then present global vegetation by PFT for fire disturbance and show how this compares to

observations. Finally I show the global distribution of vegetation in the context of observations considering uncertainty bounds.

Without explicit fire or LULCC disturbance, the model produces too much broadleaf vegetation compared to observations, especially over South America and SE Asia (Figure 3.27, second column). Both broadleaf and needleleaf trees are not simulated well in the high latitude boreal regions in JULES, and do not extend far enough across this region, which is not improved by adding disturbance. The introduction of LULCC generally results in a reduction in broadleaf, needleleaf and shrub vegetation, and an increase in C3 and C4 grasses (Figure 3.27, fourth column). This is as expected, with the purpose of this disturbance term being to represent crop area with C3 and C4 grasses. With LULCC, the broadleaf fraction is much improved over South America compared to observations, but is not improved in the high latitude regions. C3 grass is improved with LULCC, but the fraction is still too low, whereas shrub fraction remains too high (also shown in Fig. 5). The bare soil fraction is too high in the model, but the inclusion of LULCC has little effect on this.

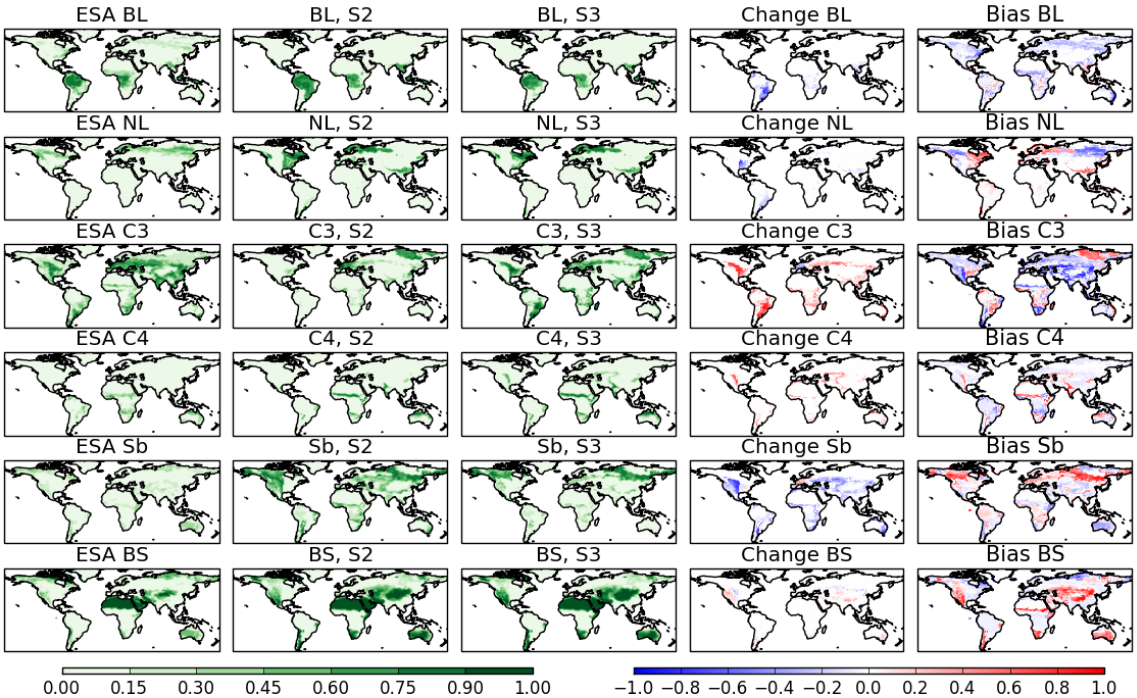

Figure 3.27: Impact of land-use change on present day (2010-2015) vegetation fractions Present day (2010-2015) vegetation fractions for the TRENDY S2 (without LULCC) and S3 experiment (with LULCC) by PFT, without fire, compared to observations. Left column shows ESA CCI observations (2010), second column shows vegetation without LULCC (S2), third column shows vegetation with LULCC (S3), fourth column shows the change resulting from LULCC (difference between column 2 and 3), and right column shows bias of S3 compared to observations (difference between column 1 and 3). BL = broadleaf, NL = needleleaf, C3 = C3 grasses, C4 = C4 grasses, Sb = shrub, BS = bare soil.

Now considering fire, compared to observations of burnt area from GFED 4.1s (including small fires) INFERNO captures the spatial extent and level of fire relatively well (Figure 3.28). INFERNO accurately simulates the areas of high fire occurrence found in GFED4.1s, especially over Africa, northern Australia, South America and SE Asia, although the model also shows high fire occurrence over India which is not seen in the observations (although combining MODIS and ATSR shows high fire counts over India, see Moritz *et al*. 2012 their figure 2).

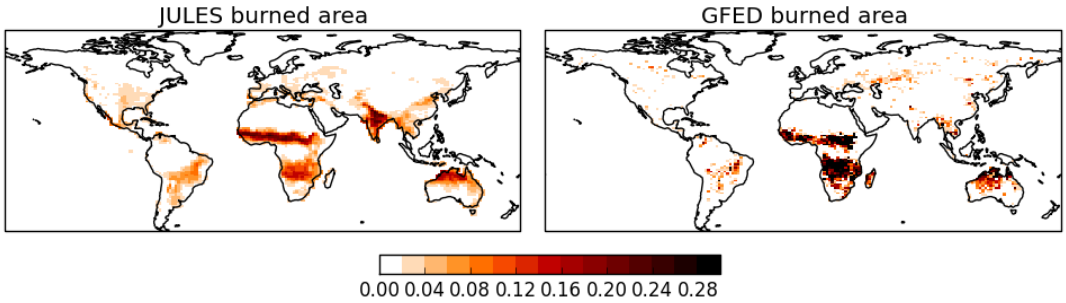

Figure 3.28: Modelled and observed burned area maps
Average 2010-2015 burned area as modelled by JULES-INFERNO (left) and average 2010-2015 burned area from GFED4.1s observations (right)

To explore this in more detail, I assessed the impact of varying population and agriculture in this region. I plotted population data to assess the spatial pattern of population used by the model compared to fire (Figure 3.29), and assessed how fire is modelled in this area with both constant population and variable population (Figure 3.30). There is little difference in the two scenarios, indicating this is not the cause of the high burnt area. I created an agricultural mask based on the input data of agricultural fraction (Figure 3.31) to apply to the fire results in order to assess what fire would look like in the model if only natural areas of vegetation were allowed to burn (Figure 3.32). This is based on the assumption that lands used for farming and agricultural would be managed and any fires that occur would be controlled. A reduction in burnt area was noticeable across all fire-prone regions, indicating this could be a potential for further model developments in the future. It improves the simulation of fire over India compared to GFED observations for example, although on a global scale burnt area is reduced too much in other regions. Here I have used grasslands as a proxy for croplands, which is how land-use is represented in the model as described in section 3.2.4, but in reality this will include a large area of wild grasslands that are unmanaged

and will in fact be subject to fires. This method would not be able to represent fires that are intentionally ignited on agricultural land either, so is a simplistic way of treating agricultural land, but is useful as a first indicator.

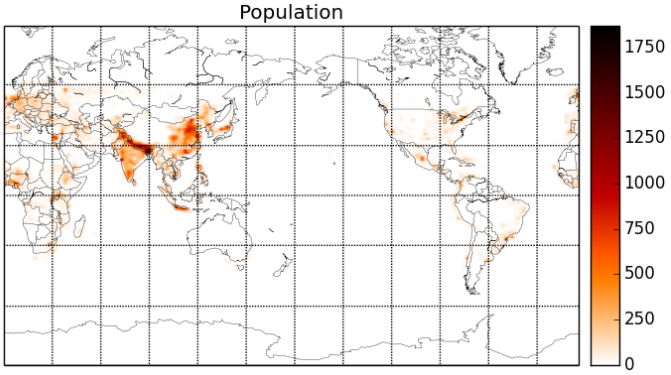

Figure 3.29: Global population data
From HYDE. Used to run JULES-INFERNO

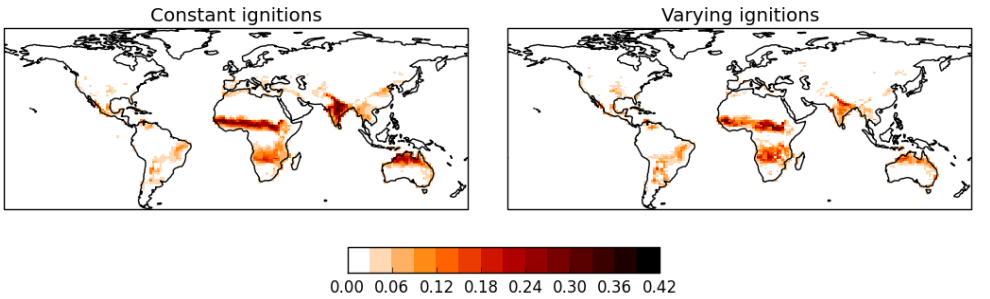

Figure 3.30: JULES burned area
With constant ignitions (left) and varying population and lightning ignitions (right), by gridbox fraction

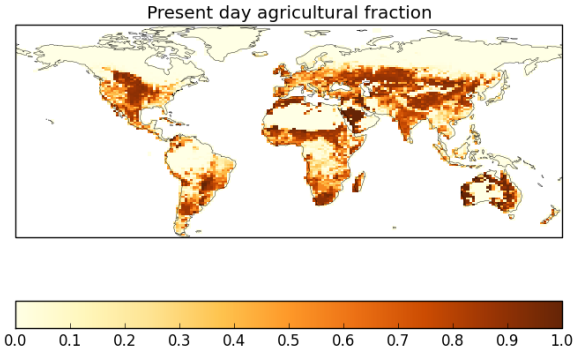

Figure 3.31: JULES present day agricultural fraction based on HYDE

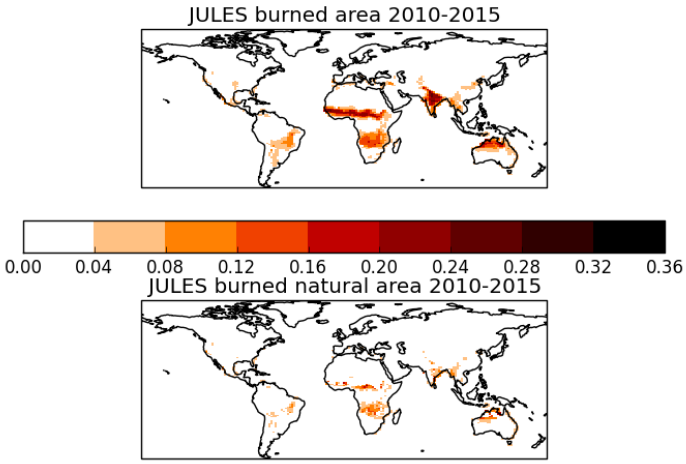

Figure 3.32: JULES natural burned area
JULES burned area including agricultural areas (top panel) and not including agricultural areas (bottom panel) by gridbox fraction

Similarly to LULCC, fire disturbance also improves the representation of vegetation cover. Without explicit fire or LULCC disturbance, the model produces too much broadleaf vegetation compared to observations, especially over South America and SE Asia (Figure 3.33, second column). This is improved over South America with fire (third column), although in other areas fire creates too much disturbance and results in tree fraction being too sparse (notably across Africa). Both broadleaf and needleleaf trees are not simulated well in the high latitude boreal regions in JULES, and do not extend far enough across this region. C3 grass fractions are generally too low compared to observations without fire, and this improves with fire and associated tuning. C4 grasses are fairly well modelled both with and without fire, but the fraction is slightly too high without fire and improved when fire is included. The shrub fraction is too high in the model compared to observations, but this is also improved when fire is included. There is too much bare soil in the model without disturbance, and this increases further with fire. The overall change as a result of fire is generally a reduction in the larger PFTs (broadleaf and needleleaf trees) and an increase in C3 grasses and bare soil (fourth column). Broadleaf trees show a loss in all regions, including the Cerrado region to the south of the Amazon, across the arid regions in Africa, SE Asia, and northern high latitudes. The changes in shrub and C4 grasses are more variable, and are region-dependent. The increase in C3 grass and bare soil reflects the burnt area as modelled by INFERNO (Figure 3.28), indicating a shift towards faster growing vegetation as a result of fire.

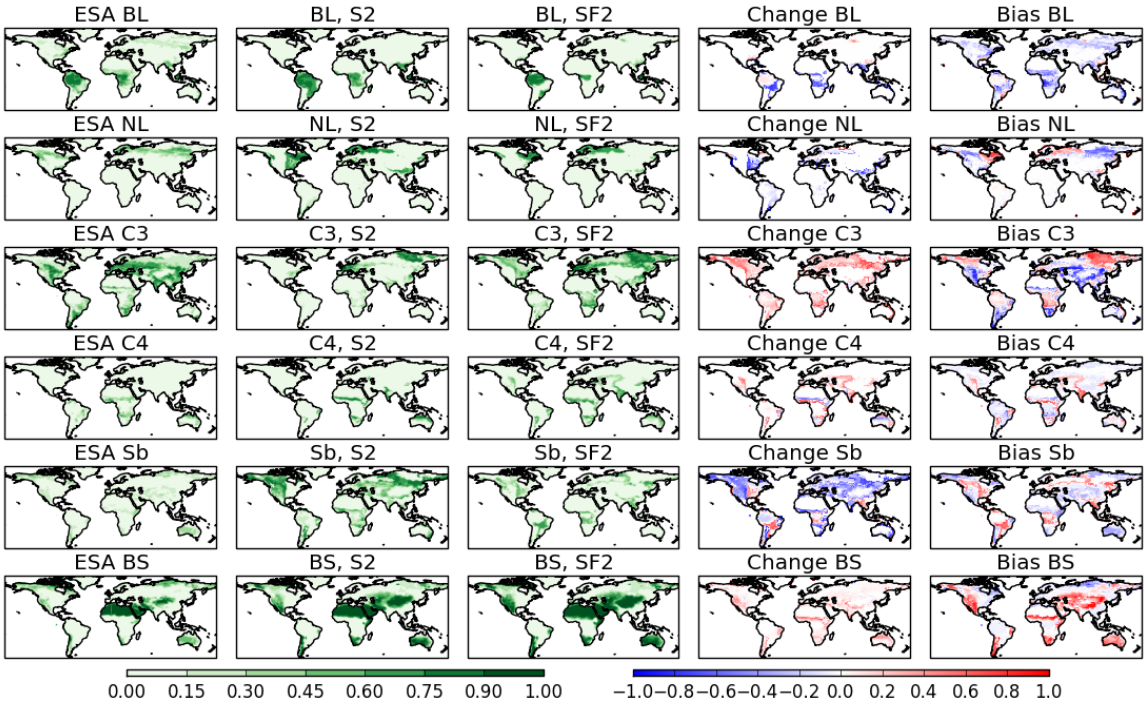

Figure 3.33: Impact of fire on present day (2010-2015) vegetation fractions
Present day (2010-2015) vegetation fractions for the TRENDY S2 experiment (no LULCC, no fire) and SF2 (fire only) by PFT compared to observations. Left column shows ESA CCI observations (2010), second column shows vegetation without fire or LULCC (S2), third column shows vegetation with fire only (SF2), fourth column shows the change resulting from fire (difference between column 2 and 3), and right column shows the bias of SF2 compared to observations (difference between column 1 and 3). BL = broadleaf, NL = needleleaf, C3 = C3 grasses, C4 = C4 grasses, Sb = shrub, BS = bare soil.

Both disturbances together (Figure 3.34) results in over-disturbance in some areas, dominated mainly by the fire response (e.g. broadleaf fractions), but C4 grass and shrub show some improvement when both disturbances are included (see also Table 3.15).

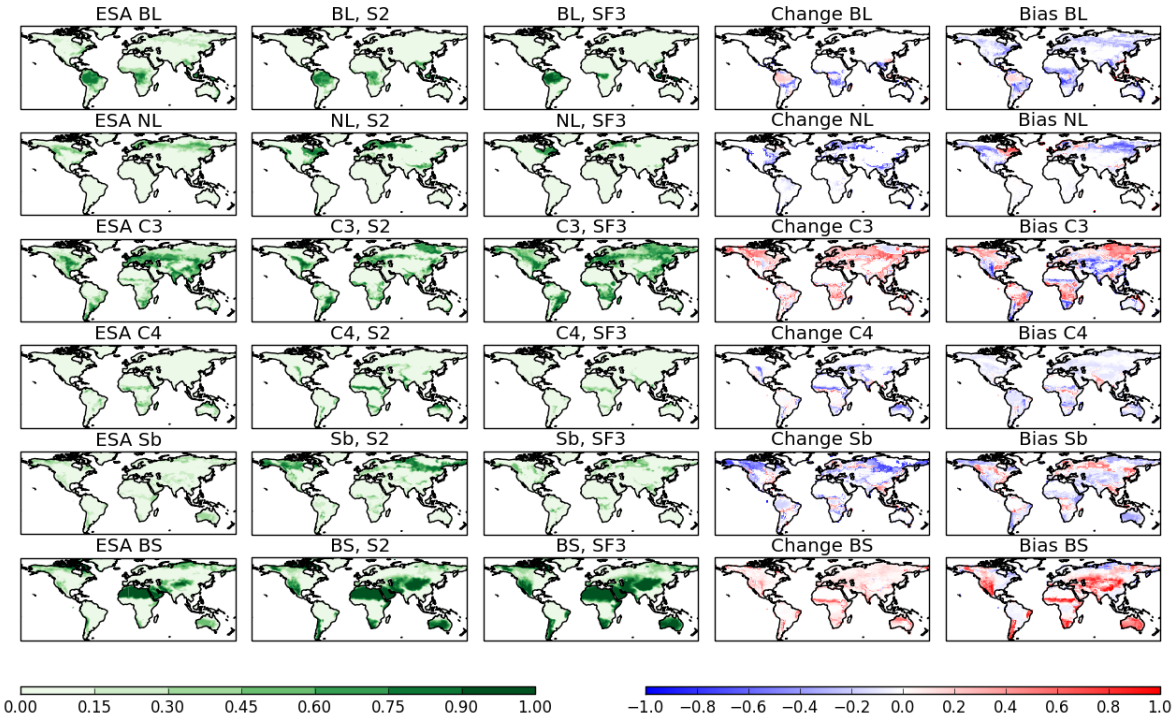

Figure 3.34: Impact of fire and land-use on present day (2010-2015) vegetation fractions Using the TRENDY S3 experiment (with LULCC) by PFT compared to observations. Left column shows ESA CCI observations (2010), second column shows vegetation without fire, third column shows vegetation with fire, and right column shows the change resulting from fire (difference between column 2 and 3). BL = broadleaf, NL = needleleaf, C3 = C3 grasses, C4 = C4 grasses, Sb = Shrub, BS = bare soil

Table 3.15: Total vegetation (percentage) globally
Totals are shown for total tree cover, shrubs, grasses and bare soil, with and without disturbance as labelled. The percentage change between experiments and percentage difference compared to ESA CCI Observations is calculated and shown in the lower rows

Global	**Trees**	**Shrubs**	**Grasses**	**Soil**
S2 no fire (S2)	26.28	23.23	16.52	33.97
S3 no fire (S3)	21.46	14.83	28.91	34.80
S2 + fire (S2F)	16.59	10.57	32.07	40.77
S3 + fire (S3F)	15.08	6.81	37.50	40.61
Observations (Obs)	23.01 (range = 22.06)	10.95 (range = 2.87)	32.94 (range = 3.40)	33.10 (range = 25.56)
% change S2 / S3F	**-42.60**	**-70.69**	**126.95**	**19.54**
% difference S2 / Obs	**13.26**	**71.83**	**-66.38**	**2.60**
% difference S3F / Obs	**-41.61**	**-46.66**	**12.94**	**20.38**

Considering the distribution by vegetation type (trees, grasses, shrubs and soil), in all cases adding disturbance to the model brings the global mean fractions of vegetation closer to observations, although bare soil increases in the opposite trend (Figure 3.35). In the case of trees and shrubs, fire plus LULCC creates too much disturbance, (42% and 47% less coverage than observations respectively), but grasses increase (13% more coverage than observations). Trees are reduced by 43% when both disturbances are included (S2 no fire compared to S3 with fire), shrubs by 71%, and grasses increase by 127% (Table 3.15), taking into account the updated terms for γ_v (Table 3.14). There is an increase of 20% in bare soil with disturbance included. Overall, adding disturbance into JULES reduces the bias of shrubs from 72% to 47%, and grasses from -66% to 13% compared to observations. However there is more variation by biome. In all cases tree fraction is simulated as too low with both fire and LULCC, although the extent of this varies. In some cases shrubs improve (in the temperate and boreal forests), but in others there is too much disturbance (tropics, savanna and temperate grasses). Grasses are generally higher than observations, except for the temperate grasses biome. Both disturbance terms reduce the tree and shrub fractions, and increase grasses and bare soil fractions. In most biomes bare soil fraction is too high compared to observations, except in the tropics and boreal regions where the fraction is well represented compared to observations.

Overall, the inclusion of these disturbance terms within JULES leads to a shift towards grass cover and a reduction in woody PFTs. This is as expected for land-use, which replaces trees with grasses as a representation of crops. The regrowth rates for trees is much slower than for grasses, which spread fast and recover quickly (see section 3), which may be an important factor in the response to fire. With continuous disturbance which varies spatially and temporally now included in the model, the vegetation seems unable to recover trees in some areas, notably around the Cerrado and Congo regions, instead encouraging the growth of grasses in their place.

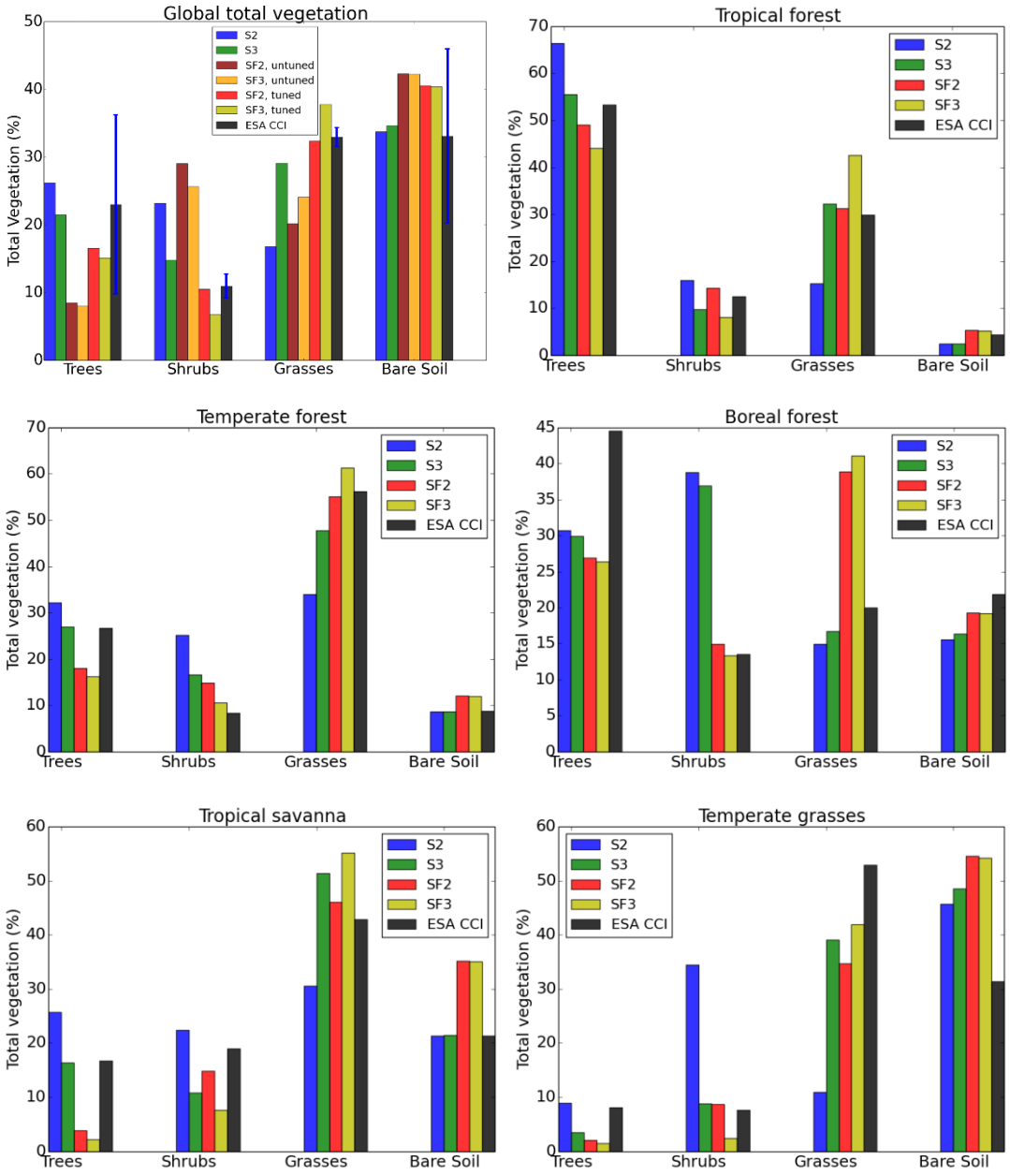

Figure 3.35: Present day (2010-2015) total vegetation (percentage)
Present day (2010-2015) total vegetation (percentage) globally (top left), and by WWF biome (5 out of 8 shown here: tropical forest, temperate forest, boreal forest, tropical savanna, and temperate grasses. Tundra, Mediterranean wood and desert not shown). Trees = total broadleaf and needleleaf trees, grasses = total C3 and C4 grasses. Top left panel includes results prior to tuning, plus uncertainty bars for the observations shown in blue.

As with all observational datasets, there are uncertainties associated with retrieving observations of land cover and the classification of these into a small number of plant functional types. The observations used here are from ESA CCI, which have been processed into the 5 PFTs used by JULES so as to be

comparable with the model output (Hartley *et al*., 2017), introducing a range of possible values for each vegetation type (Figure 3.36). The representation of vegetation distribution is further complicated by the seasonal variation, where peak growing season will have higher fraction of vegetation than low season, and high fire-risk areas will show burnt area as high bare soil in peak fire season. These uncertainties give a range of potential vegetation cover, and the developments to the representation of disturbance in JULES described here have been tuned to give reasonable distribution within this range of uncertainty as far as possible. The 'best estimate' of vegetation cover from ESA, known as the reference case, is otherwise used for comparison (see section 1.3.3 for more information).

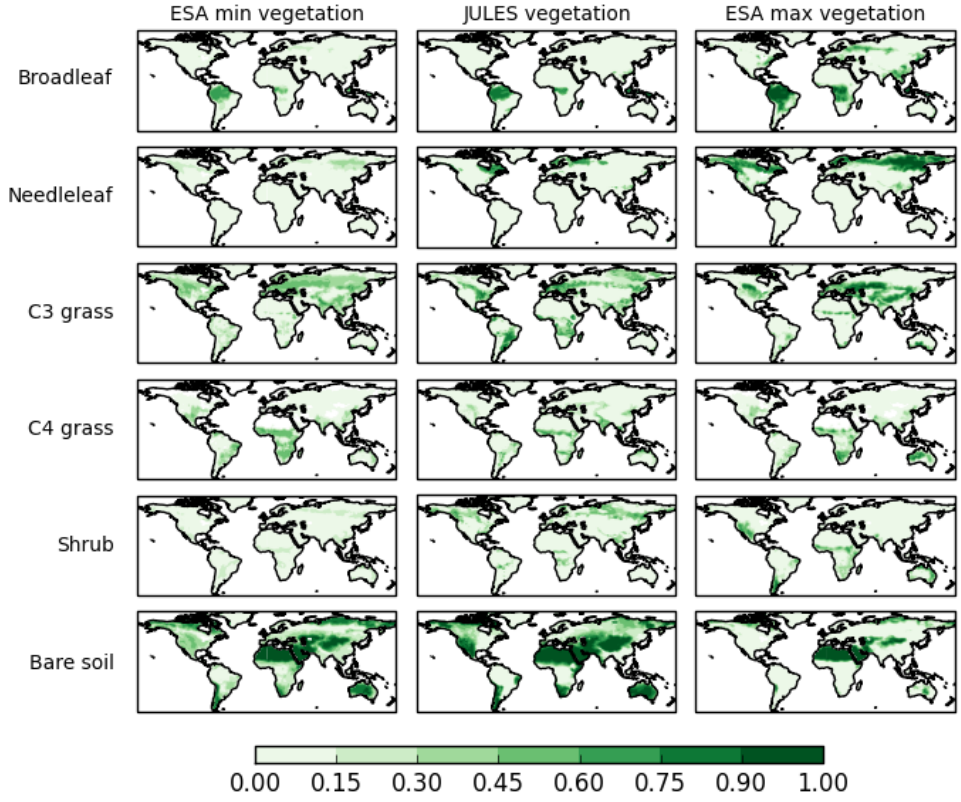

Figure 3.36: ESA Uncertainty range compared to JULES vegetation
ESA CCI minimum (left column) and maximum (right column) vegetation for each PFT within JULES. Central column shows present day (2010-2015) vegetation fraction as simulated by JULES with LULCC and fire. BL = broadleaf, NL = needleleaf, C3 = C3 grasses, C4 = C4 grasses, Sb = Shrub, BS = bare soil

As discussed in section 1.3, there is also variation across observational products and to understand how this relates to the results shown here I now consider two

other products: the WWF biomes and vegetation carbon from Avitabile *et al*. (2016).

The WWF biomes and ecoregions used in Figure 3.35 is shown here (Figure 3.37). This categorisation shows a small region of tropical forest across the Congo region, surrounded by a large area of savanna which represents trees and grasses. This is more in line with the simulations as modelled by JULES when fire is added, and agrees more with the minimum vegetation of the ESA CCI projections. This is a key point for the modelling of vegetation, where in many cases there are different classifications of the same area of vegetation within observations.

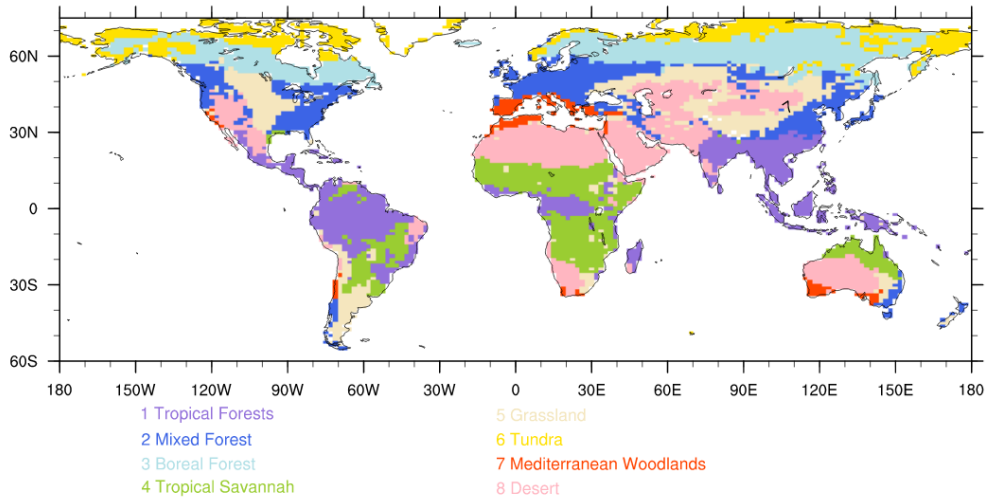

Figure 3.37: WWF biomes and ecoregions
Major global biomes based on 14 World Wildlife Fund's ecoregions. Some ecoregions have been combined to reduce the total number to 8: Tropical forests = all tropical and subtropical forests plus mangroves; Mixed forest = temperate broadleaf and mixed forests plus temperate conifer forests; tropical savannas = tropical/sub-tropical grasslands, savanna, and shrubland; Grassland = temperate grasslands, savannas, shrublands, flooded grasses, montane grasses. Reproduced from Harper *et al*. (2016), Figure 3b.

NASA's Socioeconomic Data And Applications Centre (SEDAC) use this information to produce raster data of land cover, within the 'Population, Landscape, And Climate Estimates' (PLACE) map V3 series (CIESIN, 2012)[24]. Their biome map of Africa shows good agreement with the simulation of tropical forest and savanna produced by the JULES model when fire is included (Figure 3.38). The area covered by forest is larger when fire is not included, and this is

[24] NASA PLACE maps: http://sedac.ciesin.columbia.edu/data/set/nagdc-population-landscape-climate-estimates-v3/maps?facets=region:africa

replaced by savanna when fire is included as a separate process. This is considered also for South America – see section 3.3. The model does show desert (bare soil) extending too far south compared to PLACE vegetation however.

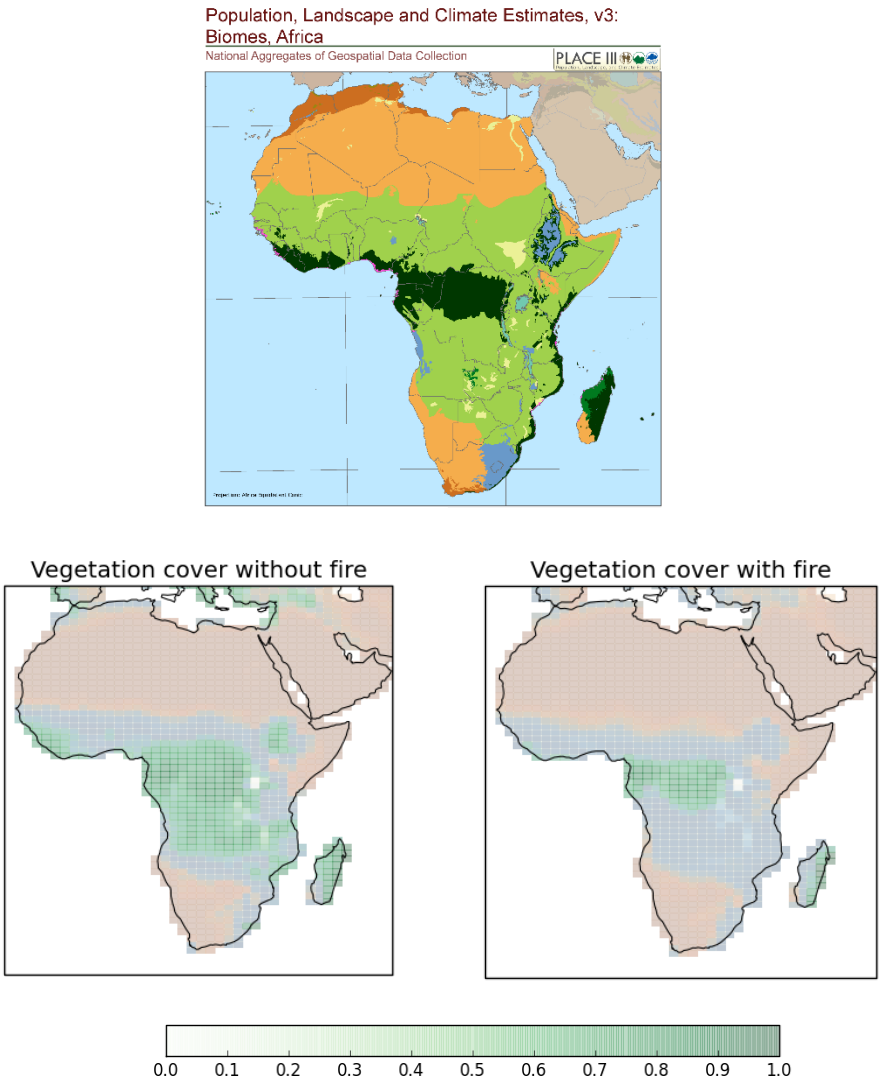

Figure 3.38: Vegetation cover over Africa
Vegetation cover from NASA's PLACE (CIESIN, 2012) biome map of Africa (top): Dark green = moist broadleaf forest, light green = grasslands, savannas, and shrublands, orange = desert and semi-deserts. Vegetation fraction in Africa as simulated by JULES (bottom row), without fire (left) and with fire (right), with no land-use change: Green= tropical broadleaf forest, blue = grasses and shrubs, brown = bare soil. Colour bar shows fraction of tree vegetation; grasses and soil fractions are not shown but use the same scale in blue and brown respectively.

I also compare the vegetation carbon as modelled by JULES with the Avitabile product, to show again that the dense vegetation carbon is spatially well-captured when fire is included in JULES (Figure 3.39).

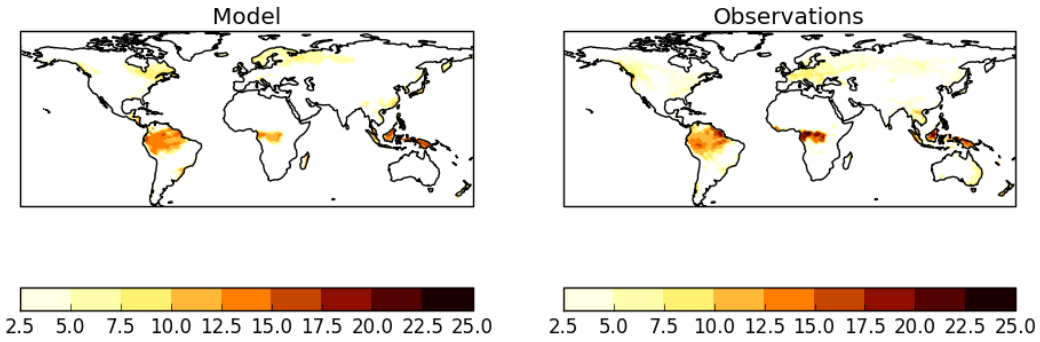

Figure 3.39: Avitabile aboveground biomass
Vegetation carbon (kg m^{-2}), as modelled by JULES-INFERNO (left panel) and observations from Avitabile *et al*. (2016) (where vegetation carbon is taken as half total biomass)

Here we can see that although there are some some differences between model output and the ESA CCI land cover product, other products show better agreement with the land cover as simulated with JULES-INFERNO.

Overall there is a shift towards increased grasses (127%) and a reduction in trees (43%). The regrowth rates for trees is much slower than for grasses, which spread fast and recover quickly (see section 3.2.3.1), which may be an important factor in the response to fire. With continuous disturbance which varies spatially and temporally now included in the model, the vegetation seems unable to recover trees, instead encouraging the growth of grasses in their place.

3.2.8 Discussion

Fire and land-use are important global disturbances, and the results presented here have shown that when considered, they have a significant impact on the modelled vegetation as represented by JULES. In all cases, including disturbance brings the vegetation fractions closer to the observations compared to no disturbance, although in some cases there is a tendency towards over-disturbance when both fire and LULCC are included, and bare soil increases too much compared to observations. Disturbance generally improves the simulation of shrubs and grasses, but tree fractions are often simulated as too sparse. LULCC mainly decreases trees and shrubs and replaces them with C3 and C4 grasses (representing crop and pasture). Fire creates a more mixed response, decreasing vegetation in the boreal regions and high burned areas, and showing an increase in grasses. Both fire and LULCC reduce the larger woody vegetation

types such as trees and shrubs when added to the model (Figure 3.33 and Figure 3.27). Without the inclusion of fire, this could result in an over-estimation in the amount of carbon released due solely to LULCC, which may have significant impact on carbon budgets.

Previous work has shown that fire may be an important contributor to the existence of savannas (Cardoso *et al*., 2008; Bond et al., 2005; Staver *et al*., 2011). The results shown here support this conclusion, showing that when fire is included in the model there is a shift towards open savanna-like states in areas that climatologically could support trees without the incidence of fire, including the Cerrado area of South Brazil, and savanna areas in Africa. Here we have shown that a large savanna region in South America is completely forested in the model without the addition of fire or anthropogenic LULCC.

It should also be noted that here I have used the ESA CCI dataset as observations. Different observational products may give different results for vegetation cover; for example the 'Population, Landscape, And Climate Estimates' (PLACE) maps V3 from NASA's Socioeconomic Data And Applications Centre (SEDAC) biome map of Africa (CIESIN, 2012), based on the WWF biomes, indicates a much larger area of 'Grassland, Savannas and Shrubland' over Africa than the ESA CCI dataset, which is approximately equal to the area modelled by JULES when fire is included (see section 1.3). However, it is important to consider regional improvements or degradation as well which can be masked in global scale analyses. It also suggests that there may be some overlap in the disturbances, which reflects the complicated nature of how fire and LULCC are often used together for land clearance. The HYDE LULCC dataset in this study has been developed from a combination of model, satellite and historical reconstructions of agricultural and population data, and the biomass quantities are noted to contain uncertainties due to lack of direct observations from the historical period (Hurtt *et al*., 2011). Some of what has been attributed to LULCC may include fire clearance, which is a key point for consideration for other DGVMs including fire and land-use together.

When interactive fire was initially added to JULES, there was a tendency towards complete dominance by shrubs and significant tree reduction. This was tuned to the observations by increasing the general disturbance term (γ) and increasing

spreading (λ) (section 3.2.4), to account for the fact that fire was previously included in the total mortality rate. Grasses spread and recover quickly with TRIFFID, whereas larger PFTs take longer to re-establish. On this timescale the tree cover is not able to recover fast enough with constant disturbance from fire, and the results indicate that fire restricts tree growth and encourages a shift towards the more responsive vegetation types. Grasses can be given a higher mortality rate to prevent over-growth, but this has been tested and results in too much bare soil for this reason. As the carbon is unable to regrow into trees, and prohibited from re-growing in shrubs and grasses, it is then transferred into the soil pools leaving larger areas of bare ground. This was evident in the various tuning tests; when fire was introduced, the trees were kept low giving very high levels of grass and shrub growth. When these were also reduced, the bare soil increased. This was the case even when fire was reduced in certain PFTs (by reducing the average burnt area by PFT), indicating that the physical properties of the model do not allow regrowth in areas that are constantly disturbed, unless disturbance ceases. The fractions were low from the start of the run (1860) as fire was included in the spin-up, and the vegetation does not recover through the transient simulation due to continual disturbance, leading to present day levels being low.

These results point to a need for faster regrowth of trees within TRIFFID to cope with disturbance, for example by representing age or mass classes within each PFT to enable a range of successional stages to be represented. It is also worth noting that the fire disturbance is high in the model compared to observations in some areas (Figure 3.28), which may lead to too much disturbance overall. In addition, there remains significant underlying complexity around the interaction of LULCC and fire as discussed in section 3.2.2. For example, agricultural land in some regions may be a cause of fire ignition, whereas in other areas may act as a fire break or generate anthropogenic fire suppression, and future development would benefit from reducing burnt area in cropland areas (Bistinas et al., 2014). One way forwards for this could be to identify the average field size based on surrounding vegetation, and mask fire in larger agricultural regions, but allow smaller fields to include the probability of burning. There will also be additional complexity around the PFTs themselves, where some species will be more fire resilient than other species, for example vegetation in high fire-risk

areas often develops thicker bark for protection from fire, whereas other species may adapt to the fire and use it as a method of reproduction (Pellegrini *et al*., 2017), and this should also be a priority next step for further model development. This may also help the problem of over-disturbance in tree fraction. Finally, we have just considered two of the main disturbances here. We have not considered windthrow, pests, and diseases etc, which for now are still aggregated into the generic large-scale disturbance term in JULES.

Overall there are still a number of regions that require improvement in the simulation of vegetation. In all of the JULES simulations there are too few needleleaf trees across the boreal regions compared to observations. With fire, notably the trees across the extratropics and savanna regions such as the Congo region in Africa is too low compared to ESA mean observations (although are more in agreement with other observational datasets). The representation of just five PFTs is a considerable simplification of the real world, and further work could develop these configurations into the 9 PFT set up by Harper *et al*., (2016). In particular, recent work has shown that the distinction between evergreen and deciduous needleleaf trees has led to an improved representation of boreal forests within JULES which could improve these simulations (Harper *et al*., 2018a). However we now have improved modelling capability and complexity, enabling us to represent more processes around the interaction of fire and vegetation, and which gives us the ability to model future changes. It is often the case that when new processes are added to a model it may result in some degradation, but the increase in capability is pushing the frontiers of current scientific modelling ability which is crucial for continued development. The new interaction of fire and vegetation has been included here without any major global degradation of vegetation cover, which is a significant advancement, and an important step towards coupling to other aspects of the Earth system.

3.2.9 Conclusion

This work has described the first steps in developing the land surface model JULES to represent fire as a separate disturbance, alongside LULCC. The disturbances contribute significantly to changes in vegetation on a global scale. Without disturbance JULES simulates too much vegetation in most PFTs compared to observations, which is generally improved with the addition of fire

and LULCC, although there is still regional variation. Disturbance generally has the effect of decreasing tree cover (43%) and shrubs (71%) and increasing grasses (127%). In places the disturbance is too high with both fire and LULCC and leads to vegetation being reduced too much. The regrowth rates in TRIFFID also mean that with constant disturbance from fire, there is a shift towards faster growing PFTs that can recover and spread quickly. The simulation of shrubs and grasses is much improved, with the bias reducing from 72% to 47%, and from 66% to 13% respectively. It is expected that fire danger will increase in the future with climate change as a result of hotter, drier conditions, but fire occurrence depends heavily on the interaction with LULCC. The developments to the model that have been outlined here now give the capability to model future interactions between fire and LULCC and the impact that this could have on future vegetation density, spread and carbon storage. Overall we have presented results for an improved representation of mechanistic processes of disturbance in JULES using a non-optimised approach, with positive results to vegetation cover. This is a significant first step in the representation of highly complex factors surrounding anthropogenic and natural disturbances in the model, and lays the foundation for future developments into Earth System Models.

3.3 Implications for Brazil

3.3.1 Introduction

Until now fire has not been represented as an explicit disturbance process in JULES. The implications of developing JULES to include this new process for vegetation distribution globally has been assessed in the previous section, and now I will focus on the implications for South America, and specifically the Amazon region in Brazil. The south east area of the Amazon is of particular interest as discussed in Chapter 1, because this ‘arc of deforestation’ is vulnerable to land-use change, and is climatically warmer and drier than the rest of the Amazon and so may be more prone to fire.

As previously discussed, most fires that occur across the Amazon are not naturally ignited from lightning, but depend on human ignitions and will only take hold when the climatic conditions and fuel are dry enough. The Amazon forest is dense and humid with high annual rainfall, and is made up of large tropical

evergreen vegetation. This makes it difficult for fires to ignite and to spread. Contrastingly, the area to the south of the Amazon forest has quite different qualities. The Brazilian Cerrado is a savanna ecosystem, climatically very different to the Amazon tropical forest biome, which supports entirely different vegetation, soils, and fire regimes. The vegetation ranges from open grasslands to sparse woody vegetation, and precipitation is lower (see Figure 1.4).

Fire can be the determinant factor in maintaining savanna vegetation in ecosystems that could otherwise support forest cover, including the Brazilian Cerrado (Moreira *et al*., 2000). Work by Staver *et al*. (2011) and Hirota *et al*. (2010), has shown that fire is an important contributor to the existence and creation of savannas. They used tree cover, climate, fire and soil data to show that on a global scale climate influences tree cover, but where climate is average (mild seasonality and intermediate rainfall), fire is the determinant of forest cover verses savanna, and that these can be alternative stable states over the Congo and Amazonia. Fire can act as a positive feedback, whereby fire suppresses the development of trees, and low tree cover provides more conducive fire conditions (see Figure 1.2). They argue that the expansion of savanna ecosystems probably occurred in a drier period in Earth's history, the Miocene 20 million years ago to 5 million years ago, at a time before humans began altering the landscape and as a result of a self-reinforcing fire-shaped landscape the savanna areas remain today even though climatically they could now support forests. This raises the question of whether we see evidence to support the theory of a fire-created savanna in Brazil in the JULES model, which I will address in this section.

3.3.2 Methods

To understand whether fire or land-use is a key driver in the evolution of the Brazilian Cerrado, I conduct four experiments with the coupled JULES-INFERNO model: 1) No disturbance, 2) only fire disturbance, 3) only land-use disturbance, 4) both fire and land-use disturbance. For each experiment the model is spun-up separately, with fire on for experiments 2 and 4, and without fire for experiments 1 and 3.

I use the same model set up as before, running JULES Vn4.9 with CRU-NCEP7 forcing data for climate and CO_2, and land-use ancillaries from HYDE (Hurtt *et al*. 2011), and new parameters for disturbance as described in Table 3.14. S2 again

refers to the CO_2 and climate forcing experiment (with land-use constant at 1860, referred to as 'No LULCC'), and S3 refers to the full CO_2, climate and land-use forcing experiment. TRIFFID is used to simulate dynamic vegetation in each scenario.

3.3.3 Results

I present the results of change in broadleaf fraction over the historical period to present day (1860-2015) over the South American continent, for each of the four experiments alongside a map showing the WWF classification of ecoregions. With no disturbance, forest extends right across Brazil joining the Amazon forest and the Atlantic forest, with no representation of the Cerrado (Figure 3.40, first column). It is only by prescribing land-use for the historical period that the Cerrado is represented, and this only changes from 1960 onwards (third column). When the new dynamic fire process is added, the model correctly simulates the Amazon forest as distinct and separate to the Atlantic forest, leaving the Cerrado region as a mix of shrub and grassland (second column). The Cerrado region is simulated mainly as shrub without any land-use (Figure 3.42), and with land-use this changes to be largely grassland from 1960 onwards which is more reflective of observations from ESA (Figure 3.41). This area is made up of a high proportion of agricultural land, which is simulated in JULES as grasses, but will also include shrubs and woody vegetation to make up the mixed-vegetation of the Cerrado (Ferreira and Huete, 2004). Another point of note is the simulation of the Atlantic forest. With land-use change (S3), at present day this is simulated in the model as a small area of forest, and predominantly grassland. Without land-use change (S2 + fire) the Atlantic forest is simulated more as broadleaf forest. Compared to the WWF biome map, the land-use change is too high in this area.

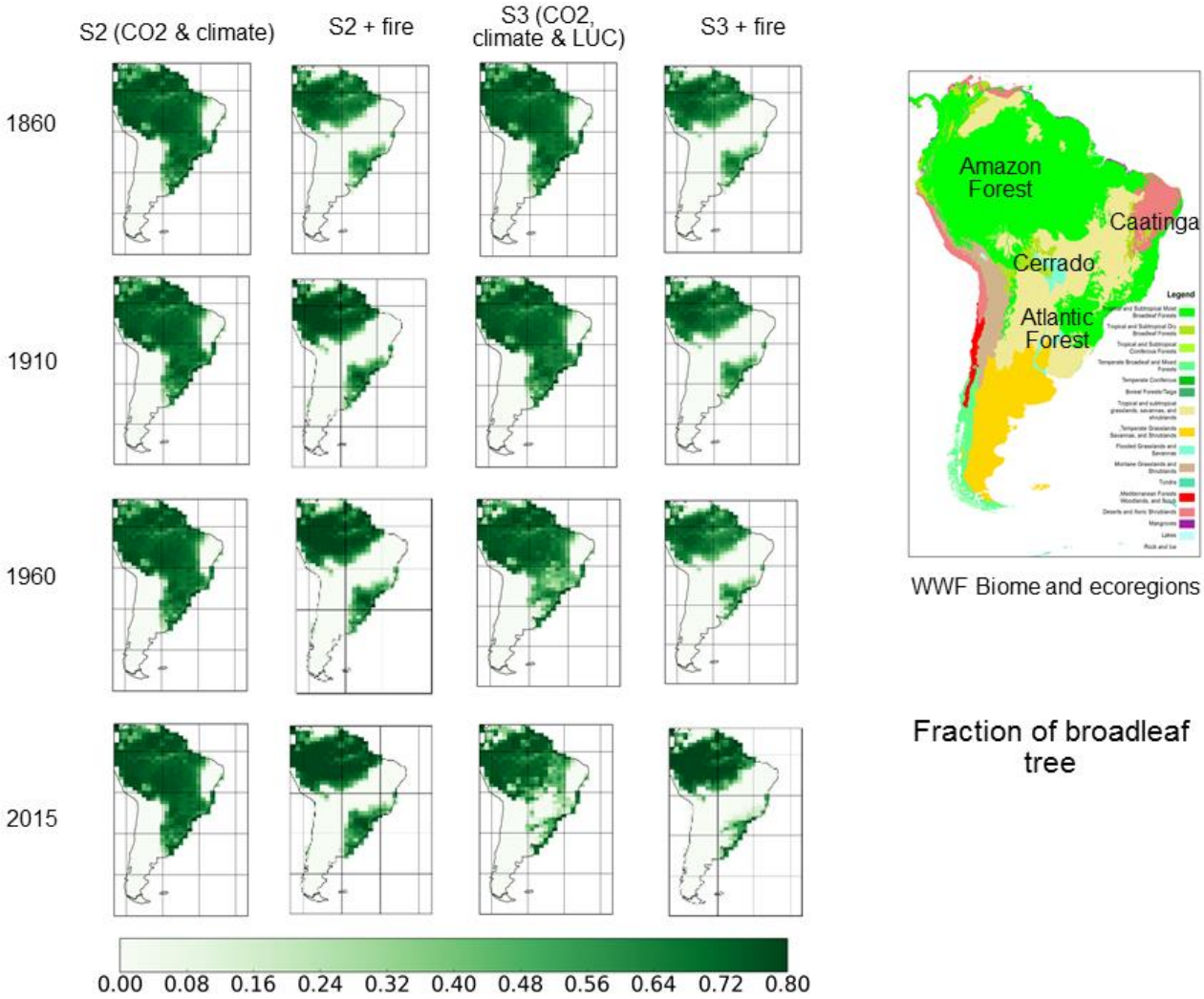

Figure 3.40: Fraction of broadleaf vegetation across South America
From 1860 to present day (rows). Columns from left to right show S2 (varying CO_2 and climate change), S2 with interactive fire, S3 (varying CO_2, climate change and land-use change), and S3 with interactive fire in JULES. Right panel shows WWF biomes and ecoregions

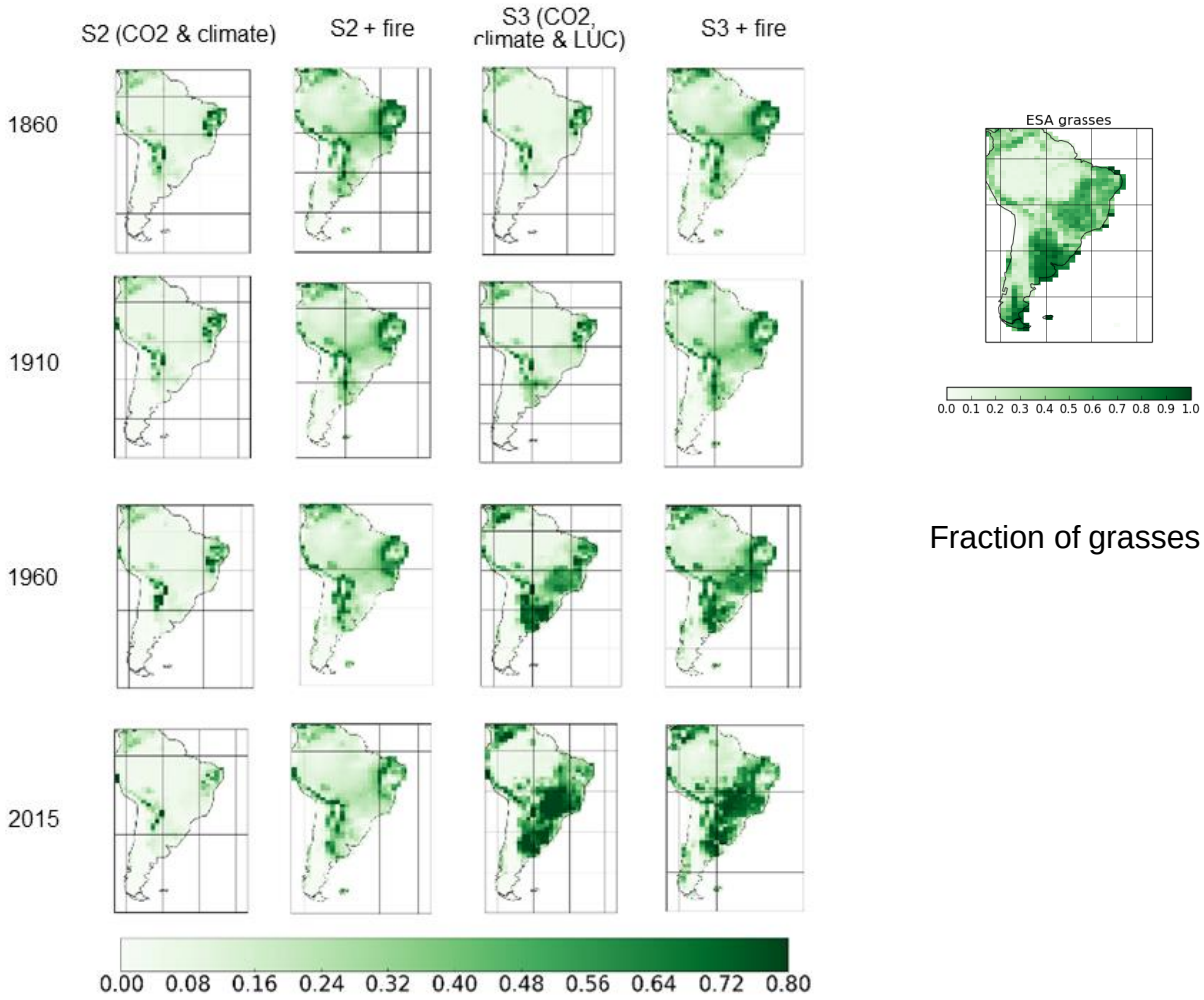

Figure 3.41: Fraction of grasses across South America
From 1860 to present day (rows). Grasses include C3 and C4. Columns from left to right show JULES S2 (varying CO_2 and climate change), S2 with interactive fire, S3 (varying CO_2, climate change and land-use change), and S3 with interactive fire. Right panel shows ESA grass fraction

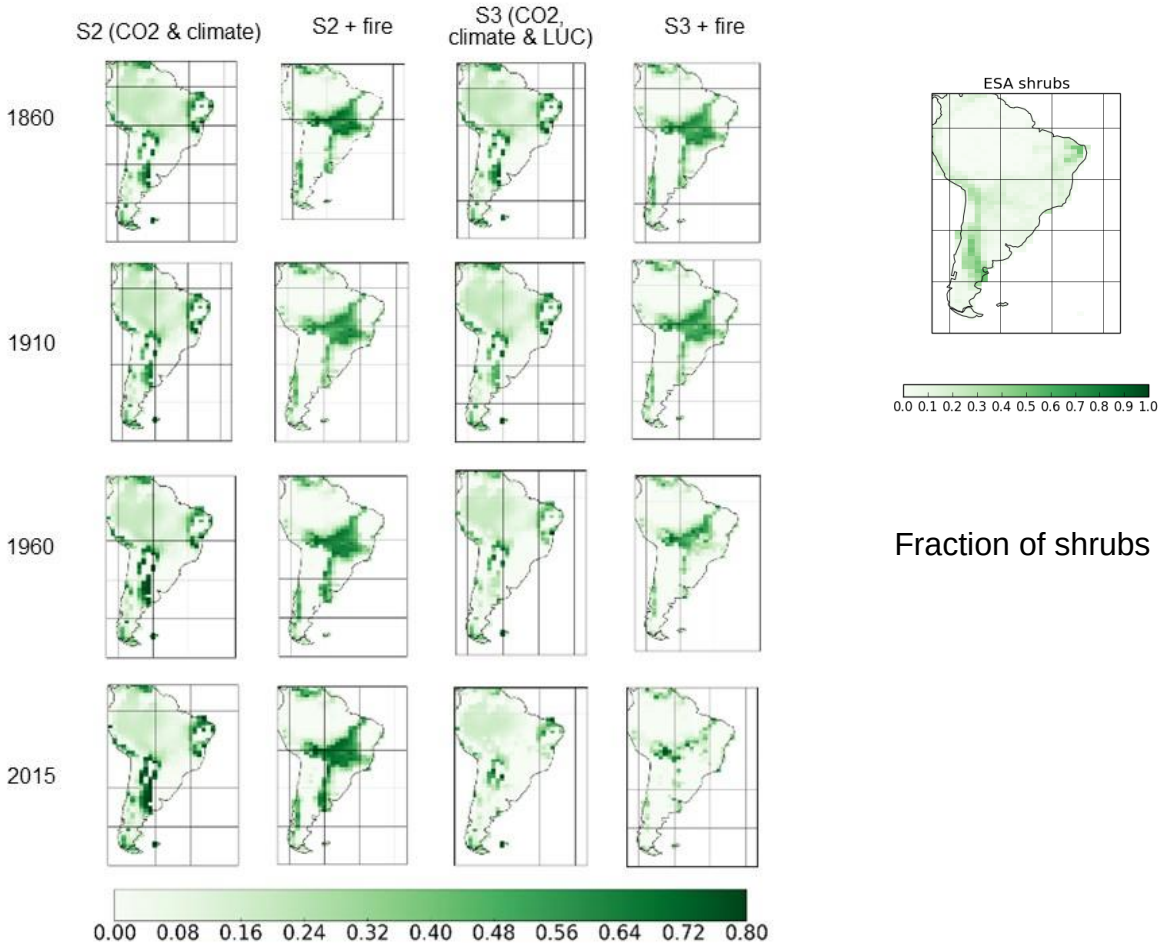

Figure 3.42: Fraction of shrub across South America
From 1860 to present day (rows). Columns from left to right show S2 (varying CO_2 and climate change), S2 with interactive fire, S3 (varying CO_2, climate change and land-use change), and S3 with interactive fire in JULES. Right panel shows ESA grass fraction

To understand the role of land-use and fire in determining the carbon flux by ecoregion in Brazil, I calculate the Net Biome Productivity (NBP) for the S2 (no land-use change) scenario, the S3 (with land-use change) scenario, and the difference between the two, without fire and with fire. NBP is calculated as Net Primary Productivity (NPP) minus soil respiration and wood product emissions from land-use change. With the new interactive vegetation-fire capability, we can now also include the role of fire, so NBP becomes NPP minus soil respiration, wood product emissions and fire emissions. NBP is a measure of the net carbon accumulated in an ecosystem and can therefore be a useful indicator of the change in the carbon sink. A positive NBP represents an overall carbon uptake, or 'carbon sink', whereas a negative value of NBP indicates an overall source of carbon. Here 'gross carbon uptake' represents the S2 scenario without land-use,

and the ‘net carbon uptake’ represents the S3 scenario with land-use, so that the ‘land-use contribution’ is S3-S2.

Without fire, the land-use emissions are relatively high, especially in the Cerrado region (Figure 3.43, bottom left plot), compared to SEEG (System for Greenhouse Gas Emissions and Removals Estimates) emissions data from Brazil (Figure 3.44). When fire is accounted for, the emissions from land-use are smaller in each ecoregion, and especially for the Cerrado, followed by the Amazon and the Pantanal. This is an important result; without fire processes included in the model, anthropogenic land-use (deforestation) is required to achieve the correct extent of forests across Brazil, resulting in very high land-use emissions from the Cerrado region. When fire is included, the model simulates the savanna region as a natural biome, and the land-use emissions from this region are reduced.

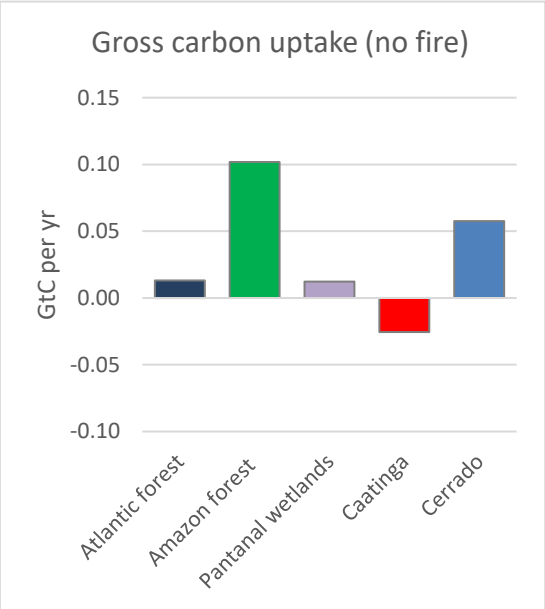

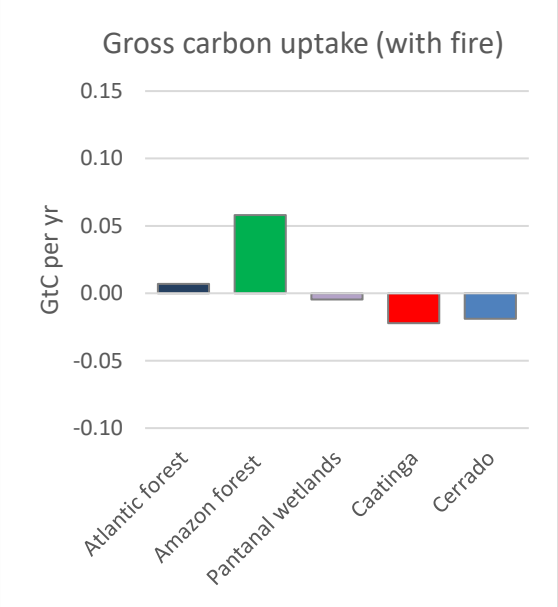

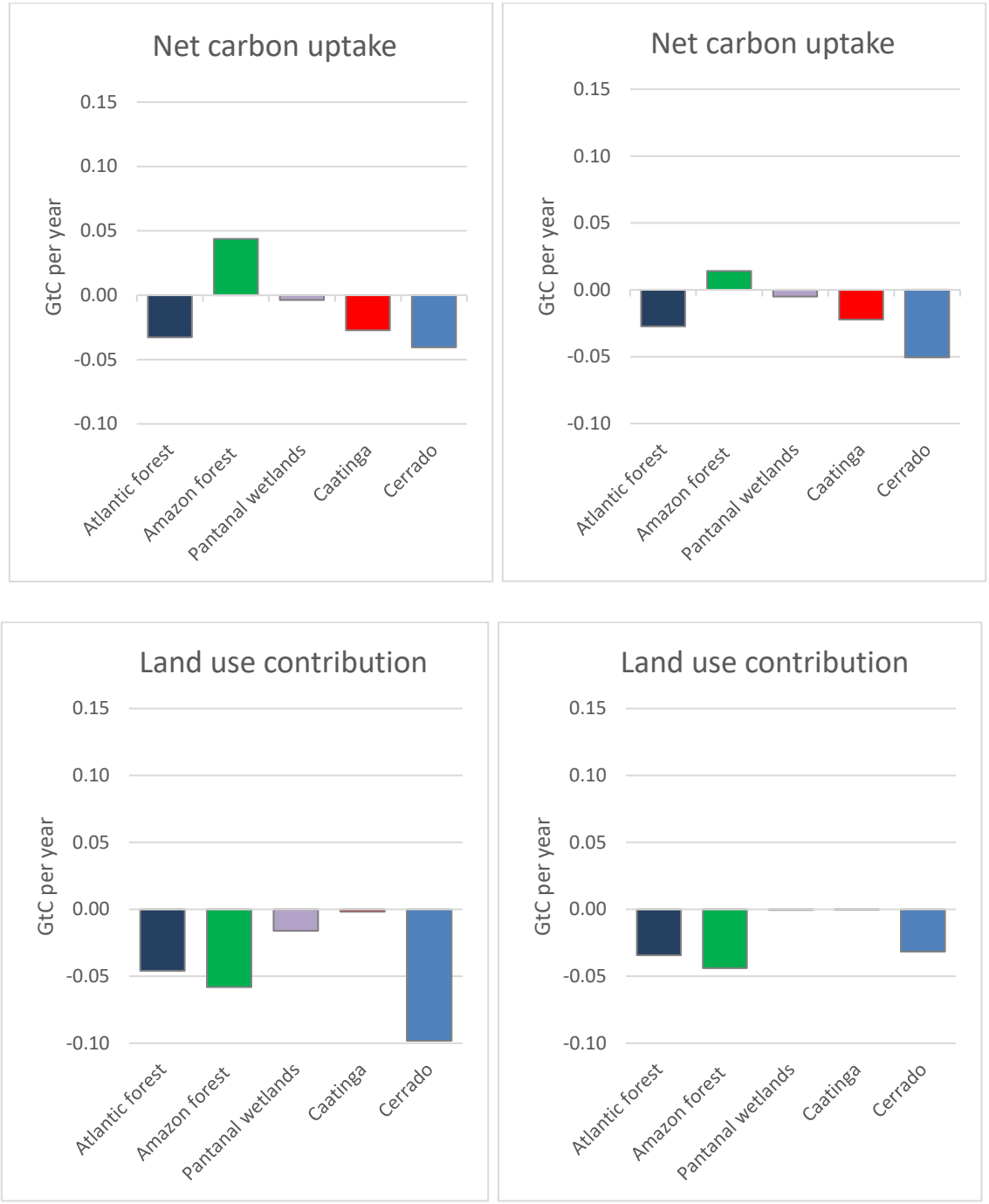

Figure 3.43: Carbon flux by ecoregion, Brazil
Carbon flux (NBP, GtC per year) in JULES by ecoregion for Atlantic forest, Amazon forest, Pantanal wetlands, Caatinga and Cerrado, 1990-2015 mean. Top row shows gross carbon uptake (S2 scenario, no land-use), middle row shows net carbon update (S3 scenario, with land-use), and bottom row shows contribution of land-use (S3-S2).

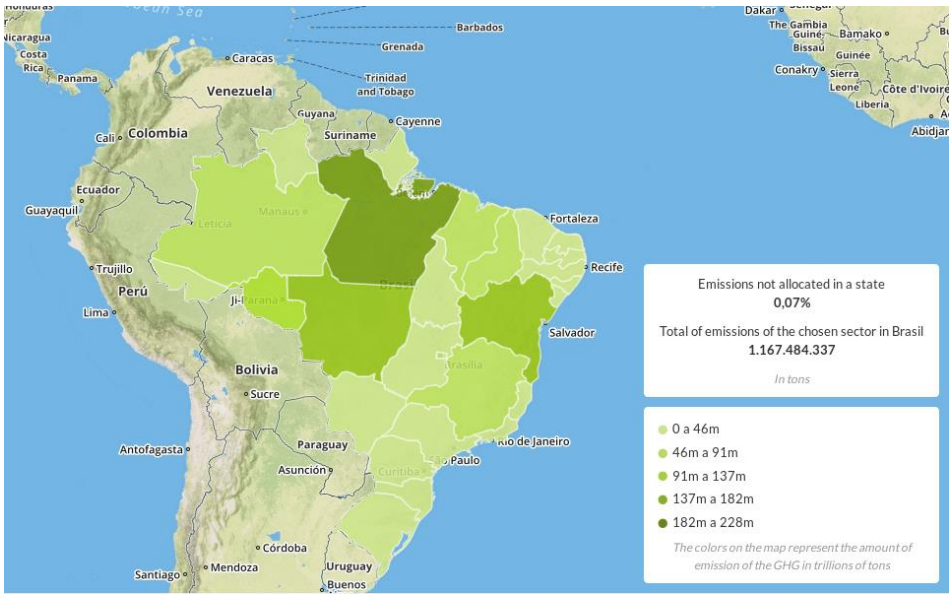

Figure 3.44: Emissions data from Brazil
Emissions from Land-use Change and Forestry (CO2e (t) GWP-AR5) by state for 2016. Data and map produced from SEEG Brazil[25]

3.3.4 Discussion and conclusions

In this section I have tested the hypothesis that fire is a key driver in the development and maintenance of the Brazilian Cerrado. Bond *et al*. (2008) suggest that a mix of resources, herbivory and fire may be responsible for limiting tree cover in C4 grasslands / savannas. Pivello (2011) asserts that in the past there have been questions over whether the Cerrado is man-made (through anthropogenic fire and deforestation) or natural. However their research argues that pollen and charcoal records show that fires were present before the arrival of humans around 12,000 years ago, and that major plant adaptations happened around 4 million years ago to accommodate frequent fire occurrence, long before human intervention. The results presented here support this study, showing that fire is a key determinant in the JULES land surface model in simulating the correct distribution of forest cover without the influence of humans changing the landscape through land-use change. When fire is included, the vegetation shifts from tropical broadleaf vegetation, which can be *climatically* supported (as shown by the S2 without fire scenario, Figure 3.40), to a mix of grasses and shrub which is what we see in reality (Figure 3.41 and Figure 3.42). Previously a large proportion of carbon emissions in this area have been attributed to LUC, as we

[25] http://plataforma.seeg.eco.br/map

see from Figure 3.43. Now that fire is accounted for, the land-use emissions from the Cerrado region in particular are much reduced. Similar results have been shown with other dynamic vegetation models, for example Hirota *et al*. (2010) used a simple climate-vegetation-fire model to show that under current climate conditions tropical forest would extend 200km further south into the savanna region without fire. The analysis for Africa here shows similar results, with the forest area extending further into the savanna region without fire (see section 3.2.7).

In conclusion, this study has shown that the impact of fire on the vegetation distribution and plant functional types is significant, especially across Brazil, and highlights the importance of being able to correctly simulate this additional disturbance process in modelling.

Chapter 4: Impacts of the 2015-2016 El Niño

4.1 Abstract

The link between El Niño events and related increases in droughts and fires is well-known. A number of studies have considered the impacts of the recent 2015-2016 El Niño and found an increase in burnt area in some regions compared to La Niña years, but no studies have yet used a dynamic land surface model to consider how conditions might have differed had the El Niño not occurred. Here I use the JULES land surface model with interactive fire from INFERNO to assess the impact of the 2015-2016 El Niño on precipitation, temperature, burnt area, and the associated impacts on the carbon sink globally and for three key regions: South America, Africa and Asia, compared to a 'no El Niño' scenario based on mean climatological drivers. I find that the model projects a higher burnt area with El Niño conditions than without in most regions globally, although the results are more complex over Africa where there are areas of both increase and decrease. The timing of the impacts in Africa is also different, with the peak occurring earlier than in South America or Asia. South America shows the largest fire response with the El Niño (13% increase in burnt area and a 21% increase in emitted carbon), and this region is projected to change from a net sink of carbon to a carbon source. Peak fire occurs from August to October across central-southern Brazil, and temperature is shown to be the main driver of the El Niño-induced increase in burnt area during this period.

4.2 Introduction

South America usually experiences a regular 'wet season' dominated by the South American Monsoon System (SAMS) from October to April, which brings heavy rains across the continent particularly from December – February (Rao *et al*., 2014). The pattern of these rains varies across the Monsoon period, with the southern regions experiencing more rain in the first part of the Monsoon and the central and east regions staying drier, with a change to more rain in central and north regions towards the end of the Monsoon (Grimm *et al*., 2003). This influences the pattern of fire across the continent, where typically peak fire is seen August – October in the central and east regions, which then reduces as the wet season progresses (see Appendix 4).

The El Niño Southern Oscillation (ENSO) which is a reasonably predictable mode of variability that occurs every 2 – 7 years, can have a large impact on this regular rainfall pattern. An ENSO event is defined as a Sea Surface Temperature (SST) anomaly compared to a baseline period of 1971-2000, centred on the equatorial Pacific Ocean in the NINO 3.4 region (5°N–5°S, 120°–170°W), that is 0.5°C or larger over three consecutive months (Trenberth, 1997, and updated by NOAA, 2003; Larkin and Harrison, 2005; Yu *et al*., 2017). ENSO years are characterised by unusually warm SSTs (El Niño) or by unusually cold SSTs (La Niña) in the Equatorial Pacific Ocean, but can have global impacts (Larkin and Harrison, 2005). It is the largest mode of variability in the climate system and the global carbon cycle (Malhi *et al*., 2018). The El Niño phase of ENSO commonly results in higher temperatures and reduced precipitation across the tropics, although the timing of this varies globally (Chen *et al*., 2017). The impacts across the continent can also be variable, for example the south of South America often experiences wetter conditions, with the northern and central-east regions experiencing drought (Stauffer, 2015; Grimm *et al*., 2003). Brazil's semi-arid northeast for example has been experiencing a severe drought since 2014, which has worsened with the 2015/16 El Niño (Stauffer, 2015), and up to 13% of the rainforest experienced extreme drought in February-March 2016 (Jiménez-Muñoz *et al*., 2016). These dry central and eastern regions overlap with the areas of highest fire occurrence for the continent, highlighting the link between El Niño conditions and increased fire activity. Figure 4.1 below shows the usual patterns of rainfall and temperature related to an El Niño event.

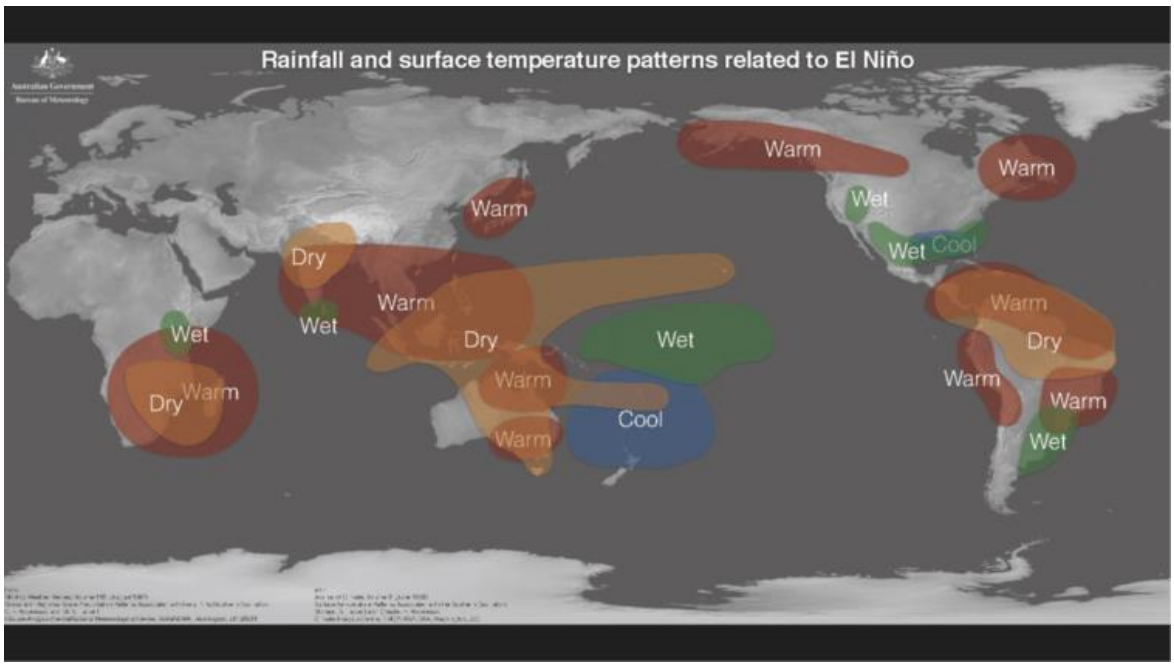

Figure 4.1: Rainfall and surface temperature during a typical El Niño event Reproduced from the Bureau of Meteorology[26].

In the last 20 years, there have been two large El Niños, and a number of smaller events. During 1997-1998 and 2015-2016, very high SST anomalies were recorded; the years 2002-2003, 2004-2005, 2006-2007, and 2009-2010 also showed higher than average SSTs (NOAA CPC[27]). Chen *et al*. (2017) shows from satellite data that during a typical El Niño cycle, fires increase across northern South America in Jan–Apr (mid- El Niño), Central America in Mar–May (mid-late El Niño), and the southern Amazon in Jul–Oct (late – post El Niño) and that overall fire emissions in pan-tropical forests increase by 133% in El Niño years compared to La Niña years (over 1997-2016).

The 2015/16 El Niño was one of the strongest on record, beating the previous highest 1997/98 record for Niño-3.4 Index, although showing lower Nino3 and Nino 1+2 Eastern values (L'Heureux, 2016). There were initial signs of the developing El Niño in 2014 before it was announced as meeting the official El Niño criteria by the Australian Bureau of Meteorology in May 2015, before peaking in late 2015 and ending in May 2016. The event has been associated with a large rise in global levels of CO_2 (Betts *et al*., 2016), most of which derives

[26] Bureau of Meteorology: http://www.bom.gov.au/climate/updates/articles/a018.shtml

[27] NOAA CPC: http://origin.cpc.ncep.noaa.gov/products/analysis_monitoring/ensostuff/ONI_v5.php

from the terrestrial tropics (Malhi *et al*., 2018), which has been attributed to different factors using satellite data that vary spatially (Liu *et al*., 2017): in tropical South America the cause has been linked to a decrease in GPP and reduced carbon uptake from reduced precipitation; in tropical Asia the increase has been linked to higher fire occurrence; and in Africa it is proposed that an increase in respiration led to increased carbon release. Other studies however show GPP as the main driver of carbon loss across the tropics as a whole, with a decline in photosynthesis (Bastos *et al*., 2018) and a 28% reduction tree growth (Rifai *et al*., 2018; Santos *et al*., 2018) evident in the Amazon. Northeast Amazonia saw a temperature rise of up to 3°C and a 200mm decrease in precipitation (Jimenez *et al*., 2018), which led to a decline in photosynthesis and resulted in a reduction in GPP (Luo *et al*., 2018). Anderson *et al*. (2018) show that repeated exposure to drought over the last 40 years has increased the sensitivity of Amazon vegetation, as demonstrated by increasingly negative Enhanced Vegetation Index anomalies, suggesting that Amazonia is becoming more vulnerable to extreme drought events.

The extent of fires across Indonesia was large with an estimated 4,604,569 hectares (using Synthetic Aperture Radar data, with an overall accuracy of 84%) burned during the 2015 fire season, predominantly started deliberately for land clearance, and much of which was over high emission-producing peatlands (Lohberger *et al*., 2018). CO_2 accounts for in excess of 90% of global fire carbon emissions each year (~2PgC total emissions), which usually peaks during El Niño years (Eldering *et al*., 2017). Recent research from Aragão *et al*. (2018) has shown that drought-induced fires in the Brazilian Amazon increased by 36% during the 2015/16 El Niño period, (calculated as the departure from the 2003 to 2015 monthly averages excluding drought years 2005, 2010 and 2015) according to MODIS data, with the study concluding that emissions from drought-induced fires are as important as emissions from LULCC and need to be included in emission inventories. The eastern Amazon was found to be the region most affected by fire (Jimenez *et al*., 2018; Burton *et al*., 2018b).

While a clear link has been found between the 2015-2016 El Niño and an increase in satellite and radar-detected fire events across a number of pan-tropical regions as outlined above, a model-based assessment of the full impact of the El Niño has not yet been done. Using an interactive fire-vegetation model

within a land surface model to assess the impacts of the 2015-2016 El Niño compared to a mean climatology enables a comprehensive investigation to be conducted into the impacts of the El Niño across a range of variables, and their associated drivers.

Here I use the JULES-INFERNO model to investigate the impact of the 2015/16 El Niño on fire, and compare this to observations of burned area to address three research questions:

1) What was the impact of the 2015/16 El Niño on fire? Did this vary globally, and why?
2) What impact did the El Niño have on the carbon sink globally and regionally when fire is taken into account?
3) How did the impacts of the 2015/16 El Niño vary spatially and in time across South America?

4.3 Methods

For this study the climatology from CRU-NCEP v7 is used to drive JULES, including precipitation, temperature, humidity, wind, air pressure and short and long wave radiation which models the observed El Niño (see section on Data Availability for suite ID). The model was run from 1860-2016 with this forcing, and then again using the mean climatology from the previous 10 years (2005-2014) to represent standard baseline conditions for 2015-2016 without the El Niño event occurrence, referred to in the results as “no El Niño” (driving data provided by Nicholas Viovy, IPSL). The experimental design used here is intended for use in investigating the impacts driven by the occurrence of the 2015/2016 El Niño, compared with a similar period without the observed SST anomaly. The period of 2005-2014 is chosen to ensure conditions are as similar as possible to 2015/16 in terms of climate and CO_2 levels, while the 10-year mean climate is chosen to even out anomalous and extreme years. The benefit using a land surface model to assess changes using a mean climatology from the previous 10-years is that CO_2 and land surface conditions still represent 2015/16, using the same initial conditions as the control experiment, making a direct comparison of El Niño meteorological conditions with ‘average meteorological conditions’ possible.

We can define the 2015/16 perturbation as dominated by the significant El Niño, and study the impacts against a 10-year baseline. Changes referred to as 'due to El Niño' throughout this study are calculated as absolute change between the two model conditions (El Niño – No El Niño) or as percentage change (El Niño – No El Niño / No El Niño x100). I have chosen to use the period July 2015 – June 2016 to study the impacts over 12 months covering the peak El Niño. This period is slightly later than the official El Niño period to capture some of the lag effect in fire response as identified by Chen *et al*. (2017). I analyse the results of the experiment to show how the impact of fire has changed as a result of the El Niño across a range of variables including burnt area and emissions using the interactive fire model INFERNO within the land surface model JULES. I use constant ignitions and land-use and then compare the results with varying ignitions and land-use. The results are analysed globally, and for three fire-prone regions; South America, Africa and Asia (see Appendix 4 for maps of each region). Observations used for comparison are from GFED4.1s including small fires (see section 1.3.1).

4.4 Results

Section 1: What was the impact of the 2015/16 El Niño on fire? Did this vary globally, and why?

The first question is addressed by assessing the burnt area in the El Niño and no- El Niño case. Here I produce simulations using the JULES-INFERNO model driven by observations and compare the results to the average climatology to show how the burnt area has changed with El Niño conditions. A direct comparison of the burnt area across the period July 2015 – June 2016 with and without El Niño shows the pattern of burnt area is very similar in both scenarios (Figure 4.2). Some increase in burnt area can be seen with El Niño across South America, Southern USA and India, whereas Saharan Africa shows a decrease.

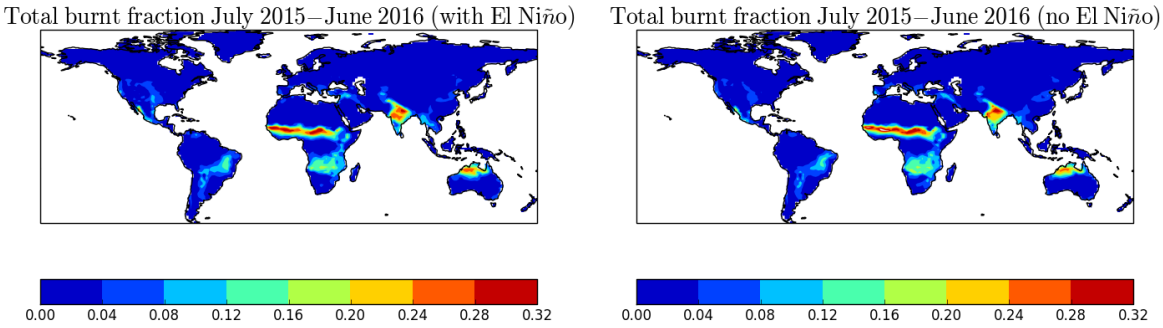

Figure 4.2: Global burnt area fraction with El Niño
July 2015 – June 2016 with El Niño (left) and without El Niño (right) simulated by JULES-INFERNO

Considering the percentage increase in burnt area with El Niño, areas of highest change can be seen across northern South America, southern USA and central-southern Australia which see up to 100% increase in some regions (Figure 4.3). Some decreases in burnt area are seen across Canada, Sahara and Southern Africa and East Asia, although these are mostly smaller than the increases.

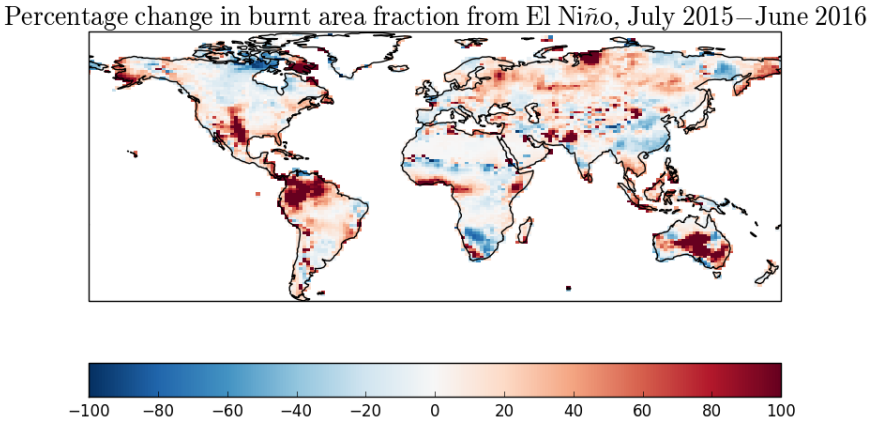

Figure 4.3: Change in burnt fraction due to El Niño
July 2015 – June 2016 simulated by JULES-INFERNO

The increase in burnt area corresponds to an increase in emitted carbon in the same regions (Figure 4.4). Globally, the total carbon emitted from fires with El Niño is 2.74 PgC, compared to 2.59 PgC in the “no El Niño” scenario, giving a total of 0.15 Pg additional carbon (6% increase) released from fires due to the occurrence of the 2015/16 El Niño.

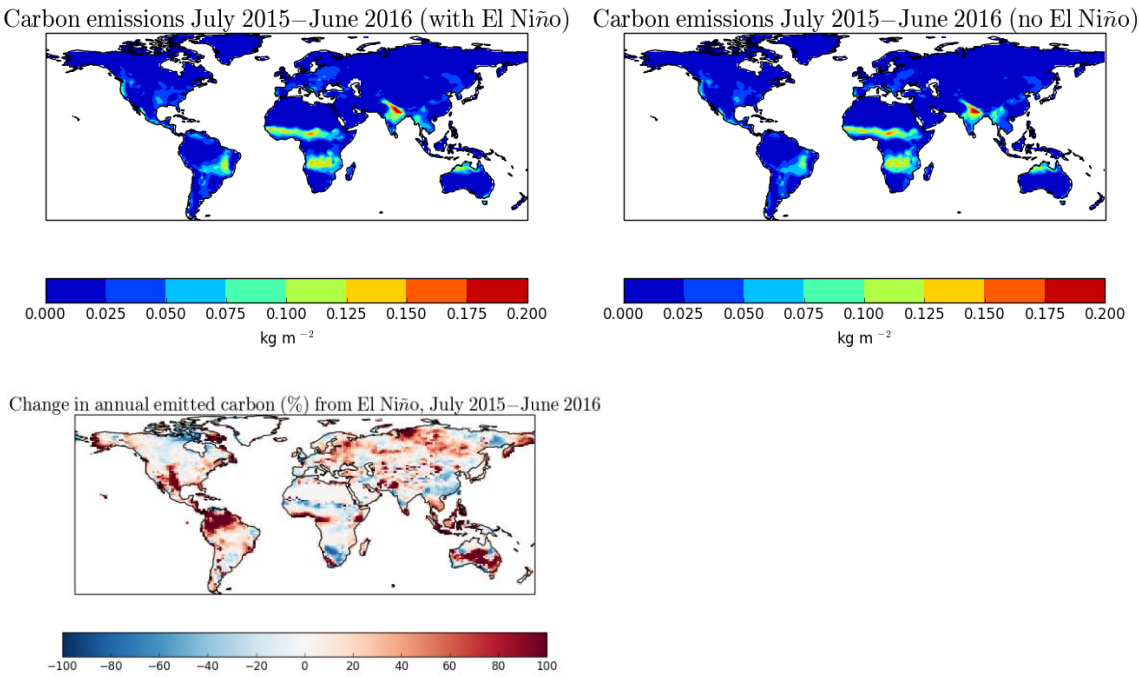

Figure 4.4: Carbon emissions from El Niño
July 2015 – June 2016 with El Niño (top left) and without El Niño (top right), and percentage change in emitted carbon due to El Niño, July 2015 – June 2016 (bottom left) simulated by JULES-INFERNO

Considering how fire occurrence changes throughout the year, the global total burnt area is higher in the latter half of 2015 with El Niño compared to no El Niño (Figure 4.5). In 2016 the El Niño signal weakens, with some months showing higher burnt area with El Niño (Jan, Feb, April), but some lower (March, May, June). As some regions show an increase in burned area and some show a decrease, the total global difference between the 'El Niño' and 'no El Niño' scenarios is not large. The global total burnt area across the year with El Niño is 4.44 Mkm^2, compared to 4.34 Mkm^2 in the scenario without El Niño, giving a total change of 0.10 Mkm^2 of burnt area due to El Niño from July 2015 - June 2016.

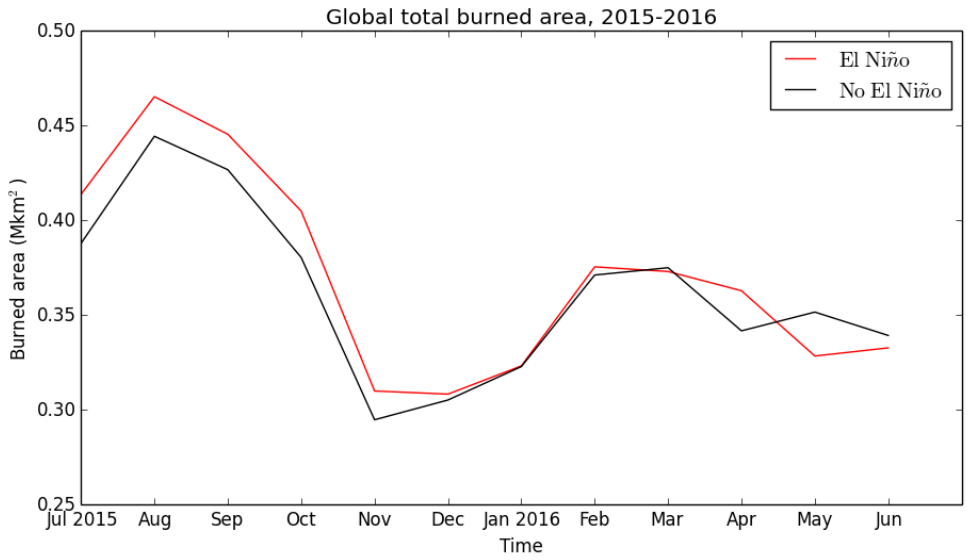

Figure 4.5: Global burnt area with El Niño
Global total burnt area (Mkm^2) with El Niño (red) and without El Niño (black), July 2015 – June 2016 simulated by JULES-INFERNO.

The global total emitted carbon from fire is higher with El Niño consistently from July 2015 to April 2016 (Figure 4.6). Similar to the burnt area, in 2016 this is more variable with slightly higher emissions at the start of the year, increasing to a peak in February. In May the emissions 'with El Niño' decrease to lower than the 'without El Niño' case. The variability reflects the changing pattern of fire occurrence globally, where the peak impacts of fire are experienced at different times in differing locations, as discussed below.

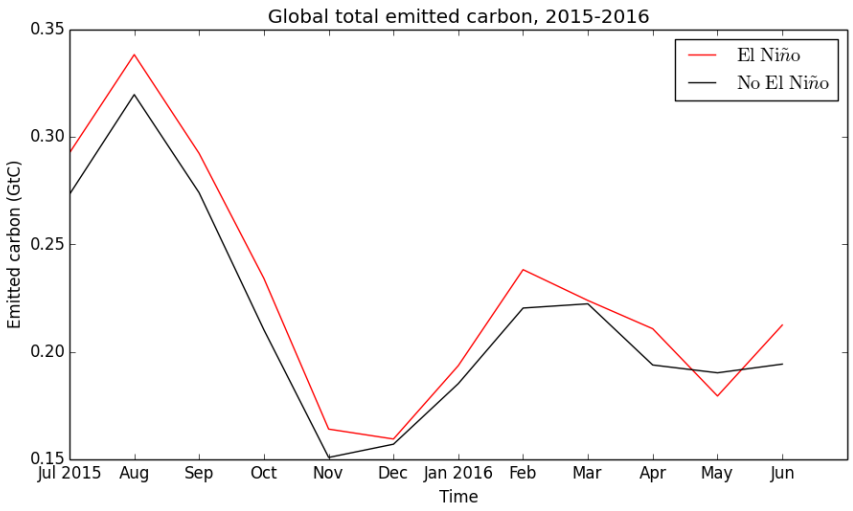

Figure 4.6: Global emitted carbon with El Niño
Global total emitted carbon from fire with El Niño (red) and without El Niño (black), July 2015 – June 2016 simulated by JULES-INFERNO

Focusing on three key regions that are important for fire occurrence - South America, Africa and Asia - Asia experiences a higher burnt area across the latter half of 2015 with El Niño, and less of an impact in 2016 (Figure 4.7). This suggests that Asia has an important influence on the global trend in burnt area in late 2015. Because there is an increase in burned area in 2015 followed by a decrease in 2016, again the total change over the period July 2015- June 2016 is small. The total burnt area with El Niño in Asia is 1.00 Mkm^2 compared to 0.99 Mkm^2 without El Niño, giving a total of 0.01 Mkm^2 of burnt area due to the El Niño.

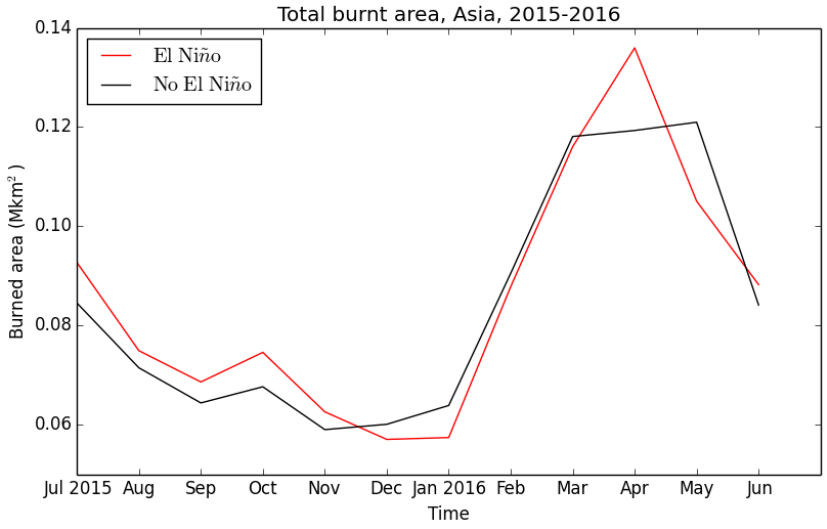

Figure 4.7: Burnt area in Asia with El Niño
Total burnt area in Asia with El Niño (red) and without El Niño (black), July 2015 – June 2016 simulated by JULES-INFERNO

The total burnt area for the African continent, conversely, is lower on average throughout the same period with El Niño (Figure 4.8). The total burnt area from July 2015 – June 2016 was projected as 1.73 Mkm^2 with El Niño compared to 1.82 Mkm^2 without El Niño. This is partly because peak fire occurred earlier across Africa than other regions (Figure 4.9). Thus comparing the entire year 2015, the burnt area with El Niño was projected as higher: 1.78 Mkm^2 with El Niño and 1.73 Mkm^2 without El Niño from January to December 2015.

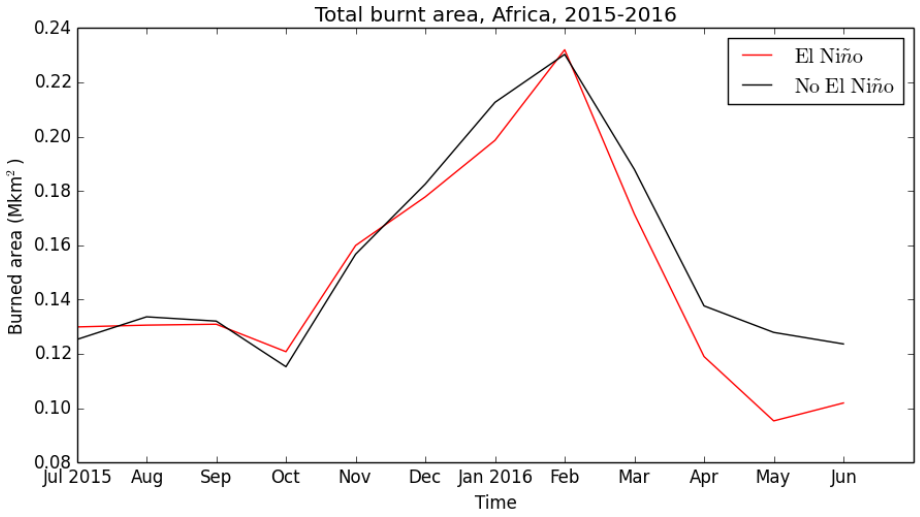

Figure 4.8: Burnt area in Africa with El Niño
Total burnt area across Africa with El Niño (red) and without El Niño (black), July 2015 – June 2016 simulated by JULES-INFERNO

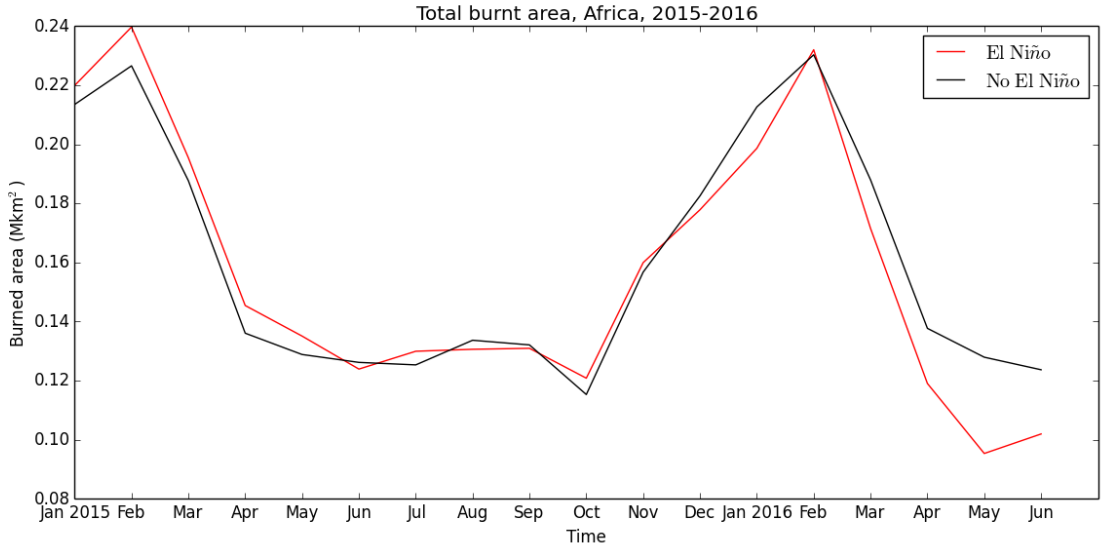

Figure 4.9: Burnt area in Africa with El Niño, 2015
Total burnt area across Africa with El Niño (red) and without El Niño (black), January 2015 – December 2015 simulated by JULES-INFERNO

Considering the South American continent, the change in burnt area due to El Niño is projected as higher than for the other two regions considered in this study. The burnt area is consistently higher with El Niño throughout the period July 2015 – June 2016 (Figure 4.10). The total burnt area over this period is 0.52 Mkm^2 compared to 0.46 Mkm^2 without El Niño, giving a total of 0.06 Mkm^2 change (13%) due to El Niño.

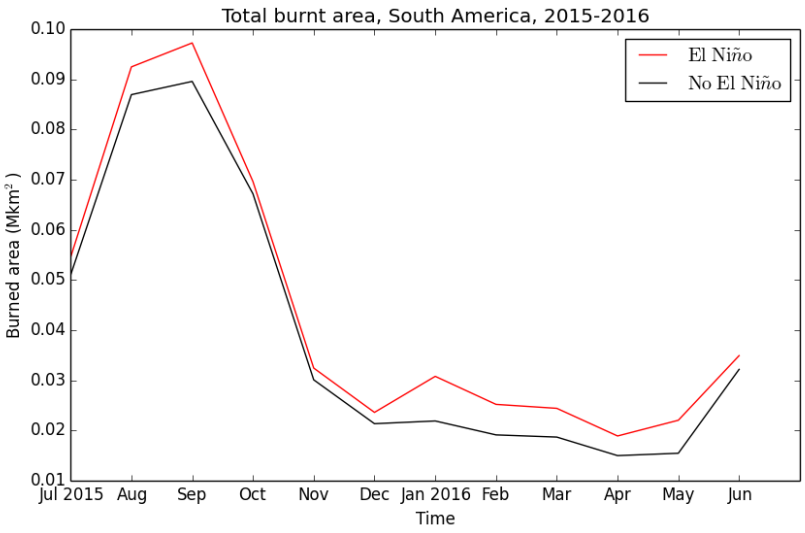

Figure 4.10: Burnt area in South America with El Niño
Total burnt area across South America with El Niño (red) and without El Niño (black), July 2015 – June 2016 simulated by JULES-INFERNO

Taking the tropics as a whole (20° South to 20° North), the burnt area is higher with El Niño through late 2015 (Figure 4.11). The total burnt area for this region is 2.42Mkm^2 with El Niño and 2.40Mkm^2 without El Niño.

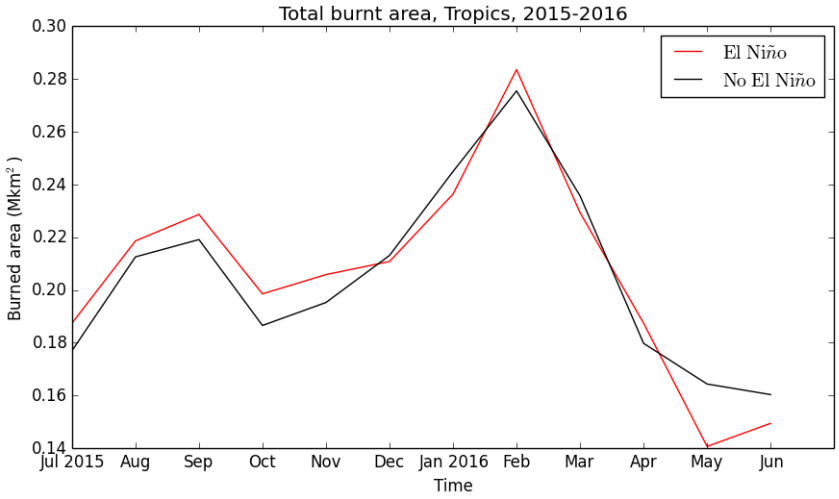

Figure 4.11: Burnt area in the Tropics with El Niño
Total burnt area for the tropics (-20 degrees to 20 degrees latitude) with El Niño (red) and without El Niño (black), July 2015 – June 2016 simulated by JULES-INFERNO

Comparing all three regions together, Figure 4.12 (upper panel) shows that the largest total burnt area is in Africa both with and without El Niño, followed by Asia and then South America, while the largest change with El Niño compared to climatology is seen in South America (Table 4.1). Peak fire in the form of burnt area is in February for Africa, April/May for Asia and September for South America. This partly results from the larger land area in Africa and Asia, so burnt

area is also calculated as a percentage of total land area by region in the lower panel at Figure 4.12. Africa still shows highest burned area at the continental peak in February, but there is higher burned area in South America than across Asia from Jules 2015- February 2016, and the fire season peak in from August to October exceeds the burnt area in both Africa and Asia for that period.

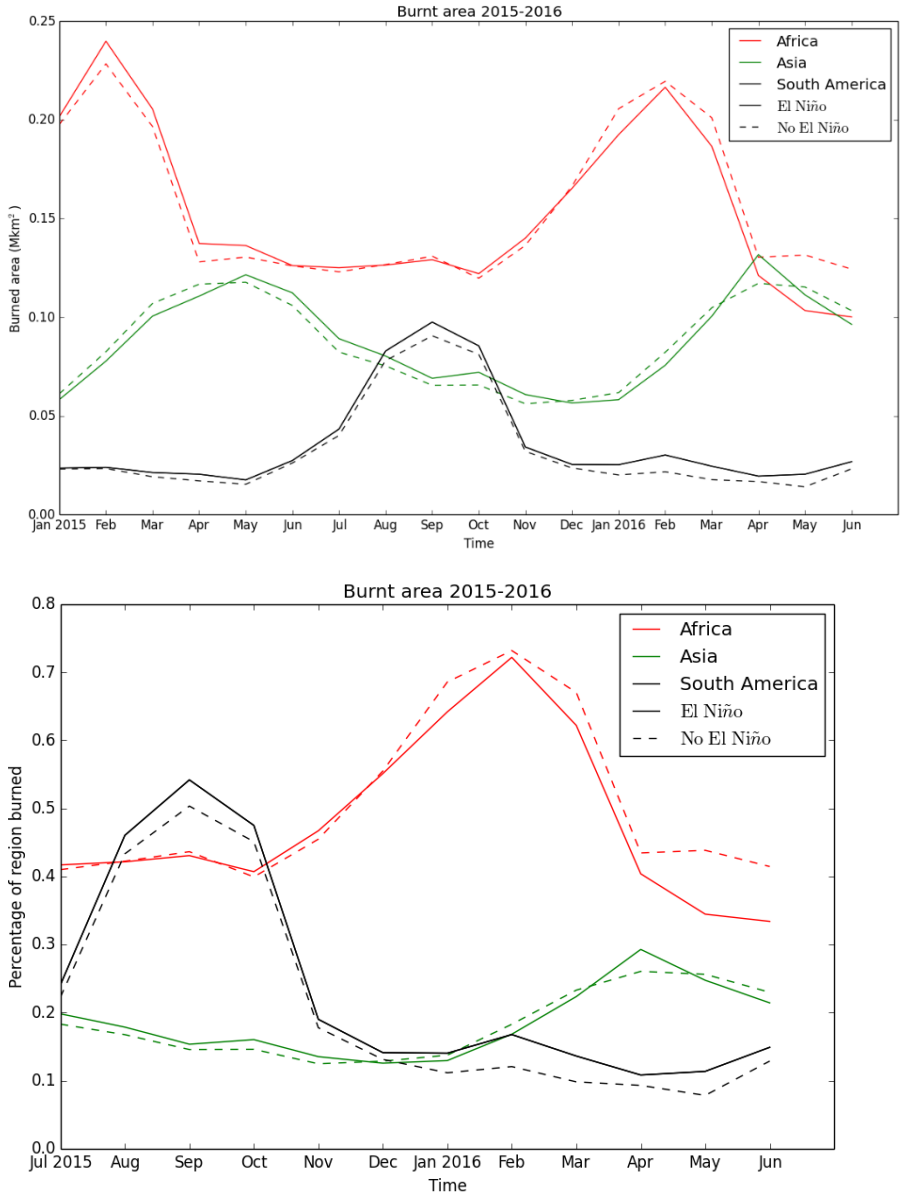

Figure 4.12: Burnt area for 3 regions
Burnt area across Africa (red), Asia (green) and South America (black). Solid lines show El Niño, dashed lines show no El Niño simulated by JULES-INFERNO. Upper panel shows total burnt area (Mkm^2), lower panel shows total burnt area as a percentage of the land area per region

Table 4.1: Summary of burnt area and emitted carbon
Globally and by region, with and without El Niño for total burnt area (Mkm^2) and emitted carbon (PgC) simulated by JULES-INFERNO

Burnt Area (Mkm^2) July 2015 – June 2016	**With El Niño**	**Without El Niño**	**Change**	**Percentage change**
Asia	1.00	0.99	0.01	1.01
Africa	1.73	1.82	-0.09	-4.95
Africa Jan-Dec 2015	1.78	1.73	0.05	2.89
South America	0.52	0.46	0.06	13.04
Tropics	2.42	2.40	0.02	0.83
Global Total	4.44	4.34	0.10	2.30
Emitted Carbon (PgC) July 2015 – June 2016	**With El Niño**	**Without El Niño**	**Change**	**Percentage change**
Asia	0.58	0.57	0.01	1.75
Africa	0.92	0.94	-0.02	-2.13
Africa Jan-Dec 2015	0.99	0.95	0.04	4.21
South America	0.46	0.38	0.08	21.05
Tropics	1.50	1.40	0.10	7.14
Global Total	2.74	2.59	0.15	5.79

The largest impact of the 2015-2016 El Niño was across South America (Figure 4.13). On average there was a global total increase in burnt area and emitted carbon with the El Niño compared to no El Niño, although some areas experienced a reduction in fire including Africa which reduced the global totals.

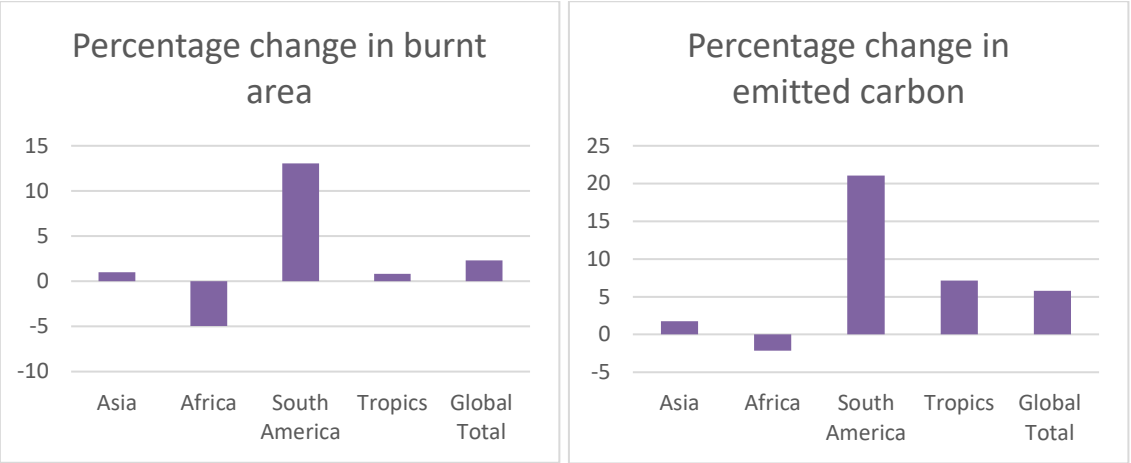

Figure 4.13: Percentage change in burnt area and emitted carbon

Considering the key drivers of the change in burnt area, across the north of the South American continent there was an increase in temperature and a decrease in precipitation and soil moisture due to the El Niño (Figure 4.14). These hotter, drier conditions are typical of the impacts that we expect to see with a strong El Niño (Figure 4.1), and have been linked to an increase in fire (van der Werf *et al*., 2004[28]). The change in burnt area across Africa however is more variable, with some regions showing an increase and some showing a decrease. Across the northern half of the continent the variability is in line with changes in precipitation, soil moisture and temperature, but there is a strong signal of decreased burnt area in the far south which does not fit this trend (Figure 4.14). In this region the precipitation and soil moisture are lower, and temperature is higher compared to the mean climatology, which would usually be expected to lead to higher burnt area, and indeed does lead to higher burnt area across other regions including South America.

[28] NASA: https://www.nasa.gov/press-release/nasa-examines-global-impacts-of-the-2015-el-ni-o

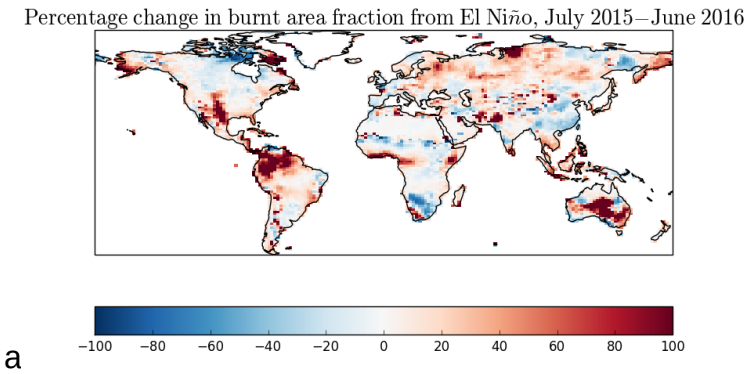

a

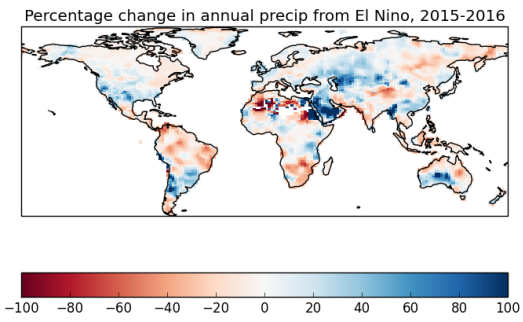

b

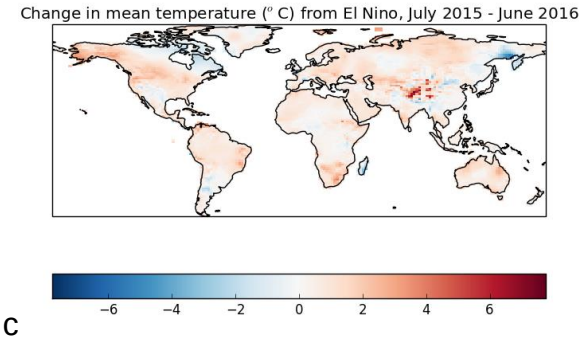

c

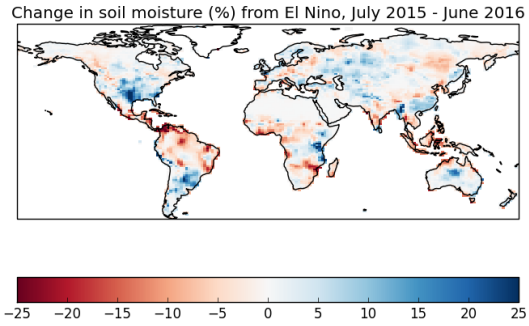

d

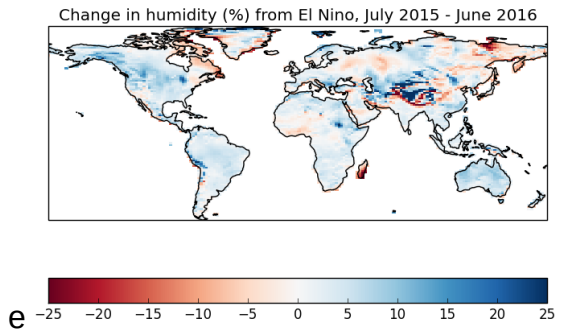

e

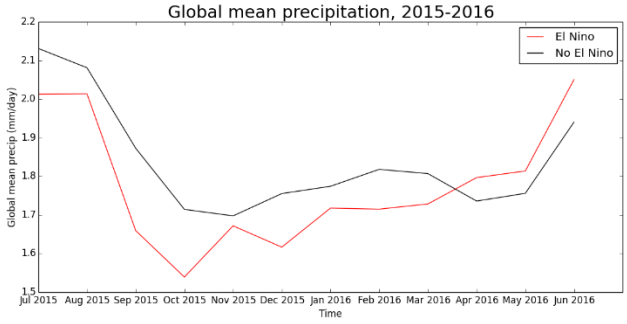

f

Figure 4.14: Drivers of burnt area with El Niño
Drivers of change in burnt area due to El Niño, July 2015-June 2016. Percentage change in burnt area (a), percentage change in annual precipitation (b), change in mean temperature (c), percentage change in soil moisture (d), percentage change in humidity (e) global mean precipitation (mm/day) time series with El Niño (red) and without El Niño (black) (f) simulated by JULES-INFERNO

Considering the flammability of vegetation across this area of southern Africa, we can see that there is a decline in flammability of grasses that seems to be driving the decrease in burnt area (Figure 4.15). Picking two points in Africa with differing fire responses, we can see there is a difference in humidity between the north and south, with higher humidity throughout the year in Namibia in the south where there is lower fire (Figure 4.16). Humidity may therefore be an important driver of fire in this region, together with a decline of fuel, as indicated by a strong decrease in grass flammability (Figure 4.15) and fraction (Figure 4.17). This is an area of semi-desert, so fuel is likely to be an important factor here.

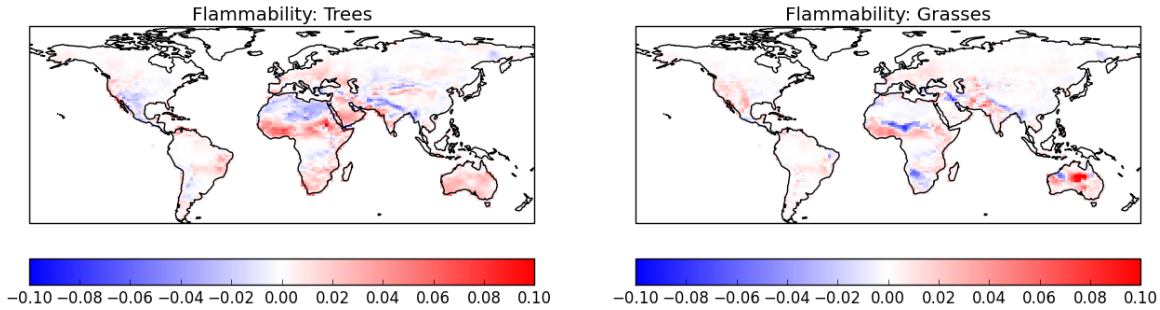

Figure 4.15: Change in flammability
Change in flammability due to El Niño for trees (left panel) and grasses (right panel) simulated by JULES-INFERNO

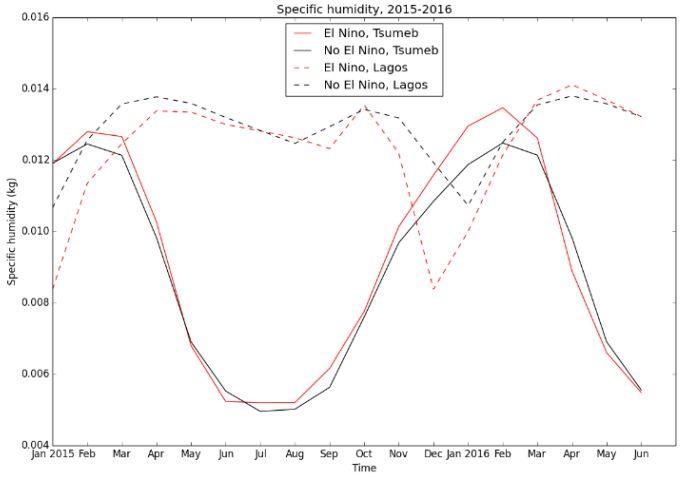

Figure 4.16: Specific humidity in two African regions
Tsumeb, Namibia (southern Africa, low fire, solid lines) and Lagos, Nigeria (North Africa, high fire, dashed lines) for El Niño (red) and no El Niño (black) simulated by JULES-INFERNO

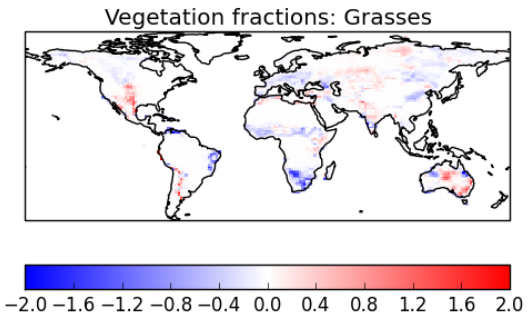

Figure 4.17: Change in fraction of grass vegetation due to El Niño simulated by JULES-INFERNO

Now considering ignition and land-use, I investigate if there is a large impact on the burnt area driven by the 2015-16 El Niño that is affected by anthropogenic change. For this experiment I repeat the simulation with S3 land-use change (varying 1860-present day) and varying ignitions based on population and lightning input data.

The initial results of burnt area fraction show some changes in the global pattern of burnt area, with a larger area burnt in USA and South America, but smaller burnt area across Saharan Africa (but with higher peak burning), India and Northern Australia (Figure 4.18).

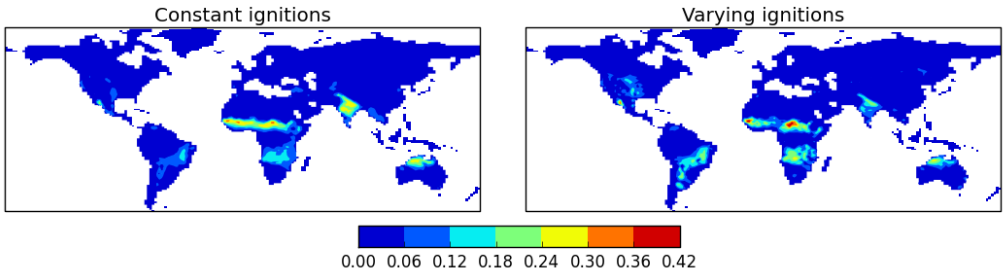

Figure 4.18: Burnt area with constant and varying ignitions
Burnt area (gridbox fraction) from July 2015 – June 2016 with constant land-use and ignitions (left panel) and varying land-use and ignitions (right panel) simulated by JULES-INFERNO

To understand the impact of these changes in the context of the El Niño event, I compare the percentage change in burnt area with El Niño with the 'no El Niño' climatology for constant and varying ignitions (as described in Chapter 3). The same pattern of increases and decreases in burnt area is seen in both cases, suggesting that the change in climatology is a more important driver of change in burnt area than anthropogenic changes (Figure 4.19).

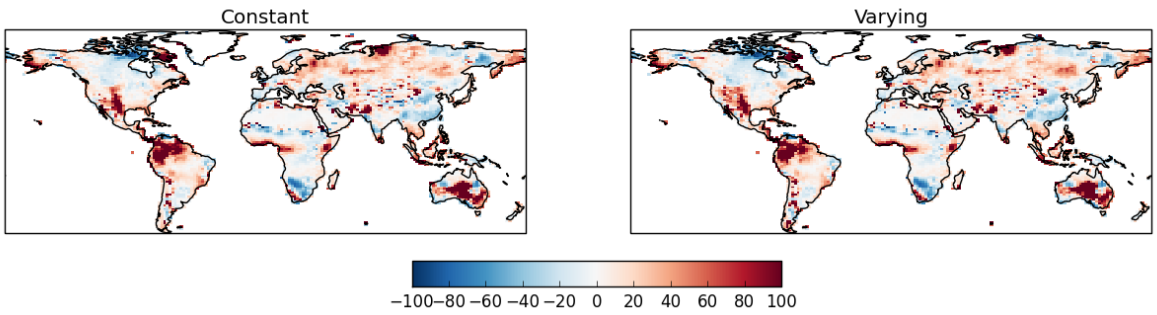

Figure 4.19: Change in burnt area with El Niño with constant and varying ignitions
Percentage change in burnt area (gridbox fraction) due to El Niño from July 2015 – June 2016 with constant land-use and ignitions (left panel) and varying land-use and ignitions (right panel) simulated by JULES-INFERNO

The monthly global burned area shows more inter-seasonal variability with varying ignitions and land-use, which is closer to the observations than constant anthropogenic drivers (Figure 4.20). This results in a smaller global total burned area, and greater variance between the El Niño and No El Niño burnt area (Table 4.2).

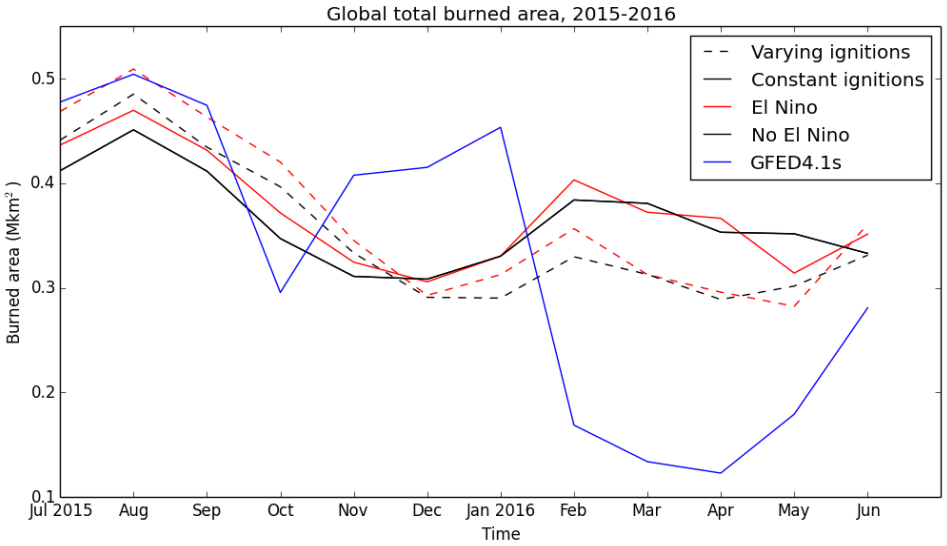

Figure 4.20: Global total burned area time series with varying ignitions
JULES simulation with varying ignitions (dotted line) and constant ignitions (solid line), with El Niño (red) and without El Niño (black). GFED4.1s observations shown in blue

Table 4.2: Change in burnt area with varying ignitions and land-use
Total annual global burned area July 2015 – June 2016 (Mkm^2) with and without El Niño simulated by JULES-INFERNO, compared to GFED4.1s observations

Burnt Area (Mkm^2) July 2015 – June 2016	**El Niño**	**No El Niño**	**Variance**	**GFED4.1s**	**Variance from obs**
Varying ignitions and land-use	4.39	4.21	0.18	3.91	0.48
Constant ignitions and land-use	4.44	4.34	0.10		0.53

For the three regions there are some changes in the seasonal variability of fire between the constant and varying ignitions and land-use (Figure 4.21). Peak burned area for Asia is in July (varying, “Asia V”) vs May (constant, “Asia C”), and for South America in October (varying, “South America V”) vs September (constant, “South America C”), whereas peak burned area for Africa is February for both constant and varying.

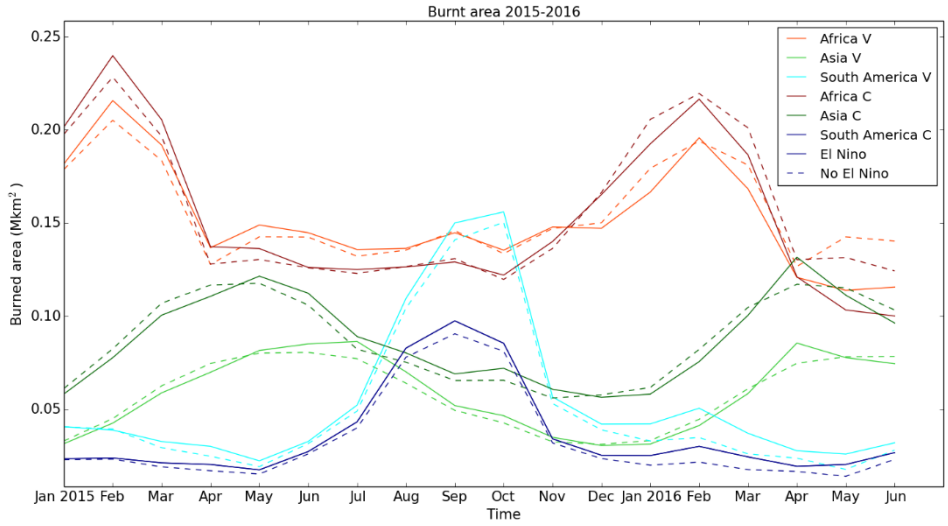

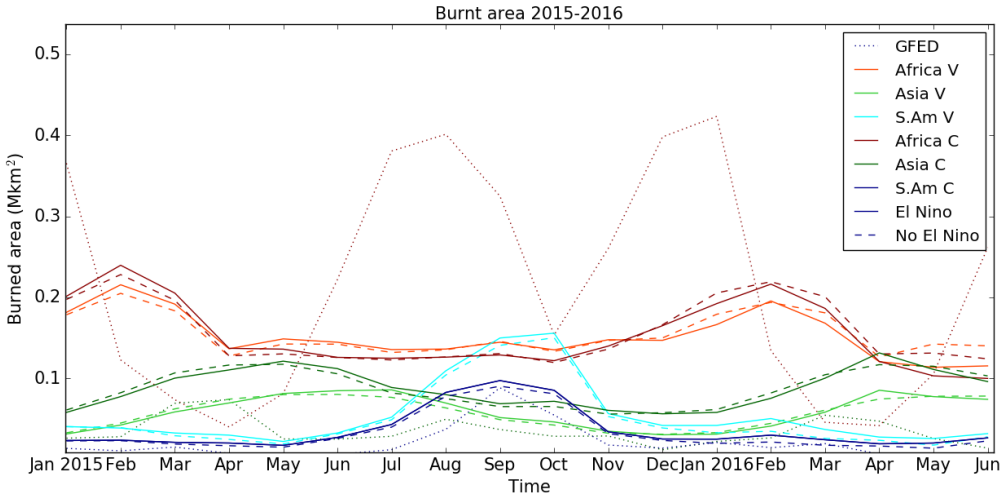

Figure 4.21: Burnt area for three regions with constant and varying input
Burnt area (Mkm^2) for Africa (red), Asia (green) and South America (blue), using constant ignitions and land-use ("C", dark colours), and varying ("V", light colours). El Niño shown with solid line, no El Niño shown with dashed line, simulated by JULES-INFERNO. Bottom plot includes GFED4.1s observations with dotted line

I compare the modelled burned area from JULES-INFERNO with GFED observations (Figure 4.22). For Asia (green), the timing of peak emissions is more closely captured with constant input (dotted line) than varying input (dashed line), but both are off by at least one month, and are higher than the observed burned area (solid line). For South America (blue), the timing and magnitude is well captured when using constant land-use and ignitions (dotted), but too high and the peak too late with varying input (dashed). For Africa (red), the modelled burned area, both with constant and varying ignitions, is much lower than observations and less variable.

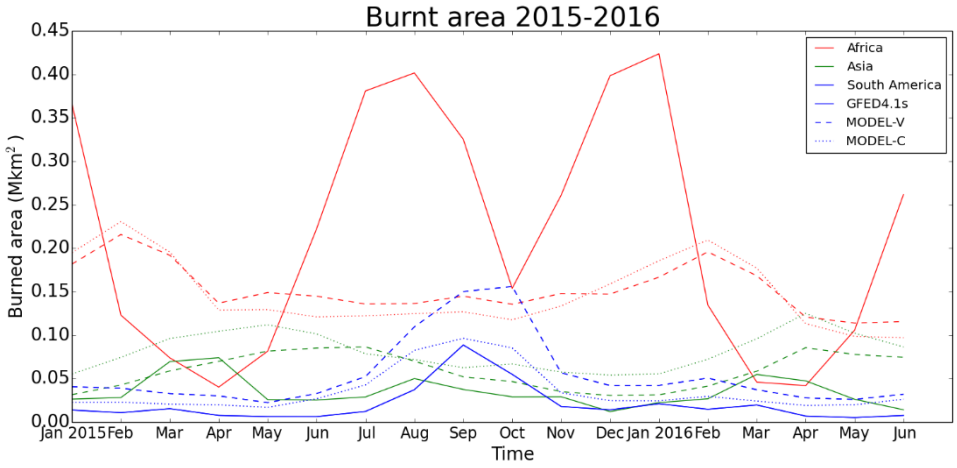

Figure 4.22: Time series of burned area for three regions with observations
Burned area (Mkm^2) as simulated by JULES-INFERNO with constant ignitions and land-use (dashed line), varying ignitions and land-use (dotted line) and GFED4.1s observations (solid line) for Africa (red), Asia (green) and South America (black) from January 2015 – December 2016 (model simulations up to June 2016 only)

Assessing the burned area across a time series it is apparent that the modelled burned area for Africa is notably lower than observations (Figure 4.22), and yet the global total burned area is higher in the model than the observations (Table 4.2). Spatially we can see that the total burned area according to GFED observations for the period July 2015 – June 2016 is focused on Africa, with areas across South America and Asia having lower burned area than simulated by the model (Figure 4.23).

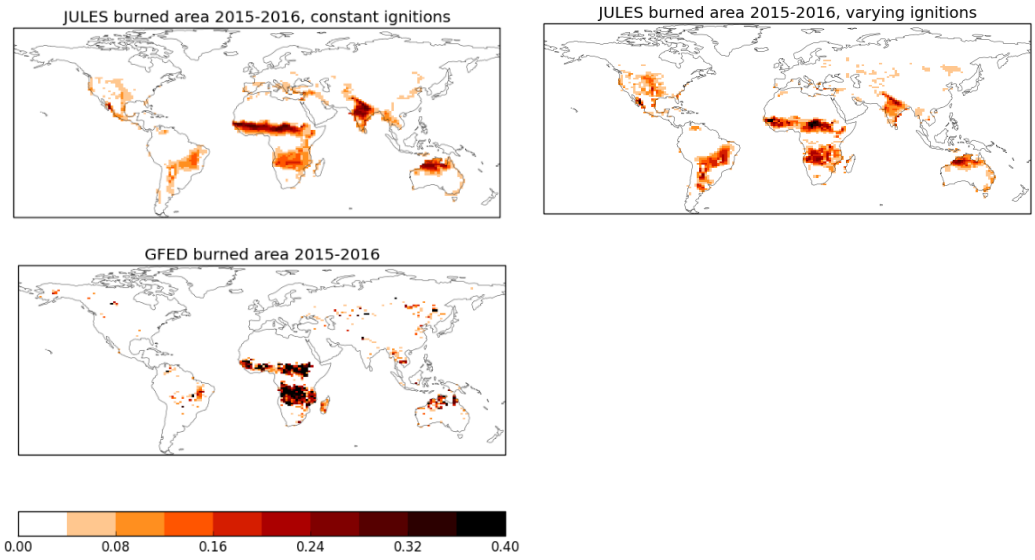

Figure 4.23: Modelled and observed pattern of burnt area
Burned fraction as modelled by JULES-INFERNO (top row) with varying land-use and ignitions (left) and constant land-use and ignitions (right) compared to GFED4.1s observations (right), for July 2015 – June 2016.

The model enables us to compare how burned area may have changed as a result of the El Niño by driving the model with the mean climatology. Comparing the total area burnt by region, the results with varying ignitions and land-use also highlight South America as the region most affected by the El Niño, and a decrease in burnt area in Africa (Table 4.3).

Table 4.3: Burnt area and emitted carbon, with anthropogenic change
Globally and by region, with and without El Niño for total burnt area (Mkm^2) and emitted carbon (PgC) simulated by JULES-INFERNO

Burnt Area (Mkm^2) July 2015 – June 2016	**With El Niño**	**Without El Niño**	**Change**	**Percentage change**
Asia	0.69	0.67	0.02	2.99
Africa	1.73	1.81	-0.08	-4.42
South America	0.78	0.70	0.08	11.43
Tropics	2.46	2.41	0.05	2.07
Global Total	4.39	4.21	0.18	4.28
Emitted Carbon (PgC) July 2015 – June 2016	**With El Niño**	**Without El Niño**	**Change**	**Percentage change**
Asia	0.43	0.43	0	0.00
Africa	0.91	0.92	-0.01	-1.09
South America	0.59	0.51	0.08	15.69
Tropics	1.47	1.38	0.09	6.52
Global Total	2.64	2.50	0.14	5.60

It is perhaps surprising that there are not larger differences between the constant and varying ignitions and land-use scenarios. The results suggest that the changes in climate are more important drivers of change in burnt area than varying ignitions and land-use in this case. This result may lend support to recent work by Aragão *et al*. (2018) showing that fire is increasingly being decoupled from anthropogenic ignition, and increasingly being driven more by climatic changes.

To answer the first research question, 'Did the 2015/16 El Niño have an impact on fire occurrence? Did this vary globally and why?' I have considered the change in burnt area and emissions globally and for three key fire-prone regions, South America, Africa and Asia. The results as simulated by the JULES-INFERNO model from July 2015 – June 2016 have shown that there was an impact on fire

occurrence due to the El Niño conditions of 2015/16, and that this impact was largest in South America where there was an increase in burnt area due to hotter, drier conditions. The response across Asia was more mixed, with some regions showing an increase and some showing a decrease, with an overall slight increase in burnt area. The response across Africa was also variable, with an overall decrease in fire over the period considered (but with higher burnt area in 2015). This decrease was dominated by a large decline in burnt area across southern Africa, which may have been driven by a combination of higher humidity and low fuel availability. These general trends do not vary with changing ignitions and land-use. To focus on the climatic changes, and as the seasonality and magnitude of burnt area over South America is better captured by constant ignitions and land-use compared to GFED observations, I will continue to use this set up for the other research questions.

Section 2: What impact did the El Niño have on the carbon sink globally and regionally?

To address the second research question, 'What impact did the El Niño have on the carbon sink globally and regionally?', I calculate the Net Biome Productivity (NBP) with and without El Niño, and then calculate the change in Gross Primary Productivity (GPP), respiration and emissions to understand what impact the El Niño has on the carbon sink in three key regions.

NBP is calculated as Net Primary Productivity (NPP) minus soil respiration, wood product emissions from land-use change, and fire emissions. NBP is a measure of the net carbon accumulated in an ecosystem and can therefore be a useful indicator of the change in the carbon sink. A negative NBP indicates that an ecosystem is a net emitter of carbon, which can happen under conditions such as large El Niño events where carbon uptake is reduced because of higher temperatures negatively impacting photosynthesis, and due to higher fire occurrence.

Here I use the last 10 years of data to explore whether the NBP in 2015/16 was unusual. I also include the previous large El Niño, 1997/98, as a comparison (Figure 4.24). The 2015/16 had the lowest NBP of any year in the series in the

second half of 2015, but from March 2016 had the second lowest with 1998 having a lower NBP. The 1997/8 El Niño conditions were focused more in the Central Pacific, whereas the 2015/16 were more focused in the East Pacific (Betts *et al*., 2018), which is a likely reason why the lowest NBP occurred at different times in each case.

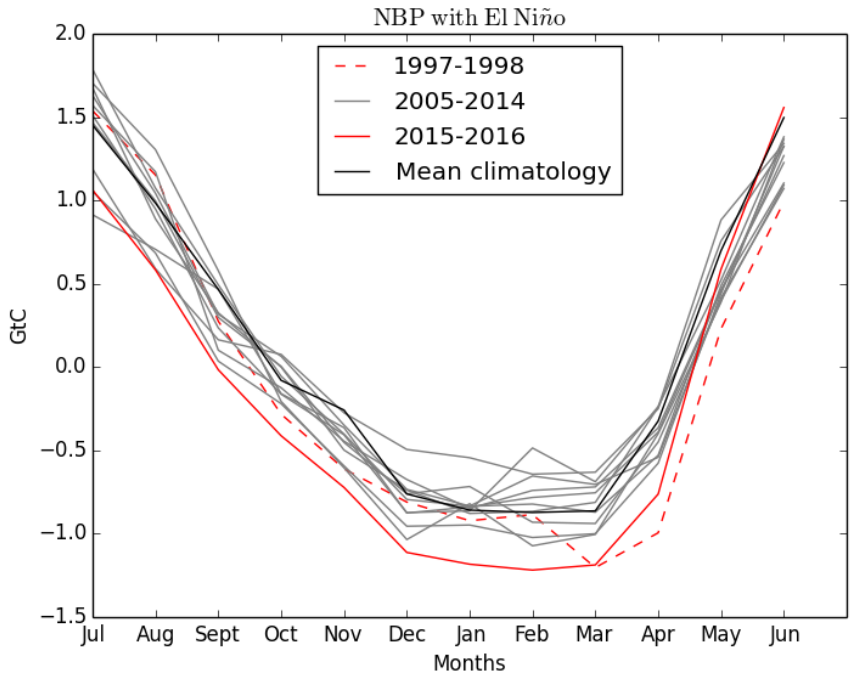

Figure 4.24: Global NBP
Global terrestrial (GtC/month) NBP for time series of 10 years from July – June. 2005-2014 shown in grey, large El Niño years shown in red (1997-1998 dashed; 2015-2016 solid), mean climatology ('No El Niño') shown in black simulated by JULES-INFERNO

Now considering net carbon flux for South America, Africa and Asia calculated as Gross Primary Productivity (GPP = carbon uptake) minus soil and vegetation respiration (carbon emissions), in all regions the net carbon flux is negative without the El Niño (Figure 4.25), indicating an overall carbon sink where carbon uptake exceeds emissions. With the 2015/16 El Niño, South America and Africa change to an overall source of carbon. Asia shows a net carbon sink both with and without El Niño, but the sink is reduced with the El Niño conditions. From Figure 4.27 we can see that this is influenced by a change in GPP and respiration (including vegetation and soil respiration). The GPP is higher than respiration in all cases without El Niño, giving an overall carbon sink, but with El Niño GPP is lower than respiration giving an overall carbon source in all cases except Asia where it results in a reduced sink. There is a reduction in both GPP and respiration in all three continents as a result of the El Niño, but the reduction in

GPP is higher than the reduction in respiration. This means less carbon is taken up, leading to a net carbon source for the South America and Africa regions, and a reduction in carbon uptake for Asia.

When fire emissions are also included, Asia and Africa turn from a sink to a source both with and without El Niño, which is higher with El Niño (Figure 4.26). South America turns from a sink to a source with El Niño. The overall emissions are higher in all cases when fire is included (Figure 4.27), as would be expected when adding in additional processes not previously accounted for.

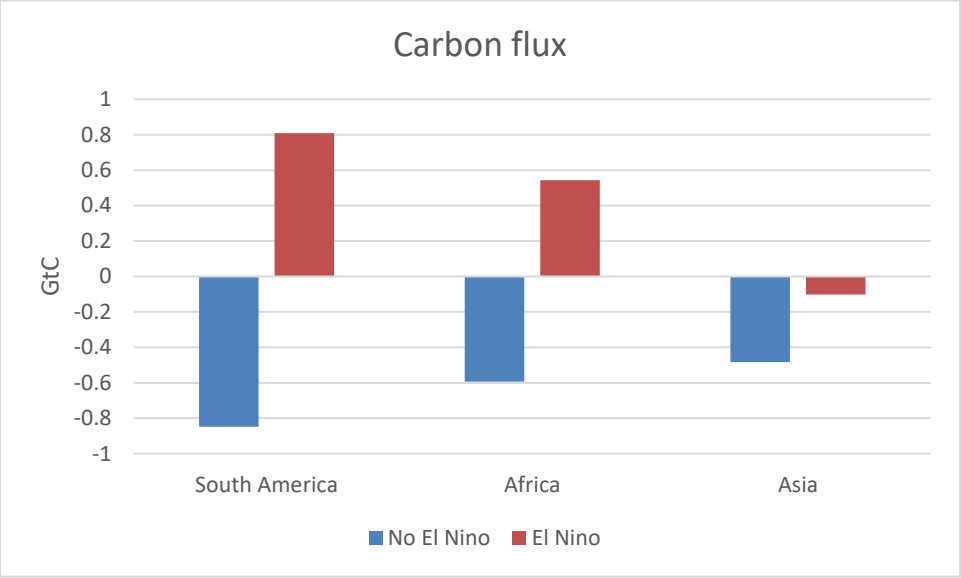

Figure 4.25: Carbon flux for three regions
Carbon flux (GtC) with (red) and without (blue) El Niño, taking account of NPP, soil and vegetation respiration simulated by JULES-INFERNO

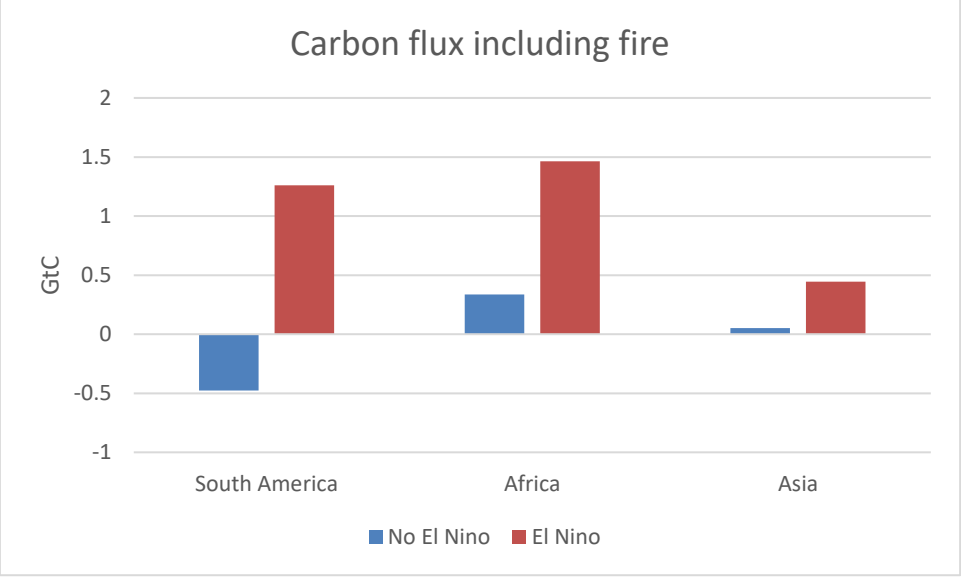

Figure 4.26: Carbon flux including fire
Net emissions (GtC) with (red) and without (blue) El Niño, taking account of NPP, soil respiration, vegetation respiration and carbon emissions from fire simulated by JULES-INFERNO

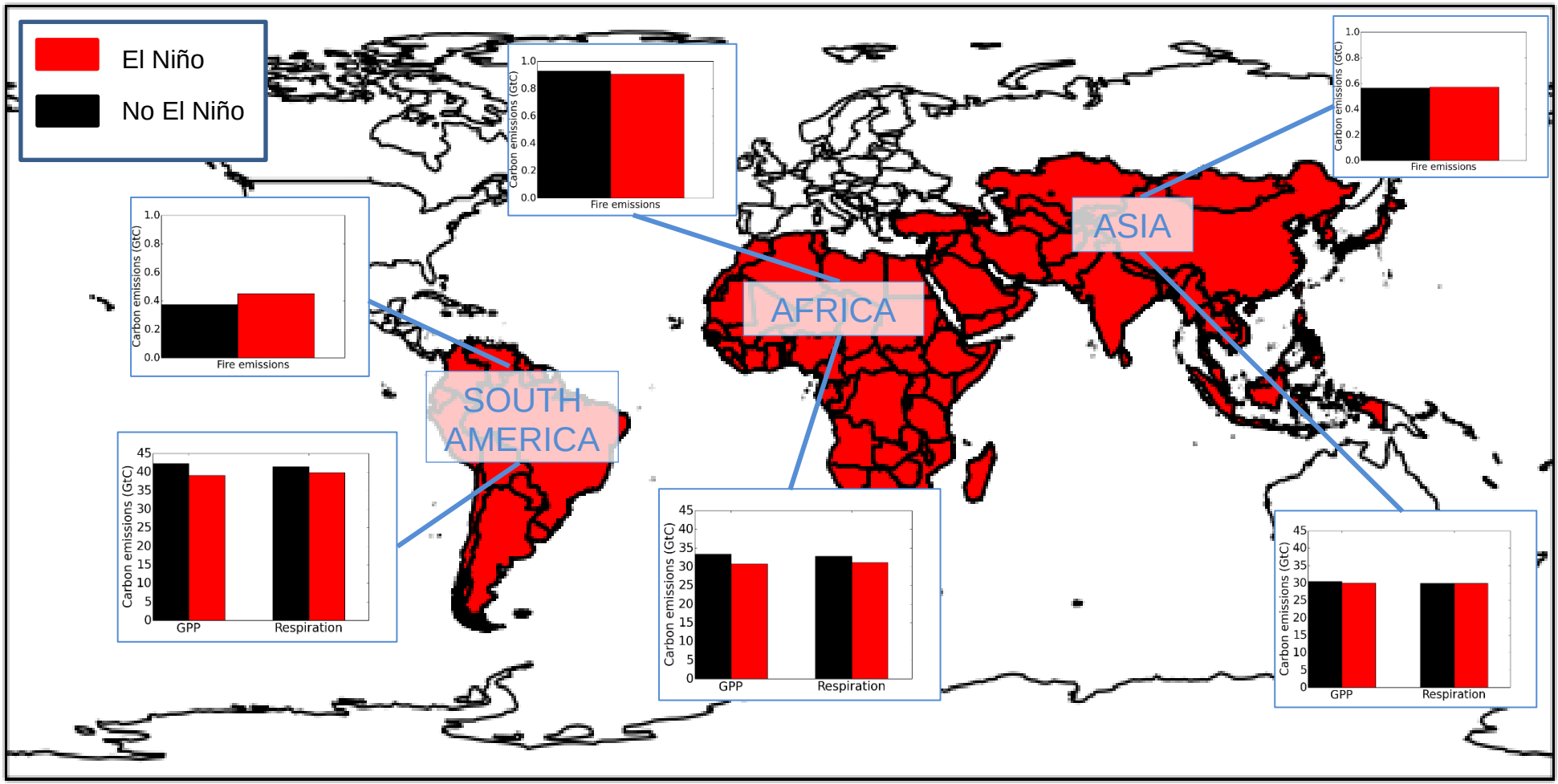

Figure 4.27: Map of carbon uptake and emissions
Map of GPP, Respiration (vegetation and soil) and carbon emissions (GtC) from fire for three key regions: South America, Africa and Asia with El Niño (red) and without El Niño (black) simulated by JULES-INFERNO

The main losses of carbon (as indicated by reduction in NBP) are found across South America and southern Africa, with other areas of loss including western Europe, Asia, and northern Australia (Figure 4.28). The drivers of these losses are spatially heterogeneous, with fire and reduction in GPP driving the losses across South America, reduction in GPP driving the loss across southern Africa, and fire driving the loss in Asia (Figure 4.29). This supports the research conducted by Liu *et al*. (2017) showing that carbon losses due to the 2015-2016 El Niño vary regionally, although the drivers here differ from their study; Liu *et al*. concluded that the main cause of carbon losses was reduction in GPP in South America, an increase in fire in tropical Asia, and respiration increase in Africa. Here the JULES-INFERNO model shows that fire is dominant in South America and tropical Asia, and reduction in GPP is dominant in Africa.

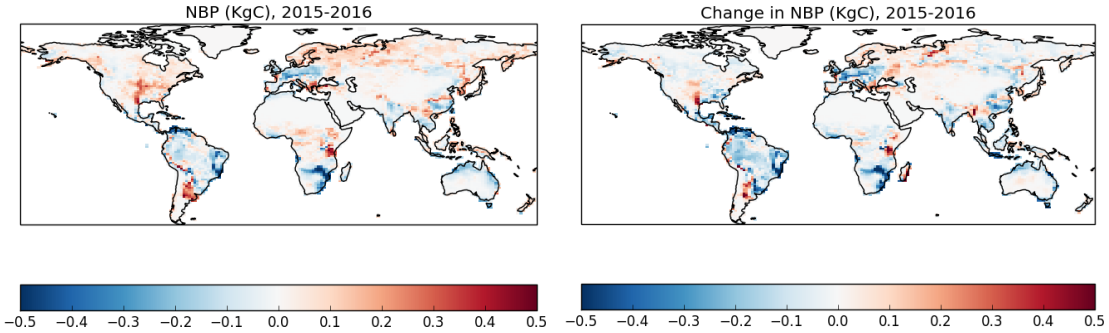

Figure 4.28: Global NBP
Net Biome Productivity (NBP) July 2015 – June 2016 (KgC) (left), and change in NBP due to El Niño (right) simulated by JULES-INFERNO

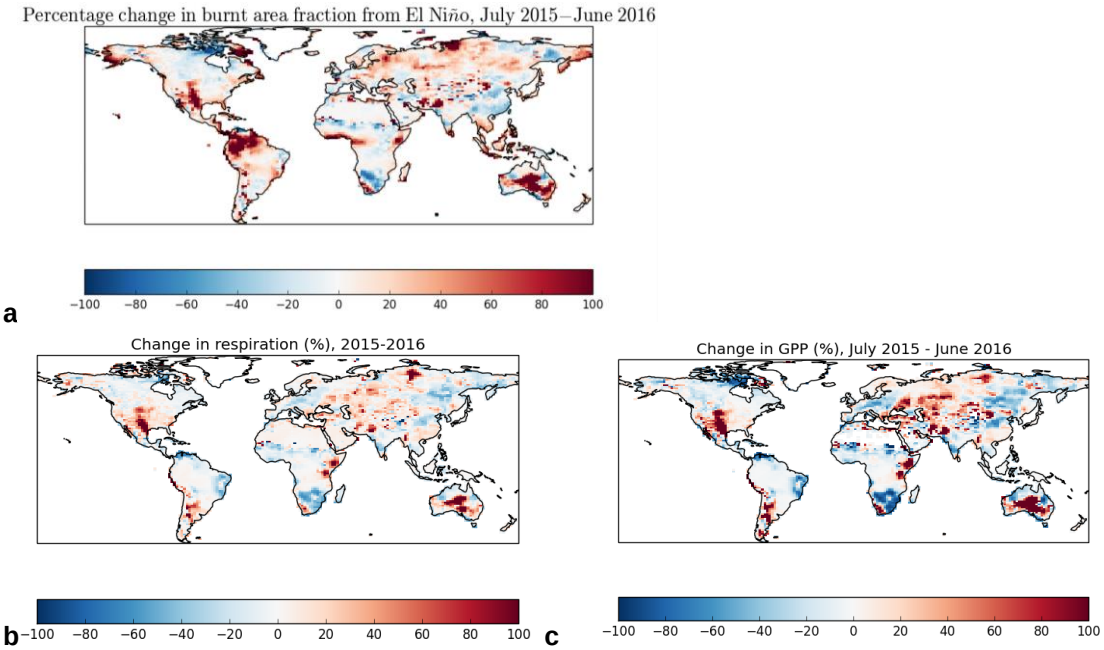

Figure 4.29: Drivers of change in NBP
Percentage change due to El Niño July 2015 – June 2016 for burnt area (a), respiration (vegetation and soil) (b), and GPP (c) simulated by JULES-INFERNO

I have considered three continents here that are important for fire contributions and known as global carbon sinks. The 2015/16 El Niño had a negative impact on the carbon sink, with the largest impact seen in the South American continent compared to Africa and Asia, dominated by decreases in GPP and increases in fire. South America turns from a sink to a source of carbon as a result of the El Niño. When fire is not included, Africa also changes from a sink to a source of carbon with El Niño, and when fire is included Africa and Asia become stronger sources of carbon due to decreases in GPP. Reduction of NBP in Africa seems to be dominated by a reduction in GPP in the south of the continent, whereas carbon losses in South America are driven by fire and GPP reduction. The response across Asia is mixed, but across tropical Asia fire also appears to be dominant.

Section 3: How did the impacts of the 2015/16 El Niño vary spatially and in time across South America?

The third research question considers how the impacts of the 2015/16 El Niño varied spatially and temporally across South America.

First I investigate whether temperature or precipitation is the largest driver of burnt area globally and for South America. I perform two new runs, the first just using the precipitation associated with observed El Niño together with the mean climatology for other climatic variables, 'ENSO-Precip', and the second just using the temperature associated with the El Niño together with the mean climatology of other variables, 'ENSO-Temp' (Figure 4.30).

Temperature is a larger driver of burnt area than precipitation in this experiment both globally and for South America. Further, the results suggest that globally the El Niño -related changes in precipitation on their own, without a rise in temperature, would in some months be sufficiently high enough to lead to a reduction in burnt area. Considering South America, temperature is an important driver of burnt area during the peak fire season August-October, but towards the end of the El Niño period over March-June this changes to precipitation being the more important driver. This coincides with the wet season in central Brazil, indicating that reduction in precipitation in the wet season is a more important

driver of fire than in the dry season where it is already hot, dry and fire-prone. On a local scale, precipitation is an important driver of changes in GPP and Net Ecosystem Exchange, whereas at larger spatial scales temperature is a more important driver as a result of two compensating water effects (Jung et al., 2017). The results here showing temperature as the dominant driver on large spatial scales may be reflective of this principle.

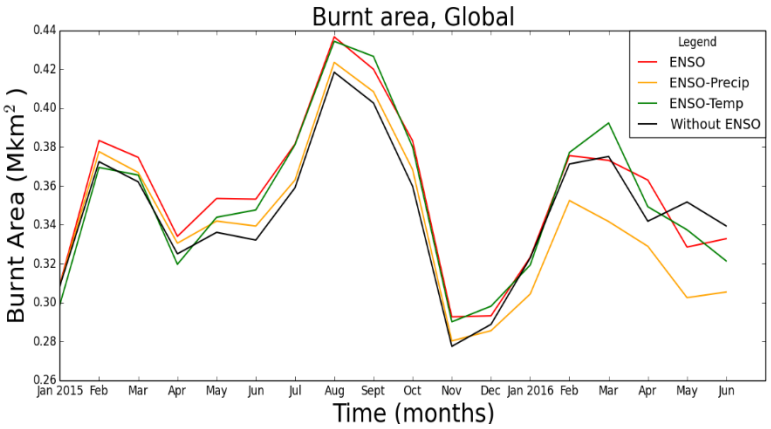

a

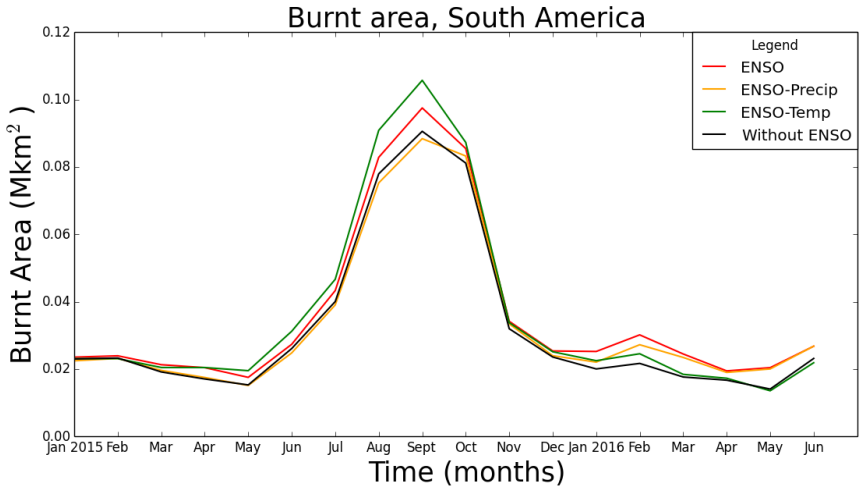

b

Figure 4.30: Drivers of burnt area globally and for South America
Burnt area (Mkm^2) globally (a) and for South America (b) from January 2015 – June 2016 simulated by JULES-INFERNO

Burnt area for South America as a whole is highest across August – October (Figure 4.31), and comparing to a year without El Niño (2013-2014) the burnt area was higher in 2014-2015 as the El Niño was beginning, and higher again in 2015-2016 with the full impact of the El Niño. Without the El Niño (dotted line) the burnt area would not have been as high as in 2015-2016 according to the

projections, but would still have been higher than the previous two years from August-October.

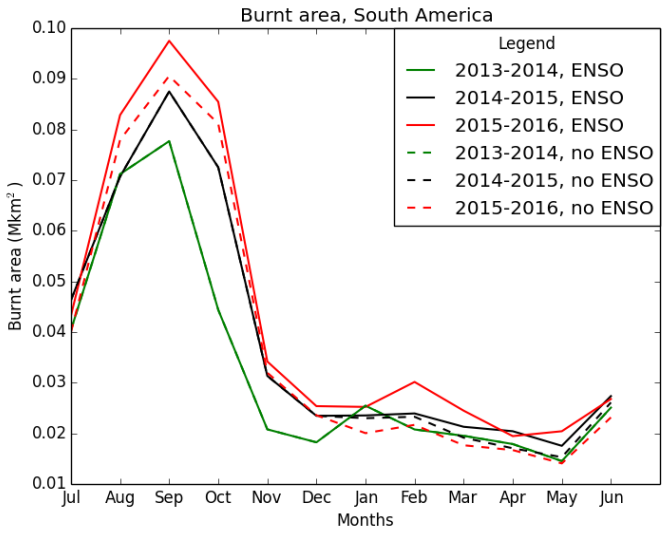

Figure 4.31: Burnt area for South America 2014-2016
Burnt area (Mkm^2) over South America from July– June for years 2013-2014, 2014-2015, and 2015-2016 with and without El Niño simulated by JULES-INFERNO

To understand how burnt area changed as a result of the El Niño across South America, Figure 4.32 shows the change in total burnt area with El Niño in 2015. We can see that the impacts on fire did change spatially, especially across Brazil, with an increase in burnt area across the Brazilian Cerrado region, but a decrease in the East. This is within the Caatinga area (Figure 1.4), and is likely driven by fuel limitation (Figure 3.36 panel d). Putting this in a global perspective, the pattern of change is mixed across all other continents as well (Figure 4.33).

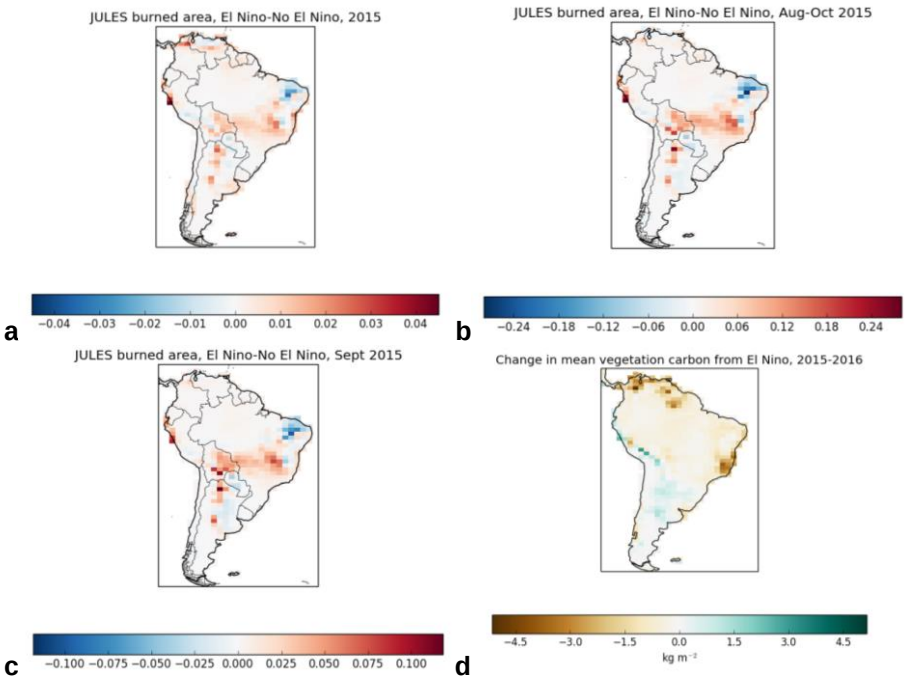

Figure 4.32: Change in burnt area in South America
Change in burnt area fraction due to El Niño across South America for 2015 (a), peak fire season Aug-Oct 2015 (b), and peak fire month September 2015 (c) simulated by JULES-INFERNO. Change in mean vegetation carbon shown in (d)

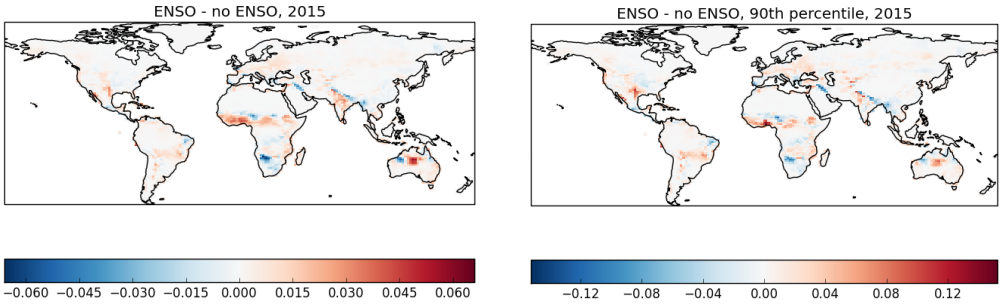

Figure 4.33: Change in global burnt area 2015
Change in total burnt area fraction (left), and at the 90th percentile (right) due to El Niño in 2015 simulated by JULES-INFERNO

Over a period of 5 years, JULES-INFERNO does not show 2015-2016 to be an outstanding year in terms of high burnt area, with 2011 showing a similar extent (Figure 4.34a). It is only when we compare to average climatology for the year ('No El Niño', black line) that the increase in burnt area due to El Niño is evident. Overall for Brazil, the El Niño shows higher temperatures (b), lower rainfall (c), and reduced soil moisture (d), which leads to an increase in burnt area (a), a decrease in plant respiration (e) and reduction in vegetation carbon (f). Comparing two regions of Brazil, one in central Amazonia (Manaus, g) and one in the Cerrado region (Primavera do Leste in the state of Matto Grosso, h), both show higher burnt area with El Niño than without, but the location in the south shows much higher total burnt area (Figure 4.34, g and h).

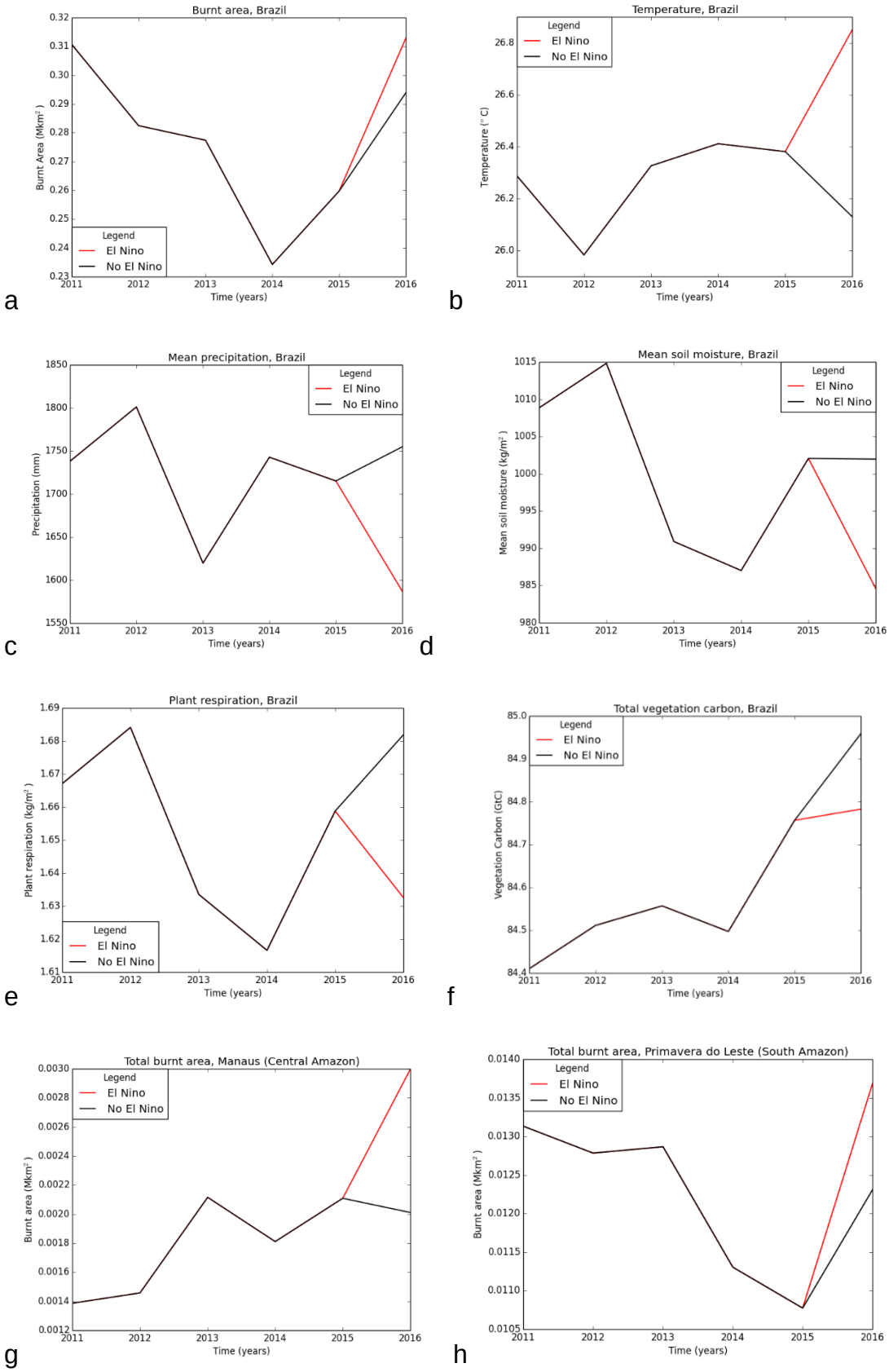

Figure 4.34: Change in key variables due to El Niño 2011-2016
Time series for 5 years 2011-2016 showing change with El Niño across a range of variables, as labelled. Manaus is taken as 1 to 5 degrees latitude, 298 to 302 longitude (62 to 58 West), and Primavera do Leste in the state of Matto Grosso, -13 to -17 degrees Latitude, 52 to 56 West, simulated by JULES-INFERNO

To answer the question of how the impacts of the 2015/16 El Niño varied spatially and temporally across South America using the JULES-INFERNO model, I have investigated burnt area over a time series and spatially across the continent from 2015-2016 using an experiment to demonstrate 'No El Niño' compared to the observed El Niño. The results have shown that the fire season was highest across August – October 2015, and that the burnt area overall was higher as a result of the El Niño. However the regional changes in burnt area were spatially heterogeneous, with the southern region of Brazil across the Cerrado showing higher modelled burnt area and the East of Brazil showing lower burnt area. Studies of two locations in Manaus and Matto Grosso in Brazil also demonstrated a higher burnt area across the South of Brazil. This picture of mixed impacts was also shown to be the case on a global scale. Investigating the driving variables that may have contributed to these results showed an overall increase in temperature, and overall decrease in mean precipitation, soil moisture, plant respiration and vegetation carbon in Brazil. An additional experiment changing only the precipitation and temperature separately showed that temperature was the more important driver of burnt area during the peak fire season in the 2015/16 El Niño.

Finally, I compare the model results to observations of burnt area from GFED4.1s to understand if the model is capturing the observed interannual variability.

INFERNO is able to capture the right order of magnitude of the global burned area and emissions, and accurately represents a peak in burnt area in August, and a drop in emissions in November (Figure 4.35 a and b).

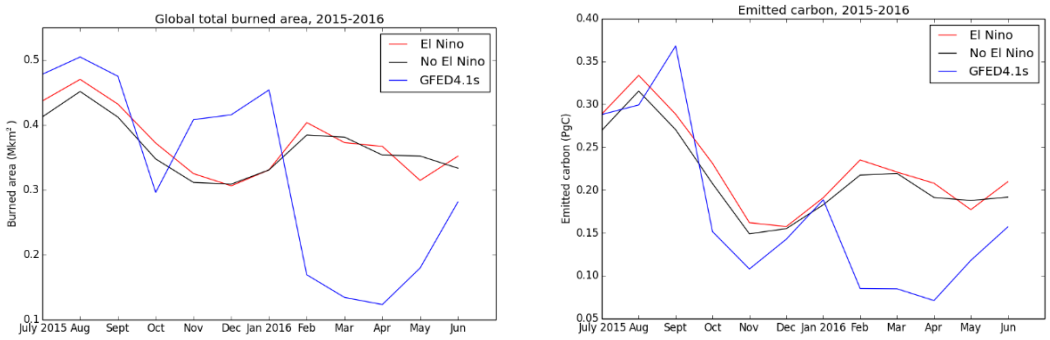

Figure 4.35: Modelled burned area and emitted carbon with observations
Global total burned area (Mkm^2) (left) and emitted carbon (PgC) (right) July – June, as modelled by JULES-INFERNO (red and black, 2015-2016) and from GFED 4.1s observations (blue)

The large drop in burnt area in February shown in the GFED observations is not captured by JULES; to check this was not an anomalous year I examined the previous five years of data to see if this pattern is repeated (Figure 4.36). A large decrease in burnt area is seen every year in the last five years in February, so this is a robust seasonal variation that is not being captured by the model. As shown previously, the global trend is dominated by large burned area in Africa (Figure 4.22), and therefore this may drive the seasonality in the observations. Peak burning in Africa for example is in July in the South, and January in the North (Roberts *et al*., 2009). In some regions burning coincides with the end of the agricultural season rather than in the peak dry season, whereas human ignition datasets used in modelling are typically based on population on an annual to decadal timescale. Therefore this may not be a model deficiency, but rather a current inability to capture seasonality of human trends in burning.

What is also apparent is that 2015-2016 was not a significant year for global total burnt area, contrary to the previous El Niño year 1997-1998 (Figure 4.36b). However the impacts of El Niño events are spatially heterogeneous, with some areas getting hotter and drier, and some experiencing increased rainfall. This results in areas of increased burnt area in some regions, and areas of decrease in other regions, which impacts the global mean. The model captures the low burned area in Sept-Oct 2013, and the peak in Sept 2011, but the high burned area of 1997-1998 does not stand out as an anomalous year in the model. The fires of the 1997/98 El Niño were dominated by widespread peatland fires which is not yet included in the model as a separate process, which may explain why 1997-1998 is not shown as an unusual year. This analysis also highlights that the change due to El Niño in the model is not large compared to natural variability.

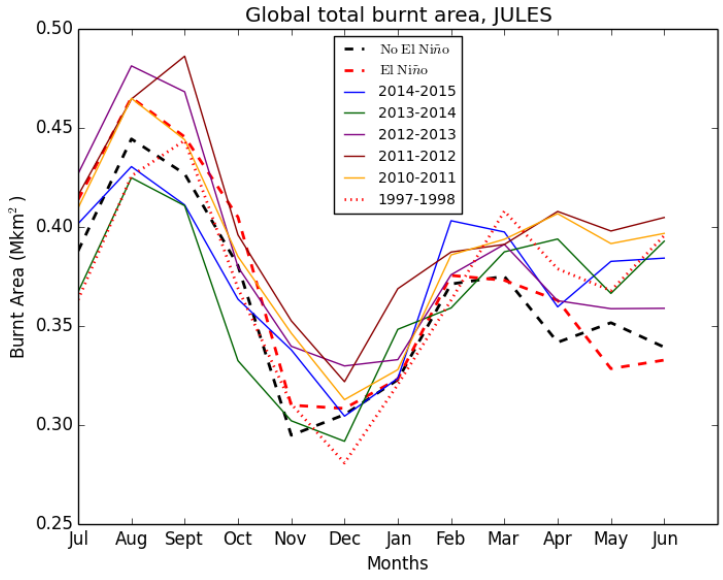

a

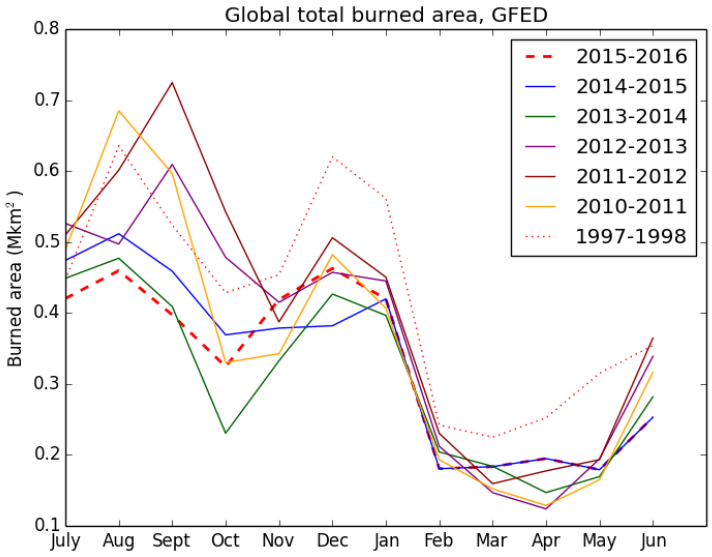

b

Figure 4.36: Global burnt area 2010-2015 with JULES and observations
Global total burnt area (Mkm^2) July-June from 2010 to 2015, plus 1997-1998 from JULES-INFERNO (a) and GFED4.1s observations (b)

To validate the model against observations over a longer time series I take data from 1997 to 2015 for burned area and emitted carbon (Figure 4.37). Again the model captures the right order of magnitude of burnt area and emissions over the period, and in some cases individual years are well modelled such as 2006-2008. From these results it is quite apparent that the global burned area is decreasing, as reported in Andela *et al*. (2017). This decline in fire is not being captured by JULES; the main suggested cause for this decline from Andela's research is the

increasing conversion of savannas into managed agricultural lands and therefore human suppression and fire management is increasing in these ecosystems. As agricultural lands are not yet represented as distinct and exempt from fire, this is a probable explanation for why the model does not show a similar downwards pathway as the observations. Spatially the places where fire occurs are captured well compared to the observations (Figure 4.38), although notably fire across India is too high as previously discussed in Chapter 3.

a

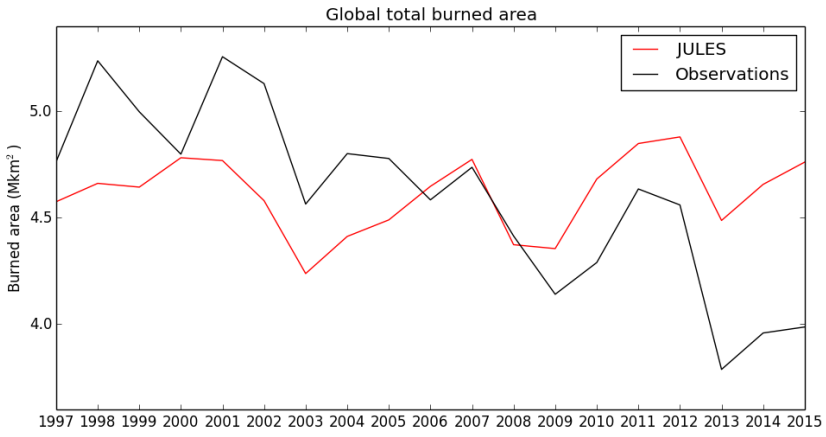

b

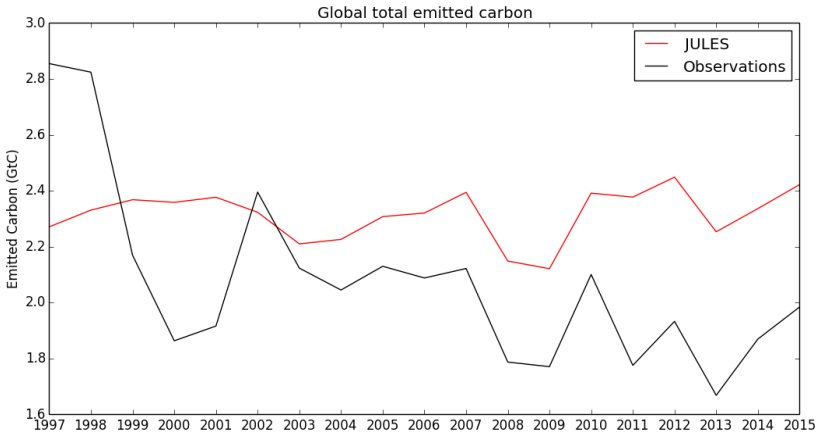

Figure 4.37: Modelled burned area and emitted carbon 1997-2015 with observations
Global total burned area (Mkm^2) (a) and emitted carbon (GtC) (b) 1997-2015, as modelled by JULES-INFERNO (red) and from GFED 4.1s observations (black)

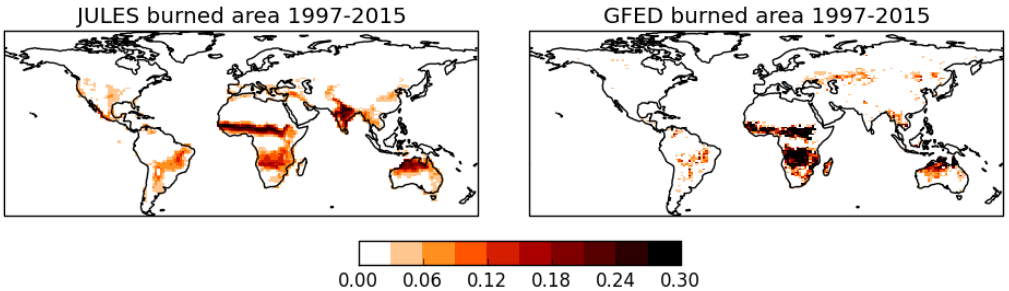

Figure 4.38: Map of modelled and observed burned area
Global total burned area fraction as modelled by JULES-INFERNO (a) and GFED 4.1s observations (b) 1997-2015 mean

4.5 Discussion

Here I have considered the impact of the 2015/16 El Niño on fire, compared to a mean climatology. The results suggest that there was an impact on fire, and this varied spatially and temporally. It is well known that the impacts of El Niño conditions vary, causing drought across Asia, some parts of Africa and northern South America, and wetter conditions across central-east Africa and western America (Met Office[29]). Both the 1997-1998 (Page *et al*., 2002) and the recent 2015-2016 (Aragão *et al*., 2018) El Niño events have been associated with an increase in fire, and the results here have shown that in some regions fire did increase with the 2015-2016 El Niño compared to a 'no El Niño' scenario.

Surprisingly, in the three regions studied here, both the GPP and the respiration decreased with El Niño in all cases. However looking at the overall impact of these changes showed that the decrease in GPP was larger than the decrease in respiration, leading to an overall decline in the uptake of carbon in all regions, exacerbated by the additional emissions from fire which are included in the calculation of NBP here for the first time. The modelled carbon emissions are in agreement with GFED observations, producing a similar order of magnitude of emissions. These results therefore have important implications for the calculation of carbon budgets using JULES which have not included fire emissions explicitly up to now, potentially reducing the remaining budget. However it should be noted again that there are uncertainties in the GFED data (see section 1.3.3), and the data have been found to underestimate burned area and emissions from the 2015/16 El Niño in Amazonia (Withey *et al*., 2018).

Focusing on Brazil, there is an overall warming and drying of the region (Figure 4.14, Figure 4.34) which gives some context to the increase in burnt area shown. It is a well-known feature of El Niño conditions that there is a drying over the Amazon region, which is associated with a weakening of the land carbon sink and thus higher rates of CO_2 growth (Humphrey *et al*., 2018).

The pattern of rainfall moves across Brazil from the West (central South America) in January, to the North from May through to July, with very low rainfall in August

[29] Met Office ENSO Impacts: https://www.metoffice.gov.uk/research/climate/seasonal-to-decadal/gpc-outlooks/el-nino-la-nina/enso-impacts

and September across central South America, correlating with the highest burned area in this region (see Appendix 4, Figure A4.1). The shift in fire occurrence is also evident across the year globally, for example the region of high burned area shifts from central Africa at the beginning of the calendar year, to Southern Africa from May through to September (see Appendix 4, Figure A4.2).

The previous large El Niño of 1997-1998 showed a large spike in carbon emissions, as shown in the GFED observations (Figure 4.37; Figure A4.11). A significant part of this was due to emissions from peatlands across Indonesia (Page *et al*., 2002). The same peak in emissions was not seen in the JULES-INFERNO model, and this points to an important development for the model to be able to represent peatland fires in future iterations.

The period of 2005-2014 used for this study was chosen to ensure conditions are as similar as possible to 2015/16 in terms of climate and CO_2 levels, while 10 years was chosen to reduce the effects of interannual variability. However this period does include the weak El Niño years of 2004-2005, 2006-2007, and 2009-2010, meaning some of the impacts of the 2015/16 El Niño may look weaker than if compared to the previous 20 years. It should also be noted that this experiment cannot be defined strictly as an attribution study for El Niño impacts, as other modes of variability may have driven changes during 2015/16. For a more complete attribution study to be conducted, El Niño events could be isolated from the historical period and compared to standard years, however this is complicated by the relatively few occurrences of El Niño events, and large range in strengths across numerous indexes that make it difficult to compare each event. We can define the 2015/16 meteorological conditions as dominated by a significant El Niño in this case, and using models we are able to compare the impacts against a 10-year mean climatology which gives us greater insight into the causes and impacts of the El Niño event.

4.6 Conclusion

In this chapter I have investigated three research questions:

1) What was the impact of the 2015/16 El Niño on fire, and did this vary globally?

2) What impact did the El Niño have on the carbon sink globally and regionally?
3) How did the impacts of the 2015/15 El Niño vary spatially and in time across South America?

The first question was addressed by using the JULES-INFERNO model with an experiment where the observed 2015/16 El Niño did not happen using the average climatology from the previous 10 years. The results showed that the burnt area was impacted by the El Niño, with some areas showing an increase in burnt area (south USA, South America, central Australia) and others showing a decrease (Africa, east Asia, west Australia). This also affected emissions in the same way. Globally burnt area was higher with the El Niño in the last half of 2015, and emissions were higher for most of the period July 2015 – June 2016. Three fire-prone regions were considered; Asia, Africa, and South America; out of these regions South America showed the largest change (increase) in burnt area with the El Niño, which was the same with both constant and varying ignitions and land-use, driven by increased temperature and reduction in moisture availability. Africa showed a negative change driven by higher humidity and lower fuel availability. Overall, the impact of the 2015/16 El Niño on fire varied by region.

To answer the second question I explored the change in NBP using the experiment with and without El Niño. I found that the year 2015-2016 had the lowest NBP in the series of 10 years, and lower for most of the year than the previous largest El Niño in 1997-1998. This resulted in converting South America and Africa from a sink to a source of carbon, and a reduction in the Asian carbon sink without fire due to decreases in GPP; with fire South America was still converted from a carbon sink to a source driven by increases in fire and decreases in GPP, and Africa and Asia became larger sources of carbon driven by reduction in GPP and increases in fire respectively. Reduction of NBP in Africa seem to be dominated by a reduction in GPP in the south of the continent. The response across Asia is mixed, but across tropical Asia fire also appears to be a dominant driver of NBP reduction. Overall the 2015/16 El Niño reduced the carbon sink globally and for each region studied.

Thirdly I considered the drivers of the El Niño globally and for South America, and found that temperature was a larger driver than precipitation. Burnt area in South America was highest in August-October, and the change due to El Niño varied

spatially with the Cerrado region in the South of Brazil experiencing an increase in burnt area and the East showing a decrease. This gave an overall increase in burnt area for the country as a whole. The El Niño caused an increase in temperature, humidity and burnt area, and overall decrease in mean precipitation, soil moisture, plant respiration and vegetation in Brazil.

The final section compared the model results to observations from GFED4.1s, and showed that the magnitude of burnt area and emissions are well modelled, but the seasonal variability in burnt area is less well captured from February – June across a year. Interannual variability is captured by the model, but the overall downward trend in burnt area is not, likely due to processes of suppression in agricultural lands not being captured yet in the model. Similarly the high burnt area in the previously large El Niño 1997-1998 was not represented in the model, likely due to lack of peat representation.

In conclusion, this chapter has shown that although 2015-2016 was not a peak year for global total burnt area or fire emissions, the El Niño had an impact on fire which varied regionally, with the highest increase in South America, which led to an overall increase in burnt area and emissions compared to a ‘no El Niño’ scenario for 2015-2016. This contributed to a reduction in the sink of carbon globally and regionally. Across South America there were both positive and negative impacts on fire due to the El Niño, but overall the burnt area increased across the continent and this had a large negative impact on the carbon sink which changed to an overall source of carbon over the El Niño period.

Chapter 5: Future projections of fire, climate and land-use change

5.1 Introduction

There is low agreement in models on whether climate change will cause fires to become more or less frequent in the future due to the complexity of interactions and feedbacks, and lack of proper representation in models (Settele *et al*., 2014; Kloster and Lasslop *et al*., 2017). With climate change we can expect to see an increase in temperatures globally, which could lead to increased fire weather conditions. However, moisture is required for adequate vegetation growth and fuel production, and future projections of rainfall are less certain. In some regions precipitation may increase substantially, which could lead to a reduction in burned area if fuel becomes too wet to burn (Prentice *et al*., 2011).

A number of studies have shown that on a global scale, fire occurrence may be decreasing. Changes in patterns of land-use including conversion of savanna land to agricultural farm lands have led to a downward trend in global fire occurrence according to Andela *et al*., (2017). Yet this can be conflated incorrectly with other aspects of the fire regime which are not necessary correlated; for example while the overall burned area has decreased, the number of fires has increased in some areas such as the Mediterranean, and in the USA national reporting shows fewer but larger fires (Doerr and Santin, 2016). In addition there is regional variation, with some areas such as the tropics having seen an increase in burned area from deforestation fires in the last half of the century (Mouillot and Field, 2005), although an important aspect of this is also the relaxation of fire suppression policies over this period (Doerr and Santin, 2016). Moritz *et al*. (2012) project a decrease in fire activity across most of the southern hemisphere using a statistical model based on CMIP3 climate projections by the end of the century, although there is little agreement on the direction of change in the nearer term to 2040, and notably there is low agreement across the east of Brazil even by 2100. The primary driver of projected decreases for tropical rainforests is an increase in precipitation. However, while CMIP3 projections show an increase in wet season precipitation and a decrease in the dry season across the Amazon in the future, the more recent CMIP5 projections

show a decrease in precipitation in both wet and dry seasons (Joetzjer *et al*., 2013; Kanikicharla[30]).

In contrast, other studies have projected increases in fire in the future. Liu *et al*. (2010) project higher fire danger by the end of the century across South America, Southern Africa and Australia, mainly due to warming and drying using the KBDI and four GCMs including HadCM3. Wu *et al*. (2015) found that burned area in eastern Europe may increase over the coming decades, based on LPJ-GUESS-SIMFIRE and LPJmL-SPITFIRE simulations. Kloster *et al*. (2012) use CLM with climate projections from ECHAM5/MPI-OM and CCSM to show projected increases in annual mean fire emissions by the end of the century, particularly in South America, mainly due to climatic changes although land-use and population changes were also factored in. They projected that overall, global carbon emissions from fire in 2075-2099 will be higher compared to present day by 17-68% due to climate change. Fire may also be a significant danger in high latitude regions in the future. Permafrost thaw has already been associated with fire events in Western Canada, creating a positive feedback with more peatland consequently exposed to further burning (Gibson *et al*., 2018). But confidence in the magnitude of radiative forcing resulting from fires is low, and based on limited studies using wide-ranging modelling techniques, we cannot even be sure of the sign of the radiative response yet (Figure 5.1). Other studies show no detectable change in future fire (Knorr *et al*., 2016).

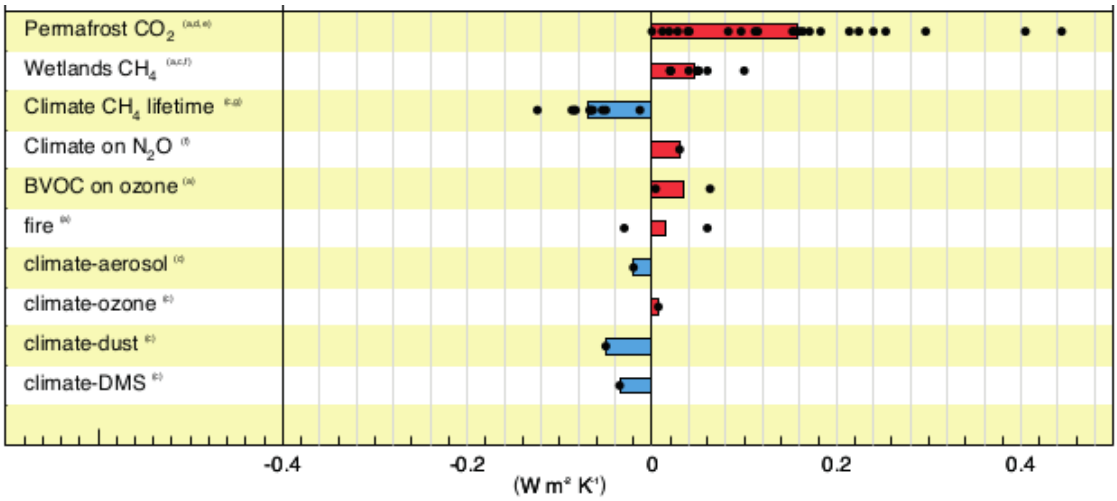

Figure 5.1: A synthesis of the magnitude of biogeochemical feedbacks on climate. Black dots represent single estimates, and coloured bars denote the mean of the dots with no weighting or likelihood estimate. There is low confidence in the magnitude of the

[30] https://unfccc.int/sites/default/files/4_krishna_sbsta.pdf

feedbacks, especially for those with few, or only one, dot. Reproduced from IPCC AR5 Figure 6.20.

HadGEM2-ES has been used in previous studies to assess future fire danger using the McArthur Forest Fire Danger Index (FFDI) to estimate how fire danger may change with different representative concentration pathway (RCP) scenarios (Betts *et al*., 2015). The results showed a general increase in FFDI under all emissions scenarios, with the greatest risk in the scenarios with highest warming (RCP8.5). Areas of particularly large increase in FFDI under RCP8.5 included eastern Amazonia. There are however added complexities associated with diagnosing fire occurrence that are not represented by indices of fire danger such as the FFDI, including fuel availability, as well as anthropogenic influences including both ignition and fire suppression, and therefore risk varies strongly by region (Ciais *et al*., 2013). To be able to represent all of these factors, an interactive land surface or Earth System Model with fire is required.

One of the primary factors in the uncertainty of future fire trends is the uncertainty in future projections of precipitation. There is large disagreement across models concerning how precipitation will change by the end of the century, in particular over South America (Figure 5.2), predominantly related to changes in sea surface temperatures and land-sea temperature differences which cause shifts in convection and convergence (Kent *et al*., 2015). However the mean trend across CMIP5 models indicates a drying across the NE of South America, in line with projections from HadGEM2-ES. Over the Amazon, this drying is largely driven by plant physiology (Chadwick *et al*., 2016), whereby plant stomata open less under higher levels of CO_2 which leads to reduced evapotranspiration (ET), and local warming and drying (Betts *et al*., 2008). While these physiological processes are represented in HadGEM2-ES, they are not yet included in all ESMs, leading to significant differences in the projections over this region.

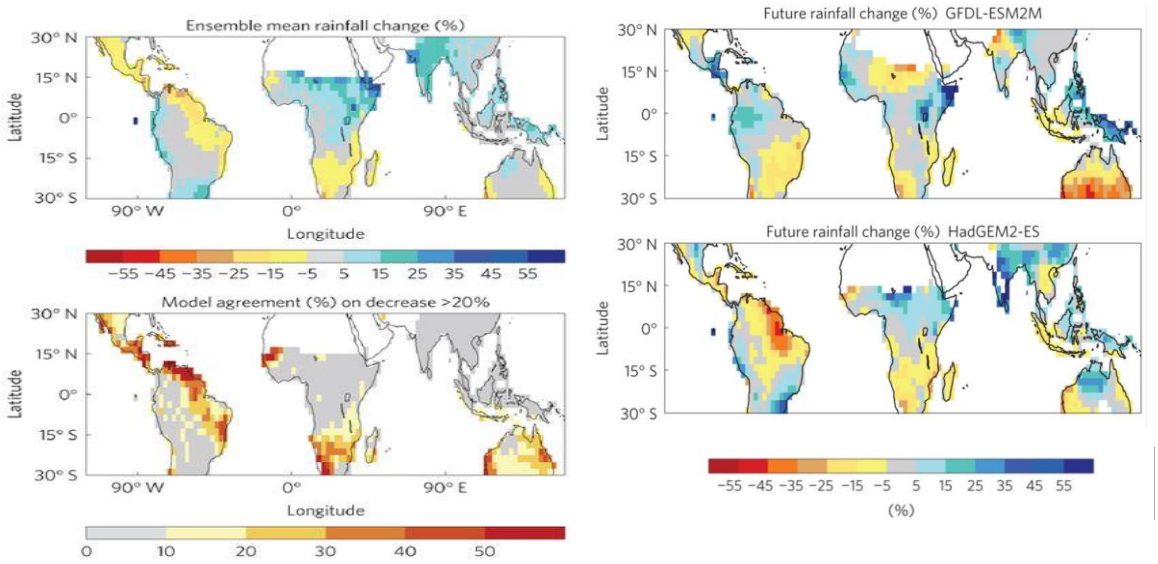

Figure 5.2: CMIP5 projections of precipitation change
Precipitation change for 2071–2100 minus 1971–2000, under the RCP8.5 emissions scenario, as follows: CMIP5 ensemble mean precipitation change (top left), model agreement on precipitation changes at a number of thresholds (bottom left), GFDL-ESM2M only (top right) and HadGEM2-ES only (bottom right). Areas where 1971–2000 precipitation is <200 mm yr−1 (top left), areas where <20 models have 1971–2000 precipitation of >200 mm yr−1 (bottom left), areas of desert and sea (right column) and are masked in white. Reproduced from Chadwick *et al*. (2016) figures 1 and 4.

While the potential for changes in fire patterns will change globally in the future, and high latitude regions may also be at increased risk under a warming climate, here I focus on Brazil as a key region associated with high uncertainty in the future.

Fire in the Amazon

Generally across central Amazon today fire is not a major threat, with high levels of moisture and few ignition sources. However, as discussed in Chapter 1, fire may be at risk of increasing in the future as a result of warming and drying over the next century with climate change (IPCC AR5), especially in the south-east Amazon where fire danger is higher, and where most models project longer and more intense dry seasons in the future (Malhi *et al*. 2008; 2009), combined with increasing land-use frontiers. A recent study by Le Page *et al*. (2017) considers the risk of understory fires increasing in the Amazon in the future with different RCP scenarios; they show that fires are projected to increase in frequency and duration, burning up to 28 times more forest by the end of the century than present day. Limiting emissions and land-use activities as per scenario RCP4.5 has some effect on reducing this to 0.9-5.4 times higher than present day, showing again the important interactions between climate and land-use in this

region. Drought years could increase fire danger further on top of this climate change signal, as was the case in the recent 2015/16 El Niño (Aragaõ *et al*., 2018).

CO_2 fertilisation may go some way towards offsetting the vulnerability of vegetation to future drought, through increased photosynthesis, carbon uptake and water use efficiency, but this may be limited by nutrient availability, and there is still a high degree of uncertainty around the size of these potential changes due to the current lack of field observations (Ciais *et al*., 2013).

Future fire danger in the Amazon will depend on both anthropogenic and climatic factors. It is estimated that currently 58% of the Amazon is too humid to support fires, but climate change may reduce this area to 37% by 2050 (Ciais *et al*., 2013) or even lower (Le Page *et al*., 2010), which will interact with human factors such as land-use, ignitions and suppression as well as changes to biomass (fuel). As stated in the IPCC AR5 report:

"Climate change alone is not projected to lead to abrupt widespread loss of forest cover in the Amazon during this century (medium confidence), but a projected increase in severe drought episodes, together with land-use change and forest fire, would cause much of the Amazon forest to transform to less dense, drought- and fire-adapted ecosystems" (Settele, 2014).

More recent work has added to our knowledge in this area, confirming the conclusions reached in the AR5 report, and providing further evidence of vulnerability of tropical forests to drought (Good *et al*., 2018).

Golding and Betts (2008) used the McArthur FFDI to calculate the change in fire danger in the Amazon with the simulated changes in climate. They found a significant increase in central and eastern Amazonia by 2020, and high fire danger for over 50% of the forest by 2080; these areas also correlate with those projected to be most impacted by deforestation as projected by the SRES scenarios of LUC. They estimated that future vulnerability to fire may depend nonlinearly on both climate change and deforestation. However, this study was also based on HadCM3, which was subsequently shown to have a dry-bias in this region.

There is still much uncertainty around how forests will respond in the future to changing climatic conditions, and how this will interact with anthropogenic factors such as land-use change and fire. Some models show high resilience of tropical forests to climatic changes, but the Amazon in particular has been shown to be one of the most vulnerable to ecosystem changes (Betts *et al*., 2015; Good *et al*., 2011), and other models have shown a higher vulnerability of tropical forests in general (Colwell *et al*., 2008; Bertrand *et al*., 2011). Recent research has suggested that when the impact of fire is included in analysis of future change over the Amazon, the potential tipping point for the Amazon forest to a savanna-like state may be lowered from the previous estimates of 40% deforestation to around 20-25% (Nobre *et al*., 2016; Lovejoy and Nobre, 2018).

Tropical forests have high ET rates, leading to increases in precipitation and cooling, and studies in Amazonia have shown that conversion of forest to agricultural pasture land has had a warming and drying effect on the region (Bonan, 2008). There are additional complexities resulting from changes to albedo, where forests have a low albedo (low reflectivity and therefore higher heat absorption) leading to warming which is offset by strong evaporative cooling, but this process is reversed when forests are converted to pastures. It can be expected that fire will have a similarly disruptive impact on biogeochemical processes, including increasing albedo and reducing ET. These non-linear interactions between vegetation and atmosphere can amplify or reduce the effects of anthropogenic climate change.

In this study, I use the land surface community model JULES (Joint UK Land Environment Simulator) (Best *et al*., 2011) with the latest version of the fire model JULES-INFERNO (Mangeon *et al*., 2016) to understand how fire danger may change in the future under three emission scenarios, RCP2.6, RCP4.5 and RCP8.5. I assess the response of vegetation to future fire using INFERNO coupled to vegetation dynamics (Burton *et al*., 2019) for the first time, to answer three key research questions:

1) How is burnt area projected to change with climate change in the future and, together with changes in land-use, what impact does this have on vegetation coverage?

2) What is the impact of different warming levels, and does the pathway to reach them alter the impacts on the land surface?
3) Could fire lead to a change in state from tropical forest to savanna by 2100?

The results are divided into three sections to answer each of these questions.

5.2 Methods

When modelling future change, it is necessary to consider how future concentrations of GHGs present in the Earth system may vary over time. To reflect current uncertainty that exists around future emission levels, climate sensitivity to those emissions, policy and mitigation options, technology, population levels, and changes in land-use, a set of Representative Concentration Pathway (RCP) scenarios were developed by the IPCC to represent a range of potential future greenhouse gas (GHG) concentration levels (see Appendix 2). If global mitigation policies are put in place, for example aiming at a high chance of limiting global mean temperature rise to 2˚C above pre-industrial (PI) levels, emissions will be reduced and the concentration pathway RCP2.6 (2.6W/m^2 radiative forcing) could be the future trajectory. On the other hand, if emissions are not curbed and we continue along a business-as-usual pathway into the future, we will see much higher concentrations greenhouse gases (GHGs), and higher radiative forcing such as represented in scenario RCP8.5 (8.5W/m^2 radiative forcing).

Underpinning these concentration scenarios are assumptions about how land-use trends may change, as discussed in Chapter 2. For example in RCP2.6, to achieve high mitigation policy targets it is assumed that large amounts of land will be converted to biofuels (see Appendix 2). In RCP8.5, a large amount of land could be converted to agriculture to feed a rapidly growing population. In other middle-ground scenarios such as RCP4.5, reforestation is implemented as an alternative mitigation measure to help draw down carbon.

In addition to variation in levels of GHGs and land-use change between scenarios, there are also different pathways for how aerosols may change in the future which varies by scenario. After reaching a peak around 2010, aerosol concentrations are projected to decrease over the twenty-first century in all

scenarios, with the strongest decline following mitigation of emissions in RCP2.6, with their associated cooling effects therefore becoming weaker (Szopa *et al*., 2012). The highest aerosol optical depth (AOD) is assumed in RCP8.5 (Figure 5.3) from high levels of emissions, leading to highest negative radiative forcing (Table 5.1). RCP4.5 follows a similar pathway to RCP8.5 until around the middle of the century, when the AOD starts to decrease faster than in scenario RCP8.5. This may have impacts on biogeophysical and biogeochemical responses (Jones *et al*., 2003), for example lower aerosol levels have been linked with a potential increase in drought conditions over the Amazon (Cox *et al*., 2008).

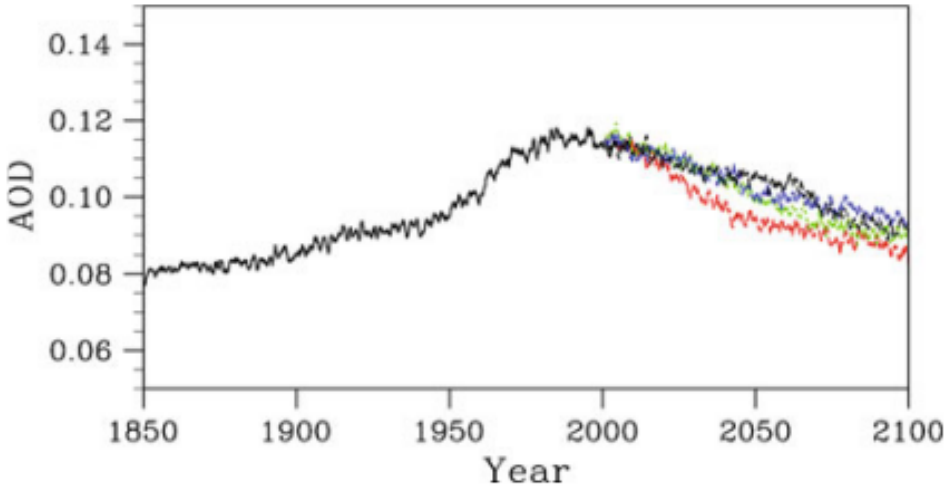

Figure 5.3: Global average aerosol optical depth
At 550 nm as simulated from CAM-chem (Community Atmosphere Model vn3.5 with interactive chemistry). Red curve = RCP2.6. Green curve = RCP4.5. Black curve = RCP6.0. Blue Curve = RCP8.5. Reproduced from Lamarque *et al*. (2011).

Table 5.1: Clear sky radiative forcing (W/m^2)
With respect to 1850 by aerosol type. Reproduced from Lamarque *et al*. (2011).

	2000	2100 RCP2.6	2100 RCP4.5	2100 RCP6	2100 RCP8.5
Black carbon	0.10	0.01	0.02	0.03	0.04
Organic carbon	−0.05	−0.02	0.00	−0.04	−0.02
Ammon. nitrate	−0.05	−0.10	−0.05	−0.07	−0.10
Sulfate	−0.81	−0.13	−0.21	−0.22	−0.29
Total	−0.81	−0.24	−0.24	−0.36	−0.37

In this experimental configuration, JULES vn4.9 at revision 9986 is driven with HadGEM2-ES model data. Three different RCP scenarios are used for GHG concentrations, aerosols and land-use; a low emissions scenario RCP2.6, a medium emission scenario RCP4.5, and a high business-as-usual emissions scenario RCP8.5. JULES was spun-up for 120 years using one-year preindustrial

climatologies of 1860 CO_2 data and land-use data from HYDE. The model was then run from 1860-2005 for the historical period with varying CO_2 and land-use, and then 2005-2100 with the full data series of CO_2 and land-use for each scenario (see 'Data availability' for fcm repository location). In this version of JULES, dynamic vegetation from TRIFFID is used, with five plant functional types, and including interactive fire and constant ignitions (see Chapter 3 for more information on the model development).

For this study, I use three RCP scenarios to assess how climate may vary by the end of the 21st Century (2090-2099) dependent on GHG concentration levels under a high, medium and low emissions pathway, and investigate what impact this has on other aspects of the climate system compared to present day (taken as 1996-2005). I run simulations with and without fire, and with and without land-use to determine the impact of drivers within the scenarios. For the 'without land-use' scenario I use varying land-use over the historical period, and then set land-use at a constant rate at 2005 for the whole future period.

While the RCP scenarios give an indication of the GHG concentration limits compatible with limiting temperature to specific levels, e.g. RCP2.6 for limiting temperature rise to 2˚C above pre-industrial levels, pertinent policy-relevant questions around possible impacts requires analysis at specific levels of warming, for example how impacts will differ at 1.5˚C compared 2˚C. I therefore consider specific levels of warming in section 2, and assess what impact the differences in pathways has on a range of variables.

Because JULES is a land surface model and temperatures are generally higher over land, model output data from the global Earth System Model HadGEM2-ES is used to define the time periods of specific levels of *global mean* warming at 1.5°C, 2.0°C and 4.0°C above pre-industrial levels (Table 5.2). For each RCP scenario, the first year at which each temperature threshold is reached is recorded (n), and the time period for that temperature is taken as n-9 to n+10 to rule out year-to-year variations in temperature change. The difference at each specific warming level using a 20-year time slice is compared to present day, which is defined here as the period 1981-2010 (where mean CO_2 is 362.43ppm and mean temperature above PI is 0.3°C). This method is based on the study by Johns (2017).

Table 5.2: Periods of specific levels of warming and associated CO_2 from HadGEM2-ES

	Pre-Industrial	**RCP85**	**RCP45**	**RCP26**
1.5°C	1861-1880	2019-2038	2025-2044	2023-2042
2.0°C	1861-1880	2032-2051	2036-2055	2048-2067
4.0°C	1861-1880	2066-2085		
CO_2 (ppm)	**PI (1861-1880)**	**RCP85**	**RCP45**	**RCP26**
1.5°C	287.93	444.49	446.58	432.36
2.0°C	287.93	498.04	474.81	441.58
4.0°C	287.93	721.81		

The third section of this study focuses on the potential for a change of state from tropical forest to savanna vegetation. For this analysis I first use a drought factor based on the Keetch Byram Drought Index (Keetch and Byram, 1986), with varying soil moisture provided by JULES (based on Holgate *et al*., 2017, as used in Burton *et al*., 2018a):

$$\boldsymbol{Drought\ factor} = \frac{\mathbf{0.191} * (\boldsymbol{SMD} + \mathbf{104}) * (\boldsymbol{N} + \mathbf{1})^{\mathbf{1.5}}}{\mathbf{3.52} * (\boldsymbol{N} + \mathbf{1})^{\mathbf{1.5}} + \boldsymbol{P} - \mathbf{1}}$$

Where P = precipitation (mm day^{-1}) and N = number of days since last rain. I use varying soil moisture to calculate the soil moisture deficit (SMD) compared to the field capacity at a depth of 1m to account for varying ecoregions. Secondly I investigate the dry season resilience (DSR) of the forest following the method of Good *et al*. (2013), which investigated the tendency of two models HadCM3 and HadGEM2-ES to project tropical forest dieback in the future based on this resilience factor. This was based on the following equation for the calculation of DSR for HadGEM2-ES:

$$\mathbf{DSR = (dry\ season\ length) + 0.25T - 0.0027CO_2 - 14.7}$$

Where T = temperature in units of °C, CO_2 is in units of ppm, and DSR is in units of months. Dry season length is defined as the number of months with less than 100mm of precipitation (Good *et al*., 2011). The calculation is applied to the tropics, defined as 20.0°S to 20.0°N. I develop this experiment to assess the impact of adding fire to the JULES model, to give an indication of whether the

representation of fire in the model reduces the resilience of the forest in the dry season, making a shift to savanna vegetation cover more likely.

5.3 Results

Section 1: How is burnt area projected to change with climate change in the future and, together with changes in land-use, what impact does this have on vegetation coverage?

Before addressing the first research question, I start by assessing the impact of using model driving data on present day burnt area. Here I am using model output data from HadGEM2-ES to drive JULES offline for both the historical and future projections in this experiment for consistency, rather than using the CRU-NCEP observational dataset which was used for historical and present day simulations in previous chapters. The driving data has a significant impact on the results; the precipitation patterns from HadGEM2-ES show a warm and dry signal along the northeast coast of South America at present day, which is not seen in the CRU-NCEP observed precipitation (Figure 5.4, panel a). Together with temperature and fuel availability (also driven by precipitation, panel b), this changes the pattern of burned area from southeast Brazil to northeast Brazil (panel c). Comparing the results with observations of burnt area, we can see that the present day model projections more accurately reflect the pattern of observed fire occurrence when the CRU-NCEP driving data is used, which will impact the future projections. As there is still a large uncertainty in how projections of precipitation will change in the future (Myneni *et al*., 2007; Ciais *et al*., 2013) as discussed in the Introduction (section 5.1), we cannot yet draw confident conclusions based on model data about the exact pattern or precise location of changes. However CMIP5 models generally agree that there will be warming and drying over this region in the future (see Figure 5.2).

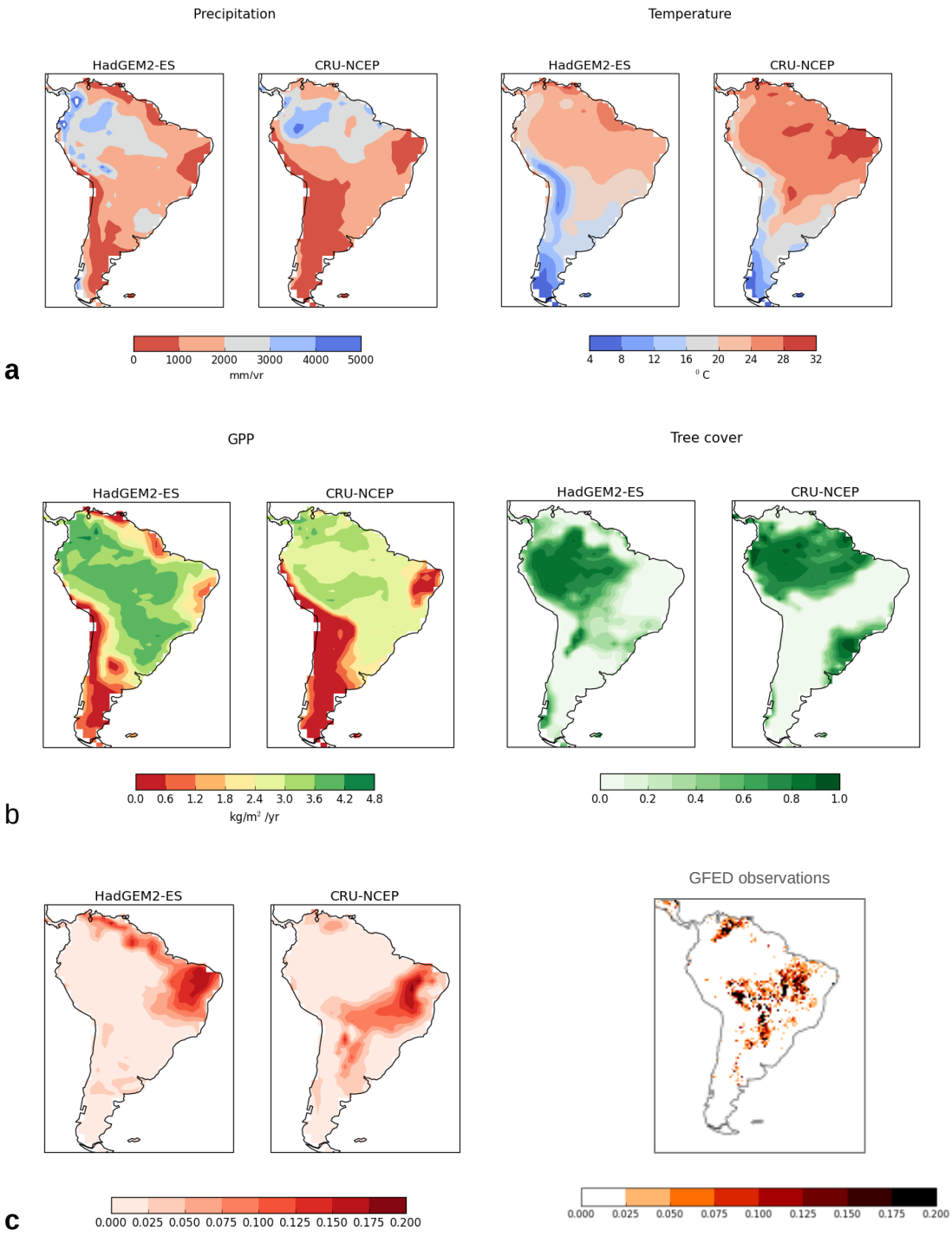

Figure 5.4: CRU-NCEP and HadGEM2-ES
Present day (2005) simulations from JULES driven by HadGEM2-ES and CRU-NCEP. (a) shows annual precipitation (mm/yr) (left) and temperature (˚C) (right); (b) shows GPP (kgC/m^2/yr) (left) and tree cover fraction (right); (c) shows burnt area fraction from HadGEM2-ES (left), CRU-NCEP (centre), and GFED4.1s observations (right) all for South America

Looking at how the global mean temperature changes over time, we can observe a slow but steady increase over the historical period, and a faster increase in temperature from around 1980 to present day along with a similar rise in carbon

dioxide (CO_2) (Figure 5.5, a and b). The future scenarios show very different rates of change, with the RCP2.6 (high mitigation) scenario warming more quickly than the higher emissions scenarios initially, but then peaking and levelling off to stabilise temperatures at around 2.0°C of warming above pre-industrial levels. The RCP4.5 scenario shows a slower rate of warming, but by 2100 temperatures stabilise at around 1.0°C higher than the RCP2.6 scenario. The 'business as usual' scenario RCP8.5 shows rapid and consistent warming reaching temperatures well above the other RCP scenarios by the end of the century. Compared to the CMIP5 ensemble, this is not an unusual pattern of temperature change, with a number of models showing this rapid rise in temperature in the RCP2.6 scenario before stabilising at 2.0°C (Figure 5.6) in response to GHG concentrations. These 'pathways' to warming may have implications for the impacts seen at 1.5°C, 2.0°C and 4.0°C, due to differences in the timing of reaching each temperature scenario as well as the assumptions made in how each level of warming is reached, as I explore further in section 2.

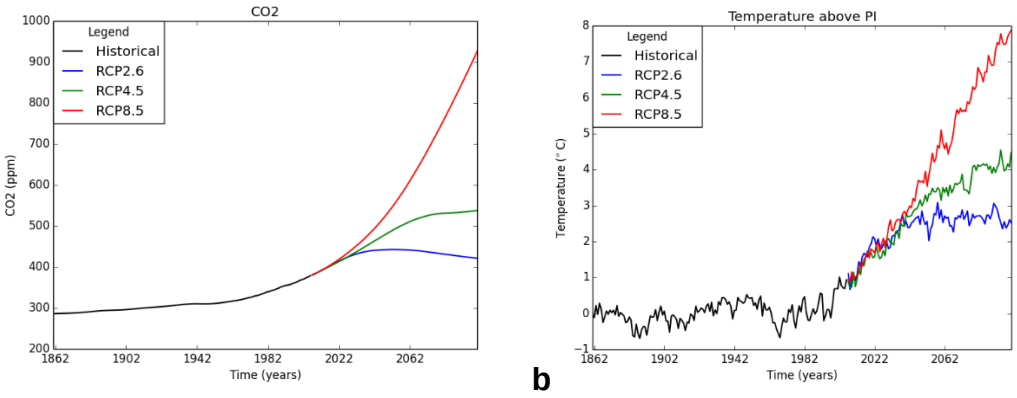

Figure 5.5: Global mean change in CO_2 and temperature
Time series of global mean change in CO_2 (parts per million) (a) and global mean temperature change over time (degrees Celsius above pre-industrial (PI) 1861-1880) (b) from JULES (land-only)

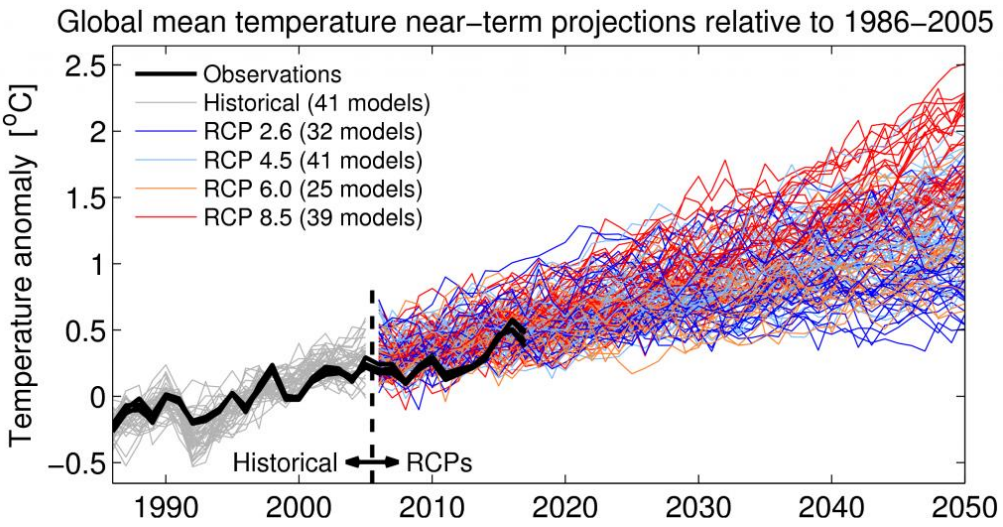

Figure 5.6: CMIP5 global mean temperature projections
Updated version of IPCC AR5 Figure 11.25a, showing time series of global mean temperature observations, and the CMIP5 model projections for different RCPs relative to 1986-2005. The black lines represent observational datasets (HadCRUT4.5, Cowtan & Way, NASA GISTEMP, NOAA GlobalTemp, BEST). Figure from Ed Hawkins Climate Lab Book[31]

Considering now the change in gross primary productivity (GPP) and burnt area over the same period (Figure 5.7 a and b), both show similar patterns of change to Figure 5.5 a and b, indicting a strong driver of temperature and levels of CO_2 with very strong increases in the RCP8.5 scenario. This is as expected for GPP, reflecting more available CO_2 for photosynthesis and thus more productivity. The global burnt area also increases with temperature, staying approximately steady over the historical period but increasing sharply in the RCP8.5 scenario.

Despite an increase in productivity, vegetation carbon declines over the historical period (panel c). From Figure 5.7 panel (d) we can see that a key driver of this change is due to increasing conversion of land for agricultural use. As discussed in Chapter 2, in the RCP4.5 scenario agricultural land-use change declines in the future and reforestation is implemented, and this leads to the highest total vegetation carbon by 2100 out of all three scenarios (c, solid lines). RCP8.5 has high land-use change, but this is somewhat compensated by an increase in productivity. The high mitigation scenario RCP2.6 has high land-use change and low productivity, leading to steady-to-declining levels of vegetation carbon. We can see by comparison that when land-use is kept constant at present day, vegetation carbon starts to increase again in all scenarios, and emulates the CO_2

[31] Climate Lab Book: https://www.climate-lab-book.ac.uk/comparing-cmip5-observations/

concentration and fertilisation effect with RCP8.5 showing the largest increase, followed by RCP4.5 and RCP2.6 (c, dashed lines).

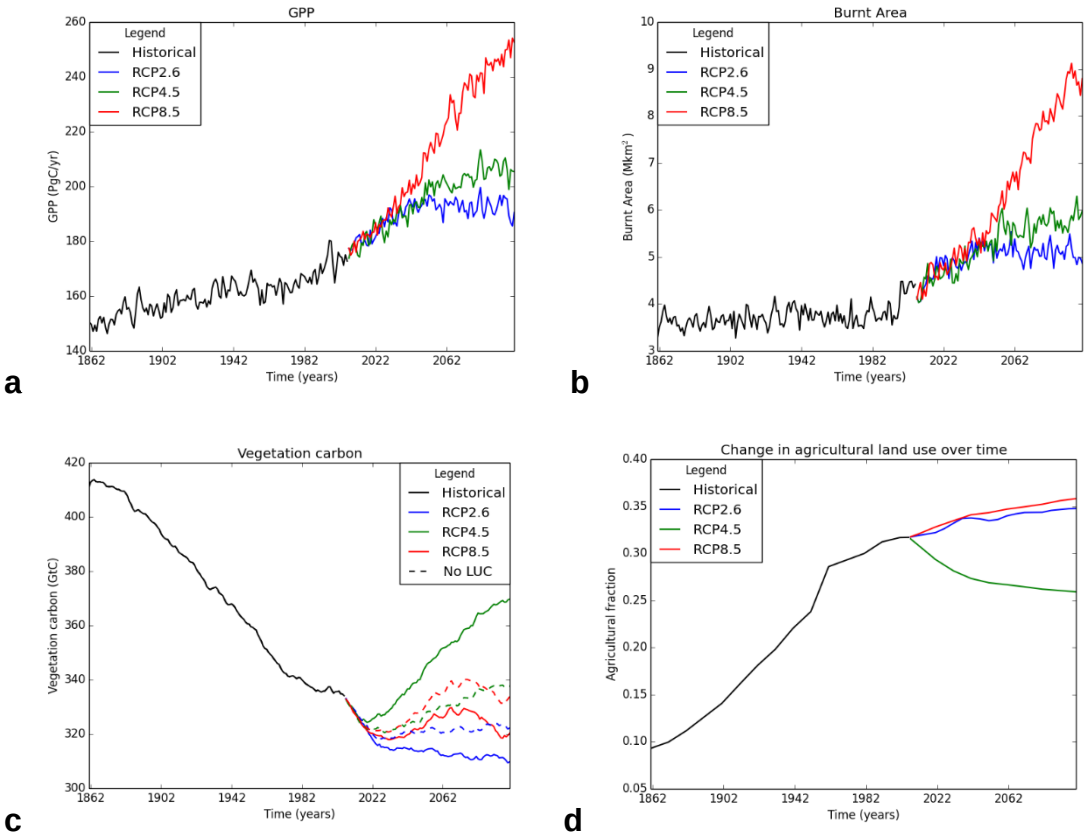

Figure 5.7: Global change over RCP scenarios 1860-2100
Panels a-c show time series of global total: (a) GPP (GtC), (b) burnt area (Mkm^2), (c) vegetation carbon (GtC) (with land-use: solid line, with 'no land-use (constant at 2005): dashed line); panel (d) shows agricultural fraction (fraction of gridbox). All panels show 1860-2100

Figure 5.8 shows how the change in burnt area is higher in the future for many areas, increasing with emission scenario. Regions around east Brazil, parts of Africa, and Europe are shown to be particularly exposed to increased fire danger, especially in scenario RCP8.5 by the end of the century. This can be compared with the McArthur Index for fire danger, as presented in Betts *et al* (2015) and in Appendix 5.

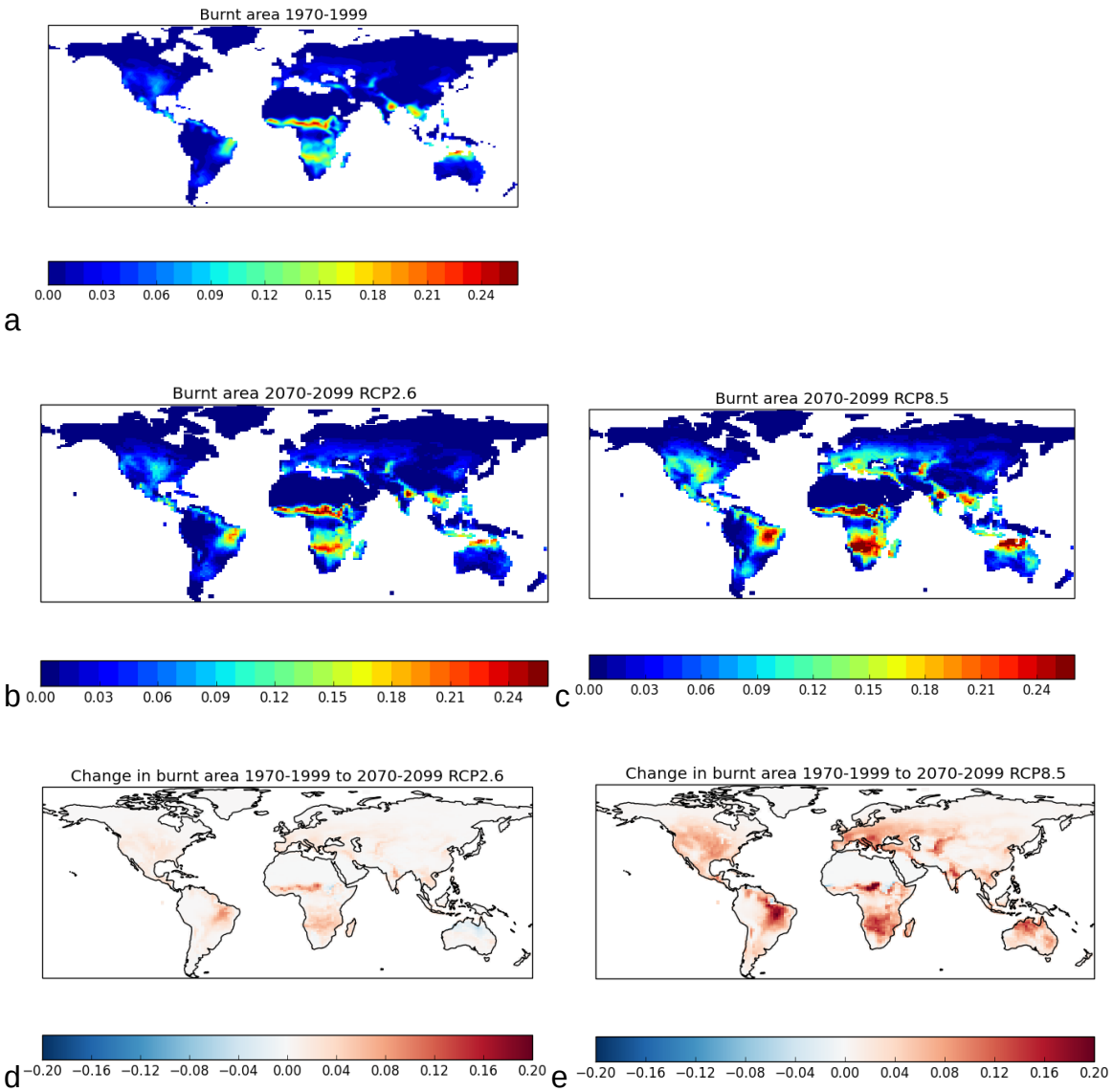

Figure 5.8: Future burnt area as modelled by JULES-INFERNO
Mean burnt area fraction 1970-1999 (a), 2070-2099 RCP2.6 (b), 2070-2099 RCP8.5 (c) change in burnt area 1970-1999 to 2070-2099 RCP2.6 (d), change in burnt area 1970-1999 to 2070-2099 RCP8.5 (e)

The impact of both fire and land-use change disturbances on total vegetation carbon is shown in Figure 5.9. Without fire or LUC, vegetation carbon generally increases globally in the future with CO_2 fertilisation, with higher increases in the higher emission scenarios, however across central Brazil there is still a decrease in carbon compared to present day (top row). This is likely because LUC is held constant at 2005 levels in this experiment, and land-use fraction is already high in this area, so there is no opportunity for high-carbon vegetation i.e. trees to regrow. In the land-use only scenario (third row), land-use decreases in RCP4.5 and as a result vegetation increases everywhere. With this exception, vegetation

carbon strongly decreases across central Brazil both from fire (second row) and LUC (third row). We can see the result of these changes specifically for Brazil below.

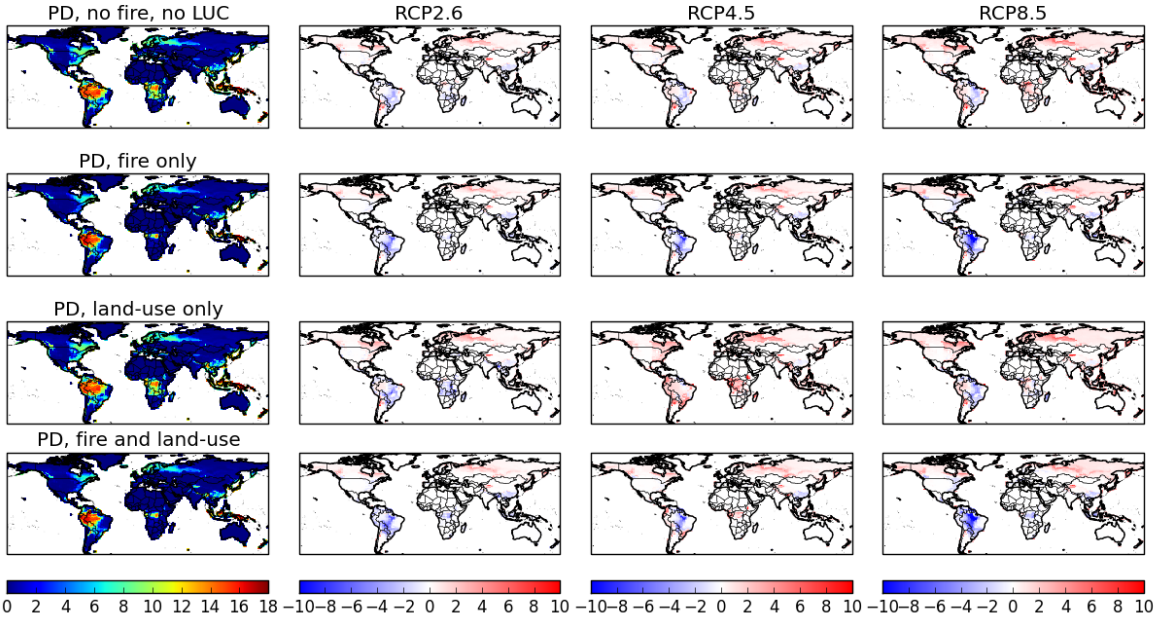

Figure 5.9: Impact of disturbance on vegetation carbon
Total vegetation carbon (kg m^{-2}) at present day (1996-2005 mean) (left column) and change compared to present day (kg m^{-2}) for three RCP scenarios (2090-2099), RCP2.6 (second column), RCP4.5 (third column), RCP8.5 (right column). Top row shows no fire with land-use at 2005, second row shows fire with land-use at 2005, third row shows LUC and no fire, bottom row shows fire and LUC

Now considering Brazil, the highest temperatures by 2100 are obviously projected in the high emissions RCP8.5 scenario, however the maximum temperature reached here is in the north of Brazil (Figure 5.10). In the RCP2.6 scenario the maximum temperature reached is lower. In the RCP4.5 scenario the maximum temperatures are seen along the Northeast coast. Considering the change in precipitation (Figure 5.11), there is a mixed response. In the RCP2.6 scenario central South America generally becomes drier, whereas in RCP4.5 the central region becomes wetter, and there is a strong drying response in the North to Northeast which is stronger again in RCP8.5. Soil moisture in the top layers exhibit a similar pattern of drying (Figure 5.12). As the East and Northeast regions experience warming and (in some areas) drying in the future, they also become more susceptible to fire. We can see the impact of this on burnt area in Figure 5.13 and Figure 5.15.

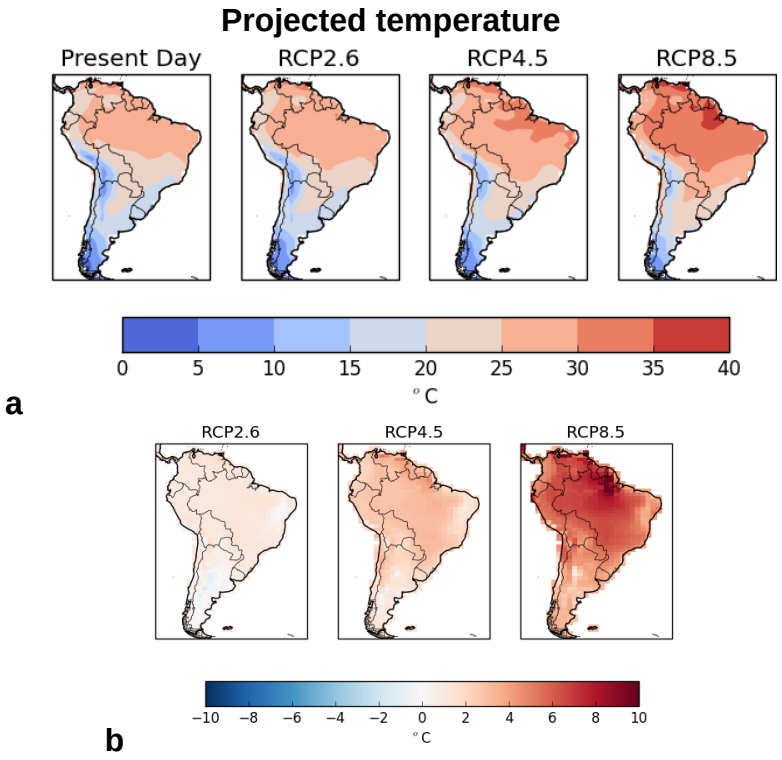

Figure 5.10: Future change in temperature
Panel (a) shows projected temperature (° C) at present day (1996-2005) and at the end of the century (2090-2099) for three future RCP scenarios. Panel (b) shows projected change in temperature from present day (1996-2005) for three future RCP scenarios.

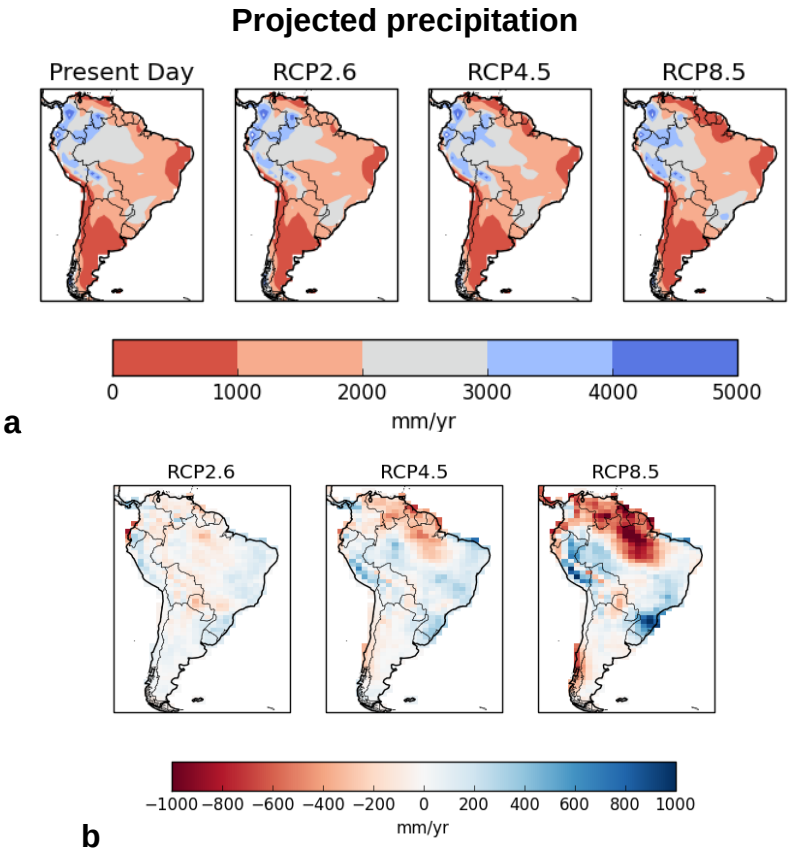

Figure 5.11: Future change in precipitation
Panel (a) shows projected precipitation (mm/yr) at present day (1996-2005) and at the end of the century (209-2099) for three future RCP scenarios. Panel (b) shows projected change in precipitation from present day (1996-2005) for three future RCP scenarios.

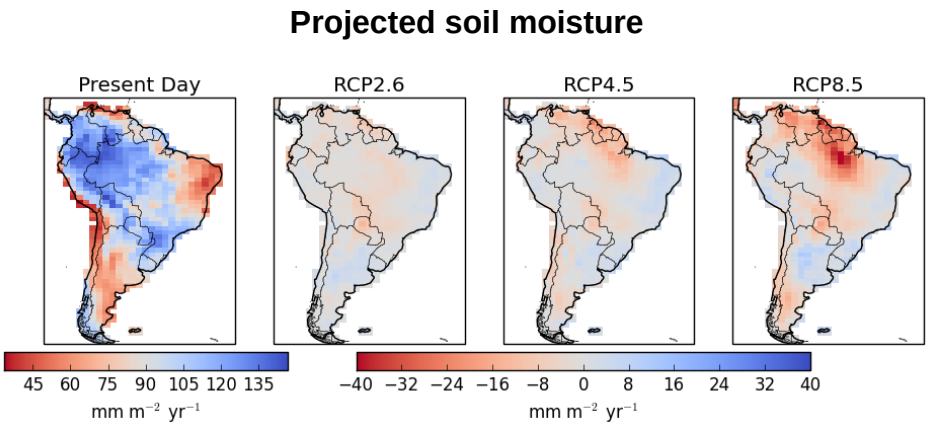

Figure 5.12: Future change in soil moisture
Mean soil moisture in top two layers of soil (mm/m^2/yr) at present day (1996-2005), and projected change from present day at the end of the century (2090-2099) for three future RCP scenarios.

The burnt area as simulated by the model is centred on the area of maximum warming and drying, and increases with temperature across the RCP scenarios (Figure 5.13). In RCP2.6 the burned area is centred on the East of Brazil; in the RCP4.5 scenario this area is widened to include the northeast as well, and in the RCP8.5 scenario a large proportion of east Brazil is at risk of fire.

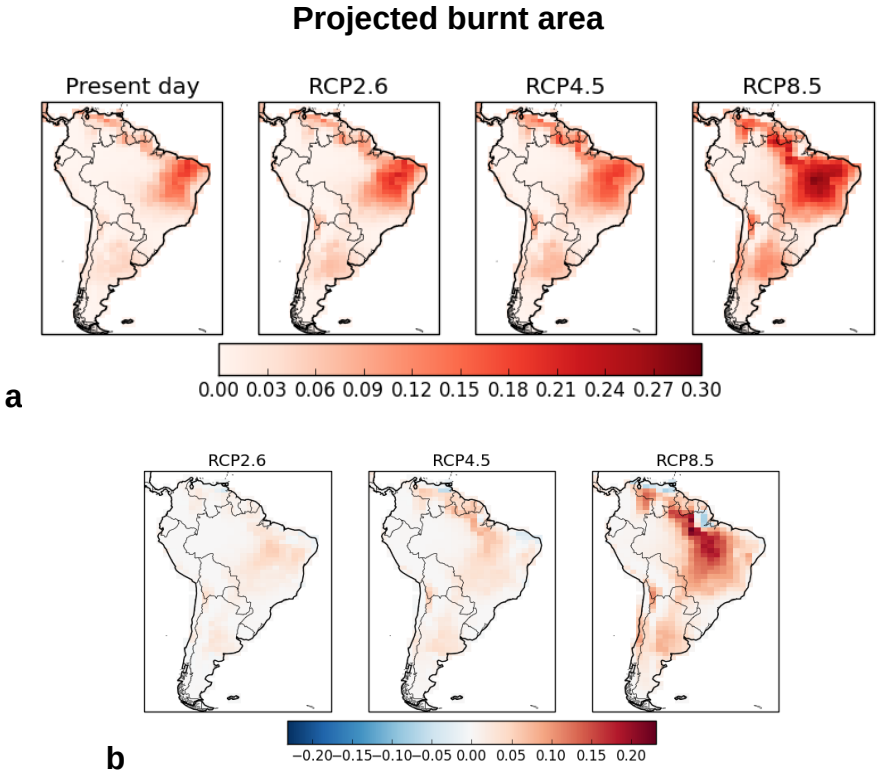

Figure 5.13: Future change in burnt area
Panel (a) shows projected burnt area (gridbox fraction) at present day (1996-2005) and at the end of the century (2090-2099) for three future RCP scenarios. Panel (b) shows projected change in burnt area from present day (1996-2005) for three future RCP scenarios.

The change in GPP over time shows much less variation between scenarios for Brazil than globally but still shows an increase in GPP for RCP8.5 (Figure 5.14a), and both GPP and burnt area (a and b) show more inter-annual variability. With fire and land-use change, vegetation carbon continues to decline in scenario RCP8.5, whereas in scenario RCP4.5 it stays roughly constant from present day to 2100 (panel c, solid lines) due much less land-use change (panel d). We can see that if land-use change was kept constant at present day, the loss of carbon from fire in RCP4.5 would not be offset as much by reforestation and would follow a similar pathway as RCP2.6 (c, dashed lines). There is more variation in land-use change between scenarios for Brazil than globally (d), with RCP4.5 showing a large decrease, RCP2.6 almost levelling, and RCP8.5 showing increasing land-use conversion to the end of the century.

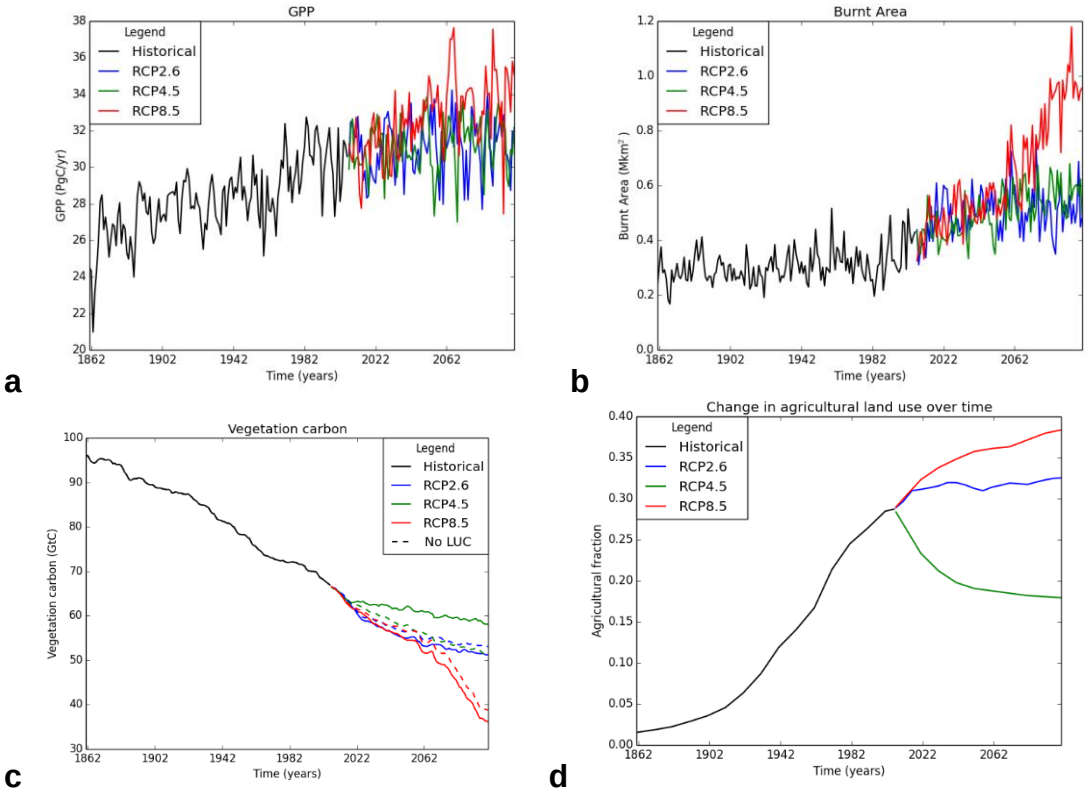

Figure 5.14: Change over RCP scenarios 1860-2100 for Brazil
Panels a-c show time series of totals for Brazil: (a) GPP (GtC), (b) burnt area (Mkm^2), (c) vegetation carbon (GtC)) (with land-use: solid line, with 'no land-use' (constant at 2005): dashed line); panel (d) shows agricultural fraction (fraction of gridbox). All panels show 1860-2100

With no disturbance, tree fraction increases in the future due to the CO_2 fertilisation effect, which is strongest in the high emission scenario RCP8.5 (Figure 5.15, top row). Adding interactive fire to the model has a significant impact

on the tropical forest area across South America (second row). Some loss of tree fraction can be seen across the northeast Amazon and across the 'arc of deforestation' to the south in RCP2.6 by 2100. With land-use the model simulates a small loss of forest in scenarios RCP2.6 and RCP8.5, and shows and increase in forest in scenario RCP4.5 again reflecting the reforestation assumptions made in this scenario (third row). Both disturbances together result in high vegetation loss dominated by fire (bottom row), although in RCP4.5 there is also some regrowth in the South of Brazil from reforestation. This is symptomatic of the assumptions around land-use that underpin the scenarios, with strong reforestation in scenario RCP4.5 (see Chapter 2, and Appendix 2). In RCP8.5 there is significant loss of around half of the Amazon forest across the East due to fire.

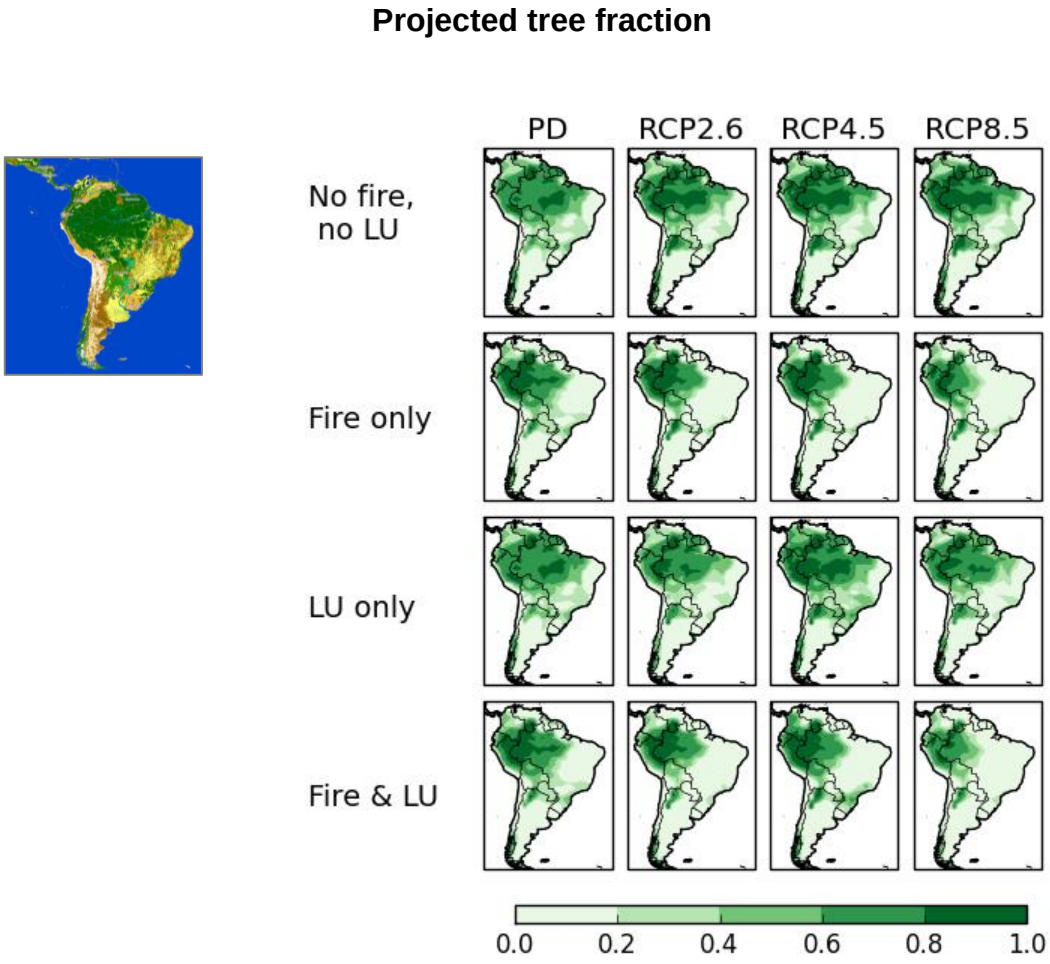

Figure 5.15: Future tree fraction
Panels show projected tree fraction at present day (1996-2005, left panels) and at the end of the century (2090-2099) for three future RCP scenarios as labelled, for 'no disturbance' (top row), 'fire disturbance only' (second row), 'land-use disturbance only' (third row), and 'both fire and land-use disturbance' (bottom row). ESA CCI Land Cover map is shown to the left for comparison with present day vegetation cover. No LUC means land-use constant at 2005.

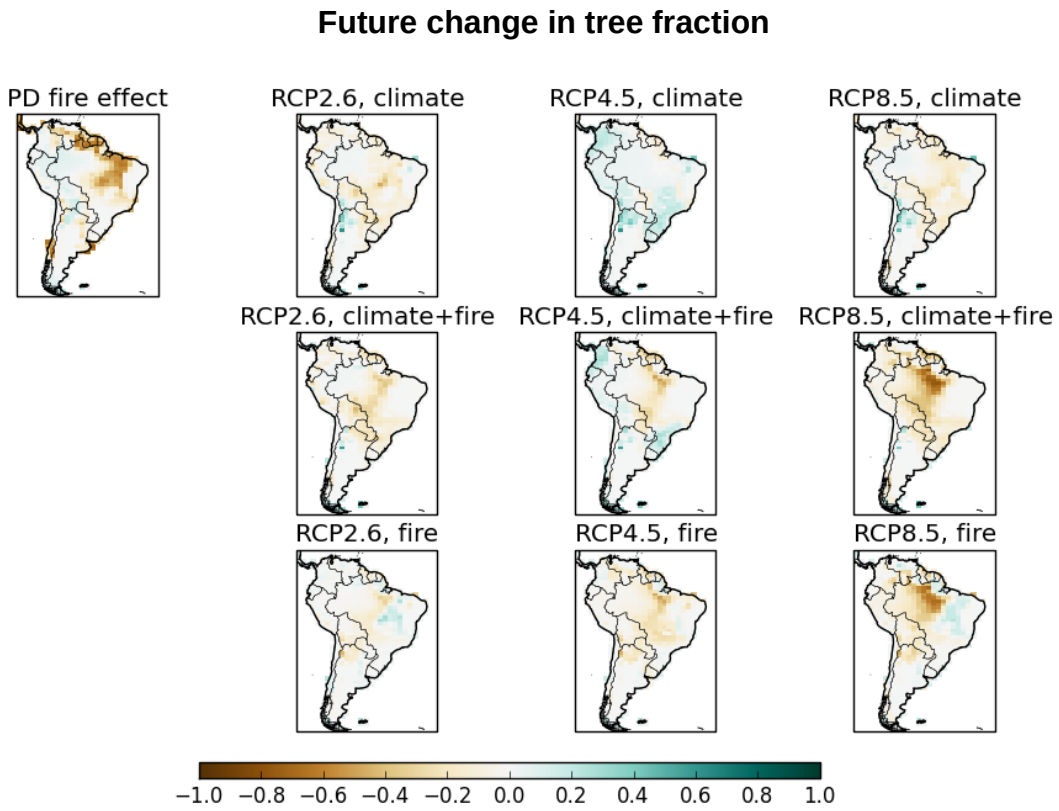

Figure 5.16: Future change in tree fraction
Change in tree (broadleaf and needleleaf) fraction: change at present day (2005) due to fire (PD fire – PD no fire) [far left]; change for each RCP scenario at 2100 from 2005 due to climate and LUC [top row]; change for each RCP scenario at 2100 from 2005 climate, LUC plus fire [centre row]; change for each RCP scenario at 2100 from 2005 due to fire (centre row minus top row) [bottom row]

In summary, the results have shown that there is a projection of increased temperature across South America in the future, which increases with higher emission scenarios. Projections of rainfall are more mixed, with a strong drying in the North of the continent, and a wetting in central regions. As a result, burnt area is projected to increase in the future in all scenarios, but with the largest increase in RCP8.5. The areas that are most vulnerable to increased fire as a result of warming and drying are eastern Brazil (in all scenarios) and the Northeast coast (mainly in RCP4.5 and RCP8.5). This has a large impact on tropical forest cover across Brazil, with a significant loss of tropical broadleaf vegetation in RCP8.5 by 2100, and some loss in the northeast and southern Amazon in RCP2.6 and RCP4.5. However it should be noted here again that this assumes that all of the vegetation within the burned area dies, which is a limitation of the current set-up and of our understanding of fire-vegetation mortality. In reality there is likely to be some level of fire resilience according to species, bark thickness and fire-tolerance; in addition CO_2 fertilisation may increase vegetation

resilience by increasing height, GPP and speed of recovery. There is some increase in forest cover in the south of the country in the RCP4.5 scenario here, which indicates the combination of fire and land-use disturbances.

Section 2: What is the impact of different warming levels, and does the pathway to reach them alter the impacts on the land surface?

In this section I explore whether these are any differences in a 1.5°C, 2°C and 4°C world according to each RCP scenario as a result of the pathway taken to achieve each level of warming, and what the overall impact of each specific level of warming is. Differences may be due to the variance in timings of reaching each specific level of warming according to CO_2 concentration (see Figure 5.5), or due to assumptions made in each scenario. For example, the treatment of land-use between scenarios varies and has large impacts on the vegetation cover (See Chapter 2), which will have biogeophysical effects such as reducing ET, and reducing precipitation patterns and local warming. The difference in aerosol levels in each scenario may also result in variation in results across specific levels of warming (Figure 5.3).

Considering temperature first (Figure 5.17), although in each scenario the global mean temperature is the same, here we can see that there are some regional differences between each RCP scenario with some areas warming more than others. There is little change across the scenarios at 1.5°C, and in particular no change over Brazil. At 2°C there are more noticeable differences across the tropics, with larger areas of South America reaching 2°C or higher in RCP4.5 and RCP8.5 than in the RCP2.6 scenario, and more of Africa projected to see above 2°C in the RCP8.5 scenario.

Change in regional temperature at global mean 1.5°C, 2.0°C and 4.0°C above pre-industrial

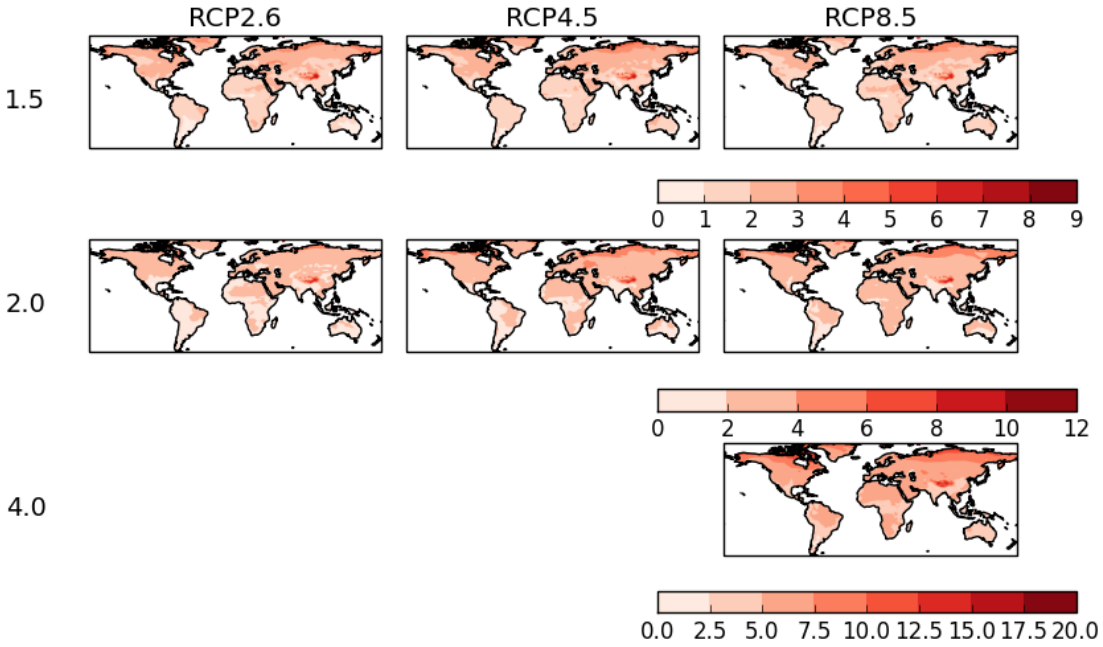

Figure 5.17: Specific warming levels of temperature
Global mean temperature change from present day (°C) at 1.5 (top row), 2.0 (centre row) and 4.0°C (bottom row) above pre-industrial, for each RCP scenario RCP2.6 (left column), RCP4.5 (centre column) and RCP8.5 (right column)

There are some noticeable differences in specific humidity (Figure 5.18) at 1.5°C, with higher humidity in RCP2.6 and RCP8.5 over the Sahara. Across South America, there is higher humidity across the west in RCP4.5 and RCP8.5, and a region of reduced humidity in central/east Brazil in RCP2.6 (see Appendix 5 for a more detailed plots). There is higher humidity in the high northern latitudes in RCP4.5 than the other scenarios. At 2.0°C, humidity is lower across central Russia in RCP4.5, but lower across the far North in RCP2.6 including across USA / Canada compared to the higher emission scenarios. At 4.0°C humidity is much increased across most of the world, with many regions seeing up to a 50% increase from present day, as would be expected with higher global temperatures.

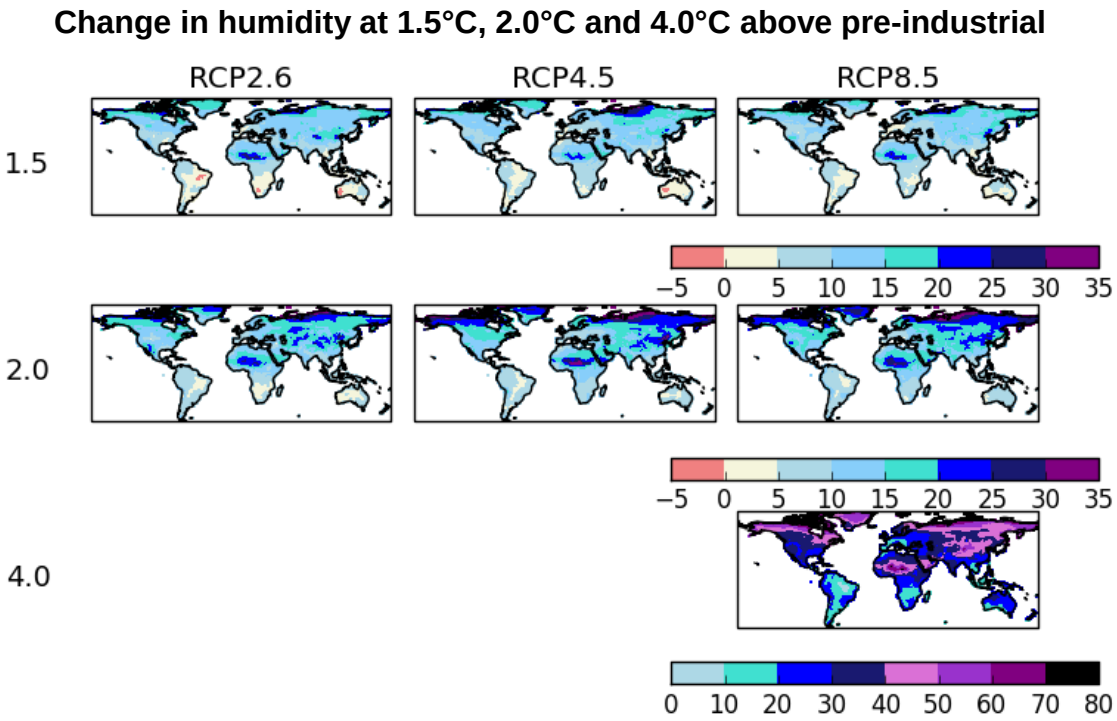

Figure 5.18: Specific warming levels of humidity
Specific humidity (percentage change from present day) at 1.5 (top row), 2.0 (centre row) and 4.0°C (bottom row) above pre-industrial, for each RCP scenario RCP2.6 (left column), RCP4.5 (centre column) and RCP8.5 (right column)

With a warmer climate, precipitation patterns would also be altered. At all levels of warming, a reduction in precipitation is observable over South America in this model, which is more pronounced with higher temperatures (Figure 5.19). At 1.5°C and 2.0°C precipitation is reduced more in scenarios RCP2.6 and RCP8.5 than RCP4.5 over South America and south east Africa. In general drying response over the Southern hemisphere in the future, and a wetting over the northern hemisphere.

Change in precipitation at 1.5°C, 2.0°C and 4.0°C above pre-industrial

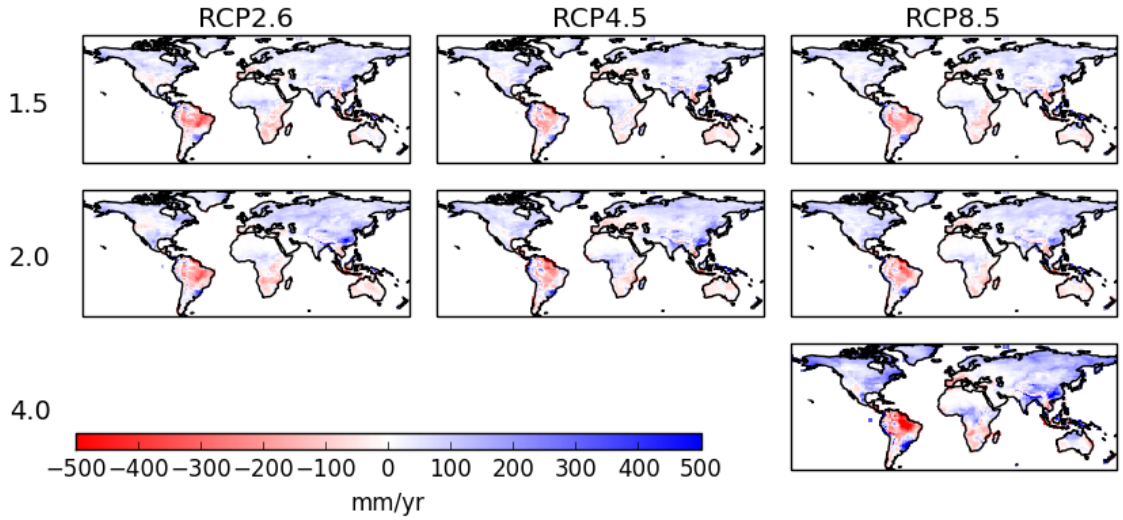

Figure 5.19: Specific warming levels of precipitation
Precipitation change from present day (mm/year) at 1.5°C (top row), 2.0°C (middle row) and 4.0°C (bottom row) above pre-industrial, for each RCP scenario, RCP2.6 (left column), RCP4.5 (centre column) and RCP8.5 (right column)

At both 1.5°C and 2.0°C of warming there is more projected burnt area in RCP2.6 and RCP8.5 than in the RCP4.5 scenario (Figure 5.20). This does not seem to be a function of land-use change, as the same pattern is seen without land-use (Figure 5.21), but corresponds with areas of higher precipitation reduction (Figure 5.19).

Change in burnt area at 1.5°C, 2.0°C and 4.0°C above pre-industrial (with land-use change)

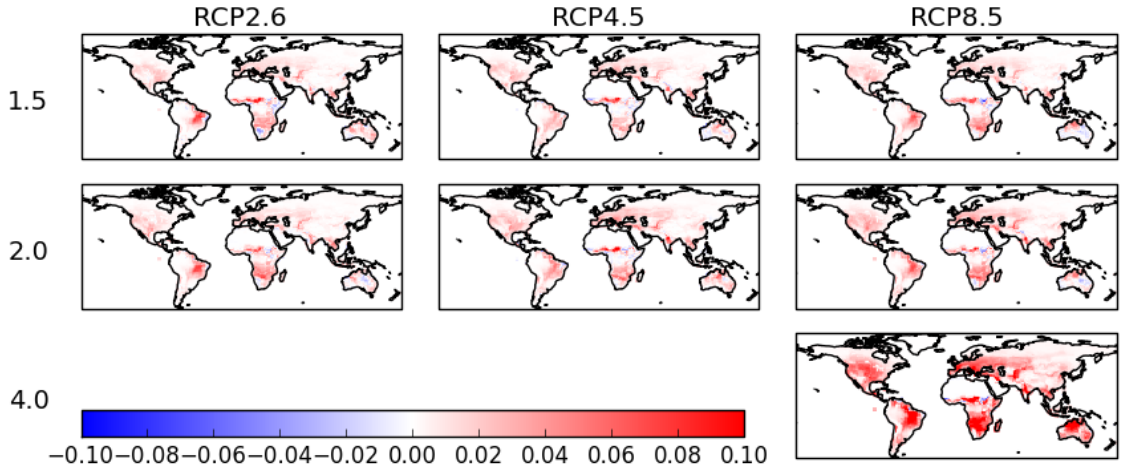

Figure 5.20: Specific warming levels of burnt area
Burnt area fraction (change in burnt area fraction from present day) at 1.5°C (top row), 2.0°C (middle row) and 4.0°C (bottom row) above pre-industrial, for each RCP scenario, RCP2.6 (left column), RCP4.5 (centre column) and RCP8.5 (right column)

Change in burnt area at 1.5°C, 2.0°C and 4.0°C above pre-industrial (no land-use change)

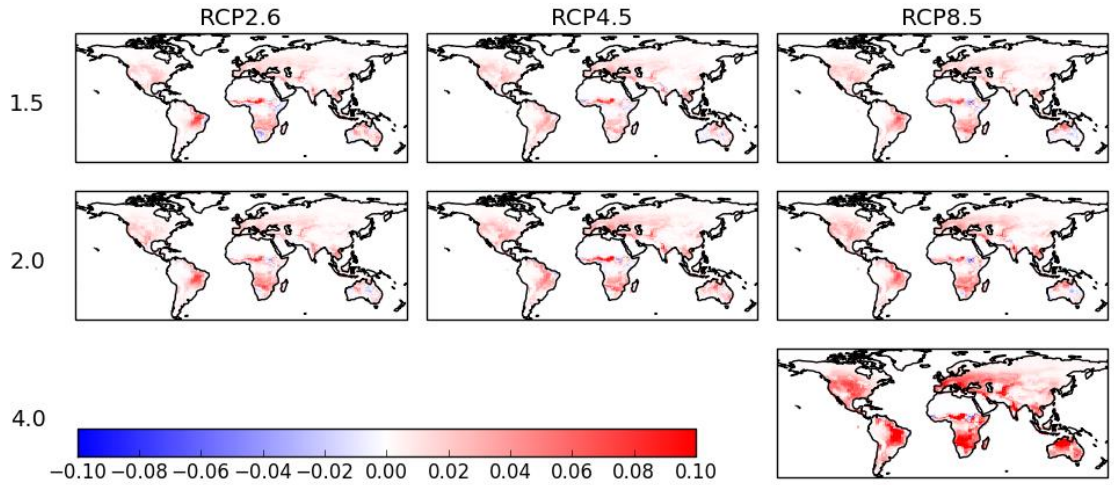

Figure 5.21: Specific warming levels of burnt area (no LUC)
Burnt area fraction (change in burnt area fraction from present day) at 1.5°C (top row), 2.0°C (middle row) and 4.0°C (bottom row) above pre-industrial for each RCP scenario, RCP2.6 (left column), RCP4.5 (centre column) and RCP8.5 (right column)

The impact on vegetation carbon is shown in Figure 5.22 and Figure 5.23. Without fire, the land-use change projections have a larger impact on the vegetation; in all scenarios there is a loss of vegetation carbon around the 'arc of deforestation' to the south and east of the Amazon, increasing with temperature. In the RCP4.5 scenario however we see an increase in carbon across western South America and central Africa, and much less of a decrease across southern Brazil than in RCP2.6 and RCP8.5. There are also some increases in the northern high latitudes of Europe and Russia which increases with temperature which will be a function of increased levels of CO_2. When interactive fire is included, there are again losses over South America centred on southern Brazil. The loss is higher in scenarios RCP2.6 and RCP8.5 as seen in Figure 5.21. There is some increase in carbon in the high latitudes, and across central Africa particularly in RCP4.5.

Change in vegetation carbon at 1.5°C, 2.0°C and 4.0°C above pre-industrial (without fire)

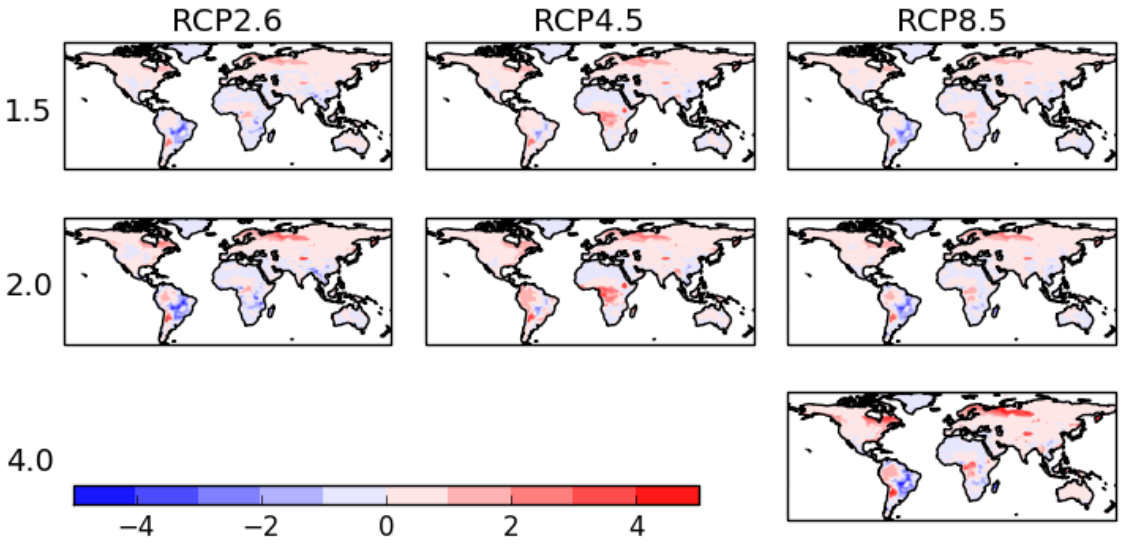

Figure 5.22: Specific warming levels of vegetation carbon, no fire
Vegetation carbon (kg m^{-2}) presented as change from present day at 1.5 (top row), 2.0 (centre row) and 4.0°C (bottom row) above pre-industrial, for each RCP scenario RCP2.6 (left column), RCP4.5 (centre column) and RCP8.5 (right column) – without fire

Change in vegetation carbon at 1.5°C, 2.0°C and 4.0°C above pre-industrial (with fire)

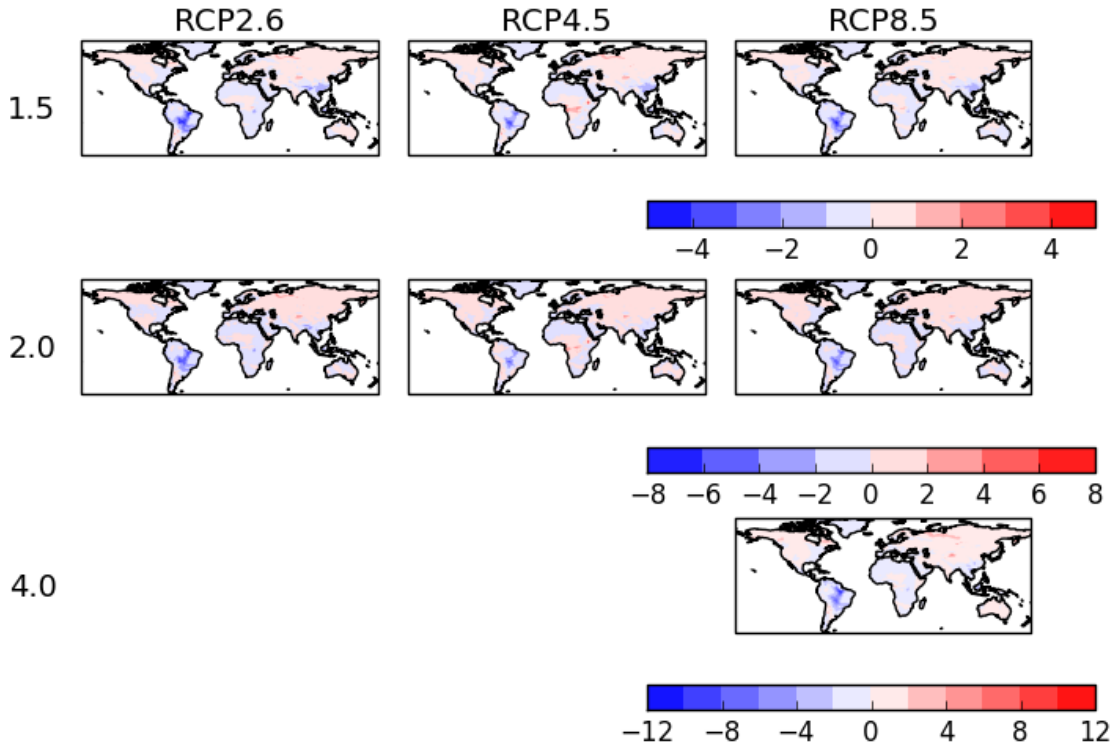

Figure 5.23: Specific warming levels of vegetation carbon, with fire
Vegetation carbon (kg m^{-2}) presented as change from present day at 1.5 (top row), 2.0 (centre row) and 4.0°C (bottom row) above pre-industrial for each RCP scenario RCP2.6 (left column), RCP4.5 (centre column) and RCP8.5 (right column) – with fire

Generally with a warmer climate we see an increase in ET (Figure 5.24), also corresponding to regions of higher precipitation (Figure 5.19). However there is spatial heterogeneity, with some regions showing a reduction in ET. With loss of forest for example (Figure 5.23), we see a reduction in ET as expected. This would lead to local changes such as increased warming and drying. At 1.5°C and 2.0°C, RCP2.6 shows the largest reduction in ET across South America, followed by RCP8.5, with RCP4.5 showing the smallest reduction. This corresponds to the areas with the largest forest losses. When fire is added to the model, these differences are still apparent at 1.5°C, but the differences between the scenarios at 2.0°C are reduced (Figure 5.25).

Change in evapotranspiration at 1.5°C, 2.0°C and 4.0°C above pre-industrial (without fire)

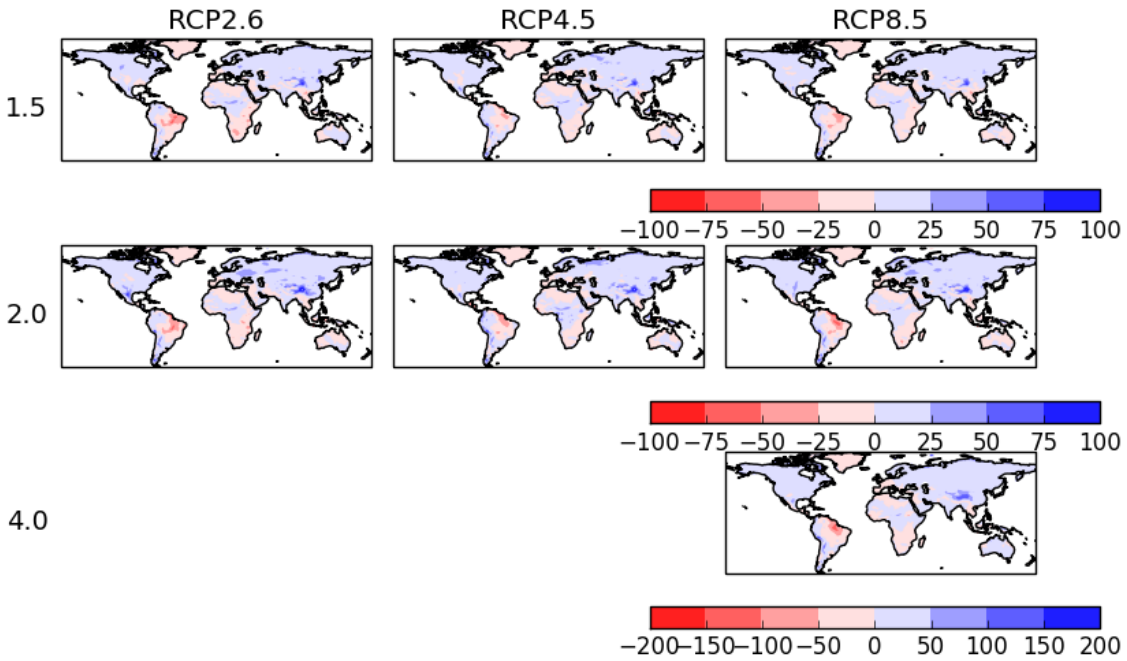

Figure 5.24: Specific warming levels of evapotranspiration, no fire
Evapotranspiration (mm yr^{-1}) presented as change from present day at 1.5 (top row), 2.0 (centre row) and 4.0°C (bottom row) above pre-industrial for each RCP scenario RCP2.6 (left column), RCP4.5 (centre column) and RCP8.5 (right column) – without fire

Change in evapotranspiration at 1.5°C, 2.0°C and 4.0°C above pre-industrial (with fire)

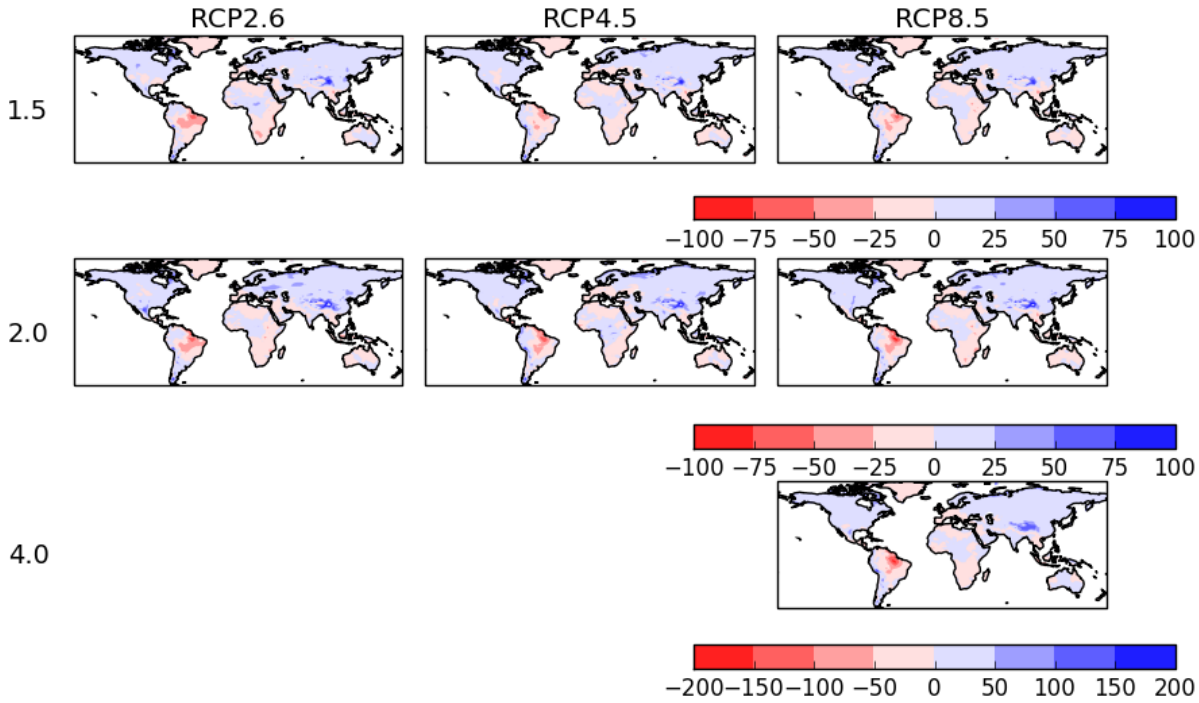

Figure 5.25: Specific warming levels of evapotranspiration, with fire
Evapotranspiration (mm yr^{-1}) presented as change from present day at 1.5 (top row), 2.0 (centre row) and 4.0°C (bottom row) above pre-indsutrial, for each RCP scenario RCP2.6 (left column), RCP4.5 (centre column) and RCP8.5 (right column) – with fire

Focusing on South America, we can see that the addition of fire reduces ET, with larger reductions at higher levels of warming (Figure 5.26). This also corresponds with larger areas of forest loss, as previously discussed. Again with reduced ET around northeast Brazil there would be increased warming and drying, creating a positive feedback with fire.

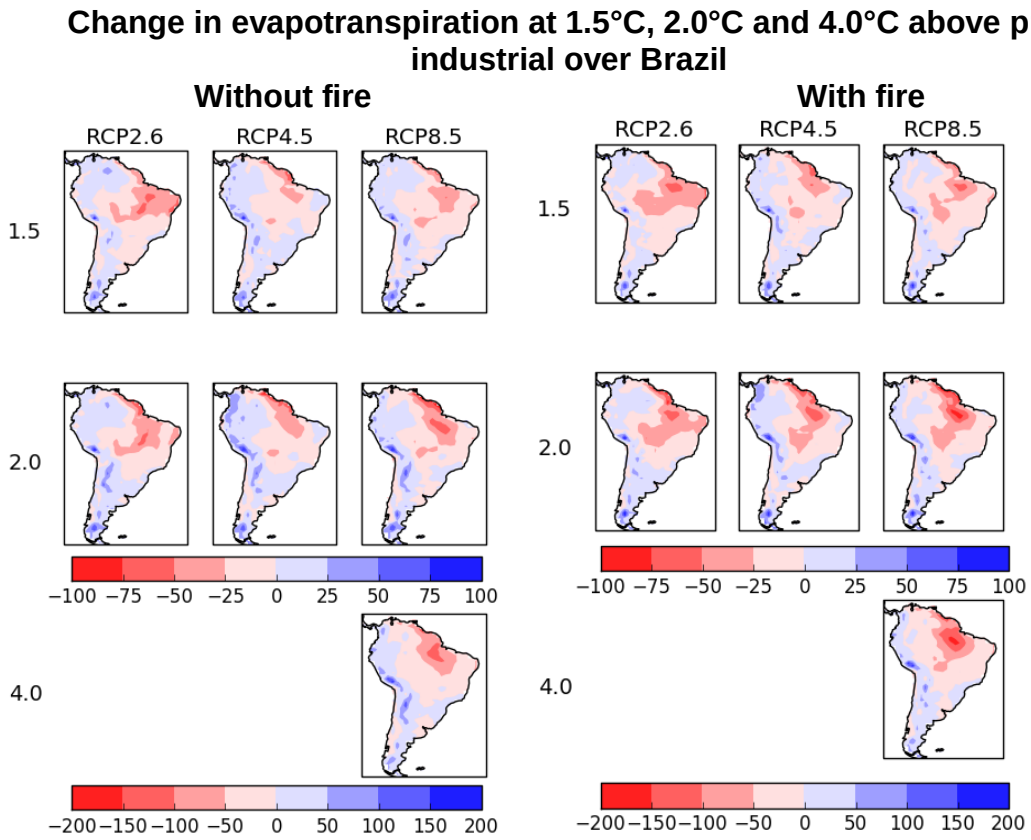

Figure 5.26: Change in evapotranspiration with fire
Evapotranspiration (mm yr^{-1}) presented as change from present day at 1.5 (top row), 2.0 (centre row) and 4.0°C (bottom row) above pre-industrial, for each RCP scenario without fire (left) and with fire (right) for South America (with LUC)

There are differences between the RCP scenarios at both 1.5°C and 2.0°C, where RCP2.6 shows larger areas of ET reduction without fire, followed by RCP8.5 and the smallest reductions in RCP4.5. With fire this is more evident at 1.5°C, whereas the differences between RCP scenarios at 2.0°C of warming are reduced. It might be supposed that these variations between scenarios is due to changes in land-use, with higher reduction in forest area in RCP2.6 and RCP8.5. However, scenario RCP2.6 still has the largest reduction in ET without fire or land-use change (Figure 5.27), indicating that changes in climate such as precipitation patterns are more dominant, which can be seen in the overlap of dry areas in Figure 5.28. However it should be noted that any changes to precipitation a result of land-use cannot be separated out here, and would need to be investigated in the coupled ESM HadGEM2-ES with and without LUC.

Change in evapotranspiration at 1.5°C, 2.0°C and 4.0°C above pre-industrial over Brazil

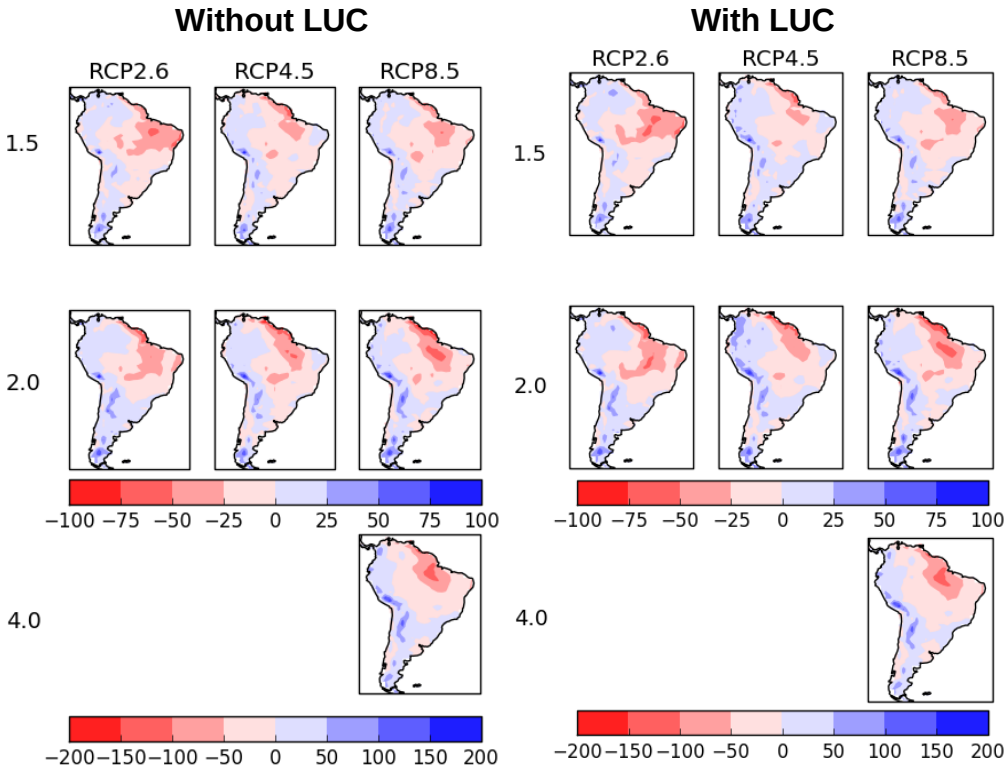

Figure 5.27: Change in evapotranspiration with LUC
Evapotranspiration (mm yr^{-1}) presented as change from present day at 1.5 (top row), 2.0 (centre row) and 4.0°C (bottom row) above pre-industrial, for each RCP scenario without LUC (left) and with LUC (right) for South America (without fire)

Change in precipitation at 1.5°C, 2.0°C and 4.0°C above pre-industrial over Brazil

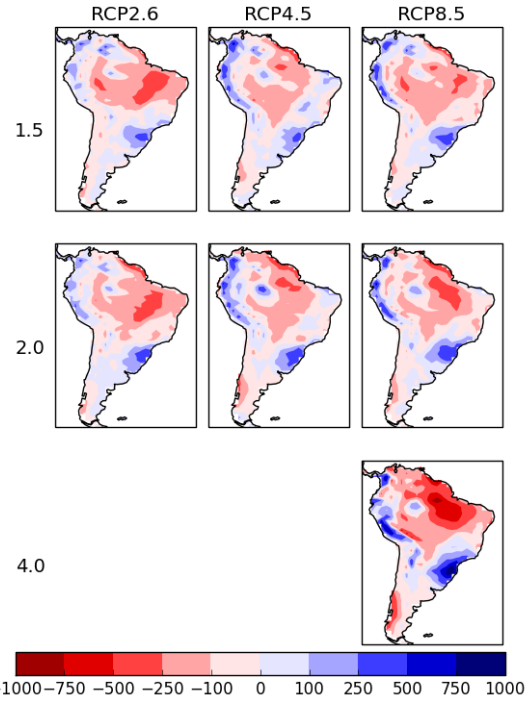

Figure 5.28: Specific warming levels of precipitation over Brazil
Precipitation (mm yr^{-1}) presented as change from present day at 1.5 (top row), 2.0 (centre row) and 4.0°C (bottom row) above pre-industrial, for each RCP scenario South America

The positive feedback resulting from reduced ET will be offset to some extent by increased albedo in areas of forest loss. The RCP4.5 scenario shows lower albedo than RCP2.6 and RCP8.5 across all levels of warming (Figure 5.29), which we can see strongly across the tropics, including across South America (Figure 5.31). This results from the higher forest area in RCP4.5, which is darker and less reflective. When fire is added, there is a similar pattern of change with RCP4.5 showing lower albedo than RCP2.6 and RCP8.5 (Figure 5.30). At 4.0°C, RCP8.5 shows an increase in albedo across most of the South American continent resulting from vegetation loss.

Change in Albedo at 1.5°C, 2.0°C and 4.0°C above pre-industrial (without fire)

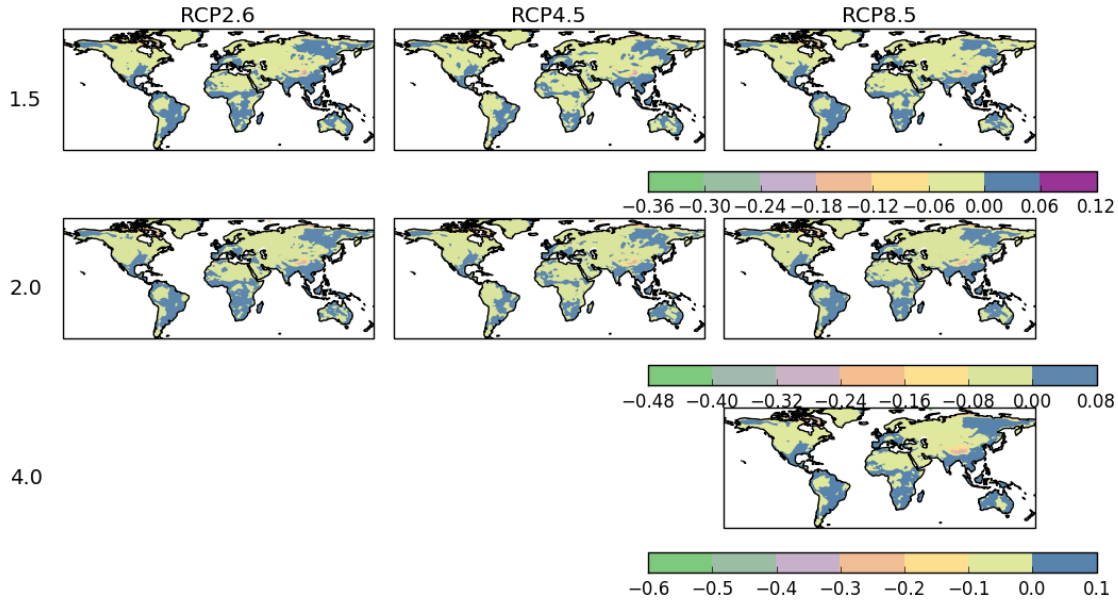

Figure 5.29: Specific warming levels of albedo, no fire
Albedo (change from present day) at 1.5 (a), 2.0 (b) and 4.0°C (c) above pre-industrial, for each RCP scenario RCP2.6 (left column), RCP4.5 (centre column) and RCP8.5 (right column) – without fire

Change in Albedo at 1.5°C, 2.0°C and 4.0°C above pre-industrial (with fire)

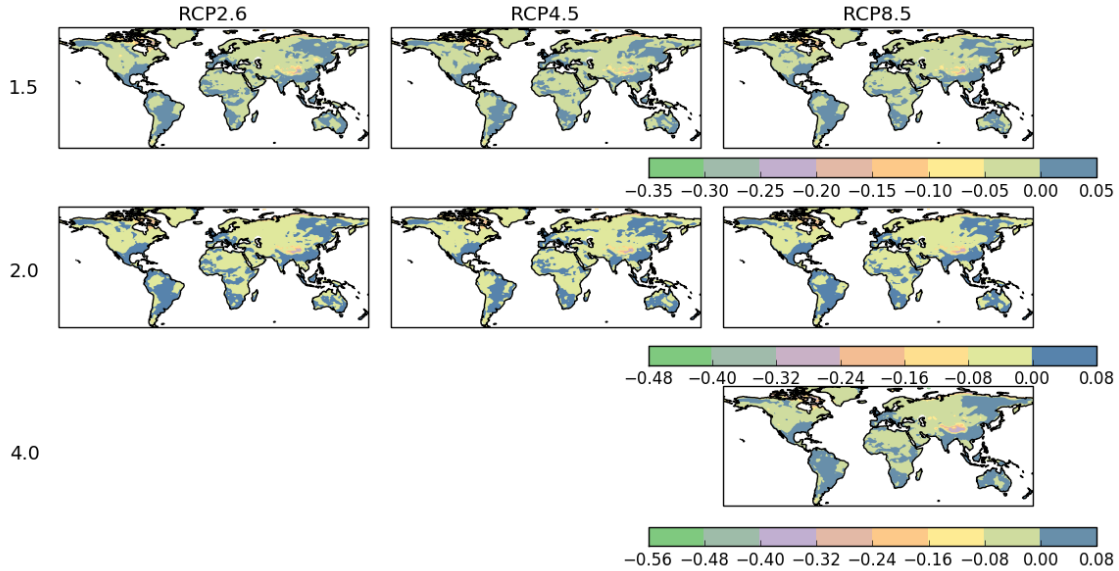

Figure 5.30: Specific warming levels of albedo, with fire
Albedo (change from present day) at 1.5 (a), 2.0 (b) and 4.0°C (c) above pre-industrial, for each RCP scenario RCP2.6 (left column), RCP4.5 (centre column) and RCP8.5 (right column) – with fire

Focusing on the changes over South America, fire generally results in an increase in albedo compared with no fire due to increased forest loss (Figure 5.31). RCP4.5 still has a lower albedo than RCP2.6 and RCP8.5, which is due to less land-use change in this scenario. We can see this is the case from Figure 5.32 where albedo the same across all RCP scenarios at all levels of warming in the 'no land-use' scenario, but increases with land-use change in the 'with land-use' scenario for RCP2.6 and RCP8.5. There are no significant changes in albedo at 1.5°C vs 2.0°C. Albedo is highest in scenario RCP8.5 at 4.0°C of warming, where forest loss is greatest from both changes in land-use (Figure 5.32) and fire (Figure 5.31).

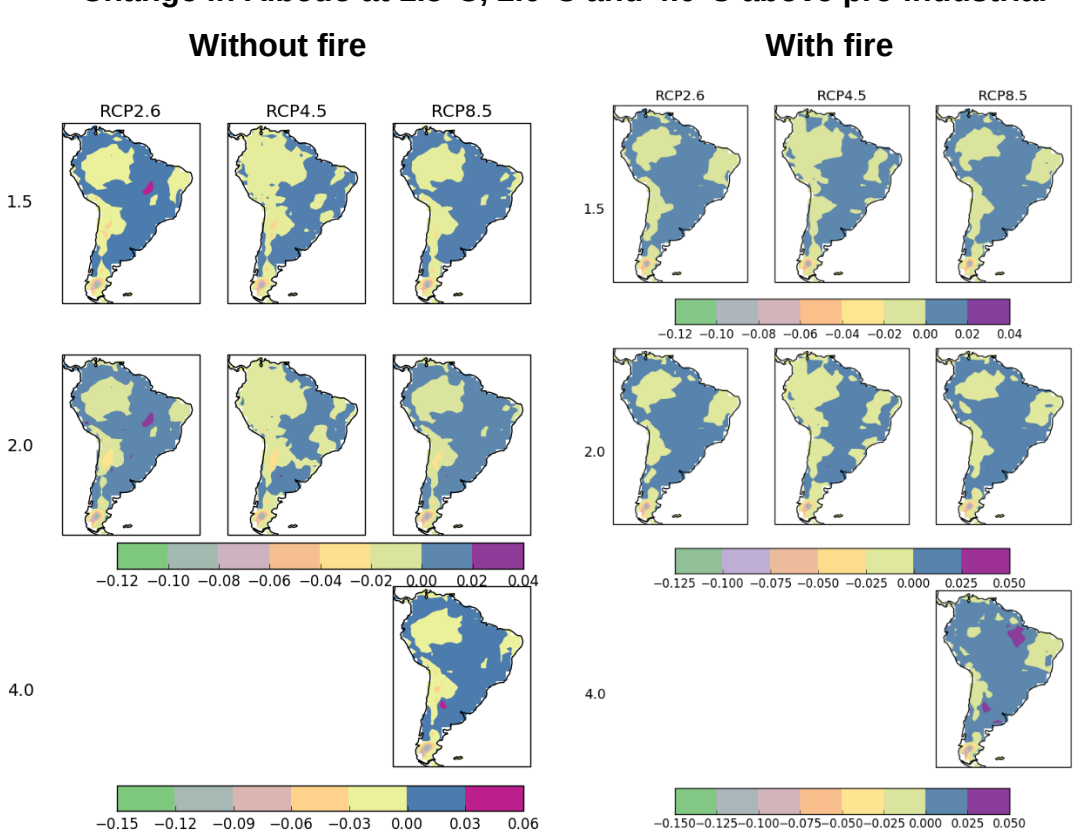

Figure 5.31: Change in albedo with fire
Albedo (change from present day) at 1.5 (a), 2.0 (b) and 4.0°C (c) above pre-industrial for each RCP scenario without fire (left) and with fire (right) for South America, including LUC.

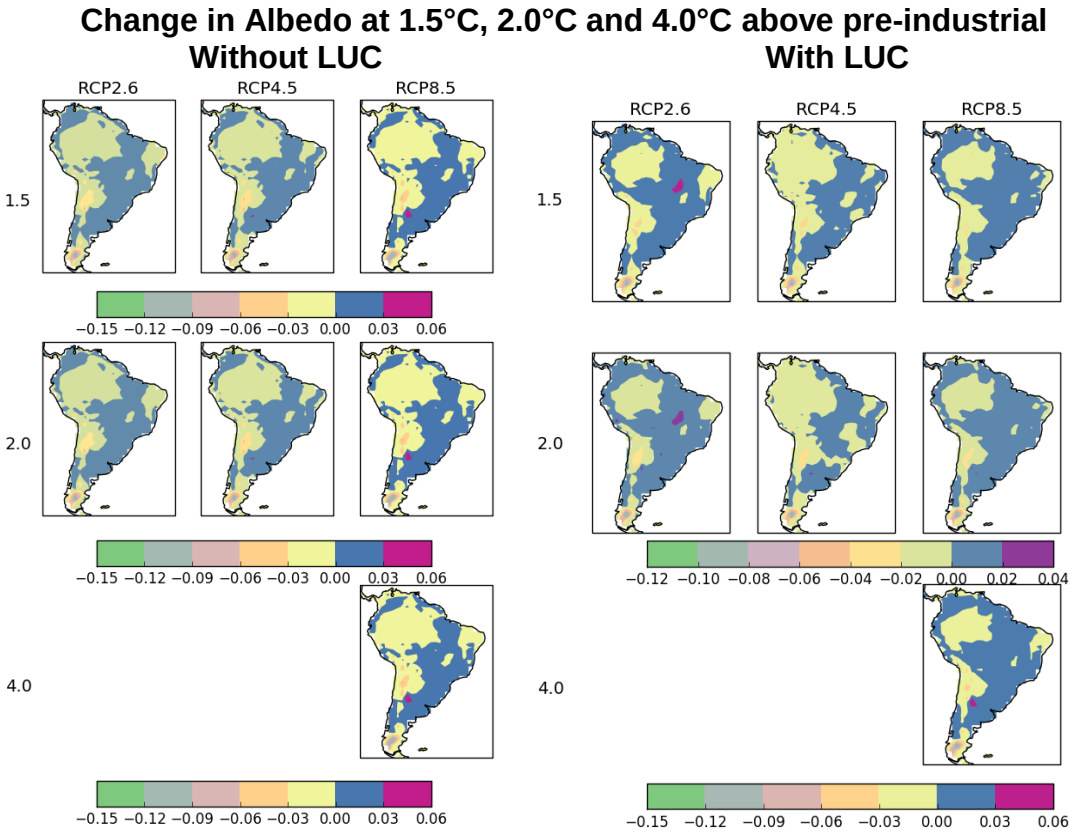

Figure 5.32: Change in albedo with LUC
Albedo (change from present day) at 1.5 (a), 2.0 (b) and 4.0°C (c) above pre-industrial for each RCP scenario without LUC (left) and with LUC (right) for South America (without fire)

I summarise the changes in key variables for each RCP scenario and each level of warming (land only from JULES output), globally and for Brazil, using bar graphs including both fire and land-use disturbances. Globally there is an increase in precipitation with higher levels of warming which varies only marginally between RCP scenarios. Over Brazil however the overall trend is drying, which is highest in scenarios RCP2.6 and RCP8.5. Burnt area also increases with warming, with the highest response at 4.0°C. Burnt area over Brazil is higher than the global average, and is higher in scenarios RCP2.6 and RCP8.5 than RCP4.5 which is driven by differences in precipitation (Figure 5.28). Global mean albedo is reduced by up to 8% in the highest warming / emissions scenario, with higher reductions corresponding to higher levels of warming. As we have seen, this is dominated by a reduction in the northern hemisphere (Figure 5.30), driven by increased vegetation carbon (Figure 5.23) from additional warming and CO_2 fertilisation. Conversely albedo increases across Brazil, in particular in RCP2.6 and RCP8.5, due to loss of forest cover from fire and LUC. Similarly ET also reflects the difference in global trends versus change in Brazil, with a global mean increase in ET but decrease over Brazil corresponding to forest loss and drying.

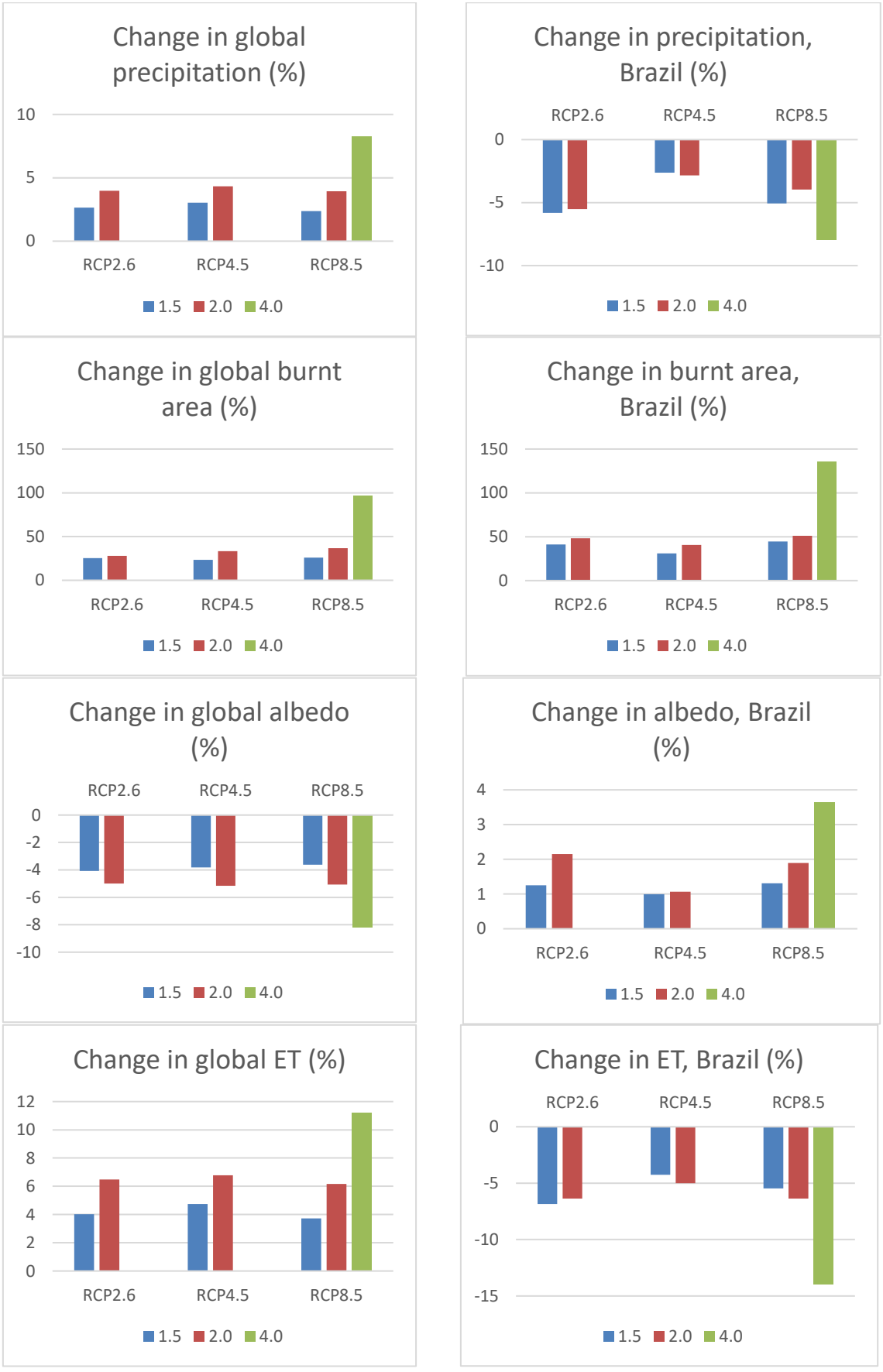

Figure 5.33: Summary of changes from present day
For each RCP scenario and level of warming (with fire and LUC). Colours indicate temperature above pre-industrial

In summary, the results have shown that the pathway to reach specific levels of warming does have an impact on local biogeophysical responses. Temperature differences between scenarios are more evident at 2.0°C than 1.5°C, where higher emissions scenarios show larger areas reaching 2.0°C or higher than lower emission scenarios. Humidity generally increases with temperature, although RCP4.5 shows less of an increase than scenarios RCP2.6 and RCP8.5 over the Sahara and Russia. Precipitation as well generally increases with warming, particularly over the northern hemisphere, but over northern South America there is a strong drying signal. There are changes in precipitation and ET patterns across each RCP scenario, which lead to differences in burnt area. Both temperature and precipitation were shown to be important drivers of burnt area, as fire increases with emissions scenario with RCP8.5 showing the largest change in burnt area. Burnt area was particularly increased in areas that are projected to become both hotter and drier, including eastern South America and southern Africa. The vegetation carbon also showed large differences between scenarios as a response of fire and land-use change, with RCP4.5 showing increases in vegetation carbon in many areas at 2.0°C in particular, and more of a dipole response in RCP2.6 and RCP8.5 especially at higher temperatures. Burnt area is high across the tropics leading to stronger reductions in vegetation carbon across all scenarios although again slightly less in RCP4.5. Forest loss from fire leads to reduced ET and a higher albedo. Overall there is a global mean increase in precipitation and ET and a reduction in albedo, whereas over Brazil the opposite response is seen with a mean decrease in precipitation and ET, and increase in albedo. Burnt area increases both globally and over Brazil, increasing with warming level.

Section 3: Could fire lead to a change in state from tropical forest to savanna?

Previous studies have suggested that warming and drying in the future, together with interactions between fire and land-use change could lead to a “tipping point” for the Amazon, where the tropical forest area transitions into a bi-stable state of forest and savanna (Settele *et al*., 2014; Lasslop *et al*., 2016). Although a strong “dieback” was very noteably shown in HadCM3 due to a strong warming and drying signal (Cox *et al*., 2000; Huntingford *et al*., 2004; Malhi *et al*., 2009),

subsequent models have shown more resilience in the forest to increases in temperature, as demonstrated here using the HadGEM2-ES driving data within JULES in the scenarios without fire. Fire has now been added into the model as an interactive vegetation feedback for the first time, and the results have shown that with this extra interaction included, a forest transition is again shown to be a worse-case scenario by 2100 following a business-as-usual scenario. However it should be noted that the vegetation response to fire is strong even in the present day, with slow recovery times following disturbance within the TRIFFID dynamic vegetation model (see Chapter 3 and Appendix 3), and stronger drying in HadGEM2 in Northeast Brazil than CRU-NCEP (Figure 5.4). There is also as yet no interaction between fire and agricultural land in terms of suppression or ignition, which has been shown to have important interactions which vary regionally (Andela *et al*., 2017).

As we have seen, fire has a large impact on forest area in the future, with large losses projected in the RCP8.5 scenario. I now consider if this may be a signal of a transition to a more savanna-like state, using land-use change and fire.

Figure 5.34 shows the change in the mean vegetation fractions in Brazil, categorised into trees, grasses and shrubs. There was a reduction in mean tree cover in the future in all scenarios, with the highest reduction in RCP8.5. In RCP2.6 and RCP8.5 this is replaced by a large increase in grasses. In RCP4.5, the shift is towards more shrub-type vegetation. Savanna can be characterised by both shrubs and grasses, implying a definite shift towards a more savanna-like state. This can be seen if we look at the pattern of vegetation cover spatially, in Figure 5.35 - Figure 5.37.

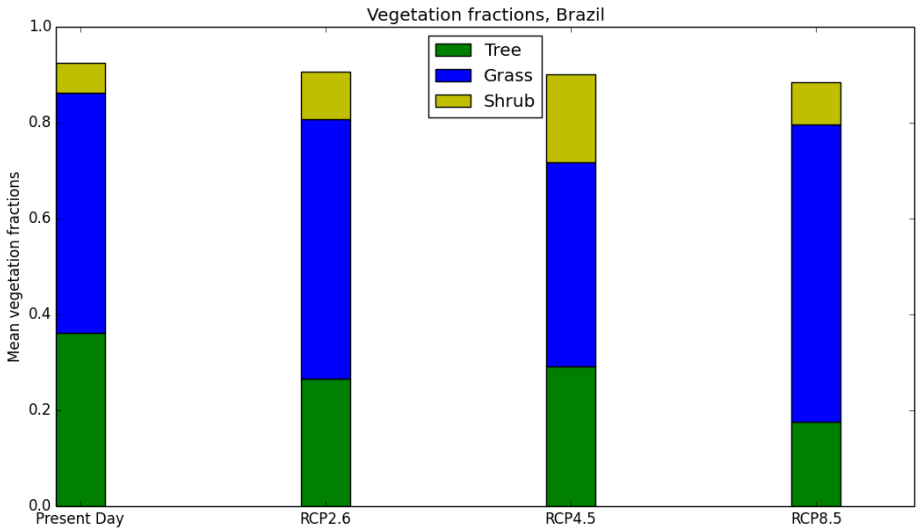

Figure 5.34: Vegetation type over time in Brazil present and future
Mean vegetation fraction at present day (2005) and at 2100 in three RCP scenarios. Trees = broadleaf + needleleaf trees; Grasses = C3 + C4 grasses.

Spatially we can see large forest losses across the South and East of the Amazon forest, especially in the high emission scenario RCP8.5 (Figure 5.35), which is replaced by grasses (Figure 5.36) and shrubs (Figure 5.37). Grasses are particularly increased in scenarios RCP2.6 and RCP8.5, and shrubs more prolific in scenario 4.5. This highlights the interaction of fire and land-use in the model, where there is large projected conversion to biofuels and cropland in this region in scenarios RCP2.6 and RCP8.5 respectively (see Chapter 2) which is represented in JULES by grasses. There is an increase in soil fraction in Eastern Brazil in scenario RCP2.6 and to a less extent RCP4.5, and in Northeast Brazil in RCP8.5 (Figure 5.38), and this increases with fire. One area in particular with a strong increase in bare soil fraction is Northeast Brazil in RCP8.5 with fire, which corresponds to a decrease in fire by 2100 (Figure 5.13) due to less available fuel.

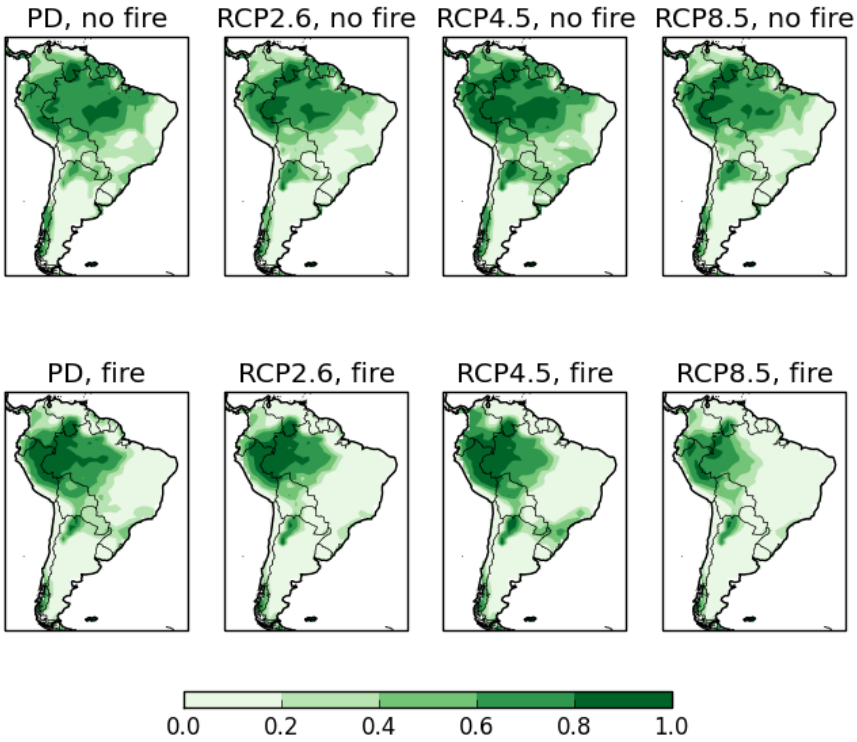

Figure 5.35: Future tree fraction with and without fire
Tree fraction (broadleaf and needleleaf), at present day (2005) and 2100 in three RCP scenarios, without fire (top row) and with fire (bottom row)

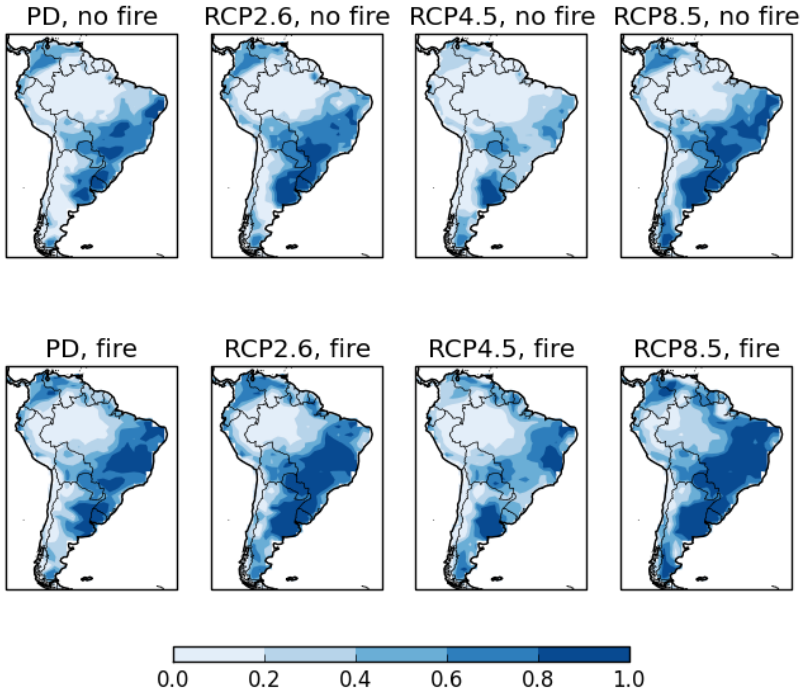

Figure 5.36: Future grass fraction with and without fire
Grass fraction (C3 and C4), from present day (2005) to 2100 in three RCP scenarios, without fire (top row) and with fire (bottom row)

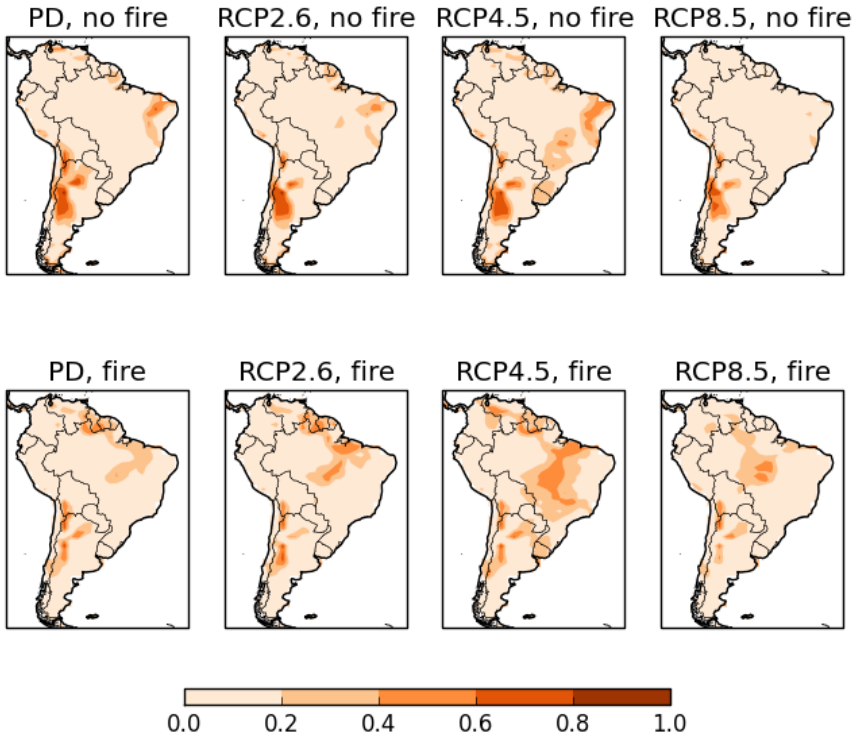

Figure 5.37: Future shrub fraction with and without fire
Shrub fraction, from present day (2005) to 2100 in three RCP scenarios, without fire (top row) and with fire (bottom row)

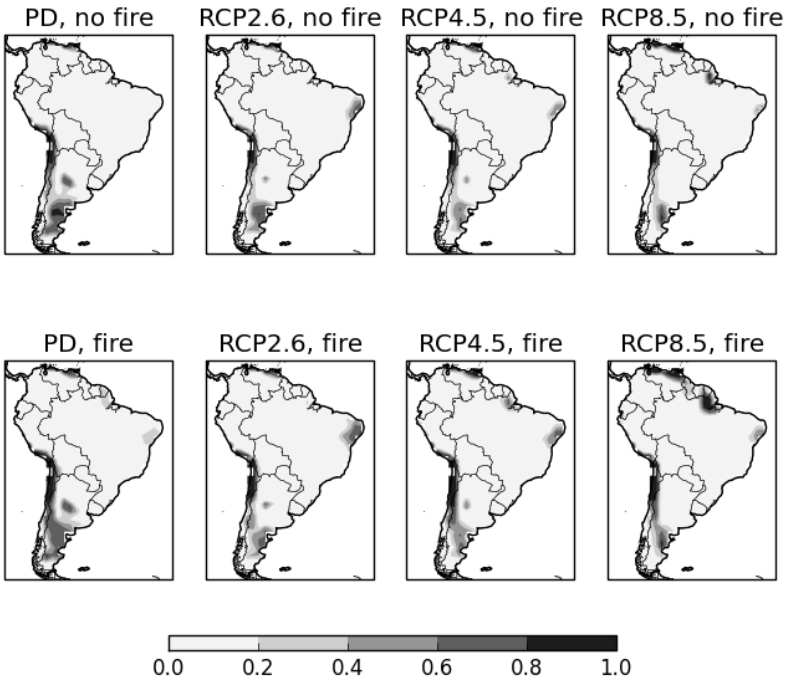

Figure 5.38: Future soil fraction with and without fire
Soil fraction, from present day (2005) to 2100 in three RCP scenarios, without fire (top row) and with fire (bottom row)

Another way to consider the potential impact of future changes in the climate is to use a drought factor to assess whether regions become more vulnerable to drought in the future with varying scenarios of climate change. Here I use a drought factor based on the Keetch Byram Drought Index (Keetch and Byram, 1986), with varying soil moisture provided by JULES (based on Holgate *et al*., 2017, as used in Burton *et al*., 2018a).

We can see from Figure 5.39 that the drought factor increases in particular in the East of Brazil in the RCP2.6 scenario, and in the Northeast region in RCP8.5, making these areas more vulnerable to forest loss and to fire. This supports the findings of Figure 5.20 where we do indeed see higher burnt area in these regions.

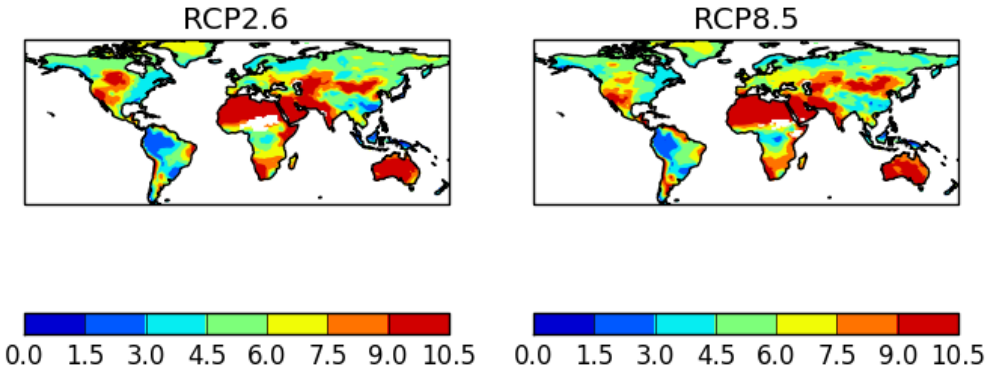

Figure 5.39: Drought factor (2100) for RCP2.6 and RCP8.5

The final experiment in this chapter is based on the work of Good *et al*. (2013), which investigated the propensity of two models HadCM3 and HadGEM2-ES to project tropical forest dieback in the future, based on the dry season resilience in each model. The results of their study showed that the dry season length was longer in HadCM3 than HadGEM2-ES, resulting in a negative impact on tropical forest cover. Here I have developed this experiment to assess the impact of adding fire to the JULES model, to give an indication of whether the representation of fire in the model gives rise to more conducive conditions for a tipping point from tropical forest cover to savanna.

The method (presented in Good *et al*., 2011) is based on a linear function of temperature, dry season length and CO_2 concentration, and quantifies the

equilibrium response of tropical forests to climate and CO_2 in order to simulate whether tropical forest is sustainable in the model under the conditions given.

The blue diagonal lines on the plots represent the threshold of dry season resilience in HadGEM2-ES without fire (right plots), which can be compared to the reduced threshold when fire is included (left plots). The different positions of the blue lines between the historical (top plots) and future (lower plots) simulations shows the effect of changing CO_2 concentration (higher CO_2 leads to increased resilience). Without fire, the highest fraction of broadleaf tree (dark green points) declines slightly in the future scenarios, although the highest emission scenario RCP8.5 shows slightly less of a decline, which is most likely due to the increased levels of CO_2 in this scenario giving rise to a fertilisation effect (Figure 5.40, right hand panels). When fire is added to the model, there is a sharper decline in high broadleaf fraction (fewer dark green points, and more red points below the blue line), which is reduced further with higher emission scenarios. The dry season resilience is thus reduced, with a longer dry season for more areas (more data points in the top of the range above 6) and lower fractions of broadleaf for the shorter dry season lengths.

Dashed lines are shown on each plot at 5 and 6 months for comparison between the fire and the no-fire scenario; the threshold of forest transition (where green points change to red) is around 6 months with fire in the historical period (top left plot), but is around 8 months without fire (top right plot). In the future simulations the threshold is around 5 months with fire, and 8 months without fire. The data suggest that the dry season resilience of the forest is reduced by about three months when fire is added to the model, leading to a higher possibility for a tipping point threshold to be reached whereby tropical broadleaf vegetation could incur a ‘dieback’ and / or transition to more grassland-savanna like vegetation, as shown in Figure 5.35 - Figure 5.37.

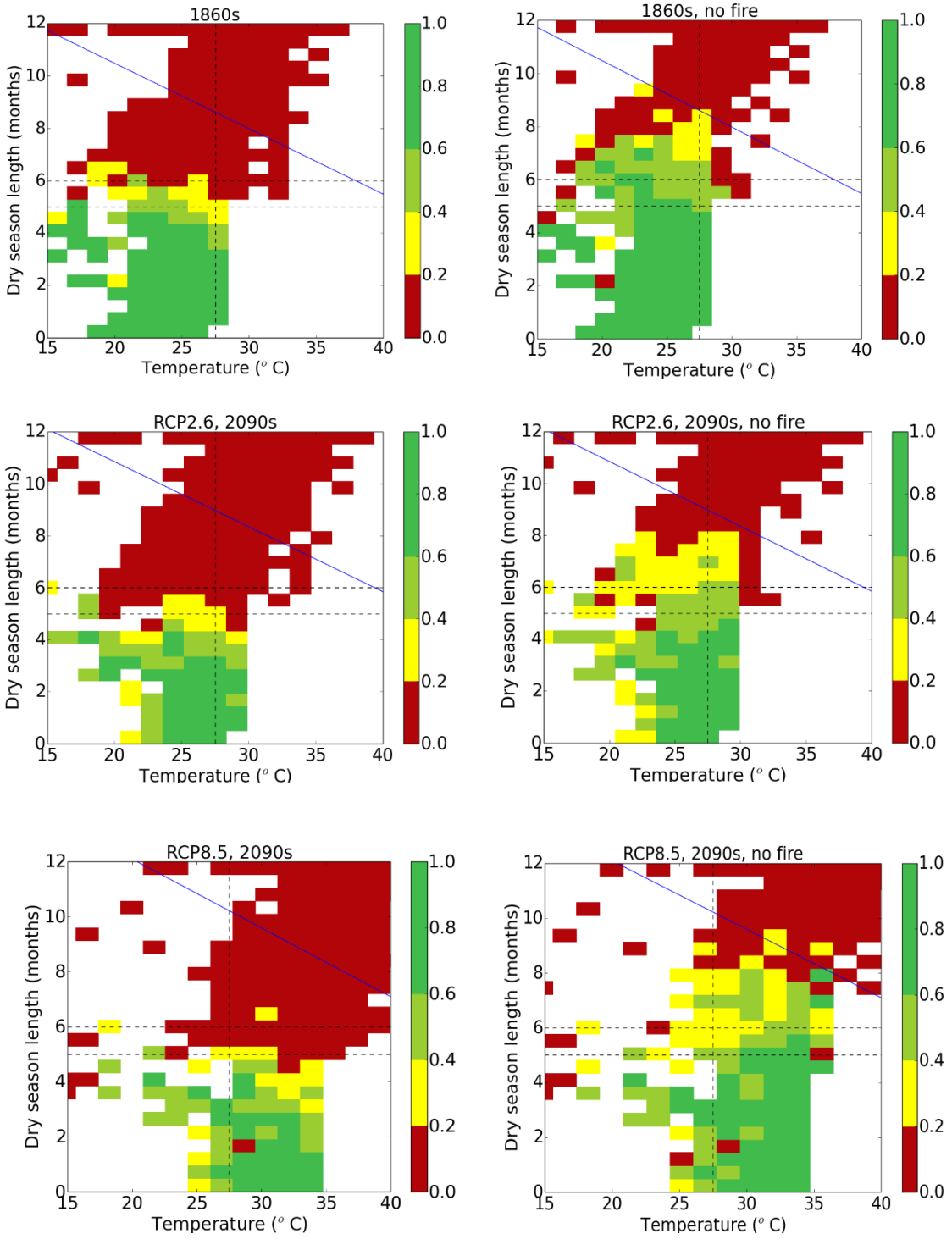

Figure 5.40: Tropical forest dry season resilience
Bioclimatic zone plots for JULES with fire (left colum) and without fire (right colum). From top to bottom, plots show 10 years of data: top row pre-industrial 1860-1869; bottom two rows 2090-2099 RCP2.6 (centre row) and RCP8.5 (bottom row). Colours represent mean broadleaf fraction (Red: BLF <0.2. Orange: 0.2 > BLF > 0.4. Light green: 0.4 < BLF < 0.6. Dark green: BLF > 0.6). Dashed lines show dry season length of 5 and 6 months, and T=27.5°C. Blue line shows dry season resilience

In summary, I have shown that adding interactive fire into the JULES model could lead to a change in state from tropical forest to savanna in the future. In the

experiments where fire is added, we can observe a shift from broadleaf vegetation cover to more grasses (RCP2.6 and RCP8.5) and shrubs (RCP4.5). We also see a shift in the East and Northeast of Brazil to hotter, drier conditions, leading to more vulnerability to drought which can lead directly to forest loss and also indirectly to forest loss through higher fire occurrence. This has implications for the resilience of the forest when fire is added to JULES, leading to higher risk of forest 'dieback'.

5.4 Discussion

Levels of CO_2 and global mean temperatures increase in the future as per the emissions scenarios, with RCP8.5 (the highest emission scenario) showing the highest CO_2 concentration and temperature rise, followed by RCP4.5, and RCP2.6 (the lowest emission scenario) showing a lower rise in CO_2 and temperature from present day to 2100 (Figure 5.5). From these factors alone we can expect multiple interactions with vegetation, for example between a fertilisation effect from higher levels of CO_2 concentration, offset by potential heat stress at higher temperatures. An increase in maximum temperatures or a lengthening of time at which higher temperatures are experienced can have a strongly negative effect on growth rates by increasing respiration, reducing stomatal conductance, and reducing photosynthesis (Schippers *et al*., 2015). These effects can be further compounded by a reduction in precipitation, leading to potentially longer and more intense dry seasons, and also by anthropogenic factors including land-use change which reduces ET and creates local warming and drying, and thus higher risk of fires which cause further forest losses. Evaporation and transpiration are important processes in maintaining the moisture required to sustain tropical rainforest ecosystems, especially where the large-scale factors for rainfall formation are weak such as in the central and Eastern Amazon (Lovejoy and Nobre *et al*., 2018). ET rates in most areas of the Central and Western Amazon increase in the dry season due to higher solar radiation, so that dry season ET is approximately equal to wet season ET even though there is less moisture available; in the South and Southeast Amazon where precipitation is lower and the dry season is longer, this is not the case and ET decreases considerably in the dry season, making these regions much more vulnerable to drought (da Rocha *et al*., 2009).

Gross Primary Productivity (GPP) shows a similar pattern of increase to temperature and CO_2, with the highest productivity in RCP8.5 (Figure 5.7a). The GPP is the amount of carbon fixed through photosynthesis, so it is expected that this will increase as the amount of CO_2 available increases in the future. However there is still large uncertainty around this process, for example nutrient limitation may reduce the CO_2 fertilisation effect significantly. A lack of ground-based data means we cannot yet be confident of how vegetation will respond to higher levels of CO_2.

Using JULES-INFERNO, I have shown that burnt area is also projected to increase in the future, closely following the same trend as temperature for the three emission scenarios (Figure 5.7b). However the projections of vegetation carbon (Figure 5.7c) show that the maximum vegetation carbon will be seen in scenario RCP4.5, and the lowest vegetation carbon in scenario RCP2.6. The lower vegetation carbon in the RCP2.6 and RCP8.5 scenarios may be caused by a number of factors, including lower plant productivity in RCP2.6 due to lower levels of CO_2, and also projected land-use changes. Land-use change is projected to be highest in these two emission scenarios, changing forest to crops to feed a high population in RCP8.5, and to biofuels for higher climate change mitigation in RCP2.6 (Settele *et al*., 2014).

Over South America, the region showing the highest projected warming is approximately over the Amazon, with RCP8.5 showing the largest change from present day (Figure 5.10). Some warming is projected over most of the continent in all scenarios, although this is low in RCP2.6. The projected change in precipitation is more varied, with some regions getting drier and some getting wetter, and these vary by scenario (Figure 5.11). In RCP2.6 there is a weak drying signal over central Brazil, whereas in RCP4.5 and RCP8.5 the drying seems to be more towards the northeast, with strong drying in RCP8.5. The projections show a signal of increased precipitation along the Southeast coast of the continent, in particular in RCP4.5 and RCP8.5. The fire disturbance in the model mirrors this trend of warming and drying of the east of Brazil, with higher burned area across the northeast coast in RCP4.5 and especially in RCP8.5 (Figure 5.13). Considering the continent as a whole, burned area is projected to increase strongly in RCP8.5, and moderately in RCP4.5 and RCP2.6. Again it should be noted that future projections of precipitation are currently not well

constrained, which will have an important impact on how fire danger will change across Brazil in the future. There will also be further interactions between fire, vegetation mortality, and agricultural land which are not fully represented by the model yet, as outlined in Chapter 3.

The results of increased burned area may seem contradictory to the declining global trend that has been seen in the observations in the last 20 years (Andela *et al*., 2017). However the global trend is dominated by a decline in areas of high burned area such as Africa, where there has been an expansion and intensification of agriculture, reducing fuel and ignitions. In the current model set-up, agricultural land is treated as the same as grassland and is thus equally flammable, and ignitions are based on population and do not take account of changes in land management practises which can alter ignition frequency. It is important to consider the results in the context of these limitations. Furthermore, while the global trend shows a decline in burned area, there are regions which have shown an increase in burned area over the last few decades, for example deforestation fires have increased burned area in the tropics exponentially (Mouillot and Field, 2005) (also see section 3.2.5 for trend analysis of the model compared to observations).

Assessing the impact of fire disturbance on broadleaf vegetation, Figure 5.15 shows some loss of the Amazon forest in RCP2.6 over the south and east. This change is more substantial in the RCP8.5 scenario, with a significant loss of forest across the eastern side. This ‘dieback’ is not seen in the model without interactive fire included (right hand panels). As outlined in Chapter 3, fire has previously only been represented in JULES as a constant disturbance and projections of future vegetation cover have therefore not taken changes in fire occurrence into account. Here it is shown that by adding fire into the model the projections of Amazon forest cover change significantly.

Assessing how the impacts change at 1.5°C, 2.0°C and 4.0°C across the RCP scenarios, we can see that there are small local differences in some of the patterns of change. This could be due to the underlying assumptions that are used in the creation of the scenarios, including difference in the way land-use is treated, and how air quality and emissions policies affect the presence of aerosols in each scenario. For vegetation carbon for example, at 1.5°C there are greater

losses of vegetation across the Southeast of the Amazon in scenarios RCP2.6 and RCP8.5, but a small loss in RCP4.5. At 2.0°C there are larger losses in the same area in RCP2.6 and RCP8.5, but there are also increases in vegetation across the northwest of the South American continent, especially in scenario RCP4.5 where the overall impact is an increase in vegetation carbon. Much of this will be a result of land-use policies, where reforestation is projected to be strong in this region in RCP4.5 (see Chapter 2:). We see more growth in the northwest region with higher temperatures, which will likely be a result of CO_2 fertilisation.

The results showed that the pathway to reach specific levels of warming does have an impact on local biogeophysical responses. Higher temperatures are projected across more of Brazil in RCP8.5 than RCP2.6 at 2.0°C of warming, and there is higher humidity in scenarios RCP4.5 and RCP8.5 than RCP2.6 at 1.5°C, but there was less of a response in precipitation between scenarios. Burnt area increased with warming levels, which was particularly increased in areas that are projected to become both hotter and drier, including eastern South America and southern Africa. Burnt area was lower in RCP4.5 than RCP2.6 and RCP8.5 at both 1.5°C and 2.0°C, especially over South America, resulting from differences in precipitation patterns. The forest loss from fire leads to reduced ET, and forest loss from both fire and land-use change leads to a higher albedo. In a fully interactive climate model we could expect this to have biogeophysical and biogeochemical effects on the atmosphere as well (including changes to levels of CO_2, temperature, precipitation, clouds and aerosols). For example, land-use change may lead to a reduction in ET and precipitation in HadGEM2-ES, which is then used to drive JULES. As JULES is used offline in this study, these potential impacts on the climate cannot be evaluated here and the results focus instead on land surface impacts.

The third part of this study has addressed the issue of whether adding a new process, fire, into the model creates an increased likelihood of a dieback response in the Amazon in the future. The results have shown that there is a substantial loss of forest from fire by 2100, especially in the higher concentration scenarios, as a result of increasing drought. This was raised as a potential concern in the IPCC AR5 report, where it was suggested that land-use change and fire could interact with changes to the climate, catalysing a transition to low-

biomass vegetation (Settele *et al*., 2014). Recent research has also suggested that when the interaction of fire and climate change are considered, the potential tipping point for the Amazon forest may be lowered from the previous estimates of 40% deforestation to around 20-25% (Lovejoy and Nobre, 2018; Nobre *et al*., 2016). Silva *et al.* (2018) found that fires have already had a negative long-term impact on carbon stores in the Amazon, reducing forest biomass by an average of 25% and inducing a permanent shift of state to altered forest dynamics. This reduction was found to be mainly driven by delayed mortality of large, high-biomass trees that failed to recover decades after a drought or fire, with their slow regrowth meaning they are unable to re-establish before the next mortality event. This has implications for the recovery of the forest in the future if drought and/or fires become more frequent. The results from this study support these hypotheses, showing tipping point behaviour at future levels of warming when fire is added to the model.

5.5 Conclusion

Through this chapter I have addressed three key research questions:

- How is burnt area projected to change with climate change in the future and, together with changes in land-use, what impact does this have on vegetation coverage?
- What is the impact of different warming levels, and does the pathway to reach them alter the impacts on the land surface?
- Could fire lead to a change in state from tropical forest to savanna?

It has been shown here that burnt area is projected to increase in the future with climate change, as a result of hotter, and in some regions drier conditions projected over Brazil by 2100. Areas that are particularly at risk are the far east of Brazil in scenario RCP2.6, the northeast in RCP4.5, and both the east and northeast of the country in scenario RCP8.5 which shows strong warming and drying. Using the interactive fire-vegetation model, this leads to significant forest loss across the east of the Amazon, with the model projecting a shift from tropical broadleaf forest to shrubs (RCP4.5) and grasses (RCP2.6 and RCP8.5). With the projected forest loss we see a decrease in ET and increase in albedo.

I have also shown that the pathway to reach specific levels of warming can have different regional impacts. At global mean temperatures of 2.0°C above pre-

industrial levels, the temperature is higher across more of Brazil in the RCP8.5 scenario than in the RCP4.5 and RCP2.6 scenario. The humidity at 1.5°C is lower in RCP4.5 than RCP2.6 and RCP8.5 across the North of Brazil. Burnt area is higher in RCP2.6 and RCP8.5 leading to greater vegetation loss; however without fire there are increases in vegetation across the Northwest of the South American continent, especially in scenario RCP4.5, and RCP8.5 at 4.0°C from CO_2 fertilisation and changes in land-use patterns. RCP4.5 shows the largest vegetation carbon growth in the future with land-use, and RCP8.5 shows larger carbon accumulation without land-use. Over South America there is a strong projected warming and drying across the East of Brazil in the high emission scenario RCP8.5, which leads to higher burnt area in this region. This results in a substantial loss of broadleaf forest across the East of the Amazon in RCP8.5, although the loss is less significant in the lower emission scenarios. These initial results seem to support the conclusion in the IPCC report that Amazon dieback is unlikely to happen as a result of climate change alone, but the interaction of warming and drying, land-use change and fire may result in a loss of dense broadleaf rainforest in this region. The vegetation loss leads to higher albedo, and lower ET across the east (RCP2.6) and northeast (RCP4.5 and RCP8.5). This ET reduction is highest in RCP2.6, followed by RCP8.5 and finally RCP4.5 at 1.5°C and 2.0°C, mirroring changes in precipitation. Finally this study has shown an increasing vulnerability of the northeast and eastern regions of Brazil to drought, and adding fire increases the risk of the forest transitioning to lower biomass vegetation especially in higher emission scenarios.

This is the first time that the interactive fire-vegetation model JULES-INFERNO has been used to assess how fire danger may change in the future and what impact this may have on the land surface biogeophysics and the tropical rainforest of Brazil. Limitations to the model include a strong response of vegetation to fire, which could be a result of a number of factors including the mortality rate of vegetation being too high, a slow regrowth rate in the dynamic vegetation model TRIFFID, and current lack of interaction with land-use (i.e. no suppression of fire in agricultural areas). To improve this work in the future, addressing these issues would be a useful step.

Chapter 6: New horizons: limiting temperature rise to 1.5˚C with SRM

6.1 Introduction

One of the central reasons why we create and use models is so that we can use them to run simulations of future scenarios. It is important to verify models against a historical period where observations are available to ensure they reproduce a realistic representation of the real world, so that we can use them to create 'new worlds' in the future. We can modify elements of the land, atmosphere, climate and oceans to see what the world may look like if emissions change, if the climate changes, if land-use activities change, and understand a range of impacts spatially and temporally. The importance of this research is in understanding the impacts in a 'safe' model environment before they occur in the real world, offering the potential for mitigation and adaptation.

One of the largest sources of uncertainty for the future of the Earth system is in how emissions may change, and the resultant impact on the climate (Nakicenovic and Swart, 2000). Together with uncertainties in emissions, we do not know exactly how population levels will change, how land-use activities will vary, and how sensitive the climate and Earth system will be to these variations. A number of future scenarios have been developed to enable us to address these uncertainties within climate model simulations, giving us possibilities for high emissions/ high population / high land-use (e.g. RCP8.5) versus low emissions / controlled population growth / mitigation through biofuels or reforestation (e.g. RCP2.6 and RCP4.5) (see Appendix 2 for explanation of underlying assumptions in RCP scenarios).

In the latest IPCC 5th assessment report, RCP2.6 is the lowest emission / highest mitigation scenario out of four highlighted for climate modelling use, which is designed to limit warming to 2°C (Figure 6.1). Most of the scenarios considered to achieve this lower level of warming are dependent on net negative emissions (van Vuuren *et al*., 2011; Fuss *et al*., 2013), mostly in the form of carbon dioxide removal (CDR) through Bioenergy Carbon Capture and Storage (BECCS). This option has the advantage of converting to non-fossil fuel energy production, as well as capturing resultant CO_2 from burnt fuel. However the total land area

required to meet the 2°C target through BECCS would be around 50% of present-day cropland area (Harper *et al*., 2018b), raising questions around the feasibility and potential conflicts with land needed for food production. An alternative option for limiting temperature rise could be through solar radiation management (SRM), which is the focus of this experiment.

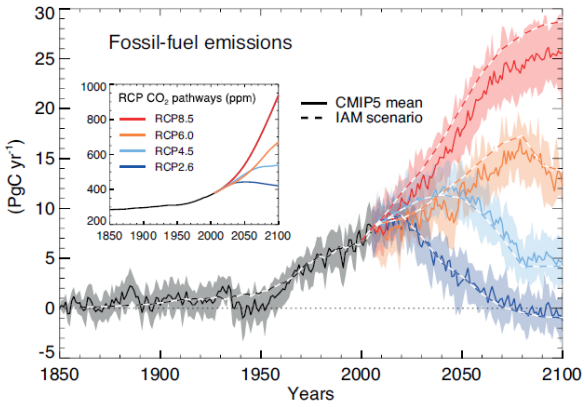

Figure 6.1: Time series of fossil fuel emissions for four RCP scenarios
Time series of compatible fossil fuel emissions simulated by the CMIP5 ESMs for the four RCP scenarios (PgC yr–1). Dashed lines represent the historical estimates and emissions calculated by the Integrated Assessment Models (IAMs) used to define the RCP scenarios, solid lines and plumes show results from CMIP5 ESMs (model mean, with 1 standard deviation shaded) (reproduced from IPCC WGI Chp6 Figure 6.25)

At the COP21 meeting in Paris in 2015, nations came together for the first time to state their commitment to keeping global mean temperature risk below 2°C above pre-industrial levels, and in a further pledge an agreement was reached to "pursue efforts to limit warming to 1.5°C". The 'Paris Agreement' was subsequently ratified by 174 countries in New York in 2016. It is now important for research to begin to understand the implications of this new target, including how it might be achieved, and what difference it could make in avoided impacts.

The remaining carbon budget consistent with a median chance of limiting warming to 2°C is ~1300 $GtCO_2$ which is likely to be exhausted in the next ~25 years. Keeping warming to 1.5°C or below gives a remaining budget of 550 $GtCO_2$ (IPCC SYN table 2.2), which could be exhausted in the next ~10 years with a 50% chance at today's emission levels from 2016, or just 5 years for a 66% chance[32]. This therefore means it would be necessary to convert to zero

[32] Met Office: http://www.metoffice.gov.uk/binaries/content/assets/mohippo/pdf/climate/cop22/theme_2-carbon-budgets.pdf

emissions much sooner in order to reach the 1.5°C target, or alternatively a scenario of overshoot and subsequent strong mitigation / negative emission methods to bring carbon back down to the required levels would be needed. Converting to zero emissions would involve rapid and substantial transformation of our energy demand and supply methods, which is unlikely to be achievable on these timescales.

One option for achieving the 1.5°C target is through SRM in the form of stratospheric aerosol injection of sulphur dioxide (SO_2). Aerosols cool the climate by reflecting incoming solar radiation, as was the case following the 1991 Mount Pinatubo eruption where global temperatures were reduced by around 0.5°C for two years following the event due to the high volume of particulate matter released into the stratosphere (Stowe *et al*., 1992). Volcanic eruptions of this nature increase Aerosol Optical Depth, which reflects incoming solar radiation more effectively than trapping the outgoing Earth radiation, producing a net cooling effect. The aerosol must be evenly distributed within the stratosphere to ensure that the particles are long-enough lived to impact global temperatures, where particles injected at lower levels in the troposphere would be precipitated out too quickly (Haywood *et al*., 2013). Figure 6.2 below shows the temperature profile for three standard RCP scenarios, with the new scenario limiting temperature to 1.5°C.

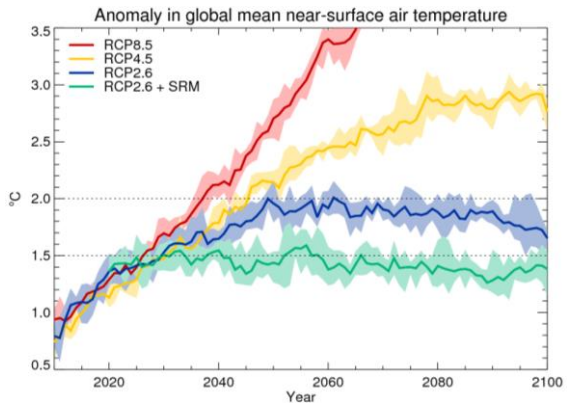

Figure 6.2: Time series of temperatures for SRM scenario
Temperature profiles for three standard RCP scenarios, together with new SRM scenario (figure courtesy of A. Jones, in Wiltshire *et al*. (in prep))

In this Chapter I explore the impacts of limiting global mean temperature rise to 1.5°C compared to 2.0°C above pre-industrial levels. For this I use the established McArthur Forest Fire Danger Index (FFDI) to enable a focus on

change in fire danger conditions as a direct result of a change in meteorological conditions in the two emissions scenarios. The SRM scenario was created using HadGEM2-ES; this is an Earth System Model, enabling atmospheric response to aerosol forcing to be simulated which could not be done in JULES. Fire indices were chosen here for the analysis in order to be able to meet the deadline for the IPCC 1.5 degree special report. The land surface scheme in HadGEM2-ES is based on MOSES-2 but is further improved to include sub-gridscale soil moisture variability (Clark and Gedney, 2008; Martin *et al.*, 2011), showing substantial improvements from previous hydrology modules compared to observations (Good *et al.*, 2013), and which is used in the FFDI calculation for soil moisture. The land surface scheme is approximately equivalent to the JULES-C configuration. A scenario limiting temperature rise to 1.5°C above pre-industrial is not yet available as a standard RCP scenario, and therefore this first-order test uses a simple fire index to assess potential impacts of limiting temperature rise to 1.5°C compared to 2.0°C. This is the first step in assessing future scenarios of fire at lower emission levels. Other factors including ignitions and biomass can introduce further complexities and uncertainties so are not considered here; however we now have the capability to include these within INFERNO and future work could address this.

6.2 Future fire danger at 1.5°C

This paper has been published in GRL, as Burton *et al*. (2018a).

6.2.1 Abstract

The commitment to limit warming to 1.5 °C as set out in the Paris Agreement is widely regarded as ambitious and challenging. It has been proposed that reaching this target may require a number of actions, which could include some form of carbon removal or Solar Radiation Management in addition to strong emission reductions. Here we assess one theoretical solution using Solar Radiation Management to limit global mean warming to 1.5 °C above preindustrial temperatures and use the McArthur fire danger index to evaluate the change in fire danger. The results show that globally fire danger is reduced in most areas when temperatures are limited to 1.5 °C compared to 2.0 °C. The number of days where fire danger is “high” or above is reduced by up to 30 days/year on average,

although there are regional variations. In certain regions, fire danger is increased, experiencing 31 more days above “high” fire danger.

6.2.2 Introduction

As climate change brings hotter, drier conditions to many parts of the world, fire danger is likely to increase in some areas. Fire is one of the most important disturbances globally, impacting vegetation, hydrological cycles, atmospheric chemistry, and the carbon cycle, as well as having socioeconomic impacts through loss of life and property (Hanston *et al*., 2016). Studies have previously attributed fire events to anthropogenic climate change, such as the Californian fires of 2014 (Yoon *et al*., 2015), showing that climate change has already increased the likelihood of fire occurrence in some areas. Other studies have shown that global fire risk may change under different emission scenarios (e.g., Betts *et al*., 2015; Gonzalez *et al*., 2010; Settele *et al*., 2014), showing in general an increase in fire danger with higher levels of climate change above 2 °C in the future, and a shift towards a more climate driven fire regime (Pechony & Shindell, 2010). However, there is inhomogeneous response, and in some areas fire risk may decrease with climate change in the future (Moritz *et al*., 2012).

At the Conference of Parties meeting in Paris in 2015 (COP21), for the first time nations across the world committed to limit global mean warming to 2.0 °C and to “pursue efforts to limit warming to 1.5°C” (UNFCCC, 2015) in an attempt to limit the negative impacts of climate change. Work is now ongoing to understand how this more ambitious climate goal might be achieved, and the potential costs, benefits, and impacts of a 1.5 °C verses a 2.0 °C world. It will also be important to fully understand the impacts of the methods used to achieve this in order to make informed choices moving forward.

For a high probability of stabilizing temperatures at 1.5 °C, it will be necessary to reduce greenhouse gas emissions substantially and rapidly (Millar *et al*., 2017). It is also suggested that this will require net negative emissions by the end of the century or sooner (Rogelj *et al*., 2016), or alternative means of limiting warming. These could be achieved through deployment of geoengineering solutions, either by removing carbon dioxide from the atmosphere (Carbon Dioxide Removal), for example, through Bioenergy Carbon Capture and Storage (Fuss *et al*., 2014; Smith *et al*., 2016) or by reducing the incoming solar radiation through Solar

Radiation Management (SRM; Kravitz *et al*., 2013; Vaughan & Lenton, 2011). However, these technologies are mostly untested, and the impacts of employing such methods of mitigation are not well understood.

One option for SRM could be in the form of stratospheric aerosol injection of sulfur dioxide (SO_2; Crutzen, 2006). Relatively small amounts of SO_2 injection would be required (Keith *et al*., 2010), and this would have reasonably quick effects on reducing global temperatures. However, it has been noted that this could alter regional climate patterns (Haywood *et al*., 2013) and hence could modify fire regimes. Here we perform the first assessment of the potential impact on global patterns of fire danger using SRM to limit global warming to 1.5 °C, compared to a 2.0 °C achieved solely through limiting the rise in greenhouse gas concentrations.

It should be noted that once injected, SO_2 emissions would need to be repeated every year to maintain temperature reduction, and if stopped, the temperature would rise sharply up to pre-SRM levels (Jones *et al*., 2013), unless greenhouse gas concentrations levels were simultaneously reduced. SRM may therefore allow some additional time for reducing greenhouse gas emissions but is viewed as an unsuitable replacement for such reductions in the long term (Keith & MacMartin, 2015). It has been shown that this termination effect would be particularly severe in high-emission scenarios such as RCP8.5, and consequently, it is impractical to consider the use of SRM in this context (McCusker *et al*., 2014). This study therefore focuses on the potential impact of employing SRM together with strong mitigation efforts using the Representative Concentration Pathway (RCP) 2.6 (van Vuuren *et al*., 2011). It should also be noted that there are a number of other potential hazards of SRM which should be taken into consideration, including negative impacts on stratospheric ozone (Keith *et al*., 2010), hydrology and regional climate (Trenberth & Dai, 2007), nutrient cycles, and vegetation loss resulting from sulfur deposition (Crutzen, 2006), and continued ocean acidification (Robock, 2008). These additional impacts are outside the scope of this paper.

6.2.3 Methods

Here we use a theoretical SRM geoengineering scenario to model the potential impacts of fire danger on a global scale at 1.5 °C compared to 2.0 °C. We use

output from the Earth System Model HadGEM2-ES (Collins *et al*., 2011; Jones *et al*., 2011) at a spatial resolution of 1.875° × 1.25°, driven by concentrations following the strong mitigation scenario RCP2.6, and in a second experiment setup a new run of RCP2.6 + SRM is initialized at 2020 and run to the end of the 21st century with SO_2 injected continuously and uniformly into the stratosphere at a height of 16–25 km in four member ensemble simulations. In the model, the SO_2 oxidizes to form a sulfate aerosol that reflects incoming solar radiation and creates a cooling effect on the climate, simulating the effect of SRM in order to keep climate warming to 1.5 °C. The results are then analyzed in terms of potential fire impacts. We use the McArthur Forest Fire Danger Index (FFDI) to compare fire danger for both scenarios RCP2.6 and RCP2.6 + SRM, using the mean from the four member ensemble runs. A period of 10 years 2061–2070 is chosen to represent the future state, as the decade at which maximum warming occurs in the RCP2.6 scenario. We also compare the results to the present-day fire danger, where present day is taken as the period 2006–2015.

The assessment of fire danger is a way of determining the risk of fire occurrence and impact in a region, in terms of ignition, rate of spread, ability to control, and potential impact, based on a number of input variables (de Groot *et al*., 2015). The McArthur FFDI (McArthur, 1967; Noble *et al*., 1980) was designed for use in Australia, but it can be used for assessing global fire danger, (Betts *et al*., 2015; Golding & Betts, 2008) and uses meteorological conditions to calculate the risk of fire occurrence in the following equation:

$$\boldsymbol{FFDI = 1.25 * D * exp\left[\frac{T - H}{30.0} + 0.0234 * V\right]}$$

where D = drought factor, T = temperature (°C), H = humidity (%), and V = wind speed (km/hr1). The drought factor (D) is calculated as follows:

$$\boldsymbol{D = \frac{0.191 * (SMD + 104) * (N + 1)^{1.5}}{3.52 * (N + 1)^{1.5} + P - 1}}$$

where P = precipitation (mm/day) and N = number of days since last rain. Here we use varying soil moisture from the Earth System Model to calculate the soil moisture deficit (SMD) compared to the field capacity at a depth of 1 m to account for varying ecoregions, based on Holgate *et al*. (2017). Soil moisture is calculated based on inputs and outputs of precipitation, snowmelt, evapotranspiration, and drainage. The land surface scheme is based on MOSES-2 (Essery *et al*., 2003) but further improved to include subgridscale soil moisture variability (Clark & Gedney, 2008; Martin *et al*., 2011).

This fire danger system is used operationally in high fire-risk areas such as across Australia as a way of providing early warning for dangerous fire events (de Groot *et al*., 2010). It provides a way of managing the resources needed for fire management and suppression and underpins evacuation plans for national safety.

Here we use daily input data to calculate the FFDI. We first present the change in key meteorological variables, temperature and precipitation (Figure 6.3). We use the 90th percentile of daily maximum temperature to understand the extremes that contribute to fire danger and the mean change in precipitation to understand the overall pattern of change. We then assess the change in the 90th percentile of fire danger between the RCP2.6 and RCP2.6+SRM scenario compared to present day, and explore how regions experiencing 'high' fire danger may change with each scenario (Figure 6.4). The results of these analyses are presented by Giorgi region (Giorgi and Francisco, 2000) (Figure 6.5).

6.2.4 Results

Compared to present day climate, the temperature increases globally in the future under scenario RCP2.6 (Figure 6.3, panel a) as expected. However, this increase is not homogenous; the mean change shows greater warming in the northern high latitudes (Figure 6.8), and at the 90th percentile the regions in central and eastern United States and NE Asia show minimal to negative change. With the application of SRM, overall the temperature decreases compared to RCP2.6, however the same regions (United States and NE Asia) show an increase in temperature (Figure 6.3, panel c). There are also regions where the change between RCP2.6 and SRM is approximately 0, such as across Scandinavia.

The change in mean precipitation is even more heterogeneous. Across the northern hemisphere the change is mostly an increase in precipitation with RCP2.6 compared to present day (panel b). Across the Southern Hemisphere, the change is mostly a decrease in precipitation with particularly strong drying across South America, except for two regions that show an increase in precipitation (east Brazil and south Brazil / Uruguay). With deployment of SRM, the results show a decrease in precipitation in many areas compared to RCP2.6, including central and eastern United States and NE Asia (panel d). However some regions show an increase in precipitation compared to RCP2.6, including Central America, a band across Brazil, central Africa, West Asia, and most of Australia. Most of the Sahara region shows no noticeable change.

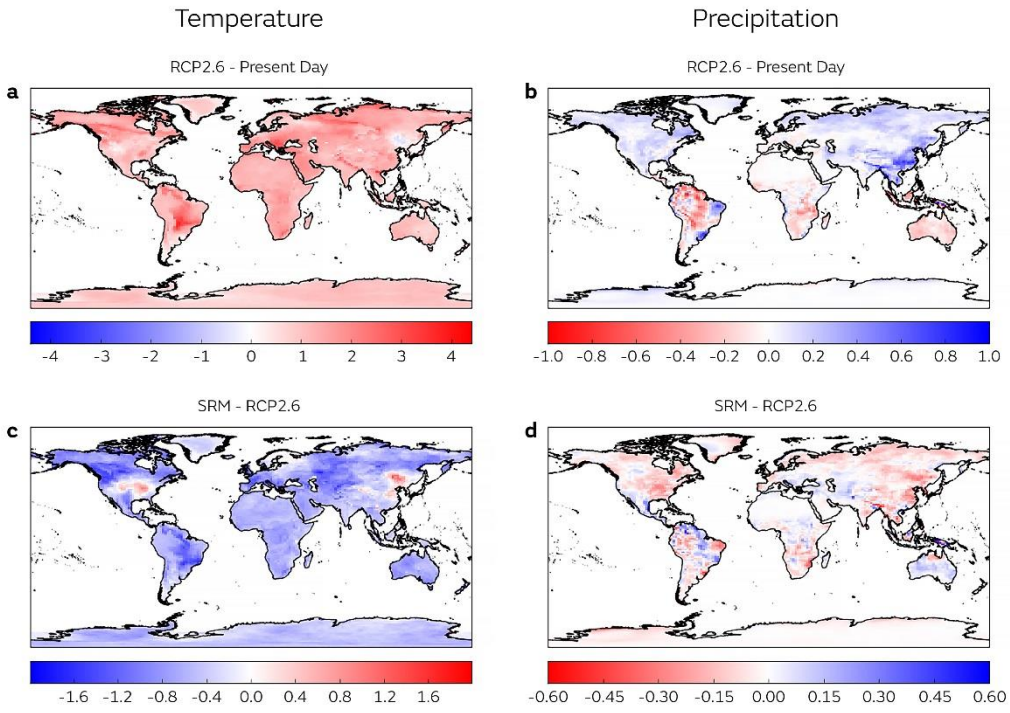

Figure 6.3. Change in daily climate variables
90th percentile of daily maximum temperature (°C) at 1.5m (left column), and mean precipitation change (mm/day) (right column). Upper row shows RCP2.6 (2061-2070) minus present day (2006-2015). Lower row shows the change in fire danger with SRM, calculated as change in RCP2.6+SRM (2061-2070) from Present Day (2006-2015) minus change in RCP2.6 (2061-2070) from Present Day (2006-2015).

We assess how the 90th percentile of fire danger may change with RCP2.6 and RCP2.6+SRM (Figure 6.4) to understand if more areas are exposed to 'high' fire danger in the future due to these meteorological changes. We also calculate if the number of days where the fire danger is 'high' or above changes between

scenarios, to understand if regions become vulnerable to dangerous fires more often.

In the present day, the Sahara, Middle East, and parts of west and central Australia show ‘severe’ fire danger (Figure 6.4, panel a), which also corresponds to the highest number of days above ‘high fire danger (panel b).

Compared to present day fire danger, RCP2.6 shows an increase in the 90th percentile of fire danger across most regions globally, with the highest change of 8 (panel c). The areas most affected by increased fire danger in this scenario include South America, Europe, Arabia and western Australia. Interestingly, there are also regions that decrease in fire danger in this scenario, such as USA and NE Asia, with the largest change of -5. These regions correspond to reduced temperatures and increased precipitation with RCP2.6 (Figure 6.3, a and b). The number of days where fire danger is ‘high’ or above is also mostly increased in RCP2.6 compared to present day (panel d), with the highest change across Southern Africa, Australia and South America, and a maximum increase of 62 days per year on average (619 days across the 10 year period). A similar pattern of decreased fire danger in the United States and NE Asia can be seen in both the change in the 90th percentile of fire danger (panel c) and the change in number of days above ‘high’ FFDI (panel d). Panel (d) also shows a decreased number of days of high fire danger across East Brazil.

Compared to present day fire danger, RCP2.6+SRM also shows an increase in fire danger for most regions in the future (Figure 6.4, panel e), although this is generally less than in the RCP2.6 scenario. However, the two regions (USA and NE Asia) that showed a decreased danger in the RCP2.6 scenario do not show as much of a decrease with SRM, and in fact some parts of these regions show higher danger with SRM in both the 90th percentile and the number of days above ‘high’ FFDI. Parts of Central America and western Asia show a marked decrease with SRM.

Overall the 90th percentile of fire danger is reduced with the application of SRM, but there are some regions that show the opposite trend (Figure 6.4, panel g). NE Asia and the Unites States show an increase in the 90th percentile of fire danger reached with RCP2.6+SRM compared to RCP2.6, with a maximum increase of 5.5. This is partly due to a decrease in fire danger seen in the RCP2.6

scenario compared to present day that is not as marked with SRM (Figure 6.4, panel c and e). Most other regions show a decrease, with the highest reduction being 3.8. In some areas there is no clear change, such as across western South America, and the northern high latitude regions. The change in number of days above ‘high’ fire danger with SRM shows a similar increase in fire danger across NE Asia, and America compared to the RCP2.6 scenario (Figure 6.4, panel h). These regions show a maximum of 31 more days at ‘high’ fire danger on average per year at 1.5°C compared to 2°C. Again the general global trend is a decrease in the number of days of ‘high’ fire danger in the RCP2.6+SRM scenario compared to RCP2.6 with a maximum reduction of 30 days per year on average, although some areas show no obvious change including central Asia.

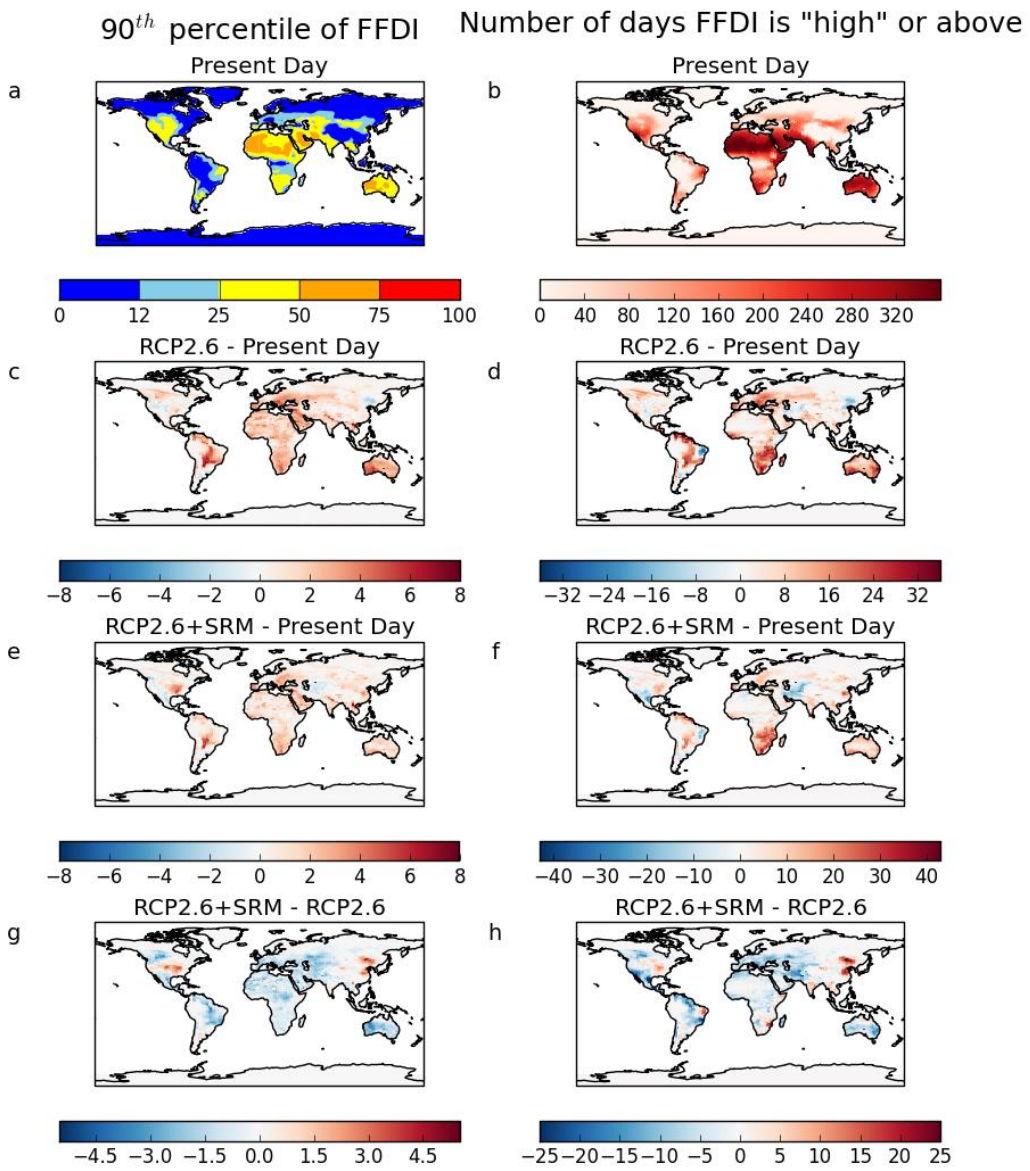

Figure 6.4. Change in fire danger
90th percentile of fire danger (left column) and number of days where fire danger is above'high' on the McArthur scale (right column). Top row shows present day (2006-2015). Second row shows the change in RCP2.6 (2061-2070) minus Present Day (2006-2015). Third row shows the change in RCP2.6+SRM (2061-2070) minus Present Day (2006-2015). The bottom row shows the change in fire danger with SRM, calculated as change in RCP2.6+SRM (2061-2070) from Present Day (2006-2015) minus change in RCP2.6 (2061-2070) from Present Day (2006-2015). Panel (a) uses the McArthur FFDI scale categories as follows: 0-11 = Low-moderate fire danger; 12-24 = High fire danger; 25-49 = Very high fire danger; 50-74 = Severe fire danger; 75-99 = Extreme fire danger; 100+ = Catastrophic fire danger.

The results show that where mean temperature reduction with SRM is minimal (Figure 6.8 panel b), and where the 90th percentile of temperature change shows an increase compared to RCP2.6 (Figure 6.3c), together with a marked reduction

in precipitation (Figure 6.3d), there is increased danger of fire for two key regions. These regions may be exposed to higher fire danger for longer periods under an SRM scenario compared to RCP2.6.

Considering the Giorgi regions, Figure 6.5 shows that in most regions overall fire danger is increased in the future under both scenarios. The largest difference in 90th percentile fire danger is in Northern Australia (NAU), where application of SRM decreases the danger overall. Southern Australia (SAU) and Central Asia (CAS) also show among the highest decreases. Other regions show small changes, such as Alaska (ALA). In some cases the fire danger is reversed, with SRM causing increased fire danger at the 90th percentile compared to RCP2.6. In East Asia (EAS), Eastern North America (ENA) and Central North America (CNA) the highest fire danger increases with application of SRM, which supports the findings in Figure 6.4. A similar trend is seen in the number of days where fire danger is high or above. This is usually lower in the SRM scenario compared to RCP2.6, but in the same regions it is increased (EAS, ENA, CNA). In some cases the overall fire danger is changed to negative with SRM, including Central Asia (CAS), Central America (CAM), and West North America (WNA).

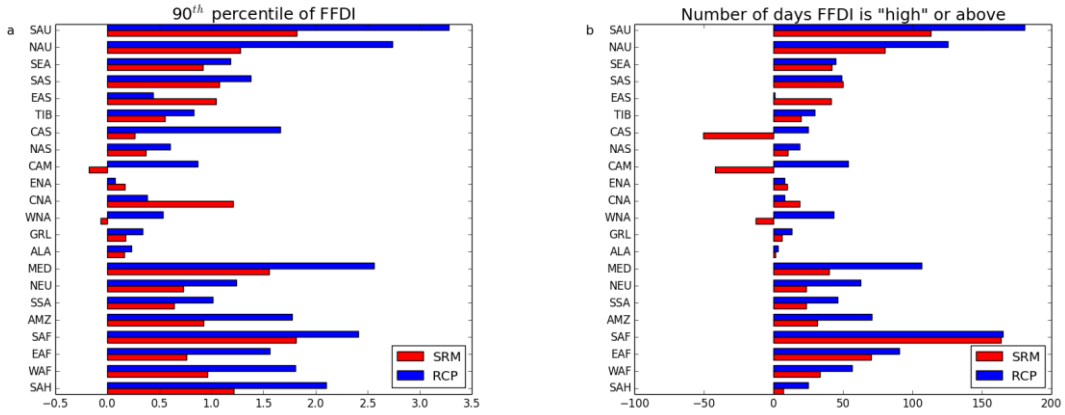

Figure 6.5. Graph of change in McArthur FFDI
From 2061-2070 compared to present day (2006-2015), for 90th percentile of fire danger (a) and number of days at 'high' fire danger or above (b). Red bars represent the RCP2.6+SRM scenario, blue bars represent RCP2.6 scenario. Full list of Giorgi regions can be found in the Supplementary Material.

6.2.5 Discussion

The results presented here have shown that in general, meteorological fire danger increases in the future (Figure 6.3 and Figure 6.4), even in a scenario of strong climate change mitigation. Here we have compared the highest mitigation

scenario from the IPCC Representative Concentration Pathway scenarios, RCP2.6 which limits committed warming to 2.0°C, with an even stricter mitigation target of 1.5°C achieved through implementation of SRM. If we were to compare this with a business as usual scenario, RCP8.5, we would likely see a significant difference in fire danger globally and regionally, with global temperatures expected to reach approximately 5.5°C above pre-industrial in this high emission scenario (Settele *et al*., 2014; Betts *et al*., 2015). This could also result in different patterns of increase / decrease in fire frequency and probability, for example Mortiz *et al*. (2012) show a reduction in fire across the tropics with future high emissions scenarios in a range of global climate models. We have compared these two mitigation scenarios here to determine if there is a difference in fire danger, if so by how much, and if this the same everywhere in the world. The results have shown that the highest fire danger, the 90th percentile of the distribution, has shifted so that more regions globally experience higher fire danger in the future under RCP2.6 compared to present day (Figure 6.3c). Regions may also experience prolonged exposure to higher levels of fire danger in the future (Figure 6.3d). However, fire danger does not increase homogenously, and some areas show decreased fire danger (some parts of USA and NE Asia). These regions would experience higher fire danger with implementation of SRM, partly due to the decrease seen in the RCP2.6 scenario. These areas show the smallest decrease in temperature, and are vulnerable to decreased precipitation and humidity with SRM (Figure 6.1 and Figure 6.8 and Figure 6.10). A decrease in precipitation as seen here may be partly due to circulation changes caused by lower temperatures, and research has also shown a direct impact of aerosols on the hydrological cycle and transport of latent heat, leading to a reduction in precipitation (Trenberth and Dai, 2007). This has direct implications for the use of aerosols in SRM methods. This highlights an important message, that although temperatures could be decreased globally by using geoengineering methods such as SRM, the impacts are not felt evenly across the world. This spatial heterogeneity in fire danger response underlines the importance of conducting a thorough assessment of potential impacts when considering new geoengineering technology, as there may be unintended and unanticipated consequences on both a regional and global scale.

The McArthur Index is useful in providing an indication of fire danger as it includes a number of meteorological variables as well as a drought index. However, it is worth noting that it was designed and calibrated for Australian vegetation (de Groot *et al*., 2006), and therefore its applicability outside of this region is less certain, where other species may have a different tolerance and resistance to fire (Golding and Betts, 2008). Moreover, there will be some bias in the fire index as a result of using model input data instead of observations. To ensure the results were not dependent on the fire index used, we also assessed the mean response with the Angström Index (Chandler *et al*., 1983) (see Supporting Material). The Angström Index is a very simple fire index using only two variables, temperature and relative humidity. The index gives very similar results, with global mean fire danger increasing in the future, and the RCP2.6+SRM scenario generally showing a smaller increase in fire danger than the RCP2.6 scenario. Similar regions also show an increase in fire danger with SRM in both the McArthur and the Angström Index. However, the largest difference in the mean fire danger in the McArthur FFDI is in Australia, whereas the largest difference in the Angström Index is in Europe, both reflecting the regions they were designed for. Many fire indices were initially designed for other regions, such as the National Fire Danger Rating System (NFDRS) in America (Bradshaw *et al*., 1983), and there may therefore be some small variations in the extent of the change using different fire indices.

It should also be noted that both indices used here provide an indication of fire danger given certain meteorological conditions, and do not take into account the availability of fuel or ignitions. For a full assessment of fire prediction using fuel, flammability and ignition, a land surface or Earth System model including fire disturbance is required. This said, the inclusion of additional inputs introduces greater uncertainty, and fire indices are therefore useful in providing a simple guide of how fire conditions may change in the future with climate change, and give an indication of how different temperature scenarios are likely to affect fire danger. They are also used operationally to manage fire danger, with the McArthur Index being used frequently in high fire-risk areas in Australia to manage dangerous fire events (de Groot *et al*., 2015).

6.2.6 Conclusion

This study has shown that there is a noticeable change in the fire danger with RCP2.6+SRM compared to RCP2.6. In most areas this change is a reduction in fire danger, with a maximum decrease of 3.8 in the 90th percentile, and 30 fewer days per year on average of high fire danger. However, the changes are not homogenous and there are regions where the fire danger is increased due to reduced precipitation and minimal temperature reduction with the implementation of SRM, in particular parts of NE Asia and the USA, and also due in part to the reductions seen in the RCP2.6 scenario which are not seen in the RCP2.6+SRM scenario. The maximum increase due to SRM is 5.5 on the McArthur FFDI and 31 more days of above 'high' fire danger per year on average. Considering the Giorgi regions, the greatest difference between the scenarios is in Australia and central Asia. In some cases the overall fire danger is changed to negative with SRM, including Central Asia (CAS), Central America (CAM), and West North America (WNA).

These results highlight the importance of thoroughly assessing all of the potential impacts on a regional scale when considering geoengineering options, to rule out any potential unintended consequences that may be caused by large scale geoengineering. The changes to key impact metrics need to be evaluated thoroughly in order to weigh them against the potential costs and risks of mitigation options such as this. The method of geoengineering chosen here also does not address CO_2 levels by itself, and additional mitigation methods would need to be simultaneously employed to reduce emissions. While it has been shown that there would be some benefits from this method of SRM in the form of an overall reduction in meteorological fire danger, the negative impacts of SRM also need to be carefully considered, and more work is needed to fully understand the potential impacts across a range of variables.

Acknowledgments, Samples, and Data

This work was supported by the European Commission's 7th Framework Programme (EU/FP7) under Grant Agreement 603864 (HELIX), and the Joint UK BEIS/Defra Met Office Hadley Centre Climate Programme (GA01101).

The HadGEM2-ES scenarios were produced by Andy Jones of the Met Office Hadley Centre, and were used for the experiments in this paper with his kind permission. Data used to calculate the results is available through BADC:

McArthur FFDI: http://dx.doi.org/10.5285/70ac55eb85344c3bb2239ed2d7b7575d

Angström Index: http://dx.doi.org/10.5285/75a7e567fe2342a493663a7a085d015e

The authors would like to thank Inika Taylor of the Met Office Hadley Centre, for her guidance on calculating the Drought Index used in this paper.

Supporting Material

This supporting information gives further analysis on the climate variables and fire indices at 1.5ºC compared to 2.0ºC. The Giorgi regions used in Figure 6.5 of the main paper are also listed here in full.

Another fire index was used in support of the work done with the McArthur Index. The aim was to ensure the results of the analysis of fire danger at 1.5°C and 2°C were not dependent on the fire index used. The results show very similar results to the McArthur Index, with overall increased fire danger with future scenarios, higher fire danger with the RCP2.6 scenario compared to RCP2.6+SRM, and the same regions showing increased fire danger with SRM.

The Giorgi regions used in Figure 6.5 are as follows:

North America:
Alaska = ALA
Greenland = GRL
Western North America = WNA
Central North America = CNA
Eastern North America = ENA
Central America = CAM

South America:
Amazonia = AMZ
Southern South America = SSA

Europe:
Northern Europe = NEU
Mediterranean = MED

Africa:
SAH = Sahara
WAF = West Africa
EAF = East Africa
SAF = South Africa

Asia:
Northern Asia = NAS
Central Asia = CAS
Tibet = TIB
Eastern Asia = EAS
Southern Asia = SAS
South East Asia = SEA

Australia:
Northern Australia = NAU
Southern Australia = SAU

The Angström Index was used to verify the results of the McArthur Index. This fire index, of Swedish origin, uses just two variables, temperature and humidity, to determine fire danger. The index uses a reverse scale where a low index value corresponds to a high fire danger, as shown in Table 6.1:

The index, I, is given by:

$$\boldsymbol{I} = \left(\frac{\boldsymbol{R}}{\boldsymbol{20}}\right) + \left(\frac{\boldsymbol{27 - T}}{\boldsymbol{10}}\right)$$

Where:

R = Relative humidity (%)

T = Air temperature (°C)

Table 6.1: The scale of fire danger used in the Angström index

Index value	Meaning
I > 4.0	Fire occurrence unlikely
4.0 > I > 2.5	Fire conditions unfavourable
2.5 > I > 2.0	Fire conditions favourable
I < 2.0	Fire occurrence very likely

Mean changes in fire danger were analysed with both the McArthur Index and Angström Index to check if there were any significant differences in the trend of change as a result of the fire index chosen. The results show that the both indices give similar results, showing an increased danger of fire with future scenarios, and a higher overall fire danger with RCP2.6 compared to RCP2.6+SRM.

The mean change in the McArthur fire index shows that there is increased fire danger in the future in all 6 domains, but that this is reduced with SRM (Figure 6.6). The largest difference between scenarios can be seen in Australia.

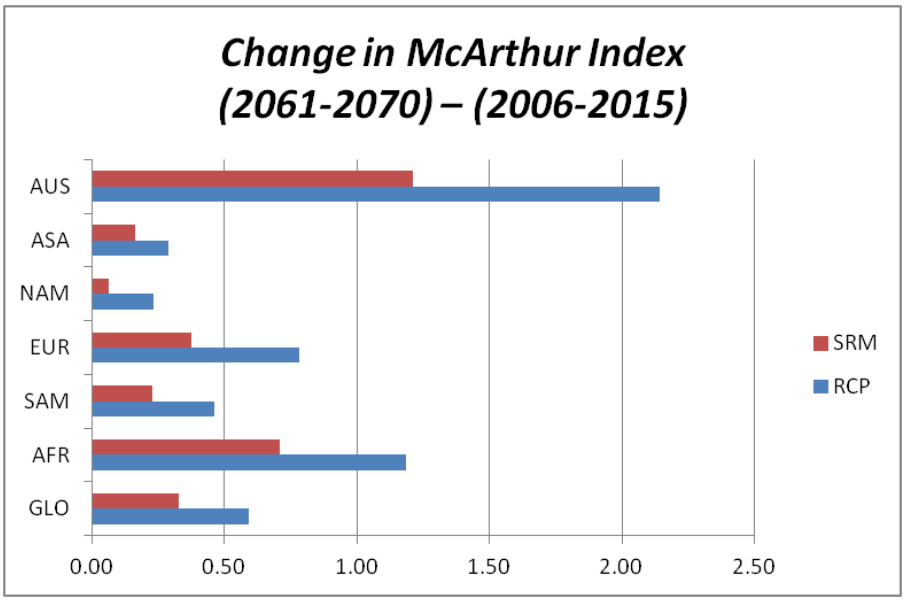

Figure 6.6: Graph of change in mean McArthur FFDI
From 2061-2070 compared to present day (2006-2015). Red bars represent the RCP2.6+SRM scenario, blue bars represent RCP2.6 scenario. Giorgi domains are as follows: AUS = Australia, ASA = Asia, NAM = North America, EUR = Europe, SAM = South America, AFR = Africa, GLO = Global.

The mean change in the fire danger was also calculated using the Angström Index to verify the change compared to the McArthur Index. The results show that the fire danger also increases in this index in the future compared to the present day, and that the fire danger is higher in the RCP2.6 scenario compared to RCP2.6+SRM in all domains and globally (Figure 6.7). The change using this index is higher in Europe, closely followed by Australia and North America.

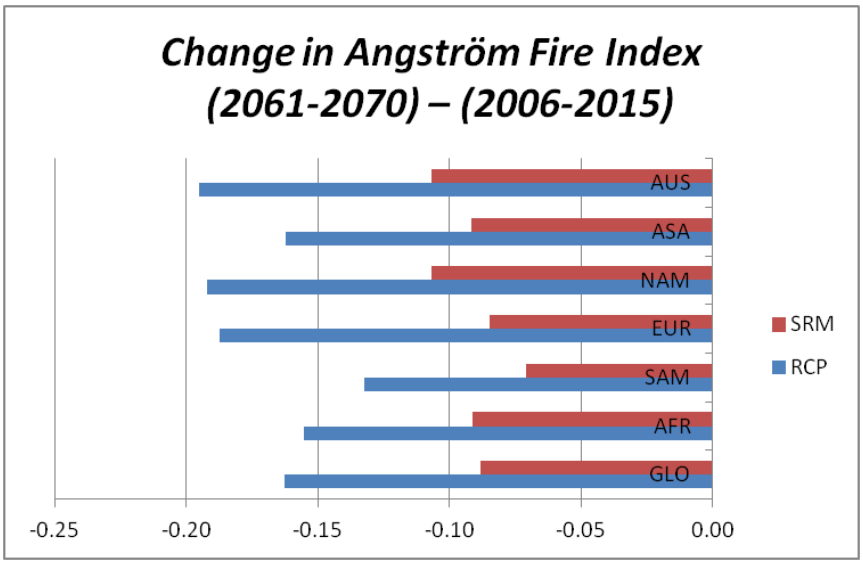

Figure 6.7: Graph of change in mean Angström Index
From 2061-2070 compared to present day (2006-2015). Red bars represent the RCP2.6+SRM scenario, blue bars represent RCP2.6 scenario. Giorgi domains are as follows: AUS = Australia, ASA = Asia, NAM = North America, EUR = Europe, SAM = South America, AFR = Africa, GLO = Global. The Angström Index uses a reverse scale, where lower numbers represent higher fire danger.

The mean values for temperature were also calculated as context for the mean fire danger:

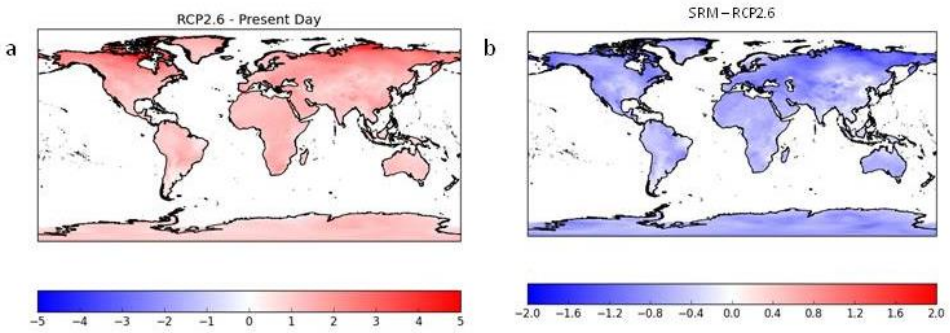

Figure 6.8 Change in mean daily maximum temperature
Temperature (°C) at 1.5m, for RCP2.6 (2061-2070) minus present day (2006-2015) (a) and RCP2.6+SRM - RCP2.6 (2061-2070) (b).

In addition to the mean values, the extremes of fire danger were also calculated for the Angström Index using the same criteria as used for the McArthur FFDI (although note that because the Angström Index scale is reversed, the 10th percentile was used instead of 90th percentile). The results show a very similar trend to those from the McArthur FFDI, and the same regions of increase with SRM.

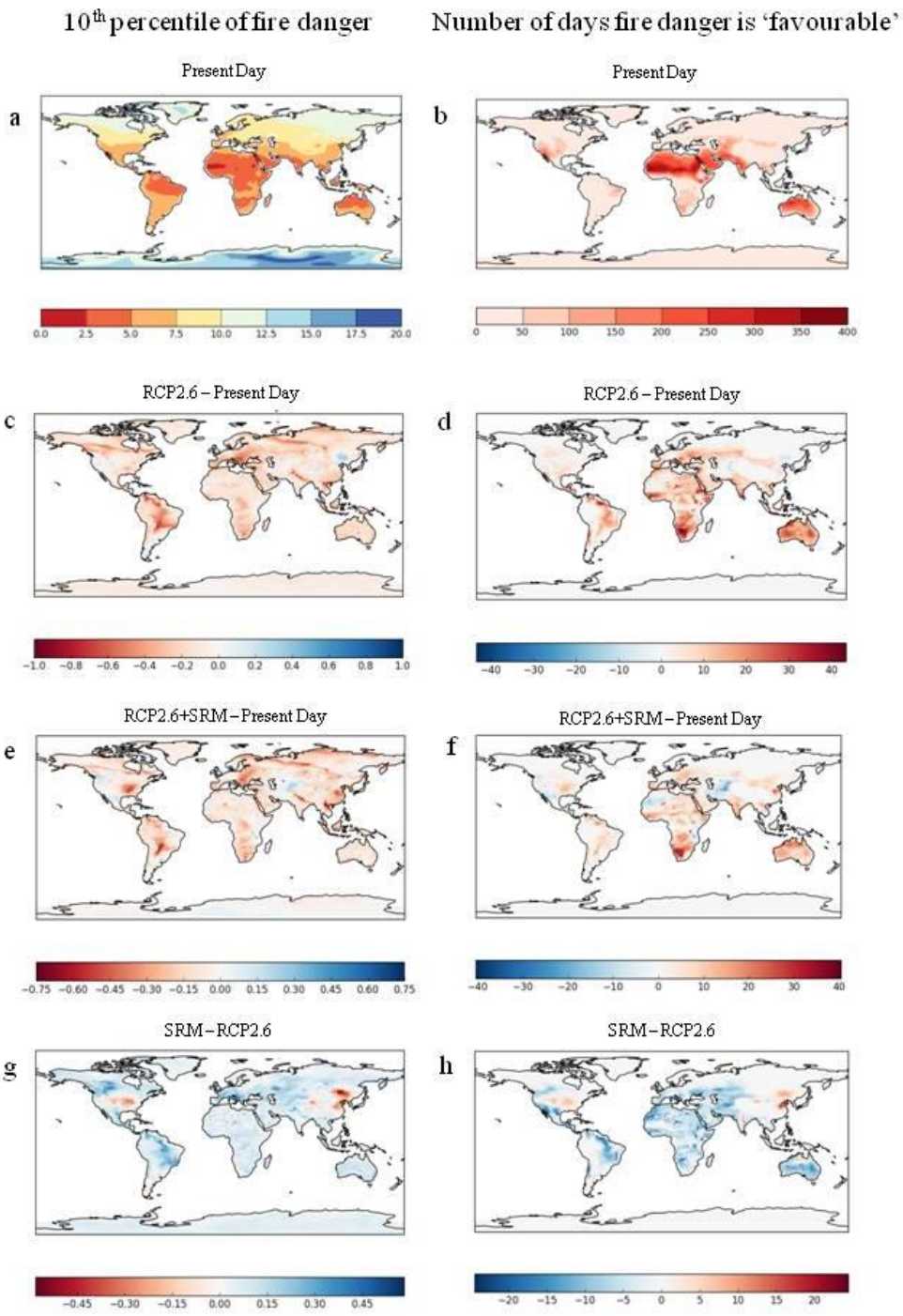

Figure 6.9: Change in fire danger using the Angström Index
10th percentile of fire danger (left column) and number of days where fire danger is below 2.5 (favourable) on the Angström Index (right column) averaged over 10 years. Top row shows present day (2006-2015). Second row shows the change in RCP2.6 (2061-2070) minus Present Day (2006-2015). Third row shows the change in RCP2.6+SRM (2061-2070) minus Present Day (2006-2015). The bottom row shows the change in fire danger with SRM, calculated as change in RCP2.6+SRM (2061-2070) from Present Day (2006-2015) minus change in RCP2.6 (2061-2070) from Present Day (2006-2015).

The other variables that contribute to fire danger have been included here to give further context to the calculations.

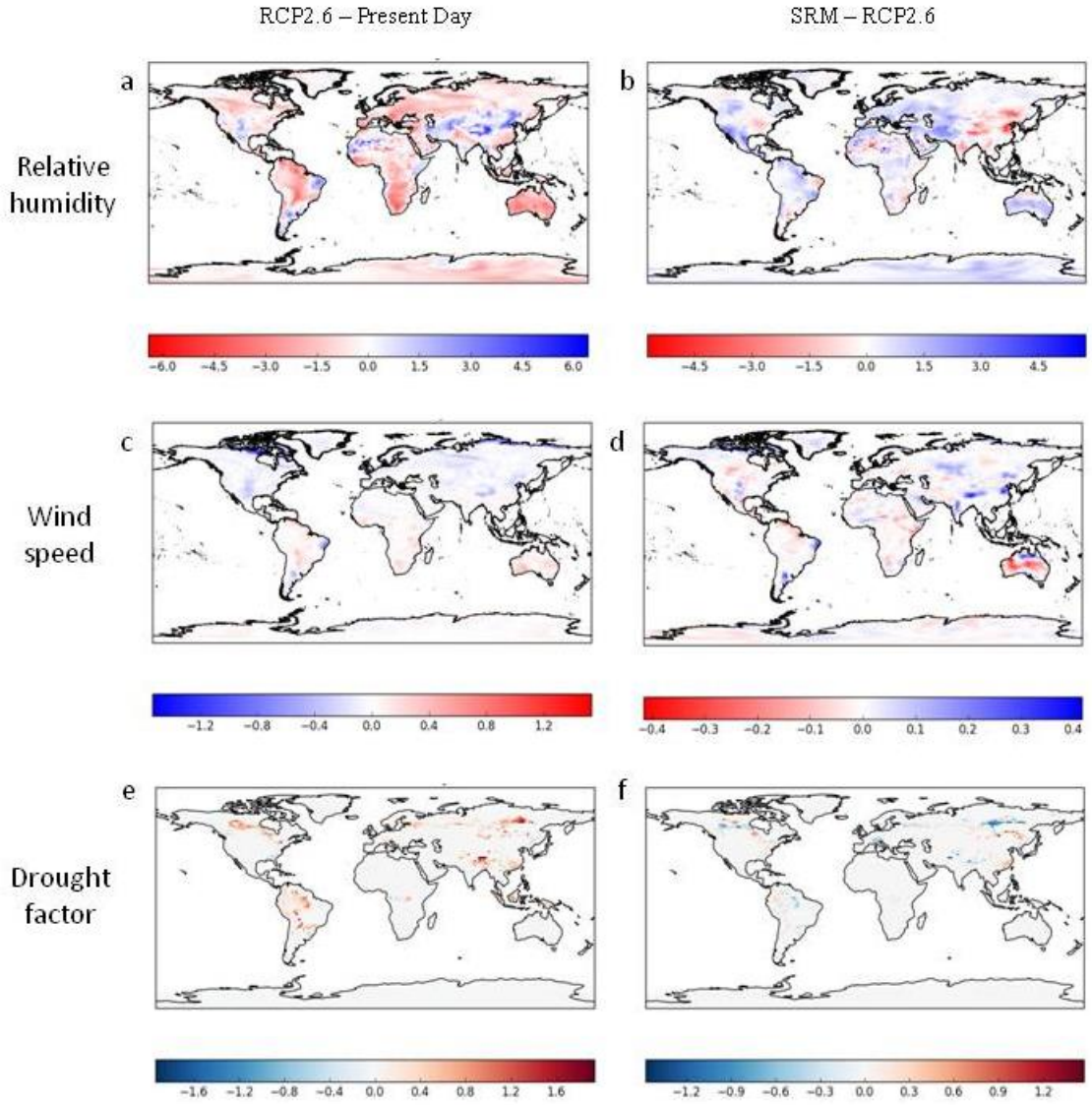

Figure 6.10: Change in humidity
Change in daily minimum relative humidity (%) (top row), daily mean wind speed (km hr-1) (middle row), and drought factor (bottom row) for RCP2.6 (2061-2070) minus present day (2006-2015) (left column) and RCP2.6+SRM - RCP2.6 (2061-2070) (right column).

Mean, minimum and maximum values of change were calculated for each change in fire danger in the main paper for Figure 6.4 (panels c-f). The results are shown below in Table 6.2.

Table 6.2: Mean, maximum and minimum values of change in fire danger, according to scenario, shown per 10 year period analysed

Maximum fire FFDI (90th percentile)			**Number of days above 'high' FFDI**		
RCP2.6 – Present Day			RCP2.6 – Present Day		
MAX	MIN	MEAN	MAX	MIN	MEAN
7.917488	-4.75938	0.262291	619	-335.5	10.02265
RCP2.6+SRM - Present Day			RCP2.6+SRM - Present Day		
7.986501	-7.61999	0.156555	369.75	-429.25	5.619522
SRM - RCP			SRM - RCP		
5.507972	-3.76442	-0.10574	310.25	-298.75	-4.40313

Chapter 7: Synthesis and conclusions

7.1 Summary of key findings

The aim of this PhD has been to understand how fire and land-use change impact vegetation cover today, and how this may change with climate change in the future, with a focus on the Brazilian Amazon, South America. In order to address this research question, I have developed the INFERNO fire model so that it interacts with dynamic vegetation within the land surface model JULES. This work enables us to represent interactive fire disturbance and mortality as a separate process for the first time in JULES, fulfilling an important missing component of the terrestrial carbon cycle. Fire has multiple impacts on the Earth system, including on vegetation, the carbon cycle, the water cycle, atmospheric chemistry, albedo and radiative forcings, which can be compounded or diminished by processes of land-use and land cover change, making it a critical disturbance factor to understand.

First I conducted an in-depth literature review to understand the context of fire and land-use globally and in the Brazilian Amazon, and outlined the current status of fire modelling. This showed that while prominent early studies showed a dieback response of the Amazon forest in the HadCM3 model due to strong warming and drying, subsequent models such as HadGEM2 have not shown such a strong sensitivity of the forest to future climate changes, and project a less intense drying signal. However these models did not include fire as a separate process. It was postulated in the IPCC AR5 report that fire could be a key missing process that has the potential to interact with drought and land-use change, to alter the ecosystem balance enough to initiate a transition to a low-biomass fire adapted vegetation such as grasses and shrubs, and other studies have shown that the Amazon is the most vulnerable tropical forest to this kind of mass tipping point. However there are few studies that have considered future scenarios of fire danger, and there is still high uncertainty about how forests may respond to changes in fire and climate. A limited number of studies have used the McArthur FFDI to show that fire danger may increase in the future, but these did not include vegetation interactions. Other work has shown that fire danger may decrease in tropical regions in the future, and that we are already seeing a decrease in fire in

some areas due to increasing conversion of land to savanna through deforestation. This review gave an overview of available observations, fire indices and fire models, including potential flaws and uncertainty factors that need to be considered when using them.

I analysed available land-use datasets in Chapter 2, and showed how land-use is projected to change in the future under different emission scenarios, with high disturbance in scenarios RCP2.6 and RCP8.5, and reforestation in RCP4.5 and RCP6.0. I analysed the impact of land-use globally and for Brazil, and performed a multi-model analysis across the TRENDY models to assess the uncertainty in the land sink across biomes in Brazil, showing the largest uncertainty range in the Cerrado region. Including fire in the analysis significantly reduces the modelled emissions attributed to land-use in this region, shown later in Chapter 3.

Chapter 3 focused on model development, where I first performed initial simulations to test the capability of coupling the fire to dynamic vegetation, which showed promising results. I then described the coupling process, and the representation of the new disturbance terms in the form of equations for vegetation competition. This is the first time that fire-vegetation interactions have been included for JULES-INFERNO. The results of the coupling were shown in terms of fractional vegetation cover. Overall there was a tendency towards the faster growing PFTs with a loss of forest, and when both fire and land-use were included together there were some areas of 'over-disturbance'. The loss of woody PFTs was likely a result of slow regrowth times, and / or too high a mortality rate. Spatial distribution of vegetation improved significantly with tuning, and overall the results were mostly within the range of uncertainty from ESA observations although there were variations by biome. Across Brazil this showed an important result; without land-use or fire, climatically the model supports forest right across the savanna region. It is only with the introduction of fire or prescribed land-use that this area of savanna is correctly simulated in the model as shrub and grass. This supports the findings of Staver *et al*. (2011) and Hirota *et al*. (2011) showing that fire is a fundamental process in the development of savannas. This also impacts on our ability to quantify land-use emissions from this region. Previously in JULES a significant proportion of emissions in Brazil were attributed to land-use in the Cerrado region, due to the simulation of too much tree cover by the

model. Now fire is included, this Cerrado area is no longer simulated as broadleaf tree cover, but a mixture of grasses and shrubs without prescribed land-use change. As a result, emissions from Brazil are now higher from the Amazon than from the Cerrado region, which is more in line with the SEEG emission records.

I then used the new interactive fire-vegetation model to assess a case study of the 2015-2016 El Niño to understand the impact of climate variations on fire in Chapter 4. The year 2015/16 did not show an anomalously high burnt area or emissions according to GFED data, but I used the JULES-INFERNO model with observed climatology and with mean climatology from the previous 10 years to investigate whether the El Niño may have caused a higher burnt area than would have been the case without the El Niño event. I found that burnt area was higher with the El Niño in some areas (south USA, South America, central Australia), but lower in others (Africa, east Asia, west Australia). Globally burnt area was higher with the El Niño in the last half of 2015, and emissions were higher for most of the period July 2015 – June 2016. Three fire-prone regions were considered; Asia, Africa, and South America; out of these regions South America showed the largest change in burnt area and fire emissions with the El Niño, driven by increased temperature and reduction in moisture availability, and Africa showed a negative change driven by higher humidity and lower fuel availability. 2015-2016 had the lowest Net Biome Productivity in the series of 10 years, and was lower for most of the year than the previous largest El Niño in 1997-1998. As a result South America was converted from a net carbon sink to a source of carbon driven by decreases in GPP and increases in fire, and Africa and Asia became larger sources of carbon driven by a reduction in GPP and increases in fire respectively. I found that temperature was a larger driver of burnt area than precipitation. Burnt area in South America was highest in August-October, and the change due to El Niño varied spatially with the Cerrado region in the South of Brazil experiencing an increase in burnt area and the East showing a decrease. This gave a net increase in burnt area for the country as a whole. The El Niño caused a global mean increase in temperature, humidity and burnt area, and overall decrease in mean precipitation, soil moisture, plant respiration and vegetation carbon. This supports other research that has shown an increase in fire activity related to drought conditions e.g. Aragão *et al*. (2018). It is possible that El Niño-related droughts and increases in temperature may become more

intense in the future with climate change, which is a cause for concern for potential increases in fire during such events. Compared to GFED observations of burnt area, the model showed good overall magnitude of burnt area and emissions, but less accuracy in seasonality. The downward trend in burnt area over the last decade that is seen in the observations is not captured by the model, likely due to processes of suppression in agricultural lands not yet being represented.

I then investigated a number of scientific questions around the nature of fire and how climate change may impact its prevalence in the future, focusing on different aspects of the fire regime. I first considered how fire danger may change under 'conventional' future scenarios, using the Representative Concentration Pathways (RCPs) to assess how fire and land-use interact with high emissions and high mitigation pathways in Chapter 5. For this I used the new coupled JULES-INFERNO model to investigate potential changes in vegetation and biogeochemical processes, driven by HadGEM2-ES at RCP2.6, RCP4.5 and RCP8.5. The model projects an increase in burnt area in the future with climate change, particularly over Brazil as a result of hotter and (in some regions, such as the northeast) drier conditions, which is highest in the high emissions scenario RCP8.5. This supports the findings of Betts *et al*. (2015) in their study of future fire danger using the McArthur FFDI, and contradicts Moritz *et al*. (2012) who showed that burned area will decrease in tropical regions. In many ways this outcome might be expected, considering the same base model HadGEM2-ES is used in both this study and the Betts *et al*., (2015) study, although here I have used a more sophisticated fire model which includes vegetation interactions. It is also worth noting that HadGEM2-ES includes critical physiological processes that many of the models used in the Mortiz *et al*., (2012) study do not, which has been shown to have an important impact on the precipitation in Brazil (Betts *et al*., 2008; Chadwick *et al*., 2017), and additionally that HadGEM2-ES projections are more in line with CMIP5 model mean projections of precipitation for this region. As precipitation is a key determinant of fire danger in these model studies, it may be concluded that other CMIP5 models would also project an increase in burnt area in the future in line with this warming and drying signal over South America. However it should also be noted that these two studies do not use the same indicators of fire activity, with one using fire danger and the other using burned

area; they are therefore not directly comparable and this may be another cause of the differences in results.

In this study, the increase in burnt area and fire activity leads to significant forest loss across the east of the Amazon, with the model projecting a shift from tropical broadleaf forest to shrubs (RCP4.5) and grasses (RCP2.6 and RCP8.5). The RCP4.5 scenario assumes land-use changes in the form of reforestation, which lessens the impact of forest loss compared to the other scenarios which assume high deforestation for biofuels (RCP2.6) and agriculture (RCP8.5). With the projected forest loss there is a corresponding decrease in evapotranspiration and increase in albedo.

The pathways to warming have regional impacts as well. At global mean temperatures of 2.0°C above pre-industrial levels, the temperature is higher across more of Brazil in the RCP8.5 scenario than in the RCP4.5 and RCP2.6 scenario. The humidity at 1.5°C is lower in RCP4.5 than RCP2.6 and RCP8.5 across the North of Brazil. Over South America there is a strong projected warming and drying across the East of Brazil in the high emission scenario RCP8.5. These drivers lead to a higher burnt area in RCP2.6 and RCP8.5, and a greater vegetation loss when fire is included, resulting in a higher albedo, and lower ET across the east (RCP2.6) and northeast (RCP4.5 and RCP8.5). The results show an increasing vulnerability of the northeast and eastern regions of Brazil to drought, and the potential for the interaction of climate, land-use and fire to result in a shift from tropical forest vegetation to a mixture of shrubs and grasses in the future especially in higher emission scenarios. However the location of these transitions is not certain and will be dependent on how precipitation changes in the future, along with policies around deforestation and the use of fire.

Finally, I addressed a new future scenario considering the impact of limiting temperature rise to 1.5°C above pre-industrial levels on fire danger in Chapter 6. In 2015 the ‘Paris Agreement’ showed an international commitment to pursue efforts to keep global mean temperature rise to below 1.5°C above pre-industrial levels. For the first time this means temperature scenarios below 2°C need to be considered as part of a range of ‘realistic’ future possibilities. There is a strong argument that limiting temperature rise to below 2°C will not be possible without

some form of negative emissions which could include carbon dioxide removal (CDR) or solar radiation management (SRM), yet the impacts of implementing such methods of climate control are not yet fully understood. As a first assessment of how fire danger may change at 1.5°C compared to 2°C, I used the McArthur FFDI to investigate if limiting warming was beneficial and if so to what extent. I chose to use a fire index in this instance because it is a well-known method of assessing fire danger, widely used both in research and operationally, and allows the focus of the assessment to be purely on meteorological changes, which was the purpose of this study between 1.5°C and 2.0°C. The HadGEM2-ES model was used to enable climate interactions, using a theoretical SRM scenario where aerosol injection limits warming to 1.5°C. The results showed that generally 'high' fire danger is lower at 1.5°C compared to 2.0°C by up to 30 days per year on average. However in two regions, parts of central USA and NE Asia experience higher fire danger with up to 31 more days of 'high' fire danger on average, resulting from a lack of temperature reduction combined with drier conditions in the SRM scenario. The results indicate that further research into temperature limitation is useful and necessary, but while there may be benefits in climate mitigation on this scale, the method of mitigation is equally important and needs to be fully investigated. While other studies have used the McArthur FFDI to assess future fire danger, this is the first time fire danger at 1.5°C and 2.0°C has been assessed.

In conclusion, this PhD has contributed to the scientific understanding of fire-vegetation-climate interactions by addressing new research questions around future warming scenarios, and the 2015-16 El Niño event. In addition, JULES now has the capability to represent fire as a new and distinct disturbance process which is important for the accurate simulation of vegetation distribution. This new capability is available in the trunk of the community model, and will be available for scientists across the world to continue to use for new experiments and for further model development.

Although fire danger is decreasing globally, there is regional variation and in some cases it may increase in the future through a combination of climate change and land-use change, with the highest impacts in high emission and high land-use scenarios such as RCP8.5. Keeping global mean temperature to 1.5°C above pre-industrial levels may help reduce fire danger, but ways of reaching this

goal are important and may have negative impacts in some areas. The JULES-INFERNO model projects large increases in drought and fire in the Brazil region in South America in future high-emission climate scenarios such as RCP8.5, based on the ESM HadGEM2-ES. This has important implications for its ability to continue to act as a sink of carbon, especially in years of extreme drought and high temperatures such as El Niño events. So while deforestation rates have reduced significantly since 2004, and many models no longer show dramatic dieback scenarios as a result of climate change alone, we cannot assume that the Amazon is now 'safe' from future changes. Research must continue to assess the impacts across a complete range of Earth system processes under climate and land-use change scenarios on this important region, both for our understanding today and to ensure its continued existence in the future.

7.2 Limitations and future work

This PhD has focused on the first coupling of the fire model INFERNO to vegetation mortality within the land surface model JULES. The coupling and tuning developments as outlined in Chapter 3 have resulted in the model successfully simulating vegetation cover within an uncertainty range compared to ESA CCI observations. However the analysis showed that trees were slower to respond after disturbance than grasses and shrubs, resulting in lower tree fractions and lower vegetation carbon. This is likely to be due in part to slow regrowth times within TRIFFID which is a known issue (see Appendix 3), and one which has been prioritised for development by the JULES modelling community, and also by a project focused on developing a new vegetation dynamics scheme called RED (Robust Ecosystem Demography). The aim of RED is to introduce a new growth and morality scheme which is mass-time dependent, allowing for different sizes of vegetation and smaller trees to be sustained (Moore *et al*., 2018). Currently TRIFFID requires enough carbon for a full-height mature tree to be sustained before a forest can develop. If the new RED scheme is successful in replacing TRIFFID within JULES in the future, this will likely have a positive impact on how fire disturbance effects tree cover.

Other possible causes of lower vegetation carbon are due to burnt area being too high, for example there is currently no land-use suppression in managed agricultural areas, and/or that the assumed mortality rate is too high. Here I

assumed a direct conversion of the area burnt into vegetation mortality, where in reality this will likely vary by biome, species of vegetation (i.e. bark thickness and fire resilience), fire intensity and duration of the fire (Lasslop *et al*., 2018). As INFERNO is a simple fire model, many of these parameters are not available within INFERNO or JULES, but some method of scaling burned area by PFT to reduce the impact of fire on trees compared to grasses (e.g. Sitch *et al*., 2003) is likely to be beneficial to tree cover and to vegetation carbon, and optimising this function for JULES-INFERNO should be a priority next step for the further development and improvement of the model.

The benefit of using models is that we can simplify a large range of complex interactions into something that is manageable, for example a small range of plant functional types, however we need to be able to strike the right balance between over-simplification and over-complication, both having their drawbacks. While we probably cannot or would not want to represent every single vegetation type that exists in the real world, an obvious next step for this work would be to develop the fire-vegetation interaction with 9 PFTs within JULES, and to conduct further research around how the mortality rate and combustion completeness should be represented within each PFT. Further work after that might focus on the representation of land-use, including suppression of fire in managed land, and potentially a new way of representing ignition from deforested areas rather than based on population which would be of particular importance in areas like the Amazon.

Work is now ongoing in other projects to couple INFERNO to atmospheric chemistry, which is an important step in developing a fully interactive biogeochemistry model including modelled lighting input and interactive emissions. Future work to combine the emissions coupling with the biogeophysical interactions developed in this PhD will enable us to implement INFERNO within a full Earth System Model such as UKESM further along the line.

This PhD has focused primarily on changes to fire as a result of climate change, and the interaction of these changes with historical and projected land-use change. Early simulations with the coupled model showed that the model was not sensitive to ignitions, and therefore for the purposes of the development of the

model with vegetation mortality the focus was on fire-vegetation interactions with constant ignitions. For future simulations as well the focus has been on a changing climate and land-use across Brazil and South America, and to isolate these impacts further uncertainty around population and lightning were not included. Further work could assess how projected changes population and lightning might affect ignitions in the future and if this has any significant impact on the simulation of burnt area. Future work could also evaluate other significant drought events outside of the 2015/16 El Niño assessed here, such as the 2005 and 2010 droughts which impacted Brazil.

Although the FFDI is a useful indicator of how fire danger may change in the future at 1.5°C compared to 2.0°C, it lacks vegetation interactions, fuel input and ignitions which are now available within JULES-INFERNO. To develop this work further the SRM experiment in Chapter 6 could be repeated to include these factors. The two regions showing higher fire danger at 1.5°C comprise crop and grass lands, which in the current model set up are treated as the same and allowed to burn. If croplands were excluded from burning this may have an impact on the results and reduce burned area in these areas.

Finally another known issue with the INFERNO model is around the lack of representation of peat burning. As yet there is no representation of peat in the JULES model, yet this is an important soil type for the spread of fire and for the resultant emissions from its burning; as the prolific Indonesian fires of 1997-98 and the more recent UK moorland fires in summer 2018 have shown, these smouldering underground fires are difficult to manage and result in extensive damage. Further work could be to develop peat within JULES and couple this to INFERNO to improve the representation of these fire types.

7.3 Wider implications of this work

It was show in the last IPCC report at AR5 that models are still at the early stages of development with processes such as fire and land-use, and in particular few Earth System Models are capable of representing these interactions fully. The development of capability for biogeophysical interactions here within a land surface model lays the foundations for these processes to be implemented within a fully coupled ESM in the future. This will enable improved understanding of how

the Earth system and carbon cycle responds today to carbon emissions and uptake, and will help improve projections of future changes. There is currently a large uncertainty around exactly how much carbon is stored in the Earth system through atmosphere, land and ocean sinks, and by improving our ability to model more processes we can improve our understanding of how carbon has been absorbed historically and how this may change in the future, as well as supporting land and fire management practises.

We are not yet sure how forests will respond in the future to a changing climate, increases in CO_2, how precipitation and nutrient availability will change, and how these factors interact with fire and land-use. Will forests such as the Amazon continue to take up carbon and act as an important global sink with CO_2 fertilisation stimulating additional growth, or will factors such as increasing fire, drought, dry season length, deforestation and nutrient limitation act to increase death and respiration, tipping the forest into a source of carbon to become a positive feedback of climate warming?

An improved understanding of the Earth system now and in the future means we can better inform and support the development of climate policies around mitigation and adaptation to a changing climate. Ultimately this ensures our society can maintain resilience to future challenges, and enables us to take action against further change, ensuring the future survival and diversity of our global ecosystems.

Appendices

Appendix 1: Fire and drought indices

The Met Office Fire Severity Index (FSI) is an assessment of how severe a fire could become if started, based on information such as wind speed, temperature, time of year and rainfall (http://www.metoffice.gov.uk/public/weather/fire-severity-index/#?tab=map). This is measured on a scale of 1-5 (1 = low severity, 5 = exceptional fire severity). More common, is a fire danger index which gives an indication on the risk of a fire starting in a certain location, as outlined in section 1.4.

Drought indices are used as sub-models in the McArthur Forest Fire Danger Index (FFDI) and the Canadian Fire Weather Index (FWI) to give more context to the calculations with the aim of making them more realistic to current conditions. The examples below for some of these drought indices are based on information from Mantzavelas *et al*. (2006). The FWI includes three drought induces as part of the risk calculation:

Fine Fuel Moisture Code (FFMC)

Represents the moisture level in the top of litter layer, 1.2cm deep, which gives an indication of the ease of ignition from 0 (high moisture, low flammability) to 100 (dry fuel, high flammability). It is calculated from rainfall, relative humidity, wind speed and temperature.

Duff Moisture Code (DMC)

Represents the moisture level in the deep litter layer, 7cm deep. Higher values = dry litter and high fire danger/spread. It is calculated from rainfall, relative humidity and temperature.

Drought Code (DC)

Represents the moisture level in the deep compact organic matter layer, 18cm below the DMC layer. It gives an indication of the smouldering potential and of seasonal drought. It is calculated from rainfall and temperature data.

The FFDI uses the Keetch-Byram drought index as part of the risk calculation:

Keetch-Byram drought index (KBDI)

Represents a cumulative estimate of moisture deficiency in the upper soil and surface litter layers, specifically designed for use in fire-risk calculations. It is calculated from maximum daily temperature, total daily precipitation and average annual precipitation. It can be calculated in a number of ways; as outlined by Noble *et al*. (1980) and shown in section 1.4 of this thesis, or alternatively as outlined by Mantzavelas *et al*. (2006) as follows:

$$\mathbf{KBDI_t = KBDI_{t-1} + DF} \text{ (Drought factor)}$$

while:

$$\mathbf{DF = \frac{[800-KBDI_{t-1}]\,[0.968\,\exp(0.0875T+1.5552)-8.30]\,dt}{1 + 10.88\,\exp(-0.001736R)} \times 10^{-3}}$$

Where:

T = daily maximum temperature (^{o}C)
R = mean annual rainfall (mm)
Dt = is the time increment (days)
$KBDI_{t-1}$ = Keetch-Byram Drought index for time t-1

The KBDI can also be used as a stand-alone index to measure the effects of seasonal drought on fire potential.

Table A1.1: Description of moisture conditions and fire potential for relative KBDI

KBDI range	General description	Forest fire potential
0-150	Upper soil and surface litter are wet	Fire potential is minimal
150-300	Upper soil and surface litter are moist and on not contribute to fire intensity	Fire behaviour is predictable
300-500	Upper soil and surface litter are dry and may contribute to fire intensity	Fire behaviour is somewhat predictable
500-700	Upper soil and surface litter are very dry. Surface litter and organic soil material contribute to fire intensity	Fire suppression is a significant undertaking
700-800	Upper soil and surface litter are extremely dry. Live understory vegetation burns actively and contributes to fire potential	Fire behaviour is unpredictable

Sharples Fuel Moisture Index (FMI) (Sharples *et al*., 2009)

The FMI gives an estimate of moisture content of eucalypt litter which has been used as an input to measuring fire potential in southeast Australia. Compared against the more complex FFDI, it gives a remarkably accurate projection for fire danger in this region. The simple index uses the following calculation:

$$\boldsymbol{FMI = 10 - 0.25(T - H)}$$

Where:
T = Temperature (°C)
H = Relative humidity (%)

This can be combined with wind speed (U) and drought factor (D) to give a fire danger index that incorporates the effects of variable fuel availability:

$$\boldsymbol{F_D = D\frac{\max(U_0, U)}{FMI}}$$

Appendix 2: Emission scenarios

The first emission scenarios were released in 1990 ('SA90') which were used in the Global Climate Models (GCMs) for the First Assessment Report (AR1). The following table shows the development of scenarios over time with each successive assessment report.

Table A2.1: History of emission scenarios
(Source: https://www.sei-international.org/mediamanager/documents/A-guide-to-RCPs.pdf)

Year	Name	Used in
1990	SA90	First Assessment Report
1992	IS92	Second Assessment Report
2000	SRES - Special Report on Emissions and Scenarios	Third and Fourth Assessment Report
2009	RCP – Representative Concentration Pathways	Fifth Assessment Report

The SRES scenarios, released in 2000 (Nakicenovic and Swart, 2000), consist of 40 different future pathways, spanning the wide range of uncertainty in future emissions, demographic, social, economic, and technological changes (Figure A2.1).

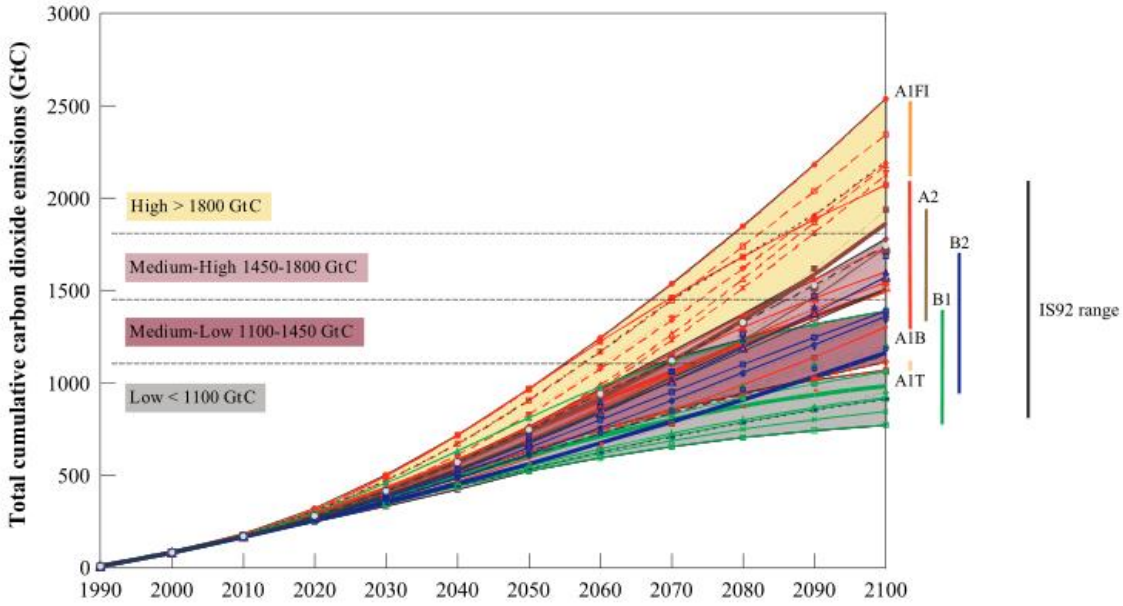

Figure A2.1: SRES scenarios of emissions over time.

Source: ***https://www.ipcc.ch/pdf/special-reports/spm/sres-en.pdf***

However the SRES scenarios avoided including any mitigation policy options for reducing greenhouse gases in the future, so in 2005 the IPCC updated these scenarios and developed what we use in climate modelling today, the Representative Concentration Pathways (RCPs). The RCPs are a consistent set of projections that only use the components of radiative forcing and do not include the direct impacts of land-use (albedo) or the forcing of mineral dust. They have been generated from four Integrated Assessment Models (IAMs), and selected from over 300 scenarios of future GHG emissions (Figure A2.2); the data provided for the scenarios is extensive, and has undergone several procedures to assure quality and consistency, to harmonize regional base year emissions to recent inventories, and to downscale the projections to 0.5 x 0.5 degree.

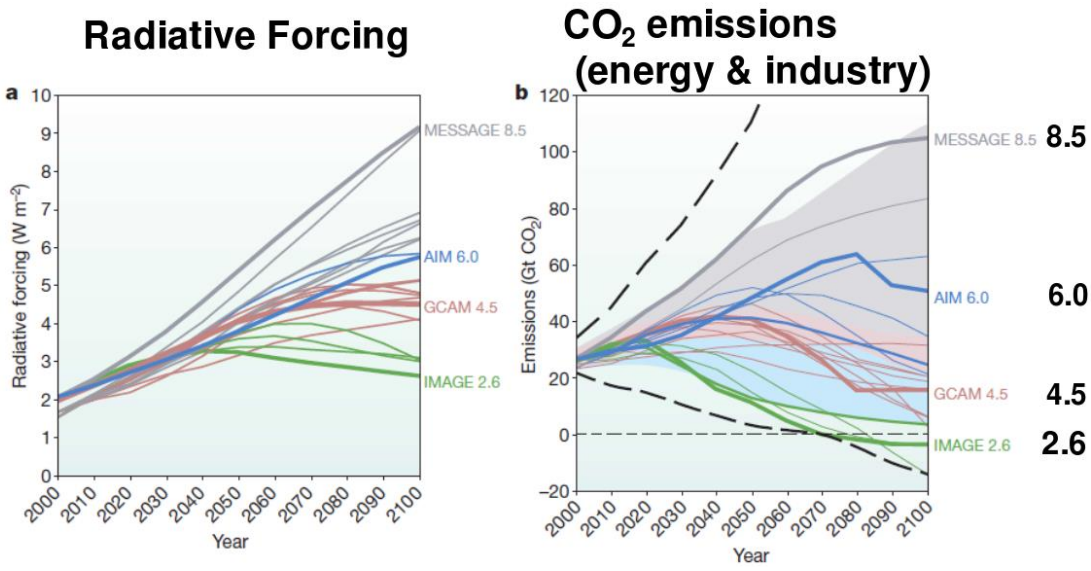

Figure A2.2: RCP radiative forcing and CO_2 emissions
Source: van Ypersele (2010)

The RCP scenarios are space and time dependent trajectories for concentrations of the full suite of GHGs and chemically active gases, as well as land -use and land cover (Moss *et al*., 2010). The scenarios are developed around the assumption that increased population levels do not necessarily imply increased fossil fuel consumption as renewable sources could be introduced, so rather than prescribing economic development, as was the case in the SRES scenarios, it is possible with the RCPs to pick a *pathway* that is compatible with 2°C of warming. Another key difference is that the RCPs are spatially explicit and provide information on a global grid at a resolution of approximately 60 kilometres. This

gives the spatial and temporal information about the location of various emissions and land-use changes. This is an important improvement as the location of some emissions affects their warming potential. The RCP scenarios are defined by their total radiative forcing pathway and level by the year 2100, where radiative forcing refers to the total energy in the system resulting from GHG concentrations and other forcing agents from all sources, measured in Watts per square meter[33], i.e. from 2.6 W/m^2 (RCP2.6) to 8.5 W/m^2 (RCP8.5). They are based primarily on atmospheric concentrations of GHGs, which can then be used in coupled carbon-cycle models to calculate emission levels associated with each level of radiative forcing. For each scenario, the level of CO_2 varies, along with levels of aerosols, and land-use change. Below is a detailed overview of the assumptions that make up each of the four RCP scenarios (from Settele *et al*., 2014).

[33] IPCC RCP overview: http://sedac.ipcc-data.org/ddc/ar5_scenario_process/RCPs.html

Table A2.2: Detailed overview of the assumptions that make up each of the four RCP scenarios (from Settele *et al.*, 2014)

RCP	Model and references	Key assumptions/drivers	Land use/cover outcomes
8.5	MESSAGE; Riahi et al. (2007)	• No climate change mitigation actions; radiative forcing still rising at 2100. • Strong increase in agricultural resource use driven by the increasing population (rises to 12 billion people by 2100). • Yield improvements and intensification assumed to account for most of production increases.	• Increase in cultivated land by about 305 million ha from 2000 to 2100. • Forest cover declines by 450 million ha from 2000 to 2100. • Arable land use in developed countries slightly decreased — all of the net increases occur in developing countries.
6.0	AIM; Fujino et al. (2006), Hijioka et al. (2008)	• Mitigation actions taken late in the century to stabilize radiative forcing at 6 W m^{-2} after 2100. • Population growth and economic growth. • Increasing food demand drives cropland expansion .	• Urban land use increases. • Cropland area expands. • Grassland area declines. • Total forested area extent remains constant.
4.5	GCAM; Smith and Wigley (2006), Wise et al. (2009)	• Mitigation stabilizes radiative forcing at 4.5 W m^{-2} before 2100. • Assumes that global greenhouse gas emissions prices are invoked to limit emissions and therefore radiative forcing. Emissions pricing assumes all carbon emissions are charged an equal penalty price, so reductions in land use change carbon emissions available as mitigation. • Food demand is met through crop yield improvements, dietary shifts, production efficiency, and international trade.	• Preservation of large stocks of terrestrial carbon in forests. • Overall expansion in forested area. • Agricultural land declines slightly due to afforestation.
2.6	IMAGE; van Vuuren et al. (2006), van Vuuren et al. (2007)	• Overall trends in land use and land cover are determined mainly by demand, trade, and production of agricultural products and bioenergy. • Expansion of croplands largely due to bioenergy production. • Production of animal products is met through shift from extensive to more intensive animal husbandry.	• Much agriculture relocates from high-income to low-income regions. • Increase in bioenergy production, new area for bioenergy crops near current agricultural areas. • Pasture largely constant.

Appendix 3: Regrowth in TRIFFID

Table A3.1. Summary of terms used in Chapter 3

Variable	Symbol	Unit	Source of variable
Combustion completeness	μ		Parameter
Competition term	c_{ij}		TRIFFID
Crop indicator	a_i		Parameter
Disturbed fraction	α	Fraction of land surface	Input Map
Fire disturbance	β_i	yr^{-1}	INFERNO
Fraction of NPP allocated to PFT area expansion	λ		Parameter
Fractional coverage	v	Fraction of land surface	TRIFFID
Large scale disturbance	γ_v	yr^{-1}	Parameter
Litterfall rate without fire or land-use change	Λ_c	kg C m^{-2} yr^{-1}	TRIFFID
Local litterfall rate	Λ_l	kg C m^{-2} yr^{-1}	TRIFFID
NPP per unit of vegetated area	Π	kg C m^{-2} yr^{-1}	JULES
PFT indices (i refers to dominant, j refers to sub-dominant vegetation types)	i, j		
Soil carbon in soil pool k	C_k	kg C m^{-2}	TRIFFID
Soil flux	f_s	kg C m^{-2} yr^{-1}	INFERNO
Vegetation carbon density	Cv	kg C m^{-2}	TRIFFID
Vegetation carbon loss due to fire	Λ_{Fire}	kg C m^{-2} yr^{-1}	TRIFFID
Vegetation carbon loss due to land-use change	Λ_{LUC}	kg C m^{-2} yr^{-1}	TRIFFID
Vegetation carbon loss due to litter, fire and land-use change	Λ_{CvLoss}	kg C m^{-2} yr^{-1}	TRIFFID

The following table had been reproduced from an unpublished study by Rebecca Oliver and Chris Jones assessing the recovery timescales of vegetation in JULES following the effects of land disturbance (agricultural abandonment). Three sites were used in the study: Harvard, USA, temperate forest; Hyytiala, Finland, boreal forest; and Manaus, Brazil, tropical forest. Following a period of spin-up, each simulation was run for approximately 1000 years, allowing for a 50 year period of disturbance, followed by 950 years of recovery from disturbance.

Table A3.2. Vegetation recovery in JULES.
Comparison of regional values associated with changes in carbon in vegetation and soil due to clearing of natural ecosystems for croplands from Houghton and Hackler (2001) with values simulated by JULES model with a 50 year period of imposed clearing for agriculture followed by abandonment. Values from Houghton and Hackler (2001) can be found at http://cdiac.ornl.gov/epubs/ndp/ndp050/ndp050appC.html
***Temperate deciduous forest (North America, China, Europe, Pacific Developed Region and North Africa and the Middle East clearing response curve from Houghton and Hackler (2001)).**
**** Boreal forest (North America, China, Europe, Pacific Developed Region and North Africa and the Middle East clearing response curve from Houghton and Hackler (2001)).**
***** Tropical equatorial forest (South and Central America clearing response curve).**
Reproduced with permission from R. Oliver and C. Jones, from their Table 2.

	Harvard*		Hyytiala**		Manaus***	
	JULES	Houghton	JULES	Houghton	JULES	Houghton
C in undisturbed veg. (Mg C/ha)	95.71	135.00	84.30	90.00	61.59	200.00
C in crops (Mg C/ha)	2.22	5.00	2.07	5.00	4.04	5.00
C in undisturbed soil (Mg C/ha)	161.00	134.00	233.69	206.00	53.16	98.00
Minimum soil C (Mg C/ha)	148.75	101.00	216.77	155.00	45.97	74.00
Recovery time vegetation (years)	749	50	950	50	+954	40
Time to min. soil C (years)	5	30	6	50	2	20
Recovery time soil from min. (years)	+1039	40	+994	35	+1002	40

Appendix 4: El Niño

Annual cycle of burned area and precipitation, 2015

JULES burned area **GFED burned area** **JULES precipitation**

January

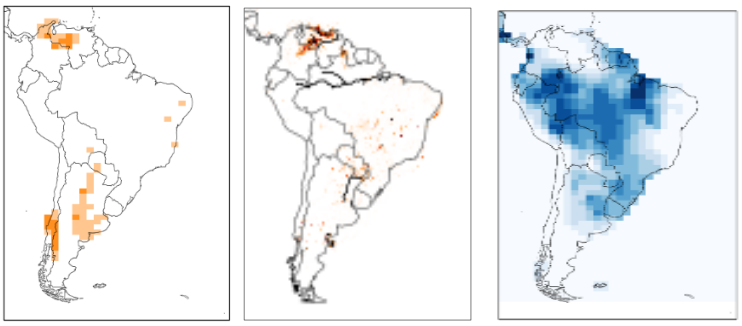

February

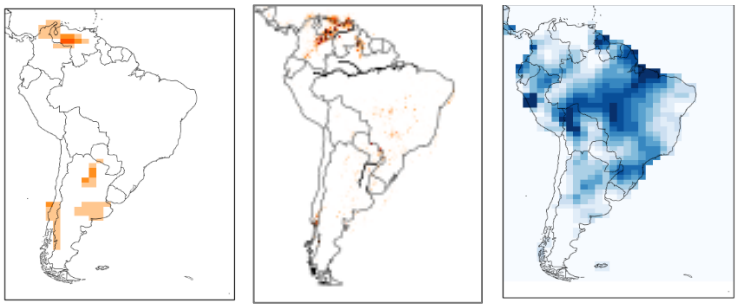

March

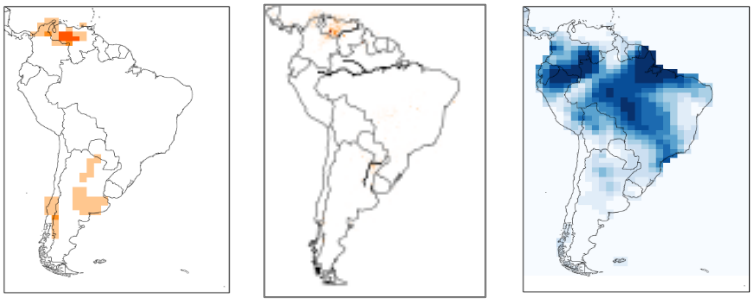

April

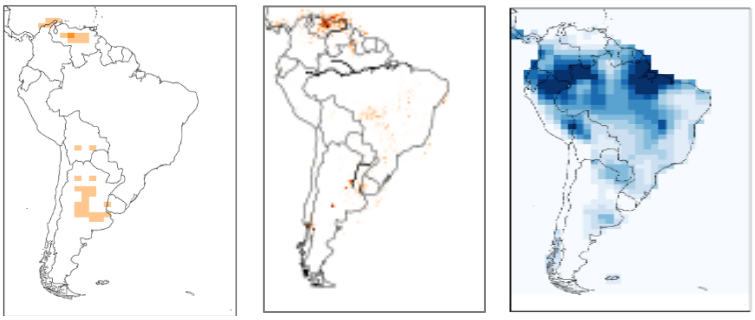

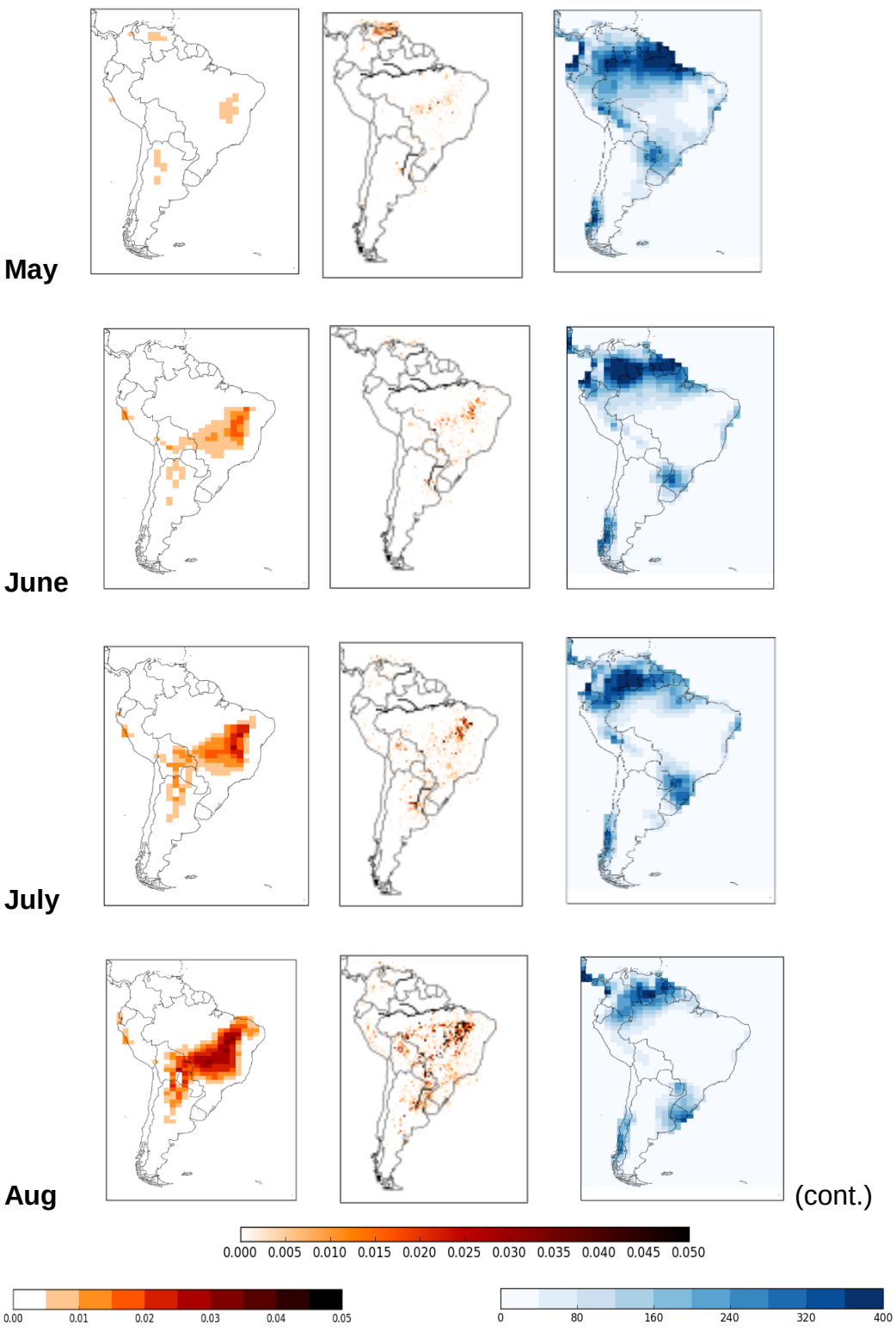

Figure A4.1: Modelled and observed burned area by month, with rainfall data
Left column: Monthly total burned area as modelled by JULES-INFERNO (fraction of gridbox). Centre column: Monthly total burned area from GFED observations (fraction of gridbox). Right column: Monthly total precipitation modelled by JULES (mm), all for South America

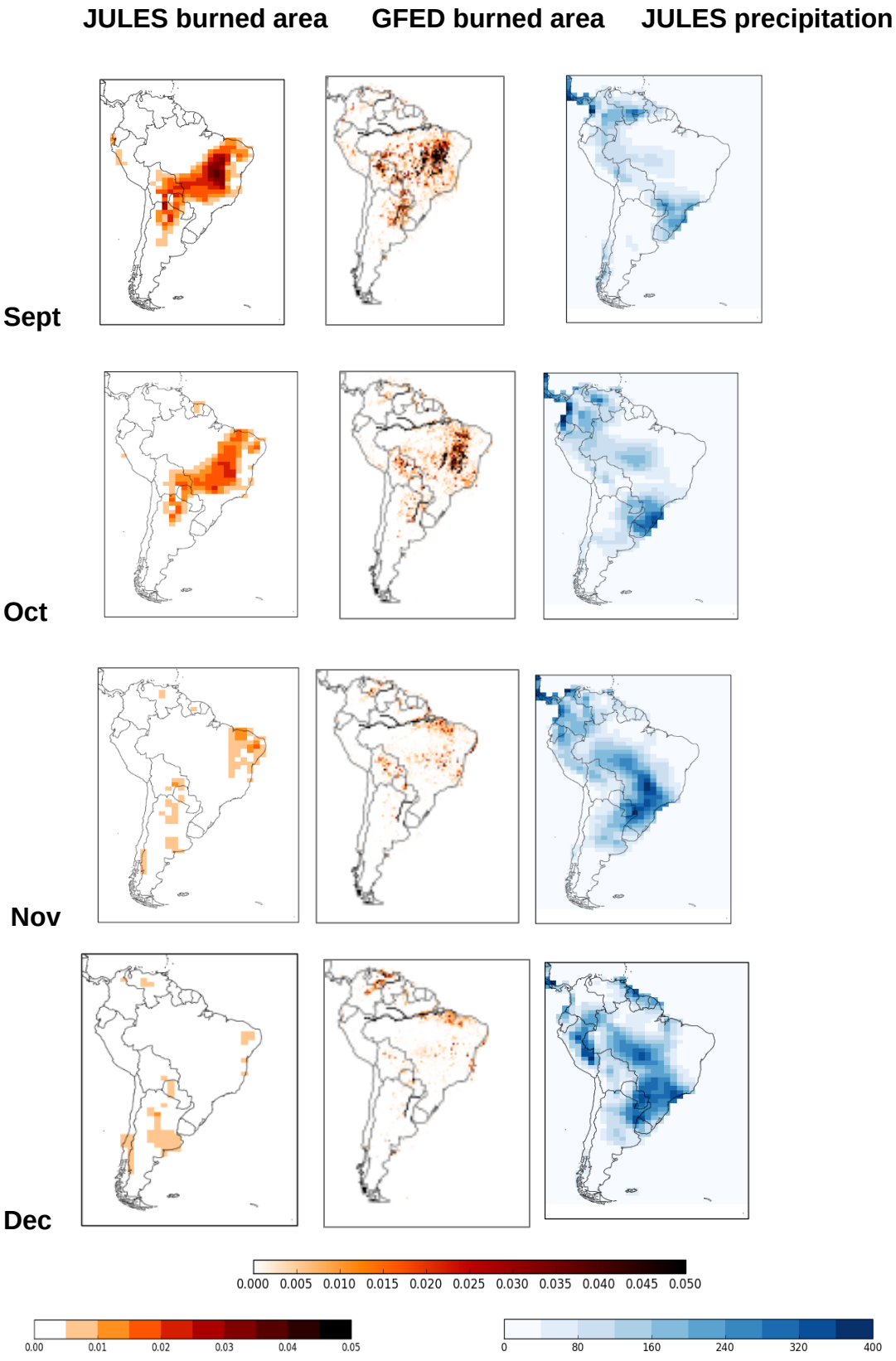

Figure A4.1: Modelled and observed burned area by month, with rainfall data
Left column: Monthly total burned area as modelled by JULES-INFERNO (fraction of gridbox). Centre column: Monthly total burned area from GFED observations (fraction of gridbox). Right column: Monthly total precipitation modelled by JULES (mm), all for South America

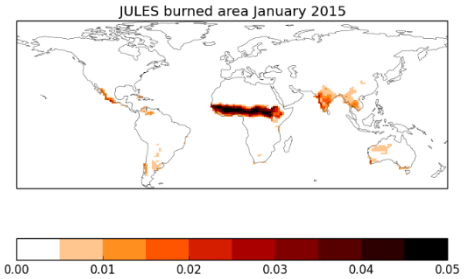
JULES burned area January 2015
0.00 0.01 0.02 0.03 0.04 0.05

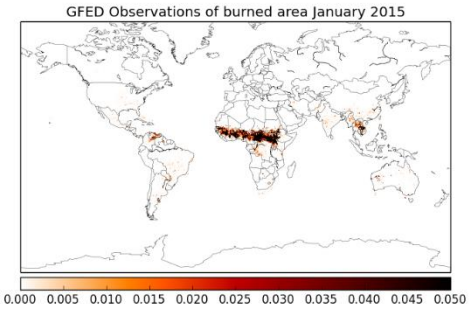
GFED Observations of burned area January 2015
0.000 0.005 0.010 0.015 0.020 0.025 0.030 0.035 0.040 0.045 0.050

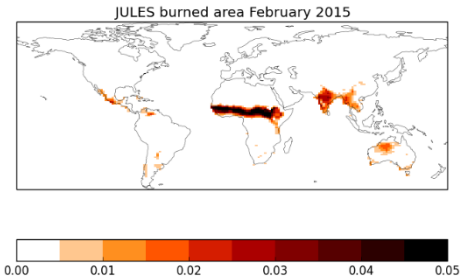
JULES burned area February 2015
0.00 0.01 0.02 0.03 0.04 0.05

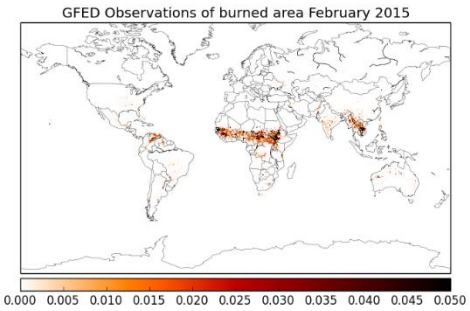
GFED Observations of burned area February 2015
0.000 0.005 0.010 0.015 0.020 0.025 0.030 0.035 0.040 0.045 0.050

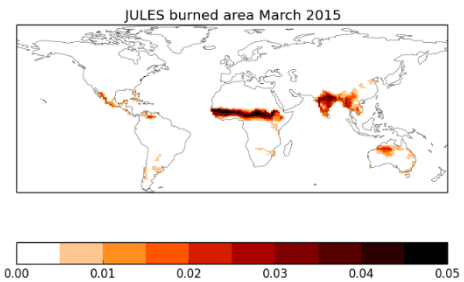
JULES burned area March 2015
0.00 0.01 0.02 0.03 0.04 0.05

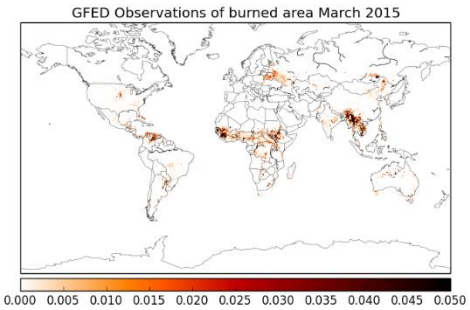
GFED Observations of burned area March 2015
0.000 0.005 0.010 0.015 0.020 0.025 0.030 0.035 0.040 0.045 0.050

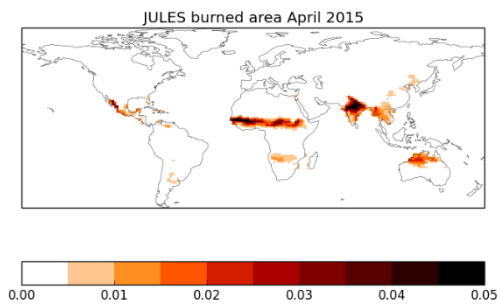
JULES burned area April 2015
0.00 0.01 0.02 0.03 0.04 0.05

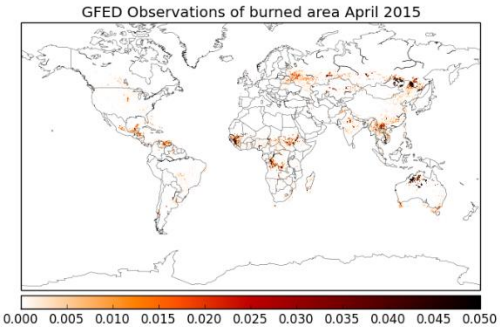
GFED Observations of burned area April 2015
0.000 0.005 0.010 0.015 0.020 0.025 0.030 0.035 0.040 0.045 0.050

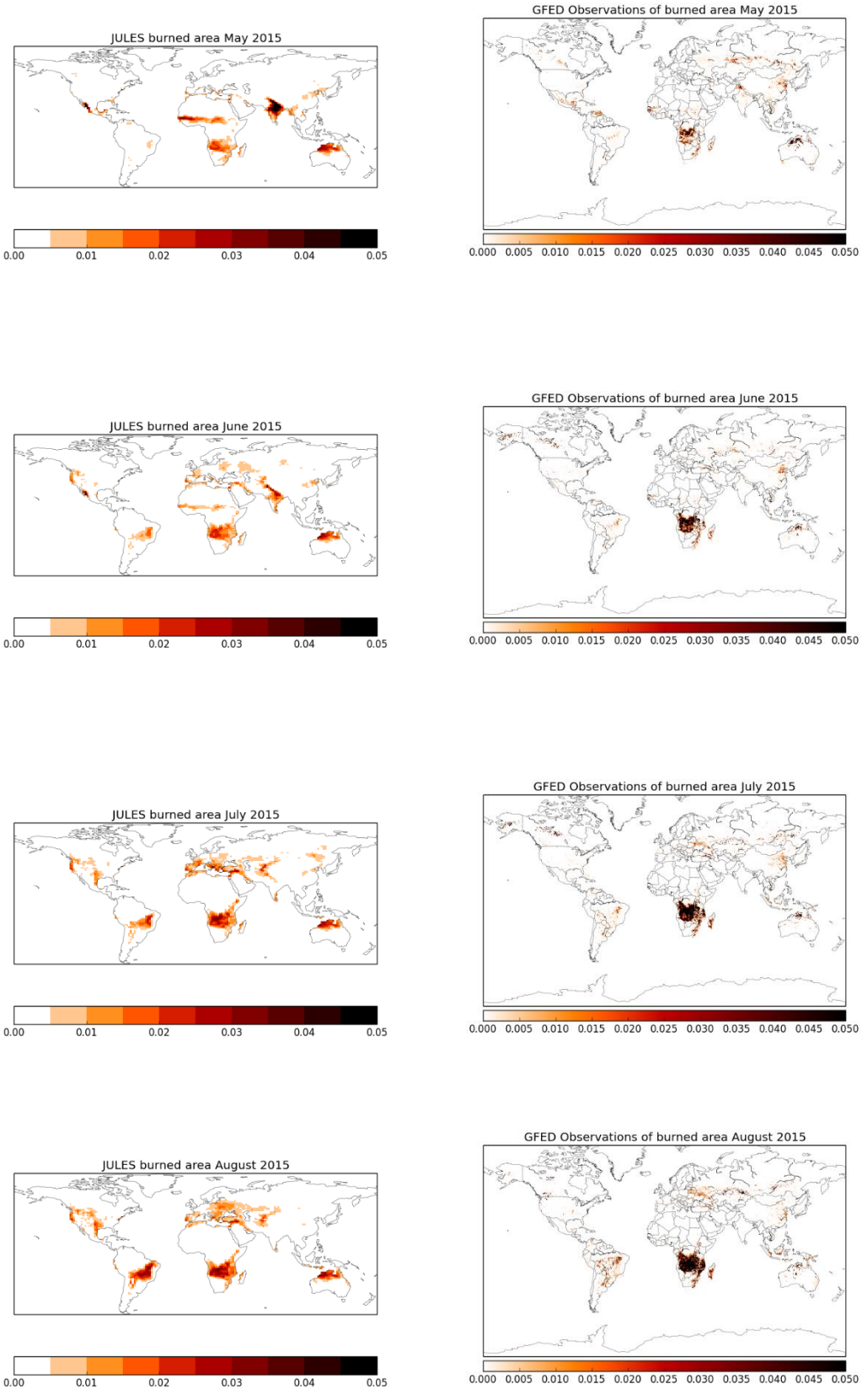

(cont.)
Figure A4.2: Global burned area by month
Left column: Monthly total burned area as modelled by JULES-INFERNO (fraction of gridbox). Right column: Monthly total burned area from GFED observations (fraction of gridbox).

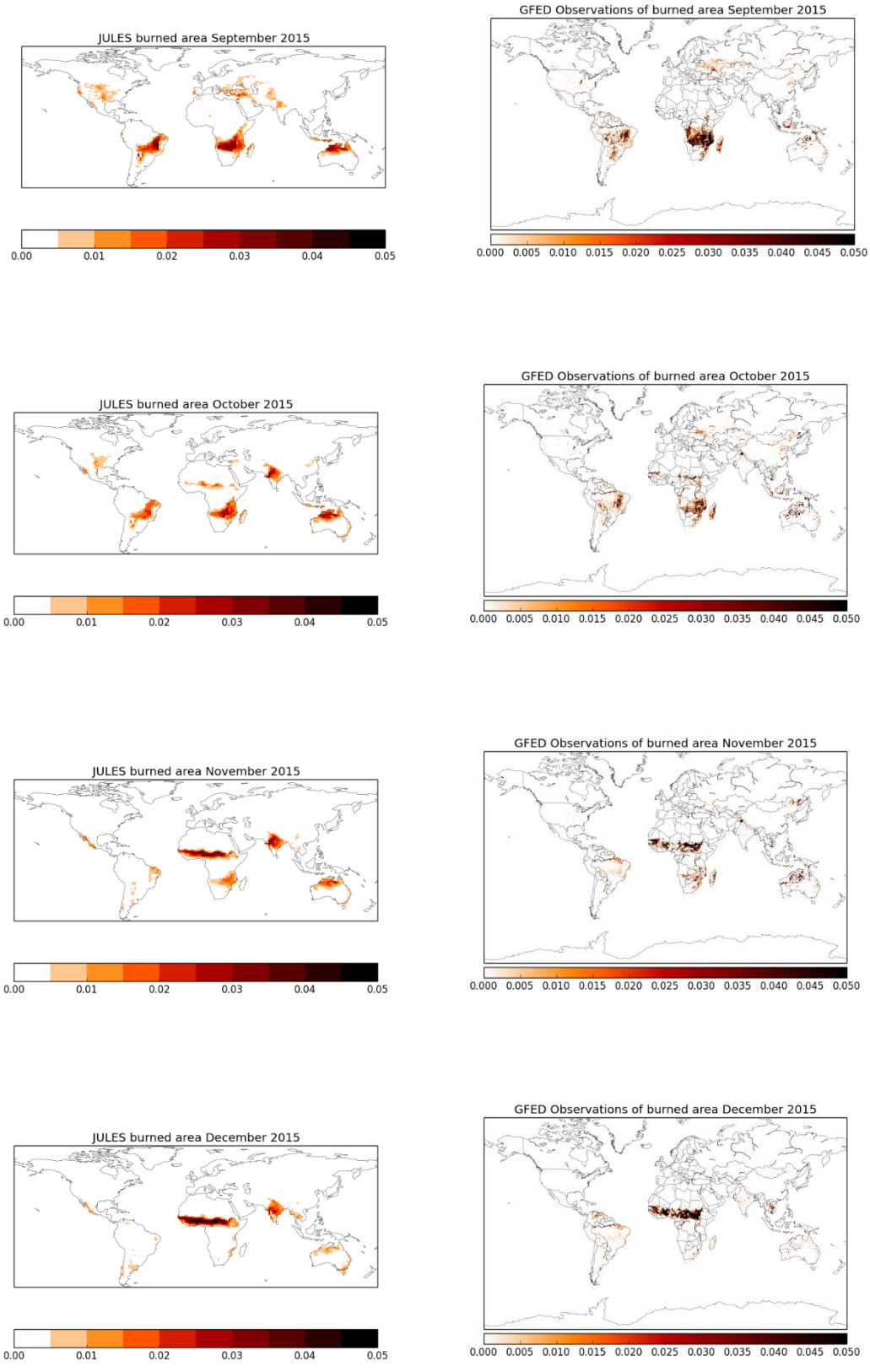

Figure A4.2: Global burned area by month
Left column: Monthly total burned area as modelled by JULES-INFERNO (fraction of gridbox). Right column: Monthly total burned area from GFED observations (fraction of gridbox).

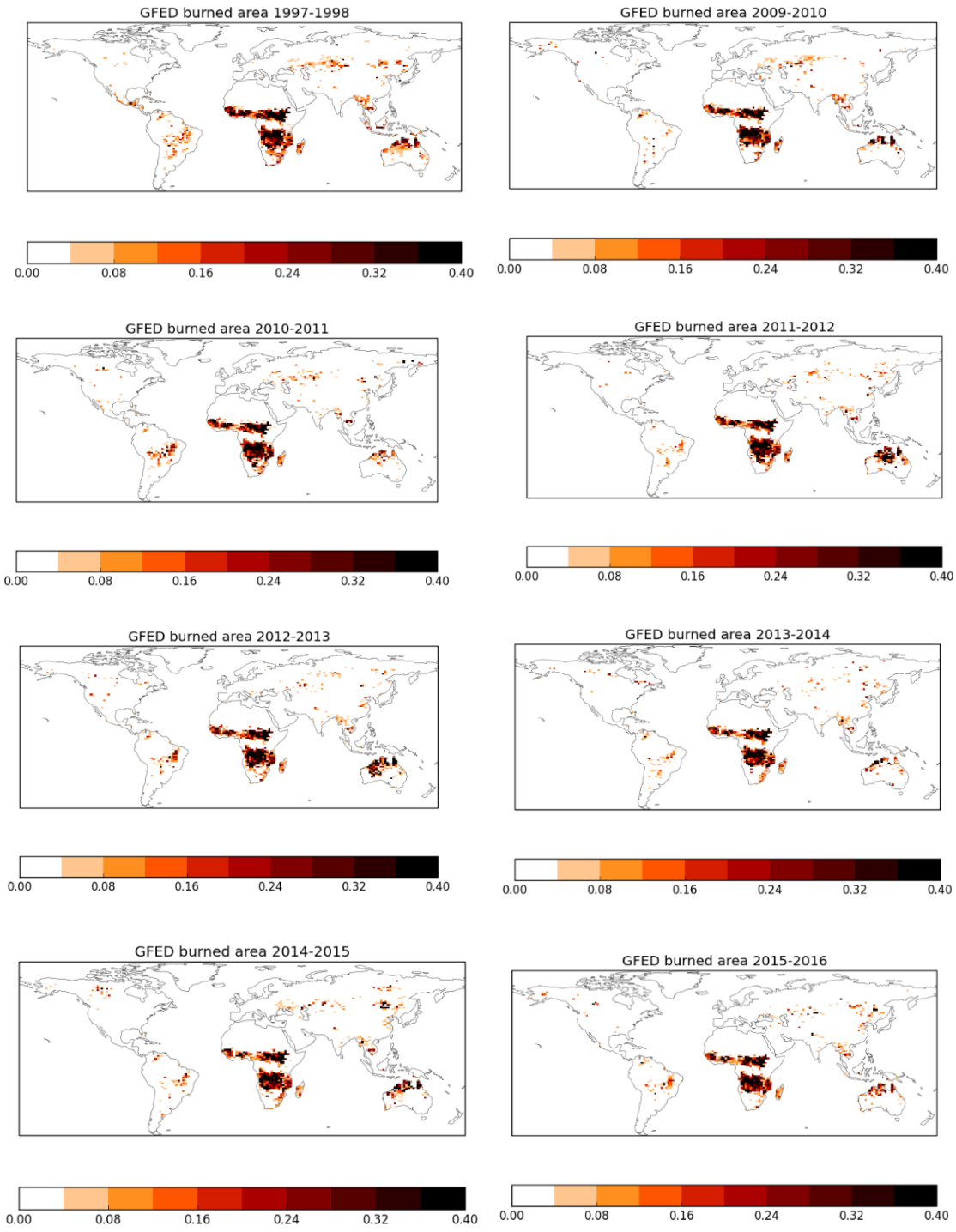

Figure A4.3: GFED Global burned area by year
GFED total burned area (fraction) from July to June, 2009 – 2016 and including 1997-1998

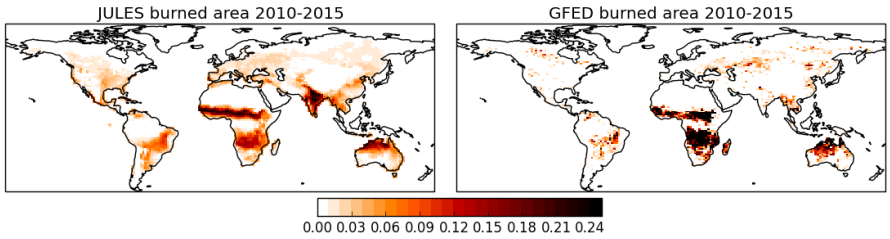

Figure A4.4: Modelled and observed global burned area
Mean annual burned area 2010-2015 (fraciton of gridbox), as modelled by JULES-INFERNO (left) and GFED4.1s observations (right), showing low fractions of burnt area

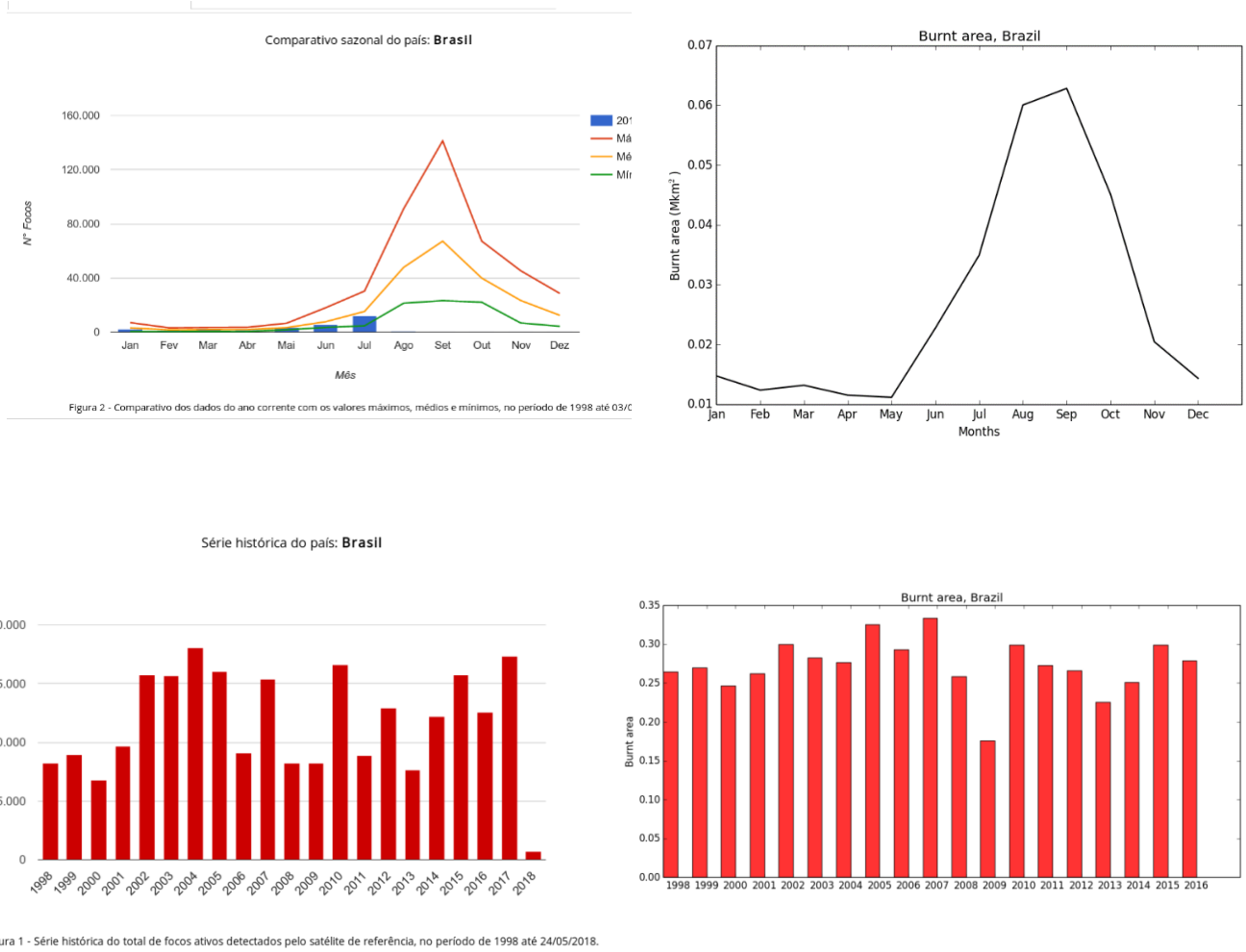

Figure A4.5: JULES burned area and INPE data
Top left: Number of fire counts in Brazil from the maximum, average and minimum values by month, in the period from 1998 to 03/08/2018 (blue line shows current year 2018). Top right: burnt area as projected by JULES by month for 2015. Bottom left: historical series of the total number of active fires detected by satellite, in the period from 1998 to 24/05/2018. Bottom right: burnt area time series as projected JULES-INFERNO, 1998-2016. INPE data is avilable from their fire moniroting programme website[34]

[34] INPE fire data: http://www.inpe.br/queimadas/portal

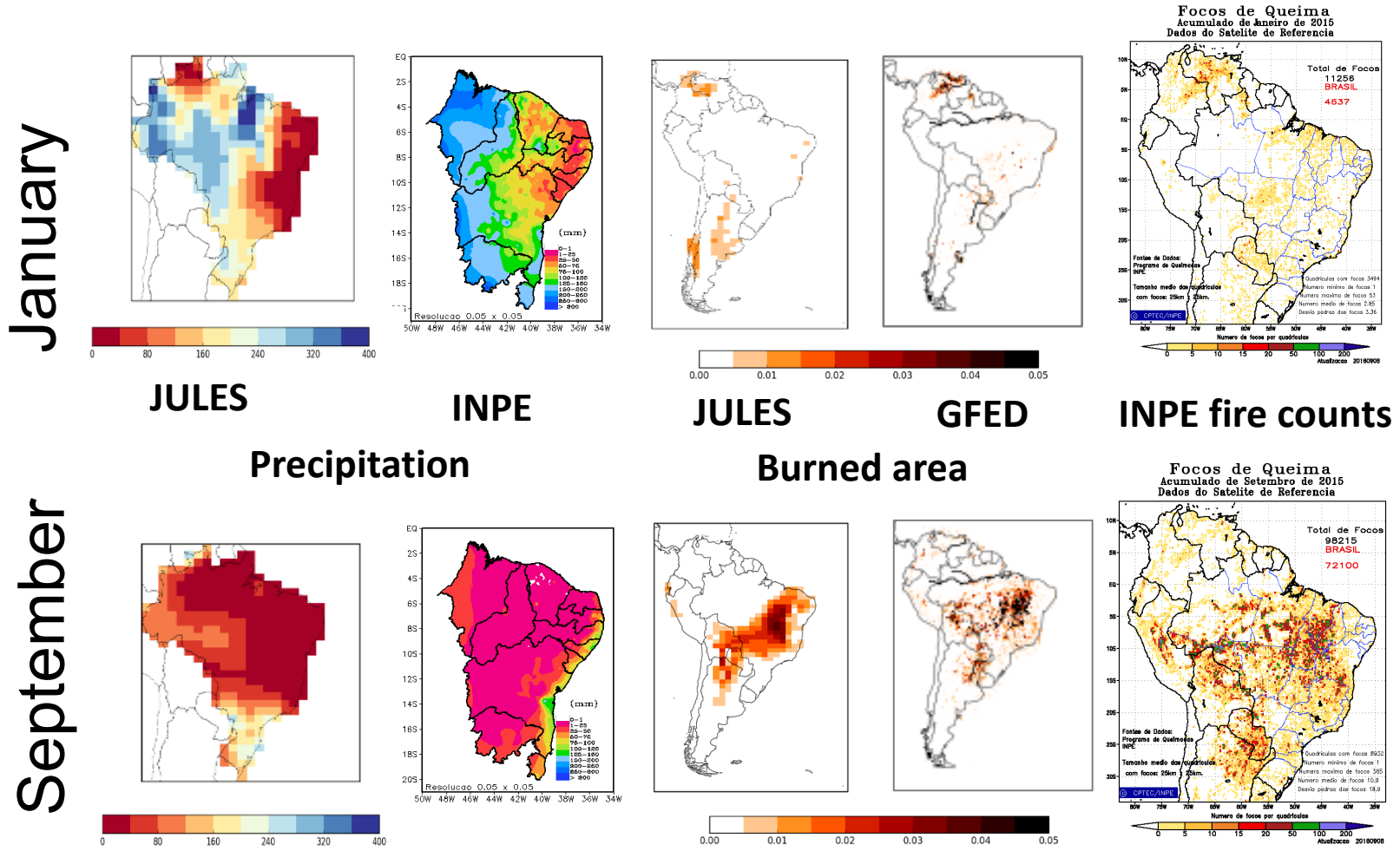

Figure A4.6: Modelled and observed burned area and precipitation
Top row shows January, bottom row shows September data. Left to right plots show: precipitation from JULES (mm), precipitation from INPE (mm), burned area from JULES (gridbox fraction), GFED (gridbox fraction), fire counts from INPE[28]. All for year 2015

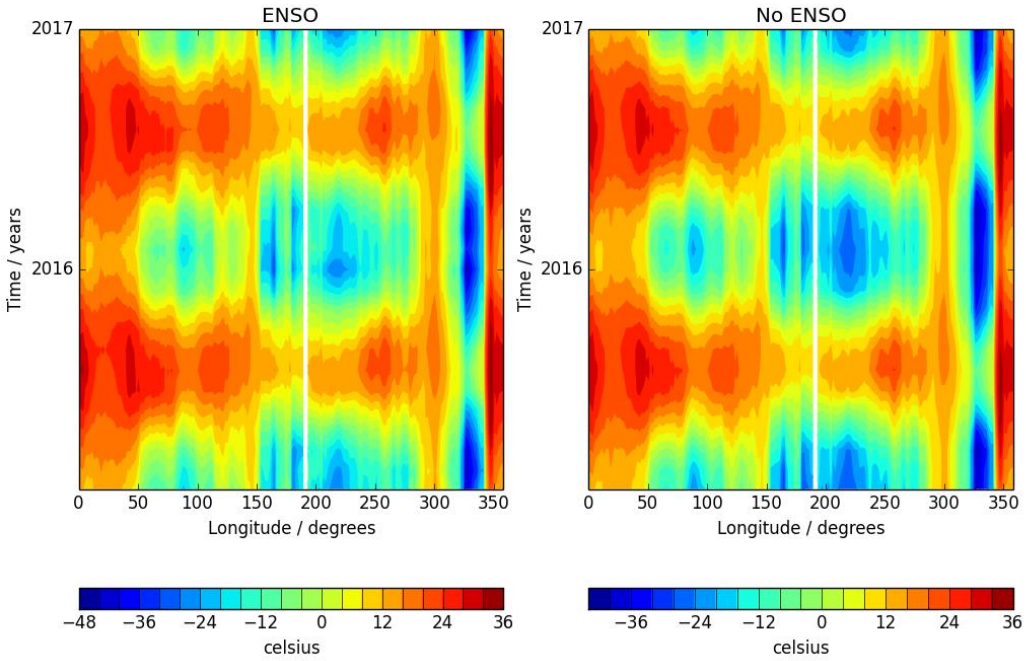

Figure A4.7: Hovmöller temperature plots with El Niño
Hovmöller plots showing difference in temperature (°C) with El Niño (left) and without the El Niño (right) 2015-2017

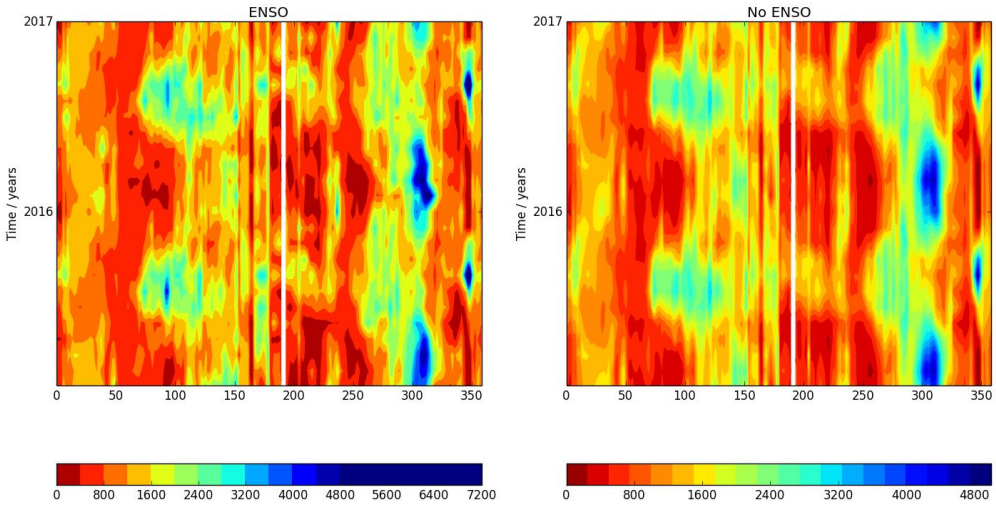

Figure A4.8: Hovmöller precipitation plots with El Niño
Hovmöller plots showing difference in precipitation (mm) with El Niño (left) and without the El Niño (right) 2015-2017

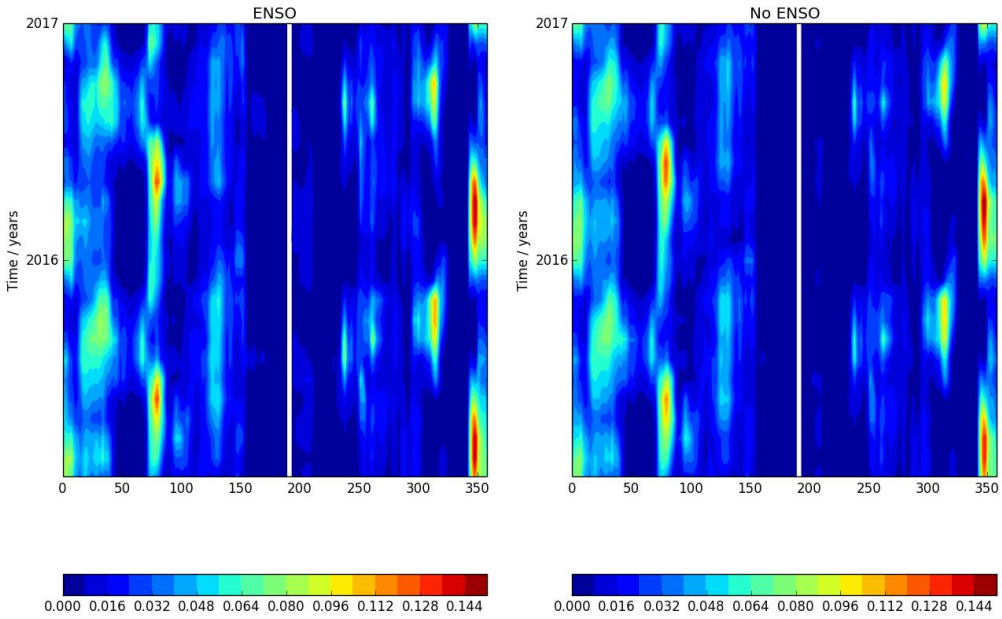

Figure A4.9: Hovmöller burned area plots with El Niño
Hovmöller plots showing difference in burnt area fraction with El Niño (left) and without the El Niño (right) 2015-2016

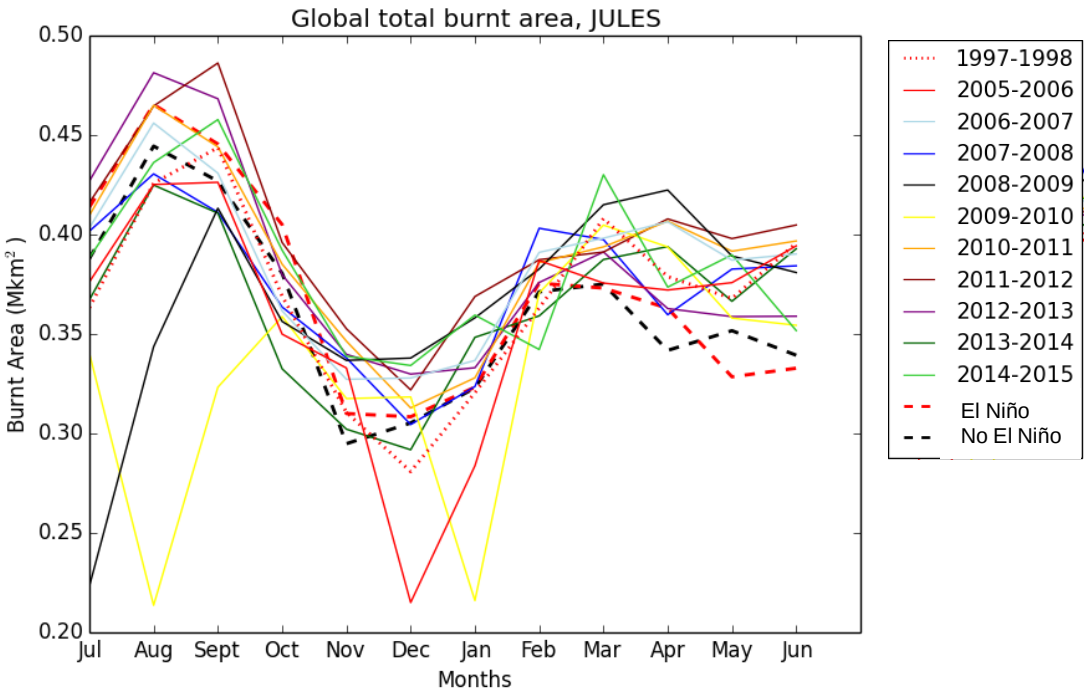

a

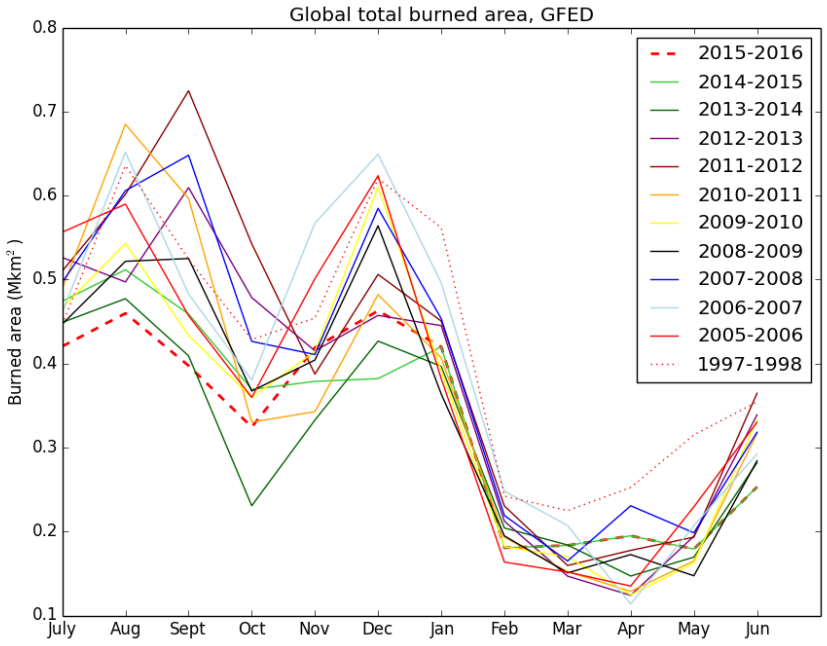

b

Figure A4.10: Global total burned area 2005-2016
Global total burnt area (Mkm^2) as modelled by JULES-INFERNO (a), and from GFED4.1s observations (b) for 2005-2016 and including previous large El Niño year 1997-1998 (as per Figure 3.35, covering additional years 2005-2010)

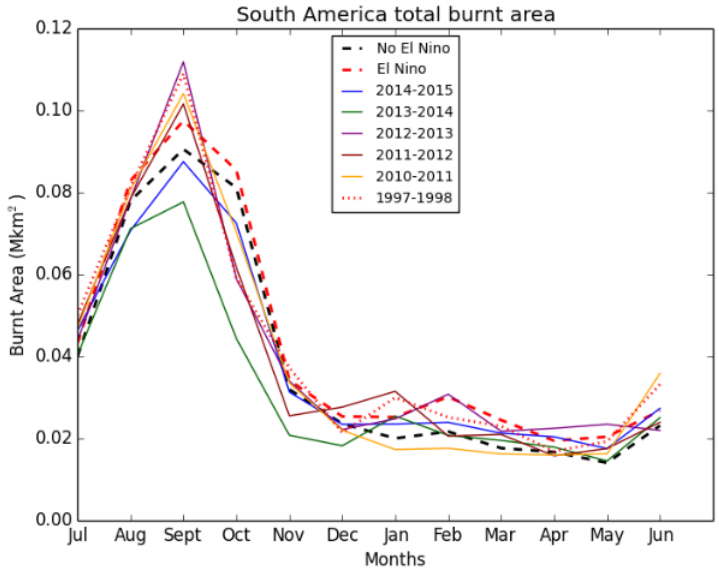

a

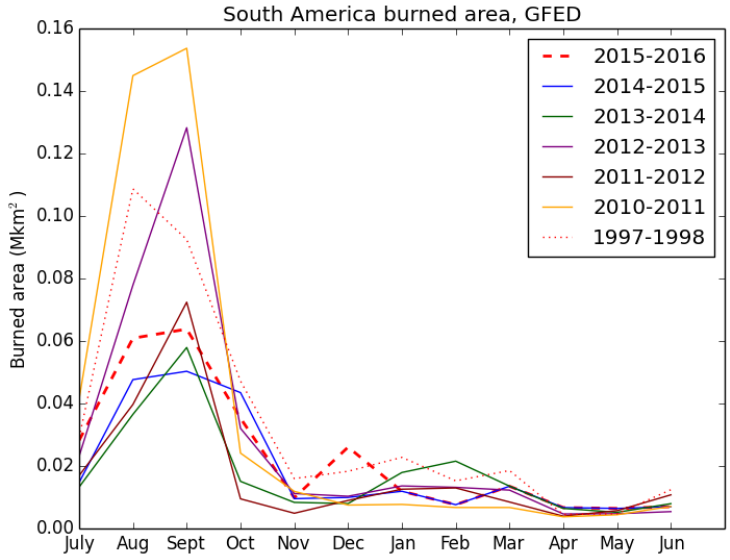

b

Figure A4.11: South America total burned area 2010-2016
Total burnt area across South America (Mkm^2) as modelled by JULES-INFERNO (a), and from GFED4.1s observations (b) for 2010-2016 and including previous large El Niño year 1997-1998 (as per Figure 3.35, for South America)

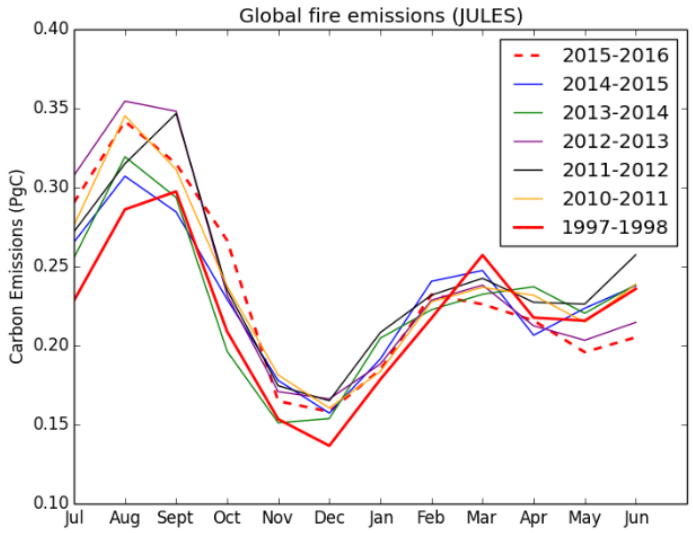

a

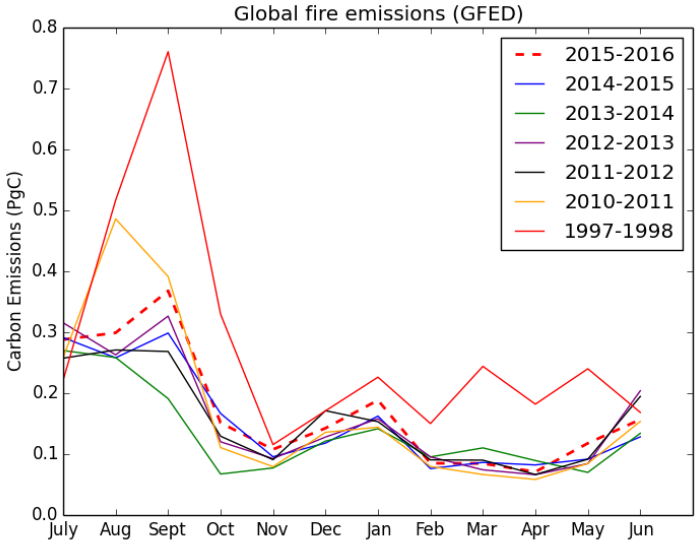

b

Figure A4.12: Global fire emissions 2010-2016
Global total carbon emissions from fire (PgC) as modelled by JULES-INFERNO (a), and from GFED4.1s observations (b) for 2005-2016 and including previous large El Niño year 1997-1998

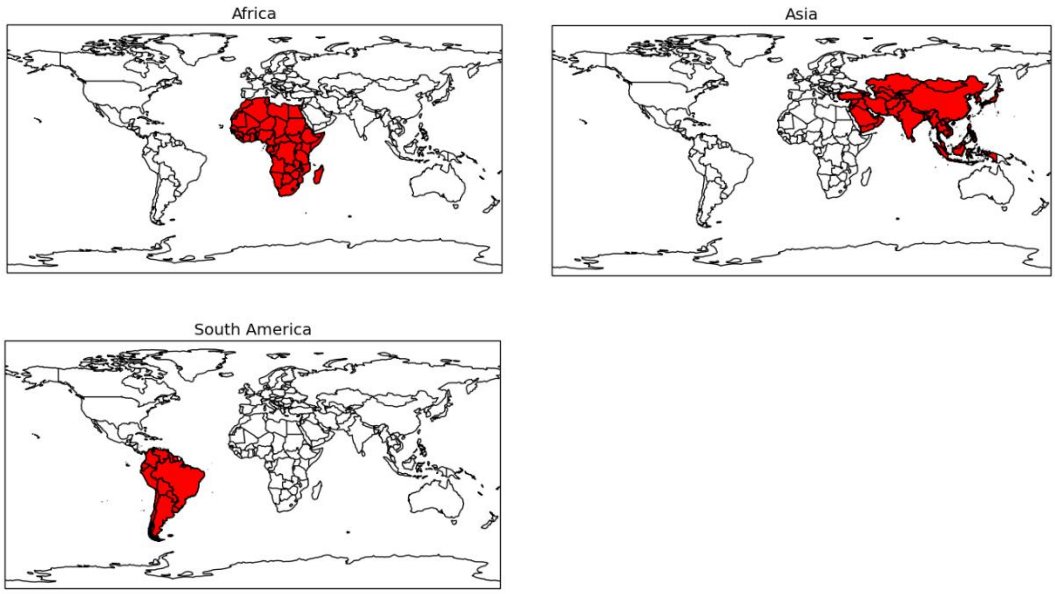

Figure A4.13: Outline of region for Chapter 4
Outline of regions for Africa, Asia and South America as used in Chapter 4 analysis

Appendix 5: Future fire danger

The HadGEM2-ES ensemble members used to drive JULES in each experiment in Chapter 5 were as follows:

RCP2.6: kaadc
RCP4.5: kaadd
RCP8.5: kaadf

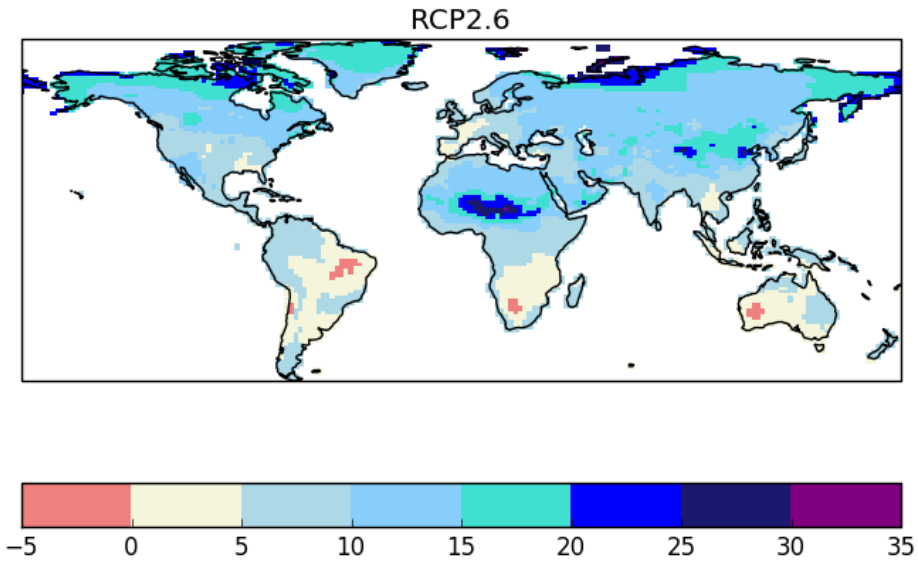

Figure A5.1: Change in humidity at 1.5°C, RCP2.6
(see Figure 5.18 for full figure)

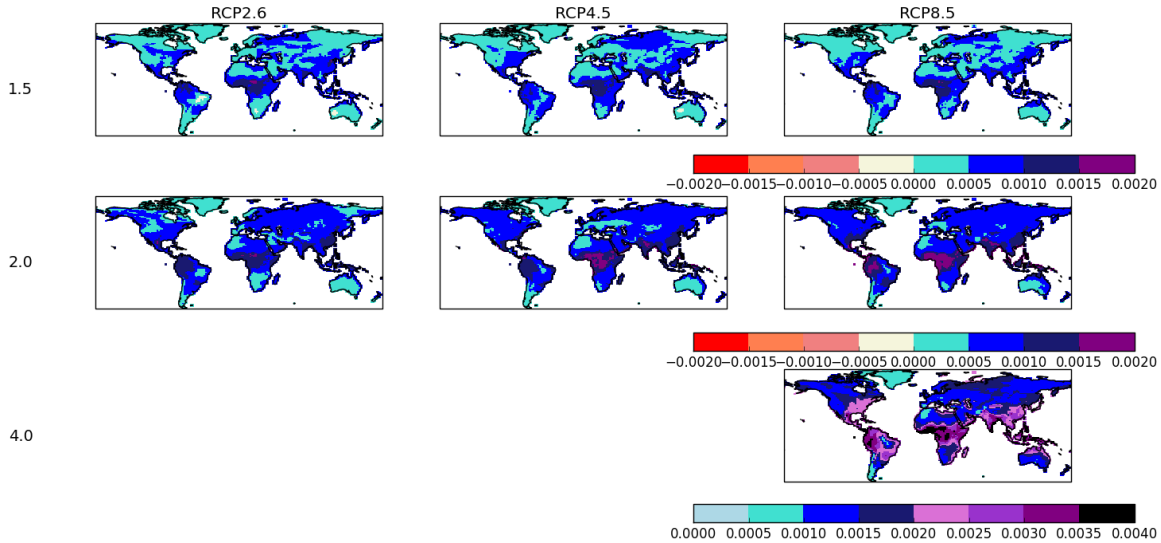

Figure A5.2: Specific warming levels of humidity
Humidity (change from present day, kg/m^2) at 1.5 (top row), 2.0 (centre row) and 4.0°C (bottom row) for each RCP scenario RCP2.6 (left column), RCP4.5 (centre column) and RCP8.5 (right column)
(see Figure 5.18 for percentage change)

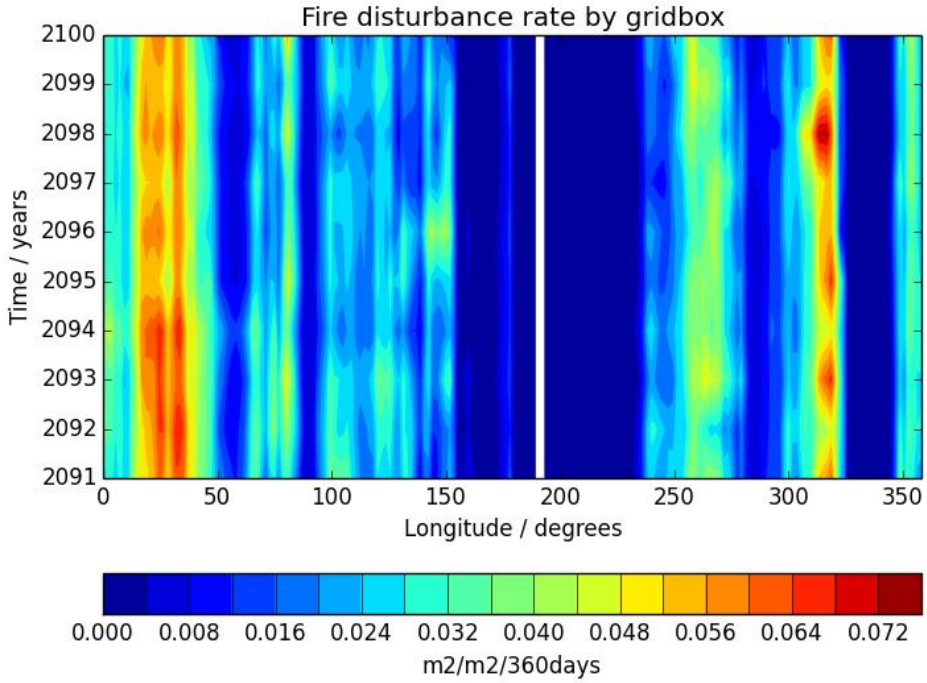

Figure A5.3: Hovmöller plot showing burnt area 2090-2099, RCP2.6

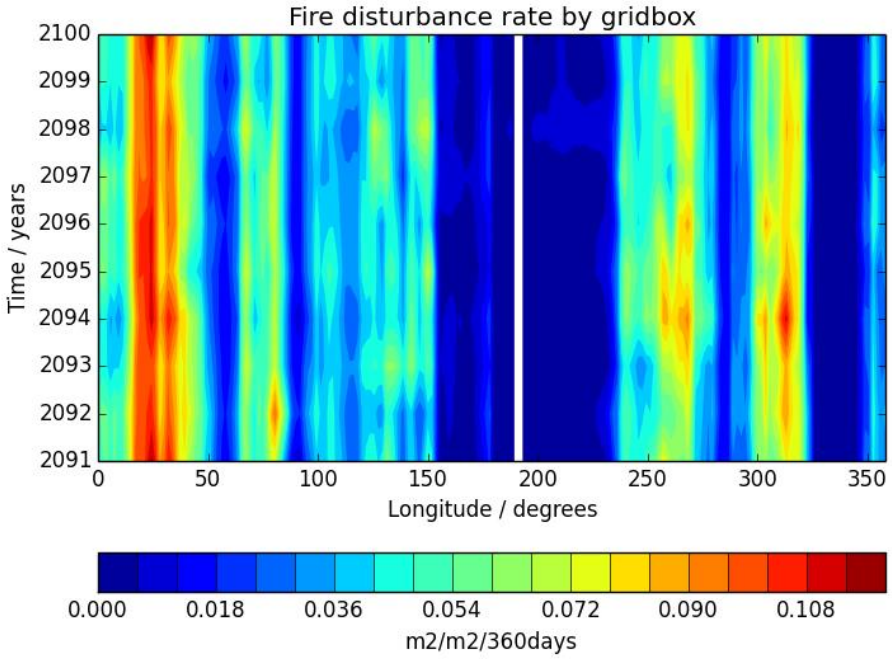

Figure A5.4: Hovmöller plot showing burnt area 2090-2099, RCP8.5

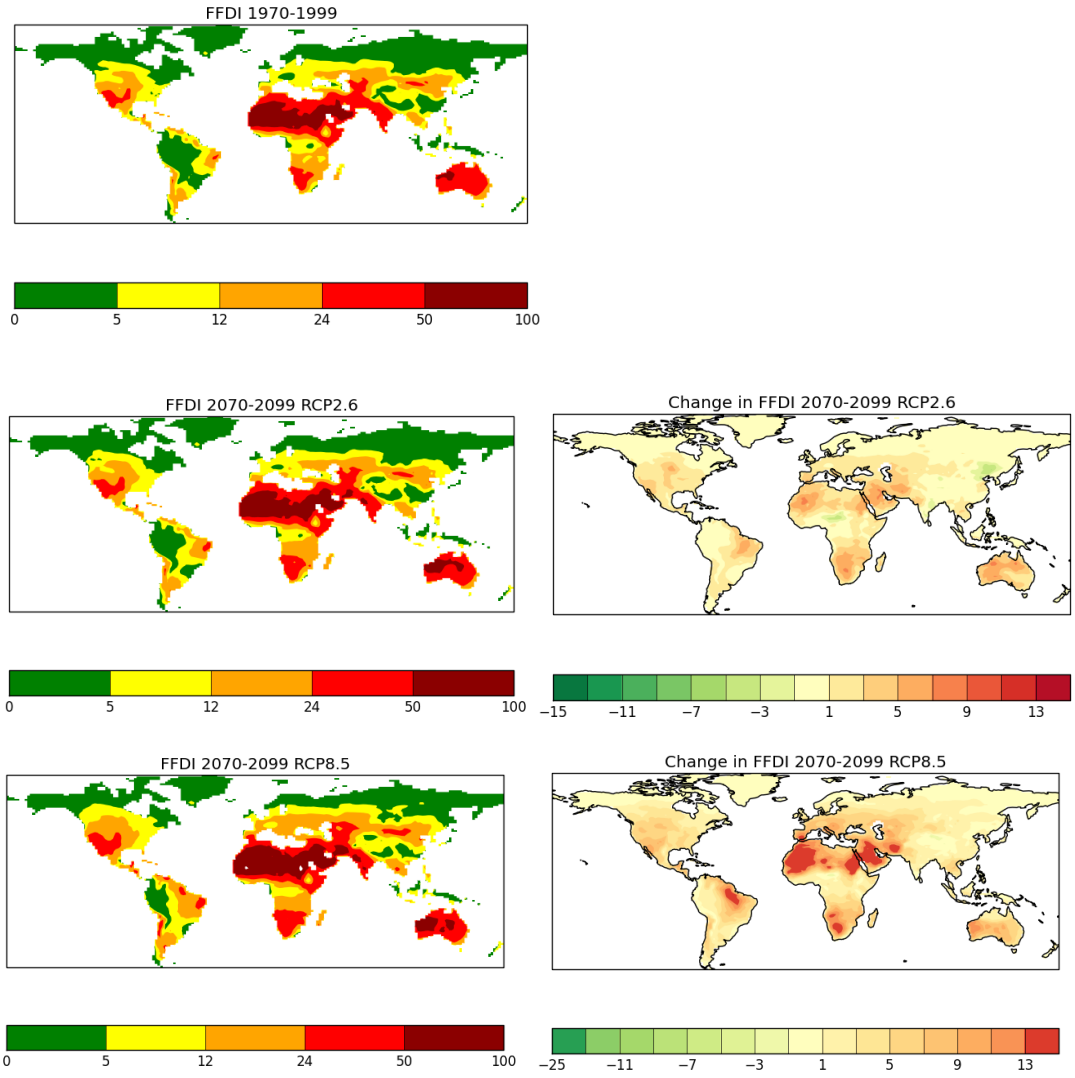

Figure A5.5 Future McArthur FFDI, varying soil moisture
As modelled by JULES with varying soil moisture 1970-1999 (a), 2070-2099 RCP2.6 (b), change in burnt area 1970-1999 to 2070-2099 RCP2.6 (c), 2070-2099 RCP8.5 (d), change in burnt area 1970-1999 to 2070-2099 RCP8.5 (e)

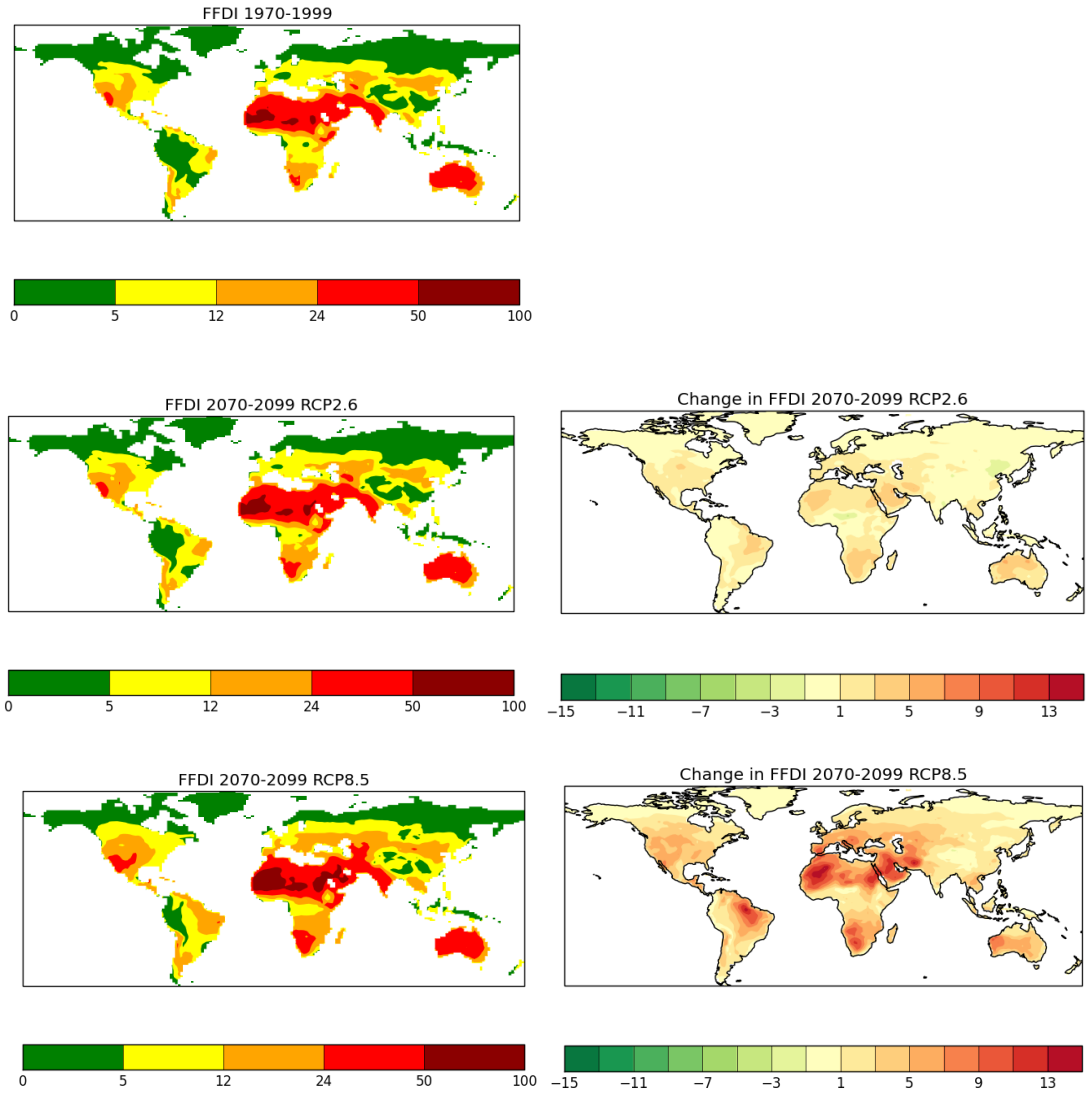

Figure A5.6: Future McArthur FFDI, constant soil moisture
As modelled by JULES with constant soil moisture (120mm) 1970-1999 (a), 2070-2099 RCP2.6 (b), change in burnt area 1970-1999 to 2070-2099 RCP2.6 (c), 2070-2099 RCP8.5 (d), change in burnt area 1970-1999 to 2070-2099 RCP8.5 (e)

Glossary

AMAZALERT	EU-funded research project that ran from 2011-2014, focused on the impacts of climate change and LUC in Amazonia. It comprised 14 partners from 6 EU countries and 3 South-American countries, including the Met Office in the UK, and INPE in Brazil.
Biogeochemical	Natural chemical processes relating to the Earth's biotic (biosphere) and abiotic (lithosphere, atmosphere, hydrosphere) environment (i.e. carbon, oxygen, nitrogen, phosphorus, sulphur, and water).
Biogeophysical	Natural biological processes relating to the Earth's geological and physical processes (i.e., plant and animal species, ecological interactions, biotic productivity; rock types, soil types, geomorphic history, sedimentation, erosion; heat, light, electrical, gravitational) (Schwartz, 1976).
C3 grass	Uses a basic process of capturing carbon using a 3-carbon molecule. Adapted to cool seasonal growth, with greater tolerance to frost, requiring less light and more moisture than C4 grass. Productivity is lower than C4.
C4 grass	Uses a more evolved process for capturing carbon, developed in the wet and dry tropics which uses a 4-carbon molecule. Adapted to warm / hot seasonal growth.
Diagnostic	A set-up mode within the model that does not affect any other variable or calculation, for example 'diagnostic burnt area' is a calculation of which areas would burn given certain meteorological conditions and given enough fuel and ignitions, but this does not affect the vegetation, atmosphere, climate or any other aspects of the Earth system.
Disturbance	Used in this thesis to refer to processes including land-use change, fire, deforestation and degradation that can impact vegetation cover.

Fire intensity	Measured by the amount of energy that is released through combustion during a fire event.
Fire severity	Measured by the amount of matter lost as a result of a fire event.
Risk	A combination of a hazard (an event e.g. fire) x exposure (whether people will be affected) x vulnerability (conditions that affect the impact such as early warning systems and infrastructure resilience)
Tipping element	Refers to a large-scale (subcontinental or larger) component of the Earth system that may induce a mass tipping point or abrupt change (Lenton *et al*., 2008). A critical threshold where a small perturbation can rapidly and qualitatively alter the state and dynamics of the system, producing large-scale and long-term consequences on human and ecological systems which persist even if the drivers of the change are abated (Settele *et al*., 2014).
TRENDY	A project comprising an international consortium of Dynamic Global Vegetation Model (DGVM) groups / land surface models aimed at investigating changes in land carbon exchange over the historical period.
MIP	Model Intercomparison Project. A range of projects focused on specific areas of research. Each MIP comprises a consortium of models that perform factorial experiments that can be compared against one another, and / or to observations where available, and can be used to create a range of uncertainty in particular areas.

Bibliography

Aguiar, A., Vieira, I., Assis, T., Dalla-Nora, E., Toledo, P., Santos-Junior, R., Batistella, M., Coelho, A., Savaget, E., Aragão, L., Nobre, C., Ometto, J. (2016). 'Land-use change emission scenarios: anticipating a forest transition process in the Brazilian Amazon'. Global Change Biology 22, 1821–1840, doi: 10.1111/gcb.13134

Ahlstrom, A. *et al*. (2015) The dominant role of semi-arid ecosystems in the trend and variability of the land CO_2 sink. *Science* **348**, 895–899

Aldersley, A., Murray, S., Cornell, S. (2011) 'Global and regional analysis of climate and human drivers of wildfire'. Science of the Total Environment 409 (2011) 3472–3481

Almeida, C.A., Coutinho, A.C., Esquerdo, J.C.D.M., Adami, M., Venturieri, A., Diniz, C.G., Dessay, N., Durieux, L., Gomes, A.R. (2016) High spatial resolution land-use and land cover mapping of the Brazilian Legal Amazon in 2008 using Landsat-5/TM and MODIS data. Acta Amazonica, Vol 46 (3), 291-302.

Alvares C.A., Stape J.L., Sentelhas P.C., de Moraes Goncalves J.L., Sparovek G. (2014) Koppen's climate classification map for Brazil. Meteorol Z. 22:711–28.

Andela, N., D. Morton, L. Giglio, Y. Chen, G. van der Werf, P. Kasibhatla, R. DeFries, G. Collatz, S. Hantson, S. Kloster, D. Bachelet, M. Forrest, G. Lasslop, F. Li, S. Mangeon, J. Melton, C. Yue & J. Randerson (2017) A human-driven decline in global burned area. Science, 356, 1356-1361.

Anderson, L., Aragão, L., Gloor, M., Arai, E., Adami, M., Saatchi, S., Malhi, Y., Shumabukuro, Y., Barlow, J., Berenguer, E., Duarte, V. (2015) 'Disentangling the contribution of multiple land covers to fire-mediated carbon emissions in Amazonia during the 2010 drought' Global Biogeochemical Cycles, 29, 1739–1753, doi:10.1002/2014GB005008

Anderson, L.O., Ribeiro Neto G, Cunha AP, Fonseca MG, Mendes de Moura Y, Dalagnol R, Wagner FH, Aragão LEOC. (2018). Vulnerability of Amazonian forests to repeated droughts. Phil. Trans. R. Soc. B 373, 20170411 (10.1098/rstb.2017.0411)

Andrews, T., Betts, R., Booth, B., Jones, C. D., and Jones, G. S. (2017) Effective radiative forcing from historical land-use change. Climate Dynamics 48, 3489-3505.

Aragão, L., Y. Malhi, N. Barbier, A. Lima, Y. Shimabukuro, L. Anderson & S. Saatchi (2008) Interactions between rainfall, deforestation and fires during recent years in the Brazilian Amazonia. Philosophical Transactions of the Royal Society B-Biological Sciences, 363, 1779-1785.

Aragão, L. & Y. Shimabukuro (2010) The Incidence of Fire in Amazonian Forests with Implications for REDD. Science, 328, 1275-1278.

Aragão, L. E. O. C., L. O. Anderson, M. G. Fonseca, T. M. Rosan, L. B. Vedovato, F. H. Wagner, C. V. J. Silva, C. H. L. Silva Junior, E. Arai, A. P. Aguiar, J. Barlow, E. Berenguer, M. N. Deeter, L. G. Domingues, L. Gatti, M. Gloor, Y. Malhi, J. A. Marengo, J. B. Miller, O. L. Phillips & S. Saatchi (2018) 21st Century drought-related fires counteract the decline of Amazon deforestation carbon emissions. Nature Communications, 9, 536.

Arora, V. & G. Boer (2005) Fire as an interactive component of dynamic vegetation models. Journal of Geophysical Research-Biogeosciences, 110.

Avitabile, V., Herold, M., Heuvelink, G. B. M., Lewis, S. L., Phillips, O. L., Asner, G. P., Armston, J., Ashton, P. S., Banin, L., Bayol, N., Berry, N. J., Boeckx, P., de Jong, B. H. J., DeVries, B., Girardin, C. A. J., Kearsley, E., Lindsell, J. A., Lopez-Gonzalez, G., Lucas, R., Malhi, Y., Morel, A., Mitchard, E. T. A., Nagy, L., Qie, L., Quinones, M. J., Ryan, C. M., Ferry, S. J. W., Sunderland, T., Laurin, G. V., Gatti, R. C., Valentini, R., Verbeeck, H., Wijaya, A. and Willcock, S. (2016): An integrated pan-tropical biomass map using multiple reference datasets, Glob Change Biol, 22: 1406–1420. doi:10.1111/gcb.13139.

Bachmann, A., and Allgöwer, B. (2002) Uncertainty propagation in wildland fire behaviour modelling, International Journal of Geographical Information Science, 16:2,115-127, DOI: 10.1080/1365881011009908

Bagley, J., A. Desai, K. Harding, P. Snyder & J. Foley (2014) Drought and Deforestation: Has Land Cover Change Influenced Recent Precipitation Extremes in the Amazon? Journal of Climate, 27, 345-361.

Barlow, J., C. A. Peres, B. O. Lagan, and T. Haugaasen (2003), Large tree mortality and the decline of forest biomass following Amazonian wildfires, Ecol. Lett., 6, 6–8, doi:10.1046/j.1461-0248.2003.00394.x.

Barlow, J., & Peres, C. A. (2008). Fire-mediated dieback and compositional cascade in an Amazonian forest. Philosophical Transactions of the Royal Society B: Biological Sciences, 363(1498), 1787–1794. http://doi.org/10.1098/rstb.2007.0013

Bastos A, et al. (2018). Impact of the 2015/2016 El Niño on the terrestrial carbon cycle constrained by bottom-up and top-down approaches. Phil. Trans. R. Soc. B 373, 20170304 (10.1098/rstb.2017.0304)

Bedia, J., Herrera, S., Gutierrez, J., Benali, A., Brands, S., Mota, B., Moreno, J. (2015). 'Global patterns in the sensitivity of burned area to fire-weather: Implications for climate change.' Agricultural and Forest Meteorology 214-215 (2015) 369–379'. http://dx.doi.org/10.1016/j.agrformet.2015.09.002

Bertrand, R., Lenoir, J., Piedallu, C., Riofrío-Dillon, G., de Ruffray, P., Vidal, C., Pierrat, J. C., and égout, J. C. (2011) Changes in plant community composition lag behind climate warming in lowland forests, Nature 479, 517–20.

Best, M., M. Pryor, D. Clark, G. Rooney, R. Essery, C. Menard, J. Edwards, M. Hendry, A. Porson, N. Gedney, L. Mercado, S. Sitch, E. Blyth, O. Boucher, P. Cox, C. Grimmond & R. Harding (2011) The Joint UK Land Environment Simulator (JULES), model description - Part 1: Energy and water fluxes. Geoscientific Model Development, 4, 677-699.

Betts, R., P. Cox, M. Collins, P. Harris, C. Huntingford & C. Jones (2004) The role of ecosystem-atmosphere interactions in simulated Amazonian precipitation decrease and forest dieback under global climate warming. Theoretical and Applied Climatology, 78, 157-175.

Betts, R. (2005) Integrated approaches to climate-crop modelling: needs and challenges. Philosophical Transactions of the Royal Society B-Biological Sciences, 360, 2049-2065.

Betts, R. A., Y. Malhi & J. T. Roberts (2008) The future of the Amazon: new perspectives from climate, ecosystem and social sciences. Philosophical Transactions of the Royal Society B-Biological Sciences, 363, 1729-1735.

Betts, R. A., N. Golding, P. Gonzalez, J. Gornall, R. Kahana, G. Kay, L. Mitchell & A. Wiltshire (2015) Climate and land-use change impacts on global terrestrial ecosystems and river flows in the HadGEM2-ES Earth system

model using the representative concentration pathways. Biogeosciences, 12, 1317-1338.
Betts, R., C. Jones, J. Knight, R. Keeling & J. Kennedy (2016) El Niño and a record CO_2 rise. Nature Climate Change, 6, 806-810.
Betts *et al*., (2018). 'A successful prediction of the record CO_2 rise associated with the 2015/16 El Niño'. Philosophical Transactions of the Royal Society B; DOI: 10.1098/rstb.2017.0301.
Bistinas, I., Harrison, S. P., Prentice, I. C., and Pereira, J. M. C. (2014): Causal relationships versus emergent patterns in the global controls of fire frequency, Biogeosciences, 11, 5087–5101, doi:10.5194/bg-11-5087-2014.
Beven, K. J.: A manifesto for the equifinality thesis, J. Hydrol., 320,18–36, https://doi.org/10.1016/j.jhydrol.2005.07.007, 2006.
Bonan, G. (2008). Forest and climate change: forcings, feedback and the climate benefit of forests. Science. 320, 5882, pp1444-1449. DOI: 10.1126/science.1155121
Bond, W., F. Woodward & G. Midgley (2005) The global distribution of ecosystems in a world without fire. New Phytologist, 165, 525-537.
Bond, W.J. (2008). What limits trees in C4 grasslands and savannas? Annu. Rev. Ecol. Evol. Syst., 39, 641–659.
Bowman, DMJS, Balch JK, Artaxo P, Bond WJ, Carlson JM, Cochrane MA, D'Antonio CM, DeFries RS, Doyle JC, Harrison SP (2009) Fire in the Earth system. Science 324:481–484.
Bradshaw, L.S., Deeming, J.E., Burgan, R.E., Cohen, J.D., (1983). The National Fire Danger Rating System: Technical Documentation. USDA For. Serv., Gen. Tech. Rep. INT-169, Ogden, UT.
Brando, P., J. Balch, D. Nepstad, D. Morton, F. Putz, M. Coe, D. Silverio, M. Macedo, E. Davidson, C. Nobrega, A. Alencar & B. Soares (2014) Abrupt increases in Amazonian tree mortality due to drought-fire interactions. Proceedings of the National Academy of Sciences of the United States of America, 111, 6347-6352.
Brandt, C. (1966) Agricultural Burning, Journal of the Air Pollution Control Association, 16:2, 85-86, DOI: 10.1080/00022470.1966.10468447
Brienen, R. J. W.; Phillips, O. L.; Feldpausch, T. R.; Gloor, E. (2015) 'Long-term decline of the Amazon carbon sink'. Nature, volume 519, pp 344-348, doi:10.1038/nature14283
Burton, C., Betts, R., Jones, C.D., Williams, K. (2018a) Will fire danger be reduced by using be reduced by using Solar Radiation Management to limit global warming to 1.5°C compared to 2.0°C? GRL, DOI 10.1002/2018GL077848
Burton C., Rifai S., Malhi Y.. (2018b). Inter-comparison and assessment of gridded climate products over tropical forests during the 2015/2016 El Niño. Phil. Trans. R. Soc. B 373, 20170406 (10.1098/rstb.2017.0406) (Luo et al., 2018).
Burton, C., Betts, R., Cardoso, M., Feldpausch, T. R., Harper, A., Jones, C. D., Kelley, D. I., Robertson, E., and Wiltshire, A. (2019): Representation of fire, land-use change and vegetation dynamics in the Joint UK Land Environment Simulator vn4.9 (JULES), Geosci. Model Dev., 12, 179-193, https://doi.org/10.5194/gmd-12-179-2019.
Butler, R. and W.F. Laurance (2009) 'Is oil palm the next emerging threat to the Amazon?' Tropical Conservation Science, 2(1), 1-10.

Cai, Y., Lenton, T., Lontzek, T. (2016). 'Risk of multiple interacting tipping points should encourage rapid CO_2 emission reduction'. Nature Climate Change. 6, 520–525 DOI:10.1038/NCLIMATE2964

Cano-Crespo, A., P. Oliveira, A. Boit, M. Cardoso & K. Thonicke (2015) Forest edge burning in the Brazilian Amazon promoted by escaping fires from managed pastures. Journal of Geophysical Research-Biogeosciences, 120, 2095-2107.

Cardoso, M., G. Hurtt, B. Moore, C. Nobre & E. Prins (2003) Projecting future fire activity in Amazonia. Global Change Biology, 9, 656-669

Cardoso, M., G. Hurtt, B. Moore, C. Nobre & H. Bain (2005) Field work and statistical analyses for enhanced interpretation of satellite fire data. Remote Sensing of Environment, 96, 212-227.

Cardoso, M., C. Nobre, D. Lapola, M. Oyama & G. Sampaio (2008) Long-term potential for fires in estimates of the occurrence of savannas in the tropics. Global Ecology and Biogeography, 17, 222-235.

Carmenta R, Blackburn GA, Davies G, de Sassi C, Lima A, Parry L, *et al*. (2016) Does the Establishment of Sustainable Use Reserves Affect Fire Management in the Humid Tropics? PLoS ONE 11(2): e0149292. doi:10.1371/journal.pone.0149292

Castello, L. & M. N. Macedo (2016) Large-scale degradation of Amazonian freshwater ecosystems. Global Change Biology, 22, 990-1007.

Cavaleri, M.A.; Reed, S.C.; Smith, W.K.; Wood, T.E.; (2015) 'Urgent need for warming experiments in tropical forests'. Global Change Biology, volume 21, issue 6, pp 2111-2121, DOI: 10.1111/gcb.12860

Center for International Earth Science Information Network - CIESIN - Columbia University (2012) National Aggregates of Geospatial Data Collection: Population, Landscape, And Climate Estimates, Version 3 (PLACE III). Palisades, NY: NASA Socioeconomic Data and Applications Center (SEDAC). http://dx.doi.org/10.7927/H4F769GP. (http://sedac.ciesin.columbia.edu/data/set/nagdc-population-landscape-climate-estimates-v3/maps)

Chadwick, R., P. Good, G. Martin & D. P. Rowell (2016) Large rainfall changes consistently projected over substantial areas of tropical land. Nature Climate Change, 6, 177-+.

Chadwick, R., H. Douville & C. B. Skinner (2017) Timeslice experiments for understanding regional climate projections: applications to the tropical hydrological cycle and European winter circulation. Climate Dynamics, 49, 3011-3029.

Chandler, C., Cheney, P., Thomas, P., Trabaud, L., Williams, D. (1983). Fire in Forestry – Forest Fire Behaviour and Effects. John Wiley & Sons, New York, Chinchester, Brisbane, Toronto, Singapore

Chapin III, S., M. Sturm, M. C. Serreze, J. P. McFadden, J. R. Key, A. H. Lloyd, A. D. McGuire, T. S. Rupp, A. H. Lynch, J. P. Schimel, J. Beringer, W. L. Chapman, H. E. Epstein, E. S. Euskirchen, L. D. Hinzman, G. Jia, C.-L. Ping, K. D. Tape, C. D. C. Thompson, D. A. Walker, J. M. Welker (2005) Role of Land-Surface Changes in Arctic Summer Warming. Science: 657-660

Charles-Dominique, P., Blanc, P., Larpin, D., Ledru, M-P., Riéra, B., Sarthou, C., Servant, M., Tardy, C (1998) Forest perturbations and biodiversity during the last ten thousand years in French Guiana. Acta Oecologica, 19, 3, 295-302. Elsevier, Paris.

Chen, Y., J. Randerson, D. Morton, R. DeFries, G. Collatz, P. Kasibhatla, L. Giglio, Y. Jin & M. Marlier (2011) Forecasting Fire Season Severity in South America Using Sea Surface Temperature Anomalies. Science, 334, 787-791.

Chen, Y., D. Morton, N. Andela, G. van der Werf, L. Giglio & J. Randerson (2017) A pan-tropical cascade of fire driven by El Niño/Southern Oscillation. Nature Climate Change, 7, 906-+.

Christidis, N., P. A. Stott, G. C. Hegerl, and R. A. Betts (2013): 'The role of land-use change in the recent warming of daily extreme temperatures' Geophys. Res. Lett.,663 40, 589–594, doi:10.1002/grl.50159.

Ciais, P., C. Sabine, G. Bala, L. Bopp, V. Brovkin, J. Canadell, A. Chhabra, R. DeFries, J. Galloway, M. Heimann, C. Jones, C. Le Quéré, R.B. Myneni, S. Piao and P. Thornton (2013): Carbon and Other Biogeochemical Cycles. In: Climate Change 2013: The Physical Science Basis. Contribution of Working Group I to the Fifth Assessment Report of the Intergovernmental Panel on Climate Change [Stocker, T.F., D. Qin, G.-K. Plattner, M. Tignor, S.K. Allen, J. Boschung, A. Nauels, Y. Xia, V. Bex and P.M. Midgley (eds.)]. Cambridge University Press, Cambridge, United Kingdom and New York, NY, USA.

CIESIN © (2012) NASA PLACE map. The Trustees of Columbia University in the City of New York. Center for International Earth Science Information. Network(CIESIN)/Columbia University. 2012. National Aggregates of Geospatial Data Collection: Population, Landscape, And Climate Estimates, Version 3 (PLACE III). Palisades, NY: NASA Socioeconomic Data and Applications Center (SEDAC). http://sedac.ciesin.columbia.edu/data/set/nagdc-population-landscape-climate-estimates-v3

Clark, D. B. and Gedney, N. (2008). Representing the effects of subgrid variability of soil moisture on runoff generation in a land surface model, J. Geophys. Res., 113, D10111, doi:10.1029/2007JD008940

Clark, D., L. Mercado, S. Sitch, C. Jones, N. Gedney, M. Best, M. Pryor, G. Rooney, R. Essery, E. Blyth, O. Boucher, R. Harding, C. Huntingford & P. Cox (2011) The Joint UK Land Environment Simulator (JULES), model description - Part 2: Carbon fluxes and vegetation dynamics. Geoscientific Model Development, 4, 701-722.

Cochrane, M. A. (2003): Fire Science for Rainforests. Nature, 421, 913-919. http://dx.doi.org/10.1038/nature01437.

Cochrane, M. & W. Laurance (2008) Synergisms among Fire, Land-use, and Climate Change in the Amazon. Ambio, 37, 522-527.

Cochrane, M. & C. Barber (2009) Climate change, human land-use and future fires in the Amazon. Global Change Biology, 15, 601-612.

Coe, M., T. Marthews, M. Costa, D. Galbraith, N. Greenglass, H. Imbuzeiro, N. Levine, Y. Malhi, P. Moorcroft, M. Muza, T. Powell, S. Saleska, L. Solorzano & J. Wang (2013) Deforestation and climate feedbacks threaten the ecological integrity of south-southeastern Amazonia. Philosophical Transactions of the Royal Society B-Biological Sciences, 368.

Collins, W. J., Bellouin, N., Doutriaux-Boucher, M., Gedney, N., Halloran, P., Hinton, T., Hughes, J., Jones, C. D., Joshi, M., Liddicoat, S., Martin, G., O'Connor, F., Rae, J., Senior, C., Sitch, S., Totterdell, I., Wiltshire, A., and Woodward, S. (2011). Development and evaluation of an Earth-system model HadGEM2. Geosci. Model Dev. Discuss., 4, 997–1062, doi:10.5194/gmdd-4-997-2011, 2011.

Collins, M., R. Knutti, J. Arblaster, J.-L. Dufresne, T. Fichefet, P. Friedlingstein, X. Gao, W.J. Gutowski, T. Johns, G. Krinner, M. Shongwe, C. Tebaldi, A.J. Weaver and M. Wehner, (2013): Long-term Climate Change: Projections, Commitments and Irreversibility. In: Climate Change 2013: The Physical Science Basis. Contribution of Working Group I to the Fifth Assessment Report of the Intergovernmental Panel on Climate Change [Stocker, T.F., D. Qin, G.-K. Plattner, M. Tignor, S.K. Allen, J. Boschung, A. Nauels, Y. Xia, V. Bex and P.M. Midgley (eds.)]. Cambridge University Press, Cambridge, United Kingdom and New York, NY, USA.

Colwell, R. K., Brehm, G., Cardelús, C. L., Gilman, A. C., and Longino, J. T. (2008) Global Warming, Elevational Range Shifts, and Lowland Biotic Attrition in the Wet Tropics, Science, 322, 258–261.

Costa, M. H. and Pires, G. F. (2010), Effects of Amazon and Central Brazil deforestation scenarios on the duration of the dry season in the arc of deforestation. Int. J. Climatol., 30: 1970–1979. doi:10.1002/joc.2048

Cox, P., R. Betts, C. Jones, S. Spall & I. Totterdell (2000) Acceleration of global warming due to carbon-cycle feedbacks in a coupled climate model. Nature, 408, 184-187.

Cox, P.M. (2001) Description of the “TRIFFID” Dynamic Global Vegetation Model. Hadley Center Technical Paper.

Cox, P., R. Betts, M. Collins, P. Harris, C. Huntingford & C. Jones (2004) Amazonian forest dieback under climate-carbon cycle projections for the 21st century. Theoretical and Applied Climatology, 78, 137-156.

Cox, Peter M.; Harris, Phil P.; Huntingford, Chris; Betts, Richard A.; Collins, Matthew; Jones, Chris D.; Jupp, Tim E.; Marengo, José A.; Nobre, Carlos A. (2008) Increasing risk of Amazonian drought due to decreasing aerosol pollution. Nature, 453. 212-215. doi:10.1038/nature06960

Crutzen, P. (2006). Albedo enhancement by stratospheric sulfur injections: A contribution to resolve a policy dilemma? Climatic Change, 77, 211-219.

Davies-Barnard, T., P. J. Valdes, J. S. Singarayer, A. J. Wiltshire, and C. D. Jones (2015): Quantifying the relative importance of land cover change from climate and land use in the representative concentration pathways, Global Biogeochem. Cycles, 29, 842–853. doi: 10.1002/2014GB004949.

De Faria, B., P. Brando, M. Macedo, P. Panday, B. Soares & M. Coe (2017) Current and future patterns of fire-induced forest degradation in Amazonia (vol 9, 095005, 2017). Environmental Research Letters, 12.

Doerr SH, Santín C. (2016) Global trends in wildfire and its impacts: perceptions versus realities in a changing world. Phil. Trans. R. Soc. B 371, 20150345.

Don, A., Schumacher, J., and Freibauer, A. (2011) ‘Impact of tropical land-use change on soil organic carbon stocks a meta-analysis’ Global Change Biol., 17, 1658-1670

Duveiller, G., Hooker, J., Cescatti, A. (2018) 'The mark of vegetation change on Earth's surface energy balance. Nature Communications, 9, 679 DOI 10.1038/s41467-017-02810-8

Eldering, A., P. Wennberg, D. Crisp, D. Schimel, M. Gunson, A. Chatterjee, J. Liu, F. Schwandner, Y. Sun, C. O'Dell, C. Frankenberg, T. Taylor, B. Fisher, G. Osterman, D. Wunch, J. Hakkarainen, J. Tamminen & B. Weir (2017) The Orbiting Carbon Observatory-2 early science investigations of regional carbon dioxide fluxes. Science, 358, 188-+.

Essery, R., Best, M., Betts, R., Cox, P., and Taylor, C. (2003). Explicit representation of subgrid heterogeneity in a GCM land surface scheme. Journal of Hydrometeorology. 4, 530–543.

FAO: Global Forest Resources Assessment 2015, Food and Agriculture Organization of the United Nations, Rome, Italy, 2015.

Fauset, S. *et al*. (2015). 'Hyperdominance in Amazonian forest carbon cycling'. Nat. Commun. 6:6857 doi: 10.1038/ncomms7857

Feldpausch TR, Phillips OL, Brienen RJ, Gloor E, Lloyd J, Lopez-Gonzalez G, Monteagudo-Mendoza A, Malhi Y, Alarcón A, Álvarez Dávila E *et al*. (2016), Amazon forest response to repeated droughts, Global Biogeochem. Cycles, 30, doi:10.1002/2015GB005133.

Ferreira, L.G., and Huete, A. R. (2004) Assessing the seasonal dynamics of the Brazilian Cerrado vegetation through the use of spectral vegetation indices, International Journal of Remote Sensing, 25:10, 1837-1860, DOI: 10.1080/0143116031000101530

Flato, G., J. Marotzke, B. Abiodun, P. Braconnot, S.C. Chou, W. Collins, P. Cox, F. Driouech, S. Emori, V. Eyring, C. Forest, P. Gleckler, E. Guilyardi, C. Jakob, V. Kattsov, C. Reason and M. Rummukainen, 2013: Evaluation of Climate Models. In: Climate Change 2013: The Physical Science Basis. Contribution of Working Group I to the Fifth Assessment Report of the Intergovernmental Panel on Climate Change [Stocker, T.F., D. Qin, G.-K. Plattner, M. Tignor, S.K. Allen, J. Boschung, A. Nauels, Y. Xia, V. Bex and P.M. Midgley (eds.)]. Cambridge University Press, Cambridge, United Kingdom and New York, NY, USA.

Fletcher, I., L. Aragao, A. Lima, Y. Shimabukuro & P. Friedlingstein (2014) Fractal properties of forest fires in Amazonia as a basis for modelling pan-tropical burnt area. Biogeosciences, 11, 1449-1459.

Foley J.A., Prentice I.C., Ramankutty N., Levis S., Pollard D., Sitch S., and Haxeltine A. (1996). An integrated biosphere model of land surface processes, terrestrial carbon balance, and vegetation dynamics. Global Biogeochemical Cycles 10(4), 603-628

Foley, Jonathan A.; Costa, Marcos Heil; Delire, Christine; Ramankutty, Navin; Snyder, Peter. (2003). Green surprise? How terrestrial ecosystems could affect earth's climate. doi:10.1890/1540-9295(2003)001[0038:GSHTEC]2.0.CO;2

Fu, R., *et al*. (2013) Increased dry-season length over southern Amazonia in recent decades and its implication for future climate projection. Proc Natl Acad Sci USA 110(45):18110–18115.

Fuss, S., J. Canadell, G. Peters, M. Tavoni, R. Andrew, P. Ciais, R. Jackson, C. Jones, F. Kraxner, N. Nakicenovic, C. Le Quere, M. Raupach, A. Sharifi, P. Smith & Y. Yamagata (2014) COMMENTARY: Betting on negative emissions. Nature Climate Change, 4, 850-853.

Gatti, L. V. *et al*., (2014): Drought sensitivity of Amazonian carbon balance revealed by atmospheric measurements. Nature 506, 76–80. doi:10.1038/nature12957.

Gibson, C. M., Chasmer, L. A., Thompson, D. K., Quinton, W. L., Flannigan, M. D., and Olefeldt, D.: Wildfire as a major driver of recent permafrost thaw in boreal peatlands, Nat. Comm., 9, 3041, https://doi.org/10.1038/s41467-018-05457-1, 2018.

Giglio, L., Randerson, J., van der Werf, G., Kasibhatla, P., Collatz, G., Morton, D., DeFries, R., (2010) 'Assessing variability and long-term trends in burned area by merging multiple satellite fire products'. Biogeosciences, 7, 1171–1186, 2010

Giglio, L., Randerson, J. T., and Werf, G. R. (2013): Analysis of daily, monthly, and annual burned area using the fourth generation global fire emissions database (GFED4), J. Geophys. Res.- Biogeo., 118, 317-328.

Gillett, N. P., Weaver, A. J., Zwiers, F. W. & Flannigan, M. D. (2004) Detecting the effect of climate change on Canadian forest fires. Geophys. Res. Lett. 31 L18211 10.1029/2004GL020876

Giorgi, F. and R. Francisco (2000). Uncertainties in regional climate change predictions. A regional analysis of ensemble simulations with the HADCM2 GCM, Clint. Dyn. 16, 169-182

Golding, N. & R. Betts (2008) Fire risk in Amazonia due to climate change in the HadCM3 climate model: Potential interactions with deforestation. Global Biogeochemical Cycles, 22.

Gonzalez, P., Neilson, R.P. , Lenihan, J.M., and Drapek, R.J. (2010). Global patterns in the vulnerability of ecosystems to vegetation shifts due to climate change. Global Ecology and Biogeography 19: 755-768.

Good, P., Jones, C., Lowe, J., Betts, R., Booth, B., & Huntingford, C. (2011). Quantifying environmental drivers of future tropical forest extent. Journal of Climate, 24, 1337–1349.

Good, P., Jones, C., Lowe, J., Betts, R., Gedney, N. (2013) Comparing tropical forest projections from two generations of Hadley Centre Earth system models, HadGEM2-E

Good, P., Lowe, J., Ridley, J., Bamber, J., Payne, T., Keen, A., Stroeve, J., Jackson, L., Srokosz, M., Kay, G., Harper, A., Kruijt, B., Burke, E., Abbott, B., O'Connor, F., Minshull, T., Turley, C., Williamson, P. (2014). Post-AR5 literature review on large-scale systems with potential for abrupt and/or irreversible change. AVOID2 publication report

Good, P., J. Bamber, K. Halladay, A. Harper, L. Jackson, G. Kay, B. Kruijt, J. Lowe, O. Phillips, J. Ridley, M. Srokosz, C. Turley & P. Williamson (2018) Recent progress in understanding climate thresholds: Ice sheets, the Atlantic meridional overturning circulation, tropical forests and responses to ocean acidification. Progress in Physical Geography, 42, 24-60.

Goulart, A. C., Macario, K. D., Scheel-Ybert, R., Alves, E. Q., Bachelet, C., Pereira, B. B., … Feldpausch, T. R. (2017). Charcoal chronology of the Amazon forest: A record of biodiversity preserved by ancient fires. Quaternary Geochronology, 41, 180–186.

de Groot, W.J., Goldammer, J.G., Keenan, T., Lynham, T.J., Brady, M.A., Justice, C.O., Csiszar, I.A., O'Loughlin, K. (2006). Developing a global early warning system for wildland fire. Proceedings of the IV International Conference on Forest Fire Research (Coimbra, Portugal). D.X. Viegas, ed. CD-ROM. Elsevier BV: Amsterdam.

de Groot, W.J., Goldammer, J.G., Justice, C.O. Lynham, T.J., Csiszar, I.A., and San-Miguel-Ayanz, J. (2010). Implementing a Global Early Warning System for Wildland Fire. Proceedings of the IV International Conference on Forest Fire Research (Coimbra, Portugal). D.X. Viegas, ed. CD-ROM. Elsevier BV: Amsterdam.

de Groot, W.J.; Wotton, B.M.; Flannigan, M.D. (2015). Wildland fire danger rating and early warning systems. (Pages 207-228 in Hazards and Disasters Series: Wildfire Hazards, Risks and Disasters. (Chapter 11). Douglas Paton, volume editor. Amsterdam, Netherlands.

Grimm, A.M., (2003): The El Niño Impact on the Summer Monsoon in Brazil: Regional Processes versus Remote Influences. J. Climate, 16, 263–280, https://doi.org/10.1175/1520-0442(2003)016<0263:TENIOT>2.0.CO;2

Gupta, Avijit (2007). Large rivers: geomorphology and management. John Wiley and Sons. p. 31. ISBN 978-0-470-84987-3

Hantson, S., A. Arneth, S. Harrison, D. Kelley, I. Prentice, S. Rabin, S. Archibald, F. Mouillot, S. Arnold, P. Artaxo, D. Bachelet, P. Ciais, M. Forrest, P. Friedlingstein, T. Hickler, J. Kaplan, S. Kloster, W. Knorr, G. Lasslop, F. Li, S. Mangeon, J. Melton, A. Meyn, S. Sitch, A. Spessa, G. van der Werf, A. Voulgarakis & C. Yue (2016) The status and challenge of global fire modelling. Biogeosciences, 13, 3359-3375.

Harper, A., P. Cox, P. Friedlingstein, A. Wiltshire, C. Jones, S. Sitch, L. Mercado, M. Groenendijk, E. Robertson, J. Kattge, G. Bonisch, O. Atkin, M. Bahn, J. Cornelissen, U. Niinemets, V. Onipchenko, J. Penuelas, L. Poorter, P. Reich, N. Soudzilovskaia & P. van Bodegom (2016) Improved representation of plant functional types and physiology in the Joint UK Land Environment Simulator (JULES v4.2) using plant trait information. Geoscientific Model Development, 9, 2415-2440.

Harper, A. B., Wiltshire, A. J., Cox, P. M., Friedlingstein, P., Jones, C. D., Mercado, L. M., Sitch, S., Williams, K., and Duran-Rojas, C. (2018a): Vegetation distribution and terrestrial carbon cycle in a carbon-cycle configuration of JULES4.6 with new plant functional types, Geosci. Model Dev. Discuss., https://doi.org/10.5194/gmd-2017-311.

Harper, A. B. *et al*. (2018b) Land-use emissions play a critical role in land-based mitigation for Paris climate targets, Nature Communications, doi:10.1038/s41467-018-05340-z

Hartley, A., MacBean, N., Georgievski, G., Bontempts, S. (2017) Uncertainty in plant functional type distributions and its impact on land surface models. Remote Sensing of Environment, ISSN 0034-4257, https://doi.org/10.1016/j.rse.2017.07.03.

Haywood, J., A. Jones, N. Bellouin & D. Stephenson (2013) Asymmetric forcing from stratospheric aerosols impacts Sahelian rainfall. Nature Climate Change, 3, 660-665.

Hirota, M., Nobre, C., Oyama, M.D. & Bustamante, M.M.C. (2010). The climatic sensitivity of the forest, savanna and forest-savanna transition in tropical South America. New Phytol., 187, 707–719.

Hirota, M., Holmgren, M., Van Nes, E. H., and Scheffer, M. (2011) 'Global resilience of tropical forest and savannah to critical transitions'. Science, 334, 232–235, doi:10.1126/science.1210657

Hoffmann, W., and Jackson, R., (2000). 'Vegetation–Climate Feedbacks in the Conversion of Tropical Savanna to Grassland'. AMS, May 2000. DOI: http://dx.doi.org/10.1175/1520-0442(2000)013<1593:VCFITC>2.0.CO;2

Holgate, C., van Dijk, A., Cary, G., and Yebra, M. (2017). Using alternative soil moisture estimates in the McArthur Forest Fire Danger Index. International Journal of Wildland Fire. 26(9) 806-819 https://doi.org/10.1071/WF16217

Houghton R. A. (1999) The annual net flux of carbon to the atmosphere from changes in land-use 1850–1990*. Tellus B, 51, 298-313.

Houghton R. A., Hackler J. L. (2001) Carbon flux to the atmpsphere from land-use changes: 1850 - 1990. ORNL/CDIAC-131, NDP-050/R1, Carbon Dioxide Information Analysis Center, U.S. Department of Energy, Oak Ridge National Laboratory, Oak Ridge, Tennessee, U.S.A., 86.

Humphrey, V., Zscheischler, J., Ciais, P., Gudmundsson, L., Sitch, S., Senevirantne, s. (2018) Sensitivity of atmospheric CO_2 growth rate to observed changes in terrestrial water storage. Nature, 560, 628-631. https://doi.org/10.1038/s41586-018-0424-4

Huntingford, C., P. Harris, N. Gedney, P. Cox, R. Betts, J. Marengo & J. Gash (2004) Using a GCM analogue model to investigate the potential for Amazonian forest dieback. Theoretical and Applied Climatology, 78, 177-185.

Hurtt GC, Frolking S, Fearon MG, Moore B, Shevliakova E, Malyshev S, Pacala SW, Houghton RA (2006) The underpinnings of land-use history: three centuries of global gridded land-use transitions, wood harvest activity, and resulting secondary lands. Global Change Biol 12:1208–1229

Hurtt, G., L. Chini, S. Frolking, R. Betts, J. Feddema, G. Fischer, J. Fisk, K. Hibbard, R. Houghton, A. Janetos, C. Jones, G. Kindermann, T. Kinoshita, K. Goldewijk, K. Riahi, E. Shevliakova, S. Smith, E. Stehfest, A. Thomson, P. Thornton, D. van Vuuren & Y. Wang (2011) Harmonization of land-use scenarios for the period 1500-2100: 600 years of global gridded annual land-use transitions, wood harvest, and resulting secondary lands. Climatic Change, 109, 117-161.

Jimenez JC, Barichivich J, Mattar C, Takahashi K, Santamaría-Artigas A, Sobrino JA, Malhi Y. (2018). Spatio-temporal patterns of thermal anomalies and drought over tropical forests driven by recent extreme climatic anomalies. Phil. Trans. R. Soc. B 373, 20170300 (10.1098/rstb.2017.0300)

Jiménez-Muñoz, J. C., C. Mattar, J. Barichivich, A. Santamaría-Artigas, K. Takahashi, Y. Malhi, J. A. Sobrino, and G. van der Schrier (2016), Record-breaking warming and extreme drought in the Amazon rainforest during the course of El Niño 2015–2016, Sci. Rep., 6, 1–12.

Joetzjer, E., Douville, H., Delire, C. *et al*. Clim Dyn (2013) 41: 2921. https://doi.org/10.1007/s00382-012-1644-1

Johns, T. (2017). Assessing mean climate change in 1.5°, 2° and 4° worlds: a comparison of results from HELIX high-resolution AGCM experiments with the CMIP5 multi-model ensemble. HELIX Technical Report.

Johnson, E.A. (1992): Fire and the vegetation dynamics: studies from the North American boreal forest. Cambridge studies in ecology. Cambridge University Press, Cambridge.

Jolly, M., Cochrane, M., Freeborn, P., Holden, Z., Brown, T., Williamson, G., Bowman, D. (2015). 'Climate-induced variations in global wildfire danger from 1979 to 2013'. Nature Communications, 6:7537. DOI: 10.1038/ncomms8537

Jones, A., Haywood, J. M., Alterskjaer, K. Boucher, O., Cole, J. N. S., Curry, C. L., Irvine, P. J., Ji, D., Kravitz, B., Kristjansson, J. E., Moore, J. C., Niemeier, U., Robock, A., Schmidt, H., Singh, B., Tilmes, S., Watanabe, S., and Yoon, J.-H. (2013). The impact of abrupt suspension of solar radiation management (termination effect) in experiment G2 of the Geoengineering Model Intercomparison Project (GeoMIP). J. Geophys. Res., 118, 9743-9752, doi:10.1002/jgrd.50762

Jones, C. D., P. M. Cox, R. L. H. Essery, D. L. Roberts, and M. J. Woodage (2003), Strong carbon cycle feedbacks in a climate model with interactive CO2 and sulphate aerosols, Geophys. Res. Lett., 30, 1479, doi: 10.1029/2003GL016867, 9.

Jones, C.D., Lowe, J., Liddicoat, S., Betts, R. (2009) 'Committed terrestrial ecosystem changes due to climate change'. Nature Geoscience 2, 484 – 487. doi:10.1038/ngeo555

Jones, C., J. Hughes, N. Bellouin, S. Hardiman, G. Jones, J. Knight, S. Liddicoat, F. O'Connor, R. Andres, C. Bell, K. Boo, A. Bozzo, N. Butchart, P. Cadule, K. Corbin, M. Doutriaux-Boucher, P. Friedlingstein, J. Gornall, L. Gray, P.

Halloran, G. Hurtt, W. Ingram, J. Lamarque, R. Law, M. Meinshausen, S. Osprey, E. Palin, L. Chini, T. Raddatz, M. Sanderson, A. Sellar, A. Schurer, P. Valdes, N. Wood, S. Woodward, M. Yoshioka & M. Zerroukat (2011). The HadGEM2-ES implementation of CMIP5 centennial simulations. Geoscientific Model Development, 4, 543-570.

Jung, M., M. Reichstein, C.R. Schwalm, C. Huntingford, S. Sitch, A. Ahlström, A. Arneth, G. Camps-Valls, P. Ciais, P. Friedlingstein, F. Gans, K. Ichii, A.K. Jain, E. Kato, D. Papale, B. Poulter, B. Raduly, C. Rödenbeck, G. Tramontana, N. Viovy, Y.-P. Wang, U. Weber, S. Zaehle, N. Zeng (2017) Compensatory water effects link yearly global land CO2 sink changes to temperature. Nature, 541, pp. 516-520

Justice, C. O., Townshend, J. R. G., Vermote, E. F., Masuoka, E., Wolfe, R. E., Saleous, N., *et al*. (2002). An overview of MODIS Land data processing and product status. Remote Sensing of Environment, 83,3−15.

Kasikowski, T., Venevsky, S., Falloon, P., Poulter, B., Betts, R., Boucher, O., Golding, N. 'Development and optimisation of a scheme for simulating burnt area in a climate model' (unpublished)

Keetch, John J.; Byram, George M. (1968). A Drought Index for Forest Fire Control. Res. Pap. SE-38. Asheville, NC: U.S. Department of Agriculture, Forest Service, Southeastern Forest Experiment Station. 35 p.

Keith, D., E. Parson & M. Morgan (2010). Research on global sun block needed now. Nature, 463, 426-427.

Keith, D. & D. MacMartin (2015) A temporary, moderate and responsive scenario for solar geoengineering. Nature Climate Change, 5, 201-206.

Kent, C., R. Chadwick, and D.P. Rowell, 2015: Understanding Uncertainties in Future Projections of Seasonal Tropical Precipitation. J. Climate, 28, 4390–4413, https://doi.org/10.1175/JCLI-D-14-00613.1

Kirchmeier-Young, M. C., F. W. Zwiers, N. P. Gillett, A. J. Cannon, 2017. Attributing extreme fire risk in Western Canada to human emissions. Climatic Change, 144, 365-379.

Klein Goldewijk (2001). Estimating global land-use change over the past 300 years: The HYDE Database. doi:10.1029/1999GB001232

Klein Goldewijk, Beusen, A. , van Drecht, G. and de Vos, M. (2011), The HYDE 3.1 spatially explicit database of human-induced global land-use change over the past 12,000 years. Global Ecology and Biogeography, 20: 73-86. doi:10.1111/j.1466-8238.2010.00587.x

Klein Goldewijk, and Verburg, P. (2013) Uncertainties in global-scale reconstructions of historical land-use: an illustration using the HYDE data set. Landscape Ecology, Vol 28, No.3 March 2013. Springer DOI 10.1007/s10980-013-9877-x

Knorr, W., L. Jiang, A. Arneth, Climate, CO2 and human population impacts on global wildfire emissions. Biogeosciences 13, 267–282 (2016). doi:10.5194/bg-13-267-2016

Kloster, S., N. Mahowald, J. Randerson, P. Thornton, F. Hoffman, S. Levis, P. Lawrence, J. Feddema, K. Oleson & D. Lawrence (2010) Fire dynamics during the 20th century simulated by the Community Land Model. Biogeosciences, 7, 1877-1902.

Kloster, S., N. Mahowald, J. Randerson & P. Lawrence (2012) The impacts of climate, land-use, and demography on fires during the 21st century simulated by CLM-CN. Biogeosciences, 9, 509-525.

Kloster, S., and Lasslop, G.: Historical and future fire occurrence (1850 to 2100) simulated in CMIP5 Earth System Models (2017) Global and Planetary Change 150: 58-69, 2017.

Koele, N., Bird, M., Haig, J., Marimon-Junior, B. H., Marimon, B. S., Phillips, O. L., … Feldpausch, T. R. (2017). Amazon Basin forest pyrogenic carbon stocks: First estimate of deep storage. Geoderma, 306, 237–243. https://doi.org/10.1016/j.geoderma.2017.07.029

Kravitz B, Forster PM, Jones A, Robock A, Alterskjær K, Boucher O, Jenkins AKL, Korhonen H, Kristjánsson JE, Muri H, Niemeier U, Partanen A-I, Rasch PJ, Wang H, and Watanabe S, (2013). Sea spray geoengineering experiments in the Geoengineering Model Intercomparison Project (GeoMIP): Experiment design and preliminary results, J. Geophys. Res., 118, 11175-11186, doi:10.1002/jgrd.50856

Kriegler, E., Hall, J., Held, H., Dawson, R., Schellnhuber, H. (2009) 'Imprecise probability assessment of tipping points in the climate system'. PNAS vol. 106, no. 13 5041–5046, doi: 10.1073/pnas.0809117106

Kucharik C.J., Foley J.A., Delire C., Fisher V.A., Coe M.T., Lenters J., Young-Molling C., Ramankutty N., Norman J.M., and Gower S.T. (2000). Testing the performance of a dynamic global ecosystem model: Water balance, carbon balance and vegetation structure. Global Biogeochemical Cycles 14(3), 795-825.

Kuhlbrodt T, C. G. Jones, A. Sellar, D. Storkey, E. Blockley, M. Stringer, R. Hill, T. Graham, J. Ridley, A. Blaker, D. Calvert, D. Copsey, R. Ellis, H. Hewitt, P. Hyder, S. Ineson, J. Mulcahy, A. Siahaan and J. Walton (2018): The low-resolution version of HadGEM3 GC3.1: Development and evaluation for global climate. Journal of Advances in Modeling Earth Systems, in review.

L'Heureux, M. (2016). 'The 2015-16 El Niño'. Science and Technology Infusion Climate Bulletin NOAA's National Weather Service. 41st NOAA Annual Climate. Diagnostics and Prediction Workshop, Orono, ME, 3-6 October 2016. http://www.nws.noaa.gov/ost/climate/STIP/41CDPW/41cdpw-MLHeureux.pdf

Lamarque, J.F., Page Kyle G, Meinshausen M, Riahi K, Smith S, van Vuuren DP, Conley AJ, Vitt F (2011) Global and regional evolution of short-lived radiatively-active gases and aerosols in the Representative Concentration Pathways. Climatic change. doi: 10.1007/s10584-011-0155-0

Lambin, E., H. Geist & E. Lepers (2003) Dynamics of land-use and land-cover change in tropical regions. *Annual Review of Environment and Resources,* 28**,** 205-241

Larkin, N. K., and D. E. Harrison (2005), Global seasonal temperature and precipitation anomalies during El Niño autumn and winter, Geophys. Res. Lett., 32, L16705, doi: 10.1029/2005GL022860.

Lasslop, G., V. Brovkin, C. H. Reick, S. Bathiany, and S. Kloster (2016) Multiple stable states of tree cover in a global land surface model due to a fire-vegetation feedback, Geophys. Res. Lett., 43, 6324–6331,doi:10.1002/2016GL069365.

Lasslop, G., Moeller, T., D'Onofrio, D., Hantson, S., Kloster, S. (2018) Tropical climate-vegetation-fire relationships: multivariate evalutation of the land surface model JSBACH. Biogeoscience, 15, 5969-5989, 2018. https://doi.org/10.5194/bg-15-5969-2018

Latif, M., and N.S. Keenlyside, (2008) 'El Niño/Southern Oscillation response to global warming'. Proceedings of the National Academy of Science of the

United States of America, Vol 106, No. 49. 20578–20583, doi: 10.1073/pnas.0710860105
Laurance, W. (1998) 'A crisis in the making: responses of Amazon forest to land-use and climate change'. Perspectives, TREE vol. 13, no. 10
Laurance, W. F., Vasconcelos, H. L., Lovejoy, T. E. (2000): Forest loss and fragmentation in the Amazon: implications for wildlife conservation, Oryx 34:39 – 45.DOI: 10.1046/j.1365-3008.2000.00094.x, 2000.
Lenton, T. M.; Held, H.; Kriegler, E.; Hall, J. W.; Lucht, W.; Rahmstorf, S.; Schellnhuber H. J. (2008) 'Tipping elements in the Earth's climate system'. Proceedings of the National Academy of Sciences of the United States of America, 105(6), 1786–1793
Le Page, Y., G. R. van der Werf, D. C. Morton, and J. M. C. Pereira (2010): Modeling fire-driven deforestation potential in Amazonia under current and projected climate conditions. J. Geophys. Res. Biogeosci., 115, G03012
Le Page, Y., D. Morton, C. Hartin, B. Bond-Lamberty, J. Pereira, G. Hurtt & G. Asrar (2017) Synergy between land-use and climate change increases future fire risk in Amazon forests. Earth System Dynamics, 8, 1237-1246.
Le Quéré, C., Robbie M. Andrew, Josep G. Canadell, Stephen Sitch, Jan Ivar Korsbakken, Glen P. Peters, Andrew C. Manning, Thomas A. Boden, Pieter P. Tans, Richard A. Houghton, Ralph F. Keeling, Simone Alin, Oliver D. Andrews, Peter Anthoni, Leticia Barbero, Laurent Bopp, Frédéric Chevallier, Louise P. Chini, Philippe Ciais, Kim Currie, Christine Delire, Scott C. Doney, Pierre Friedlingstein, Thanos Gkritzalis, Ian Harris, Judith Hauck, Vanessa Haverd, Mario Hoppema, Kees Klein Goldewijk, Atul K. Jain, Etsushi Kato, Arne Körtzinger, Peter Landschützer, Nathalie Lefèvre, Andrew Lenton, Sebastian Lienert, Danica Lombardozzi, Joe R. Melton, Nicolas Metzl, Frank Millero, Pedro M. S. Monteiro, David R. Munro, Julia E. M. S. Nabel, Shin-ichiro Nakaoka, Kevin O'Brien, Are Olsen, Abdirahman M. Omar, Tsuneo Ono, Denis Pierrot, Benjamin Poulter, Christian Rödenbeck, Joe Salisbury, Ute Schuster, Jörg Schwinger, Roland Séférian, Ingunn Skjelvan, Benjamin D. Stocker, Adrienne J. Sutton, Taro Takahashi, Hanqin Tian, Bronte Tilbrook, Ingrid T. van der Laan-Luijkx, Guido R. van der Werf, Nicolas Viovy, Anthony P. Walker, Andrew J. Wiltshire, Sönke Zaehle (2016), Carbon Budget 2016. *Earth System Science Data,* 8**,** 605-649
Le Quéré, C., Robbie M. Andrew, Pierre Friedlingstein, Stephen Sitch, Julia Pongratz, Andrew C. Manning, Jan Ivar Korsbakken, Glen P. Peters, Josep G. Canadell, Robert B. Jackson, Thomas A. Boden, Pieter P. Tans, Oliver D. Andrews, Vivek K. Arora, Dorothee C. E. Bakker, Leticia Barbero, Meike Becker, Richard A. Betts, Laurent Bopp, Frédéric Chevallier, Louise P. Chini, Philippe Ciais, Catherine E. Cosca, Jessica Cross, Kim Currie, Thomas Gasser, Ian Harris, Judith Hauck, Vanessa Haverd, Richard A. Houghton, Christopher W. Hunt, George Hurtt, Tatiana Ilyina, Atul K. Jain, Etsushi Kato, Markus Kautz, Ralph F. Keeling, Kees Klein Goldewijk, Arne Körtzinger, Peter Landschützer, Nathalie Lefèvre, Andrew Lenton, Sebastian Lienert, Ivan Lima, Danica Lombardozzi, Nicolas Metzl, Frank Millero, Pedro M. S. Monteiro, David R. Munro, Julia E. M. S. Nabel, Shin-ichiro Nakaoka, Yukihiro Nojiri, X. Antonio Padín, Anna Peregon, Benjamin Pfeil, Denis Pierrot, Benjamin Poulter, Gregor Rehder, Janet Reimer, Christian Rödenbeck, Jörg Schwinger, Roland Séférian, Ingunn Skjelvan, Benjamin D. Stocker, Hanqin Tian, Bronte Tilbrook, Ingrid T. van der Laan-Luijkx, Guido R. van der Werf, Steven van Heuven, Nicolas

Viovy, Nicolas Vuichard, Anthony P. Walker, Andrew J. Watson, Andrew J. Wiltshire, Sönke Zaehle, and Dan Zhu (2018), Global Carbon Budget 2017. Earth System Science Data Discussions, DOI: 10.5194/essdd-2017-123.

Li, F., X. Zeng & S. Levis (2012) A process-based fire parameterization of intermediate complexity in a Dynamic Global Vegetation Model. Biogeosciences, 9, 2761-2780.

Li, F., S. Levis & D. Ward (2013) Quantifying the role of fire in the Earth system - Part 1: Improved global fire modeling in the Community Earth System Model (CESM1). Biogeosciences, 10, 2293-2314.

Liu, Y.; Stanturf, J.A.; Goodrick, S.L. (2010). Trends in global wildfire potential in a changing climate. Forest Ecology and Management 259:685-697 doi:10.1016/j.foreco.2009.09.002

Liu, J., K. Bowman, D. Schimel, N. Parazoo, Z. Jiang, M. Lee, A. Bloom, D. Wunch, C. Frankenberg, Y. Sun, C. O'Dell, K. Gurney, D. Menemenlis, M. Gierach, D. Crisp & A. Eldering (2017) Contrasting carbon cycle responses of the tropical continents to the 2015-2016 El Niño. Science, 358, 191-+.

Lohberger S, Stängel M, Atwood EC, Siegert F. (2018) Spatial evaluation of Indonesia's 2015 fire-affected area and estimated carbon emissions using Sentinel-1. Glob Change Biol. ;24:644–654. https://doi.org/10.1111/gcb.13841

Lovejoy and Nobre (2018) Amazon Tipping Point. Science Advances 21 Feb 2018: Vol. 4, no. 2, eaat2340 DOI: 10.1126/sciadv.aat2340

Luo X, et al. (2018). The impact of the 2015/2016 El Niño on global photosynthesis using satellite remote sensing. Phil. Trans. R. Soc. B 373, 20170409 (10.1098/rstb.2017.0409)

Malhi, Y., Roberts, J.T., Betts, R.A., Killeen, T.J., Li, W., Nobre, C.A. (2008). 'Climate Change, Deforestation, and the Fate of the Amazon'. Science, Vol. 319 no. 5860 pp. 169-172. DOI: 10.1126/science.1146961

Malhi, Y., Aragão, L., Galbraith, D., Huntingford, C., Fisher, R., Zelazowski, P., Sitch, S., McSweeney, C., Meir, P. (2009) 'Exploring the likelihood and mechanism of a climate-change-induced dieback of the Amazon rainforest'. Proceedings of the National Academy of Sciences of the United States of America. vol. 106 no. 49, 20610–20615, doi: 10.1073/pnas.0804619106

Malhi, Y., Rowland, L., Aragão, L., & Fisher, R. A. (2018). New insights into the variability of the tropical land carbon cycle from the El Niño of 2015/2016. Philosophical transactions of the Royal Society of London. Series B, Biological sciences, 373(1760), 20170298. doi:10.1098/rstb.2017.0298

Mangeon, S., A. Voulgarakis, R. Gilham, A. Harper, S. Sitch & G. Folberth (2016) INFERNO: a fire and emissions scheme for the UK Met Office's Unified Model. Geoscientific Model Development, 9.

Mangeon, S. (2017) Developing and evaluating a global model for landscape fires. PhD thesis, Imperial College London.

Mangeon, S., N. Andela, A. Arneth, D. Bachelet, C. Burton, S. Hantson, G. Folberth, M. Forrest, G. Lasslop, F. Li, J. Melton, S. Mousafeiris, S. Sitch, G.R. van der Werf, and A. Voulgarakis (in prep) Addressing the Fuel Consumption biases in Global Fire Models

Mantzavelas, A., Apostolopoulou, I., Lazaridou , T., Partozis, T., Topaloudis, T., Lampin, C., Borgniet, L., Bouillon, C., Brewer, S., Curt, T., Ganteaume, A., Jappiot, M., Defossé, G., Gómez, F., Lencinas, D. (2006) Deliverable

5.1-1-33 ‘Method to assess with good spatial accuracy the meteorological and fuel moisture components of the fire risk’. Fire Paradox, project
Marengo, J.A. (2006). On the hydrological cycle of the Amazon basin: a historical review and current state-of-the-art. Rev. Brasil. Meteorol. 21, 1–19.
Marengo, J.A., Souza, C., Thonicke, K., Burton, C., Halladay, K., Betts, R., Alves, L., Soares, W. (2018) Climate variability, land use and change over the Amazon Region: current and future trends. Frontiers in Earth Science, section Interdisciplinary Climate Studies) https://doi.org/10.3389/feart.2018.00228
Marenco, F., Johnson, B., Langridge, J., Mulcahy, J., Benedetti, A., Remy, S., Jones, L., Szpek, K., Haywood, J., Longo, K., Artax, P. (2016) ‘On the vertical distribution of smoke in the Amazonian atmosphere during the dry season’. Atmos. Chem. Phys., 16, 2155–2174, doi:10.5194/acp-16-2155-2016
Marlon, J. R., P. J. Bartlein, C. Carcaillet, D. G. Gavin, S. P. Harrison, P. E. Higuera, F. Joos, M. J. Power & I. C. Prentice (2008) Climate and human influences on global biomass burning over the past two millennia. Nature Geoscience, 1, 697-702.
Martin, G. M., and Coauthors (2011). The HadGEM2 family of Met Office Unified Model Climate configurations. Geosci. Model Dev., 4, 723–757.
McArthur, A.G., (1967). Fire Behaviour in Eucalypt Forests. Department of National Development, Forestry and Timber Bureau, Canberra. Leaflet No. 107.
McCusker, K.E., Armour, K.C., Bitz, C. M., and Battisti, D. S. (2014). Rapid and extensive warming following cessation of solar radiation management. Environmental Research Letters, 9 024005 (9pp). doi:10.1088/1748-9326/9/2/024005
McEvedy, Colin, and Richard Jones, Atlas of World Population History (New York: Penguin, 1978)
Myneni RB, *et al*. (2007) Large seasonal swings in leaf area of Amazon rainforests. Proc Natl Acad Sci USA 104(12):4820–4823
Millar, R. J., J. S. Fuglestvedt, P. Friedlingstein, J. Rogelj, M. J. Grubb, H. D. Matthews, R. B. Skeie, P. M. Forster, D. J. Frame & M. R. Allen (2017). Emission budgets and pathways consistent with limiting warming to 1.5ºC. Nature Geosci, 10, 741-747.
Mooney, H. A. Ed. (1977) Convergent in Chile and California Mediterranean Climate Ecosystems. Dowden, Hutchinson & Ross, Inc. Stroudsberg Penn.
Moore, J., Zhu, K., Huntingford, C., Cox, P. (2018) Equilibrium forest demography explians the distribution of tree sizes across North America. Environmental Research Letters, 13, 084019 DOI: https://doi.org/10.1088/1748-9326/aad6d1https://doi.org/10.1088/1748-9326/aad6d1
Moran, E. (1993). Deforestation and Land-use in the Brazilian Amazon. Human Ecology, 21(1), 1-21. http://www.jstor.org/stable/4603072
Moreira, A. G. (2000), Effects of fire protection on savanna structure in Central Brazil. Journal of Biogeography, 27: 1021-1029. doi:10.1046/j.1365-2699.2000.00422.x
Moritz, M., M. Parisien, E. Batllori, M. Krawchuk, J. Van Dorn, D. Ganz & K. Hayhoe (2012) Climate change and disruptions to global fire activity. Ecosphere, 3.

Morton D., Le Page, Y., DeFries, R., Collatz, G., Hurtt, G. (2013) Understorey fire frequency and the fate of burned forests in southern Amazonia. Phil Trans R Soc B 368: 20120163. http://dx.doi.org/10.1098/rstb.2012.0163

Moss, Richard H; Edmonds, Jae A; Hibbard, Kathy A; Manning, Martin R; Rose, Steven K; *et al*. (2010) The next generation of scenarios for climate change research and assessment. Nature; London 463.7282. 747-56

Mouillot, F. and Field, C.B. (2005) Fire history and the global carbon budget: a 1° × 1° fire history reconstruction for the 20th century. Glob. Chang. Biol. 11, 398–420. doi:10.1111/j.1365-2486.2005.00920.xMyhre, G., D. Shindell, F.-M. Bréon, W. Collins, J. Fuglestvedt, J. Huang, D. Koch, J.-F. Lamarque, D. Lee, B. Mendoza, T. Nakajima, A. Robock, G. Stephens, T. Takemura and H. Zhang, 2013: Anthropogenic and Natural Radiative Forcing. In: Climate Change 2013: The Physical Science Basis. Contribution of Working Group I to the Fifth Assessment Report of the Intergovernmental Panel on Climate Change [Stocker, T.F., D. Qin, G.-K. Plattner, M. Tignor, S.K. Allen, J. Boschung, A. Nauels, Y. Xia, V. Bex and P.M. Midgley (eds.)]. Cambridge University Press, Cambridge, United Kingdom and New York, NY, USA.

Nakicenovic N, Swart, R, eds (2000) in Special Report on Emissions Scenarios (Intergovernmental Panel on Climate Change, Washington, DC)

Nelson, A. and K.M. Chomitz (2011): Effectiveness of strict vs. multiple use protected areas in reducing tropical forest fires: a global analysis using matching methods. PLoS ONE, 6(8), e22722, doi:10.1371/journal.pone.0022722.

Nepstad, D. C., Stickler, C. M. and Almeida, O. T. (2006), Globalization of the Amazon Soy and Beef Industries: Opportunities for Conservation. Conservation Biology, 20: 1595-1603. doi:10.1111/j.1523-1739.2006.00510.x

Nepstad, D., Stickler, C., Soares-Filho, B., Merry, F., (2008) 'Interactions among Amazon land-use, forests and climate: prospects for a near-term forest tipping point'. Philos Trans R Soc Lond B Biol Sci. 2008 May 27; 363(1498): 1737–1746. doi: 10.1098/rstb.2007.0036

Noble, I. (1980). McArthur's fire-danger meters expressed as equations. Australian Journal of Ecology, 5, 201-203. Re-publihed in July 2006 DOI: 10.1111/j.1442-9993.1980.tb01243.x

Nobre, C., Sampaio, G., Borma, L., Castilla-Rubio, J., Silva, J., Cardoso, C. (2016). Fate of the Amazon forests and the Third Way. Proceedings of the National Academy of Sciences Sep 2016, 113 (39) 10759-10768; DOI: 10.1073/pnas.1605516113

Numata, I., S. S. Silva, M. A. Cochrane & M. V. d'Oliveira (2017) Fire and edge effects in a fragmented tropical forest landscape in the southwestern Amazon. Forest Ecology and Management, 401, 135-146.

Ogden, J., Basher, L., McGlone, M. (1998): Botanical Briefing: Fire, Forest Regeneration and Links with Early Human Habitation: Evidence from New Zealand, Annals of Botany, Volume 81, Issue 6: Pages 687–696, https://doi.org/10.1006/anbo.1998.0637.

Oliver, R., and Jones, C. Land-use change: TRIFFID. *Unpublished repor*t.

Oliveras I, Román-Cuesta RM, Urquiaga-Flores E, *et al*. (2018) Fire effects and ecological recovery pathways of tropical montane cloud forests along a time chronosequence. Glob Change Biol.;24:758–772. https://doi.org/10.1111/gcb.13951

Olson, D. M., Dinerstein, E., Wikramanayake, E. D., Burgess, N. D., Powell, G. V. N., Underwood, E. C., D'Amico, J. A., Itoua, I., Strand, H. E., Morrison, J. C., Loucks, C. J., Allnutt, T. F., Ricketts, T. H., Kura, Y., Lamoreux, J. F., Wettengel, W. W., Hedao, P., Kassem, K. R. 2001. Terrestrial ecoregions of the world: a new map of life on Earth. Bioscience 51(11):933-938.

Oyama, M., Nobre, C. (2003) 'A new climate-vegetation equilibrium state for tropical South America'. Geophysical Research Letters 30 (23), 2199–2203

Page, S.E., Florian Siegert, John O. Rieley, Hans-Dieter V. Boehm, Adi Jaya & Suwido Limin (2002) The amount of carbon released from peat and forest fires in Indonesia during 1997. Nature volume 420, pages 61–65 doi:10.1038/nature01131

Pan, Y., Birdsey, R., Fang, J., Houghton, R., Kauppi, P., Kurz, W.A., Phillips, O.L., Shvidenko, A., Lewis, S.L., Canadell, J.G., Ciais, P., Jackson, R.B., Pacala, S., McGuire, A.D., Piao, S., Rautiainen, A., Sitch, S., and Hayes, D. (2011). 'A large and persistent carbon sink in the World's forests'. Science, 333(6045), 988-993

Pechony, O. & D. Shindell (2009) Fire parameterization on a global scale. Journal of Geophysical Research-Atmospheres, 114

Pechony, O., & Shindell, D. T., (2010). Driving forces of global wildfires over the past millennium and the forthcoming century. Proc. Natl. Acad. Sci. USA. 107, 19167-19170. doi:10.1073/pnas.1003669107pmid:20974914.

Pellegrini, A. F. A., Anderegg, W. R. L., Paine, C. E. T., Hoffmann, W. A., Kartzinel, T., Rabin, S. S., Sheil, D., Franco, A. C. and Pacala, S. W. (2017), Convergence of bark investment according to fire and climate structures ecosystem vulnerability to future change. Ecol Lett, 20: 307–316. doi:10.1111/ele.12725

Pfeiffer, M., A. Spessa & J. Kaplan (2013) A model for global biomass burning in preindustrial time: LPJ-LMfire (v1.0). Geoscientific Model Development, 6, 643-685.

Philips *et al*. (2009) 'Drought sensitivity of the Amazon Rainforest'. Science 323, 1344. DOI/; 10.1126/Science.1164033

Piao, S., Sitch, S., Ciais, P., Friedlingstein, P., Peylin, P., Wang, X., Ahlström, A., Anav, A., Canadell, J. G., Cong, N., Huntingford, C., Jung, M., Levis, S., Levy, P. E., Li, J., Lin, X., Lomas, M. R., Lu, M., Luo, Y., Ma, Y., Myneni, R. B., Poulter, B., Sun, Z., Wang, T., Viovy, N., Zaehle, S. and Zeng, N. (2013), Evaluation of terrestrial carbon cycle models for their response to climate variability and to CO2 trends. Glob Change Biol, 19: 2117–2132. doi:10.1111/gcb.12187

Pielke, RA (Pielke, RA); Marland, G (Marland, G); Betts, RA (Betts, RA); Chase, TN (Chase, TN); Eastman, JL (Eastman, JL); Niles, JO (Niles, JO); Niyogi, DDS (Niyogi, DDS); Running, SW (Running, SW) (2002) 'The influence of land-use change and landscape dynamics on the climate system: relevance to climate-change policy beyond the radiative effect of greenhouse gases'. Philosophical Transactions of the Royal Society of London Series A-Mathematical Physical and Engineering Sciences. 360 Issue: 1797 Pages: 1705-1719 DOI: 0.1098/rsta.2002.1027

Pinol J., Terradas J. and Lloret F. (1998) 'Climate warming, wildfire hazard, and wildfire occurrence in coastal eastern Spain'. Climate Change 38: 345-357

Pivello (2011) The use of fire in the Cerrado and Amazonian Rainforests of Brazil: Past and Present

http://www.ecologia.ib.usp.br/lepac/conservacao/Artigos/The_%20Use_%20Fire_Cerrado.pdf

Pongratz, Julia; Reick, Christian; Raddatz, Thomas; Claussen, Martin (2008). Reconstruction of global land-use and land cover AD 800 to 1992. World Data Center for Climate (WDCC) at DKRZ. https://doi.org/10.1594/WDCC/RECON_LAND_COVER_800-1992

Poulter, B., MacBean, N., Hartley, A., Khlystova, I., Arino, O., Betts, R., Bontemps, S., Boettcher, M., Brockmann, C., Defourny, P., Hagemann, S., Herold, M., Kirches, G., Lamarche, C., Lederer, D., Ottlé, C., Peters, M., and Peylin, P.: Plant functional type classification for earth system models: results from the European Space Agency's Land Cover Climate Change Initiative (2015) Geosci. Model Dev., 8, 2315-2328, https://doi.org/10.5194/gmd-8-2315-2015.

Prentice, I., S. Harrison & P. Bartlein (2011) Global vegetation and terrestrial carbon cycle changes after the last ice age. New Phytologist, 189, 988-998.

Pugh, T. A. M., Jones, C. D., Huntingford, C., Burton, C., Arneth, A., Brovkin, V., et al.: A large committed long-term sink of carbon due to vegetation dynamics. Earth's Future, 6. https://doi.org/10.1029/2018EF000935, 2018.

Rabin, S. S., S. L. Malyshev, B. I. Magi, E. Shevliakova & S. W. Pacala (2017) A fire model with distinct crop, pasture, and non-agricultural burning: Use of new data and a model-fitting algorithm for FINALv1. Geosci. Model Dev. Discuss., 2017, 1-48.

Ramankutty, Navin, and Foley, Jonathan A. (1999). Estimating historical changes in global land cover: Croplands from 1700 to 1992. doi:10.1029/1999GB900046

Randerson, J. T., Y. Chen, G. R. van derWerf, B. M. Rogers, and D. C. Morton (2012), Global burned area and biomass burning emissions from small fires, J. Geophys. Res., 117, G04012, doi: 10.1029/2012JG002128.

Rao, V., S. Franchito, M. Gan & R. Gerolamo (2014) Duration of the South America summer monsoon is increasing. Atmospheric Science Letters, 15, 110-113.

Reyer,C.P.O.; Rammig, A.; Brouwers, N.; Langerwisch, F. (2015) 'Forest Forest resilience, tipping points and global change processes'. Journal of Ecology, volume 103, Issue 1, DOI: 10.1111/1365-2745.12342

Rifai SW, et al. (2018). ENSO Drives interannual variation of forest woody growth across the tropics. Phil. Trans. R. Soc. B 373, 20170410 (10.1098/rstb.2017.0410)

Roberts, G., Wooster, M. J., and Lagoudakis, E. (2009) Annual and diurnal African biomass burning temporal dynamics. Biogeosciences, 6(5), 849–866,doi:10.5194/bg-6-849-2009.

Robock, A. (2008). 20 Reasons Why Geoengineering May Be a Bad Idea. Bulletin of the Atomic Scientists, 64, 14-18.

da Rocha HR, *et al*. (2009) Patterns of water and heat flux across a biome gradient from tropical forest to savanna in Brazil. J Geophys Res 114(G1):G00B12.

Rogelj, J., M. Schaeffer, P. Friedlingstein, N. P. Gillett, D. P. van Vuuren, K. Riahi, M. Allen & R. Knutti (2016). Differences between carbon budget estimates unravelled. Nature Clim. Change, 6, 245-252.

Saatchi, S.; Asefi-Najafabady, S.; Malhi, Y.; Aragão, L. Anderson, L.O.; Myneni, R.B.; Nemani, R. (2013) 'Persistent effects of a severe drought on

Amazonian forest canopy'. Proceedings of the National Academy of Sciences of the USA, volume 110(2): 565–570, DOI: 10.1073/pnas.1204651110

Santín, C., & Doerr, S. H. (2016). Fire effects on soils: the human dimension. Philosophical Transactions of the Royal Society B: Biological Sciences, 371(1696), 20150171. http://doi.org/10.1098/rstb.2015.0171

Santos V, Ferreira M, Rodrigues J, Garcia M, Ceron J, Nelson BW, Saleska SR. (2018). Causes of reduced leaf-level photosynthesis during strong El Niño drought in a Central Amazon forest. Glob. Change Biol. 24, 4266–4279. (10.1111/gcb.14293)

Scholze, M., W. Knorr, N. Arnell & I. Prentice (2006) A climate-change risk analysis for world ecosystems. Proceedings of the National Academy of Sciences of the United States of America, 103, 13116-13120.

Senior, C. A., Andrews, T., Burton, C., Chadwick, R., Copsey, D., Graham, T., Hyder, P., Jackson, L., McDonald, R., Ridley, J., Ringer, J., Tsushima, Y. (2016): Idealized climate change simulations with a high-resolution physical model: HadGEM3-GC2, J. Adv. Model. Earth Syst., 8, 813–830, doi: 10.1002/2015MS000614.

Seo, H. and Kim, Y. (2019): Interactive impacts of fire and vegetation dynamics on global carbon and water budget using Community Land Model version 4.5, Geosci. Model Dev., 12, 457-472, https://doi.org/10.5194/gmd-12-457-2019

Settele, J., R. Scholes, R. Betts, S. Bunn, P. Leadley, D. Nepstad, J.T. Overpeck, and M.A. Taboada, 2014: Terrestrial and inland water systems. In: Climate Change 2014: Impacts, Adaptation, and Vulnerability. Part A: Global and Sectoral Aspects. Contribution of Working Group II to the Fifth Assessment Report of the Intergovernmental Panel on Climate Change [Field, C.B., V.R. Barros, D.J. Dokken, K.J. Mach, M.D. Mastrandrea, T.E. Bilir, M. hatterjee, K.L. Ebi, Y.O. Estrada, R.C. Genova, B. Girma, E.S. Kissel, A.N. Levy, S. MacCracken, P.R. Mastrandrea, and L.L. White (eds.)]. Cambridge University Press, Cambridge, United Kingdom and New York, NY, USA, pp. 271-359.

Setzer, A. W. & R. A. Sismanoglu (2012) Risco de Fogo: Metodologia do Cálculo–Descrição sucinta da Versão 9. São Paulo: INPE.

Shakesby, R.A., Doerr, S.H. (2006) Wildfire as a hydrological and geomorphological agent. *Earth-ScienceReviews* 74, 269–307. https://www.sciencedirect.com/science/article/pii/S0012825205001467

Sharples, J.J., McRae , R.H.D., Weber R.O., and Gill A.M. (2009) 'A simple method for assessing fuel moisture content and fire danger rating' 18th World IMACS / MODSIM Congress, Cairns, Australia 13-17 July 2009 http://mssanz.org.au/modsim09

Shippers, P., Sterck, F., Vlam, M., Zuidema, P. (2015). Tree Growth variation in the tropical forest: understanding effects of temperature, rainfall and CO2. Global Change Biology 21, 2749–2761, doi: 10.1111/gcb.12877

Silva CVJ, et al. (2018). Drought-induced Amazonian wildfires instigate a decadal-scale disruption of forest carbon dynamics. Phil. Trans. R. Soc. B 373, 20180043 (10.1098/rstb.2018.0043)

Silvério, D.V., Paulo M. Brando, Jennifer K. Balch, Francis E. Putz, Daniel C. Nepstad, Claudinei Oliveira-Santos, Mercedes M. C. Bustamante (2013): Testing the Amazon savannization hypothesis: fire effects on invasion of a neotropical forest by native cerrado and exotic pasture grasses. Phil. Trans. R. Soc. B 2013 368 20120427; DOI: 10.1098/rstb.2012.0427.

Sitch, S., Smith, B., Prentice, I.C., Arneth, A., Bondeau, A. (2003) Evaluation of ecosystem dynamics, plant geography and terrestrial carbon cycling in the LPJ dynamic global vegetation model. Glob. Chang. Biol. 9, 161–185. (doi:10.1046/j.1365-2486.2003.00569.x)

Sitch, S., C. Huntingford, N. Gedney, P. Levy, M. Lomas, S. Piao, R. Betts, P. Ciais, P. Cox, P. Friedlingstein, C. Jones, I. Prentice & F. Woodward (2008) Evaluation of the terrestrial carbon cycle, future plant geography and climate-carbon cycle feedbacks using five Dynamic Global Vegetation Models (DGVMs). Global Change Biology, 14, 2015-2039.

Sitch, S., P. Friedlingstein, N. Gruber, S. Jones, G. Murray-Tortarolo, A. Ahlstrom, S. Doney, H. Graven, C. Heinze, C. Huntingford, S. Levis, P. Levy, M. Lomas, B. Poulter, N. Viovy, S. Zaehle, N. Zeng, A. Arneth, G. Bonan, L. Bopp, J. Canadell, F. Chevallier, P. Ciais, R. Ellis, M. Gloor, P. Peylin, S. Piao, C. Le Quere, B. Smith, Z. Zhu & R. Myneni (2015) Recent trends and drivers of regional sources and sinks of carbon dioxide. Biogeosciences, 12, 653-679.

Skinner, C., Poulsen, C., Mankin, J. (2018). 'Amplification of heat extremes by plant CO2 physiological forcing. Nature Communications, 9, 1094. DOI 10.1038/s41467-018-03472-w

Smith, P., S. Davis, F. Creutzig, S. Fuss, J. Minx, B. Gabrielle, E. Kato, R. Jackson, A. Cowie, E. Kriegler, D. van Vuuren, J. Rogelj, P. Ciais, J. Milne, J. Canadell, D. McCollum, G. Peters, R. Andrew, V. Krey, G. Shrestha, P. Friedlingstein, T. Gasser, A. Grubler, W. Heidug, M. Jonas, C. Jones, F. Kraxner, E. Littleton, J. Lowe, J. Moreira, N. Nakicenovic, M. Obersteiner, A. Patwardhan, M. Rogner, E. Rubin, A. Sharifi, A. Torvanger, Y. Yamagata, J. Edmonds & Y. Cho (2016) Biophysical and economic limits to negative CO2 emissions. Nature Climate Change, 6, 42-50.

Soares-Filho, B., Nepstad, D., Curran, L., Cerqueira, G., Garcia, R., Ramos, C., Voll, E., McDonald, A., Lefebvre, P., Schlesinger, P. (2006) Modelling conservation in the Amazon basin. Nature Letters, Vol 440, doi 101038/nature04389

Soares-Filho B, *et al*. (2012) 'Forest fragmentation, climate change and understory fire regimes on the Amazonian landscapes of the Xingu headwaters'. Landscape Ecol. 27, 585–598 (doi:10.1007/s10980-012-9723-6)10.1007/s10980-012-9723-6

Song, Chao, Mei-Po Kwan, and Jiping Zhu. "Modeling Fire Occurrence at the City Scale: A Comparison between Geographically Weighted Regression and Global Linear Regression." Ed. Jason K. Levy. International Journal of Environmental Research and Public Health 14.4 (2017): 396. PMC. Web. 31 July 2018.

Spessa, A. (2009) Fire Modelling in JULES using SPITFIRE: 'Spread and Intensity of Fires and Emissions' Model. Presentation at JULES 2009 meeting http://jules.jchmr.org/content/meetings

Stauffer, C (2015) 'El Niño seen bringing drought to Brazil's north, heavy rains to south'. Reuters, Environment, 2015 (https://www.reuters.com/article/us-weather-elnino-brazil/el-nino-seen-bringing-drought-to-brazils-north-heavy-rains-to-south-idUSKBN0OB1SP20150526)

Staver, A. C., Archibald, S., and Levin, S. A. (2011) 'The global extent and determinants of savanna and forest as alternative biome states'. Science, 334, 230–232, doi:10.1126/science.1210465

ter Steege, H. *et al*. (2013) 'Hyperdominance in the Amazonian tree flora'. Science 342, 1243092

Stocker, T.F., D. Qin, G.-K. Plattner, M. Tignor, S.K. Allen, J. Boschung, A. Nauels, Y. Xia, V. Bex and P.M. Midgley (eds.)]. (2013): IPCC, 2013: Summary for Policymakers. In: Climate Change 2013: The Physical Science Basis. Contribution of Working Group I to the Fifth Assessment Report of the Intergovernmental Panel on Climate Change. Cambridge University Press, Cambridge, United Kingdom and New York, NY, USA.

Stowe, L. L., Carey, R. M. & Pellegrino, P. P. (1992) Monitoring the Mt. Pinatubo aerosol layer with NOAA/11 AVHRR data. Geophys. Res. Lett. 19, 159–162.

Szopa, S., Balkanski, Y., Schulz, M. *et al*. Clim Dyn (2013) 40: 2223. https://doi.org/10.1007/s00382-012-1408-y

Tansey, K., *et al*. (2004), Vegetation burning in the year 2000: Global burned area estimates from SPOT VEGETATION data, J. Geophys. Res., 109, D14S03, doi:10.1029/2003JD003598.

Thomas, D., Butry, D., Gilbert, S., Webb, D., Fund, J. (2017) The costs and losses of wildfires; a literature survey. US Department of Commerce, National Institute of Standards and Technology. https://doi.org/10.6028/NIST.SP.1215

Thonicke, K., S. Venevsky, S. Sitch & W. Cramer (2001) The role of fire disturbance for global vegetation dynamics: coupling fire into a Dynamic Global Vegetation Model. Global Ecology and Biogeography, 10, 661-677.

Thonicke, K., A. Spessa, I. Prentice, S. Harrison, L. Dong & C. Carmona-Moreno (2010) The influence of vegetation, fire spread and fire behaviour on biomass burning and trace gas emissions: results from a process-based model. Biogeosciences, 7, 1991-2011.

Trenberth, K. E., (1997): The definition of El Niño. Bull. Amer. Meteor. Soc., 78, 2771–2777

Trenberth, K. E., and Dai, A. (2007). Effects of Mount Pinatubo volcanic eruption on the hydrological cycle as an analog of geoengineering, Geophys. Res. Lett., 34, L15702, doi:10.1029/2007GL030524.

Turner, B.L. (1990) The Earth as transformed by human action. Professional Geographer. Volume: 40 Issue: 3 Pages: 340-341 DOI: 10.1111/j.0033-0124.1988.00340.x

Turner II, B.L., Skole, D.L., Sanderson, S., Fischer, G., Fresco, L.O., Leemans, R., (1995). Land-use and land-cover change. Science/Research Plan. Stockholm and Geneva: IGBP Report No. 35 and HDP Report No. 7, 132 pp.

United Nations / Framework Convention on Climate Change (2015). Adoption of the Paris Agreement, 21st Conference of the Parties, Paris: United Nations. FCCC/CP/2015/L.9/Rev.1

Vaughan NE & Lenton TM. (2011). A review of climate geoengoineering proposals. Climatic Change, 109, 745-790; doi: 10.10007/s10584-011-0027-7

van Vuuren, D., J. Edmonds, M. Kainuma, K. Riahi, A. Thomson, K. Hibbard, G. Hurtt, T. Kram, V. Krey, J. Lamarque, T. Masui, M. Meinshausen, N. Nakicenovic, S. Smith & S. Rose (2011). The representative concentration pathways: an overview. Climatic Change, 109, 5-31.

Venevsky, S., K. Thonicke, S. Sitch & W. Cramer (2002) Simulating fire regimes in human-dominated ecosystems: Iberian Peninsula case study. Global Change Biology, 8, 984-998.

Venevsky, S., Richard Betts, Chris Jones, Tomasz Kasikowski, Yannick Le Page, Chris Huntingford (2007) Development a prototype fire model for Hadley

GCMs, *unpublished*

Ward, D.S., Kloster, S., Mahowald, N.M., Rogers, B.M., Randerson, J.T., Hess, P.G., (2012) The changing radiative forcing of fires: global model estimates for past, present and future. Atmos. Chem. Phys. 12, 10857–10886.

Watson, R.T., Ian R. Noble, Bert Bolin, N. H. Ravindranath, David J. Verardo and David J. Dokken (Eds.) IPCC (2000) Cambridge University Press, UK. pp 375. Available from Cambridge University Press, The Edinburgh Building Shaftesbury Road, Cambridge CB2 2RU ENGLAND.

Wei X, Li Q, Zhang M, *et al*. Vegetation cover—another dominant factor in determining global water resources in forested regions (2018) Glob Change Biol.;24:786–795. https://doi.org/10.1111/gcb.13983

Westerling, A. L., Hidalgo, H. G., Cayan, D. R., and Swetnam, T. W.: Warming and earlier spring increase western U.S. forest wildfire activity., Science, 313, 940–943, doi:10.1126/science.1128834, 2006.

van der Werf, G. R., J. T. Randerson, G. J. Collatz, L. Giglio, P. S. Kasibhatla, A. F. Arellano Jr., S. C. Olsen, E. S. Kasischke (2004) Continental-scale partitioning of fire emissions during the 1997 to 2001 El Niño/La Niña period. Science 303, 73–76. doi:10.1126/science.1090753pmid:14704424

van der Werf, G. R., Randerson, J. T., Giglio, L., van Leeuwen, T. T., Chen, Y., Rogers, B. M., Mu, M., van Marle, M. J. E., Morton, D. C., Collatz, G. J., Yokelson, R. J., and Kasibhatla, P. S. (2017) Global fire emissions estimates during 1997–2016, Earth Syst. Sci. Data, 9, 697–720, https://doi.org/10.5194/essd-9-697-2017.

Veraverbeke, S., Rogers, B. M., Goulden, M. L., Jandt, R. R., Miller, C. E., Wiggins, E. B. and Randerson, J. T.: Lightning as a major driver of recent large fire years in North American boreal forests, Nat. Clim. Chang., 7(7), 529–534, doi:10.1038/nclimate3329, 2017.

Wilkenskjeld, S. Kloster, J. Pongratz, T. Raddatz, and C. H. Reick (2014) 'Comparing the influence of net and gross anthropogenic land-use and land-cover changes on the carbon cycle in the MPI-ESM'. Biogeosciences, 11, 4817–4828, DOI :10.5194/bg-11-4817-2014

Williams, M.: Deforesting the Earth (2006) from Prehistroy to Global Crisis, University of Chicago Press

Wiltshire, A., Dan Bernie, Richard A. Betts, Chantelle Burton, Pete Falloon, Jonathan M. Gregory, Jim M. Haywood, Andy Jones, Anthony C. Jones, Chris D. Jones, Ron Kahana, Jason A. Lowe, Ian Totterdall, Steven Turnock. (in prep) Ecosystem Services, Unconventional Mitigation and Avoiding the 1.5°C Climate Overshoot

Withey K, et al. (2018). Quantifying the immediate carbon emissions from El Niño-mediated wildfires in humid tropical forests. Phil. Trans. R. Soc. B 373, 20170312 (10.1098/rstb.2017.0312)

White, A., M. Cannell & A. Friend (1999) Climate change impacts on ecosystems and the terrestrial carbon sink: a new assessment. Global Environmental Change-Human and Policy Dimensions, 9, S21-S30.

Wu, M., Knorr W, Thonicke K, Schurgers G, Camia A, Arneth A. Sensitivity of burned area in Europe to climate change, atmospheric CO2 levels and demography: a comparison of two fire-vegetation models. J Geophys Res: Biogeosci. (2015);120:2256–72. doi: 10.1002/2015JG003036.

Yin, L., Fu, R., Shevliakova, E. *et al*. Clim Dyn (2013) 41: 3127. https://doi.org/10.1007/s00382-012-1582-y

Yoon, J. H., Wang, S.-Y. S., Gillies, R. R., Hipps, L., Kravitz, B. and Rasch, P.J. (2015). Extreme fire season in California: A glimpse into the future? [in "Explaining Extremes of 2014 from a Climate Perspective"]. Bull. Amer. Meteor. Soc, 96 (12),S5 –S9.

Yu, L., S. Zhong, W. E. Heilman, and X. Bian (2017), A comparison of the effects of El Niño and El Niño Modoki on subdaily extreme precipitation occurrences across the contiguous United States, J. Geophys. Res. Atmos.,122,7401–7415, doi:10.1002/2017JD026683

Zemp, D. C., C.-F. Schleussner, H. M. J. Barbosa, and A. Rammig (2017), Deforestation effects on Amazon forest resilience, Geophys. Res. Lett., 44, doi:10.1002/2017GL072955

Zhang, K.; Castanho, A.; Galbraith, D.R.; Moghim, S.; Levine, N.; Bras, R.L.; Coe, M.; Costa, M.H.; Malhi, Y.; Longo, M.; Knox, R.G.; McKnight, S.; Wang, J.; Moorcroft, P.R. (2015) 'The Fate of Amazonian Ecosystems over the Coming Century Arising from Changes in Climate, Atmospheric CO2 and Land-use'. Global Change Biology (2015) 21, 2569–2587, doi: 10.1111/gcb.12903

Zhang, Y., R. Fu, H. B. Yu, Y. Qian, R. Dickinson, M. Dias, P. L. D. Dias & K. Fernandes (2009) Impact of biomass burning aerosol on the monsoon circulation transition over Amazonia. *Geophysical Research Letters,* 36**,** 6.

Zhang, Y. and Wiltshire, A. (2014) 'The impact of land-use change on terrestrial carbon flux in China'. Met Office report, unpublished

CSSP Reports and Deliverables

Parts of this work have also been based on deliverables submitted as part of the Newton Funded Met Office Climate Science for Service Partnership project Brazil (CSSP Brazil), as follows:

D1.1.1 Burton, C. and Cardoso, M. (2017) 'Assessment report of fire modelling over Brazil (Chapter 1 section 5 'Fire Models')

D3.4.1 Burton, C., and Cardoso, M. (2017) 'Report on land-use in INLAND and JULES' (Chapter 2 'Land-use and land surface modelling')

D1.1.5 Burton, C., Betts, R., Cardoso, M., Feldpausch, T., Harper, A., Jones, C., Robertson, E. and Wiltshire, A. (2017) 'Fire developments in UKESM code base' (Chapter 3, section 2 'Representing disturbance in JULES')

Websites (marked as footnotes in text where appropriate):

Accuweather cost of 2017 Californian fires https://www.accuweather.com/en/weather-news/accuweather-predicts-2017-california-wildfire-season-cost-to-rise-to-180-billion/70003495

AMAZALERT deliverables: http://www.eu-amazalert.org/publications/deliveryreports

Bureau of Meteorology El Niño Impacts: http://www.bom.gov.au/climate/updates/articles/a018.shtml

Cal Fire http://www.calfire.ca.gov/

CCST: http://www.ccst.inpe.br/projetos/inland/

Climate Lab Book: https://www.climate-lab-book.ac.uk/comparing-cmip5-observations/

ESA CCI https://www.esa-landcover-cci.org/?q=node/175

Fire Science Project, 'Fire History and Climate Change', Chapter 3: https://www.firescience.gov/JFSP_fire_history.cfm

Fire vegetation adaptation: https://www.britannica.com/list/5-amazing-adaptations-of-pyrophytic-plants

FSSI: http://www.ess.uci.edu/~amazonfirerisk/ForecastWeb/SAMFSS2016.html

GFED data: https://daac.ornl.gov/VEGETATION/guides/fire_emissions_v4.html

GFED data fire emissions: https://www.geo.vu.nl/~gwerf/GFED/GFED4/tables/GFED4.1s_C.txt

Global Carbon Project historical emissions: http://www.globalcarbonproject.org/carbonbudget/17/data.htm

GLOBSCAR: http://due.esrin.esa.int/page_project24.php

HYDE: http://themasites.pbl.nl/tridion/en/themasites/hyde/introduction/index-2.html

INPE fire data: http://www.inpe.br/queimadas/portal

IPCC LUC: http://www.ipcc.ch/ipccreports/sres/land_use/index.php?idp=24

IPCC RCP overview: http://sedac.ipcc-data.org/ddc/ar5_scenario_process/RCPs.html

Kanikicharla UNFCCC CMIP projections: https://unfccc.int/sites/default/files/4_krishna_sbsta.pdf

Met Office Carbon Budgets http://www.metoffice.gov.uk/binaries/content/assets/mohippo/pdf/climate/cop22/theme_2-carbon-budgets.pdf

Met Office, ENSO impacts
https://www.metoffice.gov.uk/research/climate/seasonal-to-decadal/gpc-outlooks/el-nino-la-nina/enso-impacts

MODIS: http://modis-fire.umd.edu/index.php

NASA Amazon fires:
https://earthobservatory.nasa.gov/Features/AmazonFire/amazon_fire2.php

NASA El Niño impacts: https://www.nasa.gov/press-release/nasa-examines-global-impacts-of-the-2015-el-ni-o

NASA PLACE maps: NASA PLACE maps:
http://sedac.ciesin.columbia.edu/data/set/nagdc-population-landscape-climate-estimates-v3/maps?facets=region:africa

NOAA CPC:
http://origin.cpc.ncep.noaa.gov/products/analysis_monitoring/ensostuff/ONI_v5.php

PRODES:
Funded by the Brazilian Ministry of Science, Technology and Communications (MCTIC) through the "Monitoramento Ambiental da Amazônia" (Environmental Monitoring of Amazônia) program at INPE:
http://www.obt.inpe.br/OBT/assuntos/programas/amazonia/prodes
https://www.arcgis.com/home/item.html?id=4160f715e12d46a98c989bdbe7e5f4d6

RECON land cover: http://cera-www.dkrz.de/WDCC/ui/Entry.jsp?acronym=RECON_LAND_COVER_800-1992

SEEG Brazil: http://plataforma.seeg.eco.br/map

Swaling: http://www.exmoor-nationalpark.gov.uk/living-and-working/info-for-farmers-and-land-managers/swaling

TRENDY: http://dgvm.ceh.ac.uk/

UKESM: https://ukesm.ac.uk/

US CENSUS BUREAU – impacts of 2017 Californian fires
https://www.census.gov/topics/preparedness/events/wildfires/2017-ca-wildfires.html

Wildfire deaths: http://newsinfo.inquirer.net/148611/wildfires-kill-339000-people-per-year-study

WWF ecoregions: https://www.worldwildlife.org/publications/terrestrial-ecoregions-of-the-world

Data availability

The JULES code used in these experiments is freely available on the JULES trunk from version 4.8 (revision 6925) onwards. Driving data for JULES comprises short and longwave radiation, precipitation, air temperature, air specific humidity, wind, and air pressure.

The rose suite used for the experiments in Chapter 3 is u-ap845, using JULES at Vn4.9 r9986. The set up uses a configuration of JULES based on JULES-TRENDY with the addition of fire, driven with CRU-NCEP data, HYDE land-use, Brooks and Corey soil hydraulics, at N96 resolution (140km grid size / 2 degrees resolution).

The rose suite used for the experiments in Chapter 4 is u-an205, using JULES at Vn4.9 r9522. As above, the set up uses a configuration of JULES based on JULES-TRENDY with the addition of fire, using HYDE land-use data, Brooks and Corey soil hydraulics, at N96 resolution (140km grid size / 2 degrees resolution). This experiment uses driving data based on CRU-NCEP, but modified as described in the Methods section of the Chapter to simulate an additional 'No El Niño' state using a mean climatology from the previous 10 years for 2015/2016.

The rose suite used for the experiments in Chapter 5 is u-as280, using JULES at Vn4.9 r9986. As above, the set up uses a configuration of JULES based on JULES-TRENDY with the addition of fire, using Brooks and Corey soil hydraulics, at N96 resolution (140km grid size / 2 degrees resolution). This experiment uses driving data from HadGEM2-ES, which uses the land surface scheme MOSES2, which is approximately comparable to the JULES-C configuration, including dynamic vegetation. The future scenarios use the RCPs for CO_2 concentration and land-use change for RCP2.6, RCP4.5 and RCP8.5.

Chapter 6 uses data from HadGEM2-ES, with an additional SRM scenario using SO_2 aerosol injection to limit future temperature rise to 1.5°C above pre-industrial levels, as described in the chapter. The model output was then used to compute the McArthur FFDI and Angström Indices. The fire index data is available through BADC at:

McArthur FFDI: http://dx.doi.org/10.5285/70ac55eb85344c3bb2239ed2d7b7575d

Angström Index: http://dx.doi.org/10.5285/75a7e567fe2342a493663a7a085d015e

All JULES suites and code are available on the JULES FCM repository: https://code.metoffice.gov.uk/trac/jules (registration required).

Data acknowledgements

Thanks to Inika Taylor of the Met Office Hadley Centre, for her guidance on calculating the Drought Index used in chapter 6. Thanks to Andy Jones also of the Met Office Hadley Centre for his kind permission to use the HadGEM2-ES scenarios with SRM that he produced. Thanks also to Nicolas Viovy and Philippe Ciais who created the CRU-NCEP datasets used to run JULES.